SHORT PAPERS IN—

Analytical methods

Cartographic techniques

Coastal geohydrology

Economic geology

Geochemistry

Geochronology

Geophysics

Ground water

Mineralogy

Petrology

Paleontology

Quality of water

Rock mechanics

Sedimentation

Soil moisture

Stratigraphy

Surface water

GEOLOGICAL SURVEY RESEARCH 1969

Chapter B

GEOLOGICAL SURVEY PROFESSIONAL PAPER 650–B

GEOLOGICAL SURVEY RESEARCH 1969

Chapter B

GEOLOGICAL SURVEY PROFESSIONAL PAPER 650-B

Scientific notes and summaries of investigations in geology, hydrology, and related fields

UNITED STATES GOVERNMENT PRINTING OFFICE, WASHINGTON: 1969

UNITED STATES DEPARTMENT OF THE INTERIOR

WALTER J. HICKEL, Secretary

GEOLOGICAL SURVEY

William T. Pecora, Director

For sale by the Superintendent of Documents, U.S. Government Printing Office
Washington, D.C. 20402 – Price $2.75

CONTENTS

GEOLOGIC STUDIES

Cartographic techniques

HYDROLOGIC STUDIES

Ground water

Surface water

Relation between surface water and ground water

Quality of water

Geochemistry of water

Coastal geohydrology

Soil moisture

INDEXES

GEOLOGICAL SURVEY RESEARCH 1969

This collection of 40 short papers is the first published chapter of "Geological Survey Research 1969." The papers report on scientific and economic results of current work by members of the Conservation, Geologic, and Water Resources Divisions of the U.S. Geological Survey.

Chapter A, to be published later in the year, will present a summary of significant results of work done during fiscal year 1969, together with lists of investigations in progress, reports published, cooperating agencies, and Geological Survey offices.

"Geological Survey Research 1969" is the tenth volume of the annual series Geological Survey Research. The nine volumes already published are listed below, with their series designations.

Geological Survey Research 1960—Prof. Paper 400
Geological Survey Research 1961—Prof. Paper 424
Geological Survey Research 1962—Prof. Paper 450
Geological Survey Research 1963—Prof. Paper 475
Geological Survey Research 1964—Prof. Paper 501
Geological Survey Research 1965—Prof. Paper 525
Geological Survey Research 1966—Prof. Paper 550
Geological Survey Research 1967—Prof. Paper 575
Geological Survey Research 1968—Prof. Paper 600

ORIGIN OF SOME AMPHIBOLITES IN WESTERN NORTH CAROLINA

By ARTHUR E. NELSON, Beltsville, Md.

Abstract.—Many bodies of amphibolite are interlayered with metasedimentary rocks in western North Carolina. Statistical data, field studies, and chemical affinities between these amphibolites and known ortho-amphibolites and basic igneous rocks strongly suggest that most of the amphibolites are ortho-amphibolites, rather than para-amphibolites. It is not known whether the rocks were originally intrusive bodies, basic tuffs, or lava flows, but probably many of the bodies represent thin-bedded pyroclastic deposits of basaltic composition and basalt flows that were interbedded with more felsic rocks. Others represent intrusive rocks of gabbroic origin, and some may represent dolerite dikes.

Many bodies of amphibolite are present in a relatively high grade metamorphic terrane in the south-central part of the Knoxville 1° by 2° quadrangle in North Carolina (fig. 1). The origin of these amphibolites is enigmatic, as it is difficult to distinguish ortho-amphibolites from para-amphibolites. Keith (1907a, b), who mapped parts of the Knoxville quadrangle, believed that the amphibolites originated from igneous rocks but stated that this would be difficult to prove.

This report presents the results of recent field and chemical studies that might help to determine the origin of these amphibolites. The chemical relations used are principally those suggested by Leake (1964), and the statistical approach is that of Shaw and Kudo (1965).

GENERAL GEOLOGIC SETTING

Much of the Knoxville quadrangle is underlain by a Precambrian gneiss-schist complex, consisting mainly of layered felsic gneisses, mica gneisses and schists, metasandstones, quartzo-feldspathic gneisses that are highly segregated into quartz-feldspar planar streaks, and migmatites. In addition, numerous bodies of both amphibolite and granite gneiss are present within the complex. Locally, small bodies of dunite and serpentinite are associated with the amphibolites. Rocks of the complex were referred to by Keith (1907a) as the Carolina gneiss, and the amphibolite bodies were called the Roan gneiss. These names are, however, no longer in use. Overlying these rocks are younger Precambrian units of the Ocoee Series (Hadley and Goldsmith, 1963), and, in the southwest corner of the quadrangle, rocks of the Ocoee Series are overlain by younger metasedimentary rocks of the Murphy marble belt indicated on figure 1 by (pЄ–Pz).

Most amphibolites in the Knoxville quadrangle occur within the older gneisses and schists. Amphibolites are not as commonly observed in the Ocoee rocks, and they have rarely been observed in the post-Ocoee rocks of the Murphy marble belt (Van Horn, 1948, p. 15–17). Field evidence suggests that the amphibolite bodies in the study area shown in figure 1 were subjected to the same regional metamorphism and deformation as the surrounding rocks.

Hadley and Goldsmith (1963, p. B107) indicated that rocks immediately north of the report area, within the Knoxville quadrangle, are polymetamorphic. Field and laboratory studies also suggest that the rocks in the report area have been subjected to several episodes of metamorphism. Most of the rocks are in the kyanite-muscovite-quartz and sillimanite-almandine subfacies of the almandine amphibolite facies of regional metamorphism (Fyfe and others, 1958, p. 230–231).

After an early period of deformation and regional thermal metamorphism, the rocks were further deformed and, in places, isoclinally folded. This later deformation (Hadley and Goldsmith, 1963, p. B107), which produced regional structures with a dominant northeast trend, was superposed upon previous structures, and locally the resultant fold pattern is most complex.

DISTRIBUTION AND DESCRIPTION OF THE AMPHIBOLITES

The amphibolite bodies range from thin discontinuous layers or bands less than half an inch thick, to pods, lenses, and boudinaged bodies several feet or more in length, to larger rather massive units several miles or more in length. Only the larger amphibolite

U.S. GEOL. SURVEY PROF. PAPER 650-B, PAGES B1-B7

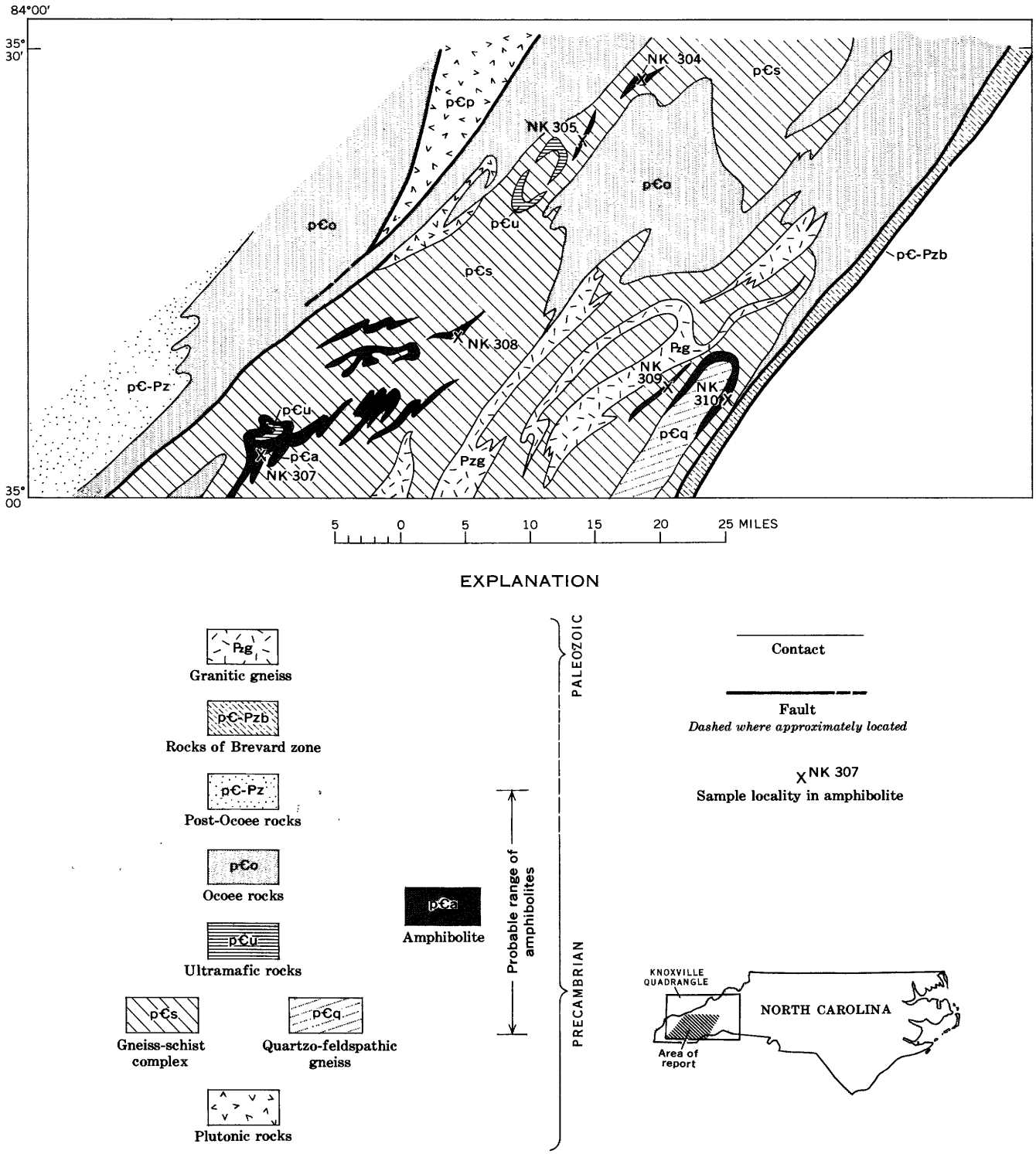

FIGURE 1.—Generalized geologic map of part of the Knoxville 1° by 2° quadrangle in North Carolina and South Carolina.

bodies are shown in figure 1. Almost all bodies of amphibolite are interlayered and conformable with the more felsic units of the gneiss-schist complex. The proportion of amphibolite to more felsic rock varies widely. In places, a thin band of amphibolite is present in a thick sequence of felsic rock; elsewhere, amphibolite predominates, and only a thin lens of felsic material is present. Commonly, however, layers of amphibolite that range from 6 inches to 4 or 5 feet in thickness alternate with similar thicknesses of more felsic rocks. Many of the layered amphibolite bodies are striped. This feature results from metamorphic segregation of felsic and mafic constituents into thin, alternating, light and dark layers.

The bodies of amphibolite conform to the regional structure, and they, like the surrounding rocks, are locally folded. The folds range from small crenulations to minor folds seen in outcrop and to larger folds determined only by mapping. Many interlayered units, consisting both of amphibolite and the surrounding rock types, have been subjected to metamorphic segregation, shearing, and tectonic thinning. All the observed amphibolites have a foliation which is parallel to that of the intercalated rocks. Foliation is highly developed in the thinner amphibolite layers, whereas in the central parts of some of the larger bodies it is indistinct and the rocks appear massive. The contacts between the amphibolite bodies and adjacent rocks are usually sharp, but some appear gradational. Almost all the contacts are parallel to the regional foliation; only one small amphibolite body was observed that was discordant with the regional planar structures.

The amphibolites range from medium gray to greenish black and usually are fine to medium grained; only rarely are they coarse grained. In places, highly biotitic zones are present as distinct layers within the amphibolites, and locally there are distinct felsic segragations as well as streaks of silexite. In addition to alined hornblende crystals, thin blades or rods of felsic and quartz segregations are also commonly alined in the foliation plane, forming lineations. These linear structures, which parallel fold axes, are presumed to be "b" lineations.

The amphibolites are composed principally of hornblende and plagioclase and lesser amounts of quartz, biotite, garnet, and magnetite; sphene and apatite commonly are present in trace amounts. Rarely, chlorite is present as an alteration product of hornblende; sericite, which is sparse, occurs as tiny patches on some plagioclase grains; and epidote and calcite are likewise rare. Generally, hornblende and plagioclase make up 80 percent or more of the rock; hornblende makes up 88 percent of one sample.

Most of the textures are xenomorphic, but in places lepidoblastic textures also occur. The minerals are mostly fine to medium grained, ranging from 0.3 to 4 millimeters in length; they are rarely coarse grained.

The hornblende is green to brownish green, commonly poikilitic, and calcium rich. It is anhedral to prismatic, and X-ray diffraction patterns show that it has a structure similar to tremolite, a feature common to may hornblendes of varying composition (Deer and others, 1962, p. 203). The plagioclase ranges from An_{23} to An_{33} and generally is finer grained than the hornblende. The biotite is brownish red and appears to have replaced hornblende. In some outcrops, sulfides, mostly pyrite, were observed.

FIELD RELATIONS

Almost all amphibolite bodies and their planar structures are parallel to the lithologic layering and gneissic structure of the enclosing gneisses and schists. The compositional layering in the host rocks probably represents strata of the premetamorphic rock sequence. Thus, the included amphibolitic bodies that alternate with the layered gneiss could be interpreted as part of the original rock sequence. In the absence of primary sedimentary structures, however, parallelism between amphibolite bodies and host rocks is not an absolute criterion upon which to base the conclusion that the amphibolites were originally sedimentary rocks. Lithologic layering or banding can also be produced by metamorphic segregation or tectonic intercalation of slices of one rock into another, especially along such planes of weakness as bedding or schistosity. In addition, parallel banding can also result from transposition of rocks during intense deformation. Although many of the amphibolite bands are not folded, some appressed fold hinges have been observed within them and in the host rocks as well, indicating that the bands have been intensely deformed and are probably transposed. In a few places, the amphibolites have boudinage structure suggesting that, at least locally, the rocks have undergone considerable extension. Thus, if some of the banded amphibolite bodies were originally mafic dikes in the country rocks, their present parallelism with the more felsic gneisses could probably be a result of extension and transposition of the dikes during deformation.

AGE RELATIONS

The amphibolite bodies in the gneiss-schist complex in the Knoxville 1° by 2° quadrangle (fig. 1) were first described by Keith (1905, 1907c), who believed they were Precambrian in age. Kulp and Poldervaart

(1956) discussed the metamorphic events and age relations of rocks in the Bakersville–Roan Mountain area, which is northeast along strike in the same tectonic block as the rocks of this report; they suggest that the Roan gneiss (layered amphibolites) was metamorphosed prior to the intrusion of some ultramafic rocks, but indicate that both rock types are Precambrian in age. Then, between the emplacement of the ultramafic rocks and a period of regional metamorphism at or near the end of the Ordovician, The Bakersville–Roan Mountain metadolerite dike swarm was emplaced.

In the report area, those amphibolite bodies that are relatively thin and interlayered with rocks of the gneiss-schist complex are believed to be time equivalent to rocks that Kulp and Poldervaart referred to as Roan gneiss; the larger more massive amphibolite bodies, which are closely associated with ultramafic rocks in the report area, are believed to be equivalent in age to the late Precambrian ultramafic rocks of Kulp and Poldervaart. The metadolerite dike swarm does not appear to have an analog in the report area. However, if deformation that accompanied the Late Ordovician(?) metamorphic event was more intense in the report area than in the Bakersville–Roan Mountain area, individual dolerite dikes, if originally present, probably cannot be distinguished from older amphibolite bodies. Thus, it seems highly probable that amphibolite bodies of the report area represent those formed during several episodes spanning a time interval that includes part of the Precambrian and that extends into the lower Paleozoic.

The metadolerites and some ortho-amphibolites of the Bakersville–Roan Mountain area were described by Wilcox and Poldervaart (1958) and are similar in chemical composition to the amphibolites of this report.

CHEMICAL RELATIONS

Table 1 presents six new chemical analyses, and table 2 presents semiquantitative spectrographic analy-

TABLE 1.—*Chemical and modal analyses of amphibolites from a part of the Knoxville quadrangle in western North Carolina and chemical analyses of two sedimentary rocks and one basalt flow for comparison*

[Samples analyzed by methods described by Shapiro and Brannock (1962). Analysts: Paul Elmore, Sam Botts, Gillison Chloe, Lowell Artis, Hezekiah Smith, James Kelsey, and J. L. Glenn. Symbols: Tr., trace; *, trace of chlorite]

Field No.	NK 304	NK 305	NK 307	NK 308	NK 309	NK 310	Shale [1]	Magnesian [2] limestone	Basalt [3]
Lab. No.	W168622	W168623	W168624	W168625	W168626	W168627			
Chemical analyses									
SiO_2	48.9	49.8	49.9	47.9	48.6	48.9	45.89	3.24	48.8
Al_2O_3	8.1	16.0	15.5	15.8	14.0	15.2	13.24	.17	14.4
Fe_2O_3	1.4	2.1	3.5	4.8	4.3	3.9	3.88	.17	4.4
FeO	8.4	8.4	7.1	9.7	9.0	7.6	----------	.06	4.6
MgO	16.3	7.0	8.3	5.3	5.5	4.6	2.12	20.84	5.4
CaO	11.8	9.9	10.4	10.4	9.2	11.3	12.09	29.58	8.3
Na_2O	.82	2.4	2.6	2.5	1.7	2.5	.47	----------	2.3
K_2O	.92	.80	.23	.50	.49	.32	2.31	----------	5.1
H_2O-	.08	.05	.07	.06	.62	.40	1.38	.30	.3
H_2O+	.74	.71	.63	.78	2.0	1.8	4.16		2.2
TiO_2	.96	1.7	.78	1.3	4.0	3.2	.52	----------	.72
P_2O_5	.55	.16	.00	.07	.37	.37	.17	----------	.58
MnO	.28	.09	.15	.16	.07	.06	----------	----------	.15
CO_2	.11	<.05	.10	<.05	<.05	<.05	10.38	45.54	2.4
Organic matter	----------	----------	----------	----------	----------	----------	3.47	----------	----------
Sum	99	99	99	99	100	100	100.08	99.90	99
Powder density by air pycnometer	3.05	2.96	3.00	3.08	3.02	3.00	----------	----------	----------
Bulk density	3.05	2.96	3.00	3.08	3.02	3.00	----------	----------	----------
Modal analyses (volume percent)									
Quartz	----------	3	5	8	6	2	----------	----------	----------
Plagioclase	Tr	25	17	25	16	30	----------	----------	----------
Hornblende	*88	67	*74	*60	*72	50	----------	----------	----------
Biotite	8	5	Tr	1	Tr	----------	----------	----------	----------
Epidote	----------	----------	4	3	----------	14	----------	----------	----------
Garnet	----------	Tr	----------	----------	----------	----------	----------	----------	----------
Magnetite	1	----------	Tr	3	3	Tr	----------	----------	----------
Accessory minerals (includes sphene and apatite)	3	Tr	Tr	Tr	3	4	----------	----------	----------

[1] From Clarke (1924, p. 552). [2] From Clarke (1924, p. 579). [3] From Nelson (1966b).

EXPLANATORY NOTES FOR TABLE 1

NK 304. Massive amphibolite layer (one of several amphibolite layers in quartzo-feldspathic gneiss) exposed on road, 0.3 mile north of Pleasant Balsam Church in Hazelwood 7½-minute quadrangle, North Carolina. Very dark greenish gray to black, medium to coarse grained. Consists of about 88 percent hornblende that is greenish brown, ranges from anhedral to subhedral, and is commonly poikilitic. Other minerals include about 8 percent biotite, some opaque minerals, apatite, garnet, and sphene. Chlorite is incipiently developed along edges of some hornblende grains. In hand specimen, amphibolite appears almost massive, but in outcrop a faint foliation is observed.

NK 305. Massive amphibolite exposed on a new road, 0.15 mile southeast of Willits in the Addie 7½-minute quadrangle, North Carolina. Locally mixed and streaked with quartzo-feldspathic gneiss. Dark greenish gray, fine to medium grained, and in places, segregated into thin felsic and mafic bands. Xenomorphic texture. Hornblende and sodic andesine together form 92 percent of rock; other minerals include biotite, quartz, and garnet, which locally occur in isolated clusters. An opaque mineral, probably magnetite, and sphene and epidote occur in trace amounts. Hornblende is brown, usually anhedral, and commonly poikilitic. Sodic andesine is about same size as hornblende and contains a few isolated patches of sericite. Foliation is moderately developed.

NK 307. Massive amphibolite exposed near Glade Gap, 0.2 mile from east edge of Shooting Creek 7½-minute quadrangle, North Carolina. Part of body is closely associated with dunite. Medium to dark greenish gray, mostly medium grained. Xenomorphic texture. Locally faintly segregated into thin felsic and mafic bands. Hornblende, which makes up 74 percent of rock, is mostly anhedral, brownish green, somewhat poikilitic, and is larger in size than associated calcic oligoclase. Other minerals include quartz, epidote, and chlorite. Sparse chlorite is formed along margins of some hornblende grains. Sphene and opaque minerals occur in trace amounts. Foliation well developed.

NK 308. Partly streaked, massive amphibolite exposed on U.S. Route 64, north 0.3 mile from Salem Church in Corbin Knob 7½-minute quadrangle, North Carolina. Dark greenish gray to black, mostly medium grained. In places, thin discontinuous streaks of felsic segregations of plagioclase and quartz are common and give a striped appearance to rock. Hornblende, calcic oligoclase, and quartz are principal constituents. Hornblende is brownish green, ranges from anhedral to subhedral, and is locally poikilitic. Oligoclase is smaller than hornblende and is commonly aggregated with quartz, forming felsic streaks. Minor amounts of biotite, apatite, magnetite, and epidote, and traces of both calcite and chlorite are present. In general, amphibolite is well foliated.

NK 309. Thin-layered amphibolite exposed on U.S. Route 64, half a mile from east edge of Cashiers 7½-minute quadrangle, North Carolina. Rock shows interlayering of biotite felsic gneiss and other amphibolites. Dark greenish gray, fine to medium grained, amphibolite has a general salt-and-pepper appearance. Segregation of felsic and mafic constituents is common and locally gives rock a striped appearance. For most part, amphibolite has xenomorphic texture, but locally is lepidoblastic. Hornblende, which makes up about 72 percent of rock, is brown with a green tint and is largest grained mineral present. Other minerals include calcic oligoclase, quartz, biotite, sphene, and magnetite. In places, minerals are elongate in plane of foliation.

NK 310. Thin layer of amphibolite exposed on U.S. Route 64, about 0.55 mile from east edge of Lake Toxaway 7½-minute quadrangle, North Carolina. Part of a layered sequence of biotite felsic gneiss and thin-layered amphibolite. Dark to medium-gray, fine-grained; mostly a xenomorphic texture and a striped appearance that is due to the segregation of some of its felsic and mafic constituents. Hornblende and calcic oligoclase are principal minerals. Hornblende is green to brownish green and mostly anhedral. Epidote is uniformly distributed; quartz, apatite, and magnetite are irregularly distributed. Trace amounts of chlorite and sericite. Foliation well developed.

ses of amphibolite samples collected in the study area (fig. 1). These samples are believed to be representative of the amphibolites in the area. The analyses correspond in composition to analyses of basalts (Nockolds, 1954). The amphibolites are calcium rich; aluminum content, except for one sample, varies little; sodium is the dominant alkali, as potassium is present in rather small quantities. Only one sample (NK 304) can be considered magnesium rich; in the other samples, total iron exceeds magnesium. Titanium oxide generally exceeds 1 percent (table 1). Semiquantitative spectrographic analyses (table 2) indicate that the amphibolites have, on the average, a higher content of Cr and Ni than do the more felsic gneisses in the area (Nelson, unpub. data).

Amphibolites in the report area are characterized, therefore, by having relatively moderate to high values of Cr, Ni, and Ti and low Niggli *k* ratios (Niggli, 1954, p. 12–14).

TABLE 2.—*Semiquantitative spectrographic analysis of amphibolites from a part of the Knoxville quadrangle in western North Carolina*

[Results are reported in percent to the nearest number in the series 1, 0.7, 0.5, 0.3, 0.2, 0.15, 0.1, and so forth, which represent approximate midpoints of interval data on a geometric scale. The assigned interval for semiquantitative results will include the quantitative value about 30 percent of the time. Analyst: W. B. Crandell. 0, looked for but not detected]

Field No. Lab. No.	NK 304 W168622	NK 305 W168623	NK 307 W168624	NK 308 W168625	NK 309 W168626	NK 310 W168627
Ba	0.02	0.007	0.002	0.002	0.01	0.01
Be	.00015	0	0	0	0	0
Co	.005	.0015	.005	.003	.002	.003
Cr	.15	.01	.015	.007	.007	.0015
Cu	.007	.007	.0015	.007	.007	.005
Ga	.0007	.0015	.001	.0015	.0015	.0015
La	.005	0	0	0	0	0
Mo	0	0	0	.0003	0	0
Nb	0	0	0	0	.0005	.0005
Ni	.05	.005	.01	.007	.007	.002
Pb	0	.001	0	0	0	0
Sc	.005	.002	.005	.005	.002	.003
Sr	.005	.015	.01	.007	.02	.03
V	.015	.01	.02	.015	.02	.015
Y	.002	.002	.002	.002	.003	.003
Yb	.0002	.0002	.0002	.0002	.0003	.0003
Zr	.015	.005	.003	.003	.01	.01

Leake (1964) indicated that amphibolites having a high Cr, Ni, and Ti content and low Niggli *k* values are almost certainly igneous in origin; they probably were derived from basalts, dolerites, or basic tuffs. He mentioned that amphibolites with low Cr, Ni, and Ti values and with high Niggli *k* values can be of either igneous or sedimentary origin. Evans and Leake (1960) made a study of layered amphibolite bodies from Ireland and suggested a chemical means for determining their origin. As no completely diagnostic abundance criteria for major- or minor-element distribution are presently known for distinguishing the various amphibolites, Leake (1964) suggested that trends of variation—rather than absolute concentrations—in the amounts of elements in amphibolites compared with similar trends of known igneous and sedimentary rocks are most useful in determining para-amphibolites from ortho-amphibolites.

Figure 2 shows the plots of Niggli *mg* versus *c* values (Niggli, 1954) of various amphibolite samples, the fields for pelitic rocks and Karroo dolerites of South Africa (basic igneous rocks), and the variation trend of the basic igneous rocks (Leake, 1964, p. 241). Because the amphibolites from the Knoxville quadrangle have a rather wide range of *mg* values, plots for individual samples are shown. These plots follow the trend of variation of basic igneous rocks quite closely.

Figure 3 shows plots of Niggli *mg*, *c*, and *al-alk* values for individual amphibolite samples and gives the field and variation trend for basic igneous rocks (Karroo dolerite samples) (Leake, 1964, p. 243). The field for typical pelitic and semipelitic rocks is shown for comparison. Plots for amphibolite samples from the Knoxville quadrangle and vicinity follow fairly closely the variation trend of the basic igneous rocks.

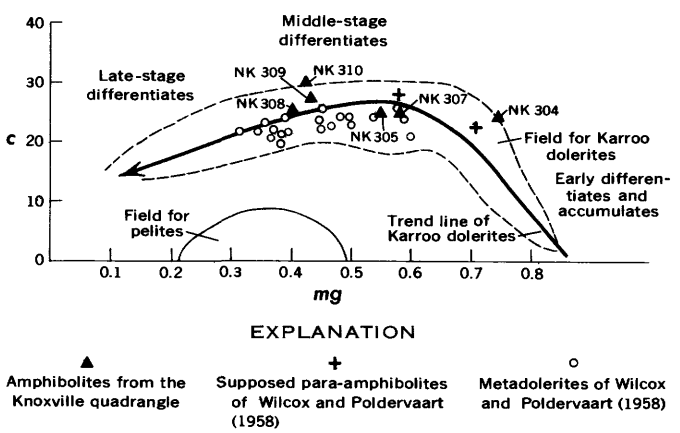

FIGURE 2.—Niggli *c* (CaO) and *mg* (MgO/FeO+MnO+2Fe_2O_3+MgO) variation diagram comparing amphibolites from the Knoxville quadrangle and vicinity with Karroo dolerites (basic igneous rocks). Fields for Karroo dolerites and pelitic rocks are from Leake (1964).

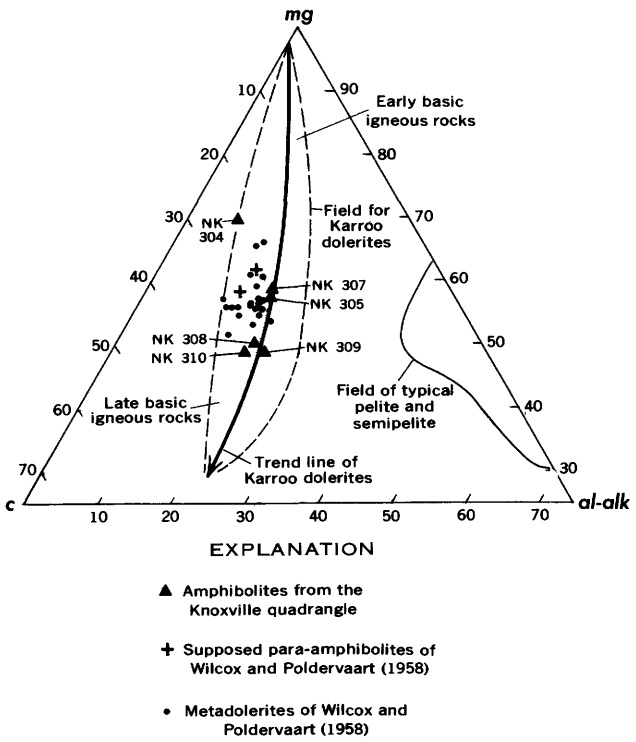

FIGURE 3.—Niggli *mg*, *c*, and *al* (=Al_2O_3)—*alk* (=Na_2O+K_2O) ternary variation diagram comparing amphibolites from the Knoxville quadrangle and vicinity with the Karroo dolerites (basic igneous rocks). Fields for pelite and semipelite and for Karroo dolerites are from Leake (1964).

According to the analyses (table 1) the amphibolites of the report area apparently were not derived from shales (calcareous), because the amphibolite samples have a high total iron and magnesium content and low CO_2 content. Also, they do not seem to have been derived from magnesian limestones (table 1), because the magnesium plus calcium content of the amphibolite samples is not high enough. In addition, the absence of tremolite and diopside and the presence of only trace amounts of calcite, further indicate that the amphibolite bodies were not derived from calcareous or dolomitic shale.

According to figures 2 and 3, the chemical nature of these amphibolites is similar to that of basic igneous rocks. The close coincidence of the amphibolite plots to the trend lines for basic igneous rocks in both figures 2 and 3 strongly suggests an igneous origin for these amphibolites. The chemical comparisons suggest that they could have been derived from gabbros or basalts, but there is no evidence whether they were originally lavas, tuffs, or intrusive rocks.

Shaw and Kudo (1965, p. 423–435) suggest a statistical approach to determining para-amphibolite from ortho-amphibolite. To accomplish this, they list several discriminant functions—X_1, X_2, and X_3 to be

applied to the abundance levels of major oxides and minor elements in a given amphibolite. The appropriate functions were applied to the major oxides and minor elements listed in tables 1 and 2. Values for the function using the major oxides show that all but two samples can be classed as ortho-amphibolite; values for one function using minor elements indicate that all but one sample should be classed as ortho-amphibolite, and values for the other function for minor elements indicate that all samples are ortho-amphibolite.

Sample NK 307, tentatively classed as para-amphibolite by the discriminant function for major oxides, is from the largest amphibolite body in the area; this body is in part interlayered with and closely associated with dunite and is therefore believed to be of igneous origin. Samples NK 307 and 308, classed as para-amphibolite by the major-oxide discriminant, have a moderate to low Cr content, moderate to high Ni content, moderate TiO_2 content, and low Niggli k values. Therefore, according to chemical criteria, these samples could be derived from rocks of igneous parentage.

CONCLUSIONS

Although they are not conclusive, field, chemical, and statistical studies suggest that most amphibolites in the south-central part of the Knoxville quadrangle are ortho-amphibolites rather than para-amphibolites, but it is not known whether these rocks were originally intrusive bodies, basic tuffs, or lava flows. Undoubtedly these basic igneous rocks formed during a long span of time that began in the Precambrian and possibly extended into the early Paleozoic. Probably many of the amphibolite bodies represent thin-bedded pyroclastic deposits of basaltic composition and basalt flows that were interbedded with more felsic rocks. An analog of this type of deposition is in north-central Puerto Rico, where much of the area is underlain by bedded basaltic tuff and basalt of Cretaceous age, interbedded with more felsic deposits and volcanic sandstone and siltstone (Nelson, 1966a, p. 6–11; 1966b; Nelson and Monroe, 1966, p. 3–8).

Undoubtedly, some of the larger, massive coarse-grained amphibolite bodies, especially those closely associated with dunite, represent intrusive rocks of gabbroic composition, and some of the thinner amphibolite bodies may represent doleritic dikes.

REFERENCES

Clarke, F. W., 1924, The data of geochemistry, 5th ed.: U.S. Geol. Survey Bull. 770, 841 p.

Deer, W. A., Howie, R. A., Zussman, J., 1962, Rock-forming minerals, v. 2, Chain silicates: New York, John Wiley and Sons, 379 p.

Evans, B. W., and Leake, B. E., 1960, The composition and origin of the striped amphibolites of Connemara, Ireland: Jour. Petrology, v. 1, no. 3, p. 337–363.

Fyfe, W. S., Turner, F. J., and Verhoogen, John, 1958, Metamorphic reactions and metamorphic facies: Geol. Soc. America Mem. 73, 259 p.

Hadley, J. B., and Goldsmith, Richard, 1963, Geology of the eastern Great Smoky Mountains, North Carolina and Tennessee: U.S. Geol. Survey Prof. Paper 349–B, p. B1–B118.

Keith, Arthur, 1905, Description of the Mount Mitchell quadrangle, North Carolina–Tennessee: U.S. Geol. Survey Geol. Atlas, Folio 124, 10 p.

——— 1907a, Description of the Nantahala quadrangle [North Carolina–Tennessee]: U.S. Geol. Survey Geol. Atlas, Folio 143, 12 p.

——— 1907b, Description of the Pisgah quadrangle [North Carolina–South Carolina]: U.S. Geol. Survey Geol. Atlas, Folio 147, 8 p.

——— 1907c, Description of the Roan Mountain quadrangle [North Carolina–Tennessee]: U.S. Geol. Survey Geol. Atlas, Folio 151, 12 p.

Kulp, J. L., and Poldervaart, Arie, 1956, The metamorphic history of the Spruce Pine district [North Carolina]: Am. Jour. Sci., v. 254, p. 393–403.

Leake, B. E., 1964, The chemical distinction between ortho- and para-amphibolites: Jour. Petrology, v. 5, no. 2, p. 238–254.

Nelson, A. E., 1966a, Cretaceous and Tertiary rocks in the Corozal quadrangle, northern Puerto Rico: U.S. Geol. Survey Bull. 1244–C, 20 p.

——— 1966b, Significant changes in volcanism during the Cretaceous in north-central Puerto Rico, *in* Geological Survey Research 1966: U.S. Geol. Survey Prof. Paper 550–D, p. D172–D177.

Nelson, A. E., and Monroe, W. H., 1966, Geology of the Florida quadrangle, Puerto Rico: U.S. Geol. Survey Bull. 1221–C, 22 p.

Niggli, Paul, 1954, Rocks and mineral deposits: San Francisco, W. H. Freeman and Co., 559 p.

Nockolds, S. R., 1954, Average chemical compositions of some igneous rocks: Geol. Soc. America Bull., v. 65, p. 1007–1032.

Shapiro, Leonard, and Brannock, W. W., 1962, Rapid analysis of silicate, carbonate, and phosphate rocks: U.S. Geol. Survey Bull. 1144–A, p. A1–A56.

Shaw, D. M., and Kudo, A. M., 1965, A test of the discriminant function in the amphibolite problem: Mineralog. Mag., v. 34, p. 423–435.

Van Horn, E. C., 1948, Talc deposits of the Murphy marble belt: North Carolina Div. Mineral Resources Bull. 56, 54 p.

Wilcox, R. E., and Poldervaart, Arie, 1958, Metadolerite dike swarm in Bakersville–Roan Mountain area, North Carolina: Geol. Soc. America Bull., v. 69, p. 1323–1367.

LAWSONITE BLUESCHIST FROM NORTH-CENTRAL OREGON

By DONALD A. SWANSON, Hawaiian Volcano Observatory,
Hawaii National Park, Hawaii

Abstract.—Lawsonite blueschist crops out in two windows of pre-Albian metamorphic rocks near Mitchell, north-central Oregon. It is associated with serpentine in one of the windows, and with chert, quartzite, crystalline limestone and marble, and mafic metavolcanic rocks in both windows. The blueschist strikes northeast and lies along the projected trend of similar rocks in the Klamath Mountains. The occurrence of the blueschist near Mitchell supports the suggestion by Warren Hamilton and W. B. Myers that the Klamath trend extends northeastward across Oregon and follows the late Paleozoic or Mesozoic continental margin.

Lawsonite blueschist was found in two windows of metamorphic rocks of pre-Albian, probably pre-Cretaceous, age during reconnaissance geologic mapping in north-central Oregon. These localities of blueschist are the first ones reported from either east of the Cascade Mountains or the area between southwest Oregon (Diller, 1898, 1903; Koch, 1966) and the Northern Cascades in Washington (Misch, 1966). (Optical and X-ray studies have shown that a specimen of schist from eastern Oregon termed "glaucophanitic" by Thayer and Brown (1964, p. 1257), kindly loaned me by T. P. Thayer, contains deep-blue-green hornblende, not glaucophane.) The blueschist is briefly described here because its regional setting is of interest to geologists studying pre-Tertiary structural trends and conditions of metamorphism in western North America.

The blueschist crops out on the walls of Myers Canyon (SW¼ sec. 13, T. 11 S., R. 21 E.), 3 miles north of Mitchell, Oreg., and in a belt extending south and eastward from Tony Butte, about 6 miles northeast of Mitchell (fig. 1). The rocks at Tony Butte lie along the strike of the rocks in Myers Canyon (Bowers, 1953; Wilkinson and Oles, 1968). Exposures are best in Myers Canyon and are easily reached by either a short walk down the canyon from State Highway 207 or a jeep road up the canyon from its mouth on Bridge Creek (fig. 1). The Tony Butte locality is accessible by jeep roads up Shoofly Creek or Girds Creek.

According to Wilkinson and Oles (1968), the pre-Tertiary metamorphic rocks (which include the blueschist) unconformably underlie 9,000 feet of shale, sandstone, and conglomerate of late Early Cretaceous (early Albian) and, possibly, early Late Cretaceous (Cenomanian) age. The blueschist is associated with subordinate amounts of chert, quartzite, crystalline limestone and marble, and mafic metavolcanic rocks at both localities, and with serpentine at Tony Butte. It is not clear whether the blueschist and associated rocks are in depositional or structural contact, owing to strong deformation and intense shearing along the contact. Poorly preserved fusulinids from crystalline limestone in Myers Canyon indicate a Permian, possibly early Permian, age (Wilkinson and Oles, 1968). The schistosity of the blueschist is highly contorted, but in general it strikes northeast, parallel to the dominant structural grain in this part of Oregon.

Most of the primary texture in the blueschist is destroyed, but aggregates of lawsonite in one sample from Myers Canyon occur as pseudomorphs after plagioclase phenocrysts in a porphyritic metabasalt. Thin alternating quartz- and muscovite-rich layers in another sample suggest interbedded silt and clay. The texture of other blueschist in the area resembles that of metagraywacke in textural-zone 3 of Blake, Irwin, and Coleman (1967). Textures and mineral assemblages correspond to those of upper type-II and type-III glaucophane schists of Coleman and Lee (1963).

The four blueschist samples examined by petrographic and whole-rock X-ray methods contain blue amphibole and lawsonite, together with varying amounts of white mica, chlorite, quartz, calcite, and

U.S. GEOL. SURVEY PROF. PAPER 650-B, PAGES B8-B11

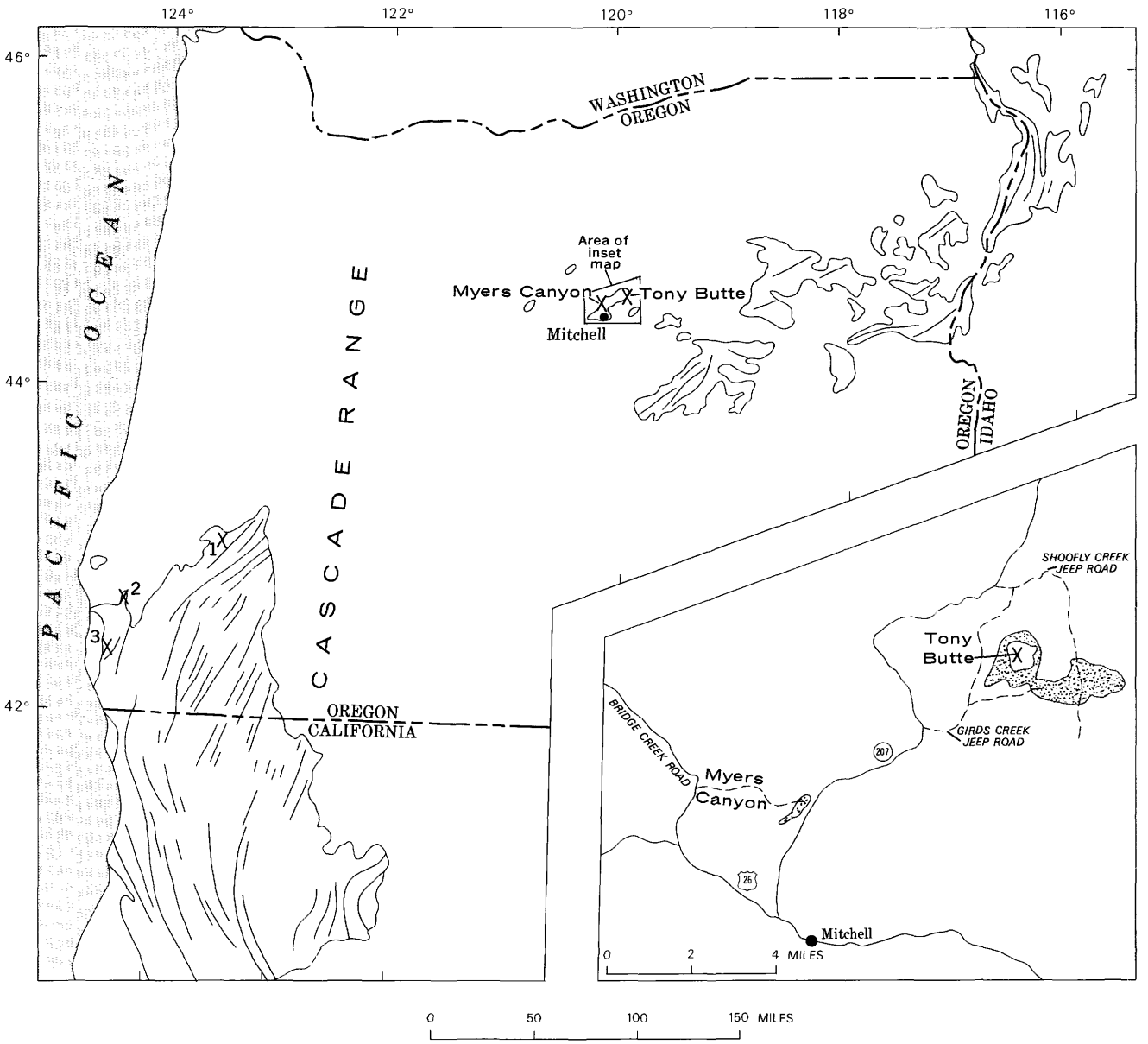

FIGURE 1.—Index map showing regional setting of lawsonite blueschist near Mitchell, Oreg. Outcrop areas of dominantly pre-Tertiary rocks and their pre-Tertiary structural trends (slightly modified from Cohee, 1961) are outlined in Oregon and adjacent parts of California and Idaho. Numbers indicate occurrences of blueschist in southwest Oregon: *1*, Winston locality (Diller, 1898); *2*, Powers locality (Diller, 1903); *3*, Signal Buttes locality (Koch, 1966; R. G. Coleman, written commun., 1968). Stippled areas of inset map portray pre-Albian metamorphic rocks that contain lawsonite blueschist in Mitchell area.

traces of albite. Neither pumpellyite nor aragonite was identified, although both are common in some blueschist terranes elsewhere.

Blue amphibole makes up about 10 to 60 percent of the blueschist sampled. Most of it is finely fibrous and may be crocidolite (fibrous riebeckite), but in one sample from Myers Canyon it is well-crystallized crossite on the basis of axial plane $\perp$ (010) and $\beta \approx C$. Pleochroism of the crossite is relatively slight, so its composition may be close to that of glaucophane. The crossite crystals lie within the plane of schistosity but are broken at the crests of folds in the schistosity, indicating deformation after crossite crystallization.

Lawsonite, identified by its X-ray pattern and distinguished from zoisite in thin section by its two perfect cleavages, makes up about 4 to 30 percent of the blueschist. The crystals are nearly colorless, only faintly pleochroic in shades of yellow brown, and have the prismatic shape characteristic of lawsonite. The lawsonite occurs as aggregates replacing plagioclase phenocrysts, as irregular areas in the matrix, and as single isolated crystals, particularly in white-mica- and chlorite-rich areas. The single crystals lie in or close to the plane of foliation.

White mica and chlorite occur as feltlike aggregates that commonly contain crossite or crocidolite and lawsonite. Calcite fills veinlets and occupies irregular patches in the matrix. It has an optic angle of $<5°$ and is therefore probably a secondary mineral unrelated to inversion from aragonite, the normal high-pressure carbonate in blueschists (Boettcher and Wyllie, 1967; Coleman and Lee, 1962). Albite occurs as tiny scattered crystals in the matrix and as narrow veinlet fillings. A green prismatic mineral occurs in one sample but is too sparse (<0.5 percent) to be identified on a whole-rock diffraction pattern. It is too fine grained for optical identification, but judging from its mineral association, the mineral is most likely either pumpellyite or an acmitic clinopyroxene.

The lawsonite blueschist near Mitchell bears importantly on the understanding of the tectonic development of the Pacific Northwest because of the unusual conditions governing blueschist metamorphism and the restricted geographic occurrence of blueschists. Experimentally determined stability fields of diagnostic blueschist minerals suggest that, during blueschist metamorphism, temperatures are the same as those of greenschist metamorphism but pressures are far higher. Commonly quoted pressure-temperature conditions are on the order of 6 to 9 kilobars and 200°C to 300°C (Ernst, 1965; Coleman, 1967; Blake and others, 1967). Petrologists disagree on the geologic environment leading to such conditions. Some attribute them to rapid, deep burial (Ernst, 1965); others suggest a combination of deep burial and an extremely low geothermal gradient (Bailey and others, 1964); still others relate the formation of blueschists to tectonic overpressures, particularly at the sole of large thrust plates (Blake and others, 1967; Coleman and Lee, 1962, Coleman, 1967). Whatever the environment, it appears to be one that is developed exclusively along continental margins or in island arcs (Plas, 1959; Ernst, 1965; Coleman, 1967). If this is true for the lawsonite blueschist near Mitchell, the continental margin during late Paleozoic or Mesozoic time must have passed through north-central Oregon, as many geologists have suggested on the basis of the distribution of late Paleozoic and Mesozoic eugeosynclinal rocks (Dickinson, 1962; Dickinson and Vigrass, 1964; Hamilton, 1963).

The lawsonite blueschist near Mitchell is of further interest because it crops out along the projected strike of pre-Tertiary lawsonite blueschist and other rocks in the Klamath Mountains of northwestern California and southwestern Oregon. Hamilton (1963) and Hamilton and Myers (1966) have proposed that the pre-Tertiary rocks in the Klamaths are, or once were, continuous with pre-Tertiary rocks in northeastern Oregon beneath a cover of Tertiary rocks, although Thayer and Brown (1964) have disagreed with this concept. The blueschist near Mitchell neither proves nor disproves this proposed correlation, but it is supporting evidence for it, in view of the unusual pressure-temperature conditions necessary for lawsonite blueschist metamorphism. Furthermore, the blueschist-serpentine association so common in the Klamaths (Blake and others, 1967) is duplicated near Tony Butte, where Bowers (1953, p. 64–65) reports "dikes" of serpentine intruding metamorphic rocks, some of which are blueschist. On the basis of present fieldwork, I interpret this serpentine to be in fault slivers, not dikes, just as it is in the Klamaths. Rock types associated with the blueschist and serpentine are also comparable in the two areas, and structural trends are similar.

It is of interest that the blueschist localities in both southwestern and north-central Oregon lie along the northwestern (oceanic) side of the pre-Tertiary outcrop belts (fig. 1), whereas metamorphic rocks within the interior (continental side) of the belts are of higher grade (higher temperature of formation), predominantly greenschist and amphibolite facies (Thayer and Brown, 1964; Brown and Thayer, 1966; R. G. Coleman, written commun., 1968).

Pre-Tertiary metamorphic rocks crop out elsewhere in central and northeastern Oregon (Walker and

King, 1969), where it might prove fruitful to search for lawsonite blueschist in light of its occurrences near Mitchell and its regional tectonic significance.

REFERENCES

Bailey, E. H., Irwin, W. P., and Jones, D. L., 1964, Franciscan and related rocks and their significance in the geology of western California: Calif. Dep. Nat. Resources Div. Mines Bull. 183, 171 p.

Blake, M. C., Jr., Irwin, W. P., and Coleman, R. G., 1967, Upside-down metamorphic zonation, blueschist facies, along a regional thrust in California and Oregon; *in* Geological Survey Research 1967: U.S. Geol. Survey Prof. Paper 575–C, p. C1–C9.

Boettcher, A. L., and Wyllie, P. J., 1967, Biaxial calcite inverted from aragonite: Am. Mineralogist, v. 52, nos. 9 and 10, p. 1527–1529.

Bowers, H. E.,1953, Geology of the Tony Butte area and vicinity, Mitchell quadrangle, Oregon: Oregon State Univ., Corvallis, M.S. thesis.

Brown, C. E., and Thayer, T. P., 1966, Geologic map of the Canyon City quadrangle, northeastern Oregon: U.S. Geol. Survey Misc. Geol. Inv. Map I–447, scale 1:250,000.

Cohee, G. V., (chm.) and others, 1961, Tectonic map of the United States: U.S. Geol. Survey and Am. Assoc. Petroleum Geologists, scale 1:2,500,000.

Coleman, R. G., 1967, Glaucophane schists from California and New Caledonia: Tectonophysics, v. 4, p. 479–498.

Coleman, R. G., and Lee, D. E., 1962, Metamorphic aragonite in the glaucophane schists of Cazadero, California: Am. Jour. Sci., v. 260, no. 8, p. 577–595.

——— 1963, Glaucophane-bearing metamorphic rock types of the Cazadero area, California: Jour. Petrology, v. 4, no. 2, p. 260–301.

Dickinson, W. R., 1962, Petrogenetic significance of geosynclinal andesitic volcanism along the Pacific margin of North America: Geol. Soc. America Bull., v. 73, no. 10, p. 1241–1256.

Dickinson, W. R., and Vigrass, L. W., 1964, Pre-Cenozoic history of Suplee-Izee district, Oregon—Implications for geosynclinal theory: Geol. Soc. America Bull., v. 75, no. 10, p. 1037–1044.

Diller, J. S., 1898, Description of the Roseburg quadrangle, [Oregon]: U.S. Geol. Survey Geol. Atlas, Folio 49.

——— 1903, Description of the Port Orford quadrangle, [Oregon]: U.S. Geol. Survey Geol. Atlas Folio 89.

Ernst, W. G., 1965, Mineral parageneses in Franciscan metamorphic rocks, Panoche Pass, California: Geol. Soc. America Bull., v. 76, no. 8, p. 879–914.

Hamilton, Warren, 1963, Overlapping of late Mesozoic orogens in western Idaho: Geol. Soc. America Bull., v. 74, no. 6 p. 779–788.

Hamilton, Warren, and Myers, W. B., 1966, Cenozoic tectonics of the western United States: Rev. Geophysics, v. 4, no. 4, p. 509–549.

Koch, J. G., 1966, Late Mesozoic stratigraphy and tectonic history, Port Orford–Gold Beach area, southwestern Oregon coast: Am. Assoc. Petroleum Geologists Bull., v. 50, no. 1, p. 25–71.

Misch, Peter, 1966, Tectonic evolution of the northern Cascades of Washington State—A west-Cordilleran case history, *in* Gunning, H. C., ed., Symposium on tectonic history and mineral deposits of the western Cordillera in British Columbia and neighboring parts of the United States: Canadian Inst. Mining Metall. Spec. Paper, v. 8, p. 101–148.

Plas, L. van der, 1959, Petrology of the northern Adula region, Switzerland (with particular reference to glaucophane-bearing rocks): Leidse Geol. Med., v. 24, pt. 2, p. 415–602.

Thayer, T. P., and Brown, C. E., 1964, Pre-Tertiary orogenic and plutonic intrusive activity in central and northeastern Oregon: Geol. Soc. America Bull., v. 75, no. 12, p. 1255–1262.

Walker, G. W., and King, P. B., 1969, Geologic map of Oregon: U.S. Geol. Survey Misc. Geol. Inv. Map I–595, scale 1:2,500,000. [In press]

Wilkinson, W. D., and Oles, K. F., 1968, Stratigraphy and paleoenvironments of Cretaceous rocks, Mitchell quadrangle, Oregon: Am. Assoc. Petroleum Geologists Bull., v. 52, no. 1, p. 129–161.

328–687 O—69——2

OLIGOCENE RHYOLITE IN THE DENVER BASIN, COLORADO

By G. A. IZETT, G. R. SCOTT, and J. D. OBRADOVICH, Denver, Colo.

Abstract.—A rhyolite tuff formerly included in the Dawson Arkose of Late Cretaceous and Paleocene age is of early Oligocene age and constitutes a separate map unit. Biotite from the rhyolite has a potassium-argon age of 34.8 ± 1.1 m.y.

The paucity of extrusive rhyolitic rocks of early Tertiary age in Colorado led the writers to study stratigraphic relations and to collect rock samples for isotope age determinations of a purported lower Tertiary rhyolite tuff near Castle Rock, Colo. This rock is the only rhyolite assigned an early Tertiary age on the geologic map of Colorado (Burbank and others, 1935). An isotope age determination made on a sample of the rhyolite verifies stratigraphic relations that suggest a middle Tertiary rather than an early Tertiary age as previously thought. Biotite separated from the rhyolite has a potassium-argon age of about 35 million years, which is early Oligocene. The Oligocene is currently believed to have begun 37–38 million years ago (Harland and others, 1964, p. 260).

Outcrops of the rhyolite tuff extend from an area about 6 miles north of Castle Rock, Colo., south to a point a few miles north of Monument, Colo. The outcrop area lies along the east side of the Front Range in the central part of the Denver basin (fig. 1). At most places the tuff caps mesas underlain by the Dawson Arkose of Late Cretaceous and Paleocene age (Brown, 1943), but a few miles southeast of Castle Rock it is overlain by lower Oligocene Castle Rock Conglomerate. The rhyolite outcrops are part of a once-continuous ash flow probably less than 50 feet thick that was extruded onto an Eocene(?) erosion surface cut on the Dawson Arkose. According to Richardson (1915), the erosion surface dips northeast about 75 feet per mile.

Richardson (1915, p. 9) included the rhyolite tuff that we date here as early Oligocene in the "extreme upper part" of the Dawson, and he assigned an early Eocene age to the Dawson. At critical outcrops, about 4 miles southeast of Castle Rock, "20 to 30 feet of fine-textured arkose lies between the rhyolite and the base of the Castle Rock conglomerate" (Richardson, 1915, p. 7). In these outcrops the friable fine-grained arkose stratigraphically above the rhyolite, thought by Richardson to be Dawson, is interpreted by the writers to be part of the overlying Castle Rock Conglomerate. Although the arkose is fine grained and less well indurated than the typical coarse Castle Rock Conglomerate, it probably represents an early alluvial facies of the Castle Rock that was deposited soon after extrusion of the rhyolite ash flow. The Dawson and the

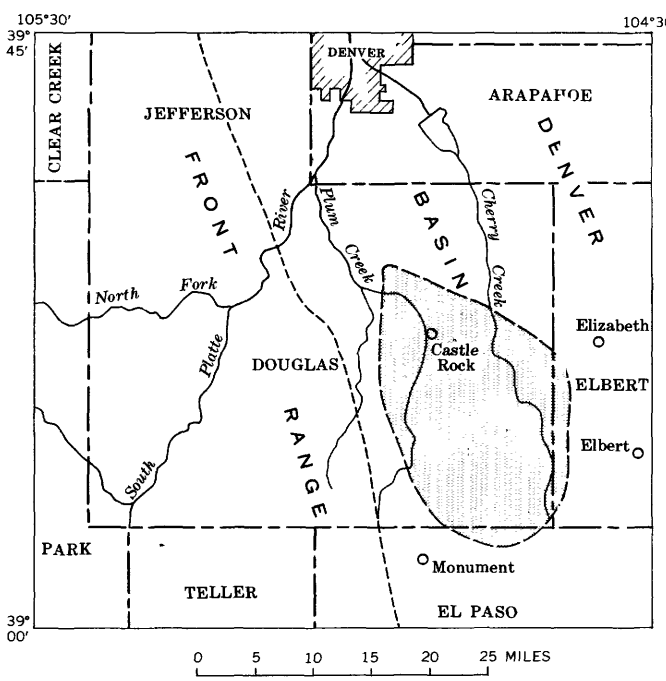

FIGURE 1.—Index map showing Castle Rock and other places mentioned in text. Shaded area shows minimum original extent of rhyolite as inferred from Richardson (1915).

U.S. GEOL. SURVEY PROF. PAPER 650-B, PAGES B12-B14

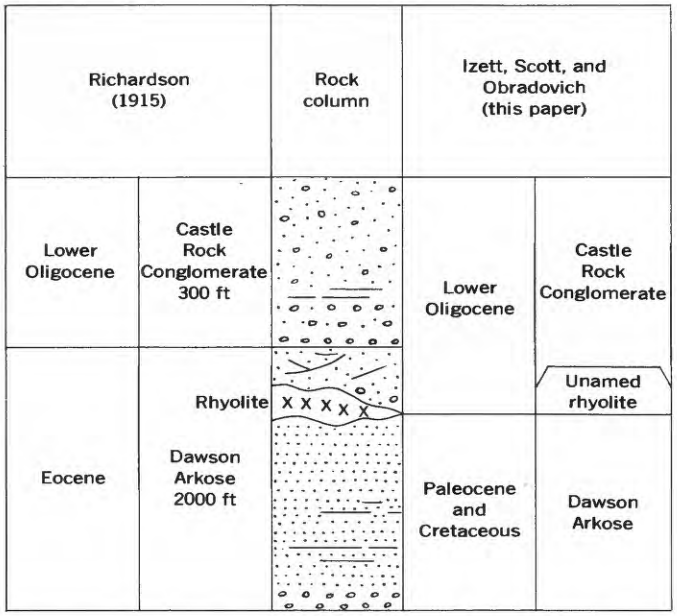

FIGURE 2.—Diagram showing redefinition of the Dawson Arkose and the Castle Rock Conglomerate, on the basis of potassium-argon age of 34.8±1.1 m.y. on rhyolite.

Castle Rock are lithologically similar because they were both derived from the Pikes Peak Granite of Precambrian age. Figure 2 shows the stratigraphic relations as interpreted by Richardson and by us.

The Castle Rock Conglomerate and the Dawson Arkose are here redefined to the extent that the 20–30 feet of friable arkosic grit above the rhyolite tuff that was included in the Dawson by Richardson (1915) is assigned to the Castle Rock; the tuff is removed from the Dawson and constitutes a separate formation (fig. 2). The rhyolite is currently being studied by Fred Welsh, a graduate student at the Colorado School of Mines, and until it is mapped and studied in detail we defer from naming the unit and establishing a type section.

The arkosic grit above the rhyolite is well exposed in the NW¼NW¼ sec. 29 and the NE¼NE¼ sec. 30, T. 8 S., R. 66 W., and there it grades upward into coarse well-indurated cliff-forming conglomerate of the Castle Rock. No fossils have been found as yet in the friable arkosic grit, but in the NE¼SW¼ sec. 18, T. 8 S., R. 66 W., C. L. Pillmore, of the U.S. Geological Survey, found remains of fossil mammals in soft sandstone interbedded in coarse conglomerate about 60 feet above the base of the Castle Rock Conglomerate. G. E. Lewis, of the U.S. Geological Survey, identified the fossils as a jaw fragment of a rhinoceros, *Trigonias* sp., and two distal humeral fragments of a titanothere of early Oligocene age. Elsewhere, the age of the Castle Rock is well established by its content of early Oligocene fossil mammals northwest of Elbert, Colo. (Richardson, 1915).

A detailed description of samples of the rhyolite from along its outcrop is beyond the scope of this paper, but certain petrographic features are described to show the lithology of the rock at the locality where we sampled it for the isotope age determinations. Richardson (1915, p. 10) demonstrated that the rock is chemically a rhyolite inasmuch as it contains about 74 percent SiO_2, 5.83 percent K_2O, and 3.72 percent Na_2O. Hand samples of the rock are light gray and contain sparse small phenocrysts of feldspar and biotite set in an aphanitic groundmass. Under a polarizing microscope the feldspars are calcic oligoclase and sanidine. $2V$ determinations made on the sanidine, using a spindle stage, range from 26° to 42° and average about 32°. The rock lacks quartz phenocrysts, but some quartz xenocrysts along with rare small xenoliths of Precambrian rock fragments were seen. Accessory minerals found in heavy-mineral concentrations include zircon, sphene, and magnetite. The groundmass of the rock is composed of devitrified glass shards that show little evidence of compaction typical of welded tuffs.

Biotite and sanidine were separated from a sample of the rhyolite collected in the NW¼NW¼ sec. 29, T. 8 S., R. 66 W., Douglas County, Colo. Figure 3

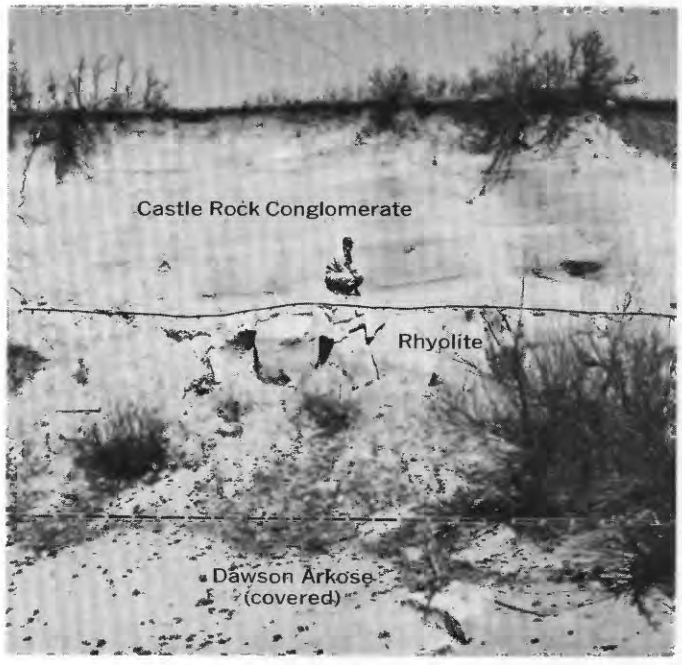

FIGURE 3.—View of the rhyolite in an abandoned quarry in the NW¼NW¼ sec. 29, T. 8 S., R. 66 W., where the sample for the isotope age determination was collected. The rhyolite is overlain by friable crossbedded fluvial arkosic grit assigned to the Castle Rock Conglomerate. The rhyolite is probably about 7 feet thick, but the base of the unit is covered by modern slopewash.

shows outcrops of the rhyolite at the sample locality. Biotite from the rhyolite has a potassium-argon age of 34.8±1.1 m.y., and sanidine from the same sample yields an age of 44.5±1.4 m.y. The data are given below.

Laboratory No.	Sample No.	Mineral	K_2O (percent)	$*Ar^{40}$ (10^{-10} moles/g)	$*Ar^{40}$ (percent)	Age (m.y.)
DKA 1441--	67G3	Sanidine	9.88	6.57	84.7	44.5±1.4
DKA 1597--	67G3	Biotite	8.14	4.21	76.7	34.8±1.1

Decay constants, K^{40}: $\lambda_\epsilon = 0.584 \times 10^{-10}$ yr^{-1}, $\lambda_\beta = 4.72 \times 10^{-10}$ yr^{-1}.
Atomic Abundance: $K^{40}/K = 1.19 \times 10^{-4}$.
$*Ar^{40}$ = radiogenic argon.

The reason for the lack of agreement between the sanidine and biotite ages was apparent after close inspection of a fraction of the sanidine used for the age determination revealed the presence of a few grains of microcline doubtless derived from Pikes Peak Granite of Precambrian age. The microcline probably was not degassed by the hot ash flow and contributed a large amount of radiogenic argon relative to the sanidine. Grain counts of a split of potassium-feldspar separate used for the age determination suggest that microcline makes up between 0.05 and 1 percent of the sample, and this amount is enough to account for the difference between the sanidine and the biotite dates. Potassium-argon dates on sanidine separated from some Tertiary ash flows that have crossed Precambrian terranes often can be unreliable. A very small amount of xenocrystic Precambrian microcline can contaminate the sanidine and produce an anomalously old age. The minor amount of biotite with respect to the microcline in the Pikes Peak Granite and its transport characteristics possibly may explain the lack of contaminating biotite in the rhyolite.

The source of the rhyolite may never be known with absolute assurance. The overall dip of the surface upon which the ash flow was extruded is northeast, and this suggests that the source should lie southwest of Monument, Colo., perhaps in the Front Range or farther west in South Park. Several silicic welded tuffs of middle Tertiary age occur in South Park in the Thirtynine Mile volcanic field (Epis and Chapin, 1968), and perhaps the rhyolite tuff in the Castle Rock area is a distal end of one of the lower Oligocene ash-flow sheets of the Thirtynine Mile volcanic field.

REFERENCES

Brown, R. W., 1943, Cretaceous-Tertiary boundary in the Denver Basin, Colorado: Geol. Soc. America Bull., v. 54, no. 1, p. 65–86.

Burbank, W. S., Lovering, T. S., Goddard, E. N., and Eckel, E. B., 1935, Geologic map of Colorado: U.S. Geol. Survey.

Epis, R. C., and Chapin, C. E., 1968, Geologic history of the Thirtynine Mile volcanic field, central Colorado: Colorado School Mines Quart., v. 63, no. 3, p. 51–85.

Harland, W. B., Smith, A. G., and Wilcock, Bruce, eds., 1964, The Phanerozoic time scale—A symposium dedicated to Professor Arthur Holmes: Geol. Soc. London Quart. Jour., v. 120, 458 p.

Richardson, G. B., 1915, Description of the Castle Rock quadrangle, Colorado: U.S. Geol. Survey Geol. Atlas, Folio 198, 13 p.

A HISTORIC ERUPTION OF MOUNT RAINIER, WASHINGTON

By D. R. MULLINEAUX, R. S. SIGAFOOS, and E. L. HENDRICKS,
Denver, Colo., Washington, D.C.

Abstract.—A sparsely distributed pumice that has not previously been recognized was erupted by Mount Rainier, Wash., in the 19th century. It is similar mineralogically to a more widespread and voluminous older pumice, and it has been identified only on moraines and terraces that postdate the older pumice. Limiting dates of its eruption have been obtained from a complex of Emmons Glacier end moraines. Ages of trees on moraines older and younger than the pumice indicate that the eruption occurred between 1820 and 1854.

A previously unrecognized deposit of pumice that is sparsely scattered on the flanks of Mount Rainier, Wash., can be dated, from its relation to young glacial moraines, as having been erupted during the 19th century. This pumice is the youngest yet recognized from Mount Rainier, and it represents the only known eruption of new magma by that volcano since the last major period of volcanic activity about 2,000 years ago. It also is the only geologic evidence known that indicates an explosive eruption during historic time, even though several eruptions of Mount Rainier were reported during the 19th century.

The newly discovered pumice is designated "layer X," though it actually is too sparse to form a continuous layer. It consists mostly of brown lapilli-size fragments, the largest of which have maximum diameters of approximately 2 inches. In detail, these fragments vary in both color and composition, within single lapilli as well as from one to another. Variation in color from pale brown to darker brown and brownish gray is typical. Refractive index of the constituent glass generally increases as color darkens. Variation in mineral content, however, is not clearly related to color difference. Many lapilli, including some of each color present, contain orthopyroxene and clinopyroxene but not hornblende. Most of the others, also including some of each color, are characterized by sparse to abundant hornblende in addition to the two pyroxenes.

The range in color and composition shown by pumice of layer X is virtually the same as that characteristic of pumice in the much more voluminous layer C, which is about 2,000 years old (Crandell and others, 1962). As a result, pumice from layer X cannot, at present, be differentiated from that of layer C by sample characteristics. Furthermore, pumice layer X apparently occupies only a small area within the broad distribution pattern of layer C. Where underlain by the older layer, the sparse lapilli of layer X are not distinguishable from layer C lapilli that have been brought to the surface by frost action and animal burrowing. Because of the similarity of the two pumices and the scanty occurrence of layer X, the latter has been recognized only where it is not underlain by layer C. Such conditions exist chiefly on moraines and associated stream terraces of the Garda Stade (Crandell and Miller, 1964), which are surfaces that postdate layer C.

Pumice layer X has been identified on moraines and terraces at three places: in Glacier Basin below Inter Glacier, in the White River valley below Emmons Glacier, and in the Ohanapecosh River valley below Ohanapecosh Glacier (fig. 1). Even on surfaces where the pumice is best represented, it is not abundant. Generally only a few fragments per square foot can be found, lying just beneath or within thin humus layers where humus is present or at the surface where no humus exists. The pumice is also somewhat irregularly distributed, and locally is absent in places where it might be expected to occur. For example, on one lateral moraine of Emmons Glacier that is bare of humus, the pumice was not found within a carefully searched area of several hundred square feet at one particular site, although the site lies between two other localities on the same moraine in which the pumice is of average abundance and is relatively conspicuous.

U.S. GEOL. SURVEY PROF. PAPER 650-B, PAGES B15-B18

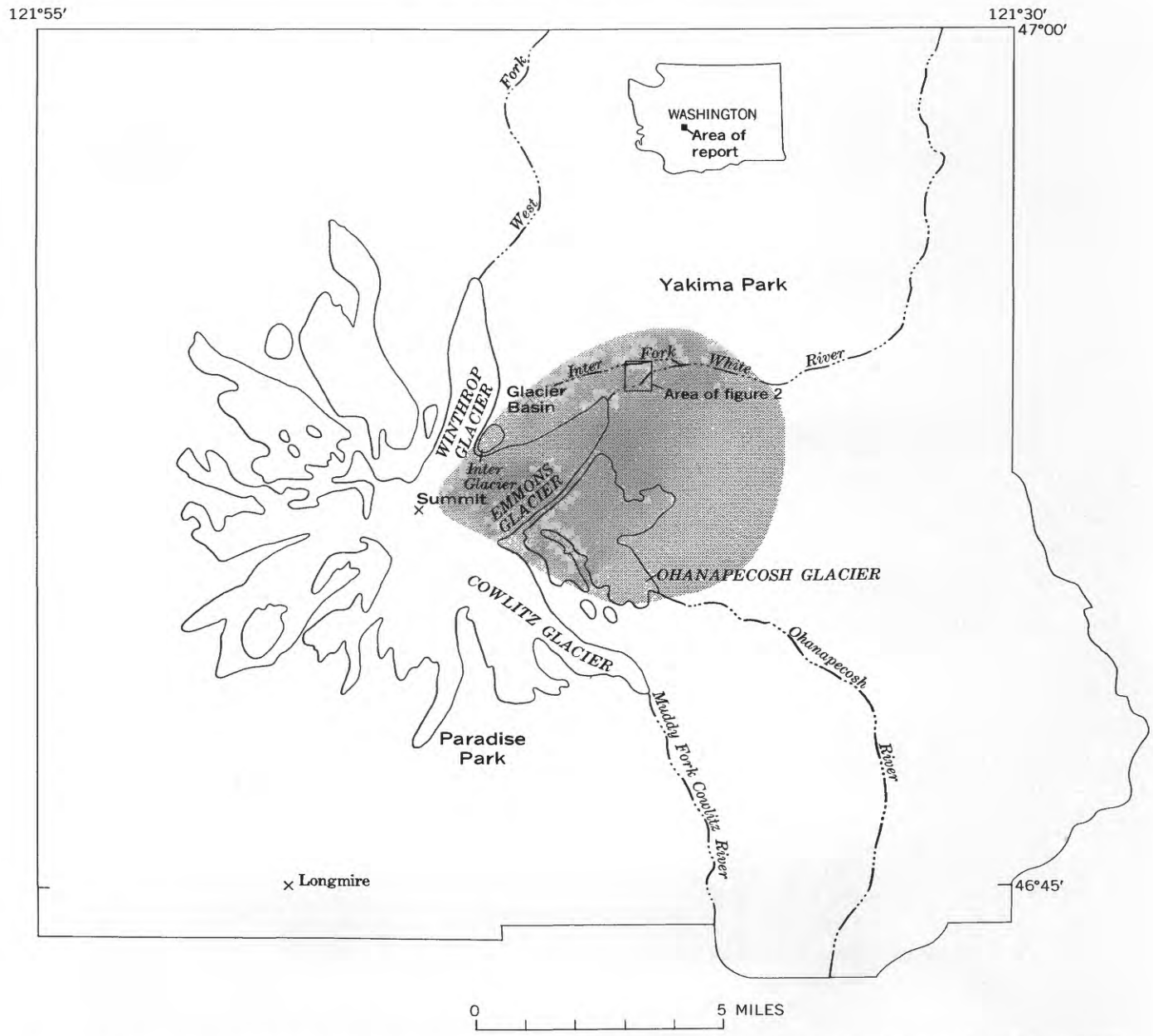

FIGURE 1.—Suggested distribution of pumice layer X (shaded area) erupted by Mount Rainier between A.D. 1820 and 1854.

Because of sparse distribution of the pumice of layer X and its similarity to lapilli of layer C, it might be suggested that layer X consists of pumice reworked from the older layer. However, such an origin seems unlikely because layer X occurs on moraines of a certain age at more than one locality, and some of the moraines form topographic highs in the middle of valley floors. The adjacent valley walls are thickly forested, and there is little likelihood that wind could have picked up significant quantities of pumice lapilli, some as large as 2 inches across, and redeposited them on moraines far out on valley floors. Neither does it seem possible that downslope movements of layer C on the valley sides could have deposited pumice on morainal ridges such as those in the center of the White River valley. Thus, the lapilli of layer X are interpreted as products of a separate eruption.

The three sites where layer X is recognized lie on the northeast and southeast flanks of the volcano (fig. 1). On both Inter Glacier and Emmons Glacier moraines, the pumice lies almost directly northeast of the summit, and it has been found as far as 6 miles from the summit in that direction. Farther north, a search

on a series of Winthrop Glacier end moraines of Garda age failed to disclose any pumice of layer X. The pumice on moraines of Ohanapecosh Glacier lies east-southeast of the summit and extends at least 5 miles from the summit in that direction. Farther south, in the valley of the Muddy Fork of the Cowlitz River (fig. 1), no pumice of layer X was seen during studies either of pumice stratigraphy or of other surficial deposits, although no specific search was conducted for it. In the area between the Emmons and Ohanapecosh moraines, no morainal or terrace surfaces of the age necessary for recognition of the pumice have been found. Thus, the distribution of layer X is not well defined. Tentatively, it is regarded as having been deposited within an east-northeast-trending lobe that encloses the known occurrences (fig. 1).

Such a distribution, chiefly east of the summit, is also common to other pumice deposits erupted by Mount Rainier, and probably results from the effect of predominantly westerly winds. The particular east-northeast pattern suggested for layer X is similar to, though much smaller than, the pattern of layer C. The area covered by layer X probably is small simply because the eruption was brief and the volume small.

The closest limiting dates for the eruption of layer X are obtained from a complex of Emmons Glacier end moraines, whose approximate ages have been determined by growth ring counts of trees on them. Sigafoos and Hendricks (1961, p. A6–A7; 1969) have shown that trees are among the first plants to grow on moraines in this area after the active ice front withdraws and a moraine becomes stable. On Emmons Glacier moraines, not more than 10 years would be expected to elapse before the first tree seedlings germinated (Sigafoos and Hendricks, 1961, p. A13). Another term of 5–20 years is allowed for growth to the height at which annual rings can be counted in cores. Simple ring counts are valid for dating, as no evidence of missing or discontinuous rings has been found. Even if such evidence exists but was not found, the error in counting surely constitutes less than 5 percent. For layer X, the older limiting date is determined from the youngest morainal ridge on which the pumice occurs; the age of the oldest sampled tree on it and allowances for delay in germination and for early growth indicate that the ridge was formed no earlier than about 1820. The younger limiting date is determined from the oldest ridge on which the pumice is absent, which definitely was formed before 1854. Thus, the pumice seems to have been erupted between 1820 and 1854.

The critical areas that provide estimates of the limiting dates for the eruption are areas 30, 9, and 49

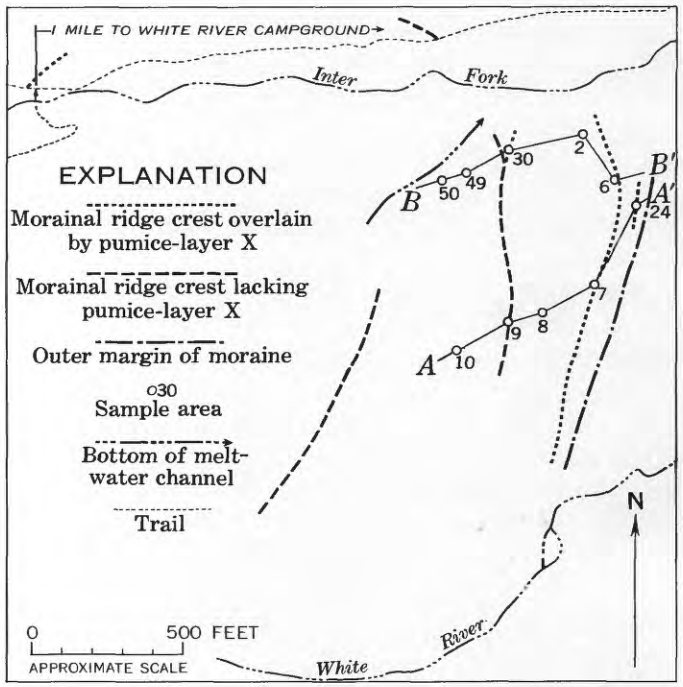

FIGURE 2.—Map of part of Emmons Glacier end moraines. Compiled by photogrammetric methods from aerial photographs taken in 1960.

shown on figures 2 and 3. Area 30 lies on the youngest ridge upon which the pumice was found. Of eight trees cored in this area, the oldest was 2 feet high in the year 1850. Allowance of the maximum of 10 years'

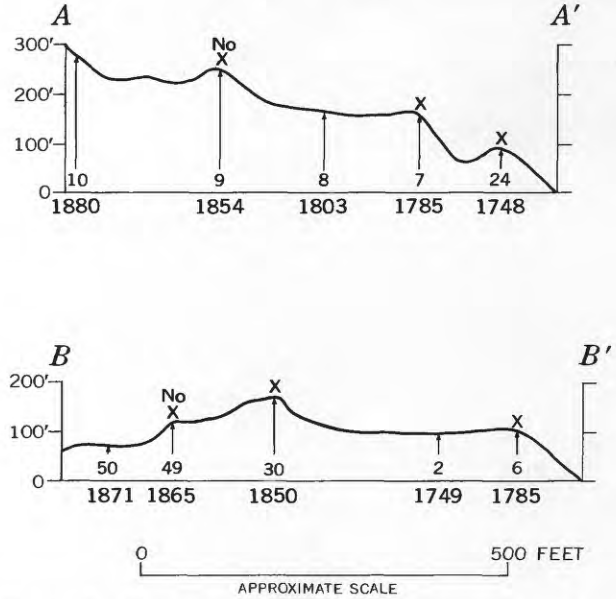

FIGURE 3.—Generalized east-west profiles across moraines and melt-water channel terraces (areas 49 and 50) below Emmons Glacier. Numbers refer to sample areas and year of growth of oldest annual ring found in the oldest tree cored. Sample areas projected to lines of profiles. Vertical exaggeration×1.05. "X" and "No X" refer to the presence or absence, respectively, of pumice layer X.

delay for germination and a maximum of 20 years for growth to a height of 2 feet gives the limiting date of 1820 for formation of this particular morainal ridge. Area 9 lies on the oldest ridge upon which the pumice is absent. The oldest of 17 trees cored on this ridge was 2 feet high in 1854. Thus, the moraine certainly was formed before 1854, and presumably some years earlier.

Area 49 is a terrace of a melt-water channel upon which pumice is absent. The channel was cut through the younger morainal ridge west of area 30; thus it is younger than the ridge. The oldest of seven trees cored in area 49 was 6 inches tall in 1865. Because the alluvial channel became stable as soon as melt-water ceased flowing, the first seedlings probably began to grow within 1–2 years. If 5 years is allowed for the tree to grow 6 inches in height, the seed would have germinated in 1860, and melt-water probably stopped flowing over the surface 1–2 years earlier. The younger limiting date provided by trees in area 49 thus supports the date provided by trees in area 9.

The eruption of layer X possibly was observed and reported. A thorough review of historical accounts of eruptions of Mount Rainier (Hopson and others, 1962) disclosed at least three reported eruptions on or after 1820 and before 1854. But because the descriptions are vague, and because even today dust from rockfalls is interpreted by many to be the product of volcanic eruptions, Hopson and his associates concluded that Mount Rainier apparently had not erupted in historic time. Now, however, pumice layer X provides substantiating geologic evidence of a 19th-century eruption. One possible date of its ejection was 1843, when Frémont (1845, p. 193) reported activity of Mount Rainier in his journals of exploration of Oregon and northern California. Frémont's account has since been cited repeatedly. Other possible times of eruption of layer X were 1846, a date for which F. G. Plummer in 1893 (see Hopson and others, 1962, p. 636) cited reports of signs of activity of the volcano, and about 1820, when John Hiaton, an Indian, was reported by Plummer to have witnessed an eruption of the mountain (Hopson and others, 1962, p. 636).

REFERENCES

Crandell, D. R., and Miller, R. D., 1964, Post-hypsithermal glacier advances at Mount Rainier, Washington, *in* Geological Survey Research 1964: U.S. Geol. Survey Prof. Paper 501–D, p. D110–D114.

Crandell, D. R., Mullineaux, D. R., Miller, R. D., and Rubin, Meyer, 1962, Pyroclastic deposits of Recent age at Mount Rainier, Washington: Art. 138 *in* U.S. Geol. Survey Prof. Paper 450–D, p. D64–D68.

Frémont, J. C., 1845, Report of the exploring expedition to the Rocky Mountains in the year 1842, and to Oregon and north California in the years 1843–1844: Washington, D.C., Gales and Seaton, printers, 693 p.

Hopson, C. A., Waters, A. C., Bender, V. R., and Rubin, Meyer, 1962, The latest eruptions from Mount Rainier volcano: Jour. Geology, v. 70, no. 6, p. 635–647.

Sigafoos, R. S., and Hendricks, E. L., 1961, Botanical evidence of the modern history of Nisqually Glacier, Washington: U.S. Geol. Survey Prof. Paper 387–A, p. A1–A20.

———1969, The time interval between stabilization of alpine glacial deposits and establishment of tree seedlings, *in* Geological Survey Research 1969: U.S. Geol. Survey Prof. Paper 650–B, p. B89–B93.

TUFFACEOUS EPICLASTIC BRECCIA AND SANDSTONE NEAR HAHNS PEAK, COLORADO, AND THEIR GENETIC IMPLICATIONS

By KENNETH SEGERSTROM and S. H. KIRBY,
Denver, Colo., Menlo Park, Calif.

Abstract.—Tuffaceous epiclastic breccia and sandstone, of latest Miocene(?) to Pliocene age, that contain abundant large clasts of altered rhyolite porphyry crop out 1 mile west of Hahns Peak, Routt County, Colo. The porphyry clasts are identical lithologically (except that they contain no pyrite) with altered intrusive porphyry (about 10 m.y.), which crops out on Hahns Peak. This newly recognized evidence indicates that airborne clasts of porphyry, plus included fragments of Cretaceous shale, were erupted from a volcanic center at Hahns Peak and dropped into a small basin floored by the Browns Park Formation, of Miocene(?) age. More or less concurrently, coarse pyroclastic debris that fell on adjacent slopes was swept into the basin as very fluid lahars and was consolidated as epiclastic basin-fill sediment. The rhyolitic eruption was halted by plugging of the vent or vents, and extrusion was succeeded by intrusion, doming, and sulfide mineralization that was centered at Hahns Peak.

Tuffaceous epiclastic breccia and sandstone are exposed on a hill which is known locally as Porphyry Mountain and is mistakenly labeled "Treasure Mountain" on some maps. The hill is about 1 mile west of Hahns Peak, Colo., between the west-trending Elkhead Mountains and the north-trending Park Range; the area is a few miles west of the Continental Divide and a few miles south of the Wyoming-Colorado boundary (fig. 1). Outcrops of the rhyolitic breccia and sandstone are restricted to Porphyry Mountain; the only similar rhyolitic rocks observed in the area during extensive coredrilling and detailed mapping occur along the margins of a breccia pipe on Hahns Peak. The tuffaceous epiclastic rocks, formerly mapped as "porphyry" on "Treasure Mountain" by Barnwell (1955, pl. 5), are evidence of a hitherto unrecognized extrusive phase of a volcano at the site of Hahns Peak. The new concept of extrusive activity at Hahns Peak influences significantly the reconstruction of geologic events since Miocene time.

STRATIGRAPHIC SETTING

The oldest rocks that crop out in the immediate vicinity of Porphyry Mountain are sandstone and siltstone of the Morrison Formation, of Late Jurassic age. These rocks are overlain by conglomerate and sandstone of the Cloverly Formation (Lower Cretaceous), which in turn are overlain by the Mancos Shale (Upper Cretaceous). The Mesozoic rocks are unconformably overlain by the Browns Park Formation of Miocene(?) age, which locally has a basal conglomerate composed largely of cobbles of Precambrian gneiss, quartzite, schist, granite, pegmatite, and vein quartz. Most of the Browns Park Formation near Porphyry Mountain consists of massive, poorly consolidated red sandstone with a clayey matrix. On Porphyry Mountain, about 400 feet of tuffaceous epiclastic breccia and sandstone overlie the red sandstone with probable angular conformity, but with possible disconformity. The Browns Park and older formations are intruded by rhyolite and rhyodacite porphyry, the radiometric age of which is about 10 million years, or early Pliocene (Bowes and others, 1968).

LITHOLOGY AND ORIGIN

The tuffaceous epiclastic rocks are well lithified and tend to weather in plates about 1–4 inches thick. They consist of ill-sorted angular fragments of dense creamy-white porphyry and dark-gray shale that range in size from fine sand to cobbles and that are set in a gray vitreous matrix. The matrix is largely opaline, but it does contain grains of quartz, feldspar, and zircon less than 1 millimeter in diameter; no glass is present. Graded bedding and block-sag structure are outstanding primary features (fig. 2*A*, *B*). Reentrants in the larger rock fragments are filled with material

U.S. GEOL. SURVEY PROF. PAPER 650-B, PAGES B19–B22

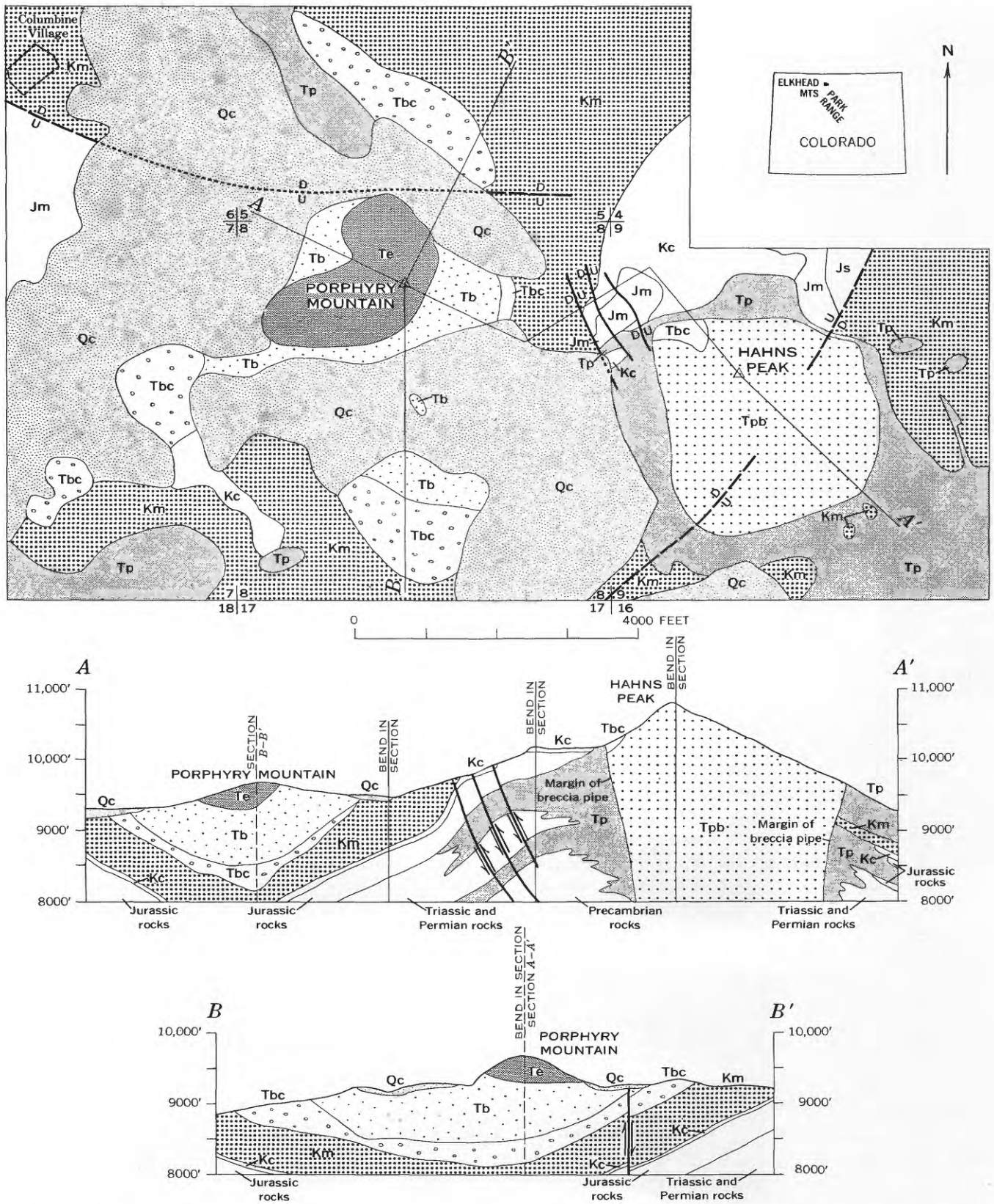

FIGURE 1.—Geologic map and structure sections, Porphyry Mountain and vicinity, T. 10 N., R. 85 W., Routt County, Colo.

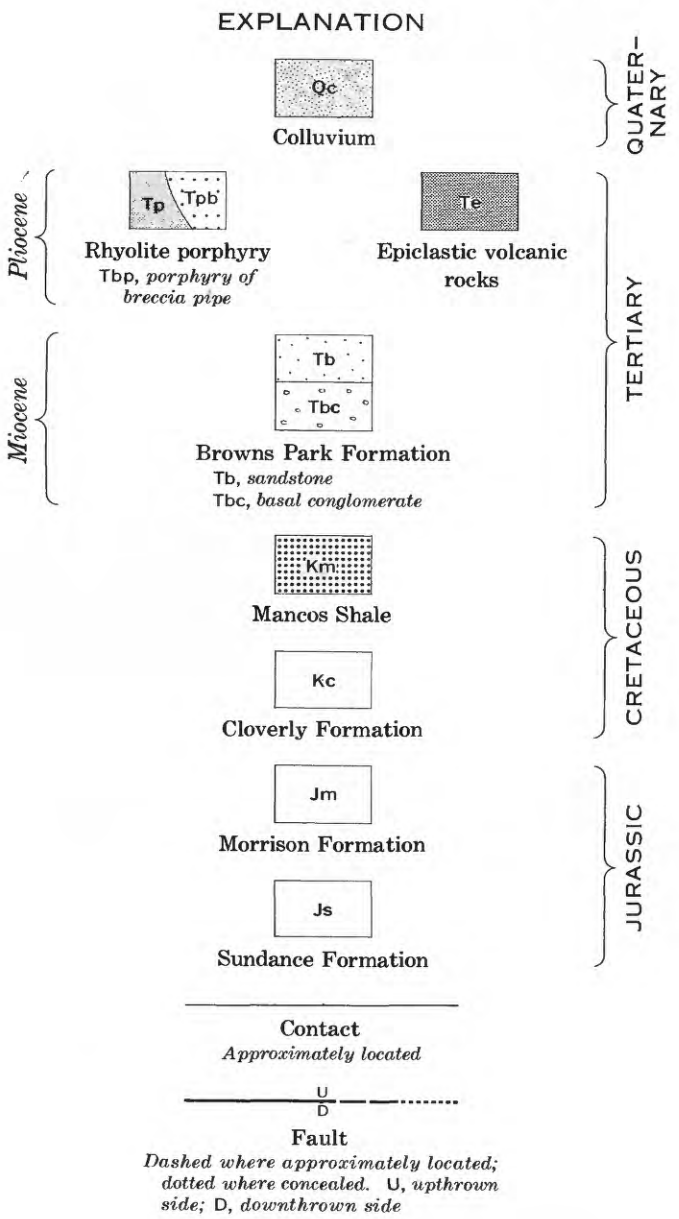

FIGURE 1.

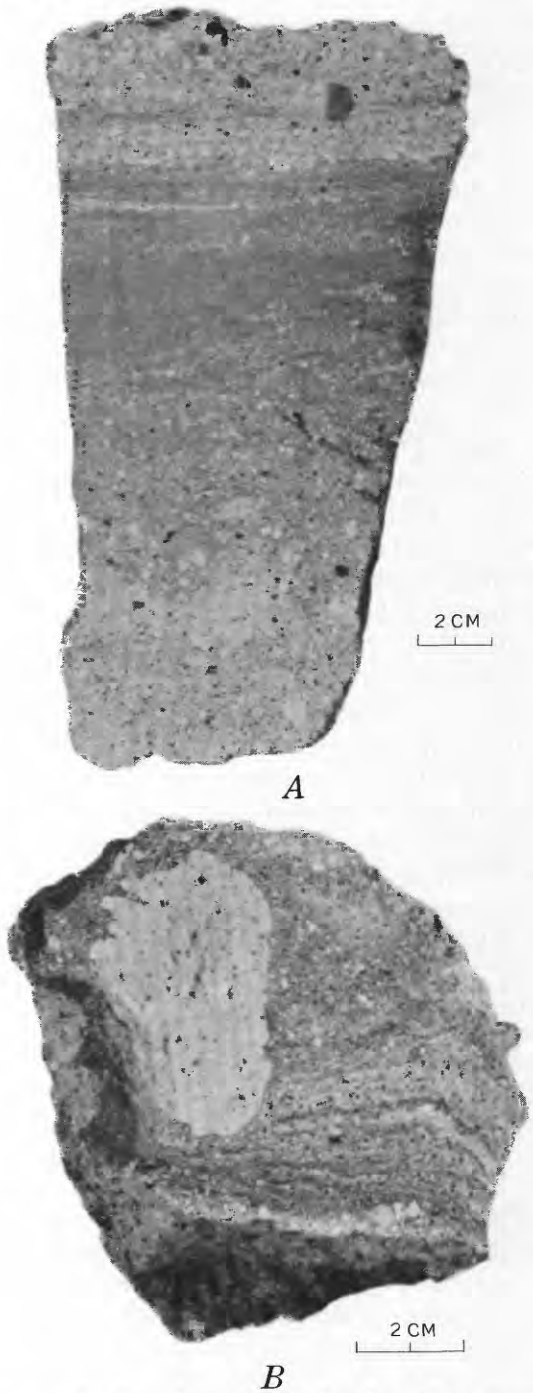

FIGURE 2.—Sawed and polished slabs of tuffaceous epiclastic breccia and sandstone. *A*, graded bedding; *B*, graded bedding and block-sag structure.

which appears to be a hardened slurry of finer grained sediment. The foregoing description is representative both laterally and vertically of the entire section of tuffaceous epiclastic rocks.

The large rock fragments range in size from 0.5 to 10 centimeters, and are composed of altered and bleached porphyry which is lithologically similar to altered intrusive porphyry at Hahns Peak. Both porphyries are buff to white, nonvesicular and replete with quartz and sanidine, and are lacking in plagioclase and biotite (which are abundant in the unaltered porphyry of the region). However, pyrite, which is ubiquitous in the altered porphyry at Hahns Peak, is absent from porphyry clasts of the tuffaceous epiclastic breccia.

The similarity of porphyry fragments in the breccia at Porphyry Mountain to the porphyry at Hahns Peak, plus the block-sag structure, suggests that the fragments are airborne products of explosive fragmentation of dense plug rock in a volcano at Hahns Peak.

Figure 2*A* bears a startling resemblance to an illustration of a sawed and polished slab from the Ohanapecosh Formation on Backbone Ridge, Mount Rainier National Park, Wash. (Fiske and others, 1963, fig. 10). The resemblance, however, is only in appearance; the pumiceous volcanic arenites in the Ohanapecosh Formation are very different in composition from the nonglassy breccia and sandstone at Porphyry Mountain. The mechanism of deposition of the rocks at Porphyry Mountain—underwater mudflows or turbidites plus direct fall of pyroclastic material—was probably similar to that of the Ohanapecosh arenites (Fiske, 1963, p. 404).

The rocks at Porphyry Mountain were deposited in flat-lying beds in a small closed basin where a considerable thickness of the Browns Park Formation had been preserved from erosion. The basin was deep enought to accommodate 400 feet or more of the tuffaceous sediment. Most of the small grains of quartz, feldspar, and zircon in the sediment probably resulted from erosion and redeposition of the Browns Park Formation. The shale fragments were certainly derived from the Mancos Shale; the large size and angularity of some of them suggest that they were blown out of the active volcano along with the porphyry fragments. The airborne material which fell on nearby slopes moved to the bottom of the basin in very fluid mudflows—probably into standing water. This mechanism of deposition would explain the similarity of bedding texture at Porphyry Mountain to that of the Ohanapecosh arenites.

STRUCTURE

The dominant structural feature of the area of figure 1 is an intrusion of porphyry centered at Hahns Peak. The intrusion consists of a central stock with branching sills. A breccia pipe occupies most of the stock (Bowes and others, 1968). The intruded sedimentary rocks dip away from the stock, thus forming a dome. Faults in the area are either radial or approximately tangential to the dome. Porphyry Mountain is in a structural and topographic basin which lies between Hahns Peak and the Elkhead Mountains to the west (fig. 1).

GEOLOGIC HISTORY

The sequence of post-Laramide events in the Hahns Peak area is believed to be as follows:

1. Deposition of the Browns Park Formation in Miocene(?) time on an inclined surface sloping gently westward from the Park Range.
2. Uplift and erosion. Doming accompanied the intrusion of porphyry bodies in the Elkhead Mountains to the west and at Hahns Peak, and a structural and topographic basin developed at the site of present Porphyry Mountain.
3. Rock alteration at Hahns Peak resulting from hydrothermal activity.
4. Explosive eruptions of altered rhyolite prophyry and associated country rock (principally shale) from a vent at Hahns Peak. Explosion rubble was deposited by direct fall on the surrounding terrain, followed by downslope movement of some of this material as mudflows which partly filled the closed basin at Porphyry Mountain.
5. Strong tilting of all rocks in the vicinity, including the tuffaceous epiclastic breccia and sandstone, caused by renewed intrusion and doming, particularly at Hahns Peak. The doming was episodic, and intervening periods of collapse in the central part of the Hahns Peak intrusive caused a breccia pipe to develop (Bowes and others, 1968).
6. Widespread silicification of intrusive and intruded rocks, and local metallization of the breccia pipe and a zone immediately adjacent to the northwest.
7. Further stripping by erosion. This resulted in an inversion of topography at Porphyry Mountain, where the highly resistant tuffaceous epiclastic rock now forms a topographic high surrounded by lower topography developed in the less resistant Browns Park Formation and Mancos Shale.

REFERENCES

Barnwell, W. W., 1955, The geology of the South Hahns Peak district, Routt County, Colorado, *in* Intermountain Assoc. Petroleum Geologists, Guidebook, 6th Ann. Field Conf., Geology of northwest Colorado, 1955: p. 73–75.

Bowes, W. A., Segerstrom, Kenneth, and Young, E. J., 1968, Disseminated lead-zinc-silver deposit at Hahns Peak, Routt County, Colorado—a preliminary report: Internat. Geol. Cong., 23d, Prague 1968, Abstracts, p. 179–180.

Fiske, R. S., 1963, Subaqueous pyroclastic flows in the Ohanapecosh Formation, Washington: Geol. Soc. America Bull., v. 74, no. 4, p. 391–406.

Fiske, R. S., Hopson, C. A., and Waters, A. C., 1963, Geology of Mount Rainier National Park, Washington: U.S. Geol. Survey Prof. Paper 444, 93 p.

ORDOVICIAN BEDDED CHERT, ARGILLITE, AND SHALE OF THE CORDILLERAN EUGEOSYNCLINE IN NEVADA AND IDAHO

By KEITH B. KETNER, Denver, Colo.

Abstract.—A large proportion of Ordovician rocks in the Cordilleran eugeosyncline forms a compositionally continuous series whose end members are bedded chert and siliceous shale. Principal minerals are quartz and illite. Illite flakes are assumed to be detrital or to be derived from detrital clay. Quartz grains are of three kinds: scattered detrital grains of silt size, scattered radiolarian tests about 0.15 mm in diameter, and matrix grains of problematic origin about 0.005 mm in diameter. The hypothesis is offered that much of the fine-grained matrix quartz in rocks of this series was formed by inorganic precipitation of quartz from marine bottom waters of nearly normal silica content.

A large proportion of Ordovician eugeosynclinal rocks in Nevada and Idaho is composed of chert, argillite, and shale. In most areas where parts of stratigraphic sections have been measured these rocks are more abundant than all other kinds of rocks combined (table 1); in other areas their proportion is unknown but very large. Principal associated rocks are quartzite, greenstone, and siltstone. Sandstone and limestone are common locally.

Rocks in the eugeosyncline in Nevada and Idaho that contain thick sequences of chert, argillite, and shale are the Clipper Canyon Group of Kay (1962), the Pinecone Formation of Kay (1960), the Willow Canyon Formation of Kay and Crawford (1964); the Vinini Formation (Merriam and Anderson, 1942); the Valmy Formation (Roberts, 1964; Gilluly and Gates, 1965); the Basco Formation of Lovejoy (1959); the Snow Canyon Formation, McAfee Quartzite, and Jacks Peak Formation of Churkin and Kay (1967); and the Phi Kappa Formation (Umpleby and others, 1930).

In the Cordilleran eugeosyncline, Ordovician chert, argillite, and shale form a continuous series, lithologically, mineralogically, and chemically. These rocks are composed principally of fine silt-sized and clay-sized grains of quartz and illite in varying proportions. Rocks in this series that contain more than 90 percent silica have conchoidal fracture and high luster, are harder than steel, and, if carbon is not too abundant, are somewhat translucent. Rocks that have

TABLE 1.—*Lithic composition, in percent, of measured partial sections of Ordovician eugeosynclinal rocks, Cordilleran eugeosyncline, Nevada*

	Formation and approximate thickness of partial section (feet)									
	1 (5,000)	2 (1,600)	3 (1,000)	4 (400)	5 (475)	6 (1,400)	7 (525)	8 (1,200)	9 (900)	Avg [1]
Quartzite	41			48	37	76	83	4	24	34
Argillite and shale	27	79	46	4	9	18	14		12	28
Chert	27	4	7	44	54	1		85	9	23
Greenstone	5							9	33	6
Siltstone			33	4		5	3		18	6
Limestone		11	13					2	1	2
Sandstone		6	1						3	1

1. Valmy Formation, Battle Mountain (Roberts, 1964).
2. Vinini Formation, Tuscarora Range (J. Fred Smith, Jr., and Ketner, (unpub. data).
3. Basco Formation, Independence Range (Lovejoy, 1959).
4, 5. Jacks Peak Formation, Independence Range (Churkin and Kay, 1967).
6, 7. McAfee Quartzite, Independence Range (Churkin and Kay, 1967).
8, 9. Snow Canyon Formation, Independence Range (Churkin and Kay, 1967).

[1] Weighted according to thickness of partial section.

U.S. GEOL. SURVEY PROF. PAPER 650-B, PAGES B23-B34

these features are called chert by most field geologists, and they are so called in this report. Rocks that contain less than 90 percent silica lack the characteristic appearance of chert and are called shale if they are fissile, argillite if they are not fissile.

The petrography of chert, argillite, and shale was studied by means of about 150 thin sections from several localities (fig. 1), 50 X-ray diffraction patterns, 50 chemical analyses, and 50 spectrographic analyses of representative samples. X-ray diffraction patterns were made by T. D. Hessin.

DESCRIPTION OF ROCK TYPES

Bedded chert

Sedimentary units in which chert is the principal rock type usually crop out as distinct ledges, a few feet to scores of feet thick. Within these units, chert beds typically average from 1 to 4 inches in thickness; a few are 12 inches thick. These beds alternate with thin shale partings commonly no more than 1 inch thick. Bedding surfaces, exposed where the relatively soft shale has weathered away, are extremely uneven. The irregularities resemble load structures (Dzulynski and Walton, 1965) except that they form on both upper and lower surfaces of the chert beds.

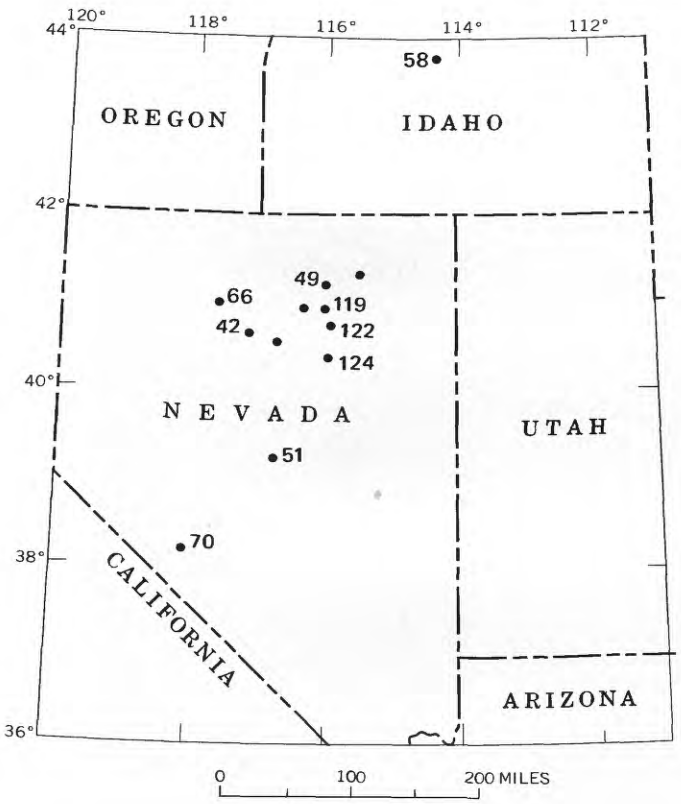

FIGURE 1.—Index map showing studied localities of eugeosynclinal chert, argillite, and shale. Numbered localities are those from which samples were obtained for chemical analysis (tables 2, 3, 4).

Within the chert beds that are separated from one another by shale partings are nonparting laminae about 1 millimeter thick. These thin laminae are caused by slightly varying concentrations of Radiolaria, illite, carbonaceous material, or detrital quartz grains.

Chert of the eugeosyncline is generally black, but much is green or greenish gray. The black and gray are ascribed to carbon or dark organic compounds and the green to illite if the dark pigments are lacking.

Principal constituents are quartz (including chalcedony), illite, organic debris, pyrite, and carbonate. The quartz content of chert ranges from 80 to 90 percent. Most of the quartz forms a mosaic of equant grains which average about 0.005 mm in diameter. Larger grains either show evidence of having been recrystallized or are detrital. The detrital grains are identified by their distinctive sharp, angular outlines.

Illite, which constitutes 5–15 percent of the chert, is not sufficiently abundant to produce fissility. Flakes generally average 5–10 microns in diameter.

Organic material is black or dark gray in hand specimen. In many specimens the organic material is so fine grained that discrete particles cannot be distinguished; its presence, however, is revealed in transmitted light by a pervasive brown color.

Pyrite in the form of cubes is dispersed throughout the chert in all areas. Commonly the cubes are less than 0.1 mm across. In some cherts pyrite cubes occupy the centers of Radiolaria. Cracks radiating from the corners of some of the larger cubes may indicate growth of pyrite after lithification.

Chert interbedded with the sparse limestone contains carbonate, usually in the form of isolated rhombs and less commonly as irregular grains.

Fossils in chert consist almost entirely of spheres about 0.15 mm in diameter (smaller diameters visible in thin sections may be off-center sections). The spheres are composed commonly of chalcedony. In a few unusually well preserved specimens, spines and nuclei are faintly discernible. These fossils are probably Radiolaria. The proportion of Radiolaria in chert is of interest because of the possibility that chert is composed of radiolarian tests. Clearly distinguishable Radiolaria rarely constitute more than 20 percent of chert, and the average is closer to 5 percent. These clearly distinguishable Radiolaria almost everywhere are whole spheres or ovoids set in a matrix of equant grains that commonly have diameters about a twenty-fifth as great as those of the Radiolaria (fig. 2). In

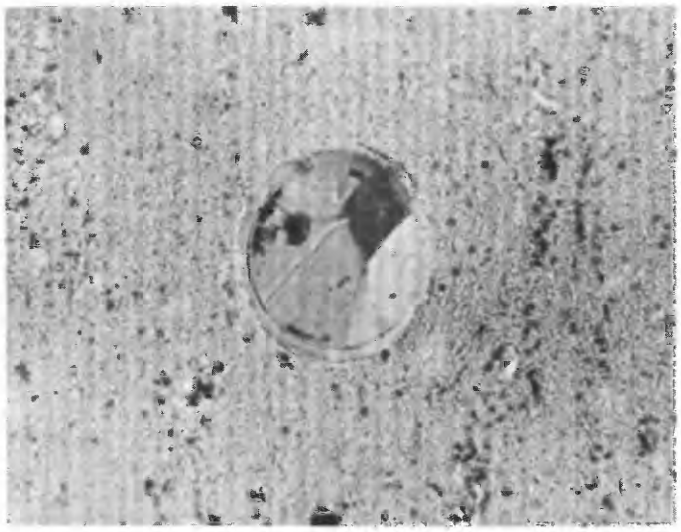

FIGURE 2.—Chert showing contrast in grain size between quartz of the matrix (salt-and-pepper texture) and radiolarian (large sphere). Site 119, crossed nicols, ×170.

some chert, barely discernible clots of quartz in a framework of organic matter can be interpreted as closely packed Radiolaria whose boundaries have become diffused and obscured by some process of recrystallization. However, the usual presence in the same rock of clearly defined Radiolaria whose outlines have not been obliterated weakens this interpretation.

The chert is notably free from the burrows, tracks, and tests of organisms other than Radiolaria. Several reasons for the apparent absence of bottom-dwelling organisms can be adduced, but the absence of graptolites is puzzling in view of their abundance in the argillite and shale that are interbedded with the chert.

Argillite

Bedding in argillite is of two types. Commonly the beds are distinctly separated from one another by thin beds of shale at intervals of an inch to a foot. These argillite beds stand out distinctly in outcrop, and flaking of the shale exposes bedding surfaces which are generally more even than those of chert beds. Within principal bedding units are laminae formed by slightly varying concentrations of Radiolaria, organic debris, detrital quartz or illite.

Argillite is generally black or dark gray, but if carbonaceous material is scanty the greenish-gray cast of illite shows up.

The quartz content of argillite ranges approximately from 40 to 80 percent. Less quartzose rocks have not been found, and those with more quartz are classed as chert. Most quartz is in the form of fitted grains about 0.005 mm in diameter, but detrital quartz grains of coarse silt size are common.

The illite content ranges from 15 to 55 percent. The illite of argillite, like that of chert, is in the form of flakes a few microns in diameter. Where argillite has been slightly heated near intrusives, the illite is recrystallized into larger flakes whose X-ray diffraction pattern is similar to that of muscovite.

Organic matter consists of discrete particles of debris or impalpable pigmentation that is brown in transmitted light. Pyrite in scattered minute cubes is ubiquitous but is nowhere abundant. Kaolinite, montmorillonite, and chlorite are sparsely present in some beds.

Fossils consist of Radiolaria, graptolites, and, less commonly, small inarticulate brachiopods. Whole distinct Radiolaria average less than 5 percent and rarely exceed 20 percent of the rock. Ghostly Radiolaria-sized clots of quartz grains are common (as they are in chert and shale) and may represent Radiolaria that have melded into the matrix by some process of recrystallization. Graptolites are common in argillites. In view of the indefinite petrographic boundary between argillite and chert, the absence of graptolites from the chert is all the more puzzling.

The thin bedding of the argillite and the absence of burrows or tracks indicate a dearth of bottom-dwelling organisms.

Shale

Normally, shale crops out so poorly that bedding features cannot be seen, but in fresh exposures and especially in drill cores, the bedding appears as alternating light- and dark-gray layers a few millimeters thick.

Like chert and argillite, the shale of the eugeosyncline is composed of quartz and illite and lesser amounts of organic matter, carbonate, and pyrite. Some shale contains a little kaolinite, montmorillonite, and chlorite.

The quartz content of shale ranges approximately from 35 to 70 percent. The quartz occurs as a matrix of interlocking grains about 0.005 mm in diameter and as scattered detrital silt.

On the average, illite is present in slightly larger quantities in shale than in argillite. It ranges approximately from 25 to 60 percent. Twenty-five percent may represent the minimum proportion of illite normally necessary to produce fissility (in a few rocks fissility is produced by an abundance of graptolites or other flaky organic debris rather than by illite).

The organic matter consists of disseminated discrete fine particles or impalpable pigments that are brown

in transmitted light. Carbonate lenses or disseminated rhombs and irregular grains are common in some shale beds that are associated with limestone. Organic matter is concentrated in the siliceous parts rather than the calcareous parts of these rocks. Pyrite cubes are a ubiquitous though minor constituent of all the shales that were studied.

Distinct Radiolaria are uncommon, but indistinct lenses of quartz and chalcedony which are common in some shale may represent the compressed remains of Radiolaria.

Graptolites are fairly common in most shale beds and are very abundant in a few. The apparent abundance of graptolites in shales as compared with that in argillites may be due to the fissility of shale, which tends to expose graptolites lying on bedding surfaces. A few very small inarticulate brachiopods occur with the graptolites.

CHEMICAL COMPOSITION OF CHERT, ARGILLITE, AND SHALE

The chemical composition of representative samples is shown in table 2, also tables 3 and 4 on page B28. A salient feature of all samples is their high silica content. This property was at first thought to represent bias in sampling introduced by an assumed failure of low-silica rocks to crop out. A special effort was therefore made to collect the softest most argillaceous-looking shale and argillite from a fresh exposure. The results of this effort are samples 2259 to 2264 from locality 119. All were above average in silica content.

Silica and alumina, as major constituents of the chert, argillite, and shale series, are naturally inversely correlative, as shown by figure 3. The rather even distribution of points on this diagram shows that the series is a continuum between definite limits. Extension of the trend line shows that theoretically a chert without any Al_2O_3 would contain 96 percent

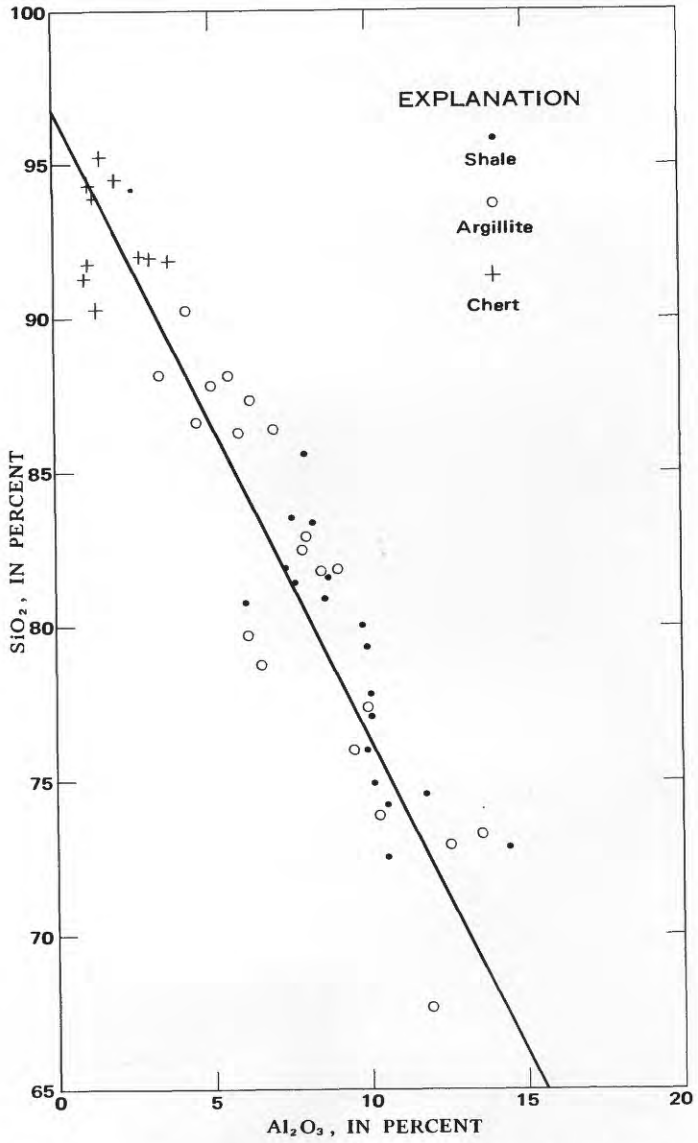

FIGURE 3.—Relation between SiO_2 and Al_2O_3 in chert, argillite, and shale.

TABLE 2.—*Chemical and spectrographic analyses, in weight*

Forty-seven additional elements were looked for but were not found or were found to occur sporadically in insignificant amounts. Chemical analyses by P. L. D. Elmore organic carbon by I. C. Frost, 1964–67; spectrographic analyess by J. C. Hamilton, N. M. Conklin, and H. G. Neiman, 1963–67]

Locality (fig. 1)	Sample No.	Chemical analyses														
		SiO_2	Al_2O_3	Fe_2O_3	FeO	MgO	CaO	Na_2O	K_2O	H_2O-	H_2O+	TiO_2	P_2O_5	MnO	CO_2	C[1]
1 122	818	94.4	1.1	0.18	0.28	0.11	0.27	0.04	0.25	0.40	1.2	0.06	0.10	0.01	<0.05	0.73
2 66	1708	94.5	1.9	.22	.20	1.0	.85	<.05	.56	.12	.48	.11	.04	.00	<.05	<.1
3 51	1842	92.1	2.7	.65	.32	.50	.45	.15	.85	.18	.82	.05	.15	.21	.08	<.1
4	1844	91.9	2.8	.69	.24	1.1	.30	.15	.85	.16	1.0	.13	.12	.10	.08	.2
5	1845	91.3	.89	4.3	.20	1.0	.25	.05	.35	.15	.71	.03	.10	.08	.08	.3
6	1846	91.9	3.6	.35	.08	.22	.09	.15	.84	.28	1.3	.20	.09	.11	<.05	.3
7	1848	93.9	1.2	.30	.20	.70	.32	.05	2.0	.18	.59	.37	.07	.08	<.05	.3
8 119	2256	91.8	1.1	.24	.18	.05	.23	.06	.60	.65	.95	.06	.08	.00	<.05	1.85
9	2669	90.3	1.3	1.7	(2)	.14	.11	.23	1.1	.45	1.4	.09	.11	.02	<.05	1.56
10 Average		92.5	1.8	0.87	0.21	0.54	0.32	0.10	0.82	0.29	0.94	0.12	0.10	0.07	±0.04	0.6

[1] Organic carbon. [2] Calculated as Fe_2O_3.

silica and 4 percent nonsiliceous, nonaluminous minerals.

COMPARISON OF ORDOVICIAN ARGILLITE AND SHALE WITH OTHER ROCKS AND SEDIMENTS

Comparison with normal shale

Comparison of analyses of Ordovician argillite and shale with published analyses of similar rocks of different ages herein called normal shale (table 5 on page B29 ; fig. 4) shows the Ordovician rocks to be unusual in several respects. Their SiO_2 content is abnormally high, but they are not merely normal shales with extra silica as is shown in table 6. In this table the SiO_2 content of average normal shale has been adjusted to the level of SiO_2 in average Ordovician argillite and shale. Although such adjustment of SiO_2 automatically reduces the Al_2O_3, MgO, and TiO_2 contents of normal shales to the level of these components in the Ordovician rocks, it fails to bring the Fe_2O_3, CaO, Na_2O, K_2O, and P_2O_5 into line. The relatively high P_2O_5 and CaO contents of the Ordovician rocks may be partly due to more abundant apatite. The relatively high content of K_2O and low content of Na_2O in the Ordovician rocks is ascribed to a higher ratio of illite to other clay minerals.

Comparison with modern oceanic sediments

Modern pelagic sediments are principally red clay, radiolarian or diatomaceous ooze, and globigerina ooze. Published analyses of these sediments indicate that red clay having a chemical composition similar to that of normal shale is a universal pelagic sediment which is varied from place to place (or time to time) by addition of carbonate or silica (tables 5, 6 on page B29; fig. 5). In other words, radiolarian ooze and diatomaceous ooze apparently are composed of red clay into which tests of Radiolaria or diatoms have settled; globigerina ooze is red clay into which tests of globigerina have settled.

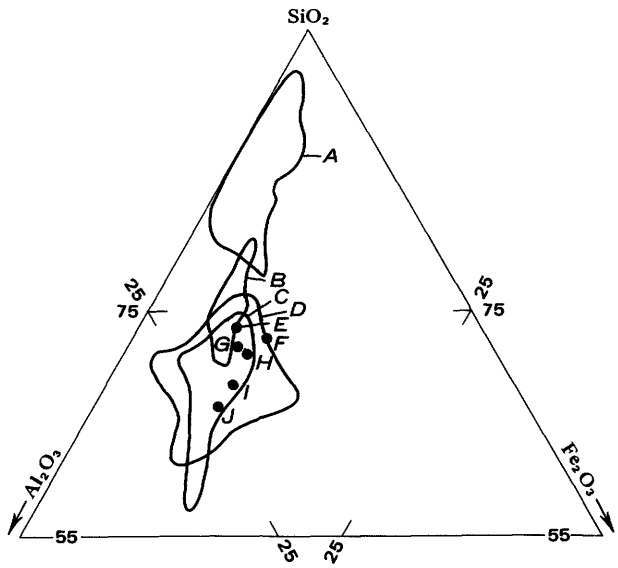

FIGURE 4.—Ratios of major oxides in normal shale, slate, and phyllite as compared with those in Ordovician argillite and shale of the Cordilleran eugeosyncline. All iron calculated as Fe_2O_3. *A*, 40 Ordovician argillites and shales of the Cordilleran eugeosyncline; *B*, 17 Pierre Shale, Cretaceous (Tourtelot, 1962) ; *C*, 18 Littleton Formation, Devonian (Shaw, 1956) ; *D*, 22 low-iron slates, Precambrian (Nanz, 1953) ; *E*, average 27 Mesozoic and Cenozoic shales (Clarke, 1924) ; *F*, average 12 phyllites (Rankama and Sahama, 1950) ; *G*, average 51 Paleozoic shales (Clarke, 1924) ; *H*, average 11 phyllites (Rankama and Sahama, 1950) ; *I*, weighted average 36 Precambrian slates (Nanz, 1953) ; *J*, average 18 phyllites (Rankama and Sahama, 1950).

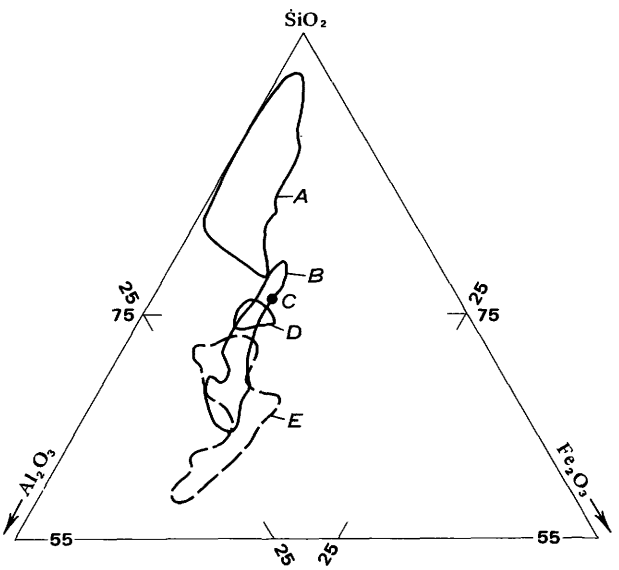

FIGURE 5.—Ratios of major oxides in siliceous oceanic sediment as compared with those in Ordovician argillite and shale of the Cordilleran eugeosyncline. All iron calculated as Fe_2O_3. *A*, 40 Ordovician argillites and shales of the Cordilleran eugeosyncline; *B*, 22 red clays (El Wakeel and Riley, 1961; Revelle, 1944) ; *C*, average 3 siliceous oozes (El Wakeel and Riley, 1961) ; *D*, 3 radiolarian oozes (Revelle, 1944) ; *E*, 18 brown clays (Goldberg and Arrhenius, 1958).

percent, of Ordovician chert of the Cordilleran eugeosyncline

S. D. Botts, Lowell Artis, G. W. Chloe, Hezekiah Smith and J. L. Glenn, 1963-67:

Spectrographic analyses								
B	Ba	Cr	Cu	Ni	Sr	V	Zr	
0.002	0.07	0.0015	0.007	0.002	0.002	0.02	0.001	
<.002	0.01	.0007	.005	<.0003	.001	.003	.001	1
.003	.05	.0007	.003	.002	.001	.003	.0015	2
.005	.15	.002	.003	.0015	.003	.007	.002	3
<.002	.15	.001	.007	.002	.0015	.005	.001	4
.005	.07	.007	.003	.0007	.0015	.015	.003	5
.002	.02	.003	.007	.002	.0015	.02	<.001	6
.003	.02	.0015	.003	.0015	.0015	.015	.003	7
.007	.015	.0015	.005	.0015	.0015	.05	.003	8
								9
0.003	0.06	0.002	0.005	0.001	0.002	0.02	0.002	10

TABLE 3.—*Chemical and spectrographic analyses, in weight percent, of Ordovician argillite of the Cordilleran eugeosyncline*

[Forty-six additioual elements were looked for but were not detected or were found to occur sporadically in insignificant amounts. Chemical analyses by P. L. D. Elmore, S. D. Botts, G. W. Chloe, Lowell Artis, and Hezekiah Smith, 1963–64; organic carbon by I. C. Frost, 1964, spectrographic analyses by J. C. Hamilton, 1963–64]

Locality (fig. 1)	Sample No.	Chemical analyses														Spectrographic analyses								
		SiO_2	Al_2O_3	Fe_2O_3	FeO	MgO	CaO	Na_2O	K_2O	H_2O-	H_2O+	TiO_2	P_2O_5	MnO	CO_2	C[1]	B	Ba	Cr	Cu	Ga	Ni	Sr	V	Zr
70	1828	81.8	5.0	1.5	1.8	1.7	3.6	0.62	0.62	0.33	1.1	0.34	0.90	0.17	0.08	0.5	<0.002	0.05	0.002	0.002	0.0007	0.002	0.015	0.007	0.003
	1827	72.8	12.5	2.0	.92	2.6	.95	.67	3.5	.72	2.2	.60	.20	.07	.09	.6	.01	.2	.005	.007	.002	.001	.007	.02	.007
	1826	73.9	10.3	2.4	.64	2.5	1.6	.10	3.1	.87	2.4	.55	.77	.04	.06	.6	.015	.1	.005	.003	.0015	.001	.007	.05	.007
	1835	78.7	6.6	.66	2.4	2.6	3.5	.62	1.3	.07	1.1	.26	.22	.17	1.2	.4	<.002	.1	.003	.001	.001	.0015	.015	.007	.003
124	553D	79.7	6.1	1.0	.42	.36	.47	.08	1.1	1.2	3.8	.28	1.2	.01	<.05	2.4	.007	.5	.005	.007	.0015	.003	.05	.02	.005
122	508	87.8	5.0	.63	.14	.49	.12	.13	1.3	.70	1.8	.25	.08	.00	<.05	.2	.007	.15	.01	.007	.0007	.0007	.005	.015	.005
	564	90.2	4.2	.36	.11	.39	.10	.11	1.1	.61	1.5	.22	.07	.00	.06	.1	.007	.1	.007	.005	.0007	.0007	.005	.01	.005
42	1701	86.2	5.7	1.1	.20	1.2	1.1	.25	2.0	.31	1.1	.25	.66	.00	.08	.3	.005	.05	.003	.005	.0007	.001	.007	.007	.003
	1706	88.1	5.5	.84	.24	.6	.32	<.05	1.9	.33	1.2	.26	.18	.00	<.05	.3	.005	.03	.003	.005	.0007	.001	.003	.007	.003
	1704	82.9	8.0	1.7	.32	1.0	.47	<.05	2.4	.37	1.4	.43	.20	.05	.15	.3	.01	.07	.005	.005	.0015	.0015	.003	.01	.005
66	1715	81.7	8.4	2.0	.40	1.0	1.0	.15	2.4	.58	1.7	.38	.33	.02	<.05	<.1	.01	.02	.005	.0015	.0015	.0003	.0015	.01	.005
	1709	87.4	6.2	.36	.28	.10	.50	.10	1.9	.36	1.4	.31	.21	.00	.10	<.1	.005	.02	.003	.0007	.001	.0003	.001	.005	.007
58	1471	73.2	13.4	.30	1.0	1.7	6.0	.75	1.4	.12	.81	.60	.30	.02	<.05	2.1	<.002	.15	.015	.003	.003	.005	.03	.03	.015
	1475	77.3	10.0	.80	2.0	2.1	1.3	1.4	2.6	.30	.70	.47	.23	.03	<.05	-------	.02	.3	.01	.01	.007	.007	.015	.05	.015
	1478	76.2	9.5	.85	1.5	1.3	1.1	.75	5.2	.12	.78	.46	.23	.02	<.05	2.0	.005	.3	.015	.01	.002	.007	.05	.05	.01
	1487	88.1	3.4	.32	.60	.92	.82	.30	1.1	.31	1.0	.19	.07	.01	<.05	3.5	<.002	.1	.007	.007	.001	.005	.01	.02	.003
119	2243	81.8	9.0	.89	.28	.82	.15	.06	3.8	.57	1.9	.55	.18	.00	<.05	.06	.015	.07	.007	.02	.002	.0015	.015	.03	.03
	2260	86.1	7.0	.50	.16	.30	.00	.10	2.2	.75	1.8	.35	.02	.00	<.05	.05	.015	.03	.007	.007	.002	.0003	.003	.07	.015
	2262	82.5	7.8	1.7	.24	.90	.16	.10	2.3	1.0	2.3	.34	.07	.00	<.05	.07	.015	.07	.005	.015	.0015	.003	.007	.015	.02
	2269	86.4	6.8	.29	.24	.85	.34	.09	1.7	.82	1.9	.40	.04	.00	<.05	.07	.007	.015	.0015	.005	<.0005	.0015	.0015	.05	.003
	2275	86.6	4.5	1.6	.14	.33	.23	.07	1.9	1.4	2.2	.21	.18	.06	<.05	.10	.015	.03	.002	.005	.0007	.0015	.003	.01	.007
49	2825	67.6	11.8	3.8	(2)	.65	.12	.09	4.6	1.6	4.3	.56	.12	.02	<.05	2.96	.03	.07	.015	.007	.003	.0015	.01	.15	.015
Average		81.7	7.6	1.0	0.7	1.1	1.1	0.3	2.2	0.6	1.7	0.38	0.3	0.03	0.1	0.8	0.01	0.1	0.006	0.006	0.002	0.002	0.01	0.03	0.01

[1] Organic carbon.
[2] Calculated as Fe_2O_3.

TABLE 4.—*Chemical and spectrographic analyses, in weight percent, of Ordovician shale of the Cordilleran eugeosyncline*

[Forty-six additional elements were looked for but were not detected or were found to occur sporadically in insignificant amounts. Chemical analyses by P. L. D. Elmore, S. D. Botts, G. W. Chloe, Lowell Artis, and Hezekiah Smith, 1963–64; organic carbon by I. C. Frost, 1964; spectrographic analyses by J. C. Hamilton, 1963–64]

Locality (fig. 1)	Sample No.	Chemical analyses														Spectrographic analyses								
		SiO_2	Al_2O_3	Fe_2O_3	FeO	MgO	CaO	Na_2O	K_2O	H_2O-	H_2O+	TiO_2	P_2O_5	MnO	CO_2	C[1]	B	Ba	Cr	Cu	Ga	Ni	Sr	V	Zr
42	1702	83.5	7.5	1.3	0.36	0.7	0.65	<0.05	2.6	0.33	1.4	0.32	0.53	0.00	0.08	0.2	0.007	0.07	0.005	0.01	0.001	0.003	0.0005	0.015	0.007
	1703	80.0	9.7	1.7	.34	.9	.25	<.05	3.1	.50	2.0	.45	.29	.00	.08	.4	.01	.07	.005	.002	.0015	.0007	.002	.007	.007
	1705	85.6	7.9	.23	.20	.6	.30	<.05	2.6	.28	1.3	.37	.36	.04	.09	.2	.007	.05	.002	.001	.001	<.0003	.002	.005	.005
51	1847	81.4	7.6	2.6	.04	.75	.30	.11	2.4	.57	1.9	.36	.46	.08	.05	.5	.007	.07	.007	.007	.001	.002	.007	.03	.007
	1849	80.8	8.6	1.8	.24	.90	.30	.17	2.5	.64	2.1	.47	.43	.00	.08	.8	.01	.1	.003	.01	.001	.003	.007	.02	.007
	1850	77.0	10.0	2.3	.40	1.6	.30	.05	3.2	1.2	3.2	.40	.20	.00	<.05	.3	.01	.07	.003	.007	.0015	.002	.005	.007	.01
70	1833	74.8	10.1	1.2	1.8	2.7	2.2	<.05	2.6	.17	2.3	.37	.34	.07	1.0	<.1	.005	.1	.005	.002	.001	.003	.005	.01	.005
	1830	74.2	10.5	1.8	1.0	2.6	1.9	.80	2.9	.74	2.0	.54	.66	.05	.09	.5	.01	.1	.005	.007	.0015	.0015	.005	.02	.005
	1831	75.9	9.8	1.5	2.0	2.6	2.4	1.1	1.2	.43	2.1	.40	.30	.08	.06	1.1	<.002	.1	.005	.0015	.001	.005	.015	.01	.002
	1832	72.7	14.2	1.8	.48	1.0	.36	<.05	5.1	.24	2.4	.65	.22	.05	.08	<.1	.005	.3	.007	.001	.002	.0007	.007	.05	.007
	1836	74.5	11.7	1.3	1.6	2.7	1.4	.85	2.8	.21	1.5	.47	.32	.06	.08	<.1	.002	.3	.005	.003	.0015	.003	.01	.02	.005
119	2253	80.7	6.0	.90	.18	.33	.32	.03	2.0	1.3	1.8	.59	.14	.00	<.05	3.78	.007	.03	.005	.003	.002	.0007	.003	.07	.007
	2259	81.8	7.3	1.3	.24	.90	1.5	.04	2.4	.86	1.8	.31	.80	.00	<.05	.11	.015	.07	.007	.015	.0015	.007	.007	.03	.02
	2261	83.3	8.1	1.0	.16	.75	.16	.17	2.6	.90	2.2	.39	.12	.00	<.05	.08	.015	.07	.007	.015	.003	.003	.007	.015	.02
	2263	79.3	9.8	1.7	.28	1.2	.15	.15	2.8	1.3	2.6	.55	.04	.00	<.05	.08	.015	.07	.007	.015	.003	.003	.003	.07	.015
	2264	81.6	8.6	1.5	.20	.86	.31	.24	2.7	.89	1.9	.36	.15	.00	<.05	.06	.015	.07	.003	.01	.002	.0003	.007	.007	.015
	2668	72.5	10.4	.79	(2)	.52	.20	.25	5.9	.70	2.5	.50	.04	.00	<.05	4.96	.015	.03	.01	.003	.003	.0015	.003	.07	.015
49	2824	77.7	10.0	1.2	(2)	.50	.20	.16	4.7	1.2	3.5	.50	.09	.00	<.05	1.17	.03	.05	.015	.005	.003	.003	.007	.07	.015
Average		78.7	9.3	1.5	0.6	1.2	0.7	0.2	3.0	0.7	2.1	0.44	0.30	0.02	0.10	0.8	0.01	0.1	0.006	0.006	0.002	0.002	0.006	0.03	0.01

[1] Organic carbon.
[2] Calculated as Fe_2O_3.

TABLE 5.—*Average chemical composition, in weight percent, of normal marine shale, oceanic sediment, extrusive igneous rock, and Ordovician argillite and shale of the Cordilleran eugeosyncline*

[Abbreviation: Tr., trace]

Kind of material	Number of analyses	Source of data	Averaged chemical analyses; carbonate, water, and carbon free									
			SiO_2	Al_2O_3	Fe_2O_3[1]	MgO	CaO	Na_2O	K_2O	TiO_2	P_2O_5	MnO
Normal marine shale												
Cretaceous shale	17	Tourtelot (1962)	68.0	17.5	6.5	2.1	0.8	1.2	2.8	0.68	0.17	0.22
Mesozoic, Cenozoic shale	27	Clarke (1924)	66.7	16.6	7.0	3.2	.2	2.2	3.2	.55	.24	Tr.
Devonian pelitic rocks	18	Shaw (1956)	63.4	20.3	7.5	2.1	.4	1.2	3.8	1.0	.14	.07
Paleozoic shale	51	Clarke (1924)	66.0	18.0	7.9	2.1	.0	1.1	4.0	.83	.16	Tr.
Total	113											
Average			66.1	18.1	7.2	2.4	0.3	1.4	3.4	0.76	0.18	Tr.
Oceanic sediment												
Siliceous ooze	3	El Wakeel and Riley (1961).	70.6	14.7	7.1	2.2	0.8	0.9	2.1	0.72	0.30	0.55
Radiolarian ooze	3	Revelle (1944)	67.6	15.2	7.4	1.0	1.4	2.0	3.5	.69	.55	.65
Red clay	12	El Wakeel and Riley (1961).	60.4	19.1	8.9	3.7	1.0	1.7	3.6	.92	.16	.52
Red clay	10	Revelle (1944)	62.2	20.0	8.7	.9	.6	1.9	3.7	.89	.20	.82
Globigerina ooze	10	El Wakeel and Riley (1961).	61.9	18.7	8.7	2.9	.9	1.7	3.4	.86	.32	.63
Globigerina ooze	20	Edgington and Byers (1942).	66.1	15.0	6.7	4.4	.2	3.0	2.7	.96	.22	.22
Total	58											
Average			64.7	17.1	7.9	2.5	0.8	1.9	3.2	0.84	0.29	0.56
Extrusive igneous rock												
Andesite, dacite, and rhyolite.	279	Daly (1933)	67.0	16.0	4.6	1.5	3.5	3.7	3.1	0.55	0.17	0.10
Ordovician rocks of the Cordilleran eugeosyncline												
Argillite and shale	40	This report	83.2	8.7	2.4	1.2	0.9	0.2	2.7	0.43	0.31	0.02

[1] All iron calculated as Fe_2O_3.

TABLE 6.—*Chemical composition, in weight percent, of normal marine shale, oceanic sediment, and extrusive igneous rock, whose silica content is adjusted to a constant value of 83.2*

[Average silica contents adjusted from average values given in table 5, this report]

Rock type and silica mixtures (adjusted to 83.2 weight percent SiO_2 content)	Chemical composition; carbonate, water, and carbon free								
	Al_2O_3	Fe_2O_3[1]	MgO	CaO	Na_2O	K_2O	TiO_2	P_2O_5	MnO
Average normal shale, 100 parts; pure silica, 102 parts	9.0	3.6	1.2	0.2	0.7	1.7	0.38	0.09	Trace
Average oceanic sediment, 100 parts; pure silica, 110 parts	8.1	3.8	1.2	.4	.9	1.5	.40	.14	0.27
Average acid to intermediate extrusive rock, 100 parts; pure silica, 96 parts	8.2	2.3	.8	1.8	1.9	1.6	.28	.09	.05
Average Ordovician argillite and shale (not adjusted)	8.7	2.4	1.2	.9	.2	2.7	.43	.31	.02

[1] All iron calculated as Fe_2O_3.

Pelagic calcareous Foraminifera and diatoms had not evolved by Ordovician time and, other conditions equal, Ordovician pelagic sediments, therefore, are likely to have been composed almost entirely of red clay and Radiolaria. On the basis of general composition and appearance, except for color, the Ordovician argillites and shales of the Cordilleran eugeosyncline could pass for lithified highly siliceous pelagic sediments. Chemical analyses, however, reveal differences similar to those between the Ordovician rocks and normal shale.

If sufficient pure silica is added to average red clay to raise the SiO_2 content of the clay to the level of SiO_2 in average Ordovician argillite and shale, the Al_2O_3, MgO, and TiO_2 contents automatically decrease to about the level of these components in the Ordovician rocks; but Fe_2O_3, CaO, Na_2O, K_2O, P_2O_5, and MnO fail to come into line. The disparity in CaO, P_2O_5, and K_2O can be explained by a greater content of apatite and a higher ratio of illite to other clays in the Ordovician rocks. The relative excess of Na_2O in modern oceanic sediment can be explained by a relative excess in the sediments of montmorillonite as opposed to illite or, perhaps, to occluded brine. Disparities in Fe_2O_3 and MnO contents are not easily explained.

Comparison with igneous rocks

Although igneous textures were not observed in thin sections of the Ordovician rocks, it is conceivable that argillite and shale are composed partly of fine-grained acid to intermediate ash derived from distant explosive volcanoes. Tables 5 and 6, and figure 6 indicate that the addition of silica to ash of intermediate to acid composition would produce deposits whose Al_2O_3 and Fe_2O_3 contents would be similar to those of Ordovician argillite and shale. However, such deposits would be deficient in MgO, K_2O, TiO_2, and P_2O_5 and would have excessive CaO, Na_2O, and MnO.

The addition of silica alone to more basic ash could not produce sediment of the right composition, and the amount of silica and other materials necessary to do so would be so great as to relegate the volcanic material to an incidental role in the formation of argillite and shale.

ORIGIN OF CHERT, ARGILLITE, AND SHALE

The uniformity of composition of normal shale and siliceous pelagic sediment of widely differing geologic ages and geographic locations (table 5; figs. 4 and 5) suggests that this composition reflects random mixtures of material from a variety of normal sources. Ordovician argillite and shale of the Cordilleran eugeosyncline differ from these normal shales and pelagic sediments in their higher ratios of quartz, illite, and probably apatite, to other minerals. Illite is assumed to be detrital or to be an altered form of other detrital clay minerals. The reasons for the predominance of illite over other clay minerals in the Ordovician rocks is unknown. The addition of unusually large volumes of volcanic ash to normal shale and pelagic clay could not bring their composition into close agreement with that of the Ordovician argillite and shale. The unique composition of the Ordovician rocks therefore must reflect unusual source areas or unusual depositional conditions bearing principally on the deposition of silica. The possible sources of silica and means of deposition are reviewed and evaluated in the following sections of this report.

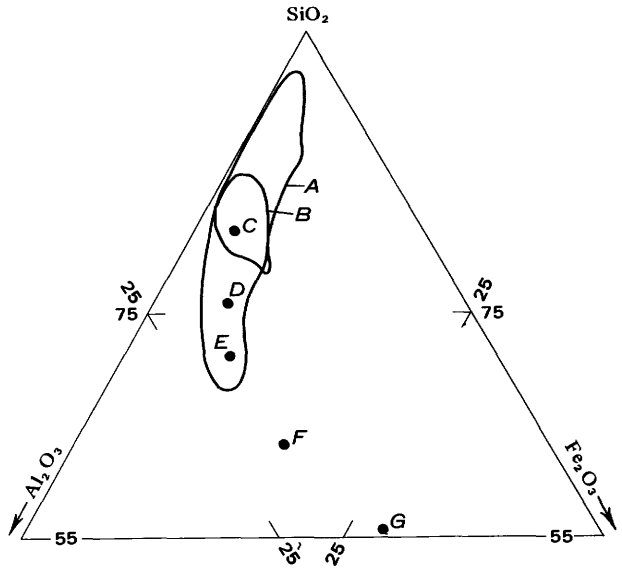

FIGURE 6.—Ratios of major oxides in igneous rock as compared with those in Ordovician argillite and shale of the Cordilleran eugeosyncline. All iron calculated as Fe_2O_3. *A*, 40 Ordovician argillites and shales of the Cordilleran eugeosyncline; *B*, 40 randomly selected rhyolites and andesites; *C*, average rhyolite (Daly, 1933); *D*, average dacite (Daly, 1933); *E*, average andesite (Daly, 1933); *F*, average basalt (Daly, 1933); *G*, average peridotite (Daly, 1933).

SOURCE OF SILICA

Streams

Streams carry silica to the sea in solution, as colloids, and as detritus. The amount carried in solution is enormous. About 4.3×10^8 metric tons of dissolved silica is presently being carried to the sea each year (Livingstone, 1963, p. 40, 41). At this rate and on the assumption that the average silica content of the sea is 6 parts per million, only 20,000 years would be required to supply the amount of silica presently in solution.

In the lower reaches of streams the amount of silica

in colloidal form is probably small relative to that in true solution. The older idea that most silica in streams is transported as a colloid (Twenhofel, 1932, p. 526) was based on faulty data and has been disproved (Krauskopf, 1956, p. 9). According to Krauskopf, silica colloids in undersaturated solutions disperse within a few days or weeks and become true solutions. The amount of clay-sized and silt-sized detrital quartz carried to the sea by streams is impossible to estimate but is probably very large.

Submarine hot springs

Commonly the silica content of hot springs is a few hundred parts per million. White (1957, p. 1640) listed 10 analyses of high-temperature hot springs in Western United States and New Zealand. Silica content ranges from 56 to 529 ppm and averages about 302 ppm. The average SiO_2 content of 12 samples of water of volcanic origin from the United States, Italy, Colombia, New Zealand, and the Philippines (Clarke, 1924) was found to be 252 ppm. White, Brannock, and Murata (1956, table 2) gave 22 analyses of samples from hot springs in Yellowstone Park and in California. The average silica content of these samples was 278 ppm.

The estimated total flow of all hot springs in the United States (Stearns and others, 1937, p. 98) is no more than 9.8×10^8 metric tons per year. If we assume an average silica content of 300 ppm, the annual discharge of silica is 2.9×10^5 metric tons. If the density of distribution of silica and the discharge of submarine hot springs are similar to the density and discharge of the continental hot springs in the United States, then 1.4×10^7 metric tons of silica is being discharged beneath the sea at the present time. If we assume a wider extent of Ordovician seas and a similar rate of flow, possibly 2×10^7 tons was discharged per year in Ordovician time. This amount is less than one-twentieth the quantity of dissolved silica now carried to the sea annually by rivers.

Submarine weathering of extrusive rock

In this process silica is supposed to dissolve from volcanic ash during its descent in the sea or from lava and ash on the sea floor. The dissolved silica is then available for precipitation under favorable conditions. Experimental work by Kennedy (1950) indicates that under the high pressures and temperatures possible in deep water at hot lava-water interfaces the solubility of silica is fairly high—several hundred parts per million. In solutions of such high concentration, silica tends to precipitate on cooling of the solution or on convection upward to zones of lower pressure unless this tendency is nullified by dilution.

There is little reason to doubt the validity of submarine silica solution, especially under conditions of high pressure and temperature, and doubtless some dissolved silica is supplied to the sea by this process. An estimation of the amount is difficult to make, but the evidence from Ordovician rocks of the Cordilleran eugeosyncline tends to minimize the importance of this source.

Analyses of pillow lava from the Valmy Formation (unpub. data, and Roberts, 1964) show normal silica-iron-alumina ratios for intermediate to basic rock. The alteration of some Ordovician greenstone may be in the direction of silica accretion rather than depletion. For example, Gilluly and Gates (1965) and Gilluly and Masursky (1965) indicated that andesine in greenstone of the Valmy Formation has been partly replaced by albite and quartz.

Fine-grained quartz of problematic origin composes, on the average, about 50 percent of the chert, argillite, and shale series. If 10 percent of the silica of greenstone were lost by reaction with sea water and precipitated to form, with other constituents, a mixed assemblage of chert, argillite, and shale, the volumetric ratio of greenstone to sediments would have to be about 10:1. The much lower ratio of greenstone to fine-grained silicic rocks in most areas and the indications that greenstone had not lost a large amount of silica compel the conclusion that the capacity of greenstone to supply the silica required by associated cherty sediments is strikingly inadequate.

Typically, chert, argillite, and shale are interlayered with one another and with siltstone, quartzite, and greenstone, but apparently with no regularity of sequence. If a cause-and-effect relationship exists, the most siliceous sediment should directly overlie greenstone consistently. Merriam and Anderson (1942) and Roberts (1964) described examples of greenstone overlain by chert, but Roberts also showed thick units of chert which do not overlie greenstone. In the Shoshone Range, Nevada (Gilluly and Gates, 1965, pl. 1), no consistent sequential relation is found. In the Palmetto Formation (Albers and Stewart, 1965), in the Toquima Formation (Ferguson, 1924), and in the Sams Spring and Petes Summit Formations (Kay and Crawford, 1964), conspicuous black bedded chert units overlie shale which, in turn, overlies quartzite.

DEPOSITION OF SILICA

Inorganic precipitation of quartz from solution

The concentration of dissolved silica in modern seas varies from near zero, in surface waters which have been depleted of silica by diatoms and other organ-

isms, to about 6 ppm (Goldberg, 1965), p. 164), 8 ppm (Sverdrup and others, 1942, p. 176), or 10 ppm (Krauskopf, 1959, p. 16) in deeper water.

The solubility concentration or saturation point of quartz in sea water is not known with certainty. Siever (1957, p. 826) calculated the value at 7–14 ppm. Gardner (1938) determined the solubility to be 6 ppm. Kennedy (as quoted by Krauskopf, 1956) estimated the solubility to be possibly less than 6 ppm, and White (as quoted by Krauskopf, 1959) reported an experimental value of 7 ppm or a little higher. Although none of these figures may be entirely reliable they agree in establishing the solubility of quartz at a figure near that of the actual concentration in modern sea waters.

Although quartz does not crystallize from saturated solutions in the laboratory, failure to do so may be due simply to lack of sufficient time (Krauskopf, 1956, p. 5; Siever, 1957, p. 827); and, in the formation of sediments, lack of time on a human scale is hardly a restraining factor. Inorganic precipitation of quartz from sea water of near-normal silica content should therefore be considered as a significant source of silica in sediments.

Biochemical precipitation of opal

The solubility concentration of opal in sea water at low temperatures is several tens of parts per million (Krauskopf, 1956, 1959). Therefore, the concentration of silica in sea water is normally far below the saturation point for opal, and inorganic precipitation of opal is impossible.

Radiolaria extract silica from undersaturated, near-surface waters for building their opaline skeletons. After death of the organism the skeletons sink to the bottom and may eventually crystallize to form chert or cherty rock. The results and proof of this process are so obvious in both modern and ancient sediments that validity of this process needs little supporting argument. The danger is that the process will be overemphasized. Precambrian bedded cherts are generally free from obvious radiolarian remains and are unlikely to have formed by organic precipitation. Investigation of Holocene oceanic bottom sediments (Riedel, 1959, p. 85) indicates that biogenic precipitation commonly accounts for only a small part of the silica in Holocene radiolarian oozes and other siliceous sediments. Many samples examined in the present investigation of Ordovician rocks are devoid of any recognizable biogenic silica. In other samples, biogenic silica forms a small part of the rock and is clearly distinguishable from other silica of problematic origin. If the problematic silica is organic it must be composed of radiolarian skeletons that have been thoroughly masticated by some unknown agent that did not disturb the thinly laminated sediments.

Adsorption on settling solids

Bien, Contois, and Thomas (1959) cited evidence that soluble silica in Mississippi River water is removed from solution by adsorption on suspended solids during mixing with sea water. The ratio of adsorbed silica to detrital solids is unknown, so it is impossible to determine what sort of sediment could be formed. Presumably it would be siliceous shale or argillite rather than pure chert in which the quantity of identifiable clastic material is very low. Adsorption, and presumably deposition of at least the larger particles, occurs near mouths of rivers and accounts more easily for silica in deltaic sediments than it does for extensive geosynclinal deposits. To form bedded chert the detrital particles on which silica is adsorbed would have to be composed almost entirely of quartz.

Coagulation of colloids

Most colloidal silica in streams probably disperses and becomes a true solution before entering the sea (Krauskopf, 1956, p. 20). Any remaining colloidal silica is likely to be precipitated near the mouths of streams owing to the electrolytic property of sea water. Normally these deposits should be local, associated with near-shore sedimentary features, and flooded by detrital sediment. They should also be small owing to the scarcity of colloidal silica in streams. The process seems wholly inadequate to account for the silica in widespread geosynclinal deposits, especially deposits of bedded chert.

Mechanical concentration of siliceous detritus

Some of the larger silt-sized quartz grains in the Ordovician chert, argillite, and shale are believed to be detrital because, in contrast to the finer grained matrix of interpenetrating grains in which they lie, they are distinctly angular and are commonly well sorted and concentrated in certain beds. On the average, these grains constitute 5–10 percent of the Ordovician cherty rocks. It seems reasonable that at least an equal percentage is composed of detritus that is too fine grained to be identified as such. Conceivably all the nonbiogenic quartz is detrital. If so, either the provenance terrane was abnormally rich in finely divided quartz or some unknown process selectively winnowed out argillaceous material and moved it to an unknown place of deposition.

HYPOTHESIS

The enormous volume of dissolved silica that can be and is now being carried by streams to the sea is entirely adequate to account for large siliceous deposits. Exceptional or local sources of dissolved silica are no more necessary to account for siliceous deposits than are exceptional or local sources of lime necessary to account for limestone.

The large volume of dissolved silica entering the sea compels constant precipitation of silica. This can be accomplished by organic precipitation of opal and by inorganic precipitation of quartz. In Precambrian time, precipitation had to be by inorganic means because siliceous skeletons had not yet been developed, but in Paleozoic time inorganic and organic precipitation assumed coordinate roles.

Opaline tests are constructed by Radiolaria from silica supplied by streams to surface waters. As the Radiolaria die, their tests tend to redissolve both during descent and while lying exposed on the bottom. Where circulation near the bottom is slow, the silica content of bottom waters is built up by this process to the saturation point with respect to quartz (10 ppm or less). Quartz then begins to precipitate. It may form as crystals in bottom waters or may replace undissolved opaline skeletal materials on the bottom. In any event, inorganic precipitation continues as long as the Radiolaria keep supplying dissolved silica to bottom waters. The essential basis of this process is the wide divergence between the solubilities of opal and quartz (Krauskopf, 1956, 1959), which permits simultaneous solution of opal and precipitation of quartz.

The kind of sediment formed depends mainly on the rates of Radiolaria production and of detrital sedimentation. The rate of Radiolaria production directly governs the rate of inorganic precipitation of quartz. When the rate of detrital accumulation is high the proportion of undissolved opaline skeletons and precipitated quartz is relatively low and the resulting sediment tends to have the composition of normal shale and pelagic sediment. When the detrital rate is very low the resulting sediment tends to approach the composition of bedded chert. Intermediate rates tend to yield rocks of intermediate composition. The prevalence of siliceous rocks in the Ordovician eugeosyncline reflects two conditions—abundant dissolved silica and sparse detritus. These conditions point to unusual tectonic stability and subdued relief of borderlands.

REFERENCES

Albers, J. P., and Stewart, J. H., 1965, Preliminary geologic map of Esmeralda County, Nevada: U.S. Geol. Survey Mineral Inv. Field Studies Map MF-298.

Bien, G. S., Contois, D. E., and Thomas, W. H., 1959, The removal of soluble silica from fresh water entering the sea, *in* Ireland, H. A., ed., Silica in sediments—a symposium: Soc. Econ. Paleontologists and Mineralogists Spec. Pub. 7, p. 20–35.

Churkin, Michael, Jr., and Kay, Marshall, 1967, Graptolite-bearing Ordovician siliceous and volcanic rocks, northern Independence Range, Nevada: Geol. Soc. America Bull., v. 78, no. 5, p. 651–668.

Clarke, F. W., 1924, The data of geochemistry, 5th ed.: U.S. Geol. Survey Bull. 770, 841 p.

Daly, R. A., 1933, Igneous rocks and the depths of the earth: New York, McGraw-Hill Book Co., Inc., 508 p.

Dzulyński, Stanislaw, and Walton, E. K., 1965, Sedimentary features of flysch and greywackes: New York, Elsevier Publishing Co., 274 p.

Edgington, Glen, and Byers, H. G., 1942, Selenium content and chemical analyses, *in* W. H. Bradley and others, Geology and biology of North Atlantic deep-sea cores between Newfoundland and Ireland: U.S. Geol. Survey Prof. Paper 196, p. 151–155.

El Wakeel, S. K., and Riley, J. P., 1961, Chemical and mineralogical studies of deep-sea sediments: Geochim. et Cosmochim. Acta, v. 25, no. 2, p. 110–146.

Ferguson, H. G., 1924, Geology and ore deposits of the Manhattan district, Nevada: U.S. Geol. Survey Bull. 723, 163 p.

Gardner, L. U., 1938, Reaction of the living body to different types of mineral dusts: Am. Inst. Mining Metall. Eng. Tech. Pub., no. 929.

Gilluly, James, and Gates, Olcott, 1965, Tectonic and igneous geology of the northern Shoshone Range, Nevada, *with sections on* Gravity in Crescent Valley, by Donald Plouff, *and* Economic geology, by K. B. Ketner: U.S. Geol. Survey Prof. Paper 465, 153 p.

Gilluly, James, and Masursky, Harold, 1965, Geology of the Cortez quadrangle, Nevada, *with a section on* Gravity and aeromagnetic surveys, by D. R. Mabey: U.S. Geol. Survey Bull. 1175, 117 p.

Goldberg, E. D., 1965, Minor elements in sea water, chap. 5 *in* Riley, J. P., and Skirrow, G., eds., Chemical oceanography: New York, Academic Press, v. 1, p. 163–196.

Goldberg, E. D., and Arrhenius, G. O. S., 1958, Chemistry of Pacific pelagic sediments: Geochim. et Cosmochim. Acta, v. 13, nos. 2–3, p. 153–212.

Kay, Marshall, 1960, Paleozoic continental margin in central Nevada, western United States: Internat. Geol. Cong., 21st, Copenhagen 1960, Rept., pt. 12, p. 94–103.

———1962, Classification of Ordovician Chazyan shelly and graptolite sequences from central Nevada: Geol. Soc. America Bull., v. 73, no. 11, p. 1421–1430.

Kay, Marshall, and Crawford, J. P., 1964, Paleozoic facies from the miogeosynclinal to the eugeosynclinal belt in thrust slices, central Nevada: Geol. Soc. America Bull., v. 75 no. 5, p. 425–454.

Kennedy, G. C., 1950, A portion of the system silica-water: Econ. Geology, v. 45, no. 7, p. 629–653.

Krauskopf, K. B., 1956, Dissolution and precipitation of silica at low temperatures: Geochim. et Cosmochim. Acta, v. 10, nos. 1–2, p. 1–26.

———1959, The geochemistry of silica in sedimentary environments, *in* Ireland, H. A. ed., Silica in sediments—a symposium: Soc. Econ. Paleontologists and Mineralogists Spec. Pub. 7, p. 4–19.

Livingstone, D. A., 1963, Chemical composition of rivers and lakes, *in* Fleischer, Michael, ed., Data of geochemistry, 6th ed.: U.S. Geol. Survey Prof. Paper 440–G, p. G1–G64.

Lovejoy, D. W., 1959, Overthrust Ordovician and the Nannie's Peak intrusive, Lone Mountain, Elko County, Nevada: Geol. Soc. America Bull., v. 70, no. 5, p. 539–563.

Merriam, C. W., and Anderson, C. A., 1942, Reconnaissance survey of the Roberts Mountains, Nevada: Geol. Soc. America Bull., v. 53, no. 12, pt. 1, p. 1675–1727.

Nanz, R. H., Jr., 1953, Chemical composition of pre-Cambrian slates with notes on the geochemical evolution of lutites: Jour. Geology, v. 61, no. 1, p. 51–64.

Rankama, K. K., and Sahama, T. G., 1950, Geochemistry: Chicago, Ill., Chicago Univ. Press, 912 p.

Revelle, R. R., 1944, Marine bottom samples collected in the Pacific Ocean by the *Carnegie* on its seventh cruise, pt. 1, *of* Oceanography-II: Carnegie Inst. Washington Pub. 556, p. 1–180.

Riedel, W. R., 1959, Siliceous organic remains in pelagic sediments, *in* Ireland, H. A., ed., Silica in sediments—a symposium: Soc. Econ. Paleontologists and Mineralogists Spec. Pub. 7, p. 80–91.

Roberts, R. J., 1964, Stratigraphy and structure of the Antler Peak quadrangle, Humboldt and Lander Counties, Nevada: U.S. Geol. Survey Prof. Paper 459–A, p. A1–A93 [1965].

Shaw, D. M., 1956, Major elements and general geochemistry, pt. 3 *of* Geochemistry of peletic rocks: Geol. Soc. America Bull., v. 67, p. 919–934.

Siever, Raymond, 1957, The silica budget in the sedimentary cycle: Am. Mineralogist, v. 42, nos. 11–12, p. 821–841.

Stearns, N. D., Stearns, H. T., and Waring, G. A., 1937, Thermal springs of the United States: U.S. Geol. Survey Water-Supply Paper 679–B, p. 59–206.

Sverdrup, H. U., Johnson, M. W., and Fleming, R. H., 1942, The oceans, their physics, chemistry, and general biology: New York, Prentice-Hall, Inc., 1087 p.

Tourtelot, H. A., 1962, Preliminary investigation of the geologic setting and chemical composition of the Pierre shale, Great Plains region: U.S. Geol. Survey Prof. Paper 390, 74 p.

Twenhofel, W. H., 1932, Treatise on sedimentation; Baltimore, Md., Williams & Wilkins Co., 926 p.

Umpleby, J. B., Westgate, L. G., and Ross, C. P., 1930, Geology and ore deposits of the Wood River region, Idaho: U.S. Geol. Survey Bull. 814, 250 p.

White, D. E., 1957, Thermal waters of volcanic origin: Geol. Soc. America Bull., v. 68, no. 12, pt. 1, p. 1637–1657.

White, D. E., Brannock, W. W., and Murata, K. J., 1956, Silica in hot-spring waters: Geochim. et Cosmochim. Acta, v. 10, nos. 1–2, p. 27–59.

NOTES ON THE GEOLOGY AND PALEOHYDROLOGY OF THE BOULDER CITY PLUTON, SOUTHERN NEVADA

By R. ERNEST ANDERSON, Denver, Colo.

Work done in cooperation with the U.S. Atomic Energy Commission

Abstract.—The Boulder City pluton, a composite granitoid Tertiary intrusive mass exposed for more than 10 square miles in the extreme northern Eldorado Mountains, Nevada-Arizona, is bounded mostly by faults. It locally intrudes Patsy Mine Volcanics, and is capped by Mount Davis Volcanics. On the basis of stratigraphic and isotopic data, the pluton has an age ranging from Eocene(?) to Miocene(?). The pluton and adjacent rocks are crossed at an altitude of about 2,400 feet by a horizontal red-brown cliff-forming zone that was probably colored by deposition of ferric oxide from ground-water solutions as an ancient water table fluctuated over an interval of about 100 feet. Subsequent downcutting by the Colorado River has exposed the pluton to a depth of about 1,800 feet below this zone, and thus reveals that the pluton is probably not a laccolith or sill-like mass as has been previously suggested.

During his reconnaissance geologic investigations of the area extending 50 miles southward from Lake Mead to Davis Dam, Arizona-Nevada, Longwell (1963) recognized a Tertiary intrusive mass, the Boulder City pluton, east of Boulder City, Clark County, Nev. Longwell (1963, p. E17) concluded that the mass was an unroofed sill or laccolith whose base was generally conformable on lavas of the Golden Door Volcanics of Eocene(?) to Miocene(?) age. As mapped by Longwell, much of the exposed pluton stands above its surroundings as a capping of a sinuous ridge that extends from Boulder City eastward for about 3 miles. The rocks beneath the mass are conspicuously iron stained and have a layered appearance. Evidence is presented in this report suggesting that the pluton is at least three times larger than shown by Longwell (1963, pl. 1) and that the iron-stained zone interpreted by him as a lava floor is a paleohydrologic feature that has resulted from deposition of ferric oxide from ground-water solutions. The iron-stained zone lies mostly within the pluton but is seen in other rocks also.

The exposed part of the Boulder City pluton covers about 10 square miles in the extreme northern Eldorado Mountains, Nev. (fig. 1). A small part extends into Mohave County, Ariz. Scattered exposures of plutonic rocks that are similar to those of the main mass occur for 8 miles west of the area of figure 1 in the southern River Mountains and northern McCullough Range. The Boulder City pluton may be at least twice as large as indicated on figure 1 if the scattered exposures to the west are parts of a broad pluton that is connected in the shallow subsurface with the main mass.

The eastern part of the pluton is well exposed along the Black Canyon of the Colorado River and its tributary canyons which dissect it to a depth of more than 2,000 feet to form a rugged topography. The topography is much more subdued westward where, although well exposed locally, the pluton tends to be onlapped and partly concealed by younger rocks, alluvium, and windblown sand.

GEOLOGY OF THE PLUTON

The Boulder City pluton is a nonfoliated composite mass ranging in composition from quartz monzonite to granite. Most of the mass consists of gray fine- to medium-grained biotite-hornblende-bearing granitoid rock, much of which is faintly porphyritic. Coarse-grained granitoid phases are sparse. The faintly porphyritic texture is produced mostly by plagioclase with overgrowths or mantles of potassium feldspar. Numerous dark clots and inclusions that occur in the granite also have a porphyritic texture that has resulted from randomly oriented long phenocrysts of

U.S. GEOL. SURVEY PROF. PAPER 650-B, PAGES B35-B40

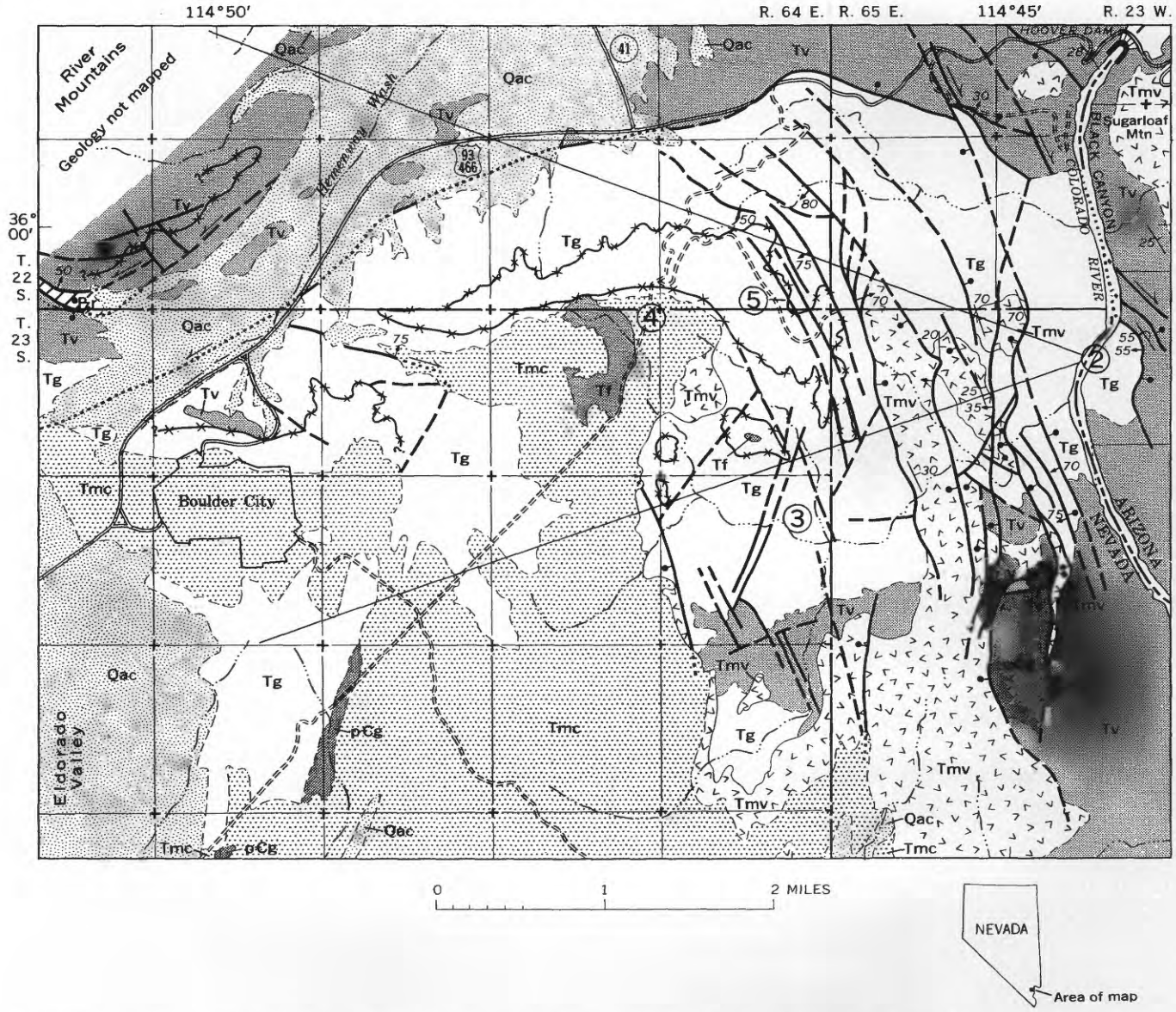

FIGURE 1.—Preliminary geologic map of the Boulder City pluton. Circled numbers show locations of photographs in figures 2, 3, 4, and 5; field of view of figure 2 is indicated by radiating lines. Base from U.S. Geological Survey quadrangle maps: Boulder City, 1958; Black Canyon, 1959; Henderson, 1952; Hoover Dam, 1953.

hornblende. In both textural types the groundmass commonly has a pseudo-ophitic texture produced by euhedral plagioclase grains encased or partly encased in anhedral quartz and alkali feldspar. This texture is seen as a modification of the more normal granitoid texture. The granitoid interior of the pluton commonly grades to porphyritic aphanites at the margins.

The pluton intrudes rocks believed equivalent to the Patsy Mine Volcanics, the oldest of several widespread sequences of volcanic strata mapped and described by Longwell (1963). Basalt, rhyodacite, tuffaceous sedimentary rocks, and coarse clastic rocks of the Mount Davis Volcanics (Longwell, 1963) are deposited on what appears to be a rather featureless erosion surface developed on the pluton (fig. 2). The absolute age of the Patsy Mine Volcanics is not known, but it is believed to be more than 26 million years on the basis of a K–Ar age obtained on granite that intrudes it (Armstrong, 1964). A K–Ar age of 15 m.y. was obtained on a probable feeder dike for Mount Davis lavas (Armstrong, 1964). A K–Ar age of 17 m.y. was obtained on the Boulder City pluton (Longwell, 1963). These data suggest a Miocene age for the pluton.

Only a few of the many faults that cut the pluton are shown on figure 1. Faults are less abundant in the western part than in the eastern part where, locally,

EXPLANATION

Qac

Alluvium and colluvium

Tmc Tf

Muddy Creek Formation

Tmc, *sedimentary rocks (Longwell, 1963)*
Tf, *Fortification Basalt Member*

Tmv

Mount Davis Volcanics

Includes lavas ranging from rhyodacite to basalt and interstratified coarse clastic and tuffaceous sedimentary rocks

Tg

Granite and quartz monzonite

Tv

Lava, flow breccia, and tuff

Includes rocks equivalent to Patsy Mine and Golden Door Volcanics

Pz

Sedimentary rocks

Mostly limestone

Gneiss, schist, and pegmatite

Contact

Dashed where approximately located

75

Fault, showing direction and amount of dip

Dashed where approximately located; dotted where concealed. Bar and ball on downthrown side; arrow indicates direction of lateral component

Trace of intersection between ground surface and uppermost level of ancient water table

25

Strike and dip of bedding or flow layering

FIGURE 1.

QUATERNARY

TERTIARY

PALEOZOIC

PRECAMBRIAN

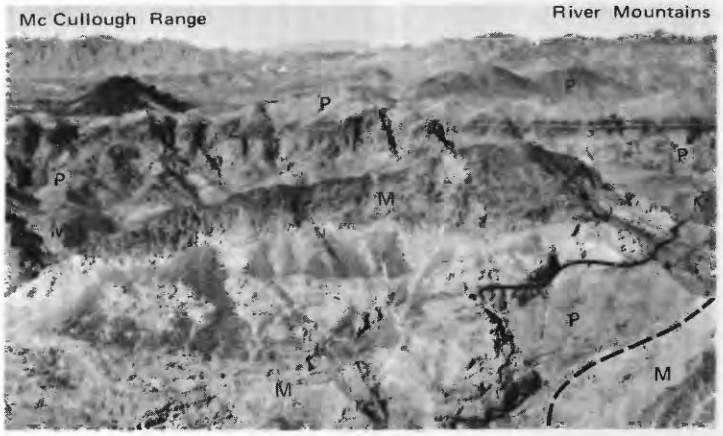

FIGURE 2.—Low-angle aerial view of banded cliff-forming paleohydrologic zone (Z) in Boulder City pluton (P). Light-colored bedded rocks and overlying dark lavas in foreground are Mount Davis Volcanics (M) deposited on the eroded pluton; other Mount Davis rocks are downfaulted in middle distance (faults are concealed). Dark cone at left consists of a basalt lava cap on granite. Small white objects slightly to right and beyond the cone are water-storage tanks in Boulder City. Field of view and camera position are indicated by lines radiating from ② on figure 1. Photograph by William Belknap, Boulder City.

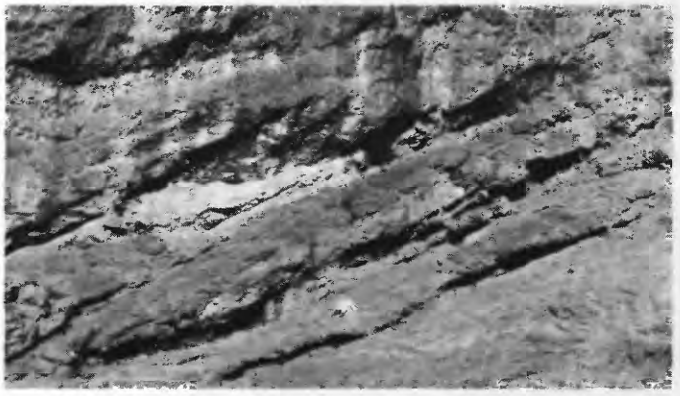

FIGURE 3.—View northward of brecciated and pseudostratified granite along low-angle west-dipping fault exposed in canyon bottom marked by ③ in figure 1. At least three similar fault zones occur at higher levels on the adjacent canyon walls; none are shown on figure 1. The fault zones are generally stained reddish brown by ferric oxide, and where they are nearly horizontal they can be easily mistaken for the iron-stained zone that is the main subject of this report. Scale is indicated by hammer in bottom center.

the fault density in plan is as high as 20 per square mile. The faults have diverse attitudes and many dip gently. They are commonly marked by broad zones of brecciated rock (fig. 3) and, where closely spaced, the entire rock mass is brecciated. Blocks of Mount Davis Volcanics are dropped deep into the pluton along faults that trend north and northwest (fig. 1).

Many dikes, ranging from andesite porphyry to sugary-textured microgranite, cut the pluton. These are emplaced along fractures that range from horizontal to vertical; along these fractures postintrusion movement is commonly indicated by brecciated dike rock.

Intrusive contacts

Unambiguous intrusive contacts between the pluton and older rocks are rare. South-southwest of Boulder

City fine-grained porphyritic border facies of the pluton intrude gneiss, schist, and pegmatite of Precambrian age along a north-northeast-trending contact that appears to dip steeply. The pluton grades to a medium-grained equigranular to faintly porphyritic granitoid rock within a few hundred feet of this contact. The areal extent of the Precambrian rock is unknown owing to onlap of younger rocks from the east. The Precambrian rock may be an elongate roof pendant.

In the southern part of the mapped area the pluton is shown intruding a band of volcanic rocks (lava, flow breccia, and tuff, fig. 1), which divide the mass into two parts at the present level of exposure. The volcanic rocks are mostly propylitically altered greenish-gray to purplish-gray andesite and basaltic andesite lavas and flow breccias. Locally, near intrusive contacts, they are argillized and (or) silicified and bleached to light gray, pale yellow, or pink. Where the effects of alteration are moderate to slight, and in the very few localities where the rocks are unaltered, they closely resemble Patsy Mine Volcanics. The pluton appears to grade to fine-grained border facies near contacts with volcanic rocks, but in many places the contacts are obscured by the presence of younger dikes (not shown on fig. 1) which have field characteristics common to both the volcanic rocks and the border facies. In many places contacts are further complicated by numerous faults and by the effects of alteration. Notwithstanding these complications, intrusive contacts dip gently northward at several localities along the northern and southern margins of the band of volcanic rocks; this dip suggests that the volcanic rocks form a north-dipping layer within the pluton. In Black Canyon, contacts dip northerly at the higher elevations and southerly near the water level; these dips suggest that the volcanic rocks there form a wedge that extends northward into the pluton. No evidence that the pluton is floored by the volcanic rocks was found.

Fault contacts

In the hills west of Hoover Dam the northern contact of the Boulder City pluton is marked by a fault zone 40 feet to several hundred feet wide; along this fault zone the pluton and adjacent gently dipping volcanic rocks are intensely brecciated and locally highly altered. Shear planes within the zone have diverse trends, but most of them parallel the generalized fault trace shown on figure 1 and have steep to moderate northerly dips; locally some have steep southerly dips. To the west the fault zone is mostly buried by alluvium and colluvium. The fault trace shown there (fig. 1) marks the approximate boundary between brecciated plutonic rock on the south and brecciated volcanic rock on the north, as determined from scattered exposures in Hemenway Wash and at the margin of the adjacent bedrock. Locally the plutonic rock is so highly comminuted that it resembles the volcanic rock. Slickensides and corrugations on several steep fault surfaces plunge at low angles; this low-angle plunge indicates a lateral component at least in the late stage of movement along the fault zone. The relative ages of the pluton and volcanic rocks are not known.

To the east where the fault trace leaves U.S. Highway 93 and plunges into Black Canyon, the contact relationships are complicated by several northwest-trending tear and reverse faults and by aphanitic dikes that parallel or strike into the generalized trend of the contact (not shown on fig. 1). Near the river level the contact is largely buried by waste and talus from dam excavations. The pluton there may be intrusive into rocks resembling Patsy Mine Volcanics. Higher on the west canyon wall, however, the contact is a fault. Much of the volcanic rock faulted against the pluton in that area is rhyolitic ash-flow tuff similar to tuff in the Golden Door Volcanics (Longwell, 1963). The faulted contacts preclude determination of the age relationships between the pluton and the Golden Door Volcanics. The contact relationships that led Longwell in his reconnaissance study (1963, p. E17) to conclude that the Golden Door rocks are older do not appear to be valid (see discussion of paleohydrology).

The eastern contact in Arizona is a north-northwest-trending moderately west dipping reverse fault against which the downfaulted volcanic strata have been dragged and locally overturned. Presumably the northward extension of this fault lies buried in the Colorado River channel. Other more steeply dipping reverse faults of similar strike displace volcanic rocks against the pluton farther south on the Nevada side of the river.

PALEOHYDROLOGY

A very conspicuous and persistent nearly horizontal reddish-brown zone cuts across the medium- to light-gray Boulder City pluton at an altitude of about 2,400 feet. The zone varies in thickness from 20 to 150 feet. In the southernmost exposures (fig. 1) it appears to have a gentle southwesterly dip toward Eldorado Valley, and in the northern part it appears to dip gently northward toward Lake Mead. Rocks within it are generally more resistant to erosion than are those above or below and thus the zone tends to form a con-

FIGURE 4.—Concordant level of iron-stained zone in pluton (P) and adjacent coarse clastic rocks (C); clastic rocks are composed of detritus shed from and deposited against the pluton; view is to east from point marked ④ on figure 1.

spicuous steep-faced cliff (fig. 2). The red-brown is virtually absent above the zone, and therefore the upper contact is sharp. The lower contact is less sharp because red-browns of lower intensity persist below it. It is especially vague in areas of widespread brecciation, such as the north-central part of the pluton.

A less distinct horizontal cliff-forming zone is visible at an altitude of about 2,600 feet in the River Mountains north of Boulder City where it has a gentle northeasterly component of dip toward Lake Mead. There is scarcely any color contrast associated with the zone in the River Mountains because it cuts across dark-gray to black andesite lavas.

Three miles east-northeast of Boulder City the resistant red-brown zone extends from the pluton westward into adjacent coarse clastic rocks deposited against the pluton (fig. 4). Because the top of the iron-stained zone (the horizon shown on fig. 1) is topographically higher than the contact between the sedimentary rock and granite, these two lines do not intersect on figure 1.

In the pluton and adjacent rocks the reddish-brown color results from secondary ferric oxide that fills fractures and coats fractured rock surfaces. Locally it penetrates the unfractured rock and coats the constituent grains, causing little or no alteration of the grains. In rock that is highly brecciated by faults the ferric oxide acts as a cementing agent. Alternating resistant and nonresistant layers, which in some places are accentuated by superposed alternations in the intensity of red-brown coloration, are produced in the brecciated rocks by variations in the degree of cementation. From a distance this layering looks much like crude bedding in a coarse clastic rock. At several localities where the layering cuts across discrete brecciated fault zones, it almost masks the fault trend (fig. 5). Nonbrecciated rocks lack layering but locally exhibit a faint color banding. In areas of little or no brecciation the granitic rock can be traced uninterrupted from the medium-gray cap through the red-brown zone into the gray granite below. The granites above and below the zone are petrographically indistinguishable and are interpreted as parts of the same mass.

The fact that the resistant red-brown zone projects through the area at a nearly consistent altitude without regard for rock type or structure suggests that it was formed by deposition of iron oxide from groundwater solutions. It slopes gently toward adjacent lowlands as would be normal for a water table. It records an interval of water-table fluctuation that existed subsequent to deposition of clastic beds and basalt lava of the Muddy Creek Formation (Longwell, 1963) and prior to the establishment of the present course of the Colorado River. The Fortification Basalt Member of the Muddy Creek Formation has been dated at 10 m.y. by the K–Ar method (Damon, 1965). Dates on basalts that flowed into the canyon of the Colorado River (Damon, 1965) indicate that the present river course is at least 2.6 m.y. old

CONCLUSIONS

The Boulder City pluton is exposed over about 10 square miles and probably extends over an equal or greater area in the subsurface. The fact that in Black Canyon it is eroded to a depth of more than 2,000 feet indicates that the pluton is probably not a laccolith or sill-like mass floored on Golden Door Volcanics as

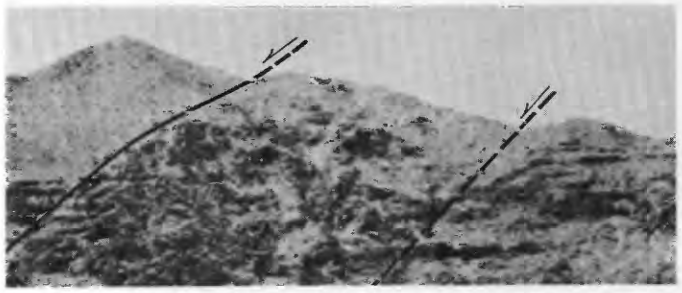

FIGURE 5.—Layered brecciated plutonic rock. Layering is best developed adjacent to faults; area between faults is darkened by iron staining, but because of its unbrecciated condition shows little or no layering; location marked by ⑤ on figure 1. Height of exposure is about 200 feet.

suggested by Longwell (1963). Although older volcanics locally dip gently beneath the pluton, there is no evidence suggesting it is floored by these volcanics. An abundance of faulted contacts and onlap by younger rocks precludes determination of the true size and shape of the pluton.

Most exposures consist of fine- to medium-grained granitoid rocks that range from quartz monzonite to granite. Border facies are porphyritic aphanites similar to the numerous dikes that cut the pluton. The pluton and adjacent rocks are highly faulted and brecciated, especially in the eastern part of the mapped area.

The pluton intrudes Patsy Mine Volcanics. It was uplifted and its cover removed by erosion prior to the extrusion on its surface of the Mount Davis Volcanics believed to be of Miocene(?) age.

The persistent horizontal red-brown-layered cliff-forming zone, interpreted by Longwell (1963) as the base of the pluton, is interpreted here as a paleohydrologic feature formed by the deposition of iron oxide minerals from ground water at or near the level of an ancient water table. It is somewhat similar to iron-stained bands produced in the McAfee Adamellite (Inyo batholith) along the frontal fault scarp of the White Mountains, Calif. (Emerson, 1966). According to Emerson (1966) the bands there were produced by weathering during repeated uplift on a recent fault.

The red-brown zone in southern Nevada cuts across the Boulder City pluton at an altitude of 2,400 feet, which is 1,800 feet above the lowest visible exposure of the pluton in the channel of the Colorado River. The zone extends from the pluton into adjacent coarse clastic rocks deposited on the pluton and also cuts across volcanic rocks in the southern River Mountains. Isotopic data indicate that the paleohydrologic feature formed some time between 2.6 and 10.6 m.y. ago.

REFERENCES

Armstrong, R. L., 1964, Geochronology and geology of the eastern Great Basin in Nevada and Utah: Yale Univ., Ph. D. thesis, 317 p.

Damon, P. E., 1965, Correlation and chronology of ore deposits and volcanic rocks—U.S. Atomic Energy Comm. Contract AT(11–1)–689, Ann. Prog. Rept. COO–689–50: Arizona Univ., Geochronology Labs., 60 p. plus app.

Emerson, D. O., 1966, Granitic rocks of the Mount Barcroft quadrangle, Inyo batholith, California-Nevada: Geol. Soc. America Bull., v. 77, no. 2, p. 127–152.

Longwell, C. R., 1963, Reconnaissance geology between Lake Mead and Davis Dam, Arizona-Nevada: U.S. Geol. Survey Prof. Paper 374–E, p. E1–E51.

ACCESSORY SPHENE FROM HYBRID ROCKS OF THE MOUNT WHEELER MINE AREA, NEVADA

By DONALD E. LEE,[1] ROBERT E. MAYS,[2] RICHARD E. VAN LOENEN,[1] and HARRY J. ROSE, JR.,[3] [1]Denver, Colo., [2]Menlo Park, Calif., [3]Washington, D.C.

Abstract.—Chemical data, unit-cell parameters, and optical properties are listed for 14 accessory sphenes recovered from hybrid granitoid rocks exposed north of the Mount Wheeler mine, White Pine County, Nev. The environment of these sphenes is well known from a careful field and laboratory study that included chemical, spectrographic, normative, and modal analyses for each of the rocks from which they were separated. These sphenes contain a rather large assemblage of rare-earth and other minor elements, and their physical properties and major- and minor-element contents do not show the same obvious response to whole-rock chemistry observed for their coexisting allanites and zircons. Four sphenes contain detectable amounts of Bi, and 13 sphenes contain Mo in the general range of 7–20 parts per million; the sphene structure appears to be a preferred site for the Bi and the Mo present in these rocks. All 14 sphenes contain a much less basic (and heavier) assemblage of rare earths than do the allanites that coexist with them.

Granitoid rocks crop out a few miles north of the Mount Wheeler mine in the southern part of the Snake Range, about 50 miles southeast of Ely, Nev. These rocks are exposed in intrusive contact with Prospect Mountain Quartzite, Pioche Shale, and Pole Canyon Limestone, all of Cambrian age (Drewes, 1958). They range in composition from grandiorite with a CaO content of more than 4.5 percent to quartz monzonite with a CaO content of about 0.5 percent, and a detailed field and laboratory study (Lee, unpub. data) has shown that this range in composition is related to magmatic assimilation of the chemically diverse host rocks. The change from high to low CaO values is rather systematic over a horizontal distance of about 3 miles, and other major elements (and most minor elements) tend to vary either directly or inversely with CaO. Amounts of quartz, microcline, plagioclase, and biotite respond to the major-element chemistry of these hybrid rocks. With a few notable exceptions the well-defined chemical and mineralogical gradients exposed are much what one would expect to find in a series of differentiates. The relation between the chemistry and accessory-mineral contents of these rocks was described by Lee and Dodge (1964), who found a sympathetic increase of sphene with CaO.

This paper presents minor-element analyses and optical data for 14 accessory sphenes recovered from these hybrid rocks. We also list major-element data for 13 of these sphenes and unit-cell parameters for 8. The location, major- and minor-element analyses, norms, and modes for the granitoid rocks from which these constituent sphenes were recovered will be presented in a later paper. The chemistry and physical properties of some of the accessory minerals coexisting with these sphenes have been discussed by Lee and Bastron (1967) and Lee, Stern, Mays, and Van Loenen (1968).

SPHENE ANALYSES AND PHYSICAL PROPERTIES

After the preliminary work described by Lee and Dodge (1964), the sphene concentrates were ground to −150 mesh (about 100 microns) and washed in tapwater to remove material smaller than about 40 microns. Purification was achieved by centrifuging repeatedly in methylene iodine and by use of the Frantz isodynamic separator. As the final step in the cleaning, each sphene fraction was subjected to ultrasonic vibration in distilled water for about an hour. With the exception of sample 190–MW–61, each sphene analyzed was at least 99 percent pure. During optical study of the analyzed fractions no discrete grains of impurity were found, but when each fraction was observed in oil with an index refraction equal to the α index of the sphene, tiny euhedral inclusions were found in some of the grains. From their optical properties these inclusions appear to be zircon and apatite, minerals that tend to be closely associated with sphene in these rocks.

U.S. GEOL. SURVEY PROF. PAPER 650-B, PAGES B41–B46

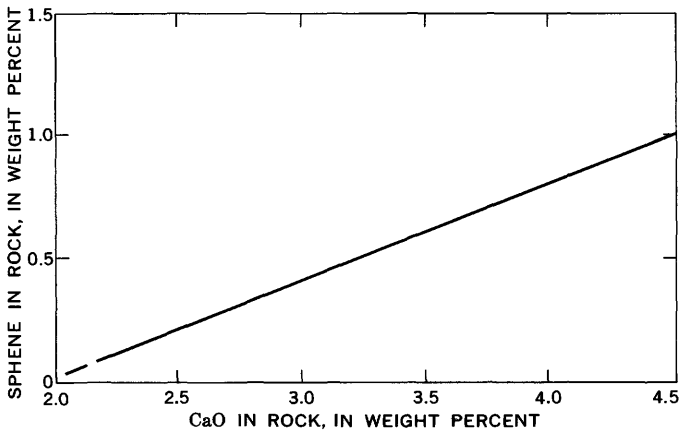

FIGURE 1.—Relation between contents of CaO and accessory sphene in hybrid granitoid rocks of the Mount Wheeler mine area, Nevada.

As background for the following discussion, the general relation between weight percentages of sphene and CaO in these hybrid rocks is shown in figure 1. However, although almost all rocks having less than 2.2 percent CaO are practically devoid of sphene and the most mafic rocks generally contain the most sphene, we emphasize that the relation shown in figure 1 is idealized and is not nearly as systematic and well defined as the covariance between amounts of CaO and other accessory minerals such as apatite, allanite, and zircon (Lee and Dodge, 1964).

Optical properties and unit-cell parameters

The sphenes analyzed are listed (table 1) according to CaO content of the rocks from which they were recovered. The α refractive indices are all in the rather narrow range of 1.895–1.910. Optic axial angles were not systematically determined, but from inspection during mineral purification work all appear to be 25–35(+), and all grains checked show the typically strong sphene dispersion, with r>v. Unit-cell parameters (table 1) were calculated for eight of the analyzed sphenes by least-squares refinement of powder diffractometer data, using an internal standard of CaF_2 and a self-indexing computer program developed by Evans, Appleman, and Handwerker (1963). All the results are in rather good agreement with the data for sphenes listed by Deer, Howie, and Zussman (1962, p. 69).

Major elements

Thirteen of the sphenes were analyzed for SiO_2, Al_2O_3, TiO_2, total iron(as Fe_2O_3), and CaO by means of X-ray fluorescence (table 1). In general the major-element chemistry is rather similar from one sample to another. The TiO_2 contents of these sphenes tend to increase as these hybrid rocks become more mafic (fig. 2), but variations in amounts of other oxides appear to be random and unrelated to chemical differences among whole rocks.

Sphene 27–DL–61, highest in TiO_2 and CaO and lowest in SiO_2, also is the only one in table 1 recovered from a large xenolithic mass, where assimilation is relatively incomplete. Related investigations in the area show that hornblende is dominant over biotite in such xenolithic masses where assimilation is only incipient. The high TiO_2 content of sphene 27–DL–61 probably results at least in part from the dearth of coexisting biotite, for where biotite is well developed it is the main reservoir of the TiO_2 present in the area's hybrid rocks, much as has been described for granitoid rocks elsewhere by Znamensky (1957). If we assume that sphene in the more mafic parts of the main intrusive phase originally formed in equilibrium with larger amounts of hornblende (since replaced by biotite), the same reasoning outlined for sphene 27–DL–61 might also help to explain the TiO_2 trend shown in figure 2. The tendency for hornblende in hybrid rock to be replaced by biotite as assimilation proceeds has been recognized by many previous writers.

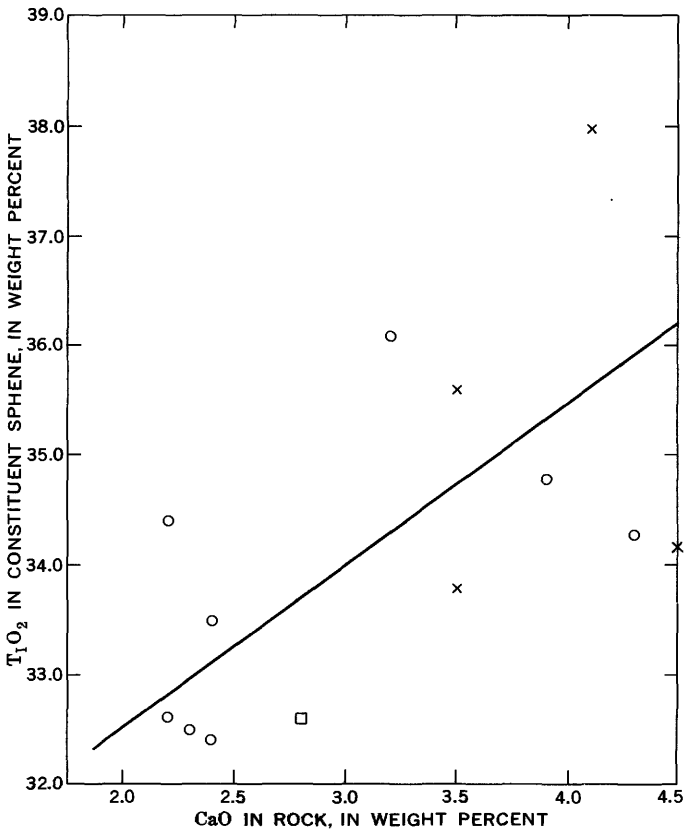

FIGURE 2.—Relation between CaO content of rock and TiO_2 content of constituent sphene. ○, sample from main intrusive phase; ×, xenolith; □, lamprophyre.

TABLE 1.—*Analytical data and physical properties for accessory sphenes from the Mount Wheeler mine area, Nevada*

[Samples arranged in order of increasing CaO content. CaO analyses by Paul Elmore, Samuel Botts, H. Smith, and Gillison Chloe. Indices of refraction: α determined in sodium light by the immersion method, β and γ not determined. Cell parameters were obtained by least-squares refinement of powder diffractometer data by R. E. Van Loenen, using a self-indexing computer program developed by Evans, Appleman, and Handwerker (1963). The internal standard was CaF_2. Margin of error for a, b, and c was ±0.004 A. Semiquantitative spectrographic analyses by R. E. Mays. Results are based on their identity with geometric brackets whose boundaries are 1.2, 0.83, 0.56, 0.38, 0.26, 0.18, 0.12, and so forth, and are reported arbitrarily as midpoints of these brackets, 1., 0.7, 0.5, 0.3, 0.2, 0.15, 0.1, respectively. The precision of a reported value is approximately plus or minus one bracket at 68-percent, or two brackets at 95-percent confidence]

Sample No.	190-MW-61	14-MW-60	36-DL-61	8-DL-61	40A-MW-60	31-DL-61	150-MW-60 [1]	152-MW-61	40B-MW-60 [2]	126-MW-61 [2]	43-DL-61	27-DL-61 [2]	16-MW-60	98-DL-62 [2]
CaO in rock (weight percent).	1.2	2.2	2.2	2.3	2.4	2.4	2.8	3.2	3.5	3.5	3.9	4.1	4.3	4.5
α Index of refraction														
α (±0.005)	1.900	1.902	1.900	1.902	1.900	1.895	1.900	1.905	1.908	1.900	1.903	1.910	1.902	1.898
Cell parameters														
a		6.544	6.549	6.546	6.543	6.546	6.551	Not determined			6.543	Not determined		6.539
b		8.696	8.701	8.698	8.703	8.700	8.699				8.674			8.703
c		7.435	7.439	7.437	7.436	7.437	7.435				7.435			7.433
Volume (±0.2A³)	367.0	367.6	367.2	367.1	367.3	367.9					366.2			366.9
β (±2′)		119°50′	119°52′	119°52′	119°54′	119°52′	119°44′				119°49′			119°51′
Major element oxides (determined by X-ray fluorescence)														
SiO_2		35.6	31.9	31.0	34.0	30.8	32.9	31.5	35.3	33.9	34.6	27.0	30.1	31.1
Al_2O_3		3.70	3.60	3.60	3.75	3.60	3.40	3.06	3.20	2.90	3.00	3.30	3.65	3.60
TiO_2		32.6	34.4	32.5	32.4	33.5	32.6	36.1	33.8	35.6	34.8	38.0	34.3	34.2
Fe_2O_3 [3]		1.90	1.65	1.80	1.85	2.25	1.90	1.65	1.70	1.85	1.60	2.25	1.75	2.20
CaO		26.2	26.1	25.2	26.6	27.5	27.0	27.6	26.0	27.1	25.6	30.2	26.4	26.6
Semiquantitative spectrographic analyses (weight percent) [4]														
Mg	0.15	0.02	0.01	0.03	0.02	0.03	0.03	0.05	0.007	0.015	0.03	0.03	0.15	0.05
Na	.03	----	----	.03	----	----	----	----	----	.1	.02	----	.1	----
P	.15	----	----	.15	----	----	----	----	----	----	----	----	----	----
Mn	.07	.07	.07	.07	.07	.07	.05	.05	.07	.07	.07	.07	.05	.07
Ba	.007	.001	----	.002	.002	.005	.03	.005	.0005	.0007	.03	.07	.01	.001
Be	----	----	----	----	.0003	----	----	----	----	.0003	----	----	----	----
Bi	.01	.002	----	----	----	----	.002	.002	----	----	----	----	----	----
Cr	.002	.005	.005	.005	.005	.005	.003	.007	.0007	.003	.01	.02	.007	.0015
Cu	.0015	----	.002	.0005	.0007	.0007	.001	.0015	----	.0005	.0005	.002	.002	.0005
Ga	.001	----	----	----	.001	----	.001	.001	.0007	.001	----	----	----	.007
Mo	.0007	.0007	.0007	.002	.002	.002	.0015	.0015	.0015	.002	.015	----	.001	.002
Nb	.07	.15	.15	.1	.1	.07	.1	.1	.1	.1	.1	.1	.07	.05
Pb	.015	.0015	----	----	.002	.002	.001	.007	----	----	----	.002	----	----
Sc	.05	.005	.005	.007	.005	.007	.02	.007	.01	.007	.005	.01	.002	.007
Sn	.03	.02	.02	.02	.02	.03	.02	.02	.02	.015	.015	.03	.015	.02
Sr	.002	.003	.003	.003	.01	.003	.015	.007	.003	.005	.005	.002	.007	.003
Th	.7	----	----	----	----	----	----	.05	----	----	----	----	----	----
U	.2	----	----	----	----	----	----	----	----	----	----	----	----	----
V	.15	.2	.2	.2	.2	.15	.15	.15	.15	.2	.15	.2	.15	.15
Zr	.2	.07	.07	.03	.07	.07	.07	.1	.05	.1	.07	.07	.07	.1

[1] Sphene from lamprophyre.
[2] Sphene from xenolith.
[3] Includes total iron.
[4] Leaders (----) indicate that element was looked for but not found.

Minor elements

The minor-element contents of these sphenes (except for rare earths) are listed in table 1. The suite of elements represented is rather large, although it is well recognized that the sphene structure often carries significant amounts of elements not represented in the type formula. (See, for example, Zabavnikova, 1957; Deer and others, 1962).

As noted previously, the sample of sphene 190–MW–61 analyzed probably was less than 99 percent pure, but minor-element data for it are included here because it is the only sphene fraction we were able to obtain from a rock having less than 2.2 percent CaO. Only about 10 milligrams of this mineral was recovered from more than 1,000 grams of crushed rock. The sphene grains were etched and pitted, suggesting disequilibrium with other minerals present in the rock.

Each of the other 13 sphenes analyzed was more than 99 percent pure. However, in view of the fact that some of the tiny inclusions already described probably are zircon, some of the Zr content shown in table 1 may not be present in the sphene structure. For example, as little as 0.1 percent zircon contamination would be equivalent to about 700 parts per million Zr. The high P content is not so readily explained, but it seems likely that P might be part of the structures of some sphenes in table 1, even though some of the tiny inclusions described appear to be apatite, because about 0.8 percent apatite would be required to produce a P content of 1,500 parts per million.

The most notable aspect of the hybrid rock exposed north of the Mount Wheeler mine area is the large number of rather systematic chemical and mineralogical trends that have been found to accompany the general change from felsic to mafic representatives. Even major- and minor-element contents of constituent accessory minerals exhibit these trends. Such systematic differences, if indeed they are present in these sphenes, are not great enough, however, to be apparent from the semiquantitative data in table 1. These sphenes (with the exception of sample 190–MW–61 already described) are well crystallized and are usually seen in thin section as well-formed euhedra. There is nothing to indicate that any of these sphenes is secondary or deuteric.

In view of the summary works cited above, the significance of most of the minor-element data in table 1 is evident, but the Mo and Bi values deserve comment. Sphene must have scavenged most of the Mo present in the magmatic environment, for the element was rarely detected in any minerals coexisting with these sphenes. Sphene must have scavenged Bi too, for this element was not detected in any other minerals present in these rocks.

Rare earths

Rare-earth contents of the sphenes are listed in table 2, along with calculated atomic percentages of the rare-earth assemblage present in each sphene. Also listed for each is the quantity Σ La + Ce + Pr (in atomic percentage of total rare-earth elements) as a numerical index of the composition and of the stage of fractionation attained by the rare-earth elements. This quantity sigma (Σ La + Ce + Pr) was introduced by Murata, Rose, and Carron (1953) in a study of the total range of variation in the composition of monazite with respect to the rare-earth elements. Later studies (especially Murata and others, 1957) confirmed that this quantity sigma is meaningful in comparing such analyses, and it has therefore been used (table 2) in appraising the rare-earth contents of accessory minerals that coexist with the sphenes.

Some 21 allanite and 13 monazite samples from these hybrid rocks have sigma values that vary from 61.3 to 80.9 atomic percent, which is an appreciable range of composition in terms of the rare-earth elements (Lee and Bastron, 1967). Moreover, sigma values of the allanites and monazites vary directly with CaO content of their host rocks, and allanites from the most mafic rocks show a concentration of the most basic rare earths (La, Ce, and Pr). Rare-earth contents of 25 accessory zircons from these hybrid rocks are much smaller than amounts listed for the sphenes in table 2, but generally they express the same trend as that shown by the allanites and monazites; that is, the heavier lanthanides are present in largest amounts in zircons from the more felsic rocks, whereas the lighter and more basic lanthanides increase in abundance with increasing lime content of the rock (Lee and others, 1968).

The analyses of sphenes in table 2 fail to express the same trend, for the sigma values of the sphenes are not very obviously related to the CaO contents of the rocks from which they were recovered. Were the trend for sphenes as well defined as for allanites, monazites, and zircons, it would be clearly shown by even the semiquantitative data in table 2. Sphenes, then, do not show the regular minor-element trends found in minerals coexisting with them.

Each sphene in table 2 has a sigma value much lower than that of its coexisting allanite (Lee and Bastron, 1967), indicating a much less basic and heavier assemblage of rare earths in the sphenes. In discussing the distribution of rare earths in accessory sphene, Uskov (1967) concluded, after a study of sphenes collected from several widely diverse geologic environments, that the chemistry of the rock-forming medium is more important than crystallochemical selection in determining

TABLE 2.—*Rare-earth contents of accessory sphenes from the Mount Wheeler mine area, Nevada*

[Semiquantitative spectrographic analyses by R. E. Mays. General limitations of the method are given in table 1]

Sample No	190-MW-61	14-MW-60	36-DL-61	8-DL-61	40A-MW-60	31-DL-61	150-MW-60 [1]	152-MW-61	40B-MW-60 [2]	126-MW-61 [2]	43-DL-61	27-DL-61 [2]	16-MW-60	98-DL-62 [2]
CaO in rock (weight percent)	1.2	2.2	2.2	2.3	2.4	2.4	2.8	3.2	3.5	3.5	3.9	4.1	4.3	4.5
Rare earths in sphene (weight percent)														
Y	0.15	0.3	0.3	0.2	0.2	0.2	0.15	0.2	0.2	0.2	0.2	0.3	0.15	0.15
La	.1	.07	.07	.05	.05	.05	.02	.03	.07	.1	.05	.05	.02	.07
Ce	.5	.2	.2	.2	.5	.5	.15	.2	.5	.5	.5	.5	.15	.5
Pr	.05	.07	.07	.05	.07	.07	0	.02	.1	.1	.07	.07	0	.1
Nd	.3	.7	.7	.5	.5	.5	.1	.3	.7	.7	.7	.7	.15	.7
Sm	.07	.2	.2	.3	.3	.15	.05	.15	.3	.3	.2	.5	.07	.2
Eu	0	.02	.02	.03	.03	.03	.01	.02	.02	.03	.03	.03	.01	.03
Gd	.03	.07	.07	.2	.2	.15	.05	.1	.2	.2	.2	.5	.05	.15
Tb	0	0	0	.005	.005	0	0	0	.005	.005	.005	.015	0	.005
Dy	.03	.07	.07	.15	.2	.1	.05	.1	.15	.15	.1	.2	.05	.1
Ho	.005	.02	.02	.02	.02	.015	.005	.01	.02	.02	.015	.015	.005	.015
Er	0	.03	.03	.03	.03	.03	0	.02	.03	.02	.02	.05	0	0
Tm	.007	.015	.015	.007	.007	.005	0	.007	.007	.007	.007	.01	.002	.005
Yb	.015	.015	.02	.015	.015	.015	.007	.015	.015	.01	.015	.02	.007	.02
Lu	.005	0	0	.003	.003	.003	0	.003	.003	0	0	.003	0	0
Total	1.262	1.780	1.785	1.760	2.130	1.818	0.592	1.175	2.320	2.342	2.112	2.963	.664	2.045
Total rare-earth elements in sphene (atomic percent)														
Y	17.9	25.0	24.9	17.7	14.7	16.9	36.0	25.4	13.5	13.3	14.7	15.8	32.6	11.5
La	7.7	3.7	3.7	2.8	2.3	2.7	3.0	2.5	3.0	4.3	2.4	1.7	2.7	3.4
Ce	37.8	10.6	10.6	11.2	23.3	26.8	22.9	16.2	21.4	21.2	23.3	16.8	20.6	24.3
Pr	3.7	3.7	3.7	2.7	3.3	3.8	0.0	1.6	4.2	4.2	3.3	2.4	0	4.8
Nd	22.0	36.0	35.9	27.3	22.6	26.0	14.7	23.5	29.1	28.8	31.6	22.8	20.0	33.0
Sm	5.0	9.8	9.8	15.7	13.0	7.5	7.0	11.3	12.0	11.9	8.7	15.6	9.1	9.1
Eu	0	.97	.96	1.6	1.3	1.5	1.5	1.5	.79	1.2	1.3	.94	1.3	1.4
Gd	2.0	3.5	3.5	10.0	8.3	7.1	6.8	7.2	7.6	7.5	8.3	15.0	6.2	6.5
Tb	0	0	0	.25	.21	0	0	0	.18	.18	.20	.42	0	.19
Dy	1.9	3.2	3.2	7.2	8.0	4.7	6.6	7.0	5.5	5.4	4.0	5.8	6.0	4.2
Ho	.32	.89	.89	.96	.79	.67	.64	.70	.73	.71	.58	.42	.57	.61
Er	0	1.3	1.3	1.4	1.2	1.3	0	1.4	1.1	.71	.78	1.4	0	0
Tm	.42	.67	.67	.31	.27	.22	0	.46	.24	.24	.26	.27	.18	.19
Yb	.94	.67	.88	.71	.60	.66	.86	1.0	.54	.36	.58	.56	.75	.81
Lu	.32	0	0	.17	.13	.15	0	.24	.12	0	0	.09	0	0
Total	100.0	100.0	100.0	100.0	100.0	100.0	100.0	100.0	100.0	100.0	100.0	100.0	100.0	100.0
Σ(La+Ce+Pr)	49.2	18.0	18.0	16.7	28.9	33.3	25.9	20.3	28.6	29.7	29.0	20.9	23.3	32.5

[1] Sphene from lamprophyre dike.
[2] Sphene from xenolith.

fractionation of rare earths in sphene. For the hybrid rocks in the Mount Wheeler mine area, in contrast, crystallochemical selection was more important than the chemistry of the rock-forming medium. In the terminology of Uskov, our sphenes contain a "selective yttrium" (as opposed to "selective cerium") assemblage of rare earths.

SUMMARY AND CONCLUSIONS

In the hybrid granitoid rocks exposed north of the Mount Wheeler mine the abundance of sphene tends to increase directly with lime content of the rock. However, when sphenes are compared to other minerals from the same rocks, their physical properties and major- and minor-element contents show relatively little response to whole-rock chemistry.

These sphenes contain a rather large assemblage of rare earths and other minor elements. They scavenged Mo and Bi, and they contain a heavier, less basic assemblage of rare earths than do the coexisting allanites.

REFERENCES

Deer, W. A., Howie, R. A., and Zussman, J., 1962, Rock-forming minerals—v. 1, Ortho- and ring silicates: New York, John Wiley & Sons, Inc., 333 p.

Drewes, H. D., 1958, Structural geology of the southern Snake Range, Nevada: Geol. Soc. America Bull., v. 69, no. 2, p. 221–239.

Evans, H. T., Jr., Appleman, D. E., and Handwerker, D. S., 1963, The least squares refinement of crystal unit cells with powder diffraction data by an automatic computer indexing method [abs.]: Am. Cryst. Assoc. Ann. Mtg., 1963, Program and Abs., no. E–10, p. 42.

Lee, D. E., and Bastron, Harry, 1967, Fractionation of rare-earth elements in allanite and monazite as related to geology of the Mount Wheeler mine area, Nevada: Goechim. et Cosmochim. Acta, v. 31, no. 3, p. 339–356.

Lee, D. E., and Dodge, F. C. W., 1964, Accessory minerals in some granitic rocks in California and Nevada as a function of calcium content: Am. Mineralogist, v. 49, nos. 11–12, p. 1660–1669.

Lee, D. E., Stern, T. W., Mays, R. E., and Van Loenen, R. E., 1968, Accessory zircon from granitoid rocks of the Mount Wheeler mine area, Nevada, *in* Geological Survey Research 1968: U.S. Geol. Survey Prof. Paper 600–D, p. D197–D203.

Murata, K. J., Rose, H. J., Jr., and Carron, M. K., 1953, Systematic variation of rare earths in monazite: Geochim. et Cosmochim. Acta, v. 4, no. 6, p. 292–300.

Murata, K. J., Rose, H. J., Jr., Carron, M. K., and Glass, J. J., 1957, Systematic variation of rare-earth elements in cerium-earth minerals: Geochim. et Cosmochim. Acta, v. 11, no. 3, p. 141–161.

Uskov, M. N., 1967, O Kristallokhimicheskikh osobennostiyakh raspredeleniya redkikh zemel' aksessornom sfene [Crystallochemical features of the distribution of rare earths in accessory sphene], p. 94–103 *in* Nantishin, M. N., and others, eds., Konstitutsiya i svoistva mineralov, no. 2 of series Khimicheskii sostav i svoistva mineralov: Kiev, Akad. Nauk Ukrayin SSSR, Ukrayin Otdel. Vses Mineral. Obshch., 137 p.

Zabavnikova, I. I., 1957, Diadochic substitutions in sphene: Geochemistry (English translation of Geokhimiya), no. 3, p. 271–278.

Znamensky, E. B., 1957, On the distribution of titanium in granites: Geochemistry (English translation of Geokhimiya), no. 2, p. 131–135.

MICROINDENTATION HARDNESS OF MEMBERS OF THE LUDWIGITE-VONSENITE SERIES

By B. F. LEONARD, Denver, Colo.

Abstract.—Microindentation hardness distinguishes members of the ludwigite-vonsenite series from one another and aids in estimating their Fe^{+2} content. Microindentation hardness varies directly with Mg, inversely with Fe^{+2}. Locality, weight percent Fe^{+2}+Mn (in parentheses), and mean HV_{50} for four analyzed members are: Willis (0.5), 1254; Gorman (~16), 952; Riverside (28.7), 956; Jayville (42.0), 838. Gorman ludwigite behaves anomalously. Composition and microindentation hardness for the four members are best related by the equation $x=593.4-186.9 \log_{10} y$, where x is weight percent Fe^{+2}+Mn, and y is maximum HV_{50}. Qualitative properties of the indentations are of minor use in distinguishing the members.

Microindentation hardness provides an additional means of distinguishing the members of the ludwigite-vonsenite series from one another and estimating their Fe^{+2} content. This note supplements an earlier study (Leonard and others, 1962) of the isostructural series, whose generalized formula is $(Mg, Fe^{+2}, Mn)_2 (Fe^{+3}, Al)BO_5$. Sample descriptions, chemical analyses, optical data in transmitted and reflected light, and X-ray powder data for four members of the series are given in that paper. The same analyzed specimens, numbered the same way, are the raw material of this note.

Earlier, Lebedeva (1961, p. 109; 1963, p. 111, No. 234) reported the microindentation hardness of one ludwigite at 50-gram load as 537–588, mean 567. Pudovkina (Pudovkina and others, 1966, p. 34) recently reported the microindentation hardness of 23 samples of ludwigite as 588–1008, bimodal anisotropy 656 and 914; load is unspecified. The chemical composition and locality of Lebedeva's and Pudovkina's samples are not stated.

Equipment and procedures used in measuring microindentation hardness of members of the ludwigite-vonsenite series are summarized in the headnote of table 1. Defective indentations and those less than three diagonal lengths from the edge of the test grain were rejected. The vonsenites were first tested at 100-gram load because this is the standard load accepted by the Commission on Ore Microscopy of the International Mineralogical Association. The ludwigites were tested at 50-gram load because some grains were too small to accommodate the standard 100-gram load. The vonsenites were then tested at 50-gram load to provide consistent data for the series. A 50-gram load applied to members of the series gives mean diagonal lengths that are undesirably close to 10 microns, the lower limit taken by W. Uytenbogaardt[1] as suitable for measurement because the error of reading the diagonal lengths of small indentations approaches ±2 percent with a measuring ocular of the sort used in this investigation. However, the choice here is between non-ideal measurements or none at all.

Microindentation hardness is a load-dependent property whose value commonly but not invariably increases with decreasing load. The common effect seems to be illustrated by the data in table 1, paired Nos. 3 and 3a, 4 and 4a. However, a test of the significance of the difference between the means of the paired measurements made at 50- and 100-gram load shows that the difference is not statistically significant for the pair 3–3a and is doubtfully significant for the pair 4–4a. For the latter pair the difference is significant at the 90-percent confidence level only. In contrast, the difference between the means of measurements made at 50- and 100-gram loads on the two different vonsenites 3–4 and 3a–4a is significant at the 95-percent confidence level. If the microindentation hardness data of table 1 are used in conjunction with reflectivity to identify vonsenites, preference should be given to the more reliable values determined on the larger indentations made at 100-gram load.

Additional information on the techniques and results of microhardness determination is given by

[1] W. Uytenbogaardt, 1967a, Principles of micro-indentation hardness measurement: Free Univ. Amsterdam, Dept. Mineralogy and Petrology, Inst. Earth Sci. Pub., 8 p. [mimeographed].

U.S. GEOL. SURVEY PROF. PAPER 650-B, PAGES B47–B52

Bowie (1967, p. 131–158), Cameron (1961, p. 73–81), Demirsoy (1968, p. 51–70), Gahm (1967), Lebedeva (1963), Nakhla (1956), Pärnamaa (1963), Povarennykh (1963, p. 243–270), Tertsch (1960), Toubeau (1963), W. Uytenbogaardt,[1 2] Young and Millman (1964), and others.

Two conventions for deriving the mean and range of microindentation hardness values are followed in the literature. According to convention 1, adopted by most workers, one finds the hardness value for each indentation from the mean length of its diagonals by using tables appropriate for the load, or by calculating the hardness value from the applicable formula. For Vickers hardness, the formula is

$$HV = \frac{1854.4\ P}{d^2},$$

where P is the load in grams (or *pond* in some European works) and d is the mean length of the diagonals in microns. The resulting value is sometimes expressed as "kilograms per square millimeter," sometimes as a dimensionless unit; the latter seems preferable to me. (It is convenient to use the symbol HV_{100}, HV_{50}, * * *, to indicate Vickers hardness at 100-gram load, 50-gram load, * * *, respectively.) The range of HV is then taken as the extremes of the individual HV values, and the mean is the arithmetic mean of the individual values. According to convention 2, recently adopted by some workers, one averages the lengths of the short diagonals of all indentations, averages the lengths of the long diagonals of all indentations, and then finds the HV values corresponding to the squares of these averaged diagonal lengths. The mean HV, or midrange, is then taken as one-half the sum of the extreme values. Both conventions yield means that are virtually identical, but the range reported according to convention 2 is considerably restricted because of

[2] W. Uytenbogaardt, 1967b, Results of Vickers hardness measurements on ore minerals, achieved in different laboratories since 1956: Free Univ. Amsterdam, Dept. Mineralogy and Petrology, Inst. Earth Sci. Pub., Second summary, 12 p. [mimeographed].

TABLE 1.—*Microindentation hardness of analyzed members of the ludwigite-vonsenite series*

[Leitz Durimet microhardness tester fitted with rotating stage; Vickers diamond indenter, nonpolarized light, green filter; specimens hand lapped with ¼-micron diamond abrasive, mounted on plasticine, and leveled; descent and indentation periods 15 seconds each; 15 indentations per sample, each indentation diagonal measured twice]

	Ludwigite		Vonsenite			
	1 WBM/541	2 L/60/WTSL	3 L/55/WTSV-3	4 J2.21	3a L/55/WTSV-3	4a J2.21
$Fe^{+2}+Mn$ ---------- weight percent	0.5	~16	28.7	42.0	28.7	42.0
Load ---------- grams	50	50	50	50	100	100
Orientation effects minimal						
Convention 1:						
Range of HV from individual indentations	1049–1486	795–1197	810–1027	766–891	689–1003	707–803
Mean HV	1254	952	956	838	883	756
Convention 2:						
Range of HV from mean maximum and minimum lengths of diagonals of individual indentations.	1197–1283	857–1072	927–985	810–874	858–894	724–782
Mean HV	1240	946	956	842	876	753
Orientation effects distinct						
Convention 1:						
Sections $\perp c$ [1] (8 indentations):						
Range HV	1049–1283	795–965				
Mean HV	1175	879				
Sections $\parallel c$ [2] (7 indentations):						
Range HV	1255–1486	891–1197				
Mean HV	1345	1036				
Convention 2:						
Sections $\perp c$ [1] (8 indentations):						
Range HV	1145–1225	857–891				
Mean HV	1185	874				
Sections $\parallel c$ [2] (7 indentations):						
Range HV	1314–1379	985–1072				
Mean HV	1346	1028				

Samples of Leonard, Hildebrand, and Vlisidis (1962):
1. NW Willis quadrangle, Montana.
2. Gorman district, California.
3. Riverside, Calif. (type locality of vonsenite). For HV, polished section 3 of the original specimen was used, instead of polished section 4, to provide abundant grains in random orientation.
4. Jayville, N.Y.

[1] y axis of indentation $\parallel a$.
[2] y axis of indentation $\parallel c$.

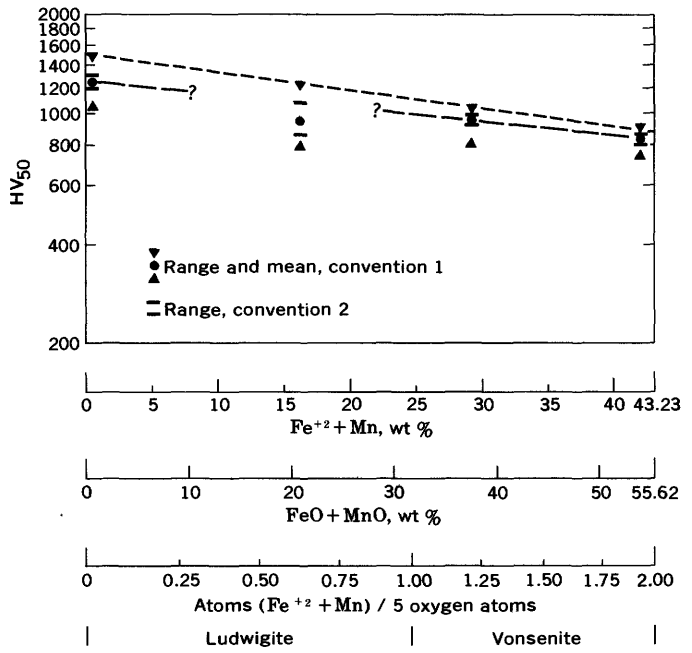

FIGURE 1.—Microindentation hardness (Vickers hardness at 50-gram load), ludwigite-vonsenite series.

the stage at which the averaging of diagonals is carried out. Some workers report only a range, without specifying the convention adopted; from their extreme values one can derive only the midrange. The different ranges obtained according to conventions 1 and 2 are reported in table 1 and shown on figure 1.

The dependence of HV_{50} on chemical composition within the ludwigite-vonsenite series is striking. The correlation between composition and maximum HV_{50} is nearly linear, the two variables defining a line whose equation is

$$x=593.4-186.9 \log_{10} y, \quad (1)$$

or

$$\log_{10} y=3.17470-0.00535x, \quad (1a)$$

where x is weight percent Fe^{+2}+ Mn, y is maximum HV_{50} according to convention 1. Solving equation 1 gives weight percent Fe^{+2}+ Mn with a precision of ±2 weight percent. The data can be better accommodated in equations derived by least-squares fitting, but the anomalous behavior of Gorman ludwigite (No. 2) makes this manipulation of doubtful value.

For three members of the series (Nos. 1, 3, 4), the two variables almost perfectly determine a line whose equation is

$$x=734.9-237.0 \log_{10} y, \quad (2)$$

or

$$\log_{10} y=3.10084-0.00422x, \quad (2a)$$

where x is weight percent Fe^{+2}+Mn, y is mean HV_{50}. Equations (2) and (2a) use data reckoned according to convention 1. The corresponding equations for data of convention 2 are

$$x=764.3-246.9 \log_{10} y \quad (3)$$

$$\log_{10} y=3.09544-0.00405x. \quad (3a)$$

Solving equation 2 or 3 gives weight percent Fe^{+2}+Mn with a precision of ±0.3 weight percent. Equations 2 and 3 come so close to defining the same line that data obtained by one convention can be substituted in equations derived for the other without significant change in the calculated results.

The fourth analyzed member (No. 2, from the Gorman tin district, Kern County, Calif.) behaves anomalously. Its mean HV_{50} falls well below the straight line determined by the other three members (fig. 1), and its logarithmic range of HV_{50} exceeds that of the other members. Moreover, it alone yields a high proportion of perfect, unfractured indentations (table 2). Leonard, Hildebrand, and Vlisidis (1962) earlier showed that other properties of Gorman ludwigite, notably the dispersion of its mean reflectivity, were anomalous with respect to those of the other members. We suggested (p. 556–557) that tin might be the cause, for its concentration is considerably higher in Gorman ludwigite (1.2 percent Sn) than in the other members (≤0.x). The manner in which partial substitution of foreign elements in a crystal lattice affects the microindentation hardness of a substance has been studied by several workers, but the results for different substances are conflicting. Thus the tin content of Gorman ludwigite may be suggested as a cause of its anomalous microindentation hardness, as it was for anomalous dispersion of reflectivity, but the true cause remains unknown. Certainly the anomaly is real and is not due to accidents of specimen preparation or measurement.

Possibly the anomaly presented by the mean HV_{50} of Gorman ludwigite (No. 2) lies in the derivation of the mean itself, rather than in the composition of this member. Crystals of Willis ludwigite (No. 1) and aggregates of Gorman ludwigite (No. 2) are markedly elongate $\|c$. HV_{50} for these members is significantly higher on sections $\|c$ than on sections $\perp c$. The ranges of measurements observed on the mutually perpendicular sections supplement each other to form the total range for each member. Mean HV_{50} for these members is arbitrarily taken as the mean of 7 indentations $\|c$ on elongate sections and 8 indentations $\|a$ on sections $\perp c$, as there seems to be no widely acceptable procedure for reporting the mean HV of minerals showing markedly preferential crystallographic development. In contrast, the abundant equant grains of the two vonsenites present many sections that are randomly oriented. The ideal approach for all members would perhaps be to determine the

crystallographic orientation optically, in reflected light, and then measure HV in an equal number of orientations $\|a$, b, and c on prime sections. For minerals embedded in their natural matrix, such an approach would be both difficult and tedious. Because the arbitrary weighting yields a credible mean for Willis ludwigite, it should do so for Gorman ludwigite, unless some other factor—here inferred to be Sn content—intervenes.

Using equations 2 or 3 to estimate the composition of ludwigites in the range 10 to 22 weight percent $Fe^{+2}+Mn$ leads to an error of +13 weight percent. Until this part of the plot can be checked by measurement of the microindentation hardness of appropriate Sn-free samples, it seems preferable to emphasize the anomalous behavior of Gorman ludwigite rather than to use it as a control point in the series. At present, appropriate samples are not available. One can only wish that the suites of samples used in the excellent studies by Brovkin, Aleksandrov, and Nekrasov (1963) and by Nekrasov (1966) might be combined with the suite investigated here.

Though the microindentation hardness of Gorman ludwigite is anomalous relative to that of other members of the series investigated here, the presence of appreciable Sn in a ludwigite of this Fe^{+2} content is not unexpectable. Nekrasov's (1966, p. 191–197) chemical and X-ray study of Sn in 95 ludwigites and vonsenites from skarns of the northeast U.S.S.R. showed a remarkable, consistent concentration of Sn in ludwigites containing 17 to 25 weight percent Fe^{+2}. Within this restricted compositional range the ludwigites contain 0.57 to 1.33 weight percent Sn, averaging 0.79 percent. The distribution of Sn in the total sample population is nearly symmetrical about this peak value. The total compositional range that was sampled is 2 to 42 weight percent Fe^{+2}, and the samples are distributed rather homogeneously. Nine samples from areas outside the northeast U.S.S.R. are uniformly low in Sn (trace to 0.128 weight percent), but none of the nine happens to fall within the range of 17 to 25 weight percent Fe^{+2}. (See Nekrasov, 1966, fig. 66 and analytical data in table 57, p. 193–194; the diagram is more readily available in Nekrasov and others, 1965, p. 52.) Experimental synthesis of Sn-bearing ludwigites by Nekrasov and others (1965) demonstrates that Sn is readily taken up in the crystal lattice of ludwigites having this favorable Fe^{+2} content, the maximum quantity being 18.5 weight percent Sn in synthetic ludwigite containing 20.8 weight percent Fe^{+2}. The relatively high Sn content of Gorman ludwigite is reasonably representative of the largest group of natural ludwigites and vonsenites studied to date, and so is the low Sn content of the other members investigated here.

TABLE 2.—*Quality of indentations in analyzed members of the ludwigite-vonsenite series*

[Results are in percent]

	1 WBM/ 541	2 L/60/ WTSL	3 L/55/ WTSV-3	4 J2.21	3a L/55/ WTSV-3	4a J2.21
Load, grams	50	50	50	50	100	100
Fractures:						
None	0	44	0	0	0	0
Very slightly fractured	10	4	18	25	21	33
Slightly fractured	50	39	70	69	58	67
Defective; discarded	40	13	12	6	21	0
Shapes (edges) of usable indentations:						
Straight	0	5	47	67	100	100
Very slightly concave	12	10	47	33	0	0
Concave	88	85	6	0	0	0

Qualitative differences in the testing behavior of members of the series are also evident (table 2). As noted above, only Gorman ludwigite (No. 2) yields a high proportion of perfect indentations. Most indentations on members of the series show one or a few short fractures. These radiate from one or more corners of each indentation and are slightly oblique to the indentation diagonals. Cleavage oblique to the diagonals is weakly developed at one corner of some indentations in the vonsenites. Roughly half the indentations at 100-gram load in Riverside vonsenite (No. 3a) show, in addition to rare or sparse linear fractures, small conchoidal fractures along one edge. In some grains, the conchoidal fractures fail to develop until the test load has been released for a minute or longer. Conchoidal fractures are absent from indentations made at 50-g load in this vonsenite. Mg-rich ludwigite (No. 1) is brittle; 40 percent of the tests cause severe deformation, mostly by complete shattering of the grains, though these were many times larger than the indentations made in them. Fe^{+2}-rich vonsenite (No. 4) gives rather uniformly good indentations. Intermediate members (Nos. 2, 3) show a low proportion of defective indentations.

Indentation shape distinguishes the ludwigites (Nos. 1, 2) from the vonsenites (Nos. 3, 4). All indentations are nearly equant, but the edges of all indentations in ludwigite are very slightly to distinctly concave, whereas those in vonsenite are straight at 100-gram load (Nos. 3a, 4a) and straight or very slightly concave at 50-gram load (Nos. 3, 4). Load clearly affects indentation shape in these vonsenites.

The dependence of microindentation hardness on composition in the ludwigite-vonsenite series is beyond doubt. Hardness varies directly with Mg, inversely with $Fe^{+2}+Mn$. Presumably the relation is so

readily demonstrated because (excepting Sn-bearing Gorman ludwigite) Mg and Fe^{+2} are the only significant compositional variables in R^{+2}, and Fe^{+3} and Al are the only ones in R^{+3}. Aluminum varies almost rectilinearly from 2.2 weight percent in Mg-rich ludwigite to 0.8 weight percent in Fe^{+2}-rich vonsenite, and Mn does not exceed 0.x weight percent in any member (data of Leonard and others, 1962, p. 531–533 and fig. 3).

Several other simple series of opaque to quasiopaque Fe-Mg minerals show microindentation hardness varying directly with Mg content, inversely with F^{+2} content. The simplest of these is the ilmenite-geikielite series studied by Cervelle (1967), in which 6 of 10 analyzed members closely fit a line whose equation, calculated from Cervelle's data, is $x=116.7 \log_{10} y - 320.7$, where x is weight percent MgO, y is mean HV at 100, 200, and 300 grams. The remaining four members are aberrant, without evident reason but perhaps because the total number of indentations measured was rather small. Cervelle (1967, p. 18) cautioned against using microindentation hardness to estimate composition within the series; he found mean reflectivity to be more suitable.

Chromites studied by Demirsoy (1968, p. 61 and fig. 84) and by Cameron and Desborough (1964) show a similar direct relation between microindentation hardness and Mg content, but one may infer that their examples are complicated by the presence of both Fe^{+2} and Fe^{+3}, as well as Al, in major amounts. Thus the plots of Demirsoy's data for microindentation hardness and reflectivity show considerable scatter. Cameron and Desborough (1964, p. 212) found a nice correlation among cell edge (indirectly representing composition), microindentation hardness, and reflectivity (the last varying inversely with Mg content). Their chromites are transitional to Ti-bearing magnetite containing ulvöspinel inclusions. Twenty-one analyzed chromites studied by Mozafari (1967) are magnesian varieties. Aluminum and Fe^{+3}, as well as Cr, Fe^{+2}, and Mg, vary widely within the suite. Mozafari found no systematic relation between microindentation hardness and composition.

Data for the magnetite-magnesioferrite series are incomplete, but the individual observations of Rumyantsev (1965) for nearly pure magnetite, Sinyakov (1966) for magnetite containing 10–13 percent MgO, and Burke (*in* Uytenbogaardt[3]) and Demirsoy (1968, fig. 102) for unanalyzed magnesioferrites, when combined, illustrate a similar direct relation between microindentation hardness and Mg content. The more reliable published data for common spinel and hercynite point the same way.

[3] See footnote 2.

ACKNOWLEDGMENTS

I am indebted to E. A. J. Burke, Free University, Amsterdam, Netherlands, for the inquiry that prompted this note, and to my associates G. A. Desborough and J. E. Harrison for comments on the manuscript.

REFERENCES

Bowie, S. H. U., 1967, Microscopy—Reflected light, *in* Zussman, J., ed., Physical methods in determinative mineralogy: London and New York, Academic Press, p. 103–159.

Brovkin, A. A., Aleksandrov, S. M., and Nekrasov, I. Ya., 1963, Rentgenometricheskoe izuchenie mineralov lyudvigit-vonsenitovoi serii [X-ray study of minerals of the ludwigite-vonsenite series]: Rentgenografiya Mineral'nogo Syr'ya, no. 3, p. 16–34.

Cameron, E. N., 1961, Ore microscopy: New York, John Wiley & Sons, 293 p.

Cameron, E. N., and Desborough, G. A., 1964, Origin of certain magnetite-bearing pegmatites in the eastern part of the Bushveld Complex, South Africa: Econ. Geology, v. 59, p. 197–225.

Cervelle, B., 1967, Contribution à l'étude de la série ilménite-geikielite: [France] Bur. Recherches Géol. et Minières Bull. [for 1967], no. 6, p. 1–26.

Demirsoy, Selçuk, 1968, Untersuchungen über den Einfluss der chemischen Zusammensetzung auf die spektralen Reflexionsfunktionen und Mikroeindruckhärten [der Chromitspinelle und eines Bravoit-Kristalls]: Tech. Hochschule Aachen, Dr. Ing. dissert., 95 p., 121 figs.

Gahm, Josef, 1967, A new microhardness tester: Zeiss Information, no. 62, p. 120–127.

Lebedeva, S. I., 1961, O mikrotverdosti mineralov [Microhardness of minerals]: Akad. Nauk SSSR, Inst. Mineralogii, Geokhimii i Kristallokhimii Redkikh Elementov Trudy, v. 6, p. 89–110.

———1963, Opredelenie mikrotverdosti mineralov [Determination of the microhardness of minerals]: Akad. Nauk SSSR, Inst. Mineralogii, Geokhimii i Kristallokhimii Redkikh Elementov; Moskva, Izdat. Akad. Nauk SSSR, 123 p.

Leonard, B. F., Hildebrand, F. A. and Vlisidis, A. C., 1962, Members of the ludwigite-vonsenite series and their distinction from ilvaite, *in* Petrologic studies— A volume in honor of A. F. Buddington: Geol. Soc. America, p. 523–568.

Mozafari, C., 1967, Microdureté, susceptibilité magnétique et indice de réfraction des magnésiochromites: Soc. Belge Géologie Bull., v. 76, p. 44–59.

Nakhla, F. M., 1956, The hardness of metallic minerals in polished sections: Econ. Geology, v. 51, p. 811–827.

Nekrasov: I. Ya., 1966, Geokhimiya olova i redkikh elementov Verkhoyano-Chukotskoi skladchatoi oblasti [Geochemistry of tin and rare elements in the Verkhoyansk-Chukotskii folded region]: Moskva, Akad. Nauk SSSR, Sibirskoe Otdelenie Yakutsk. Filial, Inst. Geologii, 379 p.

Nekrasov, I. Ya., Diman, E. N., Brovkin, A. A., and Konar, L. V., 1965, O novom tipe olovyannogo orudeneniya v magnezial'nykh skarnakh Severo-Vostoka SSSR [New type of

tin mineralization in magnesian skarns of the northeast USSR] : Geol. Rudn. Mest., v. 7, no. 2, p. 50–62.

Pärnamaa, Enn, 1963, On the use of Vickers microhardness (VH) in the microscopical identification of ore minerals, especially sulphides of Pb, Bi, Sb : Lund Univ. Årsskr., new ser., sec. 2, v. 59, no. 3, 51 p.

Povarennykh, A. S., 1963, Tverdost' mineralov [Hardness of minerals] : Kiev, Izdat. Akad. Nauk Ukrain. SSR, 303 p.

Pudovkina, I. A., Ryabeva, E. G., and Aksenova, E. K., 1966, Kolichestvennye metody izucheniya svoistv rudnykh mineralov i ikh primenenie [Quantitative methods of study of the properties of ore minerals and their application] : Mineral'noe Syr'e, v. 12, p. 5–52.

Rumyantsev, G. S., 1965, Composition and properties of minerals of the magnetite-jacobsite series redetected [newly observed] in the Magnetitovoye deposit (Buryat ASSR) : Doklady Acad. Sci. USSR, Earth Sci. Sec., v. 164, p. 135–138.

Sinyakov, V. I., 1966, Microhardness of magnetite from deposits of diverse origin : Doklady Acad. Sci. USSR, Earth Sci. Sec., v. 169, p. 145–147.

Tertsch, Hermann, 1960, Methoden mikroskopischer Härteprüfung, *in* Freund, Hugo, ed., Handbuch der Mikroskopie in der Technik, v. 1, pt. 2, Auflichtmikroskopie : p. 485–535.

Toubeau, G., 1963, Mesure de la microdureté Vickers des minéraux opaques et son intérêt en minéralogie : Soc. Belge Géologie Bull., v. 71 [for 1962], p. 242–267.

Young, R. B., and Millman, A. P., 1964, Microhardness and deformation characteristics of ore minerals : Inst. Mining and Metallurgy [London] Trans., v. 73, p. 437–466.

LARGER FOSSIL MAMMALS AND MYLAGAULID RODENTS FROM THE TROUBLESOME FORMATION (MIOCENE) OF COLORADO

By G. EDWARD LEWIS, Denver, Colo.

Abstract.—Two diagnostic fossil vertebrate faunas occur in the Troublesome Formation. One, lower stratigraphically and older, is equivalent to faunal elements of the *Merycochoerus* zone (Marsland Formation) of Nebraska. The second, higher stratigraphically and younger, is equivalent to faunal elements of the *Brachycrus* zone (Sheep Creek Formation) of Nebraska. If a twofold division of Miocene time be made, then these two faunas represent, respectively, the end of early Miocene time and late Miocene Time. A third fauna, the precise age of which has not been determined as yet, may be somewhat older than the two diagnostic faunas.

EARLIER WORK

Reported occurrences of vertebrate fossils from Middle Park, Grand County, Colo., were rare until 5 years ago, although such reports date back to the Territorial Surveys. The present short report deals with mammalian fossils from the Troublesome Formation, whence the first fossil mammal was reported 60 years ago (1908). Before that time the only vertebrate fossil reported from Middle Park was that by Leidy (1873, p. 267–268), who wrote:

> During Professor Hayden's expedition of 1869, a fossil was given to him as a "petrified horse hoof." The specimen was found in Middle Park, Colo., and according to Professor Hayden was probably derived from a formation of Cretaceous age. * * * The fossil in question consists of one-half of a vertebral body [centrum]

of a carnosaurian theropod dinosaur. This wretched fragment is chiefly notable as the inadequate basis for making *Allosaurus* of the Morrison Formation a synonym of *Antrodemus* (Gilmore, 1920, p. 3, pl. 1).

Cockerell (1908) was the first to report finding a fossil mammal in Middle Park, Colorado, from a

> ranch at Troublesome * * * in the course of making a well. * * * As no Miocene beds have ever been reported from this region, the discovery is a remarkable one. * * * S. A. Rohwer made a * * * search for further materials, but although he carefully examined all the surrounding region, he could not find any fossils. It seems probable that the deposit is quite local.

This specimen, strangely enough, came from an area (fig. 1) where thousands of specimens occur on the surface of the ground in "all the surrounding region"; it is a jaw fragment with two teeth of a horse that was identified for Cockerell as *Parahippus* by J. W.

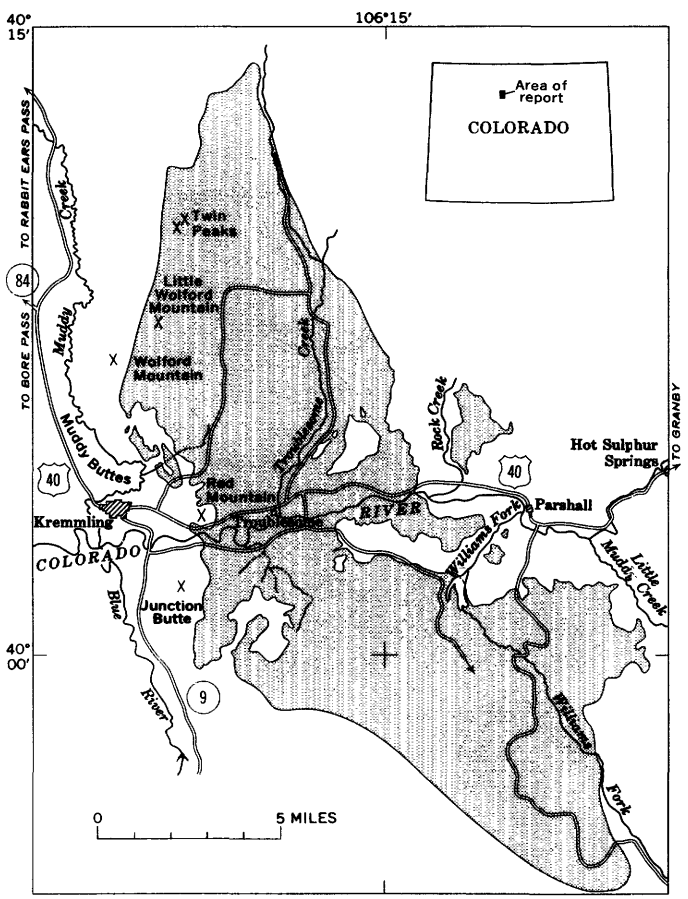

FIGURE 1.—Distribution of Miocene Troublesome Formation (stippled) near Kremmling, Grand County, Colo. (from Izett, 1968).

U.S. GEOL. SURVEY PROF. PAPER 650-B, PAGES B53-B56

Gidley and correctly assigned to middle or upper Miocene rocks.

Near Granby, Colo., about 20 miles east of Troublesome Creek, Lovering (1930, p. 74, pl. 6) reported the collection of *Blastomeryx*, a camel comparable to *Procamelus*, a large *Parahippus*, and *Moropus* cf. *M. elatus* identified for Lovering by H. J. Cook as "an Arikaree fauna * * * characteristic of the Lower Miocene." Cook's faunal list seems reasonable enough in the light of our more recent work, but his stratigraphic reference is probably too low.

Arthur Richards (1941) reported the collection of bones from what he called the Troublesome Formation; they were identified by E. C. Case as "titanothere" and "*Procamelus*" of early Oligocene and late Miocene or early Pliocene ages, respectively. This led Lovering and Goddard (1950, p. 41) to suggest that "Oligocene and late Miocene or early Pliocene fossils" occur in Middle Park. Then G. A. Izett began field studies of Middle Park in 1961; he found enough fossil vertebrates that a preliminary report was possible just 2 years later. Izett and Lewis (1963, p. B120–B121) reached "the tentative conclusion" that the "fossil vertebrate faunal elements indicate a probable middle Miocene age * * * equivalent to that of the Marsland * * * Formation of Nebraska" (see Wood and others, 1941, p. 12, 25, pl. 1), although neither the geologic nor the stratigraphic paleontologic data then available were sufficient to explain the stratigraphic relations of the several taxa.

LATER WORK

Much geological work in Middle Park has been completed since 1963 by Izett, and he, Peter Robinson, G. E. Lewis, and R. W. O'Donnell have collected many more fossil mammals. The larger mammals and the mylagaulid rodents have been studied by Lewis. Robinson, of the University of Colorado Museum, has collaborated with the U.S. Geological Survey in fossil vertebrate collection, and has studied all the micromammalian elements except the mylagaulids.

The larger mammals and mylagaulids fall into three faunal assemblages:

1. A peripheral—and possibly stratigraphically lower—assemblage occurs about 15 miles east of the main area of outcrop of the Troublesome Formation and 1 mile southwest of Granby. At this locality, we have found a distinctive microfaunal facies with large numbers of small mylagaulids reminiscent of *Promylagaulus riggsi* but perhaps more primitive in the morphological development of the cheek teeth. The age of these sediments is not certainly determinable from these mylagaulids; it may be about the same age as the Rosebud Formation of Macdonald (1963, p. 161–163), or it may be about the same age as the fauna described in the following paragraph.

2. Around the margins of the basin of deposition of the Troublesome Formation there are several localities (mapped by Izett, 1968) that have yielded faunal elements previously reported from the *Merycochoerus* zone (Marsland Formation) of Nebraska. This faunal assemblage includes *Merycochoerus matthewi*, *Merycochoerus proprius*, and *Mesogaulus* cf. *M. paniensis*. If a twofold division of the Miocene be used, this fauna indicates an age at the end of early Miocene time.

3. The more central parts of the basin of deposition of the Troublesome Formation (mapped by Izett, 1968) have yielded faunal elements previously reported from the *Brachycrus* zone (Sheep Creek Formation and some younger rocks) of Nebraska. This faunal assemblage includes *Brachycrus* cf. *B. siouxense* or *B. wilsoni*, *Protolabis angustidens*, "*Alticamelus*"-like camels, *Oxydactylus*-like camels, *Paracosoryx* sp., *Merychippus* spp., *Aphelops* cf. *A. profectus* and cf. *A. megalodus*, ?*Macrotherium* sp., and *Mylagaulus laevis* or *M. vetus*. The University of Michigan Museum of Paleontology, thanks to Curator of Vertebrates C. W. Hibbard, kindly loaned me the vertebrate fossils identified for Richards (1941) by E. C. Case. I find that the "titanothere" is in fact a large rhinoceros of the genus *Aphelops*; the "*Procamelus*" is in fact *Protolabis angustidens*. Therefore an "Oligocene and late Miocene or early Pliocene" age assignment for the Troublesome Formation is not indicated by these fossils collected by Richards. If a twofold division of the Miocene be used, this fauna indicates late Miocene age.

Lewis (1968, p. C76) has written previously that

> **the continental Miocene faunas of the United States seem to fall most naturally into a twofold rather than a threefold division; * * * Sheep Creek time seems to mark a practical datum for the beginning of late (as opposed to early) Miocene time. Recently, Sato and Denson (1967) and Denson and Izett (written commun., 1968) have demonstrated a comparable stratigraphic division; they use a twofold division of the Miocene Series in the High Plains and middle Rocky Mountains, with the boundary between the lower Miocene (Arikaree) and upper Miocene (Ogallala) marked by a change in the regimen of sedimentation that begins with the Sheep Creek Formation.**

Thus, Lewis, Denson, and Izett would place the boundary between early and late Miocene rocks between the Marsland and Sheep Creek Formations in Nebraska. This is in contrast to the threefold division used by

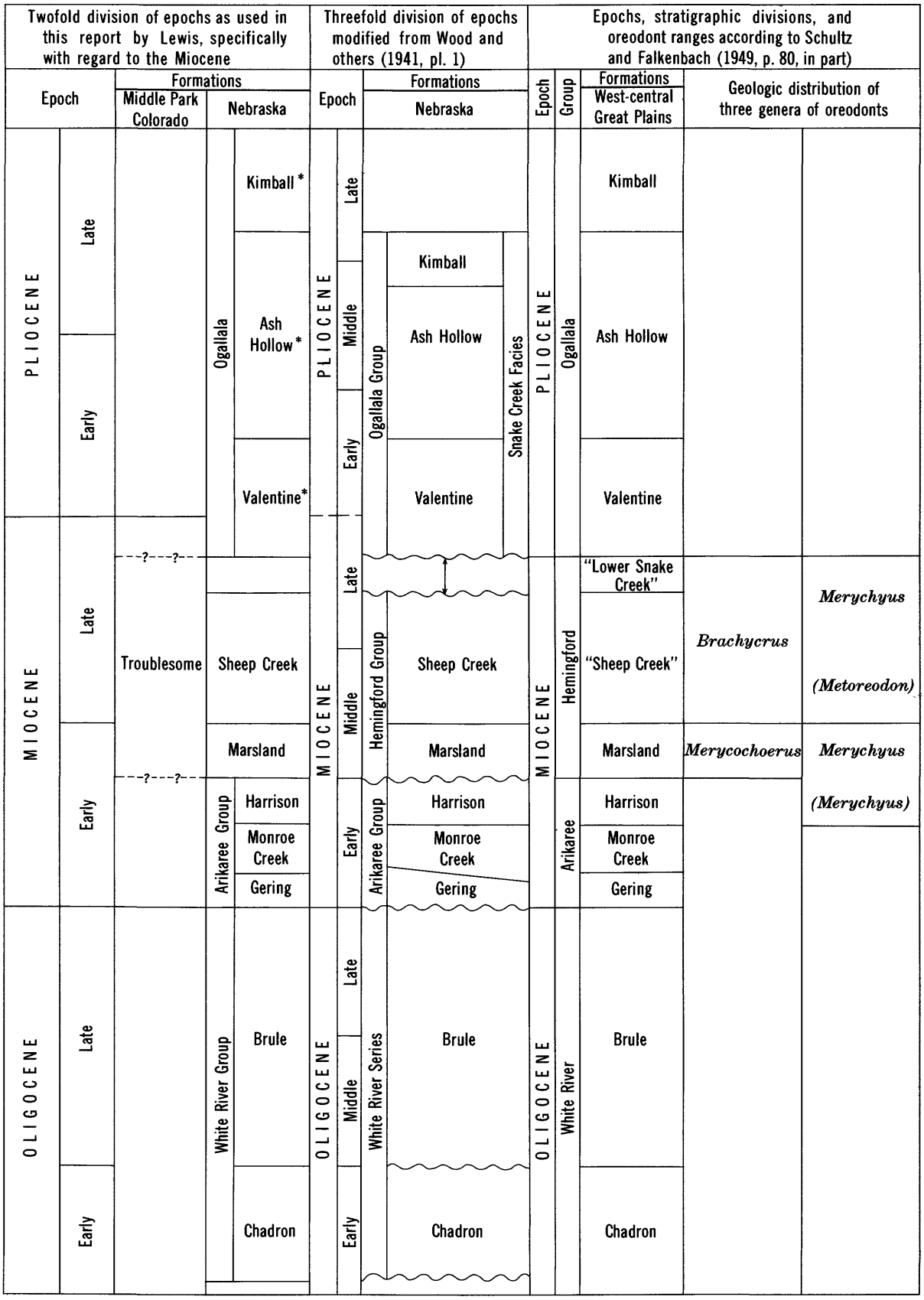

FIGURE 2.—Miocene Troublesome Formation in Colorado, and related Tertiary formations in Nebraska.

Wood and others (1941, pl. 1) according to whose scheme the Marsland and the overlying Sheep Creek together make up the middle Miocene in Nebraska. Comparison of these two arrangements may be made in figure 2 (p. B55).

REFERENCES

Cockerell, T. D. A., 1908, A new locality for Miocene mammals [*Parahippus*, Middle Park, Colo.]: Science, new ser., v. 28, p. 683.

Gilmore, C. W., 1920, Osteology of the carnivorous Dinosauria in the United States National Museum, with special reference to the genera *Antrodemus* (*Allosaurus*) and *Ceratosaurus*: U.S. Natl. Mus. Bull. 110, 159 p.

Izett, G. A., 1968, The Miocene Troublesome Formation in Middle Park, northwestern Colorado: U.S. Geol. Survey open-file report, 42 p.

Izett, G. A., and Lewis, G. E., 1963, Miocene vertebrates from Middle Park, Colorado: Art. 31 *in* U.S. Geol. Survey Prof. Paper 475–B, p. B120–B122.

Leidy, Joseph, 1873, Contributions to the extinct vertebrate fauna of the Western Territories, pt. 1 *of* U.S. Geol. Geog. Survey Terr. (Hayden) Monograph 1; 358 p.

Lewis, G. E., 1968, Stratigraphic paleontology of the Barstow Formation in the Alvord Mountain area, San Bernardino County, California, *in* Geological Survey Research 1968: U.S. Geol. Survey Prof. Paper 600–C, p. C75–C79.

Lovering, T. S., 1930, The Granby anticline, Grand County, Colorado: U.S. Geol. Survey Bull. 822–B, p. 71–76.

Lovering, T. S., and Goddard, E. N., 1950, Geology and ore deposits of the Front Range, Colorado: U.S. Geol. Survey Prof. Paper 223, 319 p. [1951].

Lugn, A. L., 1938, The Nebraska State Geological Survey and the "Valentine problem": Am. Jour. Sci., 5th ser. v. 36, no. 213, p. 220–227.

Macdonald, J. R., 1963, The Miocene faunas from the Wounded Knee area of western South Dakota: Am. Mus. Nat. History Bull., v. 125, art. 3, p. 143–238.

Richards, Arthur, 1941, Geology of the Kremmling area, Grand County, Colo.: Michigan Univ. unpub. Ph. D. thesis, 68 p.

Sato, Yoshiaki, and Denson, N. M., 1967, Volcanism and tectonism as reflected by the distribution of nonopaque heavy minerals in some Tertiary rocks of Wyoming and adjacent States, *in* Geological Survey Research 1967: U.S. Geol. Survey Prof. Paper 575–C, p. C42–C54.

Schultz, C. B., and Falkenbach, C. H., 1949, Promerycochoerinae, a new subfamily of oreodonts: Am. Mus. Nat. History Bull., v. 93, art. 3, p. 69–198.

Wood, H. E., 2d, and others, 1941, Nomenclature and correlation of the North American continental Tertiary: Geol. Soc. America Bull., v. 52, no. 1, p. 1–48.

AGE AND STRATIGRAPHIC RELATIONS OF THE TEPEE TRAIL AND WIGGINS FORMATIONS, NORTHWESTERN WYOMING

By W. L. ROHRER and J. D. OBRADOVICH, Denver, Colo.

Abstract.—In the southern Absaroka Mountains the upper part of the Tepee Trail Formation interfingers with the lower part of the Wiggins Formation. This time-transgressive contact in the Pinnacle Buttes–Togwotee Pass area migrates stratigraphically upward toward the southeast. Potassium-argon ages of about 46 m.y. on hornblendes from andesites in the basal part of the Wiggins Formation at Pinnacle Buttes indicate a late middle Eocene age. A large flora from the lower part of the underlying Tepee Trail Formation indicates that the Tepee Trail at Pinnacle Buttes is middle Eocene.

The southern Absaroka Mountains of northwestern Wyoming chiefly consist of gently dipping volcaniclastic rocks. From Togwotee Pass to East Fork these rocks comprise the greenish Tepee Trail Formation, which consists mainly of fine-grained nonresistant volcanic sedimentary rocks, and the overlying light-gray Wiggins Formation, a dominantly volcanic conglomerate.

The purpose of this report is to review stratigraphic information and age assignments of the Tepee Trail and Wiggins Formations and to present new stratigraphic information. This report is preliminary and subject to revision as more is learned about the Absaroka volcanic province.

The Wiggins Formation represents a relatively large timespan, and the Tepee Trail–Wiggins contact transgresses time. In the Pinnacle Buttes area the upper part of the Tepee Trail Formation intertongues with the lower part of the Wiggins Formation, the Tepee Trail is restricted to the middle Eocene, and the lower part of the Wiggins is also of middle Eocene age. Elsewhere, the Tepee Trail is in part of late Eocene age and the Wiggins is probably of late Eocene and early Oligocene age. The age of 45–46 million years which was established by Evernden, Savage, Curtis, and James (1964, p. 165) for the middle Eocene-late Eocene boundary is used in this report.

TEPEE TRAIL FORMATION

At the type section of the Tepee Trail Formation in the East Fork area (fig. 1), the formation consists of green or brown dominantly volcaniclastic rocks (Love, 1939). The formation is more than 1,400 feet thick, but the total thickness is unknown because the base of the formation is not exposed. The lowermost 150 feet of the Tepee Trail consists of tuff, conglomerate, siltstone, claystone, and shale, overlain by 465 feet of tuff and volcanic conglomerates and minor siltstone, shale, and claystone. The uppermost 800 feet consists of shale, sandstone, conglomerate, thin lava flows, tuff, and breccia. Love (1939, p. 74) reported that the southern and eastern exposures in the East Fork area are chiefly fine-grained fluvial tuff that coarsens to the north and northwest.

In the Du Noir area (fig. 1, area 2) the Tepee Trail Formation is 0–1,500 feet thick (Keefer, 1957, p. 193). Here the formation consists chiefly of green, olive-drab, and brown water-laid sandstone, volcanic conglomerate, shale, and tuff. The strata become progressively coarser and more conglomeratic toward the top. The thickness of the Tepee Trail varies widely owing to pre-Tepee Trail topography.

The contact between the Tepee Trail and the Wiggins was inferred throughout the Du Noir area because only a few isolated exposures of the contact were observed (Keefer, 1957, p. 194). The contact was determined chiefly on the basis of color: the predominantly dark-green strata were assigned to the Tepee Trail and the overlying light-brownish-gray strata were assigned to the Wiggins.

In the Kisinger Lakes quadrangle (fig. 1; Rohrer, 1966) the Tepee Trail Formation is about 1,800 feet thick and consists mainly of grayish-green fine-grained fluvial volcanic sedimentary rocks. The strata are interbedded claystone, siltstone, sandstone, bentonite, and mudstone. Although uncommon, red and flesh-

U.S. GEOL. SURVEY PROF. PAPER 650-B, PAGES B57–B62

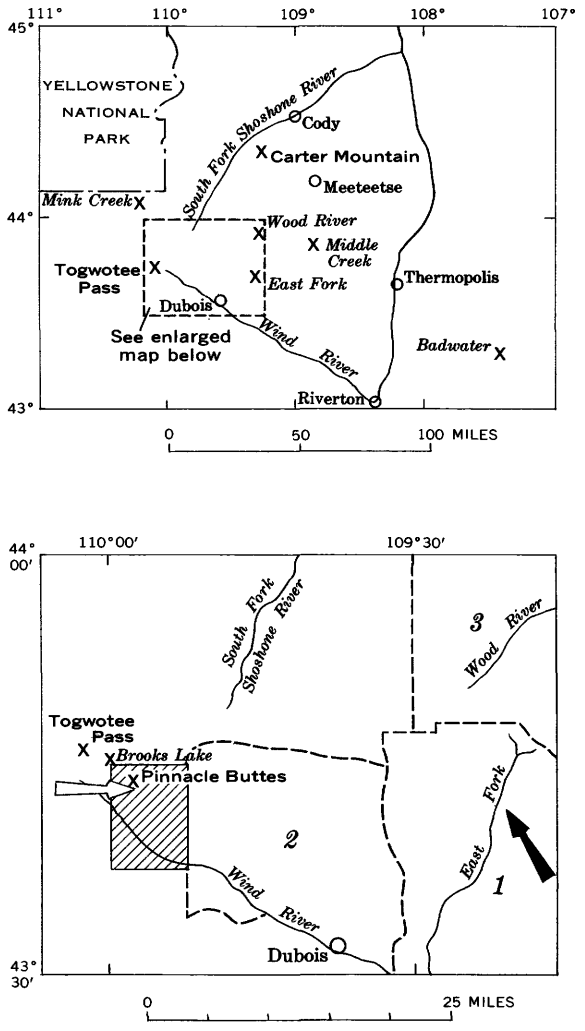

FIGURE 1.—Index maps of northwestern Wyoming, showing places mentioned in text. *1*, area mapped by Love (1939); *2*, Du Noir area mapped by Keefer (1957); *3*, area mapped by Wilson (1963, 1964). Hachured area is Kisinger Lakes quadrangle mapped by Rohrer (1966); solid arrow points to location of type section of Tepee Trail Formation; open arrow points to location of figure 2.

colored claystone, pebble conglomerate, and coal also occur in the formation.

The base of the Tepee Trail Formation in the Kisinger Lakes area was chosen at the base of a volcanic sandstone and conglomerate unit. The lowermost beds contain green, gray, and pink biotitic lapilli and chert and quartzite pebbles in a green sandstone matrix. This basal unit is ledge forming and disconformably(?) overlies a greenish-gray volcanic sandstone, which grades upward from coarse-grained sandstone to siltstone and claystone, assigned to the Wind River Formation. Although volcaniclastic rocks are not generally found in the Wind River Formation, in the area west of Du Noir Creek these rocks are common to the formation.

The lower 1,200 feet of the Tepee Trail consists of greenish-gray, grayish-green, and brownish-gray fine- to coarse-grained volcanic sandstone, greenish- and brownish-gray clayey volcanic siltstone, and gray, greenish-gray, and pale-red locally bentonitic claystone. A 35-foot-thick pale-greenish-tan, gray-weathering bentonite bed, which occurs about 280 feet above the base of the formation, may be the same bed observed by Keefer (1957, p. 192) at White Pass, in the Du Noir area (fig. 1).

The upper 600 feet contains many tongues of volcanic mudflow conglomerate and mudstone interbedded with the claystones and sandstones. These conglomerates consist of angular to rounded pebbles and small boulders of volcanic rocks and fragments of fossil wood. These coarse sediments grade southward to siltstone and claystone. Of the several conglomerate and mudstone beds in the lower 300 feet of the measured section (fig. 2), only the lowest mudstone is present 1 mile to the southeast.

At Pinnacle Buttes a distinctive bluish-green marker unit, known to the authors as the "Big Blue," occurs about 300 feet below the top of the Tepee Trail Formation (fig. 2). This marker unit, which is easily seen from the highway west of Brooks Lake Creek, is a composite unit about 32 feet thick composed of very fine to coarse andesitic sandstone, volcanic pebble conglomerate, siltstone, and claystone. The claystone contains a few plant impressions. North of Brooks Lake where the "Big Blue" crosses the valley floor, the unit contains abundant angular pebbles and cobbles of andesite. Northwest of Brooks Lake, the "Big Blue" loses much of its characteristic color and forms a resistant bench (fig. 3). The unit is a volcanic mudflow conglomerate, like those in the Wiggins, that contains angular andesite boulders as much as 6 feet in diameter.

WIGGINS FORMATION

No type section of the Wiggins Formation has been designated. However, a representative section was measured and described in sec. 20, T. 44 N., R. 104 W. (Love, 1939, p. 80). There the Wiggins consists of 989 feet of alternating volcanic conglomerate, tuff, and andesite flows. The Wiggins Formation in the Du Noir (Keefer, 1957, p. 195) and Kisinger Lakes areas is similar to that described by Love except that andesite flows are uncommon. At Pinnacle Buttes about 1,500 feet of Wiggins is present; elsewhere, the Wiggins is reported to be about 4,000 or more feet thick (Ketner and others, 1966, p. 7; Wilson, 1963, p. 17).

The Wiggins Formation at Pinnacle Buttes is an alternating sequence of brownish-gray volcanic mud-

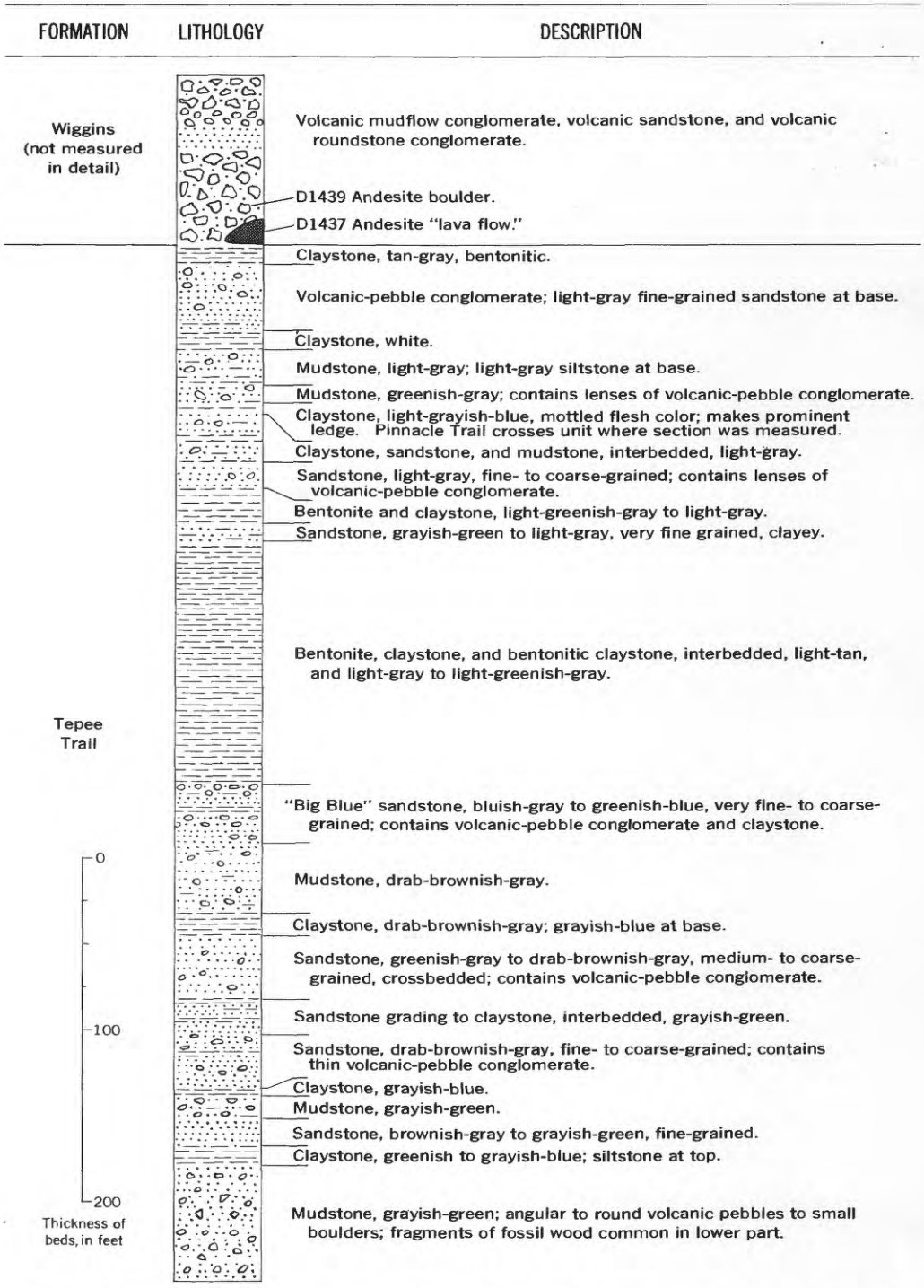

FIGURE 2.—Upper part of Tepee Trail Formation at Pinnacle Buttes in the SW¼ sec. 33, T. 44 N., R. 109 W., Kisinger Lakes quadrangle, Fremont County, Wyo.

FIGURE 3.—View looking northwest at the Togwotee Pass–Pinnacle Buttes area. Strata dip 2°–4° NE. (to the right); X, andesite sample locality. Brooks Lake, hidden by trees, is below the open hillside below the "Big Blue" bench.

flow conglomerate (about 84 percent), bluish-gray rounded volcanic stream conglomerate (about 10 percent), and fluvial tuff (about 6 percent). The mudflow conglomerate tends to be massive and in beds, commonly more than 20 feet thick, that consist of varicolored angular andesite and basalt as much as 8 feet in diameter in a tuff matrix. The fluvial tuffs are reworked fine detritus from the mudflows. Distinctive white bands, generally less than 6 feet thick, in the dissected Absaroka escarpment (fig. 3) are volcanic ash. The stream conglomerate consists of varicolored volcanic roundstones in a matrix of poorly to well-indurated angular coarse volcanic sandstone. These roundstone conglomerates are lenticular and usually less than 10 feet thick.

In the Kisinger Lakes area, the Tepee Trail–Wiggins contact is placed at the base of a sequence dominantly composed of coarse volcanic mudflow conglomerate (figs. 2, 3). The conglomerate contrasts sharply with the underlying bentonitic claystone of the Tepee Trail. No lithologic break was seen in the more than 1,000 feet of Wiggins volcaniclastic rocks, although many presumably minor disconformities are present in this interval.

The observed facies changes in the upper part of the Tepee Trail indicate that this part of the formation interfingers with the lower part of the Wiggins. The uppermost 600 feet of the Tepee Trail contains several mudflow conglomerates, some of which are described as mudstones (fig. 2). These mudstones consist mainly of an unsorted heterogeneous mixture of clay, silt, sand, and volcanic pebbles, and are probably genetically related to the coarse bouldery mudflows of the Wiggins. The "Big Blue" and the mudflow conglomerates in the Tepee Trail coarsen to the north and northwest and grade into typical coarse Wiggins-like volcanic mudflow conglomerates. These changes are similar to those indicated by Love (1939, p. 80) and Hay (1956, p. 1869).

Several discrepancies in the radiometric and fossil ages of the Tepee Trail and Wiggins Formations can be readily explained once the intertonguing of the formations and the fact that the contact of these formations migrates stratigraphically upward southeast from Togwotee Pass are recognized. These discrepancies are described in following paragraphs. The intertonguing of the Wiggins and Tepee Trail was described by Ketner and others (1966, p. 5), and K. B. Ketner and W. R. Keefer (in U.S. Geological Survey, 1966, p. *A*77) reported that local relief on the contact between these formations is more than 1,500 feet and seems to be the result of intertonguing rather than of structural complications or unconformity.

AGE

Tepee Trail Formation

The Tepee Trail was assigned a late Eocene age and was provisionally correlated with part of the Uinta Formation on the basis of a few vertebrate fossils (Love, 1939, p. 77). G. E. Lewis (oral commun., Dec. 1967) claims that these same fossils are considered equally indicative of a Bridgerian provincial age or middle Eocene age.

Late Eocene vertebrates have been reported from Tepee Trail strata in the Badwater area near Lysite, Wyo., in the northeastern part of the Wind River Basin (Black and Dawson, 1966, p. 331; Tourtelot, 1957, p. 11), and a middle Eocene flora has been reported from the lower part of the Tepee Trail Formation in the Kisinger Lakes quadrangle (Rohrer,

1966). On the basis of this fossil evidence the Tepee Trail Formation ranges in age from middle to late Eocene from west to east. Although this age range is long, the late Eocene age (45 m.y.) for vertebrates of the Badwater area is barely in that time range (Evernden, Savage, Curtis, and James, 1964, p. 189, KA 1024).

Wiggins Formation

The Wiggins was originally given a queried Oligocene age primarily on the basis of "large leg bones tentatively identified in the field as those of an Oligocene titanothere" (Love, 1939, p. 83), but the collection was lost before it was positively identified. Early Oligocene (Chadronian provincial age) vertebrates were found in the Wiggins Formation along Mink Creek (fig. 1) near the west edge of the volcanic field where the formation overlies Paleozoic and Mesozoic rocks (Love, 1956, p. 88). A reconnaissance traverse north and west of Pinnacle Buttes indicates that the Wiggins strata at Mink Creek are at most 300 feet stratigraphically higher than the basal Wiggins at Pinnacle Buttes (H. Smedes, oral commun., Oct. 1968). Such minor stratigraphic separation of beds of markedly different ages implies the presence of an unconformity.

In the Carter Mountain–Wood River area to the northeast (fig. 1), Wilson (1963) reported a vertebrate fauna of Eocene age from a clay bed in the Blue Point Conglomerate Member of the Wiggins Formation, whereas a K-Ar date from the associated trachytic ash indicates an age of 33.9±3.4 m.y. (Houston, 1964, table 3; written commun., Jan. 23, 1968). This anomalously young radiometric date is from slightly chloritized biotite and should be questioned in view of the conflicting vertebrate age.

Two andesite samples for radiometric dating were collected from the Wiggins Formation at Pinnacle Buttes (figs. 1, 2, 3). One sample is from a small andesite lava flow or sill at the base of the Wiggins, and the other is from a boulder within the volcanic mudflow conglomerate that overlies the lava. The K-Ar ages of hornblendes separated from these samples are similar and indicate a late Bridgerian provincial age or middle Eocene age. The data follow:

Sample No.	Mineral	K [1] (percent)	Ar^{40} moles/g$\times10^{-11}$	Radiogenic argon (percent)	Age (m.y.)
DKA–1437	Hornblende	0.546	4.53	76.5	46.2±1.8
DKA–1439	Hornblende	.506	4.22	61.8	46.5±2.3

[1] Isotope dilution anlyses; average of duplicates.

Thus, on the basis of radiometric dating of samples from the base of the formation and the presence of vertebrate fossils from stratigraphically higher parts, the Wiggins Formation ranges in age from latest middle Eocene to early Oligocene.

SUMMARY

On the basis of radiometric data, the lower part of the Wiggins at Pinnacle Buttes is latest middle Eocene in age; on the basis of fossil plants and the K-Ar dates, the underlying Tepee Trail Formation is of middle Eocene age in the Kisinger Lakes area. These findings do not invalidate a late Eocene age for the Tepee Trail or an early Oligocene age for the Wiggins elsewhere. An unconformity spanning considerable time may account for the contradictory ages at Pinnacle Buttes and Mink Creek. If the latter is true, the white and light-colored sequence of rocks overlying the typical green Tepee Trail strata is below the unconformity at Pinnacle Buttes (fig. 2). The Mink Creek fossils are derived from a similar light-colored sequence of rocks. The early Chadronian vertebrates in the Wiggins at Mink Creek and the new K-Ar dates indicate that the 4,000-foot-thick Wiggins Formation spans nearly 10 m.y. The Wiggins is a time-transgressive sequence. The occurrence of late Eocene vertebrates in the Tepee Trail Formation in the Badwater area requires a middle to late Eocene time-transgression for the upper Tepee Trail strata. The Tepee Trail and Wiggins Formations intertongue in the Togwotee Pass–Pinnacle Buttes area, and the formational contact migrates stratigraphically upward and eastward. These conclusions are summarized in figure 4 (p. B62).

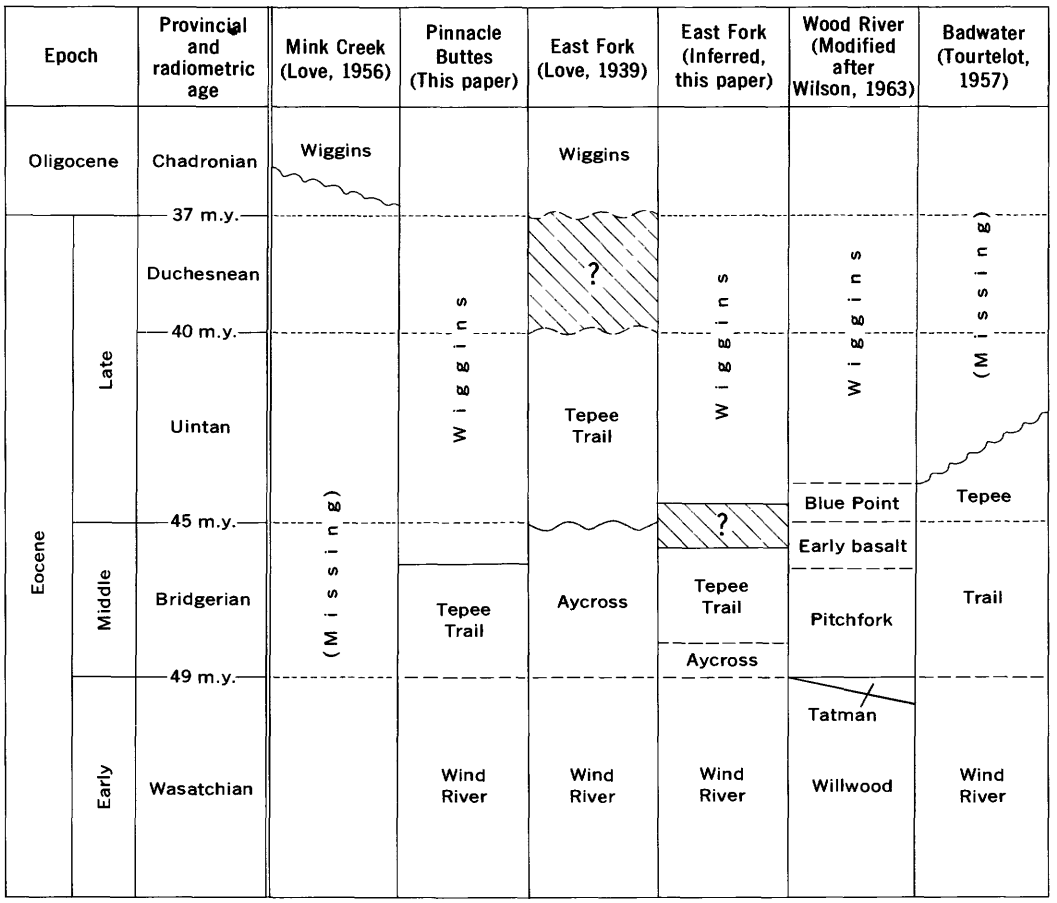

FIGURE 4.—Correlation of lower Cenozoic formations in the southern Absaroka Mountains based on fossil and radiometric ages. Radiometric ages of mammalian provincial ages are from Evernden, Savage, Curtis, and James (1964).

REFERENCES

Black, C. C., and Dawson, M. R., 1966, A review of late Eocene mammalian faunas from North America: Am. Jour. Sci., v. 264, no. 5, p. 321–349.

Evernden, J. F., Savage, D. E., Curtis, G. H., and James, G. T., 1964, Potassium-argon dates and the Cenozoic mammalian chronology of North America: Am. Jour. Sci., v. 262, no. 2, p. 145–198.

Hay, R. L., 1956, Pitchfork Formation, detrital facies of early basic breccia, Absaroka Range, Wyoming: Am. Assoc. Petroleum Geologists Bull., v. 40, no. 8, p. 1863–1898.

Houston, R. S., 1964, Non-paleontological methods of correlation of rocks of Tertiary age in Wyoming—pt. 3, The petrographic calendar: Wyoming Univ. Contr. Geology, v. 3, no. 1, p. 15–26.

Keefer, W. R., 1957, Geology of the Du Noir area, Fremont County, Wyo.: U.S. Geol. Survey Prof. Paper 294–E, p. 155–221.

Ketner, K. B., Keefer, W. R., Fisher, F. S., Smith, D. L., and Raabe, R. G., 1966, Mineral resources of the Stratified Primitive Area, Wyoming: U.S. Geol. Survey Bull. 1230–E, 56 p.

Love, J. D., 1939, Geology along the southern margin of the Absaroka Range, Wyoming: Geol. Soc. America Spec. Paper 20, 134 p.

——— 1956, Cretaceous and Tertiary stratigraphy of the Jackson Hole area, northwestern Wyoming, *in* Wyoming Geol. Assoc. Guidebook, 11th Ann. Field Conf., Jackson Hole, 1956: p. 75–94.

Rohrer, W. L., 1966, Geologic map of the Kisinger Lakes quadrangle, Fremont County, Wyoming: U.S. Geol. Survey Geol. Quad. Map GQ–527.

Tourtelot, H. A., 1957, The geology and vertebrate paleontology of upper Eocene strata in the northeastern part of the Wind River Basin, Wyoming: Smithsonian Misc. Coll., v. 134, no. 4, 27 p.

U.S. Geological Survey, 1966, Geological Survey Research 1966, Chapter A: U.S. Geol. Survey Prof. Paper 550–A, p. A77.

Wilson, W. H., 1963, Correlation of volcanic rock units in the southern Absaroka Mountains, northwest Wyoming: Wyoming Univ. Contr. Geology, v. 2, no. 1, p. 13–20.

——— 1964, Geologic reconnaissance of the southern Absaroka Mountains, northwest Wyoming—pt. 1, The Wood River–Greybull River area: Wyoming Univ. Contr. Geology, v. 3, no. 2, p. 60–77.

NEW EVIDENCE ON AGE RELATIONSHIPS OF POSSIBLE EOCENE ROCKS IN SOUTHWESTERN NORTH DAKOTA

By N. M. DENSON, Denver, Colo.

Abstract.—Stratigraphic studies in Morton, Billings, Golden Valley, Hettinger, Stark, and Slope Counties, southwestern North Dakota, indicate that generally accepted regional correlations of two stratigraphic units probably should be revised. First, a fine- to medium-grained sandstone previously correlated with the upper part of the Sentinel Butte Member of the Fort Union Formation of Paleocene age may actually be correlative with the Golden Valley Formation of early Eocene age. Second, the siliceous gray-green bentonitic siltstone and reddish brown claystone beds that unconformably overlie the Golden Valley(?) equivalent may actually be a hitherto unrecognized stratigraphic unit of late Eocene age rather than part of the White River Formation of Oligocene age as previously thought.

A relatively uniform blanketlike deposit of fine- to medium-grained brown-weathering fluviatile sandstone 150–200 feet thick caps many of the prominent buttes (Sentinel, Flattop, Saddle, Bullion, Camels Hump, and Rocky Ridge) and directly overlies important uraniferous lignite deposits in the Little Missouri River escarpment area in west-central Billings County and the northwestern part of Stark County in southwestern North Dakota (fig. 1). Most geologists, including the author, have assigned this sandstone on tenuous but permissive evidence to the Sentinel Butte Member of the Fort Union Formation of Paleocene age. The similarity, however, of the nonopaque heavy-mineral assemblages from this sandstone to those of the lower Eocene Golden Valley Formation and their marked differences from those of the underlying Fort Union Formation suggest to the author that this sandstone may be a western sandstone facies of the Golden Valley.

The nonopaque heavy-mineral assemblages from the Golden Valley Formation in secs. 8 and 11, T. 140 N., R. 90 W., 4 miles north of Hebron in Morton County, N. Dak., and from the Golden Valley(?) equivalent overlying the uraniferous deposits in the Little Missouri River escarpment area (Tps. 137–142 N., Rs. 99–100 W.; from No. 1 to No. 4, fig. 1), are characterized by the occurrence of chloritoid and blue-green hornblende. Epidote, zircon, and garnet are common constituents. By contrast, the nonopaque heavy-mineral assemblages from the underlying Sentinel Butte, Tongue River, and Ludlow Members of the Fort Union Formation locally are characterized by differing proportions of staurolite, kyanite, andalusite, tourmaline, and garnet. Chloritoid and blue-green hornblende are generally absent. Nonopaque heavy minerals are at least three times more abundant in the very fine grained sand fraction (0.062–0.125 mm) of most of the samples from the Golden Valley and its possible western sandstone correlative than in samples from the underlying Fort Union Formation. These differences indicate a marked change in the provenance of sediment during deposition of the Fort Union and Golden Valley Formations. Similar changes in sediment provenance occurred during deposition of Eocene and Paleocene rocks at many localities in the basin areas of Wyoming and Colorado (Stow, 1938, p. 157). This suggests that the blanketlike sandstone in the western part of the Williston basin, which includes the report area, is more closely allied lithologically to lower Eocene rocks than to the underlying Paleocene.

The blanketlike Golden Valley(?) sandstone rests on the stratigraphically highest lignite of the Sentinel Butte Member of the Fort Union Formation. This lignite is clearly of late Paleocene age as indicated by analyses of pollen and spores made by Harry A. Leffingwell (Union Oil Co. of California) in samples collected by the author. Three of the six carbonaceous samples yielded excellent paleontological assemblages. None of the assemblages contained Eocene index forms, and three contained species which do not range below mid-Paleocene. The carbonaceous samples studied for spore and pollen came from open-pit mines

U.S. GEOL. SURVEY PROF. PAPER 650-B, PAGES B63-B65

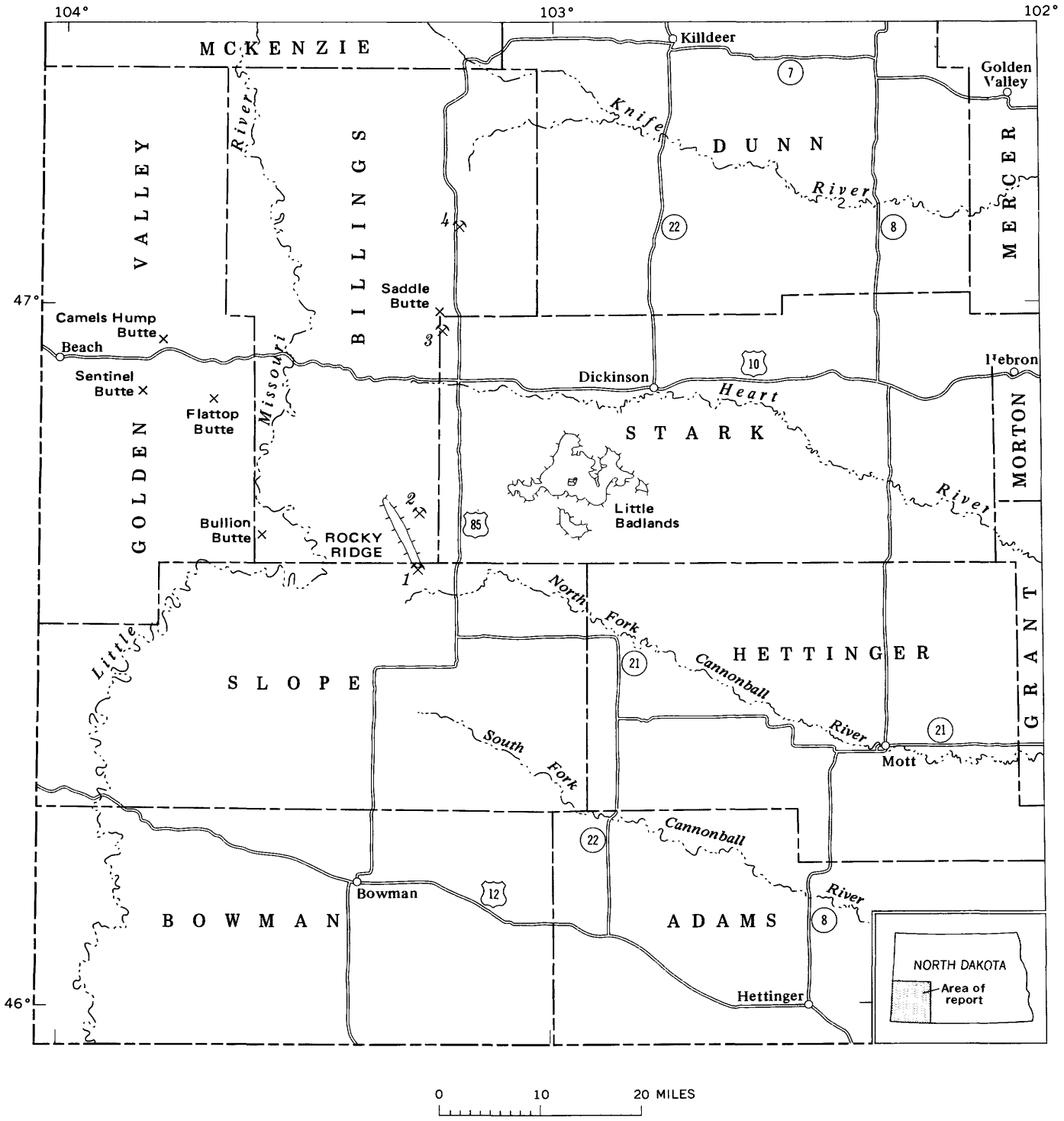

FIGURE 1.—Index map of southwest North Dakota, showing localities referred to in this report. Open-pit mines from which carbonaceous samples were taken for spore and pollen study: *1*, SE¼NW¼ sec. 5, T. 136 N., R. 100 W.; *2*, SE¼SW¼ sec. 2, T. 137 N., R. 100 W.; *3*, NW¼NE¼ sec. 7, T. 140 N., R. 99 W.; and *4*, NE¼NW¼ sec. 23, T. 142 N., R. 99 W.

in northern Slope County, eastern Billings County, and western Stark County, N. Dak. (fig. 1).

The author believes that the hard siliceous green, gray-green, and dark-gray bentonitic siltstone and reddish-brown concretionary noncalcareous claystone that unconformably overlie the blanketlike sandstone in some areas and cap some of the buttes in the Little Badlands of southwest Stark County are not the very lowest part of the White River Formation of Oligocene age as currently mapped (Benson, 1951), but that they are in reality late Eocene in age. These rocks do strikingly resemble the fossiliferous upper Eocene rocks that persist for 100 miles or more across the Granite Mountains and Bates Hole-Shirley Basin areas where locally in central Wyoming they have been incorrectly assigned to the Oligocene White River Formation (Love and others, 1955).

Further study of nonopaque heavy-mineral suites and spores in southwestern North Dakota will be necessary to corroborate the early and late Eocene age assignments suggested here. Areal mapping would assist in establishing age relationships of the rock units in the Little Missouri River escarpment area with those in the type area of the Golden Valley Formation in Mercer County, and the Little Badlands of southwest Stark County, N. Dak., where vertebrate and plant fossils clearly demonstrate the presence of rocks of early Eocene age.

Acknowledgments.—The author acknowledges, with thanks, the assistance of C. S. V. Barclay, K. Soward, and A. F. Bateman, Jr., for lithologic samples from measured stratigraphic sections of the Golden Valley Formation in Stark and Morton Counties, and H. B. Wood for samples from the thick massive sandstone directly overlying the uraniferous lignite deposits in Billings and Stark Counties, N. Dak. W. A. Chisholm identified the nonopaque heavy minerals from the Sentinel Butte Member of the Fort Union Formation, the Golden Valley Formation, and the sandstone overlying the uraniferous lignite deposits. Interpretation of field and laboratory data is the responsibility of the author.

REFERENCES

Benson, W. E., 1951, Geologic map of North Dakota southwest of the Missouri River: U.S. Geol. Survey, scale 1:500,000.

Love, J. D., Weitz, J. L., and Hose, R. K., 1955, Geologic map of Wyoming: U.S. Geol. Survey, scale 1:500,000.

Stow, M. H., 1938, Dating Cretaceous-Eocene tectonic movements in Big Horn Basin by heavy minerals: Geol. Soc. America Bull., v. 49, p. 731–762.

WHITE CLAY DEPOSITS NEAR MOUNT HOLLY SPRINGS, CUMBERLAND COUNTY, PENNSYLVANIA

By JOHN W. HOSTERMAN, Beltsville, Md.

Abstract.—In the vicinity of Mount Holly Springs are at least five deposits of white clay, all in rocks of Early Cambrian age. The only operating deposit at present is the clay pit leased by the Philadelphia Clay Co. Here, the deposit is approximately 200 feet by 1,600 feet and at least 150 feet deep. The white clay is composed of 70 percent clay, 24 percent silt, and 6 percent sand. The clay fraction is composed of kaolinite and illite in a ratio of 9:1. The white clay averages 71 percent SiO_2 and 19 percent Al_2O_3 on the pit floor but changes to 62 percent SiO_2 and 25 percent Al_2O_3 at a depth of 150 feet. Traces of alunite have been found in the deposit, indicating that the clay was probably formed in part by hydrothermal alteration.

In the vicinity of Mount Holly Springs, as many as five white clay deposits have been worked during the past 75 years. Only one of these deposits is being worked at present. This report represents a study of the mineralogical and chemical properties of the white clay in the open pit of the Philadelphia Clay Co.

These white clay deposits are composed predominantly of kaolinite and have been considered by previous workers as residuum formed by the weathering of phyllite and limestone beds. The presence of alunite in the Philadelphia Clay deposit, however, suggests that the deposits may be partly hydrothermal in origin. Also, as depth from the surface increases, the SiO_2 content decreases and the Al_2O_3 content increases, a relationship not found in a weathered profile; this further supports the probability of partial hydrothermal origin.

All the old abandoned clay deposits and the deposit of the Philadelphia Clay Co. are south and southwest of Mount Holly Springs in a narrow longitudinal valley enclosed by two parallel southwest-trending ridges (fig. 1). The ridges are composed largely of quartzite and conglomerates, and the valley is underlain by phyllites and carbonates. All these rocks are Early Cambrian in age (Stose, 1953). The two ridges, Pine Mountain and South Mountain, are the northern extension of the Blue Ridge physiographic province which extends from Pennsylvania to Georgia. The Triassic Upland of the Piedmont province lies to the southeast, and the Cumberland Valley of the Ridge and Valley province lies to the northwest.

HISTORY OF THE DEPOSITS

White clay deposits in the South Mountain area have been mined intermittently since about 1890, but no accurate production data are available. The clay was probably first recognized in the mid-1890's by prospectors looking for iron ore. Between 1890 and 1910, at least five companies mined clay in the area. Four of these companies had facilities for beneficiating the clay, which was then sold to paper mills for use as a paper filler. One company in Mount Holly Springs used the raw clay for making cream to light-buff brick (Stose, 1907, p. 330). By 1930, however, only two companies were mining clay: the Philadelphia Clay Co. had a 100-ton daily capacity mill for washing and drying clay, and the Medusa Portland Cement Co. was mining and shipping raw clay for use as a whitener in portland cement (Leighton, 1934, p. 13). In 1967, the Philadelphia Clay Co. was the only producer of clay. This company, with modern earth-moving equipment, has changed from underground mining to open-pit mining and is currently producing about 40,000 tons of raw clay a year. The clay is trucked to York and used in making hydraulic white cement.

GEOLOGY OF THE DEPOSITS

The geological and structural setting of the white clay deposits is not completely known because of the scarcity of bedrock exposures and the poorly known lithology of the Tomstown Formation. According to Stose (1953), (1) South Mountain is an anticlinal

U.S. GEOL. SURVEY PROF. PAPER 650-B, PAGES B66-B72

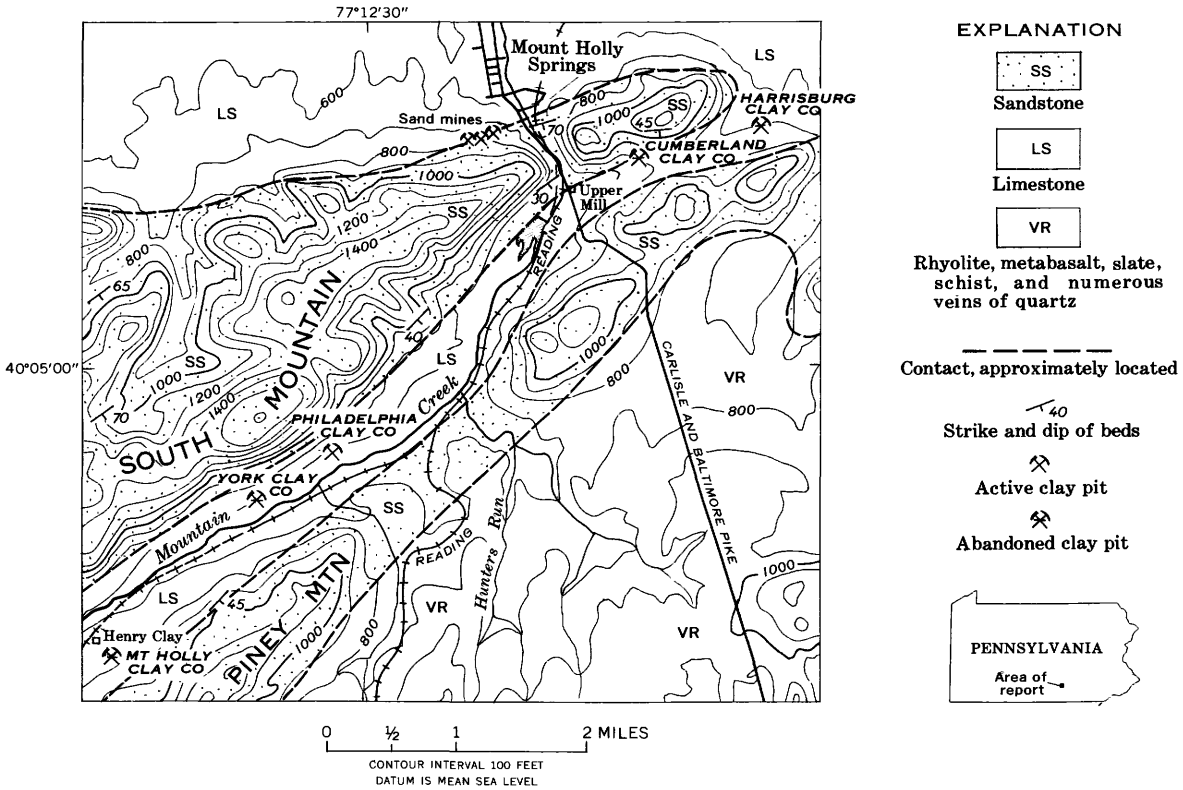

FIGURE 1.—Generalized geologic map showing location of clay deposits near Mount Holly Springs, Cumberland County, Pa. (from Stose, 1907, p. 327).

mountain underlain by Antietam Quartzite on the flanks and the Montalto Quartzite Member of the Harpers Schist in the core; (2) Piney Mountain is a homoclinal mountain composed of Antietam Quartzite, the Montalto Quartzite Member of the Harpers Schist, and Weverton Quartzite; and (3) the longitudinal valley of Mountain Creek is a synclinal one underlain by the Tomstown Formation. Freedman (1967) agrees, in general, with Stose's geologic map, but he has made two major changes in the area of the clay deposits. He believes that the quartzite underlying South Mountain is the Montalto Member of the Harpers Formation instead of the Antietam Quartzite and that there is a major fault along the southeast-facing slope of South Mountain. This fault is steeply dipping and has a relative upward movement on the northwest side. The phyllite beds exposed in the Philadelphia Clay Co. pit are tightly folded and contorted and do not form a simple syncline.

In the type locality, the Tomstown has been changed to Formation because the unit, formally called dolomite, consists of many different lithologic units. The Tomstown Formation in this area is composed of thick-bedded, dense bluish-gray dolomite, light-gray thin-bedded limestone, and light-gray phyllite. The dolomite forms a thick reddish-brown residuum composed of kaolinite and illite; the limestone weathers to a sticky yellow clay consisting of illite and kaolinite; and the phyllite weathers to a variegated silty clay containing predominantly kaolinite and some illite.

GEOLOGY OF THE PHILADELPHIA CLAY CO. DEPOSIT

All the clay deposits in the Mount Holly Springs area undoubtedly have the same geologic environment. The deposits are in the phyllite member of the Tomstown Formation, and all the deposits are about the same distance from the quartzite of the Montalto Member. Although Stose (1953) shows this contact to be normal, evidence in the Philadelphia Clay Co. clay pit, which is the only one accessible for study, indicates that it is a fault contact. This fault is probably the principal reason for the formation of these deposits.

The white clay deposit of the the Philadelphia Clay Co. is lens shaped, measuring approximately 200 feet in width at its maximum breadth and 1,600 feet in length (fig. 2); its vertical extent at depth is unknown. The northern boundary of the deposit, where it is in fault contact with the quartzite of the Montalto Member, is sharp and straight. The southern boundary is gradational, the white clay grading into

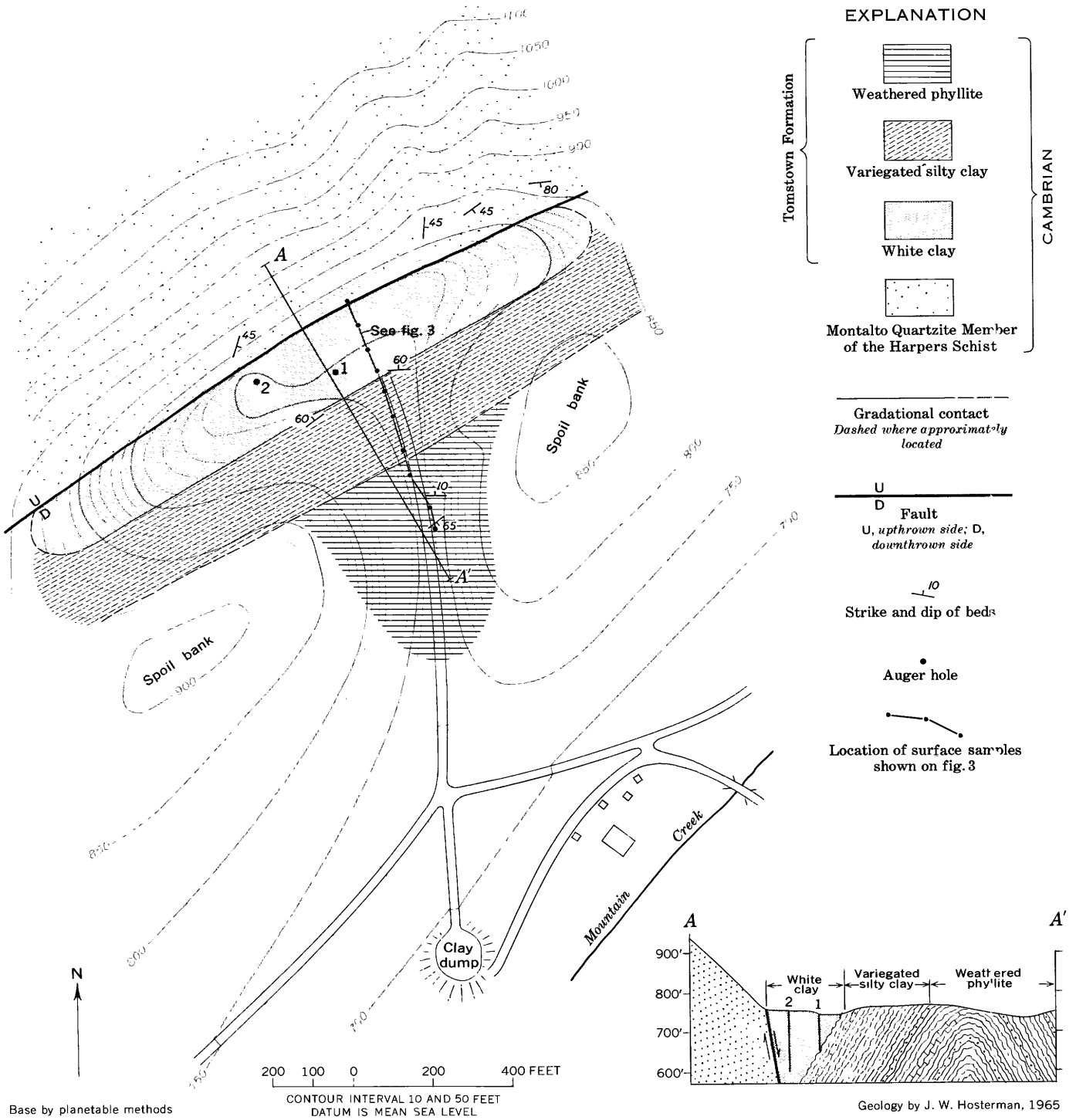

FIGURE 2.—Geologic map and section of the white clay deposit leased by the Philadelphia Clay Co. near Mount Holly Springs, Cumberland County, Pa.

yellow, pink, red, and brown silty clay. This varicolored silty clay, which is about 200 feet wide, grades into grayish-green to light-gray phyllite and calcite-veined limy phyllite of the Tomstown Formation.

Two auger holes were drilled in the floor of the pit (fig. 2). Auger hole 2 penetrated white clay for its entire length of 150 feet. Auger hole 1 penetrated white clay for a depth of 80 feet, then variegated silty clay. When the variegated silty clay contact was connected with the same contact at a depth of 80 feet in auger hole 1 (fig. 2), this contact was found to have an approximate dip of 60°. The contact does not follow the bedding planes, except locally. Assuming that the contact between the white clay and the variegated clay dips 60° NW., the white clay deposit probably wedges out against the steeply dipping fault contact at about 300 feet below the level of the pit floor (see section *A–A′*, fig. 2). The Montalto Quartzite Member along the southeast-facing steep slope of South Mountain dips 45° to 80° SE. Bedding in the white clay is not distinguishable because open-pit mining has exposed only clay that has been disturbed by previous underground mining. Adjacent to the white clay, the variegated silty clay, although very contorted, has an average dip of 60° N. This can be seen by following the thin sandy beds. The haulageway exposed an anticline in the somewhat weathered phyllite of the Tomstown Formation about 350 feet south of the white clay.

MINERALOGY AND CHEMISTRY OF THE DEPOSIT

The white clay, variegated silty clay, and weathered phyllite show progressive differences in particle-size content, clay-mineral ratio, and SiO_2 and Fe_2O_3 content (based on X-ray fluorescence analyses), as presented in table 1. In the white clay, sand and silt decrease and clay increases slightly with depth; at a depth of 100 feet below the pit floor, the clay content increases to 72 percent, and at a depth of 150 feet, the clay content is 74 percent. The sand and silt fractions of the white clay are composed chiefly of quartz and trace amounts of muscovite, hematite, and limonite. The sand and silt fractions of the variegated silty clay are composed of fine-grained quartz with hematite and limonite. The sand and silt fractions of the slightly weathered phyllite are composed of fine-grained quartz with a little muscovite, biotite, and magnetite. Some of the phyllite contains limy beds and calcite veins.

Hosterman (1969) describes how the samples were prepared for determining the partial chemical composition by X-ray fluorescence methods. The method is not as accurate as the wet-chemical method but was found to be accurate to within 10 percent of the amount of oxide present. Rose and others (1962, 1964) have described more complicated sample preparation procedures that give more accurate results.

The SiO_2 content in the rocks at the surface decreases from white clay through the variegated silty clay to the weathered phyllite, whereas both the Fe_2O_3 and K_2O contents increase. The Al_2O_3 content varies only a few percent without any discernible trend except for a slight decrease from the variegated silty clay into the weathered phyllite. The TiO_2 content remains constant (fig. 3). In addition to these chemical variations, the following mineralogical changes take place: kaolinite is most abundant in the white clay and least abundant in the phyllite; illite is least abundant in the white clay and most abundant in the phyllite. The differences in chemical and mineralogical composition may be due to weathering, but they may also be due to differences in the lithology. The Al_2O_3 content does not change very much as a result of either weathering or bulk lithology because the abundance of Al_2O_3 in naturally occurring illite can be almost as high as it is in kaolinite (Grim, 1953, p. 272).

The nature and attitude of the southern boundary of the white clay deposit are obtained from the chemical and mineralogical data obtained from auger hole 1. The vertical hole (fig. 4) was drilled within the white clay deposit approximately 60 feet from the contact with the variegated silty clay (fig. 2). The high SiO_2 and low Al_2O_3 content of the first sample is due to contamination from both quartzite and the variegated silty clay washed into the clay pit from the nearby spoil bank. The samples taken at 10- and 20-foot intervals are slightly higher in silt content

TABLE 1.—*Particle-size content, clay-mineral ratios, and content of* SiO_2, Al_2O_3, *and* Fe_2O_3 *in clay from the Philadelphia Clay Co. deposit*

	No. of samples	Sand	Silt (weight percent)	Clay	Clay-mineral ratios			SiO_2	Al_2O_3 (weight percent)	Fe_2O_3
					Kaolinite	Illite	Montmorillonite			
White clay	30	6	24	70	9	1	-------	71	19	0.4
Variegated silty clay	3	5	34	61	8	2	Trace	66	19	2.2
Weathered phyllite	5	7	33	60	1	7	2	56	18	6.3

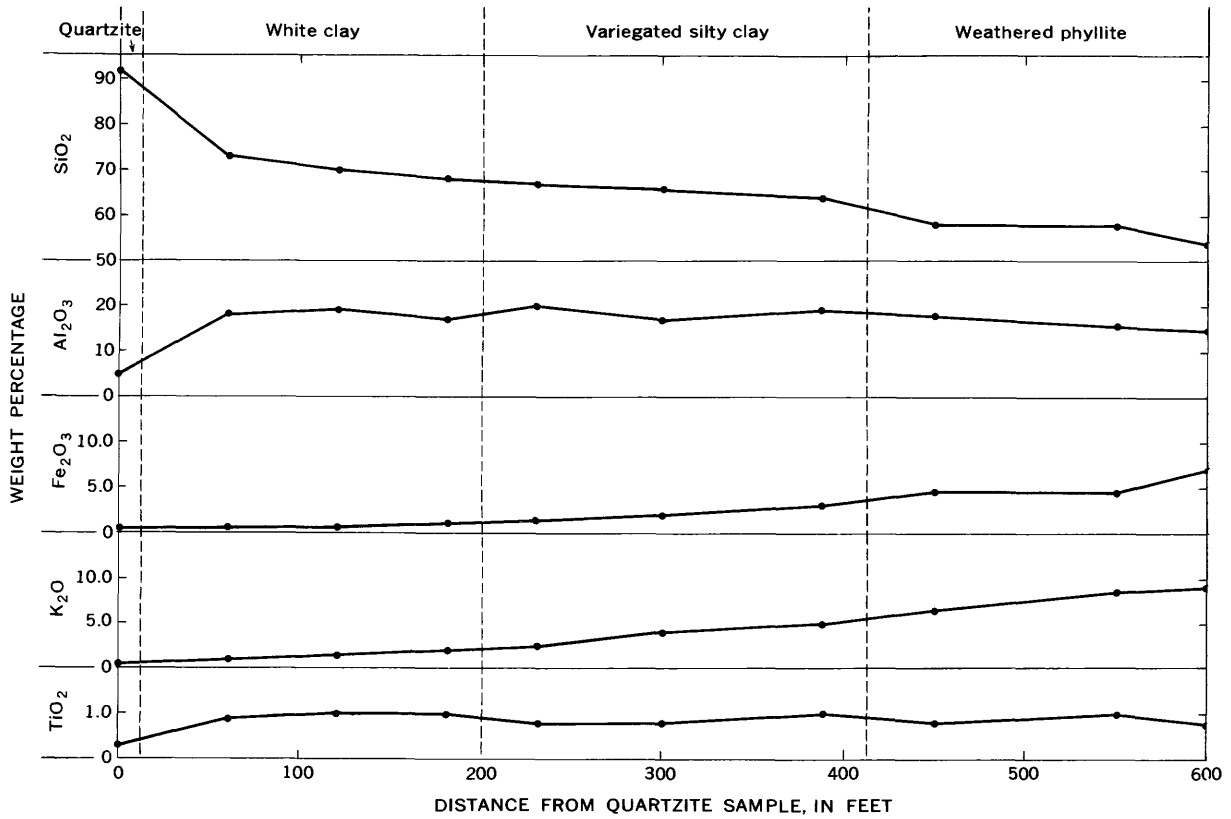

FIGURE 3.—Chemical differences between surface samples of quartzite, white clay, variegated silty clay, and weathered phyllite. Chemical analyses by X-ray fluorescence.

than the average white clay; therefore, the SiO_2 content is higher and the Al_2O_3 content is lower than the average-grade white clay. At a depth of 80 feet, the hole penetrated variegated silty clay. The boundary between the two clays is placed where there is a marked color change from white (*N*9)[1] and yellowish white (10*YR*9/1) to weak orange pink (5*YR*7/2 and 10*R*7/2). At this boundary, the Al_2O_3 content decreases markedly, and in the Fe_2O_3 and K_2O contents increases as compared with the 50 feet of white clay above it. The SiO_2 content, however, remains fairly constant, indicating no increase in the amount of sand and silt present. In addition, illite increases and kaolinite decreases. The kaolinite-illite ratio above 80 feet is 9:1 and below is 8:2. Traces of alunite were observed between 30 and 80 feet. These color, chemical, and mineralogical changes at a depth of 80 feet indicate that the white-clay-variegated silty clay contact dips approximately 60° N.

[1] Color designations are based on the "Munsell Soil Color Chart" (Munsell Color Co., 1964).

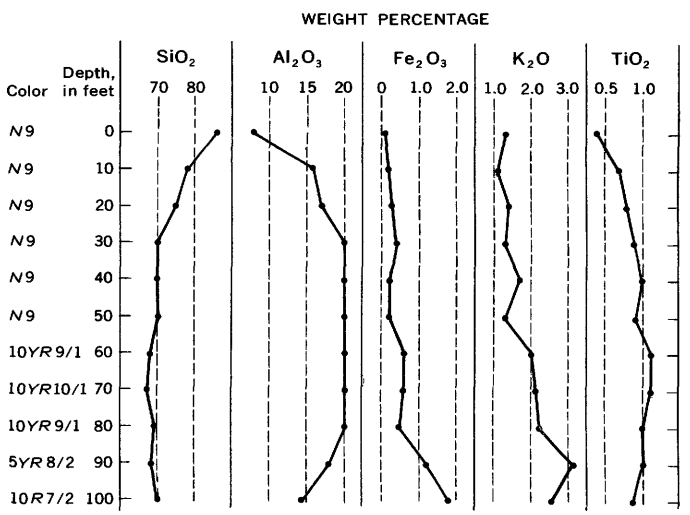

FIGURE 4.—Chemical and color changes of the white clay with depth in auger hole 1. Chemical analyses by X-ray fluorescence.

The chemical and mineralogical data obtained from auger hole 2 indicate that the Philadelphia Clay Co. deposit was not formed exclusively by weathering processes. Auger hole 2 was drilled vertically in white clay approximately 145 feet from the variegated silty clay contact (fig. 2). The high SiO_2 and low Al_2O_3 content (fig. 5) of the surface samples is possibly due to quartz contamination resulting from blasting and stripping of the Montalto Quartzite Member on the mountain slope above the clay pit. From 10 to 150 feet, the SiO_2 decreases from 72 to 62 percent, the Al_2O_3 increases from 18 to 25 percent, the Fe_2O_3 and

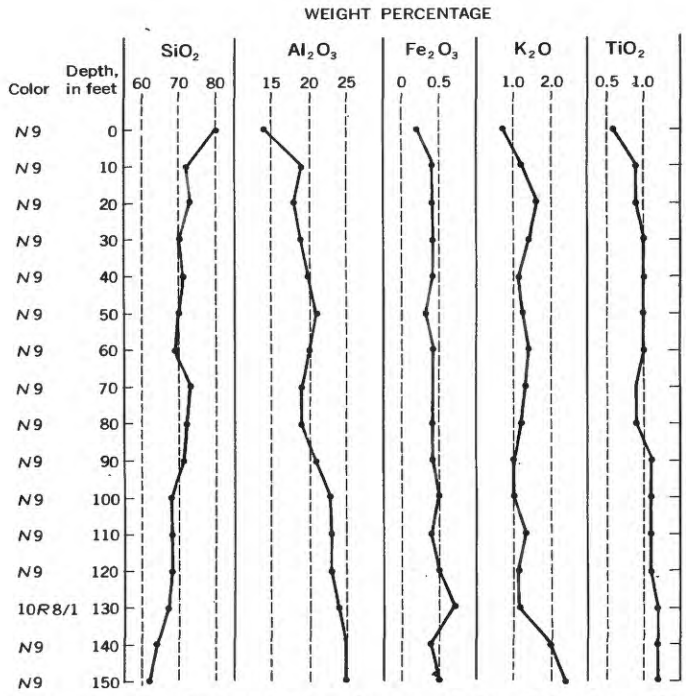

FIGURE 5.—Chemical and color changes of the white clay with depth in auger hole 2. Chemical analyses by X-ray fluorescence.

TiO_2 are relatively constant, and the K_2O is constant down to 130 feet but increases from 1.1 to 2.4 percent below 130 feet. The kaolinite-illite ratio is greater than 9:1, and the color, except for one, is white (*N*9) in all 16 samples examined. Alunite occurs in trace amounts from 40 to 130 feet and in slightly more than trace amounts from 130 to 150 feet. The only observed change in bulk lithology of the white clay from 10 to 150 feet is an increase in clay content from 70 to 74 percent. The silt content decreases from 25 to 21 percent, and the sand content is 5 percent throughout. Thus, the 5-percent increase in the amount of clay does not account for the almost 33-percent increase in $A1_2O_3$ content. The steady increase of Al_2O_3 with depth and the striking complementary SiO_2 cannot be attributed solely to differences in lithology. This increase in Al_2O_3 content with depth, however, is the reverse of the change normally observed in a weathering profile (Hosterman and others, 1960, p. 13).

ORIGIN OF THE DEPOSITS

The clay deposits in the vicinity of Mount Holly Springs could have been formed as residual clay or as hydrothermal clay deposits. The origin of the deposits by weathering was first proposed by Stose (1907, p. 323). Chemical and mineralogical evidence presented in this paper, however, suggests that these clay deposits were formed, at least in part, by hydrothermal alteration.

The surface relations suggest that the white clay deposit is a residuum formed through weathering of an argillaceous sediment. Surface waters with a high oxygen content drained from the mountain slope and penetrated the phyllite along fractures created by faulting and along bedding planes. Iron and potassium were leached from the phyllite so that illite was altered to kaolinite. The ions were carried away in solution, leaving a residual deposit of white kaolinitic clay. The iron, derived in part from the illite, but chiefly from magnetite, was precipitated from solution when the slightly acid ground water permeated the sandy carbonate beds of the Tomstown Formation. Thus, the iron ore deposits in this area, mined during the mid-19th century, were formed by supergene enrichment and are probably similar in origin to those in Virginia described by Lesure (1957, p. 98). A capping of gravel derived from the Montalto Quartzite Member has preserved these white clay deposits from being eroded away during the development of the Mountain Creek Valley.

The theory proposed by the author is that these clay deposits formed as a result of hydrothermal alteration modified by later weathering or katamorphic alteration. The occurrence of alunite, a low-temperature hydrothermal mineral (Parker, 1954, p. 42), in minor amounts has been confirmed by X-ray diffraction, differential thermal analysis, and by electron microscope examination (fig. 6). The alteration, indicated by the presence of alunite and increase in Al_2O_3 content, is more prevalent at depth than at the surface. The fault zone bordering the clay deposit provided the passageway for the ascending hydrothermal solutions.

The chemical analysis, particularly the Al_2O_3 content of auger hole 2 (fig. 5), supports the evidence of hydrothermal origin and does not support the theory that the white clay was formed exclusively as a residuum as a result of katamorphic alteration. In most weathering environments involving katamorphic alteration, SiO_2, Fe_2O_3, and K_2O are leached, whereas the Al_2O_3 increases gradationally upward from the parent material to the residual product. If the white clay is considered to be the weathered product, the variegated silty clay the intermediately weathered product, and the phyllite the parent material, then there has been normal leaching of Fe_2O_3 and K_2O both laterally and vertically, but the SiO_2 and Al_2O_3 content are the reverse of a normal weathering profile. In auger hole 2, the silt content decreases with depth from 25 percent to 20 percent; this could account for most of the decrease in SiO_2 content, which is 72 percent at 10 feet and 67 percent at 130 feet (fig. 5). Conversely,

FIGURE 6.—Electron microscope photograph of kaolinite aggregate (top) and alunite crystal (bottom) in clay sample from the 40- to 50-foot interval of auger hole 1. Photograph by E. J. Dwornik, U.S. Geological Survey.

however, the increase with depth in the amount of clay from 70 percent to 74 percent does not account for the increase in Al_2O_3 content from 18 percent at 10 feet to 25 percent at 150 feet. This represents a 5-percent increase in clay and a 33-percent increase in Al_2O_3. Alunite, $KAl_3(OH)_6(SO_4)_2$, accounts for part of this increase because it occurs only in trace amounts. The additional Al_2O_3 content could be attributed to the presence of allophane, which is amorphous to X-ray detection and almost impossible to identify by differential thermal analysis in the presence of kaolinite. Kaolinite, the most abundant mineral present, can be formed by either hydrothermal alteration or by katamorphic alteration.

The chemical and mineralogical evidence indicates that the white clay deposits near Mount Holly Springs were probably formed by hydrothermal alteration. The surface features, the presence of supergene iron ore deposits, and the weathered phyllite indicate that katamorphic alteration occurred after hydrothermal alteration.

REFERENCES

Freedman, Jacob, 1967, Geology of a portion of the Mount Holly Springs quadrangle, Adams and Cumberland Counties, Pennsylvania: Pennsylvania Geol. Survey, 4th ser., Prog. Rept. 169, 66 p.

Grim, R. E., 1953, Clay mineralogy: New York, McGraw-Hill, 384 p.

Hosterman, J. W., 1969, Clay deposits of Spokane County, Washington: U.S. Geol. Survey Bull. 1270. [In press]

Hosterman, J. W., Scheid, V. E., Allen, V. T., and Sohn, I. G., 1960, Investigations of some clay deposits in Washington and Idaho: U.S. Geol. Survey Bull. 1091, 147 p.

Leighton, Henry, 1934, The white clays of Pennsylvania: Pennsylvania Topog. and Geol. Survey Bull. 112, 19 p.

Lesure, F. G., 1957, Geology of the Clifton Forge iron district: Virginia Polytech. Inst. Bull. Eng. Expt. Sta. Ser., no. 118, 130 p.

Munsell Color Company, 1954, Munsell soil color chart: Baltimore, Md., Munsell Color Co., Inc.

Parker, R. L., 1954, Alunite alteration at Marysvale, Utah: U.S. Geol. Survey open-file report, 114 p.

Rose, H. J., Jr., Adler, Isidore, and Flanagan, F. J., 1962, Use of La_2O_3 as a heavy absorber in the X-ray fluorescence analysis of silicate rocks: Art. 31 *in* U.S. Geol. Survey Prof. Paper 450–B, p. B80–B82.

Rose, H. J., Jr., Cuttitta, Frank, Carron, M. K., and Brown, Robena, 1964, Semimicro X-ray fluorescence analysis of tektites using 50-milligram samples: Art. 157 *in* U.S. Geol. Survey, Prof. Paper 475–D, p. D171–D173.

Stose, G. W., 1907, White clays of South Mountain, Pennsylvania: U.S. Geol. Survey Bull. 315–I, p. 322–334.

——— 1953, Geologic map of the Carlisle quadrangle, Pennsylvania: U.S. Geol. Survey Geol. Quad. Map GQ–28.

POSSIBLE EXPLORATION TARGETS FOR URANIUM DEPOSITS, SOUTH END OF THE URAVAN MINERAL BELT, COLORADO-UTAH

By DANIEL R. SHAWE, Denver, Colo.

Work done in cooperation with the U.S. Atomic Energy Commission

Abstract.—Uranium deposits in Mesozoic sandstone at and near the south end of the Uravan mineral belt, Colorado–Utah, show a preferred association with zones of faults and folds. Here many large deposits in the Salt Wash Member of the Morrison Formation of Late Jurassic age occur near faults associated with collapsed salt anticlines. Unexplored areas within the belt, where favorable strata may exist near faults, are on the northeast side of Disappointment Valley 5 miles east of Slick Rock, Colo., and in a zone extending from Montezuma Canyon, Utah, to the Dolores River Canyon, Colo. Deposits in the Moss Back Member of the Chinle Formation of Late Triassic age are very large and widespread along the Lisbon Valley fault, Utah, and are related to a closed anticlinal structure. Worthy of exploration is another area where favorable host rocks likely occur in a closed anticlinal structure near faults in the vicinity of the Dolores River Canyon, 10 miles northeast of Dove Creek.

Economically important amounts of uranium have been produced from the Salt Wash Member of the Morrison Formation of Late Jurassic age and the Moss Back Member of the Chinle Formation of Late Triassic age in and near the Uravan mineral belt, Montrose, San Miguel, and Dolores Counties, Colo., and adjacent San Juan County, Utah. In the south part of the mineral belt, the area shown in figure 1, most production from the Salt Wash Member has come from the uppermost sandstone stratum, called the "ore-bearing sandstone." Where uranium ore has been mined, the ore-bearing sandstone is thick (generally more than 50 feet) and laterally extensive and it contains abundant carbonaceous plant material. Most production from the Chinle Formation has come from similarly thick and carbonaceous sandstone channel-fill layers in the lower part of the Moss Back Member at the base of the Chinle in the area of Lisbon Valley, Utah.

The uranium deposits in both the Salt Wash and the Moss Back show a strong tendency to be spatially associated with anticlines or fault zones. This strong association suggests that areas of anticlines and faults where uranium deposits are not known but where favorable host strata are likely to occur are worthy of exploration for undiscovered uranium deposits. Regardless of the multiple geologic factors that influenced localization of deposits, possibly of different ages and in different hosts, the apparent structural control suggests merit in this pragmatic approach to exploration. Three structurally favorable areas where host sandstone layers may occur are described.

Area 1 is in Disappointment Valley, San Miguel County, Colo., 5 miles northeast of Slick Rock (fig. 1), where numerous holes drilled by the U.S. Geological Survey in the mid-1950's penetrated favorable ore-bearing sandstone (Rogers and Shawe, 1962). Although few of these holes were mineralized, it is reasonable to surmise that mineralized ground occurs north and northeast of the drilled holes, and closer to the zone of faults bounding the southwest edge of the collapsed Gypsum Valley anticline. Drilling depths to penetrate the ore-bearing sandstone are a maximum of about 1,200 feet in the vicinity of the previously drilled holes, and they decrease rapidly northward.

Area 2 is part of a large area of mainly unexplored ground between the deposits exposed in Montezuma Canyon (Huff and Lesure, 1965) and those mined in the vicinity of Slick Rock farther northeast. Ore-bearing sandstone in the Salt Wash Member 5 miles west of Egnar, Colo., in the vicinity of the Deremo mine, is thick and extensive, and therefore favorable. If the favorable sandstone here extends southward to the vicinity of the zone of faults trending N. 75° E.

U.S. GEOL. SURVEY PROF. PAPER 650-B, PAGES B73–B76

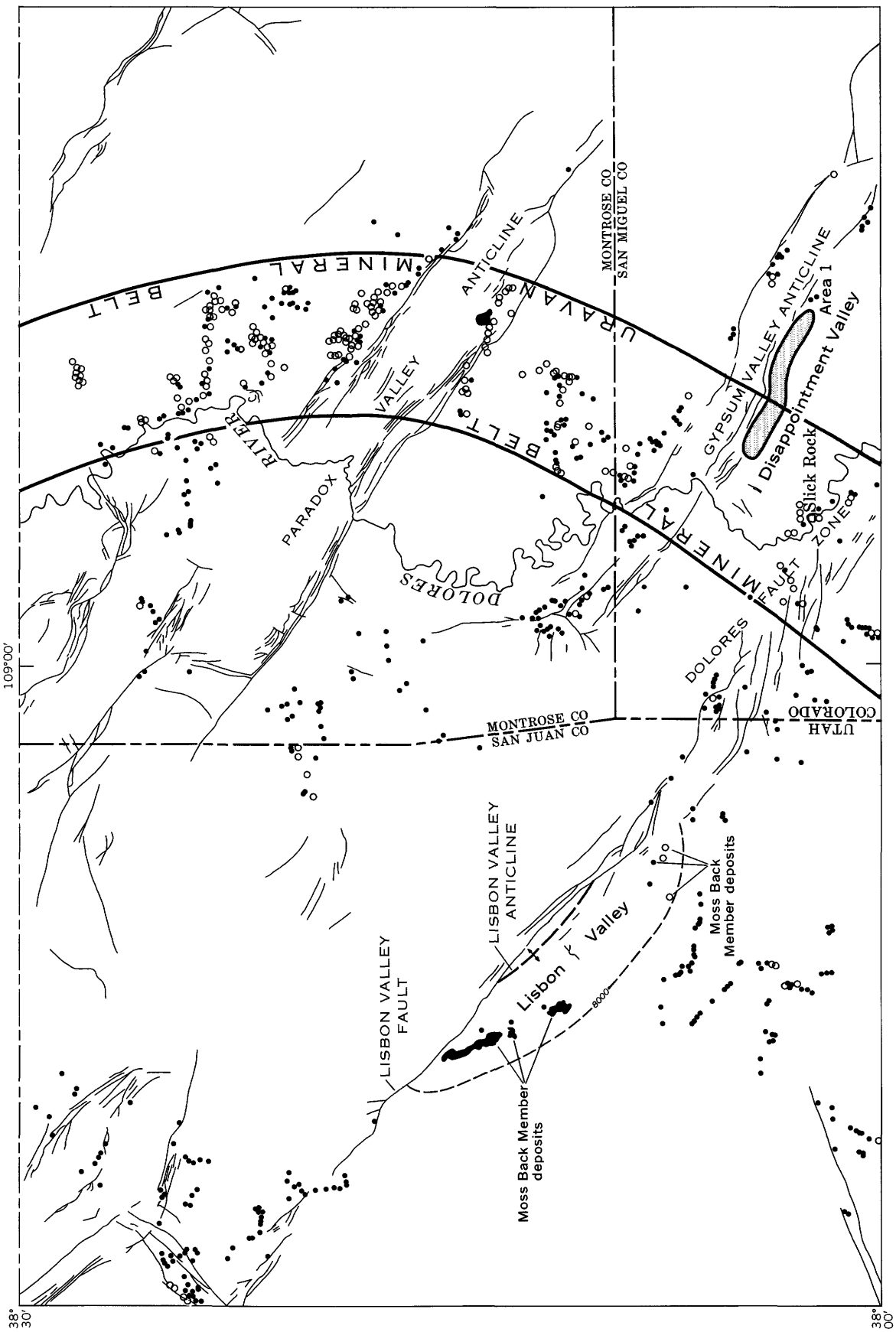
MINERAL BELT
JURAVAN BELT
ANTICLINE
MONTROSE CO
SAN MIGUEL CO
GYPSUM VALLEY ANTICLINE
Area 1
Disappointment Valley
Slick Rock
ZONE
FAULT
RIVER
VALLEY
PARADOX
DOLORES
MONTROSE CO
SAN JUAN CO
UTAH
COLORADO
LISBON VALLEY ANTICLINE
Lisbon Valley
Moss Back Member deposits
LISBON VALLEY FAULT
Moss Back Member deposits
8000
109°00'
38°30'
38°00'

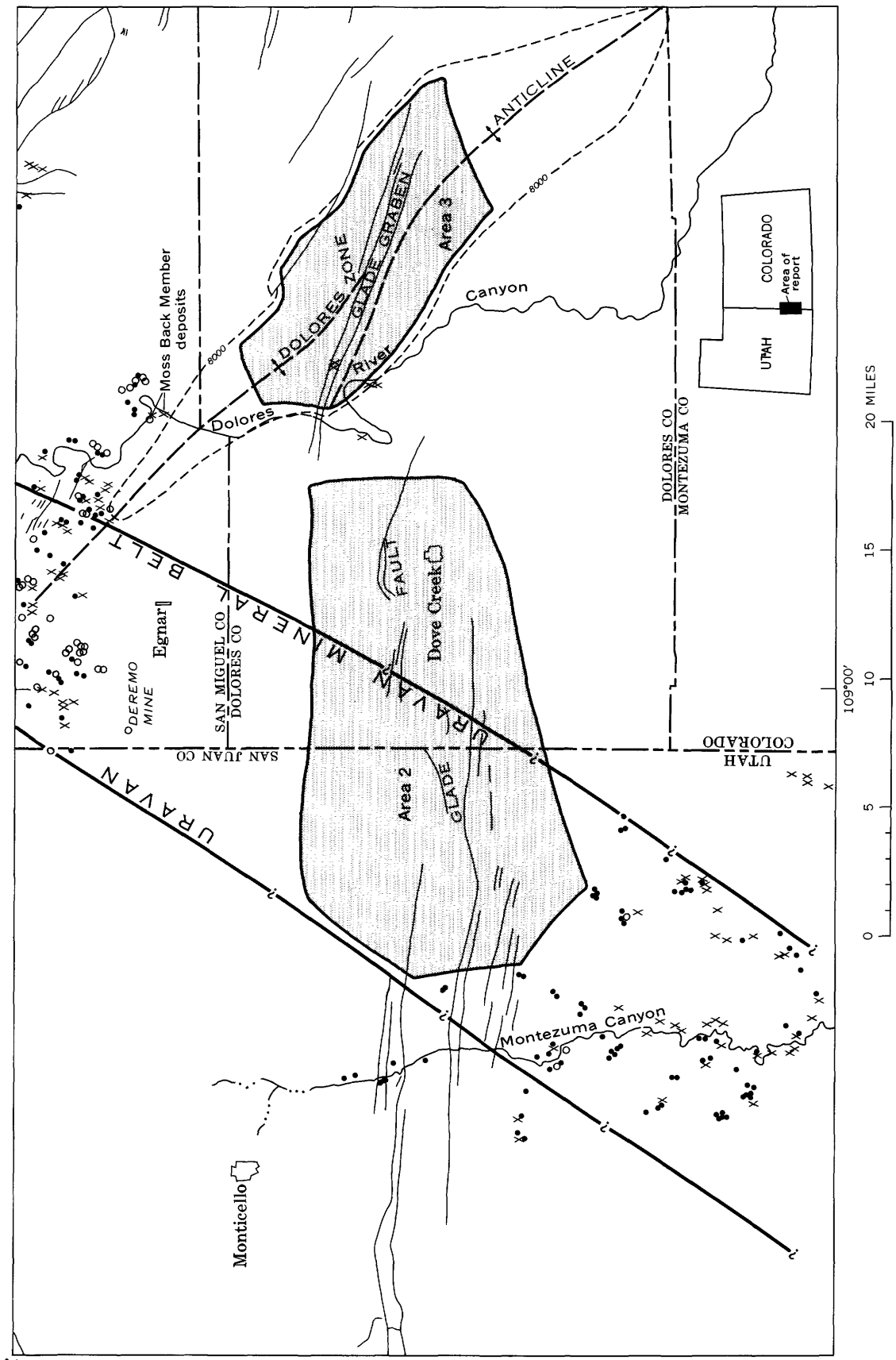

FIGURE 1.—Map showing uranium deposits, faults, and unexplored areas of possibly favorable ground near the south end of the Uravan mineral belt, Colorado-Utah. Compiled from Williams (1964) and D. D. Haynes, J. D. Vogel, and D. G. Wyant (written commun., 1968). Limits of Uravan mineral belt from Fischer and Hilpert (1952).

328-687 O—69——6

from Montezuma Canyon to the Dolores River Canyon (Glade fault zone, Shawe and others, 1959), large deposits like those centered on the Dolores fault zone in the vicinity of Slick Rock may occur in it. Interpretations concerning the deposition of favorable sandstone in the Uravan mineral belt (Shawe, 1962) suggest that this sandstone may extend into the area. Drilling depths to the target horizon are estimated to be about 750 feet.

Area 3, in the vicinity of the Glade graben where the Dolores anticline shows structural closure, should be worthy of exploration for uranium deposits in the Moss Back Member. Much uranium ore has come from mines in sandstone strata of the Moss Back Member of the Chinle Formation of Late Triassic age in the vicinity of the Lisbon Valley fault, Utah (Steen and others, 1953; Lekas and Dahl, 1956; Weir and Puffett, 1960). Ore is known in the Moss Back Member on the northeast side of the Lisbon Valley fault, but it is not shown on figure 1 because none has yet been produced there. Structure contours are closed around the Lisbon Valley anticline here, and the close correspondence of ore distribution and contours indicates an anticlinal structural control (fig. 1). Southeast of the Lisbon Valley district small uranium deposits are known in the Moss Back Member in the Dolores River Canyon near the southeastern terminus of the Dolores fault zone (Shawe and others, 1959). The deposits here lie along the axis of the Dolores anticline, and occur in thick parts of the Moss Back Member which appear to have wide extent as channellike deposits of sandstone in which carbonaceous plant material is abundant (Shawe and others, 1968, fig. 13). Abnormally high radioactivity at the base of the Moss Back is widespread in this area. Because the source area of the Moss Back has been interpreted as southeast of Slick Rock (Stewart and others, 1959), possibly favorable sandstone strata in the Moss Back lie beneath deep cover southeast of the exposures in the Dolores River Canyon. Drilling depths to penetrate the Moss Back range from a few hundred feet in the bottom of Dolores River Canyon just south of the Glade graben to at least 2,000 feet a few miles farther east.

REFERENCES

Fischer, R. P., and Hilpert, L. S., 1952, Geology of the Uravan mineral belt [Colorado Plateau]: U.S. Geol. Survey Bull. 988–A, p. 1–13.

Huff, L. C., and Lesure, F. G., 1965, Geology and uranium deposits of Montezuma Canyon area, San Juan County, Utah: U.S. Geol. Survey Bull. 1190, 102 p.

Lekas, M. A., and Dahl, H. M., 1956, The geology and uranium deposits of the Lisbon Valley anticline, San Juan County, Utah, *in* Intermountain Assoc. Petroleum Geologists 7th Ann. Field Conf., 1956: p. 161–168.

Rogers, W. B., and Shawe, D. R., 1962, Exploration for uranium-vanadium deposits by U.S. Geological Survey 1948–56 in western Disappointment Valley area, Slick Rock district, San Miguel County, Colorado: U.S. Geol. Survey Mineral Inv. Field Studies Map MF–241, 3 sheets.

Shawe, D. R., 1962, Localization of the Uravan mineral belt by sedimentation: Art. 62 *in* U.S. Geol. Survey Prof. Paper 450–C, p. C6–C8.

Shawe, D. R., Archbold, N. L., and Simmons, G. C., 1959, Geology and uranium-vanadium deposits of the Slick Rock district, San Miguel and Dolores Counties, Colorado: Econ. Geology, v. 54, no. 3, p. 395–415.

Shawe, D. R., Simmons, G. C., and Archbold, N. L., 1968, Stratigraphy of Slick Rock district and vicinity, San Miguel and Dolores Counties, Colorado: U.S. Geol. Survey Prof. Paper 576–A, 104 p.

Steen, C. A., Dix, G. P., Jr., Hazen, S. W., Jr., and McLellan, R. R., 1953, Uranium-mining operations of the Utex Exploration Co. in the Big Indian district, San Juan County, Utah: U.S. Bur. Mines Inf. Circ. 7669, 13 p.

Stewart, J. H., Williams, G. A., Albee, H. F., and Raup, O. B., 1959, Stratigraphy of Triassic and associated formations in part of the Colorado Plateau region: U.S. Geol. Survey Bull. 1046–Q, p. 487–576.

Weir, G. W., and Puffett, W. P., 1960, Similarities of uranium-vanadium and copper deposits in the Lisbon Valley area, Utah-Colorado, U.S.A.: Internat. Geol. Cong., 21st, Copenhagen, 1960, Rept., pt. 15, p. 133–148.

Williams, P. L., compiler, 1964, Geology, structure, and uranium deposits of the Moab quadrangle, Colorado and Utah: U.S. Geol. Survey Misc. Geol. Inv. Map I–360, 2 sheets.

HYDRAULIC EQUIVALENCE OF MINERALS WITH A CONSIDERATION OF THE REENTRAINMENT PROCESS

By NEIL S. GRIGG and R. E. RATHBUN, Fort Collins, Colo.

Abstract.—The concept of hydraulic equivalence has evolved to mean that grains having equal fall velocity tend to be of equivalent hydraulic value. However, calculations based on standard fall-velocity relations and Shields' criterion for critical shear stress suggest that grains having the same fall velocity but different specific gravities will require different shear stresses for initiation of motion. These calculations suggest for grains moving in traction, subject to continuous deposition and reentrainment, that equal fall velocity alone should not be a sufficient criterion to assure that the grains will be of equivalent hydraulic value.

In studies of sedimentation, the term "hydraulic equivalence" is used to describe the tendency of grains of different minerals to be deposited together. The origination of the concept of hydraulic equivalence generally is attributed to Rubey (1933a) and Rittenhouse (1943). Rubey used the idea of equal fall velocities to calculate the size distributions of magnetite and tourmaline which theoretically would be deposited with the different sizes of quartz. Rittenhouse formally defined hydraulic equivalence as the concept that a given set of hydraulic conditions will permit deposition of grains of equivalent hydraulic value. Although both Rubey and Rittenhouse pointed out that many factors in addition to fall velocity are important in determining the sizes of different minerals deposited together, the concept of hydraulic equivalence gradually has assumed the connotation that grains having equal fall velocity tend to be of equivalent hydraulic value.

It is recognized (Simons and Richardson, 1966) that fall velocity is one of the principal variables in determining the behavior of fluvial sediments. However, mineral grains undergo many cycles of deposition and reentrainment before becoming a part of an alluvial, estuarine, or littoral deposit, and particles deposited together may not be reentrained necessarily together. Thus, downstream deposits will differ from source materials as a function of the deposition and reentrainment processes.

The question of the fall velocities of quartz grains and equivalent grains of heavier minerals in quiescent water has been considered by Tourtelot (1968) as a means of estimating the size of heavy minerals, including gold, likely to be associated with quartz grains of given sizes. In the present report, existing theory is applied to the prediction of the fall velocities as well as the bed shear stresses necessary for reentrainment of spherical grains of quartz, monazite, lead, and gold. These minerals were chosen to represent the range of specific gravities of common fluvial sediments.

FALL VELOCITY

Many studies of fall velocity have been conducted, and two of the more representative and well-known studies are those of Rubey (1933b) and Report 12 of the U.S. Interagency Committee on Water Resources (1957). Rubey combined Stokes' law and Newton's impact relation and derived an equation which gives the fall velocity of a spherical grain as a function of the specific gravity and diameter of the grain and the specific gravity and viscosity of the fluid. In Report 12, extensive experimental fall-velocity data were used to obtain a graphical relation between the drag coefficient and the Reynolds number for grains of different shapes.

Figure 1 shows fall velocities in distilled water at 20.0°C. for spherical grains of quartz, monazite, lead, and gold computed from Rubey's equation and also from the drag coefficient–Reynolds number relation of Report 12. The two relations give identical results below a grain diameter of about 0.25 millimeters but conflicting results for larger diameters. The exact grain diameter at which the divergence in results begins is a function of the specific gravity, as is shown in figure 1.

U.S. GEOL. SURVEY PROF. PAPER 650-B, PAGES B77-B80

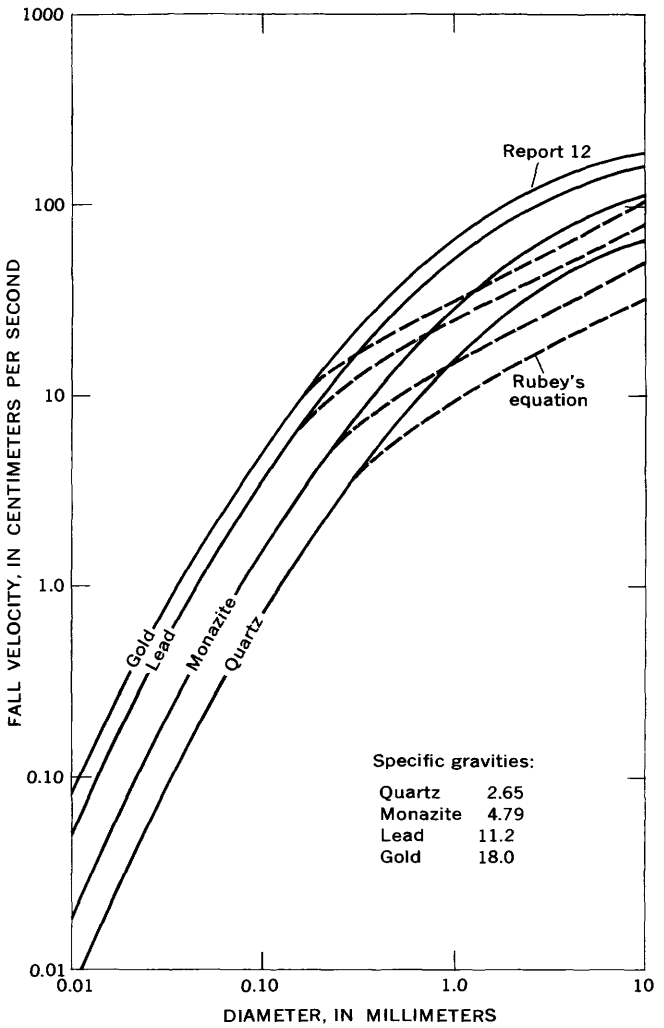

FIGURE 1.—Relation of fall velocity in water at 20°C to grain diameter for spherical grains of quartz, monazite, lead, and gold. Solid lines determined from relation given in Report 12 of the U.S. Interagency Committee on Water Resources (1957), and dashed lines determined from Rubey's (1933b) equation.

Because the relation from Report 12 is based on extensive experimental data and because Rubey's equation has never been verified extensively, it is believed that the fall-velocity data calculated from the Report 12 relation are more reliable. Hence, the fall velocities predicted by the Report 12 relation are used in the remainder of this report.

The reason for the deviation of the fall velocities predicted by Rubey's equation from those predicted by the drag coefficient–Reynolds number relation is not known. However, Rubey's equation was derived for spheres, whereas it was verified with two types of crushed grains whose fall velocities are known to deviate from the fall-velocity relations for spherical grains (Shultz and others, 1954). Blanchard (1967) found that the fall velocity–specific gravity relation predicted by Rubey's equation agreed well with the experimental fall-velocity data for spheres of different specific gravities with fall velocities in water of up to about 6 centimeters per second. For higher fall velocities for the same spheres obtained by using a fluid (acetone) with a viscosity less than that of water, he found that the experimental fall velocities were larger than the fall velocities predicted by Rubey's equation. Thus, the experimental results of Blanchard support figure 1 in suggesting that Rubey's equation predicts fall velocities that are less than the experimental values for fall velocities greater than about 6 cm/sec.

REENTRAINMENT

To define exactly when a grain is reentrained, one must specify some measure of sediment motion. A grain which is initially at rest on the bed may first oscillate slightly about its position of rest, then the grain may start to move along the bed and finally it may move by saltation and become a part of the suspended load. The complexity and the statistical nature of sediment movement are well recognized (Task Committee on Preparation of Sedimentation Manual, 1966).

A useful parameter for describing the rate of sediment transport has been given in slightly different forms by Meyer-Peter and Muller, Einstein, and Bagnold (Colby, 1964). This parameter, as presented by Einstein, is

$$\psi=\frac{(\rho_s-\rho_f)}{\rho_f}\frac{D}{R'S}, \tag{1}$$

where ψ is a function for correlating the effect of flow with the intensity of sediment transport, D is a characteristic particle diameter, ρ_s and ρ_f are the mass densities of the sediment and fluid, respectively, R' is that part of the hydraulic radius attributed to grain resistance, and S is the slope of the energy gradient which is commonly taken as the slope of the water surface.

Shields (1936) presented a criterion for beginning of motion which has become widely accepted. His criterion is presented as a relation between a dimensionless shear stress and a particle Reynolds number. The dimensionless shear stress is

$$\tau_*=\frac{\tau_c}{(\rho_s-\rho_f)gd_s}, \tag{2}$$

where τ_c is the critical bed shear stress, g is the gravitational acceleration, and d_s is the grain diameter. The particle Reynolds number is

$$R_*=\frac{U_*d_s}{\nu}, \tag{3}$$

where U_* is the shear velocity or $\sqrt{\tau_c/\rho_f}$, and ν is the kinematic viscosity of the fluid.

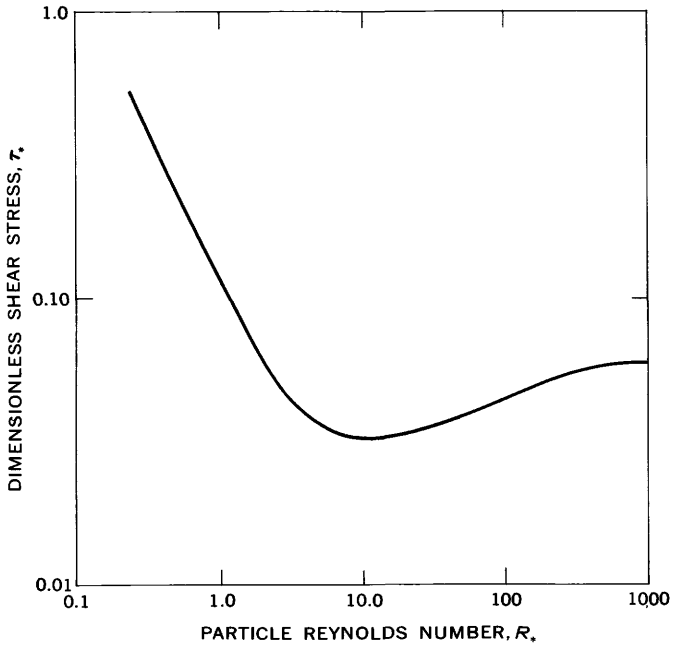

FIGURE 2.—Shields' diagram showing relation between dimensionless critical shear stress and particle Reynolds number.

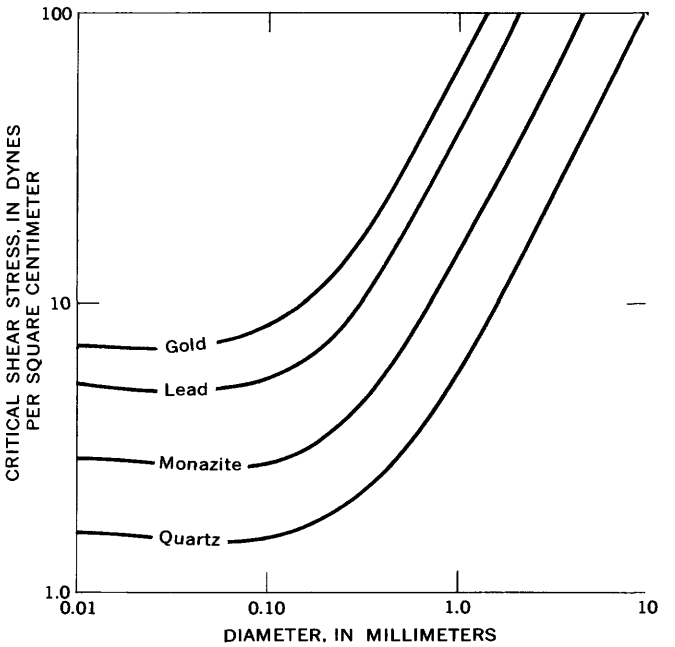

FIGURE 3.—Relation of critical shear stress in water at 20°C to grain diameter for spherical grains of quartz, monazite, lead, and gold.

Shields' relation between the dimensionless critical shear stress, τ_*, and the particle Reynolds number, R_* is shown in figure 2.

It can be shown that Shields' dimensionless critical shear stress, τ_*, has the same functional form as the inverse of Einstein's parameter ψ. While no quantitative measure of reentrainment is available in the literature, one may assume that reentrainment should be a function of the parameter τ_*. For the purpose of this report it will be assumed that a grain which has initiated motion has been reentrained. Shields' relation is used to calculate critical shear stress as a function of grain diameter.

It is recognized that Shields' criterion does not apply strictly to the smaller heavy-mineral grains among the less dense, larger quartz grains because of the hiding or shielding effect. Present theory, however, does not permit an exact treatment of the shielding problem, and Shields' criterion is used as an approximation. Hand (1967) has discussed qualitatively the problem of reentrainment of the grains of a heavy mineral.

By a trial-and-error procedure, one may calculate from Shields' criterion the critical shear stress, τ_c, as a function of grain diameter. The results of these calculations for spherical grains of quartz, monazite, lead, and gold in water at 20.0°C. are shown in figure 3. The calculated results given in figure 3 show that for a given grain diameter, the shear stress required to initiate motion is directly related to the grain specific gravity. Below a grain diameter of approximately 0.1 mm, the critical shear stress is a function of specific gravity only, whereas for grain diameters larger than 0.1 mm the critical shear stress is a function of grain diameter as well as specific gravity.

RELATION BETWEEN CRITICAL SHEAR STRESS AND FALL VELOCITY

If fall velocity is the sole criterion for hydraulic equivalence, then specific gravity and shape variables can be eliminated from consideration and mineral properties can be described entirely by a fall velocity or a fall diameter. Figure 4, which was obtained from figures 3 and 1, shows the computed relation between critical shear stress and fall velocity for spheres of quartz, monazite, lead, and gold in water at 20.0°C. For fall velocities smaller than about 2 cm/sec, the critical shear stress is dependent on specific gravity but independent of fall velocity. For fall velocities larger than 2 cm/sec, the critical shear stress is less dependent on specific gravity and more dependent on fall velocity. However, the critical shear stress becomes independent of specific gravity only for fall velocities larger than about 50 cm/sec.

CONCLUSIONS

1. Fall velocities calculated from the equation of Rubey (1933b) are identical with the fall velocities calculated from the drag coefficient–Reynolds number relation of Report 12 up to a fall diameter of about

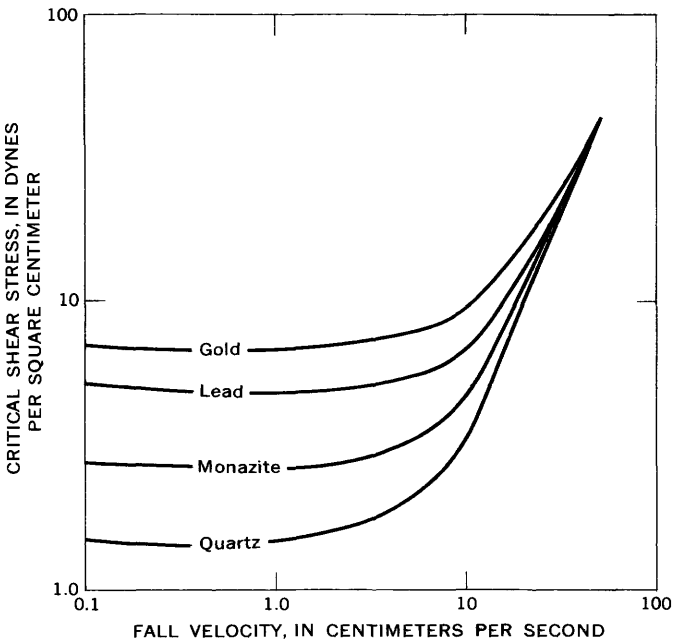

FIGURE 4.—Relation of critical shear stress to fall velocity for spherical grains of quartz, monazite, lead, and gold in water at 20°C.

0.25 mm for quartz, 0.22 mm for monazite, 0.19 mm for lead, and 0.13 mm for gold. For fall diameters larger than these values, the fall velocities predicted by Rubey's equation are less than the fall velocities calculated from the drag coefficient–Reynolds number relation. It is recommended that the drag coefficient–Reynolds number relation of Report 12 be used to determine fall velocities because it is based on a large amount of experimental data, whereas Rubey's equation has never been verified extensively.

2. Critical shear stresses calculated from Shields' criterion indicate that the critical shear stress is a function only of specific gravity for grains having diameters less than about 0.1 mm, whereas for larger grains the critical shear stress is a function of both diameter and specific gravity. The critical shear stress is a function only of specific gravity for fall velocities less than about 2 cm/sec, and is a function of both specific gravity and fall velocity for larger fall velocities. The critical shear stress becomes independent of specific gravity only for fall velocities larger than about 50 cm/sec. Conclusion 2 is a result of calculations based on available theory only, and experimental verification is necessary.

3. Fall velocity is probably the most effective parameter for measuring the dynamic response of sediment particles to hydraulic forces. However, it should be noted that the description of the reentrainment process requires more complete descriptions of particle properties than is provided by fall velocity alone. As a minimum, the specific gravity and size of a particle must be specified. The mechanics of the sediment-transport phenomena must be investigated to determine the relations governing hydraulic equivalence with respect to reentrainment. These relations, together with fall-velocity relations, will provide a framework for defining an equivalent hydraulic value for particles subjected to a given set of bed and flow conditions.

REFERENCES

Blanchard, M. B., 1967, Method for determining the density of microsize spherical particles: Geol. Soc. America Bull., v. 78, p. 385–404.

Colby, B. R., 1964, Discharge of sands and mean-velocity relationships in sand-bed streams: U.S. Geol. Survey Prof. Paper 462–A, 47 p.

Hand, B. M., 1967, Differentiation of beach and dune sands, using settling velocities of light and heavy minerals: Jour. Sed. Petrology, v. 37, no. 2, p. 514–520.

Rittenhouse, Gordon, 1943, Transportation and deposition of heavy minerals: Geol. Soc. America Bull., v. 54, p. 1725–1780.

Rubey, W. W., 1933a, The size-distribution of heavy minerals within a water-laid sandstone: Jour. Sed. Petrology, v. 3, no. 1, p. 3–29.

——— 1933b, Settling velocities of gravel, sand and silt particles: Am. Jour. Sci., 5th ser., v. 25, no. 148, p. 325–338.

Schultz, E. F., Wilde, R. H., and Albertson, M. L., 1954, Influence of shape on the fall velocity of sedimentary particles: Missouri River Division, U.S. Army Corps of Engineers, Sediment Series, no. 5, 161 p.

Shields, A., 1936, Application of similarity principles and turbulence research to bed load movement: Hydrodynamics Laboratory, California Institute of Technology, Publication 167, Pasadena, Calif., 21 p. [Translation from German by W. P. Ott and J. C. van Uchelen].

Simons, D. B., and Richardson, E. V., 1966, Resistance to flow in alluvial channels: U.S. Geol. Survey Prof. Paper 422–J, 61 p.

Task Committee on Preparation of Sedimentation Manual, 1966, Sediment transportation mechanics: initiation of motion: Am. Soc. Civil Engineers Jour., v. 92, no. HY2, p. 219–314.

Tourtelot, H. A., 1968, Hydraulic equivalence of grains of quartz and heavier minerals and implications for the study of placers: U.S. Geol. Survey Prof. Paper 594–F, 13 p.

U.S. Inter-Agency Committee on Water Resources, 1957, Some fundamentals of particle size analysis, *in* A study of methods used in measurement and analysis of sediment loads in streams: Washington, U.S. Govt. Printing Office, Rept. 12, 55 p.

RADIOCARBON DATING OF ASH DEPOSITS ON AMCHITKA ISLAND, ALASKA

By HANSFORD T. SHACKLETTE and MEYER RUBIN,
Denver, Colo., Washington, D.C.

Work done in cooperation with the Advanced Research Projects Agency, U.S. Department of Defense

Abstract.—Peat deposits on the tableland of Amchitka Island contain 3 layers of volcanic ash, each about 1–2 cm in thickness. Radiocarbon dates of discrete plant stems from these ash layers indicate that the age of the uppermost ash deposit is 725 ±250 years B.P. The two lower ash layers lie about 7 cm apart; the average of their dates is 1,845 years B.P. The amount of peat above the ash layers indicates that average rates of accumulation are approximately 0.2 cm/yr for fibrous to mucky peat, and 0.052 cm/yr for the more completely humified and compacted peat (muck). The total depth of peat at this location (2.8 m) indicates that about 3,400 years was required for the formation of this deposit. It is estimated, therefore, that this tableland has borne a vegetation mantle no longer than 4,000 years.

Amchitka Island, the largest in the Rat Island group (Aleutian Islands), has an area of 114.1 square miles (Coats, 1956, p. 86), one-half of which is tableland of several segments at different altitudes ranging from about 135 to 500 feet (Powers and others, 1960, p. 526). These segments are largely mantled with a mat of living heath and bog vegetation which overlies deposits of peat and muck that are as much as 3 meters thick. Three layers of ash, each about 1–2 centimeters thick, can be recognized in profiles of this organic deposit. The vertical distance between the ash layers is presumed to relate to the rate of peat deposition at a particular site. Perennially frozen ground (permafrost) has not been reported in the Aleutian Islands, and no effects of cryogenic processes were evident in these peat deposits on Amchitka Island.. There have been no volcanoes on this island since its emergence from the sea, which was inferred by Powers, Coats, and Nelson (1960, p. 550) to have been before late Pleistocene time.

The dating of these ash deposits allows one to determine the absolute and relative rates of peat deposition under different types of vegetation. From these rates the length of time that the present vegetation mantle has existed on this island may be estimated.

Recently combined carbon is continuously introduced into peat deposits through roots which grow downward in successive seasons; therefore, samples that represent the total material in the deposit are unsatisfactory for radiocarbon dating of the peat. In the peat profile that was studied, living roots were found 0.5 m above the bottom of the thick peat deposit. In addition, downward migration of humic substances probably distributes recently combined atmospheric carbon throughout the deposit. Carson (1968, p. 16) stated, "As is well known, peats are among the more difficult organic materials upon which to base C–14 interpretations. Annual dilution produces material of composite age, in both surface and buried mats." Dates of peat samples, therefore, ordinarily represent average ages of the organic matter in the samples, and are more recent than the age of the oldest material in the sample.

Acknowledgments.—This study was supported in part by Advanced Research Projects Agency, Department of Defense, under Order No. 938. James A. Erdman assisted in the collection and preparation of the samples.

MATERIALS AND METHODS

Trenching on Amchitka Island at an altitude of about 125 feet exposed the profile of a peat deposit 2.8 m thick which afforded an exceptionally good opportunity to obtain, from the ash layers within the deposit, samples of organic matter that were relatively free of

U.S. GEOL. SURVEY PROF. PAPER 650-B, PAGES B81–B83

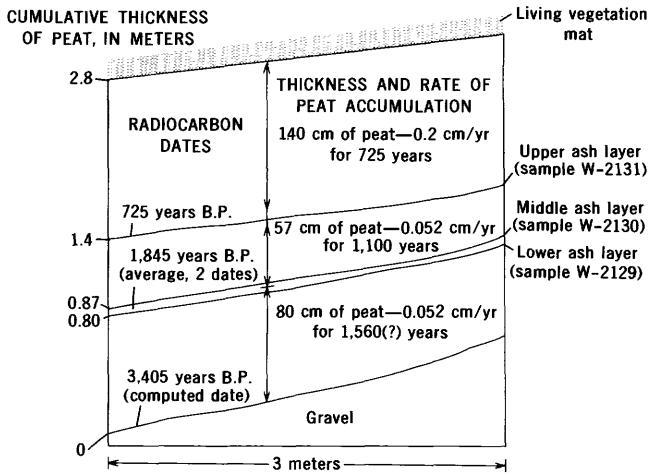

FIGURE 1.—Profile of a peat deposit on Amchitka Island, Alaska, showing the location and dates of the ash layers and the computed rates of peat deposition.

recent carbon contamination (fig. 1). This profile was of a peat composed principally of sedges (*Carex lyngbyaei*(?) and others), with some heath plants (mostly crowberry, *Empetrum nigrum*) also present. The sedge and crowberry stems were preserved as discrete plant organs that could be separated from the humified structureless mucky material and living plant roots that made up the greater part of the total deposit. These stems grow only on or just above the surface of the peat; for this reason it is known that the ash falls and the plant tissues imbedded in them are contemporaneous.

In February 1968, samples of these plant stems were removed by hand sorting from the 3 ash layers, washed to reduce gross contamination from humic materials, sealed in polyethylene bags, and in March 1968, sent to the U.S. Geological Survey's radiocarbon laboratory in Washington, D.C., for further processing and dating. Pretreatment of the stems was limited to a wash in a warm dilute HCl solution in order to remove carbonates. The usual rigorous treatment in boiling acid and alkali was eliminated because of the small size of the samples. The samples were then converted to acetylene gas and counted for 1 day in each of two proportional counters.

It should be noted that the two lower ash layers (lower and middle layers, fig. 1) were located very near each other, that the plant parts which were sampled did not lie entirely in one plane, and that at places it was impossible to determine to which ash layer a stem should be assigned. For these reasons it probably is best to consider the two lower samples as one, and to average the dates of the two samples. The time interval between the deposition of the upper and the two lower ash layers is, therefore, the only reliable measure of the rate of humified peat deposition that was obtained.

RESULTS

The age of the plant material in the upper ash layer (W–2131, fig. 1) was found to be 725±250 years B.P. (before present). The materials in the middle layer (W–2130) and in the lower layer (W–2129) were 1,950±250 and 1,740±250 years B.P., respectively. These two latter dates are averaged as 1,845 years B.P. in figure 1.

The top of the upper ash layer was 1.4 m below the ground surface, and the peat in the part of the profile above the ash layer was reddish brown and fibrous at upper levels, grading to dark-brown humified material (muck) just above the ash layer. This peat had accumulated at the approximate average rate of 0.2 centimeters/year. This rate of accumulation agrees well with that of peat in the vicinity of Fairbanks, Alaska, that was given by Heilman (1968, p. 336) as 0.25–0.38 cm/yr. Carson (1968, p. 17) reported radiocarbon ages of surface peats from the Barrow, Alaska, region to range from 4,280±160 years B.P. for the bottom layer of peat that was 10 inches thick to 395±150 years B.P. for peat 6 inches thick. An examination of the history of these peat deposits suggests that reliable rates of peat deposition in this region cannot be inferred from these data.

The more completely humified and compacted peat between the upper ash layer and the two lower ash layers accumulated in approximately 1,100 years, or at an average rate of about 0.052 cm/yr. The contrast between rates of accumulation of peat that is fibrous to mucky, and that of more completely humified muck, gives some concept of the degree of compaction and the loss of organic constituents by decomposition and leaching in lower layers of a peat deposit in the Aleutian Islands climate, if it is assumed that the deposition of organic matter on the ground surface occurred at a rather uniform rate.

About 80 cm of humified peat lay below the lower ash layer in the profile. If this layer of peat accumulated at the same rate as that described above (0.052 cm/yr), approximately 1,560 years was required for this layer to form. Thus, the estimated age of the lowermost peat in the profile is about 3,400 years. It seems likely, therefore, that the low plateaus of Amchitka Island have borne a vegetation mantle no longer than 4,000 years.

All profiles of the peat mantle that were examined on the low plateaus contained the three ash layers. The distance between the upper and the middle ash layers

in peat that was formed under the crowberry-moss-lichen heath indicates that this peat accumulates at about half the rate of that formed under sedge meadows. This difference in rate may be a measure of the difference in biomass productivity of the two plant communities, or it may only indicate that sedge-peat deposits, because of their wetter habitat, are less affected by erosion and oxidation processes.

The source of the ash that formed the three strata was not determined. These ash falls antedate the historical record of volcanic activity in the Aleutian Islands that was reported by Powers (1958, p. 64–67). Recorded activity of volcanoes on Semisopochnoi, Little Sitkin, and Kiska Islands, which are about 36, 40, and 75 miles distant, respectively, from the study site on Amchitka Island, suggests that any or all of these volcanic islands may have been the source of the ash layers in the peat profile that was studied.

REFERENCES

Carson, C. E., 1968, Radiocarbon dating of lacustrine strands in arctic Alaska: Arctic, v. 21, no. 1, p. 12–26.

Coats, R. R., 1956, Reconnaissance geology of some western Aleutian islands, Alaska: U.S. Geol. Survey Bull. 1028-E, p. 83–100.

Heilman, P. E., 1968, Relationship of availability of phosphorus and cations to forest succession and bog formation in interior Alaska: Ecology, v. 49, no. 2, p. 331–336.

Powers, H. A., 1958, Alaska Peninsula—Aleutian Islands, p. 61–75 *in* Williams, Howel, ed., Landscapes of Alaska—their geologic evolution: Berkeley, California Univ. Press, 148 p.

Powers, H. A., Coats, R. R., and Nelson, W. H., 1960, Geology and submarine physiography of Amchitka Island, Alaska: U.S. Geol. Survey Bull. 1028–P, p. 521–554.

THE AGES OF THREE URANIUM MINERALS, MOJAVE DESERT, CALIFORNIA

By D. F. HEWETT, JEROME STONE,[1] and LORIN R. STIEFF,[2]
Menlo Park, Calif.

Abstract.—The Mojave Desert region of southeastern California contains many coarse-grained quartz monzonite intrusions whose ages are important to the understanding of the region's geologic history. Betafite from one pegmatite and polycrase from another indicate ages that may range from 72 to 80 m.y., or the Late Cretaceous. Uraninite has been found in a crushed zone in quartzite about 21 miles southeast of Twenty-nine Palms.

During the post-World War II years of 1945–1955, when the search for uranium was intense, many persons from the Los Angeles area explored the Mojave Desert for deposits of radioactive minerals. Both thorium- and uranium-bearing minerals were found in many localities, and D. F. Hewett made numerous field trips from Los Angeles to examine the discoveries. By far the greater number of deposits contained thorium-bearing minerals, such as monazite, allanite, and cyrtolite, but in a few places, uranium-bearing minerals were found. It seemed advisable to collect and study these radioactive minerals in the hope that the contained uranium would permit the determination of their ages and that these ages would contribute to knowledge of the geologic history of the region.

In February 1950, betafite was identified in a pegmatite dike in the Cady Mountains, and enough was recovered to permit the determination of the isotopes of its contained lead as well as its uranium and thorium content. Its Pb^{206}/U^{238} age was calculated as 155 million years (Hewett and Glass, 1953). Soon thereafter, euxenite was found in the Pomona Tile quarry, about 40 miles southwest of the Cady Mountains. Even though sufficient euxenite was recovered for a spectrographic analysis, there was not enough for the determination of the isotopes of lead and uranium. From the content of the total lead, uranium, and thorium, the age was estimated at about 150 m.y. It was recognized in 1953 that neither estimate of the age was satisfactory.

In December 1955, Harry T. Heather, of Pasadena, Calif., brought Hewett specimens of highly radioactive rock in which the presence of betafite was readily proven. The specimens came from a pegmatite dike near Marl Spring, about 20 miles east of Baker, Calif., and the deposit was examined in December 1955 and March 1956. In January 1956, Pierre George, an amateur collector of minerals in San Gabriel, brought Hewett specimens of a uranium mineral, identified as polycrase, that he had collected from a pegmatite dike near Pearblossom, Calif.; the dike was examined soon thereafter. The Ram uranium deposit was brought to the attention of Hewett in 1956 by Cornelius Willis of Los Angeles, who was exploring it at the time.

Acknowledgments. — In recent years the positive determination of minerals and their constituent elements has demanded special skills and equipment. In the study of the minerals at the three localities in the Mojave Desert here described, several persons, all of the U.S. Geological Survey, have contributed their skills: Evelyn C. Mertie, Daphne R. Ross, and Samuel Rubinstein made the X-ray analyses; Katherine E. Valentine, the spectrographic analyses. Their contributions are acknowledged specifically in appropriate places.

The authors also acknowledge with appreciation the critical reading of the manuscript by Robert G. Coleman and Thomas W. Stern.

All field studies and geological interpretations were made by D. Foster Hewett. The program of mineral studies in Washington was guided by Jerome Stone, who did all the microscopic studies of the minerals. All the analyses of the isotopes of lead, uranium, and thorium that led to the age determinations were

[1] Present address: New York, N.Y.; formerly of the U.S. Geological Survey.

[2] Present address: U.S. Department of State, Arms Control Agency, Washington, D.C.; formerly of the U.S. Geological Survey.

U.S. GEOL. SURVEY PROF. PAPER 650-B, PAGES B84-B88

supervised by Lorin R. Stieff, aided from time to time by Thomas W. Stern.

MARL SPRING PEGMATITE

Location and accessibility

The source of the betafite and associated minerals is a pegmatite dike that crops out near Marl Spring about 10 miles southwest of the crest of Cima Dome, a conspicuous topographic feature in the southwest quarter of the Ivanpah quadrangle. The dike lies near the southern border of sec. 26, T. 13 S., R. 12 E., San Bernardino meridian, San Bernardino County.

Local geology

The pegmatite dike lies within an area of coarse-grained intrusive rock that has been called the Teutonia Quartz Monzonite (Hewett, 1956). This rock crops out over much of Cima Dome as well as a large surrounding area. As the result of study and geologic mapping of a large area, it is clear that the quartz monzonite was intruded into the highly folded and faulted Paleozoic rocks of the area, late in the epoch of orogeny that has been interpreted as Laramide. In the Cima Dome area, the quartz monzonite is a gray holocrystalline rock that shows conspicuous phenocrysts of pale-reddish orthoclase in a finer grained groundmass of white plagioclase and quartz. The only dark minerals are biotite and magnetite. In this general area, thin aplite dikes, rarely more than 6 inches thick, are widespread, but pegmatite dikes are very uncommon.

The presence of the pegmatite dike is indicated by abundant float of gray quartz and pale-reddish feldspar within an area about 20 by 30 feet. The southern border zone is shown in a pit about 5 feet in diameter, but the true shape and extent of the dike are not revealed. In the trench, the contact between the dike and the enclosing quartz monzonite is a plane that strikes N. 80° W. and dips 60° S. From this it appears that the dike is a lens that trends west and dips steeply south. At the outcrop, gray quartz seems to form about two-thirds of the dike and the remaining one-third is formed of isolated lenses of reddish microcline. In the trench a border zone about 12 inches thick adjacent to the monozonite is an intimate mixture of white albite, pale-reddish microcline, and gray quartz. It appears that this zone was originally a fine-grained mixture of microcline and quartz and that the microcline has been largely replaced by albite. The zone also contains large plates of biotite, which are not present in the unaltered pegmatite.

Minerals

An uncommon assemblage of minerals occurs locally in the reddish microcline, generally near the contact with the enclosing gray quartz. In places these minerals are entirely in the microcline, but nearby they partly line drusy cavities along its contact with the quartz.

Magnetite and ilmenite form thin plates as much as 3 inches long and ⅛ inch thick that cut through the microcline in diverse directions. The habit of these minerals is the same as that in the Pomona Tile quarry (Hewett and Glass, 1953), where the plates are thicker and longer. As at the Pomona Tile quarry, the uranium minerals—euxenite at the Pomona Tile quarry and betafite at the Marl Spring pegmatite—form grains and small crystals distributed sporadically along the plates of magnetite and ilmenite.

Allanite forms well-terminated crystals ¼ to 1 inch long in drusy cavities and embedded in the microcline near intersections of the plates of magnetite and ilmenite. The mineral has been identified by its optical properties, by its crystal form, by X-ray diffraction analysis by Daphne Ross, and by the following spectrographic analysis by Katherine E. Valentine:

Percentage	*Element*
More than 10	Fe, Si
5 to 10	Ca, Ce
1 to 5	Al, La, Th, Mg, Mn
0.5 to 1	Na, Ti, Pr
0.1 to 0.5	As, B, Na, Y

One crystal of allanite is partly replaced by bastnaesite; its identification is based upon X-ray diffraction analysis made by Samuel Rubenstein.

Crystals of cyrtolite (a metamict variety of zircon containing thorium) that rarely exceed 1 millimeter in diameter are persistently associated with the plates of magnetite and ilmenite; the identification was confirmed by X-ray analysis made by Samuel Rubenstein of material that had been heated.

Most of the betafite forms irregularly shaped grains several millimeters in diameter, distributed along the plates of magnetite and ilmenite and at their intersections; a few grains are isolated in the midst of the microcline. Several terminated octahedrons, one an inch in largest diameter, have been recovered from drusy cavities. The color of the betafite ranges from yellowish brown to dark brown; it shows adamantine luster on conchoidal fractures. By sorting, screening, and panning the finer material from the trench, about 25 grams of betafite was recovered; this was used for the isotopic age determinations.

The identification is based on the crystal form, X-ray diffraction analysis of both the natural material and

that after ignition, and by semiquantitative spectrographic analysis. By X-ray analysis the natural material yielded no pattern, but after heating it yielded "a cubic pattern, with the spacings slightly larger than those of polycrase" (Evelyn C. Mertie, written commun.). The composition determined by spectrographic analysis, by Katherine E. Valentine, is close to that of betafite:

Percentage	*Element*
More than 10	U, Nb
5 to 10	Ti
1 to 5	Ca, Th, Y
0.5 to 1	
0.1 to 0.5	Al, Ce, Dy, Er, Fe, Gd, Nd, Pb, Sm, Yb
0.05	Zr
0.01 to 0.05	Ho, Lu, Mn, Mg, Sr, Tm
0.005 to 0.01	
0.001 to 0.005	Ba, Sc
0.0001 to 0.0005	Be

By panning the fine-grained material from the trench, three brown crystals as much as 3 mm in diameter were recovered. The material is metamict; but, after heating, the crystals were identified as fergusonite by X-ray analysis made by Samuel Rubenstein. A spectrographic analysis, by Katherine E. Valentine, follows:

Percentage	*Element*
More than 10	Nb
1 to 10	Ca, Fe, Er, Gd, Ta, Th, U, Y, Si
0.1 to 1	Dy, Ho, Lu, Mg, Na, Ti, Yb

PEARBLOSSOM PEGMATITE

Location and accessibility

The Pearblossom pegmatite dike crops out on the north side of an isolated low hill on the southern border of Antelope Valley, where the valley merges with the limiting ridges of the San Gabriel Mountains, Los Angeles County, Calif. The hill lies in the SW¼ sec. 30, T. 5 N., R. 9 W., San Bernardino meridian, about 500 feet north of the Pearblossom Highway and about 1 mile southeast of the settlement of Pearblossom.

The lone hill lies within the area of the Valyermo quadrangle, which has been closely studied and geologically mapped by L. F. Noble (1954). According to Noble, the high part of the hill is composed of coarse gabbro of Jurassic(?) age that has been intruded by the Holcomb Quartz Monzonite, which he considered of Cretaceous(?) age. The contact between the monzonite below and the gabbro above is well exposed on the south slope of the hill, and the pegmatite dike extends upward from the monzonite through the gabbro so that it is revealed as a light-colored reef across the crest of the hill.

The pegmatite dike has been explored by a single shallow trench at the north edge of the hill. Here the dike is about 10 feet wide and dips west at about 45°. The rock is in part a coarsely granular and in part a finely granular mixture of pale-reddish microcline and gray quartz; it shows sporadic zones of white rock that is a mixture of albite and quartz. A traverse over the hill with a Geiger counter shows that the radioactivity of the gabbro is not significant but that the dike is slightly radioactive throughout its extent.

Minerals

Ilmenite is the most abundant dark mineral. It forms plates as much as 2 inches long and ⅛ inch thick, largely in the microline near its contact with masses of quartz. As at Marl Spring and the Pomona Tile quarry, the uranium-bearing minerals, grains, and crystals are concentrated along these plates of ilmenite. A little magnetite is present near the ilmenite.

Allanite forms small plates rather than crystals near the ilmenite plates. The mineral was determined by its optical properties and behavior before the blowpipe.

Biotite in plates as much as an inch in diameter is distributed sporadically in the feldspar-quartz rock.

Polycrase commonly forms aggregates of plates of rectangular outline either adjacent to or near the plates of ilmenite; the plates commonly range from 2 to 5 mm in longest diameter. The color is largely olive green. Some plates are cut by thin veinlets of a pale-yellow mineral whose nature has not been determined. About 20 g of the mineral has been recovered.

The identity of the polycrase is based on crystal form and on the following semiquantitative spectrographic analysis, made by Katherine E. Valentine:

Percentage	*Element*
More than 10	U, Nb
5 to 10	Ti
1 to 5	Ca, Th
0.5 to 1	
0.1 to 0.5	Ba, Ce, Fe, Nd, Pb, Si, Y
0.05 to 0.1	Al, Dy, Gd, Sm
0.01 to 0.05	Cu, Er, La, Lu, Mn, Sr, Tm, Yb, Zr
0.005 to 0.01	Mg
0.001 to 0.005	Ho, Sc
0.0005 to 0.001	Ag
0.0001 to 0.0005	Be

RAM URANIUM DEPOSIT

Location and accessibility

In 1955 uraninite was discovered in the foothills on the northern border of the Pinto Mountains, Riverside

TABLE 1.—*Lead, uranium, and thorium concentrations, and isotopic lead composition of three uranium minerals from the Mojave Desert, Calif.*

Sample and location	Concentration (percent)			Abundance of lead isotopes (atom percent)			
	Pb [1]	U [2]	Th [3]	Pb^{204}	Pb^{206}	Pb^{207}	Pb^{208}
Betafite, GS–505; Marl Spring	0. 30	18. 35	2. 80	0. 411	72. 53	9. 30	[4] 17. 75
Polycrase, GS–506; Pearblossom	. 157	14. 25	2. 94	. 039	87. 42	4. 86	[4] 7. 69
Uraninite, GS–531; Ram mine, Pinto Mountains	1. 83	74. 4			95. 085	4. 736	[5] . 177

[1] J. J. Warr, analyst, U.S. Geological Survey.
[2] Grafton J. Daniels, analyst, U.S. Geological Survey.
[3] Frank Cuttitta, analyst, U.S. Geological Survey.
[4] Maryse Delevaux, analyst, U.S. Geological Survey.
[5] Mass Assay Laboratory, Y–12 Plant, Oak Ridge, Tenn.

County, Calif. The deposit was explored vigorously during 1956–57, but the quantity recovered did not prove large enough to warrant a commercial operation. The deposit is reached by driving 10 miles eastward from the center of the town of Twentynine Palms to a fork where the main road continues to the east. At this point one turns right onto the less traveled road. About 4 miles southeast of the fork, the road enters a canyon and continues 7 miles farther to the Ram mine. Most of the explorations lie along the ridge east of the canyon, but there are several trenches west of it.

Local geology

The prevailing rock within 1 mile of the deposit is gray quartzite whose bedding is difficult to determine. Several small lenses of dark intrusive rock, which may be sills, crop out near the deposit, but they may be dikes in faults. Probably the quartzite is Precambrian, as are most of the rocks that underlie the Pinto Mountains farther west.

Minerals

Uraninite forms nearly pure masses of highly irregular shapes that weight as much as several pounds. These masses are rough lenses and pipelike bodies that are disposed in a highly erratic manner along walls that lie within a broad zone of crushed quartzite. This zone of crushed quartzite is as wide as 50 feet, but definite limiting walls are lacking. In March 1956, the uraninite exposed in the trenches was seen to be concentrated, but very irregularly distributed, along ill-defined curved walls within the crushed quartzite. Polished specimens show that the uraninite has partly replaced the quartzite and partly filled open spaces between the fragments.

The identity of the uraninite has been proven both by X-ray diffraction and by a semiquantitative spectrographic analysis, by Katherine E. Valentine, as follows:

Percentage	*Element*
More than 10	U
1	Si, Cu
0.3 to 1	Ca, Pb, Sr
0.1 to 0.3	Al, Fe
0.05 to 0.1	Be, Sc

At every place examined, the uraninite is surrounded by a layer of yellow and orange oxides of uranium. In the one sample analyzed by X-ray diffraction, the presence of uranophane was determined; but other oxides are probably present.

Small amounts of green copper minerals are persistently associated with the uranium minerals. Only chrysocolla was identified.

AGE CALCULATIONS

The quantitative data on the concentrations of Pb, U, and Th, in percentage, and the atom percent abundance of the lead extracted from the betafite, polycrase, and uraninite are given in table 1.

The ages in millions of years given in table 2 were calculated by using the procedures and constants given in the tables of Stieff and others (1959).

In the isotopic analysis of the Cima Dome betafite (GS–505), only about 2 micrograms of lead was available. The impossibly young Pb^{207}/Pb^{206} age

TABLE 2.—*Lead-uranium and lead-thorium ages, in millions of years, of three uranium minerals from the Mojave Desert, Calif.*

Sample and location	Index of common lead [1]	Pb^{206}/U^{238}	Pb^{207}/U^{235}	Pb^{207}/Pb^{206}	Pb^{208}/Th^{232}
Betafite GS–505; Marl Spring	Pb^{204}	80	76	(Impossibly young)	52
Polycrase, GS–506; Pearblossom	Pb^{204}	72	75	161	85
Uraninite, GS–531; Ram mine, Pinto Mountains	Pb^{208}	175	175	178	

[1] The isotopic abundance of the common lead used in the calculations is Pb^{204}, 1.369; Pb^{206}, 25.20; Pb^{207}, 21.26; and Pb^{208}, 52.20, from Nier's (1938, table 1) analysis of wulfenite and vanadinite, Tucson Mountains, Ariz.

(Pb^{207}/Pb^{206} value of 0.0449) appears to be related to the small amount of lead recovered for mass spectrometric analyses and is probably due to a small error in the determination of the isotope, Pb^{204}.

In the isotopic analysis of the lead from the Ram mine (GS–531) Pb^{204} was not detected. The absence of Th in this uraninite permitted the use of Pb^{208} as the index isotope in the age calculation. The highly concordant Pb^{206}/U^{238}, Pb^{207}/U^{235}, and Pb^{207}/Pb^{206} ages at 175 m.y. suggest that this procedure was justified.

CONCLUSIONS

This investigation may be regarded as a contribution to the ages of two bodies of quartz monzonite in the Mojave Desert—the Teutonia Quartz Monzonite body underlying Cima Dome and the Holcomb Quartz Monzonite near Pearblossom, 140 miles southwest. The ratios of the isotopes of lead and uranium indicate that both bodies were intruded in Late Cretaceous time.

The uraninite from the Ram mine (GS–531) is clearly deposited in a zone of crushed rock by hydrothermal solutions and at a time much younger than the host rock. The ratios of the lead uranium isotopes indicate an age of 175 to 178 m.y. (Early Jurassic), but the host is much older, undoubtedly Precambrian.

REFERENCES

Hewett, D. F., 1956, Geology and mineral resources of the Ivanpah quadrangle, California and Nevada: U.S. Geol. Survey Prof. Paper 275, p. 172.

Hewett, D. F., and Glass, J. J., 1953, Two uranium-bearing pegmatite bodies in San Bernardino County, California: Am. Mineralogist, v. 38, nos. 11–12, p. 1040–1050.

Nier, A. O., 1938, Variations in the relative abundances of the isotopes of common lead from various sources: Am. Chem. Soc. Jour., v. 60, p. 1571–1576.

Noble, L. F., 1954, Geology of the Valyermo quadrangle and vicinity, California: U.S. Geol. Survey Geol. Quad. Map GQ–50, scale 1:24,000.

Stieff, L. R. Stern, T. W., Oshiro, Seiki, and Senftle, F. E., 1959, Tables for the calculation of lead isotope ages: U.S. Geol. Survey Prof. Paper 334–A, p. 1–40.

THE TIME INTERVAL BETWEEN STABILIZATION OF ALPINE GLACIAL DEPOSITS AND ESTABLISHMENT OF TREE SEEDLINGS

By ROBERT S. SIGAFOOS and E. L. HENDRICKS, Washington, D.C.

Abstract.—Determining the age of the oldest tree growing on a recent deposit can be a reliable technique for estimating the age of the deposit. The main source of error in such an age estimate is the interval between stabilization of the deposit and germination of tree seedlings. The availability of seed, the presence of a seedbed of fine-grained material, and a favorable climate are the principal controls in the establishment of trees. These conditions are met in valley bottoms at Mount Rainier, Wash., where tree ages were compared with known ages of recently deposited moraines. Based on ages of more than 150 trees growing on surfaces of known age, the interval between sediment stabilization and tree seed germination is estimated to be 5 years for bottomland sites at Mount Rainier. Dating of a recently deposited pumice layer and determining the ages of trees growing on an underlying moraine near timberline show that the interval is longer at high altitudes than at lower altitudes.

Many geographical studies in hydrology, botany, and geology require the relative dating of landforms and deposits. Use of radiocarbon dating for many years has provided a wealth of age information. Owing to its limitations, however, the radiocarbon method can be used only to determine the age of deposits ranging from a few hundred years to a few tens of thousands of years. In the age determination of young deposits, the inherent error of this method is so large that close determination of their age is not feasible. The age of such young deposits can, however, be determined by botanical methods based on tree ages, and it is our objective here to summarize these methods.

An estimate of the age of a young deposits, then, rests primarily upon the age of the oldest tree growing on the deposit plus the interval between stabilization of the surface and germination of the tree seedling. The age of the tree is approximated by counting the annual growth rings in a section cut from the base of the trunk or, more often, by counting the rings in a core sample taken from the tree. The time required for the tree to grow to the height from which the sample was taken is another unknown interval in determining the absolute tree age. This interval can be minimized in trees no larger than 1.5 feet in diameter and no more than 200 years old by angling the sampling tool (increment borer) downward toward the trunk center. The innermost part of the sample, then, is close to ground level and either includes or is close to the first year's growth ring.

A main source of error in estimating the age of a deposit from tree ages is the interval between stabilization of the deposit and growth of tree seedlings. We intend to show that this interval is different in different places and that several conditions affect the germination of seed. Our data were collected at Mount Rainier, Wash. (fig. 1), in connection with a larger study of the history of alpine glacier activity (Sigafoos and Hendricks, 1961), and conclusions drawn apply only to Mount Rainier and the species studied.

CONDITIONS FOR SEEDLING ESTABLISHMENT

The primary control in the establishment of seedlings on a newly formed surface is the existence of a seed source close enough to provide a large volume of seed. How large this volume must be is not known. Regarding distances of dispersal, studies by the U.S. Forest Service of natural seeding in logged tracts have shown that seed of the same tree species that are abundant at Mount Rainier travel from 400 to 3,800 feet from the source (Division of Timber Management Research, 1965, p. 27, 32, 549, 688, 719). Seed of Douglas fir and noble fir travel farthest, and that of western red cedar and Pacific silver fir the shortest distance. These Forest Service data on seed dispersal suggest that the young moraines studied are well supplied with seed, because the moraines are in bottoms of valleys whose slopes are densely forested with mature trees. The distances between the sites studied and the mature, seed-producing forests range from about 250 feet at the Carbon Glacier moraines to a maximum

U.S. GEOL. SURVEY PROF. PAPER 650-B, PAGES B89-B93

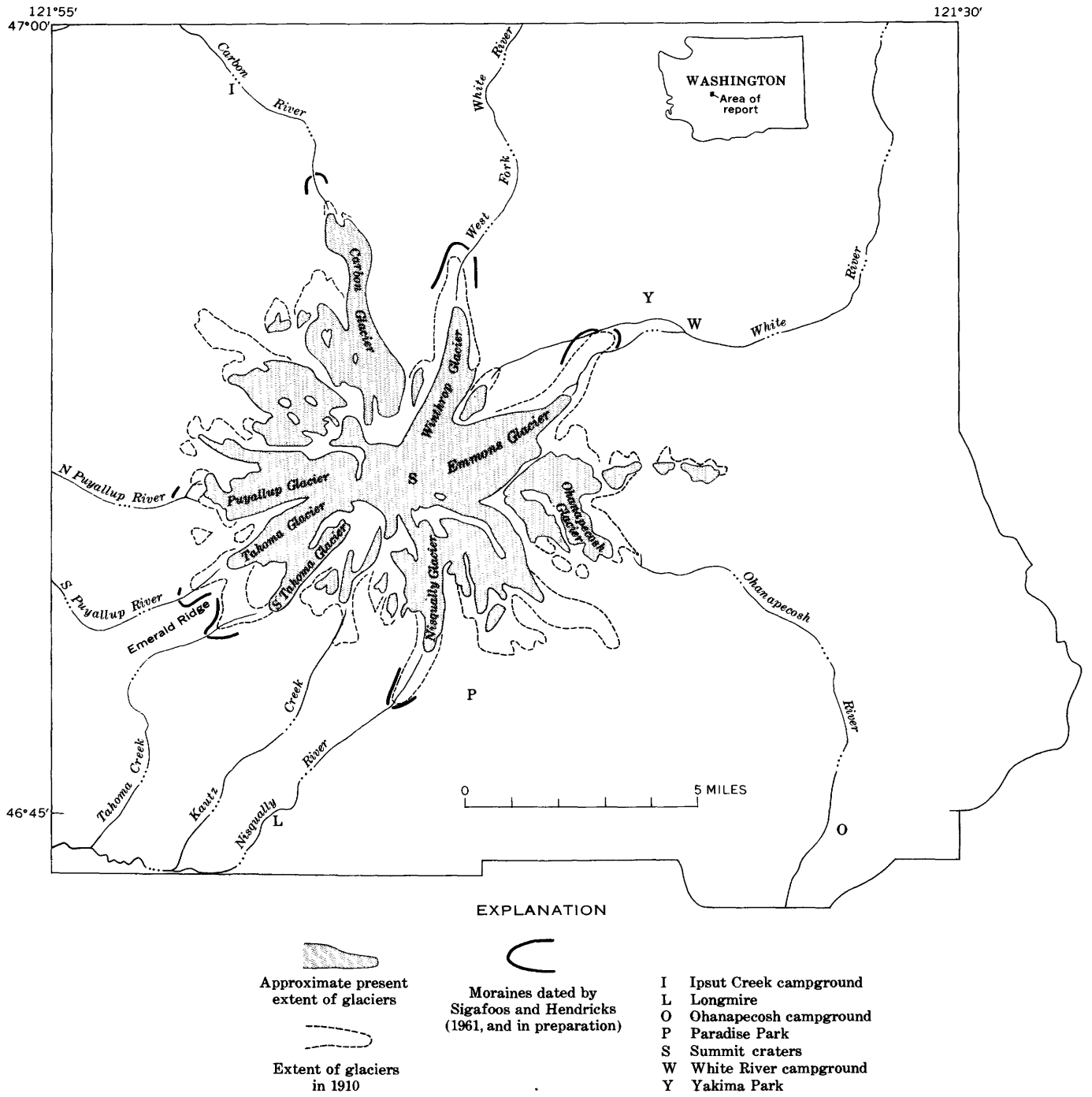

FIGURE 1.—Index map of Mount Rainier, Wash.

of about 1,000 feet at the Emmons Glacier moraines. The sites are, therefore, well within the measured distances that seed of Mount Rainier tree species will travel and are at lower altitudes than the seed source, so that sufficient quantities of seed are surely available to provide ample regeneration.

A second control is the existence of an adequate seedbed in which the seed can germinate. The characteristics of an adequate seedbed are not completely known, and certainly they differ for different species. One requirement is a fine granular material which will retain moisture. An adequate seedbed is lacking on moraines or parts of moraines that are composed solely of rock fragments several inches in diameter and larger.

Climate is the third control that affects seed germination. The length of the growing season, night temperatures, surface soil temperatures, soil moisture, and

snow-free period are among the elements believed to be most significant. Timberline at Mount Rainier ranges from 5,500 to 6,000 feet in altitude. At the valley-bottom sites between altitudes of 3,000 and 4,800 feet the presence of dense forests on surrounding slopes is positive evidence that the climate is most favorable for tree growth. Tree seedlings, here, become established as soon as the surface is stable.

In the timberline zone, however, seedlings may not become established and survive as soon as a surface is physically favorable because the harsh subalpine environment inhibits seed germination. Also, in this zone older seed trees of subalpine fir and mountain hemlock grow as widely scattered individuals and in patches; thus the quantity of seed disseminated to the new surfaces is small. Good seed crops can be expected only once in 3 years on the most favorable sites for subalpine fir (Division of Timber Management Research, 1965, p. 39) and once every few years for mountain hemlock (p. 713). The establishment of seedlings of these species requires precise climatic conditions and a good seed crop combined at a place which is favorable for germination. The frequency of coincidence of adequate climate and a heavy seed crop is probably not high. This combination of conditions apparently does not occur frequently at timberline.

CALCULATION OF INTERVAL BETWEEN SURFACE STABILIZATION AND SEED GERMINATION

The use of tree ages to estimate the age of surfaces has required attempts to determine the interval between surface stabilization and seed germination. This germination interval is calculated by sampling trees growing on surfaces whose age is known from other evidence. Intervals of 5 to 15 years seem reasonable. Intervals reported range from 5 years in southeastern Alaska (Lawrence, 1958, p. 96) to 12 years at lower altitudes of the Olympic Mountains, Wash. (Heusser, 1957, p. 144) and to 10 to 17 years in the Canadian Rockies (Heusser and others, 1954, p. 227). The intervals before seedlings become established may, however, be longer elsewhere. Bray and Struik (1963, p. 1256–1257) and Bray (1964), use an interval of 28 years and believe that the first seedlings to grow do not survive on the Canadian Glacier moraines that they studied. In his study of Nisqually Glacier moraines, Harrison (1956, p. 681–682) used both a 50- and a 30-year interval.

Our studies show that the interval differs considerably over short distances, depending upon local conditions. In the course of studying recent moraines at Mount Rainier we sampled more than 150 seedlings and saplings in 6 areas where the age of the surface was known from other evidence. The data are summarized in table 1. Some surfaces were known to have been covered with glacier ice during certain years, others were flood deposits of known occurrence; another was a roadcut on Mount St. Helens, about 50 miles southwest of Mount Rainier.

Germination on recently deposited glacial till and melt-water deposits below Nisqually and Emmons Glaciers and on flood deposits in other valleys of Mount Rainier was discussed previously (Sigafoos and Hendricks, 1961, p. A11–A13) and will only be summarized here. Seedlings were growing in fine silty sand 2,000 to 3,000 feet below timberline in the bottoms of Nisqually and White River valleys, the sides of which are heavily forested. The seed supply at these sites is ample because Nisqually River valley is within 750 feet horizontally from old-growth forest and White River valley is within 1,000 feet. In Nisqually River valley, tree seedlings started to grow 2 to 13 years after ice is known to have covered the site, whereas in White River valley they started 1 to 10 years after the disappearance of the ice. Floods and debris flows have buried parts of several valleys beneath sand and gravel, and seedlings and saplings are growing on these young deposits. A debris flow in the Kautz Creek valley on October 2, 1947, deposited silt, sand, and boulders over a broad area near the mouth of the valley. Our study indicates that they started to grow from 1 to 12 years later. This valley is bordered by dense old-growth forest and lies at altitudes between 2,300 and 2,500 feet. Seedlings started to grow on fine-grained flood-deposited material 1 to 2 years after a flood on Nisqually River on October 25, 1955.

Tree seedlings were sampled along the Carbon River where silt and sand was deposited in the forest during a flood on November 22, 1959, Of the 8 sampled trees, 7 started to grow the following summer and 1 started to grow in 1961. Here, too, the surrounding forest insured an ample seed supply and the climate is favorable because of the relatively low altitude of 2,900 feet.

Seedlings on a highway embankment on Mount St. Helens started to grow during the first summer after the grading was completed in 1962. The site is about 3,400 feet in altitude, about 2,000 to 2,500 feet lower than timberline and is underlain by pea-sized pumice and silt and fine sand-sized material.

Young trees growing in the area where seedlings were sampled along Kautz Creek have been observed annually from the date of the initial sampling, July 1958, through September 1968. They show no signs of dying and appear, on the contrary, to be growing well. If it were true that the first seedlings did not survive, then along a transect across progressively older sur-

TABLE 1.—*Summary of data and computed interval between time of ground stabilization and seed germination in areas of known history*

Area	Altitude (feet)	Number sampled	Species	Year of seed germination	Year of ground stabilization	Time interval (years)	Average interval (years)
Nisqually Glacier moraines	4,200–4,600	22	Hemlock, Douglas fir, and willow	1933–1958	1931–1956	2–13	7
Nisqually River flood-plain deposits.	3,900	Many	Douglass fir, hemlock, and noble fir.	1956–1957	1956	<1–1	1
Kautz Creek debris-flow deposits	2,500	7	Alder	1948–1958	1947	1–11	6
		4	Cottonwood	1948–1958	1947	1–11	6
		4	Willow	1955–1957	1947	8–10	9
		7	Hemlock	1949–1957	1947	2–10	6
		7	Red cedar	1952–1959	1947	5–12	7
		6	Douglas fir	1948–1952	1947	1–5	4
		4	White pine	1952–1954	1947	5–7	6
		1	Noble fir	1954	1947	7	7
Total		40					
Average							6
Emmons Glacier moraines	4,800–5,300	37	Engelmann spruce	1902–1956	1900–1955	1–25	4
		9	Alpine fir	1934–1947	1900–1945	2–30	4
		7	Mountain hemlock	1936–1956	1895–1950	6–41	9
		2	Douglas fir	1943–1944	1903–1914	30–40	35
		1	Lodgepole pine	1953	1948	5	5
		1	Hemlock	1948	1938	10	10
Total		57					
Average							6
Carbon River flood deposits	2,900	4	Douglas fir	1960–1961	1959	<1–1	1
		2	Red cedar	1960	1959	<1	<1
		2	Noble fir	1960–1961	1959	<1–1	<1
Total		8					
Average							1
Mount St. Helens road embankment.	3,400	15	Douglas fir and hemlock	1963	1962	1	1
Total		>142					
Average							5

faces, one would expect to find zones of dead seedlings or saplings, which we have not found below three glaciers.

On the basis of this evidence (table 1) we add an interval of 5 years to the number of rings counted for dating moraines below altitudes of 4,800 feet at Mount Rainier. This figure is subtracted from the sampling year; and the result, rounded to the next oldest 5 years, yields the approximate calendar date of recession of the ice from the sampling site.

We assume that the interval at the start of glacial recession in the mid-19th century was the same as that of the last 25 years for valley-bottom sites. The glaciers started to recede probably because of an amelioration of climate which probably favored seed production and germination. That the more rigorous climate that may have prevailed during glacier advances did not adversely affect trees bordering the ice is evidenced by their presence on these sites now. If the climate during a glacial advance had had an adverse effect upon tree growth, a consistent pattern of slower growth among trees close to the glaciers should be expected. Cores taken from 114 such trees failed to show a pattern of growth consistent with that expectation.

The recognition of a deposit, pumice layer X, on young surfaces on the flanks of Mount Rainier, Wash., erupted during the 19th century (Mullineaux and others, 1969) (p. B15–B18, this chapter), permits the determination of the germination interval at places where no other evidence of the surface age is available. The pumice, sparsely distributed on the northeast side of the mountain, occurs within the area of an older but lithologically similar pumice from which it cannot be distinguished. The younger pumice can be recognized only by its presence on surfaces formed after the older pumice was deposited. Close dating of morainal ridges in a complex of Emmons Glacier end moraines permitted the pumice eruption to be limited between the dates of 1820 and 1854 (Mullineaux and others, 1969) (p. B15–B18, this chapter).

At altitudes near timberline the germination interval may very well be much longer than it is at lower elevations as shown by tree ages on a young moraine below Ohanapecosh Glacier (fig. 1) between 5,600 and 5,900 feet in altitude. Pumice layer X is present on some of these moraines. The oldest of 10 trees cored on one moraine on which was found pumic layer X, which must have been formed before 1854, was 3 inches tall in 1878, proving the interval before germination of this tree to be at least 23 years.

If it is assumed that the oldest tree sampled on the Ohanapecosh Glacier moraine represents one of the

first to become established after the moraine became stabilized, then the long interval at Ohanapecosh Glacier must be attributed to the harsh subalpine environment in the vicinity of the moraine. Late-lasting snow, a short growing season, and low night temperatures inhibit germination of seedlings of subalpine fir and mountain hemlock, the two tree species that grow here.

An older moraine, bare of trees and other plants, lies just downvalley from the moraine upon which the A.D. 1878 tree is growing. This moraine consists solely of boulders ranging from less than 1 foot to 10 feet in diameter and lacks fine material. Even though it has been stable longer than the younger moraine upvalley, tree seed cannot germinate on it because of the lack of a seedbed.

The longer interval inferred for the high-altitude site at Ohanapecosh Glacier may be true for other similar sites. The oldest trees on a moraine on the east side of Emerald Ridge, between 5,000 and 5,500 feet altitude, for example, were 6 inches tall in 1857, whereas the oldest trees are 10 to 15 years older on the same moraine about half a mile southeastward and about 1,200 feet lower in altitude. At Emerald Ridge, we have no evidence other than the tree ages as to when ice receded from the moraine, and can only propose that the two parts of the moraine are the same age.

The possible reasons for discrepancies among germination intervals in different areas may lie in different combinations of controls in the establishment of seedlings. The different intervals found in different areas emphasize the need to determine the intervals in each region.

REFERENCES

Bray, J. R., 1964, Chronology of a small glacier in eastern British Columbia, Canada: Science, v. 144, p. 287–288.

Bray, J. R. and Struik, G. J., 1963, Forest growth and glacial chronology in eastern British Columbia, and their relation to recent climatic trends: Canadian Jour. Botany, v. 41, p. 1245–1271.

Division of Timber Management Research, 1965, Silvics of forest trees of the United States: U.S. Dept. Agriculture, Forest Service, Agriculture Handbook no. 271, 762 p.

Harrison, A. E., 1956, Fluctuations of the Nisqually Glacier, Mt. Rainier, Washington: Jour. Glaciology, v. 2, p. 675–683.

Heusser, C. J., 1957, Variations of the Blue, Hoh, and White Glaciers during recent centuries: Arctic, v. 10, p. 139–151.

Heusser, C. J., Schuster, R. L., and Gilkey, A. K., 1954, Geobotanical studies of the Taku Glacier anomaly: Geog. Rev., v. 44, p. 224–239.

Lawrence, D. B., 1958, Glaciers and vegetation in southeastern Alaska: Am. Scientist, v. 46, p. 89–121.

Mullineaux, D. R., Sigafoos, R. S., and Hendricks, E. L. 1969, An historic eruption of Mount Rainier, Washington, *in* Geological Survey Research 1969: U.S. Geol. Survey Prof. Paper 650–B, p. B15–B18.

Sigafoos, R. S., and Hendricks, E. L., 1961, Botanical evidence of the modern history of Nisqually Glacier, Washington: U.S. Geol. Survey Prof. Paper 387–A, p. A1–A20.

DISTRIBUTION OF MERCURY IN THE NAVAJO SANDSTONE, COLORADO PLATEAU REGION

By R. A. CADIGAN, Denver, Colo.

Abstract.—**Mercury values in the Navajo Sandstone vary regionally in a nonrandom pattern. The pattern indicates the presence of anomalous concentrations of high values which may be related to hydrologic phenomena and to economically significant mineralization. The highest values of mercury, silver, and copper were found in an elongated group of adjacent localities that are alined parallel to a regional structural lineament.**

Ninety-one samples collected from widely spaced outcrops of Navajo Sandstone in the Colorado Plateau region were analyzed for gold, copper, silver, and mercury as part of the Heavy Metals program of the U.S. Geological Survey. Seventy-eight samples contained detectable mercury, 16 contained detectable silver, 6 contained detectable copper, and none contained detectable gold. Because few values were reported for silver and copper, this is principally a report on the regional distribution of the mercury values. The samples were selected as representative of the unit and included only typical rock, barren of visible traces of ore mineralization.

The Navajo Sandstone of Jurassic and Triassic(?) age is probably a continental eolian formation (Huntington and Goldthwait, 1904, p. 203–207; Gregory, 1917; Baker and others, 1936). It lies above and intertongues with the terrestrial to marginal marine Kayenta Formation (Triassic?) and underlies and intertongues with the marine to marginal marine Carmel Formation (Jurassic). The Navajo is believed to straddle the Triassic-Jurassic time boundary (Lewis and others, 1961; Poole, 1965).

In the Colorado Plateau region (fig. 1) the Navajo Sandstone is typically a persistent relatively uniform pale-brown very fine grained to fine grained well-sorted sandstone characterized by conspicuous large-scale cross-bedding. Figure 1 shows the regional extent of the formation, its variation in thickness, areas where it has been removed by erosion, and location of the present outcrops. The unit thickens to the west, ranging in thickness from zero not far east of the Utah-Colorado border to more than 2,000 feet in southwestern and western Utah. Jobin (1962) considered the Navajo to have the largest transmissive capacity of all the hydrologic sedimentary units in the Colorado Plateau region. The direction of sediment movement

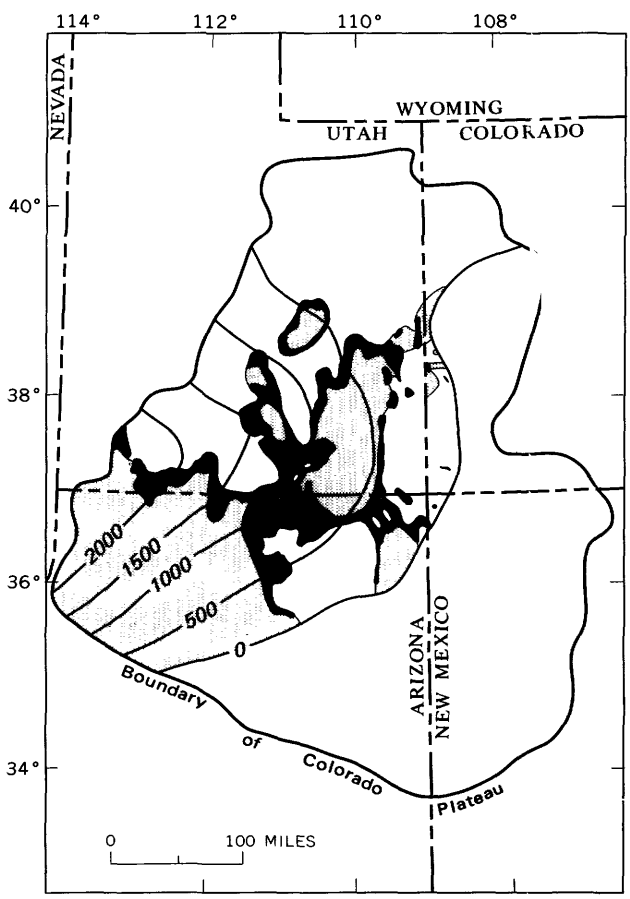

FIGURE 1.—Isopach map of the Navajo Sandstone in the Colorado Plateau region, showing outcrop and eroded areas. From Jobin (1962). Black, outcrops; stipple, eroded areas. Isopach interval 500 feet.

U.S. GEOL. SURVEY PROF. PAPER 650-B, PAGES B94-B100

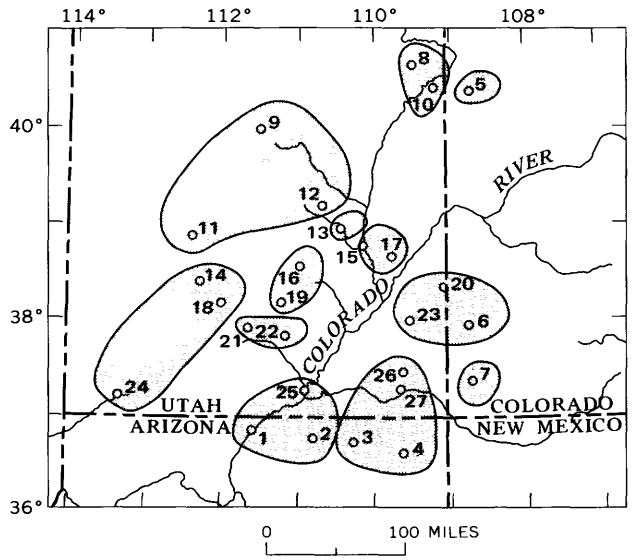

FIGURE 2.—Sample locality map. Sample localities within stippled areas are discussed in text; numbers correspond to those given in tables 1 and 2.

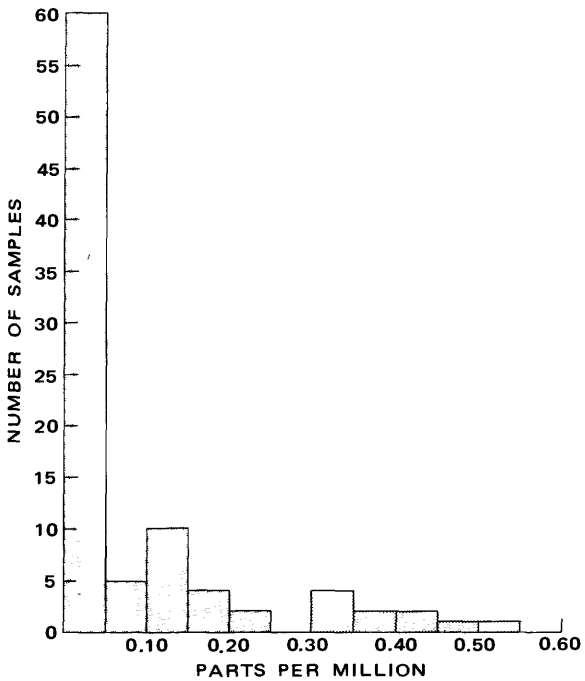

FIGURE 3.—Frequency distribution of arithmetic mercury values in 91 samples of the Navajo Sandstone. Average, 0.090 ppm; median (estimated), 0.045 ppm.

during deposition of the Navajo as interpreted from crossbed orientations by Poole (1965) was generally southeastward.

DETERMINATION OF A REGIONAL DISTRIBUTION PATTERN OF MERCURY

The 91 discrete rock samples were collected at the 27 localities shown in figure 2. The samples consisted of 86 fine-grained and very fine grained moderately well sorted to very well sorted sandstones and 5 of different lithology which are described in the footnotes to table 1. Half of the samples were collected by the author; the remainder were collected by R. F. Wilson, the late J. C. Wright, R. B. O'Sullivan, and others, while they were making stratigraphic studies and mapping in the Colorado Plateau region during 1948–66.

Sampled localities are listed by number and name in table 1. Locality names that are grouped under one number are those that have been consolidated to avoid clusters of overlapping or closely spaced dots on the sample locality map. Phi median grain size in millimeters is listed in the table and serves as a minimum lithologic description of the individual samples.

Analytical work was done at the U.S. Geological Survey Field Center, Denver, Colo. Analyses for mercury were made by W. W. Janes; those for gold by E. G. Martinez, T. A. Roemer, and A. J. Toevs; and those for silver and copper by J. D. Mensik and J. A. Thomas. The mercury determination was made by the large-volume atomic-absorption technique described by Vaughn (1967). Gold determination was made by an atomic-absorption technique (Huffman and others, 1967). Silver and copper were determined quantitatively by means of the atomic-absorption technique described by Huffman, Mensik, and Rader (1966) and by Huffman (1968).

Figure 3 illustrates the arithmetic frequency distribution of the mercury values. The number of samples is plotted over mercury content in parts per million. The values range from <0.010 to 0.500 ppm. The calculated mean or average value of the distribution is 0.090 ppm; the median value estimated from a probability graph of the cumulative frequency is 0.045 ppm. For purposes of mathematical calculation, values of <0.010 were assigned an arbitrary value of 0.005 ppm. The average mercury content of unmineralized sandstones is stated by J. H. McCarthy (oral commun., 1968) to be 20–30 parts per billion.

The statistical distribution of mercury values is highly skewed toward the low values. The term "L-shape" is sometimes used to describe such distributions, which are common in ore-grade and geochemical abundance studies. Mathematical or graphical analysis of L-shaped distributions has three major disadvantages. First, the mean or average of a small number of samples will generally overestimate the true mean of the population (Sichel, 1947, 1952); the population in this study is the Navajo Sandstone taken as a whole. Second, because of the departure from normal symmetry, measures of central tendency such as stand-

TABLE 1.—*Atomic-absorption analyses of Navajo Sandstone samples*

[Amounts (in parts per million) are shown only where they equal or exceed the detection limits which are 10 ppm for Cu, 0.2 ppm for Ag, and 0.01 ppm for Hg. Leaders (--) indicate that the amount present is less than the detection limit. Au was not detected in any sample]

Locality No. (fig. 2)	Locality name	Sample No. (each prefixed by "L")	Phi median grain size (mm)	Metal looked for (ppm) Cu	Ag	Hg
	Arizona					
1	Lees Ferry	3110	0.095	--	--	0.030
2	Navajo Canyon	3060	.141	--	--	.040
		3061	.122	--	--	.015
		3062	.094	--	--	--
3	Kayenta	3095	.105	--	--	--
		3096	.098	--	--	.030
4	Rock Point	3926	.120	--	--	--
		3927	.114	--	--	--
		3928	.075	--	0.3	--
		3929	.120	--	--	--
		3930	.111	--	--	--
	Colorado					
5	Skull Creek	2142	0.087	--	0.2	0.070
6	Horseshoe Bend	989	.115	--	--	.300
		990	.095	--	.3	.500
7	McElmo Canyon	277	.091	17	--	.460
		278	.086	11	.4	.350
		279	.075	--	--	.300
		280	.092	--	.2	.400
		281	.088	--	--	.200
		282	.084	--	.2	.400
		283	.102	--	--	.300
		284	.090	--	.7	.140
		1410	.076	--	.3	.030
	Utah					
8	Vernal	3522	0.164	--	--	--
		3523	.275	--	--	0.040
		3524	.163	--	--	--
		[1] 3525	--	--	--	--
	Brush Creek	2120	.141	--	--	.040
9	Thistle	3104	.117	--	--	.030
		3105	.169	--	--	.030
10	Cliff Creek	2516	.078	--	0.3	--
11	Meadow Creek	3067	.091	--	.3	--
		3068	.153	--	--	.020
12	Cedar Mountain	2836	.040	15	4.0	.150
		2838	.207	--	--	.140
13	Black Dragon Canyon	429	.092	--	.2,	.020
		430	.128	--	--	.220
		431	.113	--	--	.040
		432	.154	--	--	.140
		433	.138	--	--	.220
		434	.146	--	--	.160
	Utah—Continued					
14	Deer Trail Mountain	3101	.084	--	--	.020
		[2] 3102	--	--	--	.020
15	Chaffin Ranch area	2811	.153	--	--	.015
		2812	.125	--	--	.030
	VABM Butte [3]	4009	.152	--	--	.015
		4010	.158	--	--	.040
		4011	.152	--	--	.030
		4012	.165	--	--	--
	Green River	4027	.115	--	--	--
		4028	.103	--	--	.020
15	Bobbin Butte	4031	.123	--	--	.030
		4032	.124	--	--	.030
	Red Wash	4067	.137	45	--	.030
		4068	.184	220	0.2	.060
	Jeep Trail	4075	.159	--	--	.020
		4076	.161	--	--	--
16	San Rafael Swell.	1388	.119	--	--	.015
17	Sevenmile Canyon.	1399	.074	--	--	.015
		[4] 3786A	.096	--	2.0	.010
		[5] 3786B	--	39	.8	.015
18	Antimony Creek.	3074	.081	--	--	.160
		3075	.269	--	--	.040
19	Pleasant Creek	1671	.107	--	--	.100
		1672	.111	--	--	.040
		1673	.123	--	--	.100
		1674	.123	--	--	.030
		1683	.231	--	--	.140
		1684	.112	--	--	.030
		1685	.112	--	--	.140
		1686	.121	--	--	.015
20	LaSal Creek	328	.103	--	0.2	.350
		2802	.017	--	--	.015
21	Pine Creek	2925	.148	--	--	.040
		2926	.128	--	--	.060
22	Circle Cliffs area:					
	Burr Trail	1422	.180	--	--	.015
	Steep Creek	1737	.232	--	--	.040
		1738	.104	--	--	.015
		1739	.104	--	--	.080
		1740	.123	--	--	.100
		[6] 2306	.017	--	.3	--
	Silver Falls	3123	.275	--	--	.090
23	Indian Creek	959	.121	--	--	.160
		960	.100	--	--	.300
24	Leeds	2196	.238	--	--	.040
		2197	.190	--	--	--
25	Hole-in-Rock	3117	.092	--	--	.015
		3118	.158	--	--	.030
26	Butler Wash	3023	.142	--	--	.060
		3024	.142	--	--	.120
27	Comb Ridge	1432	.188	--	--	.020

[1] Siliceous concretion.
[2] Very fine grained sandstone completely cemented with quartz overgrowths.
[3] An unnamed feature, indicated by vertical-angle bench mark, shown in sec. 1, T. 24 S., R. 16 E., on U.S. Geological Survey topographic map of Green River, Utah; sample locality designated by J. C. Wright.
[4] Limestone from a shallow depression or pan on top of the formation.
[5] Silica interbedded with limestone in sample L3786A.
[6] Purple siltstone possibly derived from volcanic ash from 1-foot-thick localized lens.

ard deviation will be of questionable use. Third, graphic plots or maps cannot show detail in the lower values without expanding the higher values, which causes difficulties with scale (Williston, 1964).

An acceptable solution to these problems connected with the L-shaped distribution is the conversion of the mercury values to logarithms, a process termed by statisticians as a "log transformation." After transformation of the arithmetic distribution to a log distribution, several methods (Sichel, 1947, 1952; Miesch, 1967) are available for obtaining a statistically acceptable estimate of the mean content of mer-

cury in the Navajo. Logarithms to the base 10 are conventionally used; but in this study, done without the use of a computer, an arbitrary log scale was used. Class limits of convenience were advanced on a geometric scale, such as 25 parts per billion, 50 ppb, and 100 ppb, and each interval was assigned a log, such as 3.0, 4.0, and 5.0, as used in the method suggested by Sichel (1952, p. 272). A graphic log table was constructed on semilog paper by writing the log values along the arithmetic scale and the parts per million along the log scale. Intersection points of the assigned logs and parts per million were plotted and connected with a straight line.

This system of logarithms (actually logarithms to the base 0.00625) yields convenient class intervals as shown below:

Values of mercury (ppm)	Log_{10}	[1] $Log_{0.00625}$
0.003125	7.49485–10	0
0.00625	7.79588–10	1 00
0.0125	8.09691–10	2.00
0.025	8.39794–10	3.00
0.050	8.69897–10	4.00
0.100	9.00000–10	5.00
0.200	9.30103–10	6.00
0.400	9.60206–10	7.00
0.800	9.90309–10	8.00
(Interval)	(0.30103)	(1.00)

[1] $Log_{0.00625}$ of a number N may be obtained in the following manner:

$$Log_{0.00625}=\frac{Log_{10}N}{0.30103}+8.321919$$

Figure 4 is a histogram of the log-frequency distribution of the mercury values. The first two classes are discordant because the second class straddles the 0.010-ppm detection limit of mercury. Many of the arbitrarily assigned 0.005-ppm values may actually lie within the limits of the second class. Regardless of this discrepancy, the transformation markedly reduces the asymmetry of the original distribution. The calculated mean of the log distribution is 3.57, the antilog of which is 0.037 ppm. This estimate of the population mean compares favorably with the mean, 0.038, calculated according to the method for estimating the mean of a censored distribution described by Miesch (1967, p. B7–B8). The median, estimated graphically with probability paper, is 0.040 ppm.

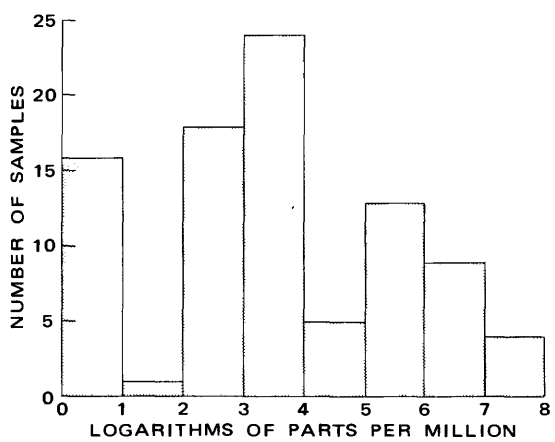

FIGURE 4.—Frequency distribution of logarithmic mercury values in 91 samples of the Navajo Sandstone.

The means or averages of the log values at each numbered map locality (fig. 2, table 1) are listed in table 2 with the number of samples, range of values, and averages of the arithmetic values. The averages of the log values are contoured in figure 5. Areas enclosed by the 4.0 contour are designated as high-mercury-content-areas and are shaded for emphasis.

The pattern produced by the contoured mercury values shown in figure 5 suggests the presence of three

TABLE 2.—*Average mercury content of Navajo Sandstone samples from localities in the Colorado Plateau region*

[Leaders indicate no range of values]

Locality No.	Locality name	No. of samples	Range (ppm)	Average mercury content (ppm)	
				Arithmetic	Logarithmic
	Arizona				
1	Lees Ferry	1		0.030	3.26
2	Navajo Canyon	3	[1] 0.005–0.040	.020	2.21
3	Kayenta	2	[1] .005– .030	.017	1.97
4	Rock Point	5		[1] .005	.68
	Colorado				
5	Skull Creek	1		0.070	4.49
6	Horseshoe Bend	2	0.300–0.500	.400	6.97
7	McElmo Canyon	9	.030– .460	.319	6.22
	Utah				
8	Vernal	5	[1] 0.005–0.40	0.019	1.88
9	Thistle	2		.030	3.26
10	Cliff Creek	1		[1] .005	.68
11	Meadow Creek	2	[1] .005– .020	.012	1.68
12	Cedar Mountain	2	.140– .145	.145	5.54
13	Black Dragon Canyon	6	.020– .220	.133	4.98
14	Deer Trail Mountain	2		.020	2.68
15	Chaffin Ranch area	14	[1] .005– .060	.024	2.59
16	San Rafael Swell	1		.015	2.26
17	Sevenmile Canyon	3	.010– .015	.013	2.13
18	Antimony Creek	2	.040– .160	.100	4.68
19	Pleasant Creek	8	.015– .140	.074	4.19
20	LaSal Creek	2	.015– .350	.233	4.54
21	Pine Creek	2	.040– .060	.050	3.98
22	Circle Cliffs area	7	[1] .005– .100	.049	3.34
23	Indian Creek	2	.160– .300	.230	6.15
24	Leeds	2	.005– .040	.022	2.18
25	Hole-in-Rock	2	.015– .023	.023	2.76
26	Butler Wash	2	.060– .120	.090	4.77
27	Comb Ridge	1		.020	2.68

[1] Values reported at less than 0.010 ppm have arbitrarily been assigned the value of 0.005 ppm to avoid zero values.

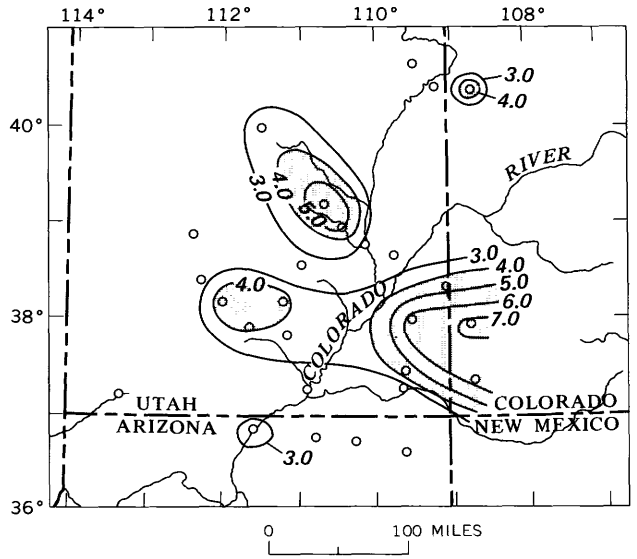

FIGURE 5.—Contour map based on the locality averages of the logarithms of the mercury values in the Navajo Sandstone. Shaded areas represent averages above 4.0, or 0.050 ppm of mercury.

generally high-content areas. The largest is in the southwestern corner of Colorado and the southeastern corner of Utah; the other two are in central and south-central Utah. The regional pattern suggests a general trend of decreasing mercury values from southeast to northwest.

The degree to which this pattern is representative of the "true" regional distribution pattern of mercury in the Navajo Sandstone cannot be tested without an additional sampling program comparable to this one. Figure 5 thus may or may not be a fair representation of the regional mercury distribution pattern, but as a preliminary sampling, it yields the following valuable information: (1) an estimate of the average mercury content; (2) a strong suggestion that the regional distribution is probably nonrandom; (3) the location of some probable regional anomalies; and (4) a suggested regional trend.

A linear trend surface was fitted to the data of figure 5 by a least squares method: the resulting surface reduces the sum of squares by only 8 percent and dips gently N. 80° W., representing a weak linear trend of values that decrease to the west-northwest. The quadratic surface, shown superimposed over the linear surface in figure 6, has the same orientation. The quadratic surface decreases the sum of squares by 41 percent and has a very highly significant correlation ($r=0.644$) with the location log averages. The regional trend of the mercury values thus appears to be curvilinear in the form of a west-northwest extending lobe.

Randomness of the regional distribution of logarithms of the mercury values was tested by means of chi-square and probability of randomness or P_r (Cadigan, 1962). For statistical purposes it was necessary to group the localities before testing so that there was a minimum of five samples per group. The resulting 12 locality groups were: 1, 2, and 25; 3, 4, 26, and 27; 5; 8 and 10; 6, 20, and 23; 7; 9, 11, and 12; 13; 15 and 17; 16 and 19; 21 and 22; 14, 18, and 24. In conformance with conventional practice the level of significance was chosen as $P_r=0.05$. Regional distributions which depart significantly from randomness will yield a P_r of 0.05 or smaller. P_r of the regional distribution of mercury was found to be <0.01, which suggests that the mercury values are not randomly distributed and that the west-northwestward trend suggested above is probably real. Such a trend then must be interpreted in terms of geologic factors.

GEOLOGICAL INTERPRETATION

The Navajo Sandstone probably contains both syngenetic and epigenetic mercury. The syngenetic mercury was probably inherited from the source of sediments and accumulated with the sediment during deposition, and it presumably shows a relationship to the thickness and orientation of the formation, as syngenetic minerals usually do. Epigenetic mercury could be related to hydrologic phenomena and thus reflect regional movement of intrastratal fluids, which would form a regional dispersion pattern. Dispersion patterns related to hydrothermal mineralization have been reported by Saukov (1946), Williston (1964), and

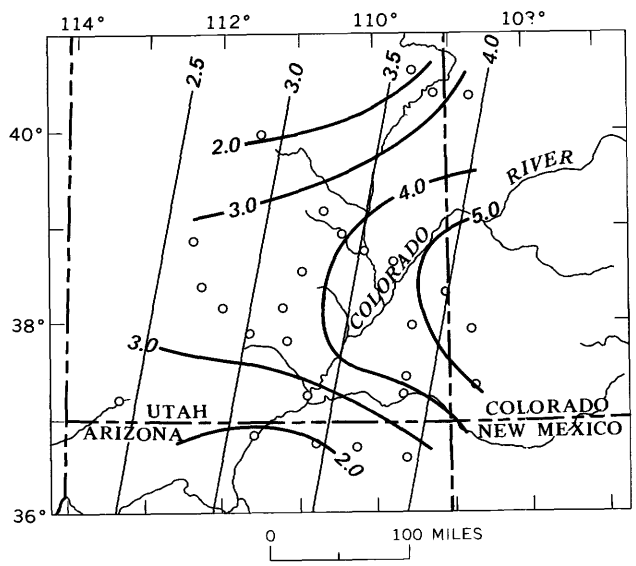

FIGURE 6.—Computed linear (lighter lines) and quadratic (heavier lines) surfaces fitted by least-squares method to data of figure 5.

Erickson, Marranzino, Oda, and Janes (1964). Such hydrothermal dispersion patterns, however, are of a much smaller scale than the regional pattern detected in this study of the Navajo Sandstone in the Colorado Plateau region.

The dominant curvilinear west-northwestward trend of the mercury values is opposite in orientation to the direction of sediment movement. This suggests that the dominant trend is related to the presence of epigenetic mercury originating from postdepositional hydrologic phenomena. The high values along the eastern edge of the Navajo suggest that this is the location, or at least the source direction, of the most important contributions of the epigenetic mercury. Perhaps the direction of movement of water within the Navajo during the time of emplacement of the epigenetic mercury was west-northwestward, toward the thickest part of the Navajo Sandstone.

The shaded high-mercury-content areas in figure 5 contain intrusive igneous centers (Ekren and Houser, 1965; Witkind, 1964) and numerous uranium deposits (Ekren and Houser, 1965, p. 61; Fischer and Hilpert, 1952). However, numerous igneous centers and uranium deposits lie outside the high-mercury areas of figure 5, and so do, for example, the Silver Reef silver-copper deposits that are accompanied by low-mercury values in the Navajo, at Leeds, Utah (loc. 24).

Figure 7 shows those localities which contain the five highest values each of silver, copper, and mercury. The underlined symbols indicate the locality of the single highest value of each of the three metals. The 15 high values are contained in 10 different samples that were collected from just 5 of the 27 localities.

No significant statistical correlations for the three metals were obtained from the individual sample values. Copper and silver values show a tendency to be positively correlated. Copper and mercury, and silver and mercury values, show a tendency to be negatively correlated within the same sample. The occurrence of the highest values in a few common localities, combined with the lack of within-sample correlation noted above, suggests that the metals are independently related to common sources. Superposition of the high metal values is probably not a chance occurrence; and the lack of within-sample correlation suggests a direct connection between sources and host rocks rather than an indirect connection involving a mercury-copper-silver solution in relative equilibrium.

It should be noted that these localities lie within, and are alined roughly parallel to the axis of, the tectonically active Pennsylvanian-Tertiary Paradox basin (Cater and Elston, 1963), a major regional unstable structural element in the central part of the Colorado Plateau.

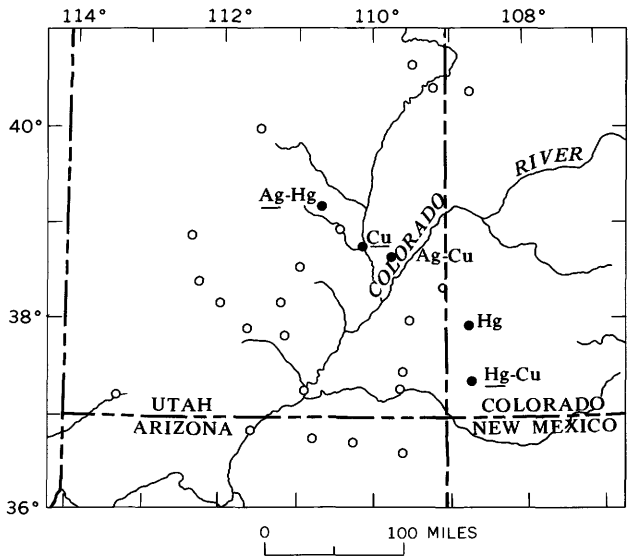

FIGURE 7.—Localities containing the five highest values of silver, copper, and mercury in samples from the Navajo Sandstone. Underlined symbols indicate locality of single highest value for each metal.

CONCLUSIONS

The following conclusions have been drawn from this reconnaissance study:

1. An extensive fairly uniform sedimentary unit, such as the Navajo Sandstone, provides an excellent opportunity to obtain a regional geochemical dispersion pattern of mercury.

2. The interpretation of mercury values is easier to make if a logarithmic transformation is done on individual sample values and if transformed values are used on maps and other graphic aids.

3. The mercury geochemical dispersion pattern produced by the Navajo Sandstone samples used in this study delineates some of the areas in the Colorado Plateau region which may warrant additional exploration for silver, copper, and uranium ore deposits.

REFERENCES

Baker, A. A., Dane, C. H., and Reeside, J. B., Jr., 1936, Correlation of the Jurassic formations of parts of Utah, Arizona, New Mexico, and Colorado. U.S. Geol. Survey Prof. Paper 183, 66 p.

Cadigan, R. A., 1962, A method for determining the randomness of regionally distributed quantitative geologic data: Jour. Sed. Petrology, v. 32, no. 4, p. 813–818.

Cater, F. W., and Elston, D. P., 1963, Structural development of salt anticlines of Colorado and Utah, p. 52–159, *in* Backbone of the Americas—Tectonic history from pole to pole, a symposium: Am. Assoc. Petroleum Geologists Mem. 2, 320 p.

Ekren, E. B., and Houser, F. N., 1965, Geology and petrology of the Ute Mountains area, Colorado: U.S. Geol. Survey Prof. Paper 481, 74 p.

Erickson, R. L., Marranzino, A. P., Oda, Uteana, and Janes, W. W., 1964, Geochemical exploration near the Getchell mine, Humboldt County, Nevada: U.S. Geol. Survey Bull. 1198–A, p. A1–A26.

Fischer, R. P., and Hilpert, L. S., 1952, Geology of the Uravan mineral belt [Colorado Plateau]: U.S. Geol. Survey Bull. 988–A, p. 1–13.

Gregory, H. E., 1917, Geology of the Navajo country—a reconnaissance of parts of Arizona, New Mexico, and Utah: U.S. Geol. Survey Prof. Paper 93, 161 p.

Huffman, Claude, Jr., 1968, Copper, strontium, and zinc content of U.S. Geological Survey silicate rock standards, *in* Geological Survey Research 1968: U.S. Geol. Survey Prof. Paper 600–B, p. B110–B111.

Huffman, Claude, Jr., Mensik, J. D., and Rader, L. F., 1966, Determination of silver in mineralized rocks by atomic-absorption spectrophotometry, *in* Geological Survey Research 1966: U.S. Geol. Survey Prof. Paper 550–B, p. B189–B191.

Huffman, Claude, Jr., Mensik, J. D., and Riley, L. B., 1967, Determination of gold in geologic materials by solvent extraction and atomic-absorption spectrophotometry: U.S. Geol. Survey Circ. 544, 6 p.

Huntington, Ellsworth and Goldthwait, J. W., 1904, The Hurricane fault in the Toquerville district, Utah: Harvard Coll. Mus. Comp. Zoology Bull., Geol. Ser. 6, p. 199–259.

Jobin, D. A., 1962, Relation of the transmissive character of the sedimentary rocks of the Colorado Plateau to the distribution of uranium deposits: U.S. Geol. Survey Bull. 1124, 151 p.

Lewis, G. E., Irwin, J. H., and Wilson, R. F., 1961, Age of the Glen Canyon group (Triassic and Jurassic) on the Colorado Plateau: Geol. Soc. America Bull., v. 72, no. 9, p. 1437–1440.

Miesch, A. T., 1967, Methods of computation for estimating geochemical abundance: U.S. Geol. Survey Prof. Paper 574–B, p. B1–B15.

Poole, F. G., 1965, Paleowinds in the western United States, p. 394–405, *in* Nairn, A. E. M., ed., Problems in palaeoclimatology, Proceedings of the NATO Palaeoclimates Conference, University of Newcastle upon Tyne, January 1963: New York, Interscience Publishers, 705 p.

Saukov, A. A., 1946, Geokhimiya rtuti [The geochemistry of mercury]: Acad. Sci. USSR Inst. Geol. Sci. Trans. 78, Mineralog.-Geochem. Ser. 17, 129.

Sichel, H. S., 1947, An experimental and theoretical investigation of bias error in mine sampling with special reference to narrow gold reefs: London, Inst. Mining and Metallurgy Trans., v. 56, p. 403–474.

———1952, New methods in the statistical evaluation of mine sampling data: London, Inst. Mining and Metallurgy Trans., v. 61, p. 261–288.

Vaughn, W. W., 1967, A simple mercury vapor detector for geochemical prospecting: U.S. Geol. Survey Circ. 540, 8 p.

Williston, S. H., 1964, The mercury halo method of exploration: Eng. Mining Jour., v. 165, no. 5, p. 98–101.

Witkind, I. J., 1964, Geology of the Abajo Mountains area, San Juan County, Utah: U.S. Geol. Survey Prof. Paper 453, 110 p.

DISTRIBUTION OF MINOR ELEMENTS IN SAMPLES OF BIOTITE FROM IGNEOUS ROCKS

By TOM G. LOVERING, Denver, Colo.

Abstract.—Two hundred samples of biotite taken from several types of igneous rocks from many localities have been analyzed by a semiquantitative spectrographic method in the laboratories of the U.S. Geological Survey. Thirty-six minor elements were detected in one or more of these samples. Ca, Na, Ti, Mn, Ba, Co, Cr, Cu, V, Sc, Ni, and Sr were detected in more than 90 percent of the samples. Biotite samples from different parent rock types show corresponding differences in concentrations of minor elements. Biotite from granitic pegmatite and pyroclastic rocks contains detectable Mo, and biotite from syenite and nepheline syenite commonly contains Ag.

Biotite is a primary silicate mineral that is easily recognized in a wide variety of igneous rocks. It is found in rocks as siliceous as granitic pegmatite and as silica deficient as peridotite and pyroxenite. Its composition is approximately $K(Mg,Fe)_3(Al,Si_3)O_{10}(OH,F)_2$. Since the development of the potassium-argon method of geochronology, many samples of biotite have been submitted to the laboratories of the U.S. Geological Survey for age determination. Splits of 165 of these biotite separates taken from representative samples of igneous rock were analyzed spectrographically by a semiquantitative spectrographic method. Data on 35 other biotite samples from igneous and metaigneous rocks analyzed by the same method for other projects are also considered in this investigation.

The distributions of the minor elements in this group of 200 samples of biotite taken from a variety of types of igneous rocks from many different localities are summarized here in the hope that they may provide information relevant to the characteristic distribution of such elements in primary magmatic biotite, and to the differences in minor element content that characterize biotite from different kinds of igneous rocks. The term "minor elements" is here used for cation elements that do not appear in the defining chemical formula for biotite.

Acknowledgments.—Thanks are due to Richard Marvin, who provided most of the biotite samples used in this study, to A. L. Sutton and Barbara Tobin, who made the analyses on this group of samples, and to Frank Dodge and Priestley Toulmin, who allowed me to include in this compilation data on their suites of biotite samples.

MINOR-ELEMENT DISTRIBUTIONS IN BIOTITE SAMPLES WITHOUT REGARD TO ROCK TYPE

Thirty-six minor elements were reported in one or more of the 200 biotite samples analyzed; these elements, and their maximum reported concentrations, are listed in table 1. Twelve of these elements were

TABLE 1.—*Maximum concentrations of the minor elements detected in 200 samples of biotite*

Element	Maximum concentration (percent)	Element	Maximum concentration (percent)	Element	Maximum concentration (percent)
Ag	0.0003	Gd	0.15	Pr	0.07
B	.003	Ho	.03	Sc	.03
Ba	7	La	.2	Sm	.07
Be	.001	Li	.15	Sn	.05
Ca	3	Lu	.015	Sr	.5
Ce	.5	Mn	3	Ti	5
Co	.015	Mo	.05	Tm	.015
Cr	.2	Na	7	V	.15
Cu	.3	Nb	.07	Y	.3
Dy	.07	Nd	.3	Yb	.005
Er	.15	Ni	.1	Zn	.07
Ga	.03	Pb	.03	Zr	.3

detected in more than 90 percent of the samples analyzed, and may thus be considered normally detected elements. Cumulative frequency distribution curves for these twelve (Ca, Na, Ti, Mn, Ba, Co, Cr, Cu, V, Sc, Ni, and Sr) are shown in figure 1. The distributions of Na, Ti, Co, and Sc are restricted, spanning less than two orders of magnitude.

The frequency distributions of the 24 remaining minor elements, which were detected in less than 90

U.S. GEOL. SURVEY PROF. PAPER 650-B, PAGES B101-B106

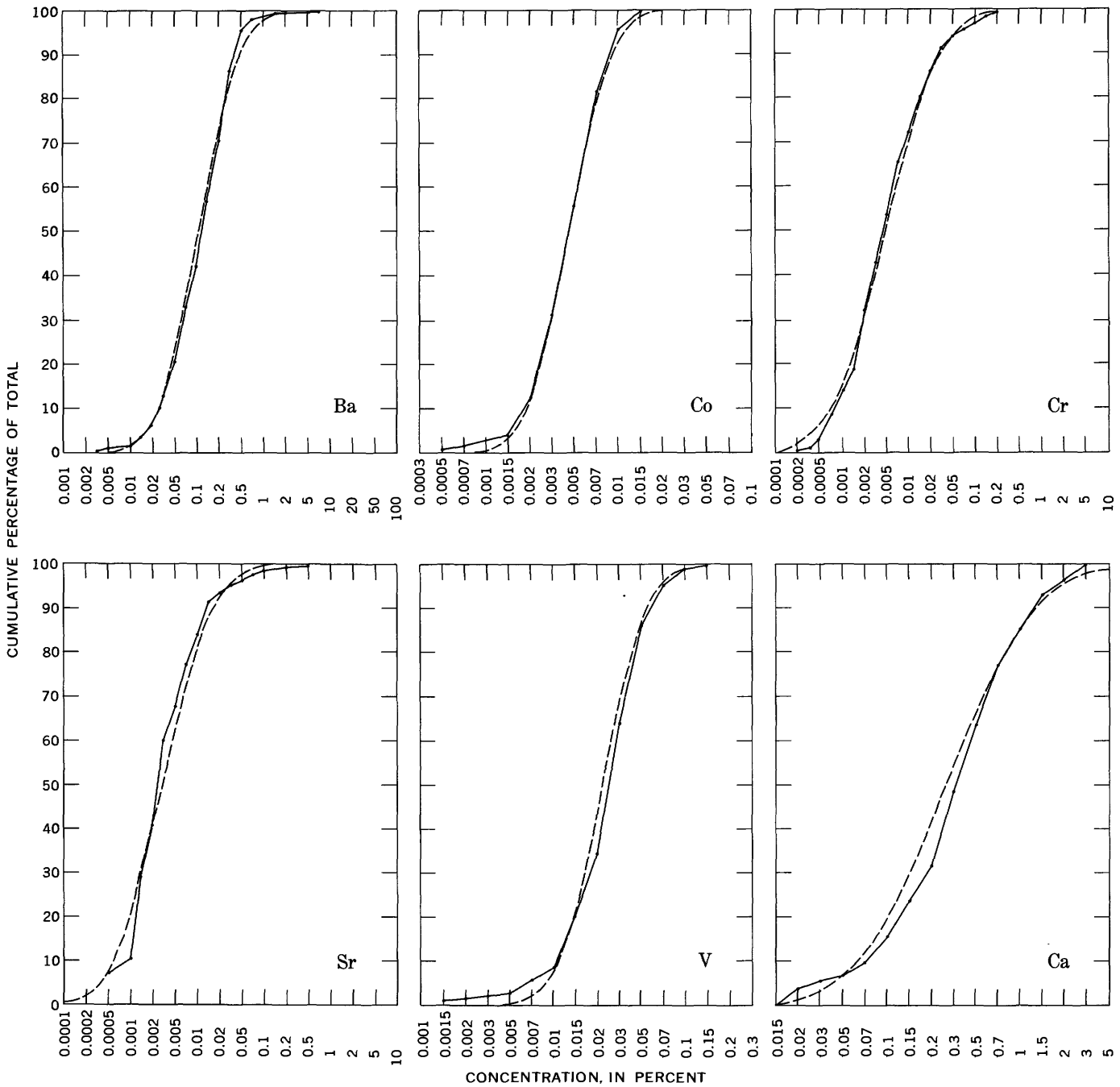

FIGURE 1.—Cumulative distribution curves of normally detected minor elements in 200 biotite samples. Solid line, cumulative sample frequency distribution; dashed line, cumulative normal frequency distribution fitted to data.

percent of the samples, cannot be specified because of their truncated nature. Data on these elements are summarized in table 2.

Several reports containing information on the composition of biotite samples have been published, but most of these pertain to biotite samples from metamorphic rocks. Nearly all the rest contain data on small groups of biotite samples separated from only a few types of igneous rocks in restricted areas, or data pertaining to only two or three elements in samples from many localities. The only published report of which I am aware that contains information on the composition of biotite derived from a variety of igneous rocks from several localities is one by Rimsaite (1964), in which the analyses of 18 biotite samples from igneous rocks in various parts of Canada are presented. Rimsaite's data were obtained with an X-ray spectrometer and are presented in tables of oxide analyses for 13 ele-

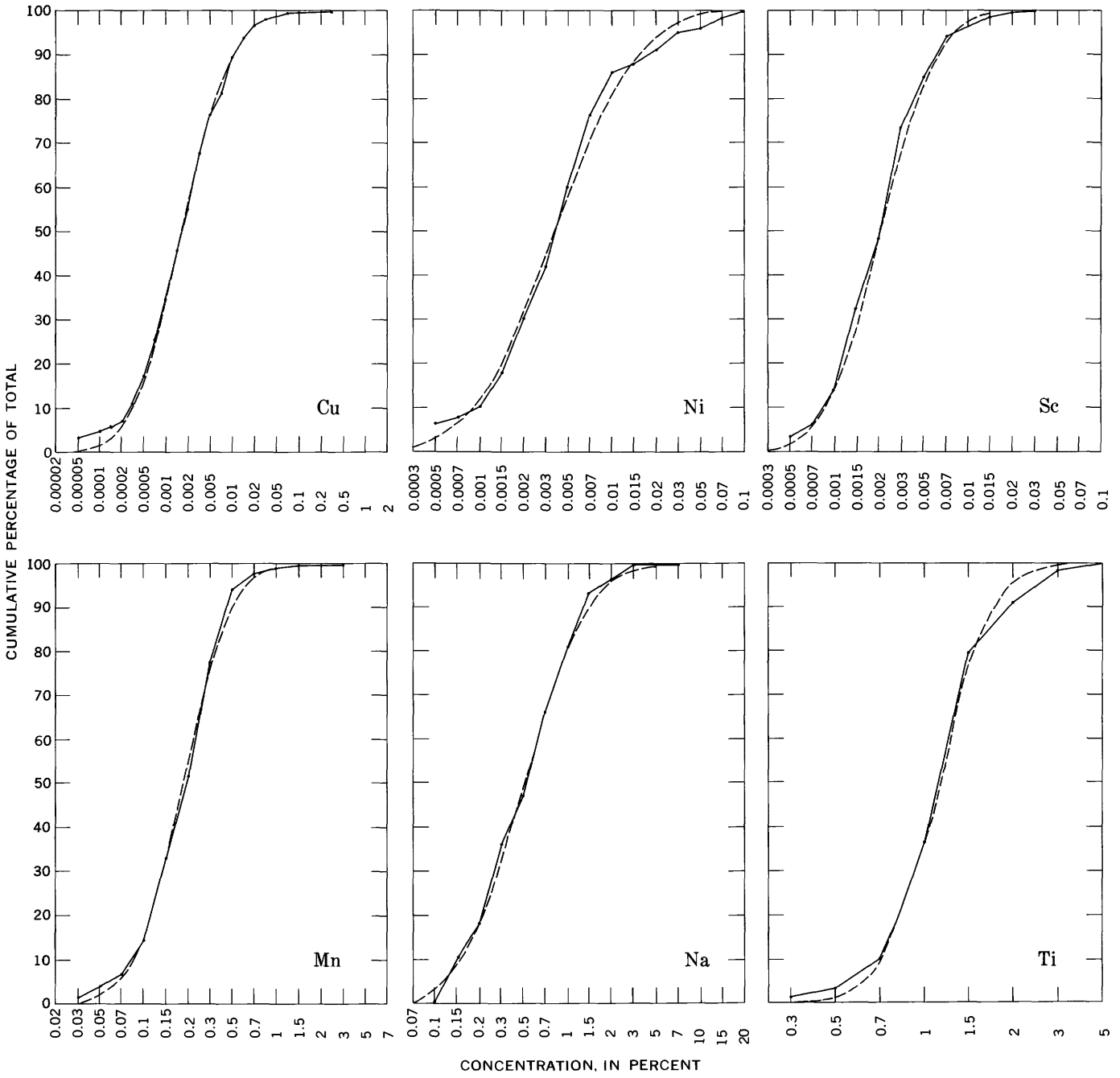

FIGURE 1.

ments. The oxides studied by Rimsaite, for which I have spectrographic data on the elements, are: TiO_2, MnO, V_2O_5, Cr_2O_3, NiO, ZnO, Ga_2O_3, CaO, BaO, and SrO. Table 3 compares the maximum, minimum, and median concentrations of these 10 elements, calculated from Rimsaite's table, with the corresponding values from my suite. The biotite samples from Rimsaite's igneous rocks in Canada show median concentrations of Ti, Mn, Ga, Ca, and Ba similar to those I found; however, her samples contain significantly more Cr, Ni, and Zn, and less V and Sr.

Descriptive and analytical data, and sample localities, on each of the 200 biotite samples, whose analyses are summarized in this report, are available elsewhere (Lovering, 1969).

MINOR-ELEMENT DISTRIBUTIONS IN BIOTITE SAMPLES FROM SPECIFIC ROCK TYPES

The suite of 200 biotite samples analyzed consists of 55 from granites, 35 from quartz monzonites, 41 from granodiorites, 10 from diorites, 9 from pegma-

TABLE 2.—*Summary of content (in percent) of minor elements not commonly detected in biotite*

Element	Median concentration	Limit of detection	Percentage of samples in which detected
Ag	<0.0001	0.0001	6.0
B	<.002	.002	3
Be	<.0001	.0001	17.5
Ce	<.015	.015	12
Dy	<.005	.005	1
Er	<.005	.005	.5
Ga	<.01	[1].01	5
Gd	<.005	.005	1
Ho	<.002	.002	1
La	<.003	.003	32.5
Li	<.01	.01	1.5
Lu	<.003	.003	.5
Mo	<.0003	.0003	24
Nb	.005	.0007	74
Nd	<.007	.007	28.5
Pb	<.001	.001	23.5
Pr	<.01	.01	1
Sm	<.01	.01	.5
Sn	<.001	.001	21
Tm	<.002	.002	.5
Y	.001	.001	50.5
Yb	<.001	[1].001	7
Zn	<.02	.02	20
Zr	.01	.001	79.5

[1] Concentrations were reported that were lower but were unreliable because of interference.

tites, 14 from mafic intrusive rocks, 16 from pyroclastic rocks, and 20 from other miscellaneous rocks. Ranges and median concentrations of 15 commonly detected elements in biotite samples from each of these rock types, except the miscellaneous group, are shown graphically in figure 2.

A recent report by Stern (1965, p. 160, 162) gives analyses of 46 biotite samples from granitic pegmatites of the Alps, for MnO, Na_2O, CaO, TiO_2, Cr, Sr, Ni, Zr, B, Be, and Ba. Because I have analyses of only 9 such samples, I have included the ranges and medians calculated from Stern's data adjacent to my own in figure 2 for comparison.

Biotite samples from granite, as compared to the entire suite of biotite samples, appear to be slightly enriched in Mn, Nb, Sc, Y, and Zr, and slightly deficient in V, Ba, Sr, and Cu. Those from quartz monzonite and granodiorite show a high median concentration for Mn, and low median concentrations for Cr, and Y. The few available biotites from diorite have high median concentrations of Ba, Mn, Cr, and Ni, and low median concentrations of Sr, Nb, and Y. The suites of biotite samples from granitic pegmatites and from mafic intrusive rocks predictably show the greatest contrast in their minor-element concentrations, as the parent rocks show the greatest diversity in composition. The biotite samples from granitic pegmatite show high median values for Nb, Sc, and Y, and low median values for Ca, Na, Ba, V, Ti, Cr, and Ni. The group from mafic intrusive rocks shows high median values for Ca, Na, Ba, Sr, Cr, Co, Ni, and Cu, and low median values for Ti, Mn, Nb, Sc, Y, and Zr. The pyroclastics, from which biotite samples were analyzed, are a heterogeneous group; however, most of them are tuffs, welded tuffs, and ash with rhyolitic or quartz latitic composition. The biotites from these rocks yielded high median values for Ca, Na, Ti, Ba, Sr, Co, Sc, and Cu; they did not yield low median values for any of the commonly detected elements.

The significance of the median values for these elements in biotites from the various rock types varies with the number and geographic distribution of the

TABLE 3.—*Summary of data on 10 minor elements in 18 biotite samples from igneous rocks in Canada, as compared to data in this report.*

[Data derived from Rimsaite (1964, table 2, p. 162); author's data in parentheses]

Element	Maximum (percent)	Minimum (percent)	Median (percent)
Ti	3.4 (5.0)	0.2 (0.3)	1.7 (1.2)
Mn	.58 (3.0)	.04 (0.03)	.31 (0.2)
V	.006 (0.15)	<.006 (0.0015)	<.006 (0.025)
Cr	.37 (0.2)	<.03 (0.0002)	.03 (0.004)
Ni	.165 (0.1)	.004 (0.0005)	.012 (0.004)
Zn	.11 (0.07)	.02 (<0.02)	.05 (<0.02)
Ga	.01 (0.03)	<.0015 (<0.01)	.003 (<0.01)
Ca	1.8 (3.0)	<.04 (0.015)	.3 (0.3)
Ba	.85 (7.0)	.045 (0.003)	.18 (0.12)
Sr	.036 (0.5)	<.0008 (<0.0005)	.0008 (0.002)

TABLE 4.—*Percentage of the biotite samples, from various types of igneous rocks, in which the less common minor elements were detected*

Element	Parent rock type							
	Granite (55 samples)	Quartz monzonite (34 samples)	Granodiorite (41 samples)	Diorite (10 samples)	Pegmatite (9 samples)	Mafic intrusive rocks (14 samples)	Alkalic rocks (6 samples)	Pyroclastics (16 samples)
Ag					22	7	83	19
B	2							25
Be	24	41		40			50	
Ce	24		2	20	22		17	19
Dy	2				11			
Er					11			
Ga	7			10	55		33	
Gd	2				11			
Ho	2				11			
La	60	18	5	30	55	7	33	56
Li	4	3						
Lu					11			
Mo	9	12			100	43	50	88
Nd	53	15	5	30	44	7	33	44
Pb	40	24	2	20	67	7	17	19
Pr				10	11			
Sm					11			
Sn	49	18	5	30	11			
Tm					11			
Yb	22	3		20				
Zn	51	6	7	10		7		

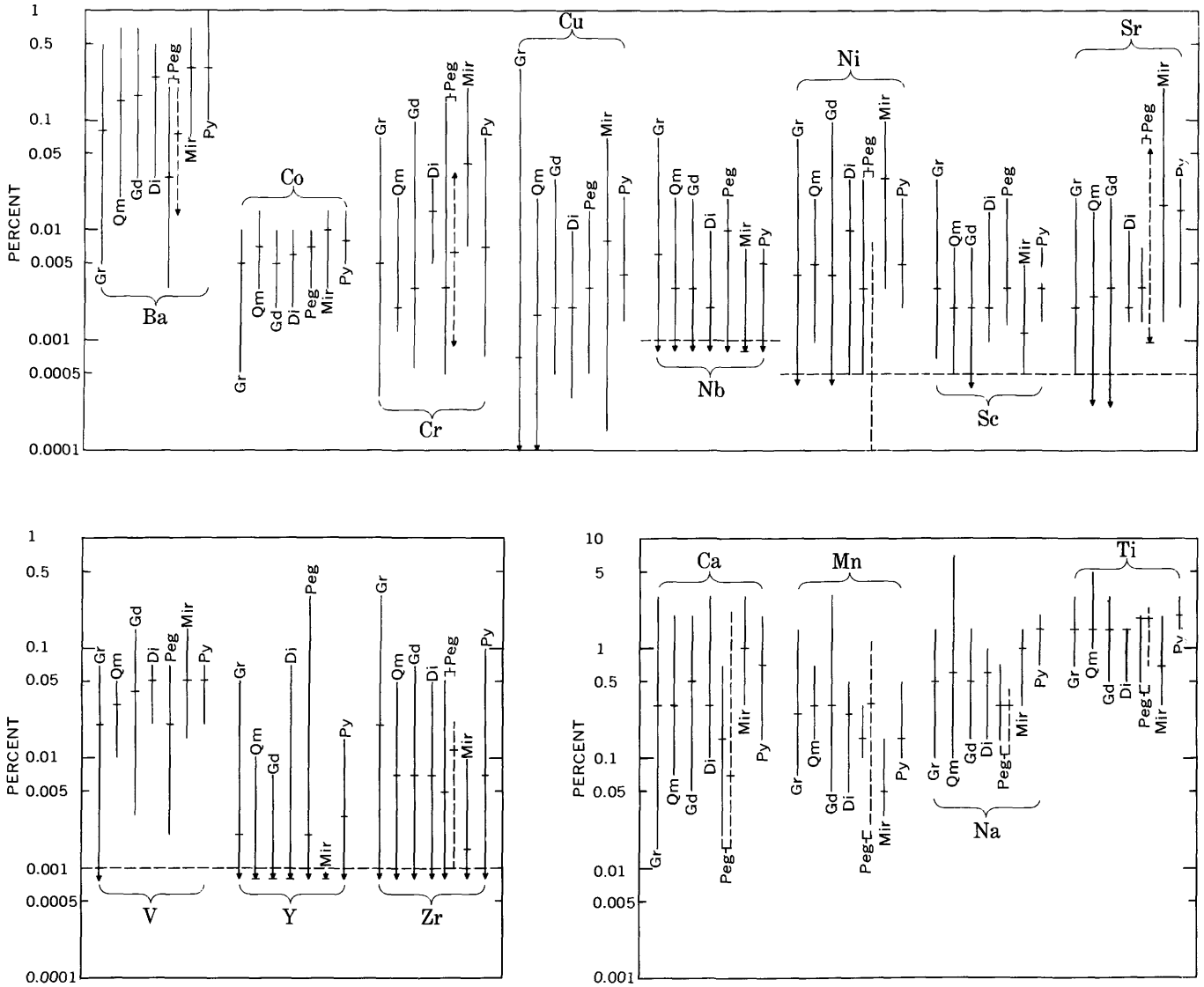

FIGURE 2.—Range of commonly detected elements in biotite samples from various rock types: Gr, granite; Qm, quartz monzonite; Gd, granodiorite; Di, diorite; Peg, pegmatite; Mir, mafic intrusive rocks; Py, pyroclastic rocks. Dashed vertical lines represent data derived from Stern (1966, tables 1a and 2). Dashed horizontal lines represent limits of detection. Tick on vertical line indicates median.

samples, and also with the overall dispersion of values for each element. The lowest median value for copper is in biotites from granites; yet the highest copper content in any sample was found in biotite from granite. Differences in median values for elements showing wide dispersion in values (Ba, Cr, Cu, Sr), in groups composed of fewer than 20 samples, may have no real significance.

Table 4 shows the proportions of biotite samples from 8 rock types, in which the occasionally and rarely detected elements were found. Although only 6 samples of biotite from alkalic rocks were analyzed, this group is included because of the unusually high concentration of certain minor elements it exhibits.

CONCLUSIONS

Interpretation of the significance of a compilation of chemical analytical data, such as the one summarized in this report, is complicated by many factors: (1) Separated biotite fractions are commonly impure, containing other minerals, as random loose grains, primary inclusions in the biotite flakes, and incipient alteration products. (2) The samples are certainly not representative of biotites in general. Specific areas and rock types are represented out of proportion to their actual frequency of occurrence. Furthermore, some rock samples from which biotite was separated were altered or otherwise atypical of any large rock mass. (3) The analytical methods used are not highly precise.

The minor-element distributions in biotite samples, summarized in this report, are suggestive of those in the primary biotite populations from which the samples were taken, but for the reasons outlined above, they cannot be considered as truly representative of these populations. For these reasons, no interpretative statistical treatment is made of the data.

Many more analyses of biotite from rocks, other than the silicic plutonic rocks, are needed to establish the characteristic distributions of minor elements in their primary biotite. The apparent concentration of Mo in biotite derived from granitic pegmatite and pyroclastic rocks, and of Ag in biotite derived from syenite and nepheline syenite (alkalic rocks, table 4) seems particularly worthy of investigation.

REFERENCES

Lovering, T. G., 1969, Distribution of minor elements in samples of biotite from igneous rocks—basic data: U.S. Geol. Survey open-file report.

Rimsaite, Jadvyga, 1964, On micas from magmatic and metamorphic rocks: Beiträge zur Mineralogie und Petrographie, v. 10, p. 152–183.

Stern, W. B., 1966, Zur Mineralchemie von Glimmern aus Tessiner Pegmatiten: Schweiz. Mineralog. Petrog. Mitt., v. 46, p. 137–188.

SUBSURFACE DEFORMATION RESULTING FROM MISSILE IMPACT

By H. J. MOORE, Menlo Park, Calif.

Work done on behalf of the National Aeronautics and Space Administration

Abstract.—Partial excavation of craters produced in indurated gypsum and alluvium by missiles with oblique trajectories revealed five distinct zones of deformation: (1) mixed breccia, (2) sanded material, (3) a zone of conjugate fractures, (4) tilted and broken material, and (5) a zone of open fractures. These zones, which are similar to those produced by explosives in natural materials, are distributed with bilateral symmetry about the plane of the missile trajectory. The sizes of the mixed breccias are in reasonable agreement with predictions using simple scaling laws derived from data on mixed breccias produced by explosives. The scaling laws do not, however, predict the difference in sizes of the mixed breccias of craters in gypsum and craters in alluvium.

Studies of craters produced by missile impact are being conducted as part of a broader program of lunar research on behalf of the National Aeronautics and Space Administration (NASA) as an aid in understanding and interpreting lunar surface features and properties. Continued lunar exploration, and manned landings on the Moon, will require additional data on impact craters, and the results of the present studies should also further studies of terrestrial impact craters. With these objectives in view, four craters were trenched to permit examination of subsurface deformation and structures.

The trenching revealed that complicated deformation accompanies formation of craters by missile impact. Materials beneath the crater floors are fragmented, compressed, sheared, and jumbled. Conjugate fractures and open fractures are found beneath the crater rims and flanks. Movement of the materials is indicated by ejection of debris, mixing of compressed material beneath the crater floor, flow-banding of some material, uplift of the ground surface, and upward rotation of fracture patterns.

Acknowledgments.—This work was done under NASA Contract R–66. J. F. McCauley aided in mapping the craters and the trenches. David Cummings and Donald Gault helped in measuring the acoustic velocities. The Command at White Sands Missile Range, N. Mex., generously supported the studies by providing photography of the craters, data on the kinetic energies of the missiles, and trenching of the craters.

METHOD OF INVESTIGATION

The craters were produced by missile impacts on two types of materials: (1) indurated gypsum dunes, and (2) alluvium with an underlying layer of gypsum. Physical properties of indurated gypsum dunes differ significantly from those of alluvium underlain by gypsum. The unconfined compressive strength of small cylinders of the indurated gypsum is about 4.1 to 5.5×10^6 dynes/square centimeter; shear-vane readings are comparable but range from 1.4 to 6.1×10^6 dynes/cm^2. The density of the indurated gypsum is generally about 1.55 grams/cubic centimeter but locally is as low as 1.37 g/cm^3. The acoustic velocity of nearby indurated gypsum dune material, measured in place, is about 0.93 kilometers/second. No mechanical data for the alluvium are available, but shear-vane readings at nearby craters in similar material are about 0.61 to 2.0×10^6 dynes/cm^2. The density of the alluvium is about 1.42 g/cm^3, and the acoustic velocity (Hans Ackermann, oral commun., 1968) is 0.23 to 0.26 km/sec.

Detailed surface topography and ejecta distribution of 3 of the 4 craters were mapped at a scale of 1:48 within 8 hours after their formation. The 2 craters in indurated gypsum dunes were trenched within several days after formation, and the 2 in alluvium 2½ months later. Trenches were mapped immediately at a scale of 1:72.5.

The kinetic energy and angle of impact of the missiles were 1.60×10^{15} ergs and near 47° from the horizontal for the craters in indurated gypsum, and 1.35

U.S. GEOL. SURVEY PROF. PAPER 650-B, PAGES B107–B112

328–687 O—69——8

TABLE 1.—*Summary data on experimental cratering*

Target material	Density (g/cm³)	Kinetic energy of missile (ergs)	Impact angle of missile (degrees)	Apparent size of crater		Volume (cm³)
				Radius [1] (m)	Depth [2] (m)	
Gypsum sand, indurated	1. 37–1. 55	1. 60×10¹⁵	47	2. 24	1. 36	9. 86×10⁶
	1. 37–1. 55	1. 60×10¹⁵	47	2. 49	1. 40	14. 4×10⁶
Alluvium and gypsum	1. 42	1. 35×10¹⁵	48	2. 20	. 97	6. 03×10⁶
	1. 42	1. 35×10¹⁵	48	[3]		

[1] Average of radii parallel and perpendicular to plane of trajectory at the original ground level.
[2] Measured from original ground surface to deepest part of crater floors.
[3] Crater not mapped because of possible interference with another experiment.

$\times 10^{15}$ ergs and near 48° for the craters in alluvium and gypsum. The experimental data are summarized in table 1.

DESCRIPTION OF CRATERS

The general characteristics of missile-impact craters have been reported previously (Moore, 1966; Moore and others, 1964) and are here summarized. The craters are depressions produced by ejection of debris as a result of impact of missiles with natural materials. For oblique trajectories, the ejecta are deposited symmetrically about the plane of the missile trajectory and are concentrated at right angles to that plane and in "down" trajectory directions (direction in which the missile was going). Very little or no ejecta is deposited "up" trajectory (direction from which the missile came).

Materials in and around the crater may be mapped and classified into seven categories: target material, thick ejecta unit, thin to discontinuous ejecta unit, tilted and broken target material, shattered target material, slope material, and fallout. Target material is the undeformed material around the craters. The thick ejecta unit is composed chiefly of fragmented target material deposited around the crater in thicknesses exceeding 3.0 to 6.0 cm. Thick ejecta also contain scattered fragments of the missile and compressed target material. The thin to discontinuous ejecta unit is composed of ejected target material with thicknesses decreasing outward from 3.0 to 6.0 cm to zero. At the outer limit of this unit, scattered ejecta cover a constant percentage of the area of the surface. Small pieces of missile are also found in this unit. A few scattered fragments may occur beyond the thin to discontinuous ejecta blanket to distances of 0.122 to 0.305 km. Tilted and broken target material is composed of coarsely fractured and rotated target material in the upper crater walls. Shattered target material is finely fractured material in the "up" trajectory wall, and slope material is talus and fallback within the crater at the angle of repose. Fallout is fine debris which settles from the air; its distribution is partly determined by the wind velocity and direction at the time of crater formation. An oblique view of a missile-impact crater is shown in figure 1.

FIGURE 1.—Oblique view of crater formed by missile impact in indurated gypsum dune. Arrow indicates trace of missile trajectory. Crater is about 4.98 m across and 1.40 m deep, and large blocks are about 0.46 m across. Note bilateral symmetry of ejecta and absence of ejecta on "up" trajectory side. Photograph courtesy of U.S. Army.

DEFORMATION ZONES

Partial excavation of the missile-impact craters showed five deformation zones (fig. 2): (1) mixed breccia, (2) sanded material, (3) a zone of conjugate fractures, (4) tilted and broken material, and (5) a zone of open fractures.

Mixed breccia

The mixed breccia (fig. 3) is composed of fragments of compressed target material and fragments of the missile in a matrix of finer debris. The fragments are

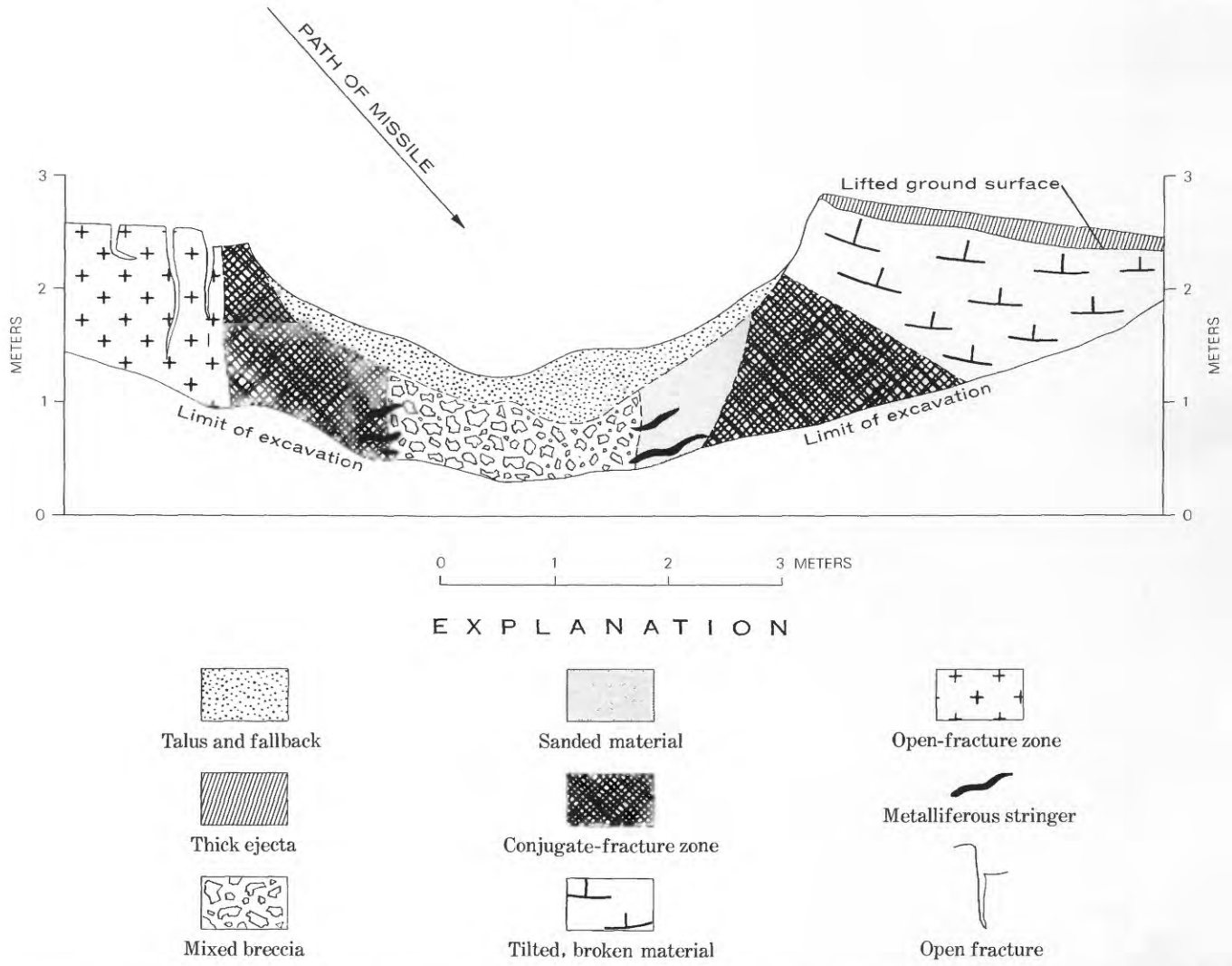

FIGURE 2.—Structure section of missile-impact crater in indurated gypsum dune, showing zones of deformation. Section is parallel to plane of missile trajectory.

jumbled, and no simple pattern can be seen. Surfaces of adjacent large fragments are rarely parallel. Fragments of both the compressed target material and missile reach dimensions of as much as 15 cm, but they are generally smaller. Many of the smooth surfaces of compressed target material are polished, striated, and grooved, showing that they have been sheared. Many surfaces of the fragments are partially coated with a thin veneer of powderlike missile material, and small pieces of the missile may be found within the fragments or embedded in the sheared surfaces. Although the maximum density of the target material is near 1.5 g/cm^3, many of the fragments have been compressed to a density as high as 2.2 g/cm^3. Many pieces of the admixed missile are twisted, bent, and striated.

Mixed breccia is located below the center of the crater floor (fig. 2). Exposed diameters of the mixed breccia beneath the craters in alluvium with an underlayer of gypsum measure 1.2 to 1.5 m across; those in indurated gypsum dunes measure 2.1 to 2.3 m across. Boundaries of mixed breccia with adjacent units are gradational; a few distinct stringers of projectile fragments originate in the mixed breccia and penetrate the sanded material (fig. 2).

Evidence of displacement of materials of the mixed breccia is ample. Fragments of sheared and compressed materials identical with those of the mixed breccia are found in the ejecta and slope material along with pieces of the missile. Although the sheared and compressed target material and projectile fragments are found chiefly in the mixed breccia and thick ejecta, a few scattered small fragments of the materials are found in the "up" trajectory directions.

In one of the craters in alluvium, where the underlying gypsum is about 0.9 m below the surface, fragments of sheared and compressed gypsum in the mixed

FIGURE 3.—Mixed breccia below crater floor. Dark fragments are pieces of missile. Note gray surfaces of some sheared-compressed gypsum which are coated with thin layer of powdered missile. Rule is about 12 inches (0.305 m) long. Photograph courtesy of U.S. Army.

breccia were displaced about 46 cm above their normal stratigraphic level. Minor amounts of gypsum were present in the ejecta.

Sanded material

The sanded material (fig. 4) is developed only in the craters in the indurated gypsum dunes. It is composed of disaggregated gypsum and small lumps of material which can be easily broken by finger pressure. No evidence of compression is found in the sanded zone, nor are pieces of the missile. Banding is developed in the sanded material near the contact with the mixed breccia, where the bands are subparallel to the contact. Toward the zone of conjugate fracturing, the banded appearance decreases and the frequency of small lumps increases laterally. This unit, where exposed, surrounds the mixed breccia on all but the "up" trajectory side, and its symmetry is bilateral about the plane of the trajectory.

As the sanded material is banded subparallel to the adjacent contacts and has the same sense of symmetry as the ejecta, it represents fabric produced by the flow of debris near the final stage of the ejection process.

Zone of conjugate fractures

The zone of conjugate fractures is characterized by a crisscross fracture pattern (fig. 5). This pattern is closely spaced near the sanded zone where fracture frequencies are about 25 to 35 fractures per linear foot. From the inner to the outer boundary of this unit, fracture frequencies decrease to about 8 fractures per linear foot and less. Near the contact with the sanded material, acute angles between fractures appear to be larger (near 70° to 60°) than those (near 60° to 50°) about a meter from the boundary. Although the two fracture sets normally intersect at one point, they are locally offset a fraction of a centimeter or so along one fracture plane or the other. Such offsets, which suggest a shearing motion, are most frequent near the sanded-material boundary. The whole fracture pattern is flexed upward below the crater rim where individual fracture planes can be followed along their curving traces.

Exposures of the zone of conjugate fracturing encircle the mixed breccia and sanded material. For the craters in indurated gypsum dunes the exposures are about 6.1 m across. For one of the craters produced in alluvium, it is about 4.6 m across, and for the fourth crater it is poorly defined.

Tilted and broken material

Widely spaced open fractures, some parallel to the ground surface and some perpendicular to it, form large blocks in the tilted and broken material. The large blocks, which are formed by tensile failure, are devoid of internal conjugate fractures and are themselves un-

FIGURE 4.—Sanded material and banding. Conjugate-fracture zone is toward left, and mixed breccia is toward right. Rule is about 12 inches (0.305 m) long. Photograph courtesy of U.S. Army.

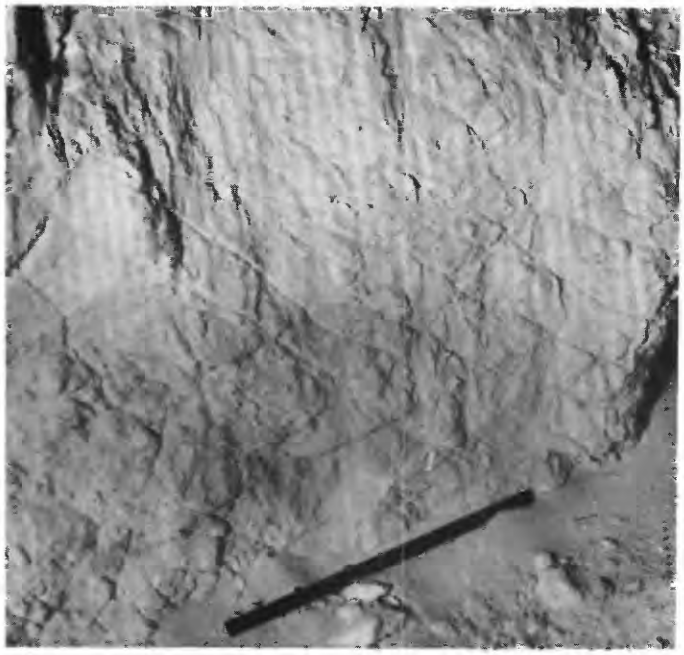

FIGURE 5.—Conjugate fractures. Sanded material to left. Rule is about 12 inches (0.305 m) long. Photograph courtesy of U.S. Army.

deformed. In contrast with lumps and pieces from the sanded material and zone of conjugate fractures, blocks of these materials can be broken only with difficulty. Beneath the crater rim, the blocks and their bounding fractures have been rotated upward.

Like the ejecta and sanded material, the tilted and broken material is present in the "down" trajectory and lateral directions, but not in the "up" trajectory direction. The uplifted ground surface with its superposed ejecta is underlain by the tilted and broken material, which, in turn, partly overlies the zone of conjugate fractures (fig. 2).

The lateral extent of tilted and broken material is difficult to establish visually, but studies on similar craters in identical materials using an engineering seismograph with a 3.05-m geophone-source spacing indicate a significant change in acoustic velocities of indurated gypsum at distances between 5.5 and 8.9 m from the crater center for radials perpendicular to the trajectory plane and radials "down" trajectory. Within a few feet of the crater rim, acoustic velocities have decreased to less than a third or a fourth of the undisturbed gypsum. Thus, significant disruption of the indurated dune materials to distances of nearly 3 to 4 crater radii is produced by the impact. No such clear change of acoustic velocity occurs around the craters in alluvium which had initially low acoustic velocities (Hans Ackermann, oral commun., 1968).

Zone of open fractures

Fractures in the zone of open fractures differ from those in the tilted and broken material and occur on the "up" trajectory side of the crater. The fractures, which are concentric with the crater rim, are nearly vertical, and although the fractures are rare, their separations are large. No evidence for upward displacement is found here; rather, materials nearest the crater rim are either not displaced or are displaced a centimeter or so downward.

COMPARISON WITH DEFORMATION PRODUCED BY EXPLOSIVES

Deformation beneath missile-impact craters is similar to that around craters produced by explosives. For example, a mixed breccia underlies the floor and walls of Teapot ESS, a crater produced in alluvium at the Nevada Test Site by a 1.2±0.5-kiloton nuclear explosive (Shoemaker, 1960, p. B424). The mixed breccia of Teapot ESS is composed of sheared and compressed alluvium in a matrix of smaller blocks and debris with pieces of glass formed by fusion of the alluvium. Although the bedding is partially preserved in this mixed breccia, individual fragments are rotated, and fragments from one horizon have been introduced into regions composed principally of fragments from another horizon. The limit of mixed breccia of Teapot ESS is 18.6 m below the center of detonation of the nuclear device. Beyond the mixed breccia the alluvium is less disturbed, but conjugate fractures are common and shear displacements are locally present beneath the uplifted ground surface near the crater rim. Thus, at Teapot ESS, deformations similar to those of the missile-impact craters are present. However, the symmetry of deformation at Teapot ESS is axial and unlike the bilateral symmetry of the deformation zones of the missile-impact craters.

Deformations like those produced by missiles are apparently common in materials shocked by explosives. Strong compression occurs near the shotpoint; obliquely fractured (conjugate fractures) material occurs next to the region of strong compression; and large broken pieces and open fractures occur beyond fractured regions (for example, see Allsman, 1960, p. 471) where tensile stresses develop in expanding stress waves and near free surfaces when tensile stress develops by reflection of stress waves. Here again, the symmetry of the deformation zones is axial, unlike the bilateral symmetry of deformation zones produced by missiles with oblique trajectories.

It is of interest to compare the exposed radii of the mixed breccia of the missile-impact craters with those

reported for five experiments using explosives with TNT weight equivalents of between about 10^{-4} tons and 1.7 kilotons (Shoemaker, 1960, p. B425). Using the cube-root scaling equation of Shoemaker (1960, p. B425) to estimate the radii of the mixed breccias, we find

$$\frac{R}{W^{1/3}}=1.74\,\frac{\text{meters}}{\text{ton}^{1/3}},$$

where R is the distance of the limit of mixed breccia measured from the origin of shock and W is the energy released, in tons of TNT equivalent.[1] Radii for the mixed breccias of the impact craters are calculated near 0.56 m and 0.59 m when the TNT weight equivalents of the missiles are taken as 3.23×10^{-2} and 3.83×10^{-2} tons, respectively. These radii are of the correct magnitude, but they are a little smaller than those observed for the impact craters, which are 0.61 to 0.76 and 1.1 to 1.2 m. Such differences can be the result of the scaling law. For example, application of scaling laws currently used at the Nevada Test Site (Nordyke and Wray, 1964, p. 678), and Shoemaker's data for Teapot ESS to establish a constant, yields

$$\frac{R}{W^{1/3.4}}=2.9\,\frac{\text{meters}}{\text{ton}^{1/3.4}}.$$

This equation predicts radii for the mixed breccias of 0.74 to 0.85 m, which falls between the ranges for the missile-impact craters.

The inability of the simple scaling laws to predict the sizes of the mixed breccias for the missile-impact craters in both indurated gypsum and alluvium is probably the result of differences in mechanical properties of the materials. Thus, the effects of rock type on crater dimensions are important in missile-impact craters as well as in explosive craters (Nordyke, 1961, p. 3348).

SUMMARY

Complicated deformation accompanies crater formation by missile impact. Several types of deformation are represented by zones beneath the crater surfaces. A mixed breccia, which lies beneath the floor, is characterized by fragments of target material that have been compressed, sheared, and admixed with pieces of the projectile. Sanded material, which partly surrounds the mixed breccia, is banded, showing that flow of debris has occurred. A zone of conjugate fractures surrounding the mixed-breccia and sanded-material zones represents less intense deformation by shearing. Tilted and broken material which lies beneath uplifted surfaces in the "down" trajectory and lateral directions is characterized by large blocks bounded by fractures parallel to, and at right angles to, the ground surface. Open fractures found near the "up" trajectory rim represent tensile breaks.

Deformations beneath missile-impact craters are similar to those around craters produced by explosives. The chief differences between the two types of craters are the presence of pieces of projectile in the mixed breccia of impact craters and contrasting symmetry of the deformation zones, bilateral for impact craters produced by missiles with oblique trajectories and axial for craters produced by explosives.

Radii of mixed breccia zones of missile-impact craters are comparable in size to those produced by explosives with equivalent energies; but differences in material properties may be responsible for differences in sizes of mixed breccias produced by impacts of equal energies.

[1] 1 kiloton of TNT releases about 4.185×10^{19} ergs of energy (Nordyke and Wray, 1964, p. 678).

REFERENCES

Allsman, P. L., 1960, Analysis of explosive action in breaking rock: Am. Inst. Mining Metall. Petroleum Engineers Trans., v. 217, p. 469–478.

Moore, H. J., 1966, Craters produced by missile impact, *in* Crater investigations, Pt. B. *of* Astrogeologic studies annual progress report, July 1, 1965–July 1, 1966: U.S. Geol. Survey open-file report, p. 79–105.

Moore, H. J., Kachadoorian, Reuben, and Wilshire, H. G., 1964, A preliminary study of craters produced by missile impacts, *in* Crater investigations, Pt. B *of* Astrogeologic studies annual progress report, July 1963–July 1964: U.S. Geol. Survey open-file report, p. 58–92.

Nordyke, M. D., 1961, Nuclear craters and preliminary theory of the mechanism of explosive crater formation: Jour. Geophys. Research, v. 66, no. 10, p. 3439–3459.

Nordyke, M. D., and Wray, W., 1964, Cratering and radioactivity results from a nuclear cratering detonation in basalt: Jour. Geophys. Research, v. 69, no. 4, p. 675–687.

Shoemaker, E. M., 1960, Brecciation and mixing of rock by strong shock: Art. 192 *in* U.S. Geol. Survey Prof. Paper 400–B, p. B423–B425.

HAWAIIAN SEISMIC EVENTS DURING 1966

By ROBERT Y. KOYANAGI, Hawaiian Volcano Observatory, Hawaii National Park, Hawaii

Abstract.—During 1966, 388 earthquakes having a magnitude of 2.0 to 4.5 occurred in the Hawaiian Islands. The foci of four-fifths of these were along structural features beneath the active Kilauea and Mauna Loa volcanoes. Nearly 100 earthquakes were felt by residents of the Island of Hawaii.

The location of earthquakes in Hawaii during 1966, compiled by the Hawaiian Volcano Observatory, U.S. Geological Survey, are graphically displayed in this report, the fifth of a series of annual reports showing the distribution of Hawaiian earthquakes (Koyanagi, 1964; Koyanagi and Endo, 1965; Koyanagi and Okamura, 1966; and Koyanagi, 1968).

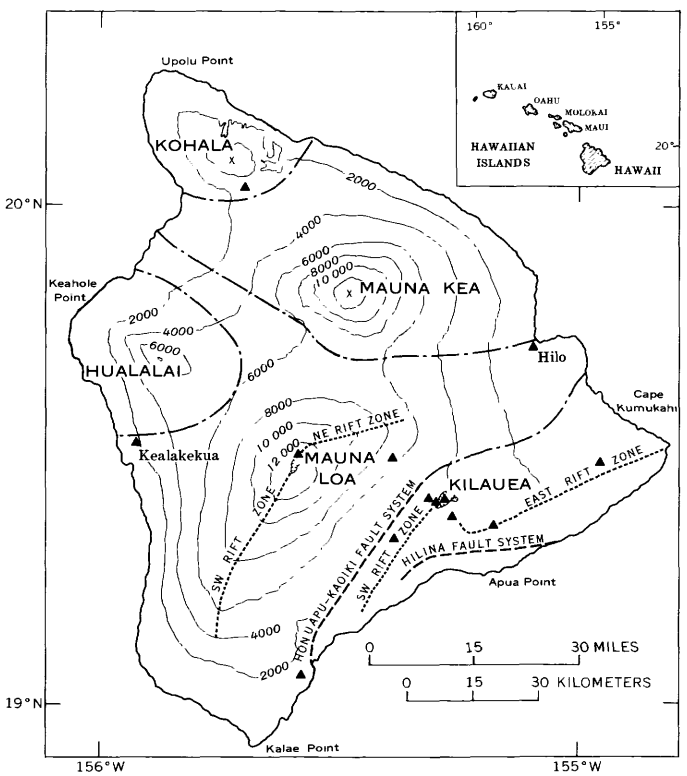

FIGURE 1.—Map of the island of Hawaii, showing the five volcanoes and their principal structural features. Dot-and-dash lines are boundaries of volcanic systems. Location of seismograph stations is indicated by closed triangles. Contour interval is 2,000 feet, and datum is mean sea level.

Earthquakes having a magnitude of 2.0 or greater that occurred beneath the five volcanoes and along the principal structural features of the island of Hawaii (fig. 1) during each quarter of 1966 are located in figure 2. Earthquakes having a magnitude of 2.0 or greater that occurred offshore along the Hawaiian Ridge from lat 18° to 23° N. and long 153° to 160° W. are plotted in figure 3. The earthquakes are plotted in 3 depth groups (less than 10, 10 to 20, and 20 to 60 kilometers) and 2 magnitude groups (2.0 to 3.5 and greater than 3.5). Also, quarterly counts and annual totals beneath the five volcanoes and offshore areas are given in figure 4.

The methods used to determine the location of the earthquakes are similar to those used in earlier reports and are subject to the same limitations. Due to traveltime anomalies and occasional recording inadequacies, a 5-km sphere of error should be allowed for the location of earthquake beneath the island of Hawaii. For events occurring offshore in areas of limited seismometric coverage, errors as large as 10 km may be expected.

CHRONOLOGY OF SEISMIC EVENTS DURING 1966

Small earthquakes numbering several tens per day occurred beneath the south flank of Kilauea during the first 3 weeks of January, as activity of the Kilauea flank eruption and seismic crisis of December 1965 (Fiske and Koyanagi, 1968) subsided. As flank seismicity decreased, however, a gradual increase in the number of shallow Kilauea caldera shocks (magnitude <2) was noticed. From less than 50 per day during the first 2 months, the average daily count rose to 80 during March, and reached a maximum in April when daily counts often exceeded 150.

U.S. GEOL. SURVEY PROF. PAPER 650-B, PAGES B113-B116

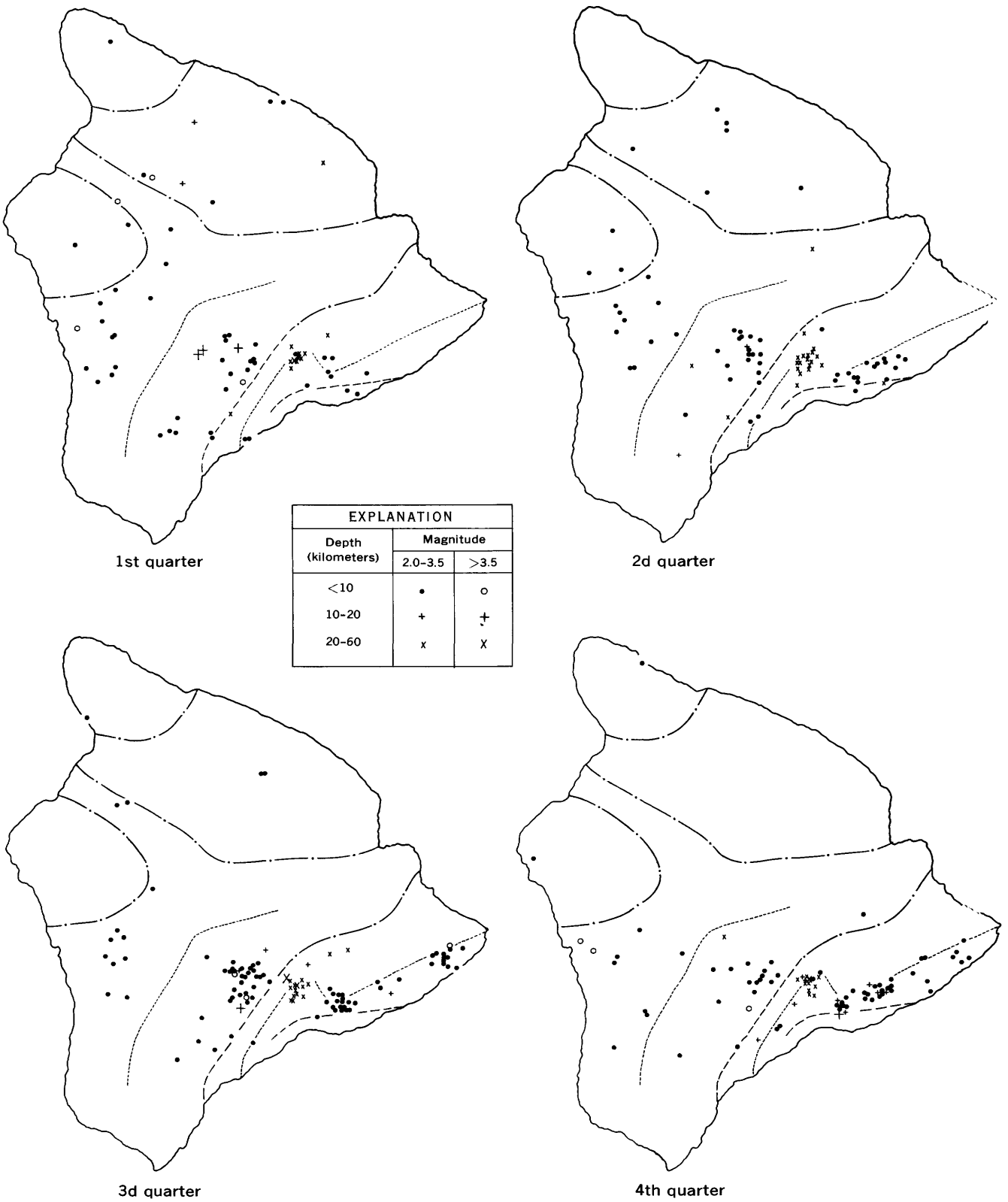

FIGURE 2.—Plot of epicenters of earthquakes having a magnitude of 2.0 or greater beneath the island of Hawaii during each quarter of 1966. Dot-and-dash lines are boundaries of volcanic systems, long-dashed lines are fault systems, and short-dashed lines are rift zones. Geographic names are shown in figure 1.

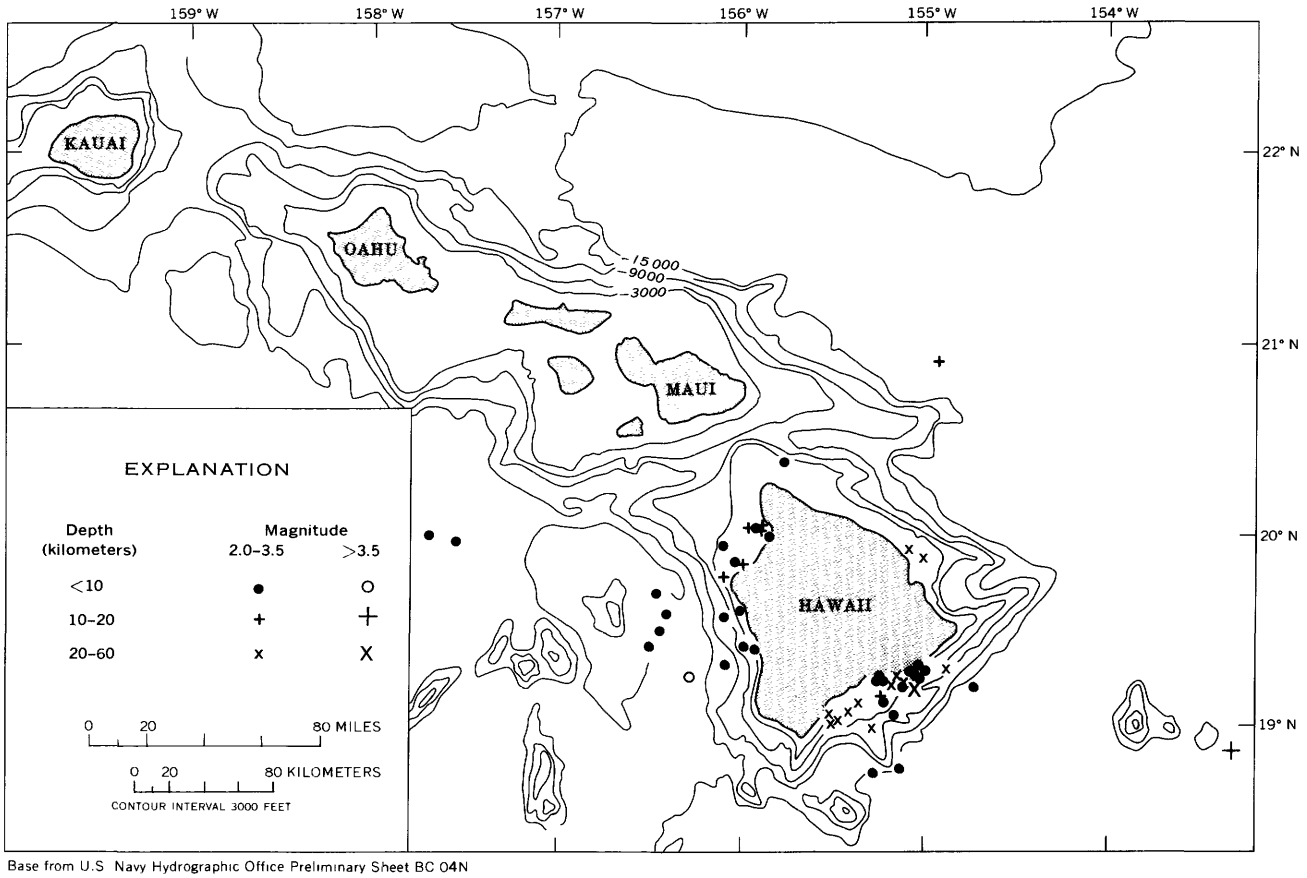

FIGURE 3.—Map of the Hawaiian Islands, showing epicenters of earthquakes having a magnitude of 2.0 or greater that occurred off the island of Hawaii during 1966.

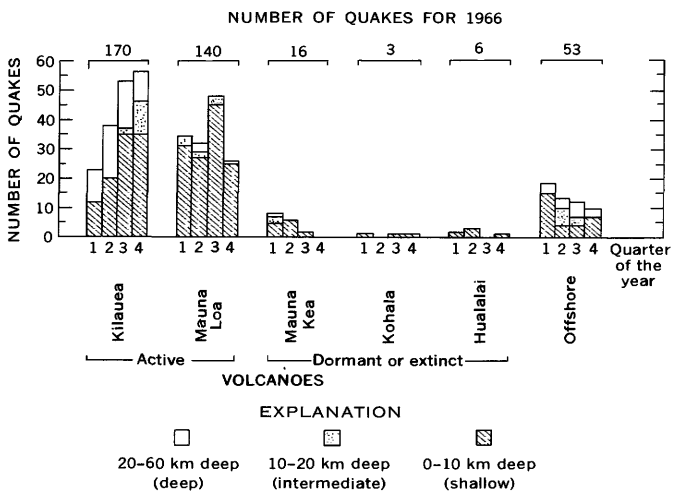

FIGURE 4.—Geographic location and the distribution, with depth, of earthquakes having a magnitude of 2.0 or greater that occurred in the Hawaiian Islands during 1966.

On July 5 a swarm of about 500 earthquakes occurred along the upper east rift and adjacent fault systems. On July 6 the largest event during this episode registered a magnitude of 2.8 at 01^h11^m and was felt in the Kilauea summit area.[1] Also in July, and extending into August, an increased level of activity was noticed along the lower east rift of Kilauea. Earthquake counts fluctuated from several per day to several tens per day. After the first week of August, seismic quiescence prevailed. A magnitude-4.5 quake from the Kaoiki fault zone proved to be the largest event of the year and was felt islandwide at 06^h33^m, September 5.

In the final quarter, activity resumed along the lower east rift. During November, the peak month of activity, 217 earthquakes having a magnitude of 0.1 to 3.5 were recorded. Five of the largest events, ranging in magnitude from 2.5 to 3.5, were felt by residents of the eastern part of the island.

SUMMARY

Of the several tens of thousands of earthquakes recorded in 1966, 388 having a magnitude of 2 or

[1] Times are in hours and minutes, Hawaiian standard time.

greater were located and plotted. Eighty percent of these larger quakes originated beneath the active Kilauea and Mauna Loa volcanoes. As in earlier years, offshore events were concentrated along the southeastern and western coasts of the island of Hawaii. The quakes were predominantly of intracrustal depths with the exception of a persistent family of Kilauean earthquakes originating from a depth of about 30 km. In all, nearly 100 shocks ranging in magnitude from 2.0 to 4.5 were felt by residents of the island. Five larger ones having a magnitude of 3.7 to 4.5 were felt islandwide; four of these occurred along the active Kaoiki fault, a scarp which marks the surface boundary of the Mauna Loa and Kilauea volcanoes.

REFERENCES

Fiske, R. S., and Koyanagi, R. Y., 1968, The December 1965 eruption of Kilauea Volcano, Hawaii: U.S. Geol. Survey Prof. Paper 607, 21 p.

Koyanagi, R. Y., 1964, Hawaiian seismic events during 1962: Art. 144 *in* U.S. Geol. Survey Prof. Paper 475–D, p. D112–D117.

——— 1968, Hawaiian seismic events during 1965, *in* Geological Survey Research 1968: U.S. Geol. Survey Prof. Paper 600–B, p. B95–B98.

Koyanagi, R. Y., and Endo, E. T., 1965, Hawaiian seismic events during 1963, *in* Geological Survey Research 1965: U.S. Geol. Survey Prof. Paper 525–B, p. B13–B16.

Koyanagi, R. Y., and Okamura, A. T., 1966, Hawaiian seismic events during 1964, *in* Geological Survey Research 1966: U.S. Geol. Survey Prof. Paper 550–C, p. C129–C132.

SEISMIC EVENTS ORIGINATING AT THE ATOMIC ENERGY COMMISSION'S NEVADA TEST SITE

By HAROLD L. KRIVOY and CONNALLY E. MEARS,
Flagstaff, Ariz.

Abstract.—Underground nuclear explosions at the Nevada Test Site (NTS) have been detected at a Flagstaff, Ariz., geophysical observatory since November 1966. Data on these manmade seismic events (shotpoint coordinates, shot times, and phase arrival times) were used to calculate a thickness of about 36 km for the crust between Flagstaff and the NTS. From the data of other observatories, as compiled and published by the U.S. Coast and Geodetic Survey, relationships are inferred which show a pattern of aftershocks following certain of the tests at the NTS.

As part of the U.S. Geological Survey's program of lunar and planetary research, systematic seismic observations have been made since November 1966 in the San Francisco Peaks area about 10 miles north of Flagstaff, Ariz. Astrogeologists are interested in earthquakes and explosions and the seismic energy that they generate because the explosionlike impacts that form lunar craters also produce seismic energy. Energy from meteorite impacts, as well as from moonquakes, may play a major role in the modification of lunar surface forms and in the production of new ones. Evidence of this may be found in certain textural features of the lunar surface revealed by Ranger spacecraft photographs (Kuiper, 1965, p. 55; Kuiper and others, 1966, p. 138). Titley (1967, p. 99) noted that these features resemble scarps and benches and debris-creep patterns that form on terrestrial materials. He suggested that the movements (slumping, landsliding, and so forth) that produce these features on Earth could be triggered on the Moon by impact-induced seismic energy.

The equipment at the Flagstaff observatory consists of a three-component set of long-period seismometers operating broad-band via electronic amplification and recording visibly in 24-hour pen-and-ink format. The data presented here were obtained from several sources in addition to the measurements made with these instruments. Data from the Tonto Forest Observatory, Payson, Ariz., were published by Geotech, Inc. (1966, 1967) for the U.S. Air Force Technical Applications Center. Data from other observatories were obtained from publications by the U.S. Coast and Geodetic Survey (1966, 1967). Data on underground nuclear explosions were supplied by the Office of Public Affairs, U.S. Atomic Energy Commission, Las Vegas, Nev.

RECORDED NUCLEAR EXPLOSIONS

Table 1 lists events recorded in Flagstaff that were initially identified as nuclear test explosions set off at the U.S. Atomic Energy Commission's (AEC) Nevada Test Site (NTS). Figure 1 shows the location of some of the shotpoints according to coordinates supplied by the AEC. Some preliminary identifications were erroneous, such as the first event listed in table 1, which turned out to be a natural earthquake from Colorado.

Arrivals of compressional (P_g and P_n) and transverse (S) waves are identifiable in the records of large underground explosions (fig. 2). The P_g waves result from the refraction of compressional-wave energy along some discontinuity whose depth is less than that of the base of the crust. The velocities of this energy approach that for granitic rock under pressure (Richter, 1958). The P_g waves follow the most efficient energy path, as the large displacements in figure 2 show. Their arrivals may, therefore, be read with accuracy for most of the events listed. P_n wave arrivals are much smaller and can be read with confidence on records of only the largest natural and artificial events. They are the earliest arrivals and represent energy refracted along the base of the crust (Mohorovičić discontinuity) at velocities typical of dunite.

U.S. GEOL. SURVEY PROF. PAPER 650-B, PAGES B117-B121

TABLE 1.—*Data for events recorded at Flagstaff, Ariz., that appeared to originate at the Nevada Test Site*

[Events are listed in order of increasing P_n and P_g traveltimes (and, hence, increasing distance from Flagstaff)]

Date	Shot-time or origin time (hr:min:sec)	Name of event (or comments)	Computed distance (km)[1]	Traveltimes (sec)	
				P_g	P_n
4/4/67	22:53:39.6	Colorado earthquake [2]		58	
11/18/66	15:15	Possible eastern Utah earthquake		66.4	
1/19/67	17:09	Possible aftershock of Nash		68.0	
12/13/66	21:00:00.8	New Point	420	69.4	
1/20/67	17:40:04.41	Bourbon	436	71.2	62.0
11/18/66	15:02:00.04	Cerise	434	72.0	
4/21/67	15:09:00.04	Chocolate	434	72.1	
5/10/67	13:40:00.04	Mickey	432	72.1	72.7
4/7/67	15:00:00.04	Fawn	435	72.4	
12/13/66	17:50			72.6	
2/23/67	18:50.0	Agile	442	73.4	63.2
5/20/67	15:00.0	Commodore	442	71.2	63.3
2/8/67	15:15:00.13	Ward	443	73.9	
4/27/67	14:45.0	Effendi	442	74.0	
1/19/67	16:45:00.04	Nash	448	74.9	64.4
3/2/67	15:00.0	Rivet III	443	74.4	65.4
5/23/67	14:00.0	Scotch	474	74.1	67.9
5/23/67	20:14:06.5	Aftershock of Scotch, lat. 37.2° N., long. 116.4° W.[2]		74.7	
11/11/66	12:00:00.14	Ajax	441	74.6	
1/5/67	12:15:23.1	Aftershock of Greeley		75.9	
12/20/66	15:30:00.08	Greeley	478	77(?)	68.1
5/26/67	15:00:01.5	Knickerbocker	481	80.0	68.6
12/13/66	18:01			85.0	
4/7/67	15:11	Possible aftershock from Fawn		90.4	

[1] Obtained by DISTAZ computer program using coordinates furnished by the AEC.
[2] Location from U.S. Coast and Geodetic Survey (1967).

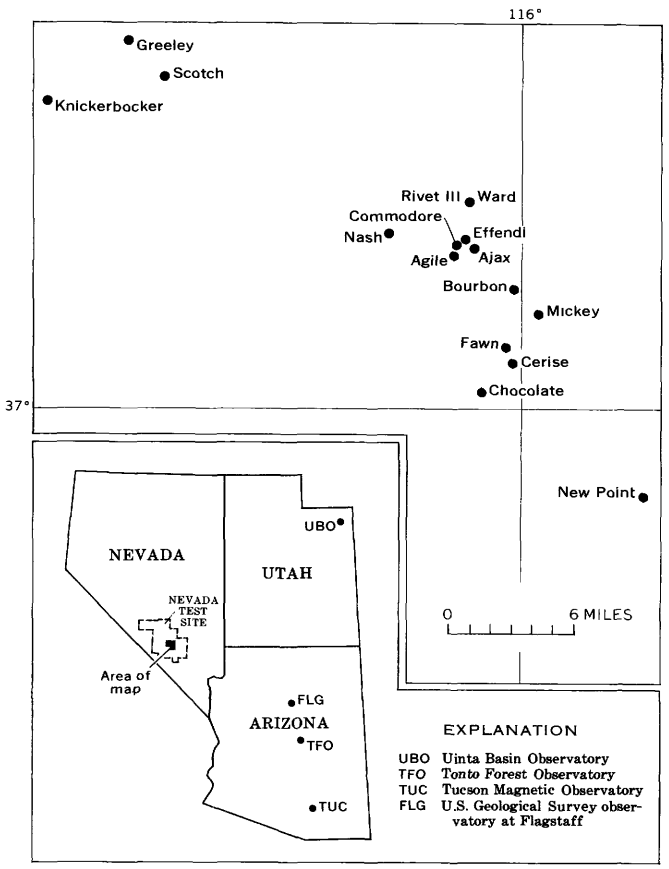

FIGURE 1.—Nevada Test Site shotpoints with inset showing recording stations.

The thickness of the crust between the NTS and Flagstaff was calculated from the traveltimes and distances of each explosion that yielded a readable p_n phase. The following equation was used (from Richter, 1958, p. 691):

$$t=\frac{\Delta \sin i + A \cos i}{V}$$

where t is p_n traveltime, Δ is the computed distance from the shotpoint to Flagstaff, i is the angle of incidence of wave path, V is the P-wave velocity in the upper crust, and $A=2d-H$, in which d is the depth to the Mohorovičić discontinuity (crustal thickness) and H is shot depth. The angle i is computed as follows: $\sin i=\frac{V}{W}$, where V is defined as above, and W is P-wave velocity at the base of the crust. In Arizona, velocity in the upper crust (V) ranges from 5.9 to 6.1 kilometers/second, and velocity at the base of the crust (W) is about 7.9 km/sec, according to work by Warren, Roller, and Jackson (1965). Shot depths are on the order of 1 km; they can be ignored if $2d$ is on the order of 70 km. The results of the computations are shown in table 2.

Errors of various sorts can detract from the validity of the computed thicknesses. Incorrect V and W values are a possible source of error; record timing and read-

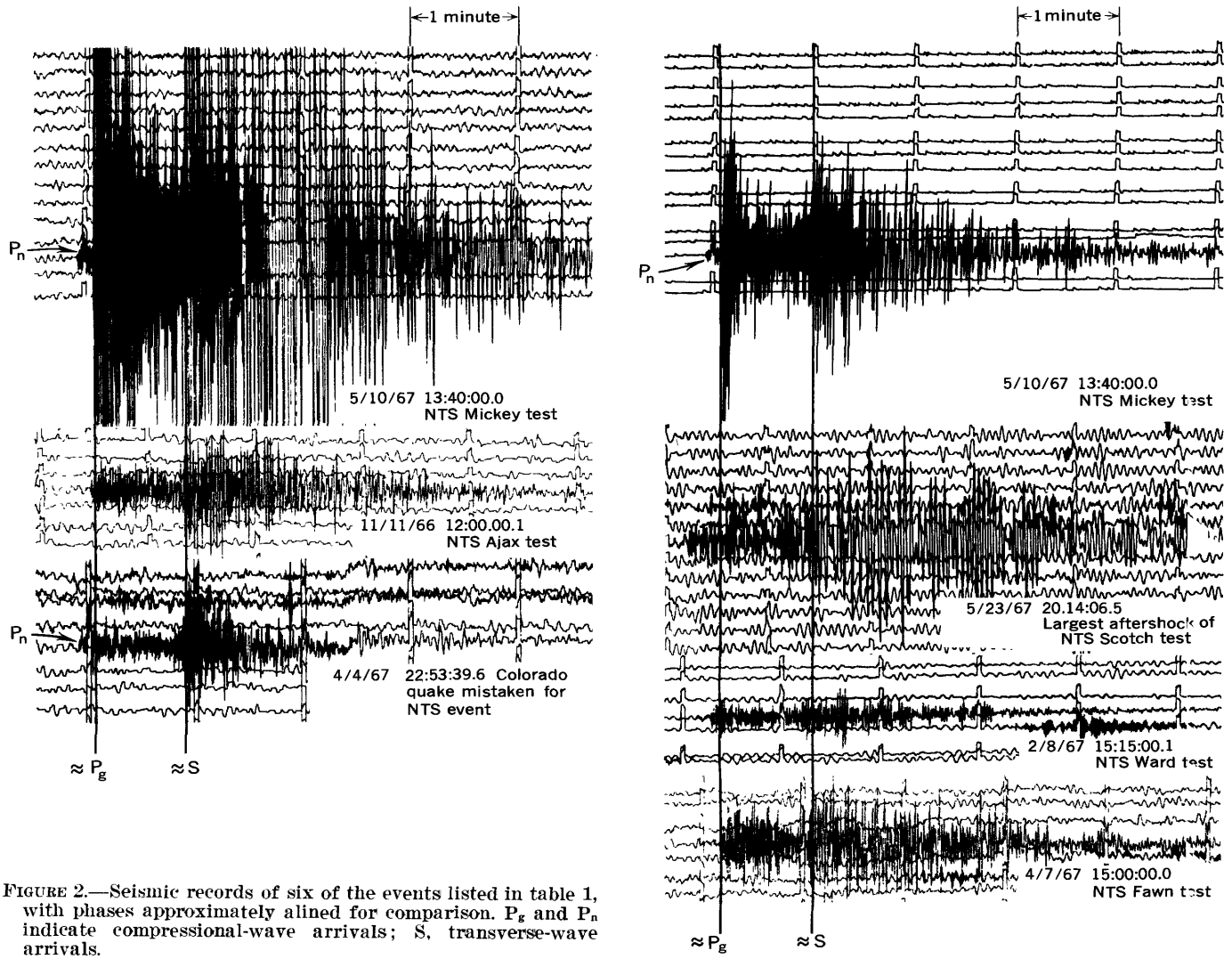

FIGURE 2.—Seismic records of six of the events listed in table 1, with phases approximately alined for comparison. P_g and P_n indicate compressional-wave arrivals; S, transverse-wave arrivals.

TABLE 2.—*Computed gross crustal thicknesses between the Nevada Test Site and Flagstaff, Ariz.*

Shot name	i (degrees)	Travel-time (P_n) (sec)	Distance (Δ) (km)	Velocity (V) (km per sec)	Crustal thickness (d) (km)
Mickey	49.4	62.7	432	6.0	37.3
Bourbon	49.4	62.0	436	6.0	31.7
Agile	49.4	63.2	442	6.0	33.6
Commodore	49.4	63.3	442	6.0	34.0
Rivet III	49.4	65.4	443	6.0	43.4
Nash	49.4	64.4	448	6.0	35.4
Scotch	49.4	67.9	474	6.0	36.9
Greeley	49.4	68.1	478	6.0	35.2
Knickerbocker	49.4	68.6	481	6.0	35.7
Average					35.9

ing are others. A 3-percent change in P_n traveltime would lead to a 26-percent change in crustal thickness readout. Flagstaff chart speed is 30 millimeters/minute, which makes possible a reading error of 0.2 second. This is equivalent to a 1-km error in crustal thickness determination. Only a multiplicity of similar events and recordings gives us confidence that any whole-second errors can be detected and accounted for.

It is often profitable to look for core reflections and conversions on records of large explosions of earthquakes. Table 3 lists events recorded at Flagstaff for which it was possible to find longitudinal reflections from the core for P and S waves, as well as core conversions and reflections of these waves. Data such as these from many stations provide clues to the nature of the Earth's mantle. On lunar records, the presence or absence of such phases could decide the validity of theories regarding the Moon's composition and structure.

AFTERSHOCKS AT THE NEVADA TEST SITE

A number of small- and moderate-intensity events seem to have been chronologically associated with some underground nuclear explosions at the NTS (table 4); we consider them to have been aftershocks.

TABLE 3.—*Readings from the records of nine of the largest events from the Nevada Test Site, with predicted traveltimes for comparison*

[A time notation (elapsed time from P), in minutes (m) and seconds (s), indicates presence of a strong readable phase; X, presence of a possible phase; NO, no reading justifiable]

	PcP 7m22s	ScP 10m05s	PcS 10m35s	ScS 14m25s
Predicted traveltimes				
1966				
Dec. 20	X	10m04s	X	X
1967				
Jan. 19	7m22s	X	NO	NO
20	X	X	NO	NO
Feb. 23	7m23s	10m06s	10m32s	14m26s
Mar. 10	X	NO	NO	NO
20	X	X	NO	X
23	X	X	10m38s	NO
23 (aftershock)	X	NO	NO	NO
26	X	10m14s	10m33s	X

PcP—P wave reflected at core.
ScP—S wave converted to P at core.
PcS—P wave converted to S at core.
ScS—S wave reflected at core.

TABLE 4.—*Chronological list of all events recorded at Flagstaff, or at other observatories, that appeared to originate at Nevada Test Site*

Date	Approximate origin time (hr:min:sec)	Name or type of event	Stations reporting [1]
1966			
Nov. 11	12:00:00.14	Ajax	FLG, TUC, ALQ, BMO
18	15:02:00.04	Cerise	FLG, BMO
18	15:15	Possibly eastern Utah.	FLG, BMO, UBO, WMO
Dec. 13	17:50	Unknown origin	FLG, BMO
13	18:01	do	FLG, BMO
13	21:00:00.8	New Point	FLG, BMO
20	15:30:00.08	Greeley	FLG, BMO, UPS, Univ. Wash.
20	16:52:28.7	Aftershock (Greeley).	TFO, UBO, BMO, C&GS
20	18:04:04.0	do	TFO, UBO, BMO, WMO, C&GS
20	18:16	do	TFO
20	19:01	do	TFO
20	19:31	do	TFO
20	21:52	do	TFO
21	01:20:01.0	do	TFO, UBO, CPO, C&GS
21	01:40	do	TFO
21	02:14:26.8	do	TFO, UBO, C&GS
21	03:12	do	TFO
21	05:26	do	TFO, UBO
21	05:57	do	TFO, UBO
21	06:02:05.5	do	TFO, UBO, BMO, C&GS
21	12:56:59.8	do	TFO, UBO, C&GS
21	14:37:29.6	do	TFO, UBO, BMO, C&GS
21	19:03:42.9	do	TFO, C&GS
21	19:11	do	UBO
22	07:05:23.1	do	TFO, C&GS
22	12:59:14.6	do	TFO, UBO, C&GS
22	16:02	do	TFO, UBO
Dec. 22	17:30:01.1	do	TFO, UBO, C&GS
23	04:57:09.3	do	TFO, UBO, C&GS
23	23:43	do	TFO, UBO
24	00:50	do	TFO
30	18:52:37.9	do	TFO, UBO, C&GS
1967			
Jan. 3	07:07	do	TFO, UBO
5	12:15:23.1	do	TFO, UBO, BMO, C&GS, FLG
8	08:15	do	TFO
16	07:48	do	TFO
19	16:45:00.04	Nash	FLG, TUC, BMO, UPS, Univ. Wash.
19	17:09	Aftershock (Nash?).	FLG, BMO
20	17:40:04.41	Bourbon	FLG, TUC, BMO, UPS
Feb. 8	15:15:00.13	Ward	FLG
14	01:08:27.0	Natural quake	UBO, C&GS
23	18:50:00	Agile	FLG, TUC, BMO, UPS, Univ. Wash.
Mar. 2	15:00:00	Rivet III	FLG, TUC, BMO
Apr. 4	22:53:39.6	Natural quake, southwestern Colorado.	FLG, ALQ, C&GS, UBO, TFO, WMO, BMO
7	15:00:00.04	Fawn	FLG, TUC, ALQ, BMO
7	15:11	Aftershock (Fawn).	FLG, TUC, BMO
21	15:09:00.04	Chocolate	FLG, TUC, ALQ, BMO
27	14:45:00	Effendi	FLG, TUC, ALQ, BMO
May 10	13:40:00.04	Mickey	FLG, TUC, ALQ Univ. Wash., BMO
13	15:53	Probable natural quake.	TFO
18	22:42	do	TFO, UBO
20	15:00:00	Commodore	FLG, TUC, ALQ, BMO
23	14:00:00	Scotch	FLG, TUC, ALQ, TFO, BMO
23	17:52:04.1	Aftershock (Scotch).	FLG, TFO, ALQ, TFO, UBO, C&GS
23	20:14:06.5	do	FLG, TUC, ALQ, TFO, UBO, BMO, WMO, C&GS
26	15:00:01.5	Knickerbocker	FLG, TUC, BMO
26	19:00	Possible aftershock (Commodore).	UBO, TFO

[1] FLG=U.S. Geological Survey observatory at Flagstaff, Ariz.
TUC=Tucson Magnetic Observatory, Ariz.
ALQ=Albuquerque Seismological Observatory, N. Mex.
BMO=Blue Mountain Observatory, Oreg.
UBO=Uinta Basin Observatory, Utah.
WMO=Wichita Mountain Observatory, Okla.
UPS=Uppsala Network, Sweden.
C&GS=U.S. Coast and Geodetic Survey stations, probably in Nevada.
TFO=Tonto Forest Observatory, Ariz.
CPO=Cumberland Plateau Observatory, Tenn.

The three-letter designations are assigned by the U.S. Coast and Geodetic Survey, which periodically publishes station locations, elevations, and related data.

See footnote at end of table.

The Greeley event and the shocks that followed it provide the best such relationship because the testing schedule was uncrowded prior to this test and enough time elapsed after it to permit a hypothetical aftershock sequence to run its course before new tests were held. Furthermore, several of Greeley's suspected aftershocks were noted by geologists working near ground zero, thus verifying a spatial relationship as well as a chronological one.

Regions of active seismicity and of recent fault movement are numerous in Nevada. Seismicity at the NTS has been intensively studied by the U.S. Coast and Geodetic Survey on behalf of the AEC. This work should result in a better understanding of the frequency and location of small, local earthquakes. However, until such information becomes available, we cannot dismiss the possibility that the aftershocks discussed herein are actually natural local earthquakes and that their association with nuclear explosions is fortuitous.

CONCLUSIONS

Shotpoint coordinates and shot times of underground nuclear explosions were used to calculate crustal thickness from arrivals of seismic waves recorded at a single seismic observatory. Determinations such as these could be reinforced by similar studies at other observatories. On a global scale, cooperation between seismic observatories has produced valuable new facts regarding the Earth's constitution. Data on the constitution of the Moon and other planets could be obtained by means of automated continuous-recording observatories, which would also contribute information on the frequency, size, and location of natural quakes and impact shocks.

The circumstantial evidence tabulated herein suggests that large energy release may result in secondary release similar to the main-shock-aftershock sequence observed in earthquake seismology. More intensified study of this phenomenon, given the opportunity provided by the AEC testing program, promises to yield important clues to the nature of earthquake and aftershock mechanisms.

REFERENCES

Geotech, Inc. (Div. of Teledyne), 1966, 1967, The registration of earthquakes: Garland, Texas, v. 5, no. 11, v. 6, no. 3.

Kuiper, G. P., 1965, Interpretation of Ranger VII records, *in* Ranger VII, pt. 2, Experimenters' analyses and interpretations: Pasadena, California Inst. Technology, Jet Propulsion Lab. Tech. Rept. 32-700, p. 9-73.

Kuiper, G. P., Strom, R. G., and Le Poole, R. S., 1966, Interpretation of the Ranger records, *in* Ranger VIII and IX, pt. 2, Experimenters' analyses and interpretations: Pasadena, California Inst. Technology, Jet Propulsion Lab. Tech. Rept. 32-800, p. 35-248.

Richter, C. F., 1958, Elementary seismology: San Francisco and London, W. H. Freeman & Co., 768 p.

Titley, S. R., 1967, Seismic energy as an agent of morphologic modification on the Moon, *in* Astrogeologic studies ann. prog. rept., July 1, 1965 to July 1, 1966, pt. A: U.S. Geol. Survey open-file report, p. 87-103.

U.S. Coast and Geodetic Survey, 1966, 1967, Preliminary determination of epicenters: Rockville, Md., nos. 57-66 to 42-67.

Warren, D. H., Roller, J. C., and Jackson, W. H., 1965, Seismic refraction survey in the vicinity of the Tonto Forest Seismological Observatory, Arizona [abs.]: Am. Geophys. Union Trans. v. 46, no. 1, p. 155.

SEISMIC INVESTIGATIONS ON CAPE COD, MARTHA'S VINEYARD, AND NANTUCKET, MASSACHUSETTS, AND A TOPOGRAPHIC MAP OF THE BASEMENT SURFACE FROM CAPE COD BAY TO THE ISLANDS [1]

By ROBERT N. OLDALE, Woods Hole, Mass.

Abstract.—Seismic data from coastal southeastern Massachusetts show one or two layers of unconsolidated sediments of Holocene to Late Cretaceous age over a basement of crystalline and sedimentary rock of pre-Mesozoic age. The basement surface slopes gently seaward and is cut by deep valleys.

Seismic studies were made on Martha's Vineyard and Nantucket in the fall of 1967, and on Cape Cod in the spring of 1968, to determine the subsurface geology and depths to pre-Mesozoic basement. Three seismic layers characterized by compressional wave velocities that generally fall between 1.5 and 1.8 kilometers per second (L_1), 1.8 and 2.4 km/sec (L_2), and 4.5 and 6.5 km/sec (L_3) were identified. The L_1 and L_2 layers are composed of unconsolidated sediments of Holocene to Late Cretaceous age. The basement is composed of crystalline rock of Paleozoic or Precambrian age or in some places consolidated sedimentary rock of late Paleozoic to Cretaceous age. Figure 1, a topographic map of the basement surface beneath Martha's Vineyard, Nantucket, Vineyard and Nantucket Sounds, Buzzards Bay, Cape Cod and Cape Cod Bay, was drawn from data obtained in this study and from published and unpublished data on depths to basement.

METHODS

Seismic lines were laid out on beaches because the beaches provided straight lines as much as 1,200 meters long and were remote from buildings and dense vegetation. In addition, explosive charges could be placed at the water table to provide excellent energy coupling, and blast holes were quickly erased by wave action.

All seismic profiles were of the inline refraction type and were made using a 12-channel portable refraction amplifier and oscillograph. At most sites on Martha's Vineyard and Nantucket, geophones were spaced 50 m apart; shotpoints were placed 50 m and, wherever posible, 350 m from the first geophone, giving seismic lines 600 and 900 m long. At Great Point on Nantucket (*31*, fig. 1) the seismic line was further extended by placing shotpoints 580 and 600 m from the first geophone. Four to 12 pounds of explosive were used at each shotpoint. All seismic lines were reversed.

Field procedures varied only slightly on Cape Cod. Shorter lines and closer geophone spacing were used because of the shallower depth to basement. Line length ranged from 183 to 546 m, and geophone spacing was 15.2, 30.5, and 50.0 m. Several profiles were not reversed because buildings were near one end of the line. Dynamite charges were reduced to 1–2 pounds with no loss of record quality.

The thickness of the seismic layers was computed using the critical-distance method (Heiland, 1940, p. 508), recorded velocities of the L_1 and L_2 layers, and approximate true velocities $\frac{2(V_u \times V_d)}{V_u + V_d}$ for basement. On Martha's Vineyard and Nantucket, where the basement was not recorded, a velocity of 5.6 km/sec was assumed for basement, as this was the average value of the basement velocities previously recorded on Cape Cod (Oldale and Tuttle, 1964, 1965); the critical distance for the basement was assumed to be at least the distance from the shotpoint to the last geophone. All lines were within 1 m of sea level, and either the computed thickness of the L_1 layer or the sum of the thicknesses of the L_1 and L_2 layers was considered to be the altitude of the basement surface. Where the basement was not recorded, computed thicknesses represent minimum values for the altitude of the basement surface.

Compressional wave velocities were measured directly on sediments of Late Cretaceous age that crop out at Gay Head cliffs (fig. 1). Seismic lines with a

[1] Contribution No. 2169 of the Woods Hole Oceanographic Institution.

U.S. GEOL. SURVEY PROF. PAPER 650-B, PAGES B122-B127

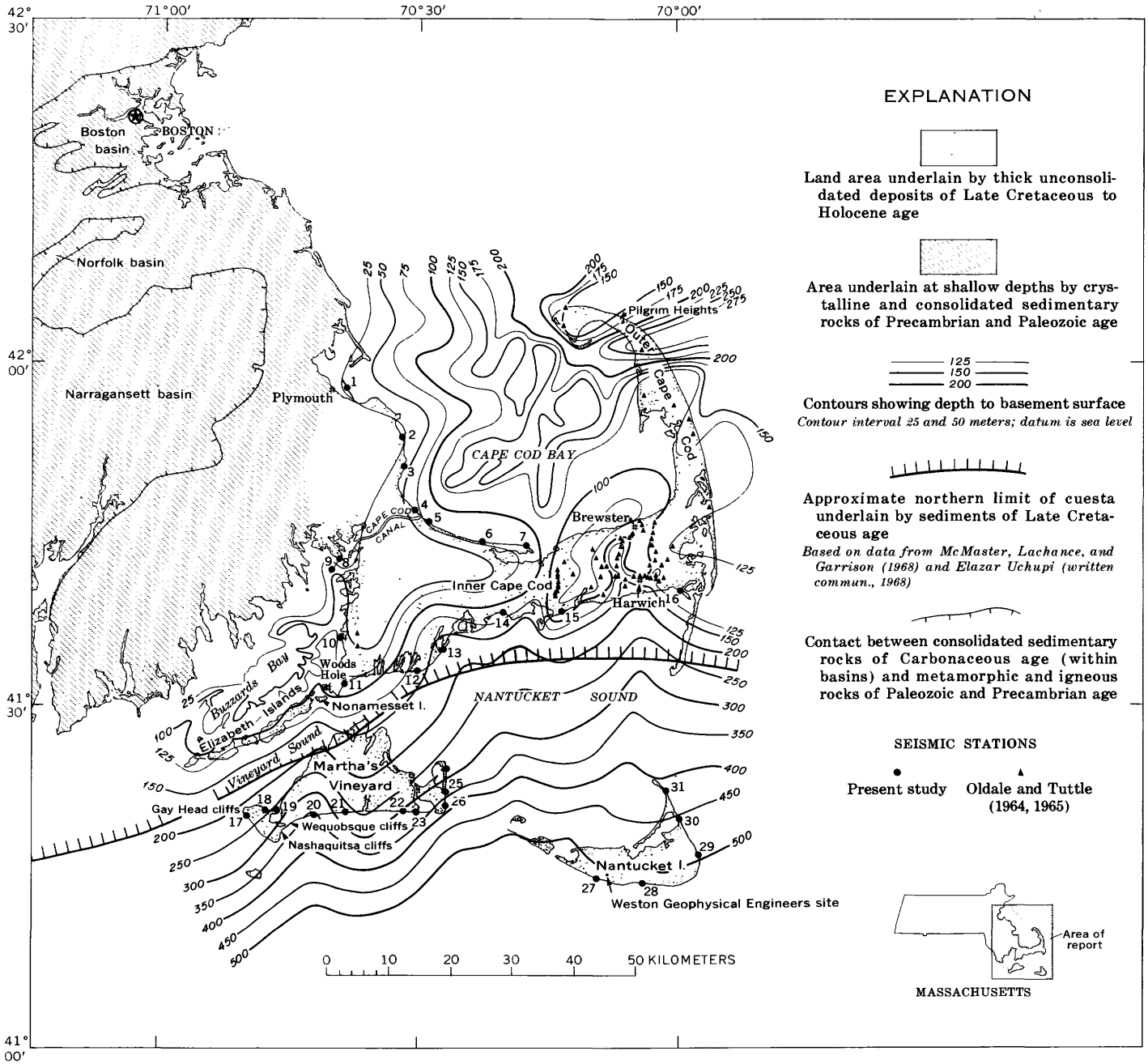

FIGURE 1.—Topography of the basement surface as inferred from seismic data. Contours in Cape Cod Bay modified from Hoskins and Knott (1961). Contours in Buzzards Bay based on data from Bunce and Phinney (1959) and Bunce (written commun., 1968). Data points for Buzzards Bay are not shown as they are too closely spaced for this scale.

geophone spacing of 1.5 m were laid directly on outcrops of red clay and black carbonaceous sandy clay. An upper-layer velocity of 0.3 to 0.6 km/sec and a lower-layer velocity of 0.8 to 1.2 km/sec were recorded. These velocities, considerably below others recorded on the islands, are similar to velocities recorded on weathered, unsaturated, and unconsolidated sediments elsewhere (Tuttle and others, 1961, p. C254; Oldale and Tuttle, 1964, p. D118; 1965, p. D102–D103).

Interpretation of the refraction seismic data for the sites studied in this report is controlled in large part by two conditions: (1) the compressional wave velocities recorded on the L_1 and L_2 layers fall within a range that would include saturated and unconsolidated sediments regardless of lithology and geologic age; and (2) except for the contact between basement and unconsolidated sediments of post-Paleozoic age, acoustic boundaries may not correspond to geologic time boundaries. These conditions have been noted elsewhere. For example, at Harwich, Mass., (fig. 1) a single velocity was recorded on a section composed of saturated sand and gravel underlain by coarse to clayey silt (Oldale and Tuttle, 1965, p. D102). In a borehole at Pilgrim Heights (fig. 1), the boundary between sand and gravel of Pleistocene age and sand and silt of Eocene(?) age occurred at a depth of 26 m (Zeigler and others, 1960) and the acoustic boundary occurred at a 53-m depth (Oldale and Tuttle, 1964, p. D119). On Block Island, R.I., the contact between sandy drift of Pleistocene age and clay of Late Cretaceous age generally occurred below the acoustic boundary (Tuttle and others, 1961, p. C255). Therefore, the presence of pre-Pleistocene to post-Paleozoic unconsolidated deposits must be inferred from something other than seismic data.

RESULTS

The uppermost layer (L_1) is thought to be unconsolidated deposits of Late Cretaceous to Holocene age. At most profiles the velocities measured on this layer were between 1.5 and 1.8 km/sec. At three profiles the velocities in the uppermost layer were low: Stoney Point dike (*9*, fig. 1), 1.3 km/sec; Scusset Beach (*4*, fig. 1), 1.3 km/sec; and Town Neck (*5*, fig. 1), 1.0 km/sec. At Chappaquoit Beach and Cedar Bushes (*10* and *2*, fig. 1) a velocity of 1.95 km/sec was recorded on the L_1 layer at one end of the profiles.

The L_1 layer is thinnest at the southwest end of the Cape Cod Canal and along the shore of Cape Cod Bay north of the canal (fig. 1). A few tens of miles west and north of the canal crystalline rocks of Paleozoic and Precambrian age crop out along the shores of Buzzards Bay and Cape Cod Bay. In general, the L_1 layer thickens seaward; beneath outer Cape Cod this layer ranges from 120 to more than 190 m in thickness (Oldale and Tuttle, 1964, p. D118), and beneath Martha's Vineyard and Nantucket it ranges from 95 to more than 500 m in thickness. In some places these are minimum thicknesses, because the top of the L_1 layer is as high as 90 m above sea level a short distance inland.

A layer (L_2) that has velocities intermediate between those inferred to represent the uppermost layer and the basement was recorded at several profiles on Cape Cod and Martha's Vineyard and at one profile on Nantucket. The L_2 layer is inferred to be compact till or coastal plain deposits. Velocities in this layer ranged from 1.8 to 2.4 km/sec, except at Town Nick (*5*, fig. 1) where the layer had a velocity of 1.6 km/sec (fig. 2). On Cape Cod the L_2 layer ranged from 34 to 136 m in thickness; on Martha's Vineyard it ranged from 215 to at least 260 m in thickness, and on Nantucket it was at least 180 m thick.

Velocities inferred to represent basement were recorded at all profiles on Cape Cod and at three profiles on Martha's Vineyard. Seismic lines on Nantucket were not long enough to record basement, but an unreversed profile by Weston Geophysical Engineers (fig. 1; written commun., 1967) showed basement that had a velocity of 5.7 km/sec overlain by 515 m of L_1 material. Basement velocities on Cape Cod generally ranged from 4.5 to 5.8 km/sec. Velocities considerably lower than those measured elsewhere on the basement were recorded at Black Pond (*3*, fig. 1), 3.8 km/sec; at Long Point (*1*, fig. 1), 4.3 km/sec; and at South Cape Beach (*12*, fig. 1), 4.1 km/sec. Basement velocities on Martha's Vineyard were 5.6 km/sec at Tisbury Great Pond (*21*, fig. 1), 5.4 km/sec at Chilmark Pond (*20*, fig. 1), and 5.8 km/sec at Sheep Pen Pond (*25*, fig. 1). Topography and altitude of the basement surface are shown by the contour map (fig. 1).

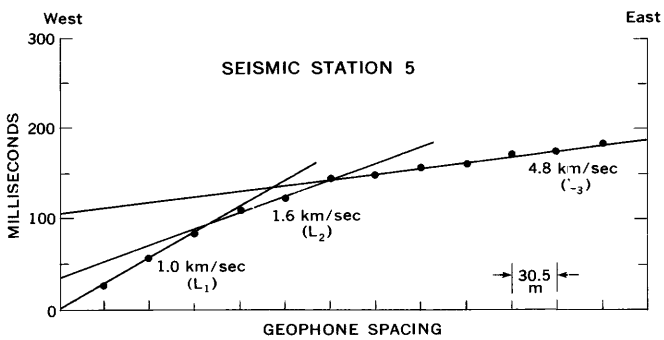

FIGURE 2.—Unreversed traveltime curve showing L_1, L_2, and basement (L_3) velocities recorded at Town Neck (*5*, fig. 1). The L_1 velocity is inferred to be fresh- and salt-water peat.

The uppermost layer (L_1) on Cape Cod is in most places glacial drift composed of fluvial and deltaic sand and gravel, lacustrine clay and silt, and sandy to clayey till. The drift is overlain in some places by rather thin deposits of Holocene age—beach, dune, and peat deposits. On outer Cape Cod (fig. 1) the L_1 layer is composed in part of unconsolidated sand and silt of Eocene age (Zeigler and others, 1965, p. R302; Oldale and Tuttle, 1964, p. D120). Elsewhere, coastal plain deposits of Pleistocene to Late Cretaceous age may form a part of the L_1 layer beneath the glacial drift, as preglacial deposits have been reported in Cape Cod Bay (Hoskins and Knott, 1961, p. 338), in Scituate (Chute, 1965), and on Nonamesset and Martha's Vineyard Islands (Woodworth and Wigglesworth, 1934, p. 14, 17).

The low velocities of the L_1 layer at Stoney Point dike and Scusset Beach are not clearly understood, but may be caused by thick artificial fill dumped into these areas during the building of the Cape Cod Canal. At Town Neck the low L_1 velocity (fig. 2) is inferred to represent marine and fresh-water peat, as much as 16 m thick, underlain by glacial drift, as salt-marsh peat occurs at the surface a short distance inshore from the beach, and the L_2 velocity here (1.5 km/sec) is characteristic of the L_1 layer at most other profiles. The high L_1 velocities recorded at one end of the profiles at Chappaquoit Beach and Cedar Bushes are similar to L_2 velocities elsewhere and probably represent compact till.

South of Cape Cod and the Elizabeth Islands the unconsolidated deposits above the basement are believed to be mostly coastal plain sediments of early Pleistocene to Late Cretaceous age. A cuesta that occurs beneath Long Island, N.Y. and that is underlain by strata of Late Cretaceous age has been traced eastward into Block Island Sound (McMaster and others, 1968, p. 471) and into Vineyard Sound, and Nantucket Sound by Uchupi (written commun., 1968). In Vineyard Sound the northern limit of the Cretaceous strata, as defined by the cuesta, is just southeast of the Elizabeth Islands; in Nantucket Sound it is just south of the south shore of Cape Cod (fig. 1). On western Martha's Vineyard the coastal plain deposits that make up the L_1 layer are exposed in the cliffs at Gay Head, Wequobsque and Nashaquitsa, and in many pits inland. In eastern Martha's Vineyard and Nantucket, glacial drift and deposits of Holocene age make up the part of the L_1 layer that occurs above sea level; below sea level the L_1 layer is probably mostly coastal plain sediments of pre-Pleistocene age similar to those on Long Island and Block Island where the glacial deposits are generally less than 100 m thick (Suter and others, 1949, p. 40–45; Tuttle and others, 1961, p. C255).

On Cape Cod the L_2 layer is probably mostly glacial till similar to the till identified in boreholes at Harwich and Brewster (Koteff and Cotton, 1962), which has seismic velocities that range from 2.0 to 3.8 km/sec (Oldale and Tuttle, 1965, p. D104), and to high-velocity drumlin till found elsewhere in Massachusetts (Tuttle, 1961). The L_2 layer may also include deposits of Tertiary age similar to those inferred to occur in Cape Cod Bay, which have velocities of 1.8 to 2.4 km/sec (Hoskins and Knott, 1961, p. 339), and to those beneath Nonamesset Island, where they have a velocity of 2.7 km/sec (Hoskins, written commun., 1960).

On Martha's Vineyard and Nantucket the L_2 layer is probably of Tertiary and Cretaceous age, as it is overlain by L_1 deposits that are believed to be too thick to be composed entirely of glacial drift. The coastal plain deposits are probably similar to those that crop out in Western Martha's Vineyard, but somewhat more compact, or they may be similar to the unconsolidated deposits of Cretaceous age on Block Island that have an average seismic velocity of 1.9 km/sec (Tuttle and others, 1961, p. C254).

The lowermost layer is basement composed of pre-Mesozoic crystalline and sedimentary rock. Velocities above 4.5 km/sec are believed to represent igneous and metamorphic rocks of Paleozoic and Precambrian age similar to (1) the granite and phyllitic schist in boreholes at Harwich and Brewster (Koteff and Cotton, 1962) that have seismic velocities of 5.4 to 6.5 km/sec (Oldale and Tuttle, 1965, p. D105), (2) to the granite in a borehole at Woods Hole, and (3) to the crystalline rocks that crop out along the west shore of Cape Cod Bay north of Plymouth and along the northwest shore of Buzzards Bay (fig. 1). Offshore, in Cape Cod Bay (Hoskins and Knott, 1961, p. 335) and in Buzzards Bay (Bunce and Phinney, 1959), a layer that has velocities of 4.6 to 5.7 km/sec was identified as basement and traced to within short distances of outcrops of metamorphic and igneous rocks of Paleozoic and Precambrian age along the shore. In Narragansett Bay, R.I., velocities of 4.9 to 6.5 were inferred to represent crystalline rocks. These are overlain by consolidated sedimentary rocks of Carboniferous age which have velocities of 3.1 to 4.5 km/sec (Berg, 1963, p. 1311).

The low velocities (3.8–4.3 km/sec) recorded on Cape Cod at South Cape Beach (fig. 3), Long Point, and Black Pond fall within the range of velocities measured by Berg on the consolidated sedimentary rocks of Carboniferous age and suggest that similar

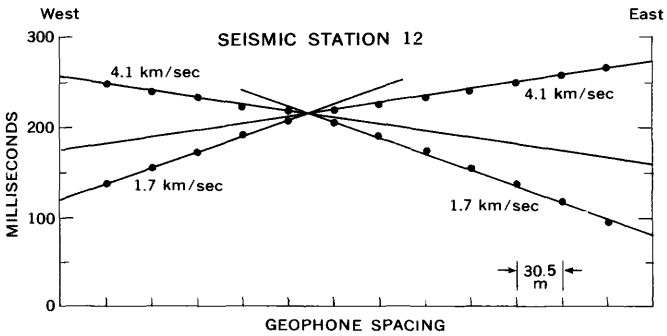

FIGURE 3.—Traveltime curves showing low basement velocities (possibly of consolidated sedimentary rock of Carboniferous or Triassic age) recorded at South Cape Beach (*12*, fig. 1).

rocks may make up a part of the basement in these areas. These velocities may also indicate the presence of sedimentary rocks of Triassic age, as velocities of about 4.0 km/sec are commonly recorded on Triassic sedimentary rocks in the Connecticut Valley (Tuttle and others, 1961, p. C254). Also, they may possibly represent consolidated sediments similar to those that have velocities of 3.4 to 4.0 km/sec in Cape Cod Bay and are inferred to be Cretaceous in age (Hoskins and Knott, 1961, p. 336–338). The low velocities may also be caused by foliated, fractured, or jointed crystalline rocks similar to the basement in two closely spaced profiles on outer Cape Cod where the velocity measured in a northerly direction was 4.3 km/sec, and in an easterly direction, 6.1 km/sec (Oldale and Tuttle, 1964, p. D120). Weathering in the upper part of the basement may also be responsible for the low velocities.

The proximity of the Narragansett, Norfolk, and Boston basins (fig. 1), which are filled with consolidated sedimentary rocks of Carboniferous age, suggests that if the low velocities represent consolidated sediments they are of Carboniferous age. However, the shallow depth of the basement at Long Point and Black Pond suggests that weathering may be the cause of low velocities in these areas.

TOPOGRAPHIC MAP OF THE BASEMENT SURFACE

The seismic data from Martha's Vineyard and Nantucket and new data from Cape Cap were combined with previous data from Cape Cod (Oldale and Tuttle, 1964, 1965), Cape Cod Bay (Hoskins and Knott, 1961), and Buzzards Bay (Bunce and Phinney, 1959; Bunce, written commun., 1968) to draw a contour map of the basement surface (fig. 1). The map is greatly generalized, for in most places there are insufficient data to show complexities in the topography. Where profiles are closely spaced, the contouring shows well-defined deep valleys and low-relief interfluve areas. The complex topography of the basement surface can best be seen on continuous seismic reflection profiles (Hoskins and Knott, 1961; Tagg and Uchupi, 1967; McMaster and others, 1968). The basement surface beneath Buzzards Bay, Vineyard Sound, Nantucket Sound, Nantucket, and Martha's Vineyard generally slopes gently south to southeast at about 10 to 15 m/km. The locations of contours along the western edge of the area agree with contours of similar values in Block Island and Rhode Island Sounds (McMaster and others, 1968, p. 470). Beneath inner Cape Cod the basement surface forms a poorly defined topographic high that trends east and separates the south-sloping basement surface beneath Nantucket and Vineyard Sounds from a rather shallow basin in the basement surface beneath Cape Cod Bay (Hoskins and Knott, 1961, p. 333). The basin appears to have drained northeast and east through a deep valley near the northern tip of Cape Cod.

The broad valleys beneath Martha's Vineyard, Nantucket, and Nantucket Sound are probably Early Cretaceous in age, for they are south of the inferred northern limit of the Upper Cretaceous deposits. If so, drainage in this area was southward during Early Cretaceous time; in contrast, during Tertiary time the area is believed to have been drained by southwest-flowing streams tributary to a major south-flowing stream in Rhode Island Sound (McMaster and others, 1968, p. 471). The valleys below inner Cape Cod and Buzzards Bay are filled with glacial deposits and were probably fluvially eroded during the Tertiary and enlarged and deepened by ice during Pleistocene glaciations. The deep valley near the north end of Cape Cod is thought to be filled in part with consolidated deposits of Carboniferous, Triassic, or Cretaceous age in part with unconsolidated deposits of Eocene age (Oldale and Tuttle, 1964, p. D120).

CONCLUSIONS

Basement beneath coastal southeastern Massachusetts is probably composed mostly of metamorphic and igneous rocks of Paleozoic and Precambrian age, similar to those that crop out to the north and west; however, part of the basement may be consolidated sedimentary rock, probably similar in age and lithology to the Rhode Island Formation of Carboniferous age that occupies the Narragansett basin. The altitude of the basement surface ranges from sea level, a short distance north of Plymouth and along much of the northwest shore of Buzzards Bay, to more than 350 m below sea level beneath southern Martha's Vineyard, and more than 500 m below sea level along the south shore of Nantucket.

The regional slope is generally south and southeast, south of Cape Cod, and north and northeast, north of Cape Cod. Locally, broad deep valleys interrupt the regional slope. The basement surface has a long history of fluvial erosion that probably began before Late Cretaceous time (Flint, 1963, p. 691). North of the cuesta underlain by sediments of Cretaceous age, the basement surface was fluvially eroded during much of the Tertiary and glacially scoured during the Pleistocene.

The unconsolidated deposits (L_1 and L_2 layers) that overlie the basement south of Cape Cod are mostly coastal plain sediments of Late Cretaceous age and, to a lesser amount, of Tertiary age. These deposits are overlain by glacial drift of Pleistocene age and small amounts of beach, dune, and peat deposits of Holocene age. On outer Cape Cod the unconsolidated deposits (all layer L_1) are composed of coastal plain deposits of Eocene(?) age overlain by stratified glacial drift of Pleistocene age and shore deposits of Holocene age. Beneath inner Cape Cod the L_2 layer is composed of high-velocity basal till, and the L_1 layer consists mostly of stratified glacial drift and minor amounts of shore deposits of Holocene age.

REFERENCES

Berg, J. W., Jr., 1963, Seismic refraction profiles, Narragansett Bay, Rhode Island: Geol. Soc. America Bull., v. 74, p. 1305–1312.

Bunce, E. T., and Phinney, R. A., 1959, Seismic refraction observations in Buzzards Bay, Massachusetts [abs.]: Jour. Geophys. Research, v. 64, p. 1096.

Chute, N. E., 1965, Geologic map of the Scituate quadrangle, Plymouth County, Massachusetts: U.S. Geol. Survey Geol. Quad. Map GQ–467.

Flint, R. F., 1963, Altitude, lithology, and the Fall Zone in Connecticut: Jour. Geology, v. 71, p. 683–697.

Heiland, C. A., 1940, Geophysical exploration: New York, Prentice-Hall, 1,013 p.

Hoskins, Hartley, and Knott, S. T., 1961, Geophysical investigation of Cape Cod Bay, Massachusetts, using the continuous seismic profiler: Jour. Geology, v. 69, p. 330–340.

Koteff, Carl, and Cotton, J. E., 1962, Preliminary results of recent deep drilling on Cape Cod, Massachusetts: Science, v. 137, p. 34.

McMaster, R. L., Lachance, T. P., and Garrison, L. E., 1968, Seismic-reflection studies in Block Island and Rhode Island Sounds: Am. Assoc. Petroleum Geologists Bull., v. 52, p. 465–474.

Oldale, R. N., and Tuttle, C. R., 1964, Seismic investigations on Cape Cod, Massachusetts: Art. 145 *in* U.S. Geol. Survey Prof. Paper 475–D, p. D118–D122.

——— 1965, Seismic investigations in the Harwich and Dennis quadrangles, Cape Cod, Massachusetts, *in* Geological Survey Research 1965: U.S. Geol. Survey Prof. Paper 525–D, p. D101–D105.

Suter, Russell, Laguna, Wallace de, and Perlmutter, N. M., 1949, Mapping of geologic formations and aquifers of Long Island, New York: New York Dept. Conserv. Water Power and Control Comm. Bull. GW–18, 212 p.

Tagg, A. R., and Uchupi, Elazar, 1967, Subsurface morphology of Long Island Sound, Block Island Sound, Rhode Island Sound, and Buzzards Bay, *in* Geological Survey Research 1967: U.S. Geol. Survey Prof. Paper 575–C, p. C92–C96.

Tuttle, C. R., 1961, Seismic high-speed till in Massachusetts [abs.]: Geol. Soc. America Spec. Paper 68, p. 288–289.

Tuttle, C. R., Allen, W. B., and Hahn, G. W., 1961, A seismic record of Mesozoic rocks on Block Island, Rhode Island: Art. 240 *in* U.S. Geol. Survey Prof. Paper 424–C, p. C254–C256.

Woodworth, J. B., and Wigglesworth, Edward, 1934, Geography and geology of the region including Cape Cod, the Elizabeth Islands, Nantucket, Martha's Vineyard, No Mans Land and Block Island: Harvard Univ. Mus. Comp. Zoology Mem., v. 52, 322 p.

Zeigler, J. M., Hoffmeister, W. S., Geise, Graham, and Tasha, Herman, 1960, Discovery of Eocene sediments in subsurface of Cape Cod, Massachusetts: Science, v. 132, p. 1397–1398.

Zeigler, J. M., Tuttle, S. D., Tasha, H. J., and Geise, G. S., 1965, The age and development of the Provincelands Hook, outer Cape Cod, Massachusetts: Limnology and Oceanography, v. 10, supp., p. R298–R311.

MICROANALYSIS WITH THE X-RAY MILLIPROBE

By HARRY J. ROSE, JR., RALPH P. CHRISTIAN, JAMES R. LINDSAY, and RICHARD R. LARSON, Washington, D.C.

Abstract.—The X-ray milliprobe, designed specifically for analysis of small selected areas generally 0.012 to 1.2 sq mm in size, using curved-crystal optics, can be used effectively for semiquantitative scanning of small grains, X-ray diffraction spindles, and selected areas within larger samples. It is particularly useful for quantitative analysis of small mineral samples. Various factors such as the shape and size of the aperture and sample mounting and preparation techniques, affect performance. Sensitivities obtainable are in the nanogram range as illustrated for iron, lanthanum, and calcium.

The conventional X-ray spectrometer using flat-crystal optics attains maximum sensitivity when a large specimen is irradiated, but its efficiency drops drastically with decrease in sample size. Curved-crystal optics, on the other hand, can achieve improved intensities by an order of magnitude, or more, over corresponding flat-crystal optics in analysis of selected small areas.

An X-ray milliprobe using curved crystals, described by Adler and Axelrod (1956), has been used mainly for semiquantitative analysis. A conventional flat-crystal unit, converted to accommodate curved-crystal optics, was built specifically for the Geological Survey by the General Electric Co. This paper presents data on flat-crystal and curved-crystal systems as they relate to microanalysis. It also discusses various factors that affect the performance and general utility of the curved-crystal system.

CURVED-CRYSTAL OPTICS

Two configurations for reflection (curved-crystal) optics are shown in figure 1, and both types satisfy the Bragg expression for diffraction: $n\lambda=2d \sin \theta$ (where n is the order number, λ is the wavelength, d is the distance between lattice planes in the crystal, and θ is the incident and reflected angle of the X-ray beam

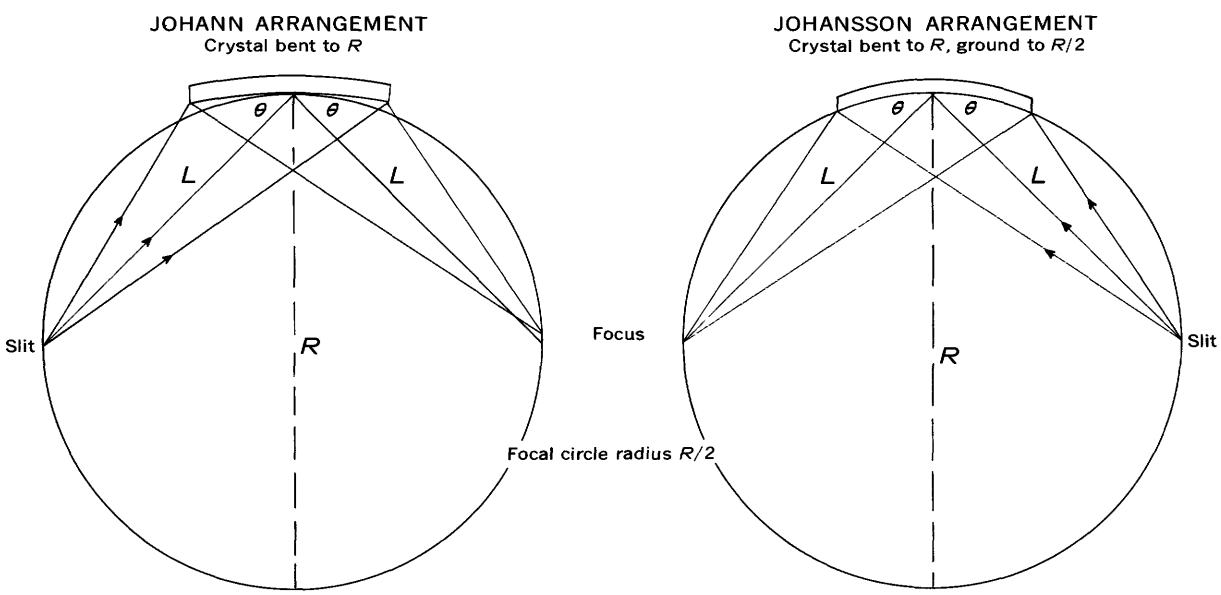

FIGURE 1.—Two arrangements for curved-crystal optics.

U.S. GEOL. SURVEY PROF. PAPER 650-B, PAGES B128-B135

to the lattice planes). In both arrangements the crystals are bent to conform to the surface of a cylinder of radius R, which is also the diameter of the focal circle. For the best possible focus, however, the concave surface of the crystal must be ground to a radius of $R/2$ as in the Johansson arrangements (fig. 1). Focus in the Johann arrangement (fig. 1) degenerates with the divergence of the crystal from the focal circle, and for this reason the Johansson arrangement is preferred whenever a bent crystal can be ground. At angles above 45°, however, the focusing defect in the Johann arrangement becomes less significant.

Most commercially available spectrometers were designed for flat-crystal optics with fixed distances for L, the distance between the secondary X-ray source slit and analyzing crystal or between the crystal and the detector slit (fig. 1). The conversion of these spectrometers for use of curved crystals, therefore, requires that R or L vary with θ according to the expression $R=L/\sin\theta$. At first glance, it would appear impractical to require a crystal of different bending radius for every change in θ for which the spectrometer would be in focus. Practically, however, approximate focus is maintained for a range of θ angles on either side of true focus. In this semifocusing arrangement, the entire 2θ range may be satisfactorily covered with several crystals of different radii. Figure 2 indicates focusing circles for three crystals and how they are made to work effectively within the fixed limitations of the spectrometer.

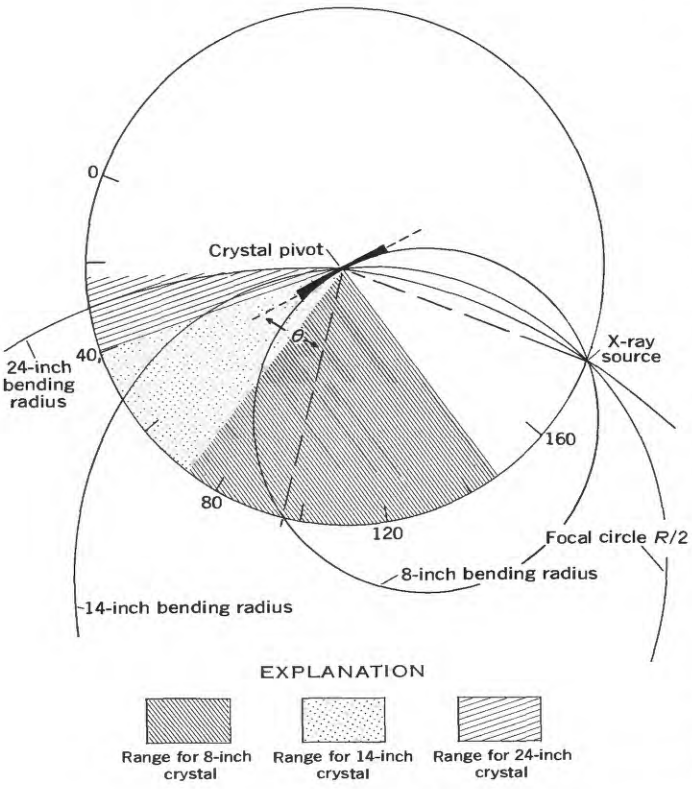

FIGURE 2.—Series of focal circles showing effective range of three crystals covering 2θ angles between 23° and 148°. Circles pass through fixed points at sample and crystal.

TABLE 1.—*Crystals currently available to the X-ray milliprobe*

Crystal [1]	Radius	Range (degrees 2θ)
LiF	Bent to 24 in. ground to 12 in.	23.0– 38.9
	Bent to 14 in. and ground to 7 in.	40.1– 69.6
	Bent to 8 in. and ground to 4 in.	73.7–148.5
Eddt	Bent to 8 in.	73.7–148.5

[1] LiF, 2*d* spacing=4.0267 angstroms; Eddt (ethylene diamine ditartrate), 2*d* spacing=8.803 angstroms.

In practice, the curved crystals have been found to improve intensities by about an order of magnitude over flat-crystal optics (Loomis and Vincent, 1967) in the analysis of selected small areas.

The automatic crystal changer for simultaneous mounting for four crystals (see table 1) is shown in figure 3. The controls for selecting the desired crystal are also shown.

COLLIMATORS AND APERTURES

X-rays are not easily focused, and to analyze small samples the cross-sectional area of the X-ray beam must be reduced by a suitable aperture. Two methods for reducing the beam size are illustrated in figure 4. An aperture can be inserted either before or after the sample. Generally, the first method is accomplished by a collar-adapter fitted to the X-ray tube into which a series of interchangeable, lead plugs with cone-shaped pinholes may be inserted (fig. 4*A*). In this system, irradiation of the sample is restricted to an area only slightly larger than the pinhole opening. The second method involves limiting the secondary X-rays as suggested by Heinrich (1962). The whole sample surface is irradiated, but only that part of the secondary X-ray beam emanating from the area defined by the aperture is measured (fig. 4*B*). The equipment for this system is shown in figure 5. The sample drawer is constructed to allow easy removal or insertion of a variety of apertures, some of which are shown. Fabricated from brass or aluminum, the cylindrical inserts have conically shaped openings between 0.005 to 0.05 inches in smallest diameter. The apertural size used depends on the spatial resolution desired.

Table 2 summarizes data obtained with various apertures on a single pellet containing 1 milligram of iron in 500 mg of cellulose. Several conclusions can be drawn from the data. The intensities and peak-to-background ratios obtained with conical apertures are

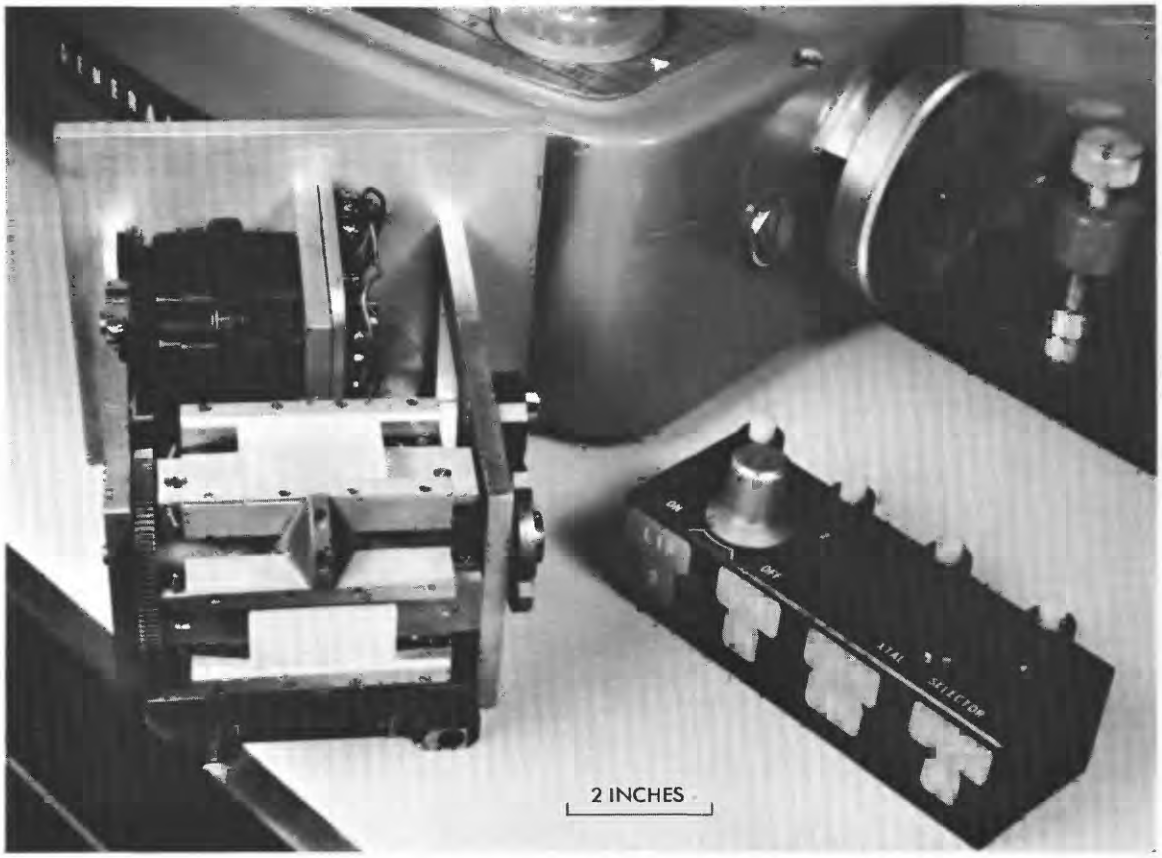

FIGURE 3.—Four-crystal changer and control panel.

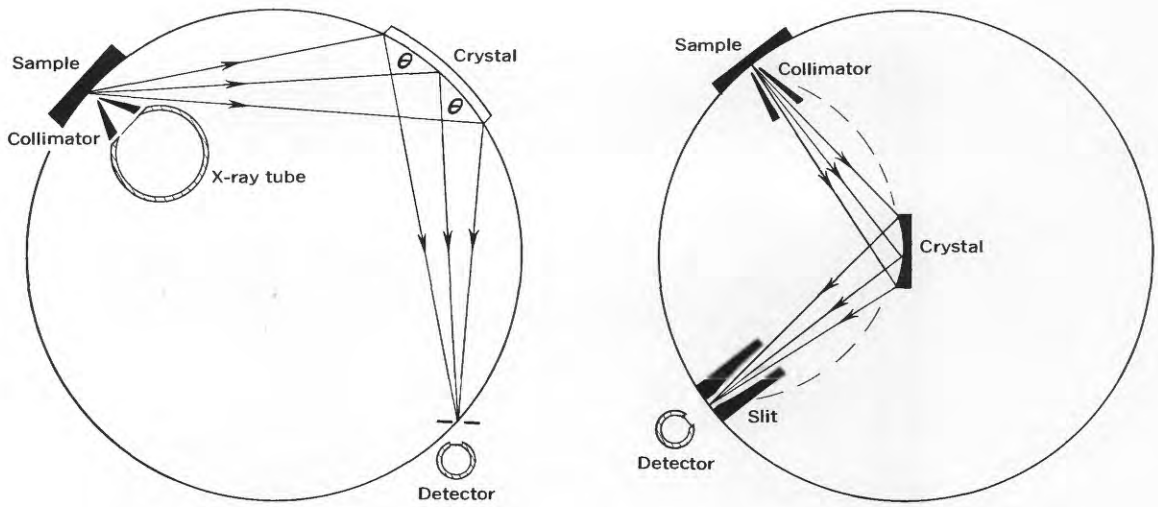

FIGURE 4.—Two methods of selected area collimation.

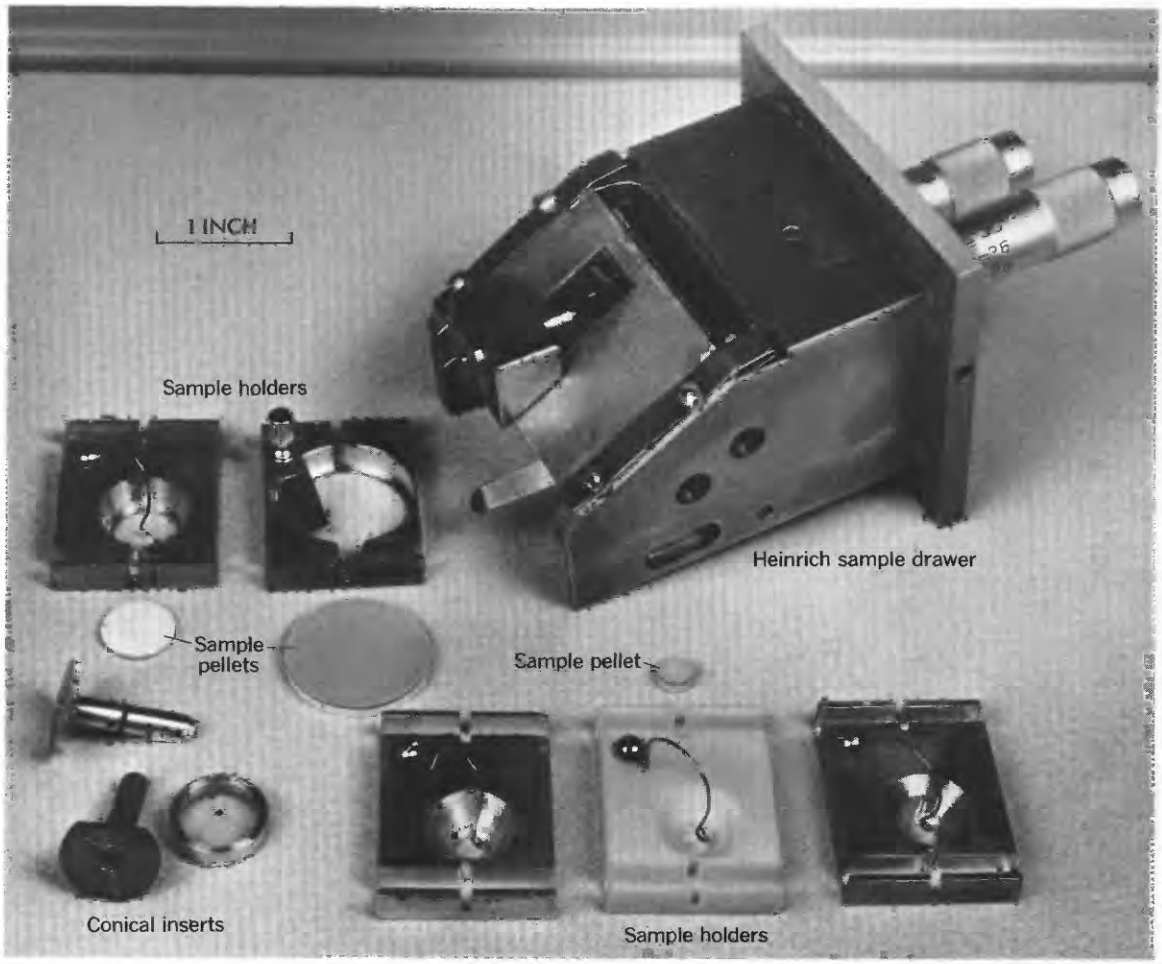

FIGURE 5.—Heinrich sample drawer, conical inserts, and assorted sample holders.

TABLE 2.—*Summary of data obtained with various apertures for the X-ray milliprobe*

[All measurements were made on the same 1-inch-dia meter pellet, which contains 1 mg of iron in 500 mg of compressed cellulose powder]

Type of aperture	Diameter (inches)	Peak (counts per second)	Background (counts per second)	Peak-to-background ratio	Area defined by aperture (square inches)	Weight of iron within defined area (milligrams)
Conical	0.05	4,800	92	52/1	0.0020	0.0025
	.03	2,180	38	57/1	.00071	.00090
	.02	1,080	12	90/1	.00031	.00040
	.01	300	3	100/1	.000079	.00010
	.005	60	.6	100/1	.000020	.000025
Cylindrical	.04	580	20	29/1	.0013	.0016

greater than those obtained with cylindrical apertures. As the aperture diameter is reduced, the peak-to-background ratio increases. In addition to the intensity data for iron, the area defined by the aperture and the weight of iron within that area are given for each aperture. All calculations exclude the dilution of iron in the powdered cellulose.

In addition to the conical apertures, vertical slits have also been devised for specific application, such as the scanning of X-ray spindles or polished surfaces in which elongated linear bands are to be studied. With the use of a vertical slit, increased counting rates result from observing a larger area of irradiation (Bertin, 1967). However, great care is required in positioning the sample with the slit, and line-to-background ratios are not improved.

SUPPORT MEDIA

Because of the varied sizes and shapes of the samples that are submitted for analysis, the types of sample holders and support media used can have significant effects on the results. Primarily because of the focusing optics, the sample must be kept at a point through which the focal circle passes, and all samples must be brought to this point. Also, small samples require a support medium that will maintain back-

ground scatter at a minimum and be free of the elements being determined in the specimen. Small fragments, chips, grains, and X-ray powder-diffraction spindles are best mounted on a thin organic film (such as polypropylene) that has been pulled taut between two aluminum hoops of slightly different diameter. To keep the sample in place, two techniques have been found to work satisfactorily. A small dot of Duco cement is placed on the organic film, and the sample is gently pressed against the cement. Care should be taken to avoid enveloping the specimen with the cementing material. Another technique is to mount a small strip of double-sided transparent tape on the organic film, and press the individual crystals onto the tape. In either method of mounting, a scan of the mounting material should be made to check for the presence of contaminants.

For semiquantitative scanning of large specimens up to one inch square, the only restrictions are that the sample be reasonably flat and less than half an inch thick. Quantitative preparations are best handled by either a fusion preparation (Rose and others, 1962, 1963) or a solution-dilution preparation (Rose and others, 1965; Rose and Cuttitta, 1968).

RELATIVE PERFORMANCE OF FLAT-CRYSTAL AND CURVED-CRYSTAL OPTICS

Though the two crystal systems cannot be compared under exactly the same conditions, the performance of each in the following two examples is significant.

Nondestructive scanning of a small specimen

Nondestructive semiquantitative scanning for the elements or rationing of elements is performed frequently on individual grains, chips, or X-ray spindles. Figure 6 illustrates the results of scanning an X-ray powder-diffraction spindle of helvite with the curved-crystal and flat-crystal spectrometers. The comparison leaves little doubt as to the greater sensitivity of curved-crystal optics when a small sample is scanned. The results are not so surprising when one considers that with flat-crystal optics, the secondary X-rays, which must be made parallel, suffer very large losses of intensity through collimation. These losses are usually offset by using a specimen large enough to utilize the full cross section of the primary X-ray beam. As the specimen size is decreased, efficiency of the flat-crystal system drops drastically, for less and less of the X-ray beam is used. The higher intensities obtained with curved crystals are attributable to the ability of the optical system to gather efficiently the diverging secondary X-rays.

Quantitative measurements on a small specimen

For quantitative analysis, the two X-ray optical systems were compared on a solution-dilution preparation (Rose and others, 1965; Rose and Cuttitta, 1968) designed to eliminate the absorption or matrix effect. A series of iron standards was prepared by adding known quantities of iron in solution to 500 mg of cellulose powder. The moist pulp was mixed thoroughly, dried overnight at 80°C., ground in a mortar, and pressed into pellets 1 inch in diameter. The calibration curves for iron obtained with each instrument are shown in figure 7. The area irradiated in the flat-crystal system was 0.786 square inch for the 1-inch pellet. Although actually slightly larger, the area of the pellet defined by the 0.05-inch-diameter conical aperture in the curved-crystal unit is 0.00196 square inch, or 1/400 of that defined by conventional flat-crystal optics. In the flat-crystal unit secondary radiation is counted from practically all the iron in the 1-mg preparation, but in the curved-crystal unit the radiation is counted from only 0.0025 mg iron. For the particular collimator and aperture chosen for each optical system, the intensity obtained favors the curved-crystal system over the flat-crystal system by 4,800/3,200 counts per second in spite of the 1/400 ratio in both sample weight and area; for the 0.1-mg-iron pellet, the counting data are 500/340 counts per second. Projection of the data to a lower limit of sensitivity based on statistics of 3δ above background (where δ equals $\sqrt{n_t}$, and n_t is the total number of the counts) indicates detection to be 1 microgram with flat crystal optics and 25 nanograms with curved-crystal optics. It should be noted that the dilution factor (500/1) has not been included in the calculations.

Figures 8 and 9 are calibration curves that were obtained on calcium and La_2O_3 from a set of prepared pellets. The data are included here to indicate the sensitivity attainable with elements that have both higher and lower atomic numbers than iron. The counting rates for lanthanum are considerably lower than for iron, but background for lanthanum is also much lower, and the peak-to-background ratio is maintained at a reasonable level.

REDUCTION OF SAMPLE SIZE

The data just presented show that the sample requirements can be reduced substantially by using pellets of smaller diameter. A series of holders designed for ¼-inch-diameter pellets was prepared. Before preparing the full set of standards, however, it was necessary to establish the minimum critical thickness. Varying quantities of the cellulose-iron mixture were used to

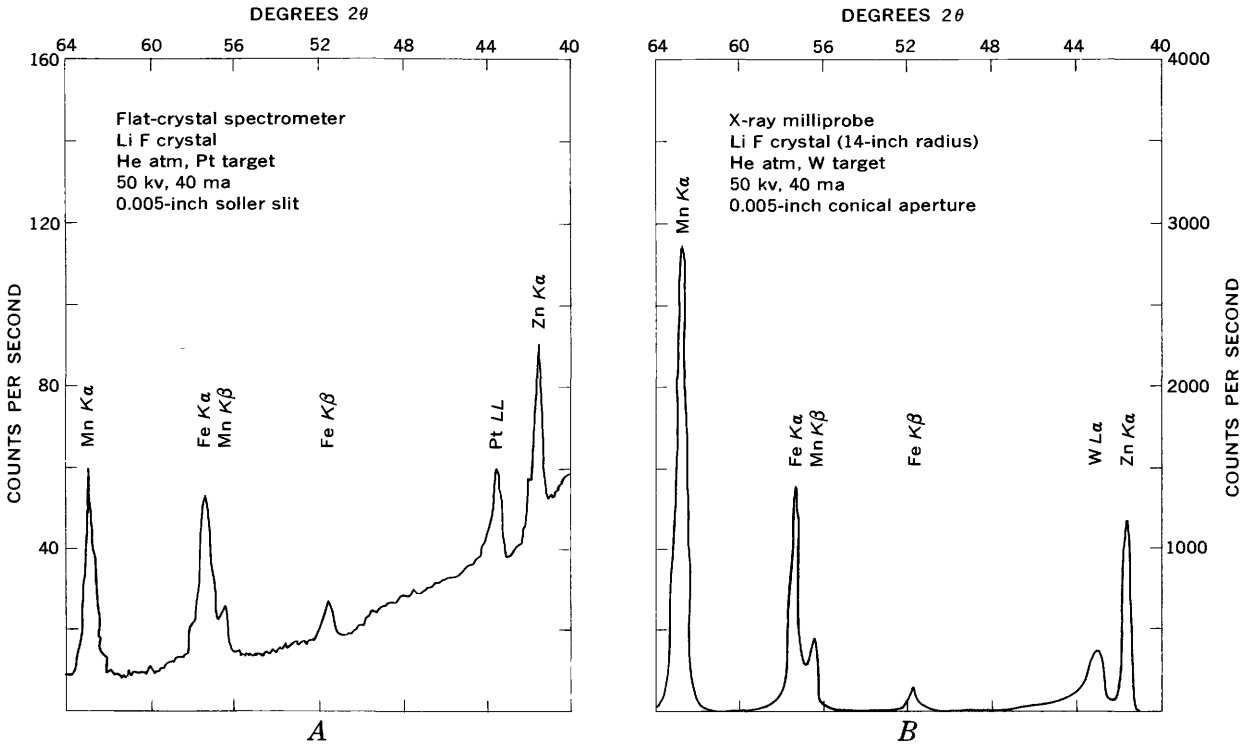

FIGURE 6.—Spectrum of X-ray powder-diffraction spindle of helvite by conventional flat-crystal (*A*) and curved-crystal (*B*) spectrometers.

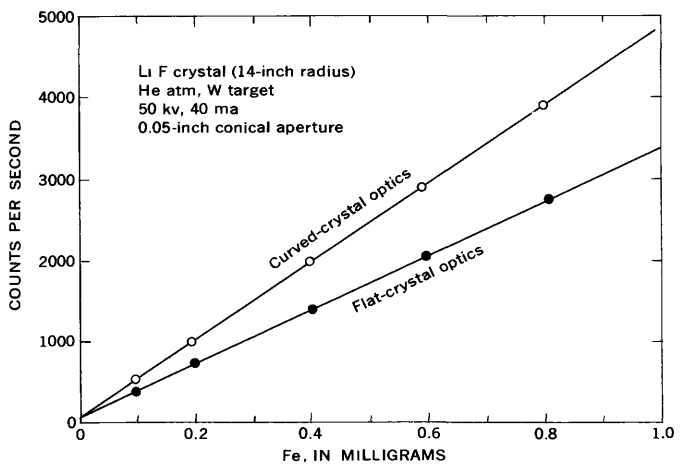

FIGURE 7.—Calibration curves for iron obtained with flat-crystal and curved-crystal spectrometers. Components for the flat-crystal system are the same as those listed in figure 6*A*.

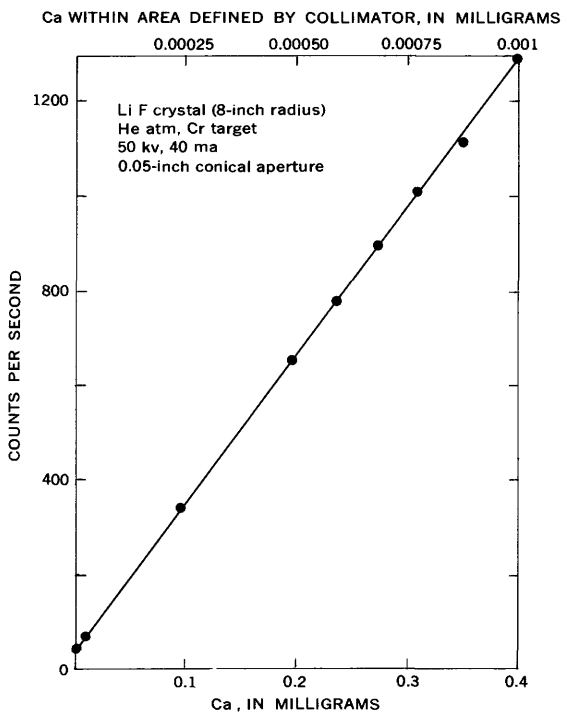

FIGURE 8.—Calibration curve for calcium obtained with a curved-crystal spectrometer.

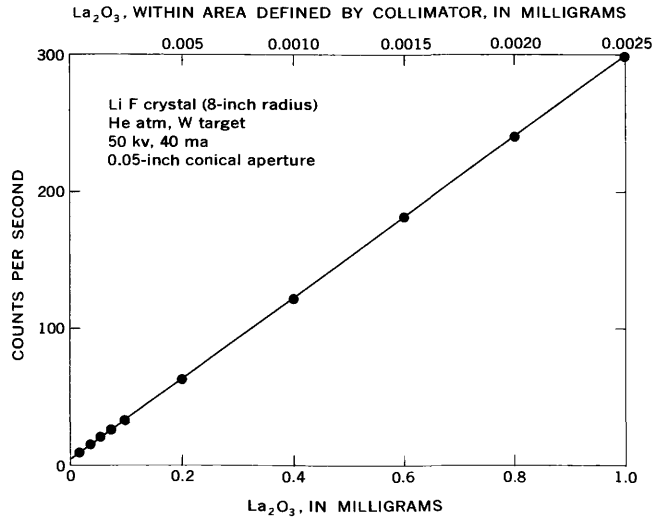

FIGURE 9.—Calibration curve for La_2O_3 obtained with a curved-crystal spectrometer.

obtain the data given in figure 10. Intensities increase with increase in sample size until the infinite thickness reached at about 35 mg of the mixture at 50 kilovolts. Beyond this point, intensity remains constant regardless of the amount of cellulose-iron mixture used.

A set of standards was prepared in the form of ¼-inch-diameter pellets using 50 mg of iron-cellulose mixture (one-tenth of that required for the preparation of the 1-inch-diameter pellets). The calibration curve for iron obtained from these smaller pellets is identical with the upper curve in figure 7, except that the weight units of the abscissa are one-tenth the values indicated.

It follows that ⅛-inch diameter pellets would attain infinite thickness at about 5 mg of mixture and would yield the same calibration cuprve as that for the 1-inch-diameter pellets. The sample weights, however, would be reduced from those given in figure 7 by 100-fold. Great care in handling such small samples is required, but the net effect is a substantial decrease in sample size.

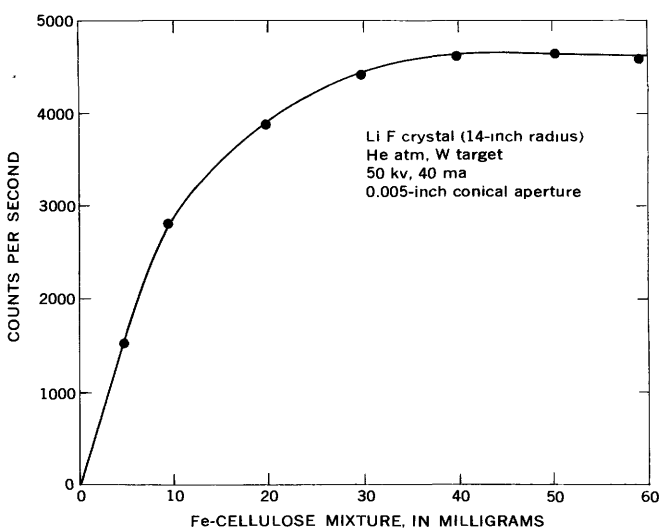

FIGURE 10.—Determination of infinite thickness for 1/4-inch-diameter pellets.

COMPARISON OF THE X-RAY MILLIPROBE AND ELECTRON MICROPROBE

Understandably, a comparison between the X-ray and electron probes can be the topic of considerable discussion. Each has several advantages, and both have a place in the analytical laboratory.

The X-ray milliprobe has the advantage of greater ease and speed of sample preparation, greater penetration of the specimen by the exciting radiation, and less dependence on surface preparation and takeoff angle. Other advantages are the ability to analyze areas of 0.012 to 1.2 square millimeters when smaller areas are not required for study, and the ability to study samples that are adversely affected by direct electron excitation or by the vacuum required by the electron microprobe. Because standards need not be as critically homogeneous as for the electron microprobe, they are more readily available to the X-ray milliprobe. Finally, corrections for electron backscatter losses, secondary excitation effects, and X-ray absorption are far more critical in quantitative determinations by the electron microprobe than by the X-ray milliprobe.

Secondary X-radiation is less intense than primary X-radiation excited by electrons, and higher orders of the K and L spectra as well as the M spectra cannot be used favorably with the X-ray milliprobe. Spatial resolution with the electron microprobe is of the order of 1-micron. The light elements, sodium to beryllium, can be detected much more readily with the electron microprobe. The microprobe is capable of obtaining useful data from backscatter, specimen current, and electron-beam-scanning imagery that cannot be obtained with the X-ray milliprobe, though X-ray scanning imagery is feasible. From the foregoing data, then, one can only conclude that the X-ray and electron probes are both welcome additions to the analytical laboratory.

REFERENCES

Adler, Isidore, and Axelrod, J. M., 1956, The curved-crystal X-ray spectrometer, a mineralogical tool: Am. Mineralogist, v. 41, p. 524–527.

Bertin, E. P., 1967, A comparison of four slit apertures for selected-area analysis with the X-ray secondary-emission spectrometer, *in* Newkirk, J. B., and Mallett, G. R., eds., Advances in X-ray analysis, v. 10: New York, Plenum Press, p. 462–473.

Heinrich, K. F. J., 1962, X-ray probe with collimation of the secondary beam, *in* Mueller, W. M., ed., Advances in X-ray analysis, v. 5: New York, Plenum Press, p. 516–526.

Loomis, T. C., and Vincent, S. M., 1967, Trace and microanalysis, chap. 37 *of* Kaelble, E. F., ed., Handbook of X-rays: New York, McGraw Hill, p. 37–1 to 37–16.

Rose, H. J., Jr., Adler, Isidore, and Flanagan, F. J., 1962, Use of La_2O_3 as a heavy absorber in the X-ray fluorescence analysis of silicate rocks: Art. 31 *in* U.S. Geol. Survey Prof. Paper 450–B, p. B80–B83.

Rose, H. J., Jr., Adler, Isidore, and Flanagan, F. J., 1963, X-ray fluorescence analysis of the light elements in rocks and minerals: Appl. Spectroscopy, v. 17, p. 81–85.

Rose, H. J., Jr., Cuttitta, Frank, and Larson, R. R., 1965, Use of X-ray fluorescence in determination of selected major constituents in silicates, *in* Geological Survey research 1965: U.S. Geol. Survey Prof. Paper 525–B, p. B155–B159.

Rose, H. J., Jr., and Cuttitta, Frank, 1968, X-ray fluorescence spectroscopy in the analysis of ores, minerals and waters, *in* Newkirk, J. B., Mallet, G. R. and Pfeiffer, H. G., eds., Advances in X-ray analysis, v. 11: New York, Plenum Press, p. 23–39.

THE DIRECT MICRODETERMINATION OF SILICON AND ALUMINUM IN SILICATE MINERALS

By ROBERT MEYROWITZ, Washington, D.C.

Abstract.—The SiO_2 and Al_2O_3 contents of 3- to 5-mg samples of common silicate minerals are directly determined spectrophotometrically by using molybdenum blue and Alizarin Red-S procedures, respectively. The samples are decomposed by sodium hydroxide fusion, and hydrochloric acid solutions of the melts are used for the determinations. The common rock-forming elements likely to be present in most silicate minerals do not interfere in the SiO_2 determinations. Fluorine in concentrations most likely to be found does not interfere in the Al_2O_3 determinations. Titanium and iron interference is overcome by adding the amounts of titanium and iron present in the sample to the standard aluminum solutions used to prepare the standard aluminum curve.

This paper is the third in a series describing micro- and semimicro-procedures (Meyrowitz, 1963, 1964) being developed by the author for the direct determination of the common rock-forming elements. The series, on completion, will provide the schematics for the complete analysis of small samples of silicate minerals. The procedures described herein are recommended for the determination of silicon and aluminum. They are based on methods described by Shapiro and Brannock (1962) for the direct determination of silicon and aluminum in silicate rocks.

Samples and standards are decomposed by fusion with NaOH in gold crucibles. The melts are leached with water, and the solutions are acidified with hydrochloric acid. Silicon and aluminum are determined spectrophotometrically by molybdenum blue and Alizarin Red-S procedures, respectively.

REAGENTS AND APPARATUS

Reagents

Sodium hydroxide pellets, ACS reagent grade: Transfer contents of previously unopened bottle to a plastic bottle and store.

Sodium hydroxide solution, 30 percent (w/v): Prepare and store in plastic bottle.

Hydrochloric acid, 6*N*.

Hydrochloric acid, 0.06*N*.

U.S. National Bureau of Standards standard soda feldspar 99a or equivalent.

Sulfuric acid, 18*N*.

Ammonium molybdate solution: Dissolve 3.75 grams of $(NH_4)_6Mo_7O_{24}\cdot 4H_2O$ in 35 milliliters of water in a plastic 50-ml beaker containing a plastic-covered magnetic stirring bar. Add 50 ml of 18*N* H_2SO_4. Mix and cool. Filter through a fast filter paper into a glass bottle. Dilute to 50 ml and mix well.

Tartaric acid solution, 10 percent: Prepare, filter if necessary, and store in plastic. Prepare fresh solution when sediment forms.

Reducing solution: Dissolve 9.0 g of sodium bisulfite, $NaHSO_3$, ACS reagent grade, in 80 ml of water in a 100-ml plastic beaker containing a plastic-covered magnetic stirring bar. Dissolve 0.7 g of sodium sulfite, Na_2SO_3, ACS reagent grade, in 10 ml of water in a 100-ml plastic beaker containing a plastic-covered magnetic stirring bar. Add 0.15 g of 1-amino-2-naphthol-4-sulfonic acid to the sulfite solution and stir until all is completely dissolved. Pour the 80-ml bisulfite solution into this combined solution with constant stirring and mix well. Filter into a plastic bottle through a fast filter paper in a plastic funnel. Dilute to 100 ml and mix well. Discard after 3 days.

Calcium chloride solution: Transfer 7 g of $CaCO_3$, ACS reagent grade, to a 250-ml beaker. Add 50 ml of water and then add dilute HCl dropwise with constant stirring until all the $CaCO_3$ is dissolved. Boil the solution for 1 to 2 minutes to remove the dissolved carbon dioxide. Cool. Filter through a fast paper, dilute to 500 ml, and mix well. Store in glass.

Hydroxylamine hydrochloride solution, 10 percent (w/v): Prepare, filter if necessary, and store in glass.

Potassium ferricyanide solution, 0.75 percent: Prepare fresh each day.

Mercaptoacetic acid solution, 1.6 percent (v/v): Prepare fresh each day.

Buffer solution: Prepare 500 ml solution to contain 100 g of sodium acetate, $NaC_2H_3O_2\cdot 3H_2O$, ACS reagent grade, and 30.0 ml of glacial acetic acid, $HC_2H_3O_2$, ACS reagent grade. Filter through a fast filter paper and store in glass.

Alizarin Red-S (alizarin sodium monosulfonate) solution, 0.05 percent (w/v): Prepare 500 ml; filter through a slow paper and store in glass.

Standard Fe_2O_3 solution, 1,000 parts per million of Fe_2O_3 in 0.12*N* HCl: Dissolve 4.91 g of ferrous ammonium sulfate hex-

U.S. GEOL. SURVEY PROF. PAPER 650-B, PAGES B136-B139

ahydrate in distilled water, add 20.0 ml of 6*N* HCl, and dilute to 1 liter.

Standard TiO_2 solution, 1,000 ppm: Prepare from U.S. National Bureau of Standards standard titanium oxide 154a as directed in "Procedure for use as a standard in colorimetry" in the certificate of analysis provided with the standard.

Apparatus

Crucibles and covers, gold, 2-ml capacity, 1.7-centimeter height, 1.7-cm top diameter, and 0.8-cm bottom diameter.

Air bath, micro. This consists of a thermostatically controlled hotplate with a vented glass dome containing an additional hole on top of dome for insertion of a glass thermometer. (See Rulfs, 1951, p. 48, fig. 2.)

Cylinders, glass, 18 millimeter outside diameter and 19 to 20 mm height. These are used to support gold crucibles in the micro hot-air bath.

Furnace, electric, temperature controlled.

Platinum sheet, for bottom of furnace.

Tweezers, with long platinum tips whose ends have been bent at right angles.

pH meter.

Spectrophotometer.

Cells, absorption, 2-cm light path.

PROCEDURE

Blank, standard, and unknown solutions are run simultaneously in duplicate. The volumetric flasks should be cleaned with 1+1 hydrochloric acid and rinsed well with water. The neck of each flask is rinsed down with water, and the contents of the flask are mixed well after the addition of each solution and reagent.

Preparation of sample solution

1. Weigh duplicate 3 to 5 mg (±0.01 milligram) <200-mesh samples of the standards in a 2-ml gold crucible.
2. Weigh 3 samples, each approximately 3.5, 4.0, and 4.5 mg, of a standard feldspar mineral in each of three 2-ml gold crucibles. A sixth gold crucible serves for the preparation of a procedural blank.
3. Using a plastic pipet, carefully add 0.50 ml of 30 percent NaOH to the bottom of the crucibles.
4. Place the crucible on the glass cylinder support in the micro air bath. Heat for 1 hour at an air-bath temperature of approximately 150°C., then for 1 hour at approximately 175°C., and finally for 2 hours at approximately 240°C.
5. Cover the crucible, place it on a platinum sheet in the electric furnace, and heat at 450°C. for 15 minutes. At the end of 10 minutes, remove from furnace, twirl to mix contents of the crucible, and replace in furnace. The cooled melt should completely cover the bottom of the crucible.
6. At end of the 15 minutes remove from furnace, place on a copper cooling block, and allow to cool to room temperature. Transfer crucible and cover to a 100-ml plastic beaker and add 10 to 15 ml of water to disintegrate the melt. Use a 4-inch plastic stirring rod to aid the preliminary solution and disintegration of the melt.
7. Add slowly with stirring 2.0 ml of 6*N* HCl, using a 2-ml Mohr pipet. Allow to stand until complete solution takes place.
8. Use platinum-tipped tweezers with right-angle tips to lift the crucible cover and then the crucible out of solution. Rinse crucible, cover, and tweezers with a fine stream of water from a plastic wash bottle.
9. Transfer the solution to a 100-ml volumetric flask. Dilute to volume and mix well. If the solution is cloudy, filter through a 7.0-cm slow filter paper,and discard the first 20 ml of filtrate.
10. Transfer the clear solution to a dry plastic bottle, and store for subsequent analysis of SiO_2 and Al_2O_3.

Determination of SiO_2

1. Transfer duplicate 10.00-ml aliquots from each of the 0.06*N* HCl solutions of procedural blank, standard feldspar, and unknown silicate mineral to 100-ml volumetric flasks.
2. Add 50 ml of water and then 2.0 ml of ammonium molybdate solution while swirling the flask during the addition of the reagent. Let stand for 10 minutes.
3. Add 4.0 ml of 10 percent tartaric acid while swirling the flask.
4. Add 1.0 ml of reducing solution while swirling the flask. Dilute to mark, mix, and let stand for at least 30 minutes.
5. Determine the absorbances at 650 millimicrons, using a 2-cm cell path. Use water as the reference solution.
6. Measure the pH of all final solutions.
7. Subtract the absorbance of the appropriate procedural blanks from the absorbance of the standard and unknown solutions to obtain the net absorbance.
8. Plot a standard SiO_2 curve from the data of the standard feldspar solutions.
9. Calculate the SiO_2 content of the unknowns from the standard SiO_2 curve.

Determination of Al_2O_3

1. Transfer duplicate 10.00-ml aliquots of 0.06*N* HCl solutions of standard feldspar and un-

known silicate mineral to each of two 100-ml volumetric flasks.
2. Add the necessary amounts of titanium and iron solutions to the standard feldspar solutions.
3. Add 5.0 ml of 0.06*N* HCl to the flasks containing the unknown solutions.
4. If the amount of acid present in the flasks containing the standard feldspar solutions is less than the equivalent of 15.0 ml of 0.06*N* H^+, add sufficient 0.06*N* HCl to reach this amount.
5. Transfer 15.0 ml of 0.06*N* HCl to each of two 100-ml volumetric flasks.
6. To all, add 2.0 ml of $CaCl_2$ solution, 1.0 ml of hydroxylamine hydrochloride, 1.0 ml of potassium ferricyanide, and 2.0 ml of mercaptoacetic acid. Allow to stand for 5 minutes.
7. Add 10.0 ml of buffer solution. Allow to stand for 10 minutes.
8. Add 10.00 ml of Alizarin Red-S solution with a transfer pipet. Dilute to mark, mix, and let stand for 45 to 75 minutes.
9. Determine the absorbances at 475 mμ, using a 2-cm cell path. Use the reagent blank prepared in step 5 as reference solution.
10. Measure the pH of all final solutions.
11. Plot a standard Al_2O_3 curve from the data of the standard feldspar solutions.
12. Calculate the Al_2O_3 content of the unknowns from the standard Al_2O_3 curve.

RESULTS AND DISCUSSION

Few silicate mineral samples are available to serve as standards for testing these procedures. Therefore, it was decided to use duplicate samples differing in weight by 5 to 20 percent whenever SiO_2 and Al_2O_3 were to be determined. Table 1 presents the results.

Common silicate minerals lack the elements that interfere in the determination of silicon. Only iron, titanium, and fluorine are normally present to affect the determination of aluminum. It was found that 0.20 ppm of F does not effect the absorbance of as much as 1 ppm of Al_2O_3. Thus, if the aliquot of solution analyzed for Al_2O_3 is equivalent to 0.5 mg of sample, as much as 4 percent F does not interfere in the determination of as much as 20 percent Al_2O_3. No experiments were made at a level lower than 1 percent Al_2O_3 or a level higher than 4 percent F.

I have found it convenient to use a feldspar such as U.S. National Bureau of Standards standard soda feldspar 99a, or standard potash feldspar 70a, as the standard material to be analyzed at the same time as the unknown silicate minerals. The data obtained for the standards are used to prepare the standard SiO_2 and Al_2O_3 curves. The amounts of titanium and iron present in these feldspars are insignificant.

Occasionally the disintegrated sodium hydroxide melt of an unknown mineral does not dissolve completely upon the addition of hydrochloric acid. However, all the silicon and aluminum does go into solution. The insoluble material is removed by filtering after the final dilution of the hydrochloric acid solution. The pH of this solution should range from 1.1 to 1.3. The concentration of H^+ is 0.06*N*.

Although the pH of the final solutions used for the determination of SiO_2 may be within a range of 1.5 to 1.8, a set of samples and standards should not differ by more than 0.1 pH unit. This will be obtained if the amount of acid present in the solution contains the equivalent of 10.0 ml of 0.06*N* HCl before the addition of the ammonium molybdate reagent. The concentration of SiO_2 in the final solution should be no more than 3.25 ppm. If the 10.00-ml portion of the 0.06*N* HCl solution of the unknown mineral is found to contain more than 325 micrograms of SiO_2, the procedure is repeated using a smaller aliquot of solution, and remembering to add sufficient 0.06*N* HCl to make up the deficiency in the amount of acid. An additional procedural blank equivalent to the smaller

TABLE 1.—*Comparison of* SiO_2 *and* Al_2O_3 *contents of various silicate minerals determined by duplicate-sample analyses*

Lab. No.	Field No.	Mineral	Weight of sample (mg)	Contents compared (percent)	
				SiO_2	Al_2O_3
154958	FB-3	Garnet	2. 84; 2. 77	39. 5; 39. 7	22. 2; 22. 4
154957	FB-5	Cordierite	3. 02; 3. 88	48. 8; 48. 8	33. 6; 34. 0
157709	25-CZ-59	Garnet	6. 75; 4. 35	36. 1; 36. 1	17. 1; 18. 0
158026	59W97-M	Heulandite	4. 56; 4. 30	63. 6; 63. 6	13. 4; 13. 4
	G-2c	Goldmanite	3. 92; 4. 02	36. 2; 37. 0	4. 85; 4. 94
161348	6-100 C″ 4-3	Celadonite	5. 25; 4. 90	51. 4; 51. 4	17. 1; 17. 2
161349	6-100 C-7	Potassium feldspar	4. 26; 3. 59	62. 7; 62. 4	18. 5; 18. 5
161350	5-507-E-2	Illite	4. 22; 4. 26	51. 2; 50. 7	28. 7; 28. 6
	36AA	Greenalite	4. 14; 5. 04	42. 1; 42. 0	7. 07; 7. 19
W-165338	DPH-77-CPX	Clinopyroxene	5. 27; 5. 78	49. 7; 49. 9	5. 67; 5. 64
Standard deviation				0. 23	0. 23

aliquot of sample solution is prepared. The amounts of SiO_2 taken for the standards should bracket or be close to the unknowns. If smaller (<10.00 ml) aliquots of the standard solution are used, similar changes are made for the amount of acid present and for the preparation of an equivalent procedural blank.

To overcome the interference of titanium and iron in the determination of Al_2O_3, approximately the same amounts of titanium and iron present in the part of the 0.06*N* HCl solution of the mineral taken for analysis are added to the standard aluminum solutions used to prepare the standard aluminum curve. Ordinarily a complete analysis is made so that the titanium and iron data are available for judging the additions. The interference of titanium in the determination of Al_2O_3 requires the preparation of a separate standard curve for each duplicate sample whenever titanium is present. If the TiO_2 concentration is less than 0.1 percent, the same standard curve can be used for both samples by using the average value for the amount of iron added to the standard aluminum solutions.

Although the pH of the final solution used for the determination of Al_2O_3 may be within a range of 4.5 to 4.7, samples and standards within a set should not differ by more than 0.1 pH unit. This will be obtained if the amount of acid present in the solution contains the equivalent of 15.0 ml of 0.06*N* HCl before the addition of the calcium chloride reagent. The concentration of Al_2O_3 in the final solution should be no more than approximately 0.95 ppm of Al_2O_3. Generally, a 10.00-ml portion of the 0.06*N* HCl solution of the feldspar is taken for the standard aluminum solution. Therefore, the volumes of titanium and iron solutions added to each standard aluminum solution must not exceed the equivalent of 5.0 ml of 0.06N H^+. This limitation must be considered when one prepares the dilute standard titanium and iron solutions to be added.

The amounts of aluminum taken for the standards should bracket or be close to the unknowns. The degree of titanium interference in the determination of aluminum depends upon the level of aluminum present, the lower the level of aluminum the greater the increase in absorbance (see Shapiro and Brannock, 1962, p. A26–A27). One cannot obtain therefore an applicable procedural blank as in the SiO_2 procedure.

REFERENCES

Meyrowitz, Robert, 1963, A semimicroprocedure for the determination of ferrous iron in nonrefractory silicate minerals: Am. Mineralogist, v. 48, p. 340–347.

——— 1964, The direct spectrophotometric microdetermination of high-level magnesium in silicate minerals—A Clayton Yellow procedure: Am. Mineralogist, v. 49, p. 769–777.

Rulfs, C. L., 1951, Quantitative semimicro inorganic procedures: Anal. Chim. Acta, v. 5, p. 46–54.

Shapiro, Leonard, and Brannock, W. W., 1962, Rapid analysis of silicate carbonate, and phosphate rocks: U.S. Geol. Survey Bull. 1144–A, 56 p.

RAPID DETERMINATION OF POWDER DENSITY OF ROCKS BY A SINK-FLOAT TECHNIQUE

By LEONARD SHAPIRO, Washington, D.C.

Abstract.—Experiments indicate that finely crushed rock ($\leq$ 80 mesh) in a heavy liquid, if not agitated, sinks or floats as large aggregates of the constituent minerals rather than as discrete grains. The "average density" of the clumped crushed material closely approximates that of the rock powder and may be determined by a simple sink-float technique. Small samples of powdered rock are centrifuged in heavy liquids in a sequence designed to bracket density with narrow limits. Only about 100 mg of sample is required to obtain density determinations within ± 0.04.

Excellent methods exist for the determination of powder density of rocks of which the most widely used is the classical pycnometer technique or some modification of it (Fahey, 1961, May and Marinenko, 1966). However, these methods require considerable care and attention, and only about three or four determinations per hour can be performed. A commercially available air compression pycnometer (McIntyre and others, 1965) is more rapid, but it requires the use of at least 50 grams of sample which may not be available. Where powder density is to be determined on large numbers of samples a saving of even a few minutes per sample can become an important factor in the choice of method.

Heavy liquids have been used for many years as a means of mineral separation, and many publications describe this approach (see, for example, Clemmons and others, 1957; Browning, 1961). Thus, at first glance, the use of sink-float methods for the determination of powder density of rocks would seem to be infeasible. Nevertheless, an investigation was made to determine the extent to which a sink-float method could be applied to density determination of rock powders.

PHYSICAL BASIS OF METHOD

Sink-float methods for determining density require no justification when applied to a pure material in either powder or lump form. Starting from the empirical observation that most rock powders can be classified within narrow limits as to their sinking or floating in liquids of known density, and thereby establishing their density, one may question why rock powders do not separate into their mineral constituents.

Two tests were made to shed some light on the mechanism:

1. An equal amount of a granite G-1, powder density 2.64, and a diabase W-1, powder density 3.00, were intermixed by tumbling, and then a dipper portion was treated with a solution of density 2.68 as described in the procedure. The entire sample sank. This procedure was repeated except that the sample and liquid were vigorously agitated prior to centrifuging. An upper and lower layer were obtained.

2. When a part of the mixture was placed in a shallow dish and a few drops of a heavy liquid were added, floating clumps consisting of different minerals were observed under a microscope. When the mixture was stirred, disaggregation into individual minerals occurred to a large degree.

From the two experiments one may conclude that, in the absence of agitation, surface adherence or clumping averages out differences in density of the rock-forming minerals.

The possible influence of micropores and degree of fineness of grind on density in porous rocks was tested by density determination of a siltstone ground to various sizes. For samples in the size range of 90 to 200 mesh, no difference in density was observed; with samples finer than 325 mesh, an increase of 0.02 in density unit was indicated, but this is within the experimental error of the procedure described and is therefore not a significant factor.

DETERMINATIVE METHOD

Heavy liquids

Prepare eight heavy-liquid mixtures according to the proportions given in table 1, from pure carbon

U.S. GEOL. SURVEY PROF. PAPER 650-B, PAGES B140-B142

TABLE 1.—*Primary heavy-liquid mixtures*

[Quantities in milliliters]

Liquid designation [1]	Carbon tetrachloride (sp gr 1.59)	Bromoform (sp gr 2.89)	Methylene iodide (sp gr 3.32)	Resultant specific gravity
A	25	22.5		2.20
B	20	29		2.36
C	14.3	35.7		2.52
D	8.3	43.7		2.68
E	2	50		2.84
F		33.3	11.5	3.00
G		20	33.3	3.16
H			50	3.32

[1] Liquid mixtures designated A, B, C, * * *, shall be termed "primary"; mixtures of adjacent primary liquids, for example, AB, BC, CD, * * *, and so forth, shall be termed "secondary."

tetrachloride (sp gr 1.59), bromoform (sp gr 2.89), and methylene iodide (sp gr 3.32). Those mixtures containing methylene iodide should be stored in amber bottles containing a small piece of copper wire to minimize light-induced decomposition, which releases iodine and darkens the liquid.

Equipment

Test tubes, 10×75 millimeters; several dozen are required.

Test-tube rack.

Small dipper capable of transferring 30–50 milligrams of sample powder.

Squeeze-type pipet suitable for transferring 0.3 milliliter of liquid.

Centrifuge.

Procedure

Transfer approximately 50 mg of sample powder (80 mesh or finer) by dipper to two test tubes and add 0.3 ml of liquid D to one of them. Do not agitate. Centrifuge for 1 minute and examine. Four results are possible: (1) the entire sample floats, (2) the entire sample sinks, (3) the sample splits to form one layer on top and one on the bottom, or (4) it disperses throughout the liquid, in which case it has an "average" density the same as density of liquid D. In some instances a small part may go in the direction opposite to that of the bulk of the sample. If the minor part is roughly 5 percent or less, it may be ignored as far as categorizing the result. If the sample floats in liquid D, add 0.3 ml of liquid C to the second tube; if it sinks, add 0.3 ml of liquid E instead. If the sample splits into two discrete layers in liquid D, add liquid C to the second tube and also add liquid E to another dipper of the sample in a third tube. Centrifuge for 1 minute and categorize as above.

If it is found that in the second liquid the sample also sinks or floats, repeat with the next liquid until it sinks in one liquid and floats in the adjoining one. At this point, mix the two primary liquids to form a secondary liquid with an intermediate density (for example, DE). Centrifuge for 1 minute and categorize.

The density difference between any two adjacent primary liquids was arbitrarily chosen to be 0.16. If the sample floats in one liquid and sinks in the adjacent liquid, the samples density is within the given 0.16 range defined by the two liquids. If the sample is denser than the mixture of the two liquids, then we can say that its density is ±0.04 of the density midway between those of the mixture (for example, secondary liquid DE) and the heavier component (liquid E). Likewise, if the sample floats in the mixture, its density is ±0.04 of the density midway between the density of the mixture (for example liquid DE) and that of its lighter component (liquid D). If the sample forms an upper and lower layer in the mixture of two liquids different in density by 0.16, then the density of the sample can be taken as the density of the liquid mixture within narrow limits.

When the sample forms two layers in one of the primary liquids, sinks in the adjacent lighter one, and floats in the adjacent heavier one, then the density of the liquid in which it split closely approximates the sample density. If the sample forms two discrete layers in two adjoining primary liquids, it obviously cannot be determined by this procedure.

DISCUSSION OF RESULTS

To test the validity of the method, densities of a set of samples submitted for rapid rock analysis were measured both by the sink-float procedure and also by pycnometer according to Fahey's (1961) method. Comparison of the results (table 2) indicates good agree-

TABLE 2.—*Comparison of results of sink-float and pycnometer methods for determining density of rocks*

Sample type	Powder density methods		Density difference
	Sink-float	Pycnometer	
Tonalite	2.86	2.82	+0.04
	2.86	2.84	+.02
Hornblende gabbro	3.08	3.06	+.02
Granodiorite	2.68	2.67	+.01
Aplite	2.60	2.59	+.01
Hornblende porphyry	2.76	2.79	−.03
Quartz muscovite with augen gneiss	2.72	2.74	−.02
Metagraywacke	2.72	2.73	−.01
	2.72	2.73	−.01
Quartz muscovite schist	2.80	2.78	+.02
Ashfall tuff	2.32	2.33	−.01
	2.24	2.24	0
	2.36	2.40	−.04
Granodiorite porphyry	2.68	2.66	+.02
Rhyodacite porphyry	2.64	2.65	−.01
	2.68	2.68	0
Plagioclase porphyry	2.84	2.80	+.04
Standard granite G–1	2.64	2.64	0
Standard diabase W–1	3.00	3.00	0

ment between the values obtained by the two methods, and that powder densities can be determined on rock powders within ±0.04 density units by the sink-float procedure described. The method may offer an attractive alternative for the determination of powder density, particularly where many samples are involved. The technique described has been applied to several hundred rocks of diverse source and type. In all but a few there was no difficulty in establishing the density.

REFERENCES

Browning, J. S., 1961, Heavy liquids and procedures for laboratory separation of minerals: U.S. Bur. Mines Inf. Circ. 8007, 14 p.

Clemmons, B. H., Jr., Stacy, R. H., and Browning, J. S., 1957, Heavy-liquid techniques for rapid evaluation of sands by prospectors and plant operators: U.S. Bur. Mines Rept. Inv. 5340, 12 p.

Fahey, J. J., 1961: A method for determining the specific gravity of sand and ground rock or minerals: Art. 283 *in* U.S. Geol. Survey Prof. Paper 424–C, p. C372–373.

May, Irving, and Marinenko, John, 1966, A micropycnometer for the determination of the specific gravity of minerals: Am. Mineralogist, v. 51, nos. 5–6, p. 931–934.

McIntyre, D. B., Welday, E. E., and Baird, A. K., 1965 Geologic application of the air pycnometer—A study of the precision of measurement: Geol. Soc. America Bull., v. 76, no. 9, p. 1055–1060.

A TRANSISTORIZED EMISSION REGULATOR FOR GAS-SOURCE MASS SPECTROMETRY

By E. E. WILSON and J. S. STACEY, Denver, Colo.

Abstract.—A transistorized circuit is described for the precise control of electron emission from the filament in a gas-source mass spectrometer. The emission current can be adjusted up to 5 milliamperes, and its regulation is better than 0.005 percent for a 10-percent line-voltage change. Normal drift of the emission current is less than 0.002 percent per hour. The electron accelerating voltage can be adjusted up to a maximum of 150 volts with regulation of better than 0.01 percent for a 10-percent change in line voltage. This level of performance helps to ensure that fluctuations in the total ion beam in a mass spectrometer during the course of an analysis are kept below ±0.1 percent.

Since 1962, the U.S. Geological Survey has designed and constructed electronic equipment associated with mass spectrometers. Many of the circuits are not commercially available and therefore may be of interest to other workers in this field. This article is the first of a series planned for publication of some of this work.

For several years we have used circuitry incorporating silicon-controlled rectifiers to regulate the filament emission in our gas-source mass spectrometers. Such circuits have proved very rugged and reliable but are quite complex and, moreover, were designed to operate from a 30-volt direct-current source. Recently we have reverted to a simpler system which uses a series regulator transistor and operates from 115-volt, 60 Hertz line input. A series regulator transistor circuit was originally used by Russell and Kollar (1960); however, our new arrangement provides better regulation for the electron accelerating voltage (EAV) by use of a more stable reference voltage and a higher gain comparison amplifier. Our experience has shown that good EAV stability is an important factor in the production of a well-stabilized ion beam in the mass spectrometer.

Three of the new units have been constructed. One of these has been used since December 1967 for lead tetramethyl analyses, and the other two have recently been installed in our argon mass spectrometers.

Figure 1 is a simplified diagram which indicates the overall operation of the emission regulator circuit; the complete circuit diagram is shown in figure 2. The total filament emission current flows through resistors R12 and R13. The resulting voltage is compared with a reference voltage ($V_{ref} \approx 7$ volts) in a comparison amplifier formed by transistors Q3, Q4, and Q5. The amplified error voltage controls the filament series regulators (Q1 and Q2). The range over which the emission current may be regulated is determined by resistors R12 and R13; for the values given, the range is from 1 to 5 milliamperes. In our lead tetramethyl mass spectrometer the emission current range is from 0.1 to 0.5 ma; this was obtained by increasing the values of R12 and R13 by an order of magnitude.

A reference voltage of 150 volts is provided for the EAV supply by Zener diode D9. This voltage is prestabilized by Zener diodes D7 and D8. The EAV itself is regulated by the series regulator transistor Q6 and the magnitude of the EAV is determined by the setting of potentiometer R16. This arrangement ensures that the shield-filament voltage is independent of emission current.

Adjustable trap and repeller voltages are derived from Zener diode D6 and are substantially independent of each other as well as of the total emission current. Diodes D1, D5 and D10 provide protection against high-voltage transients which may occur in the ion source of the mass spectrometer.

In figure 2, transformers T1 and T2 supply the various voltages required for the circuit from the 115-volt, 60 Hz line input. They are designed to operate with ion source voltages of as much as 5,000 volts. An electrostatic screen is provided between the primary and secondary windings of each transformer. Each screen is insulated from its primary winding for 5,000

U.S. GEOL. SURVEY PROF. PAPER 650-B. PAGES B143-B146

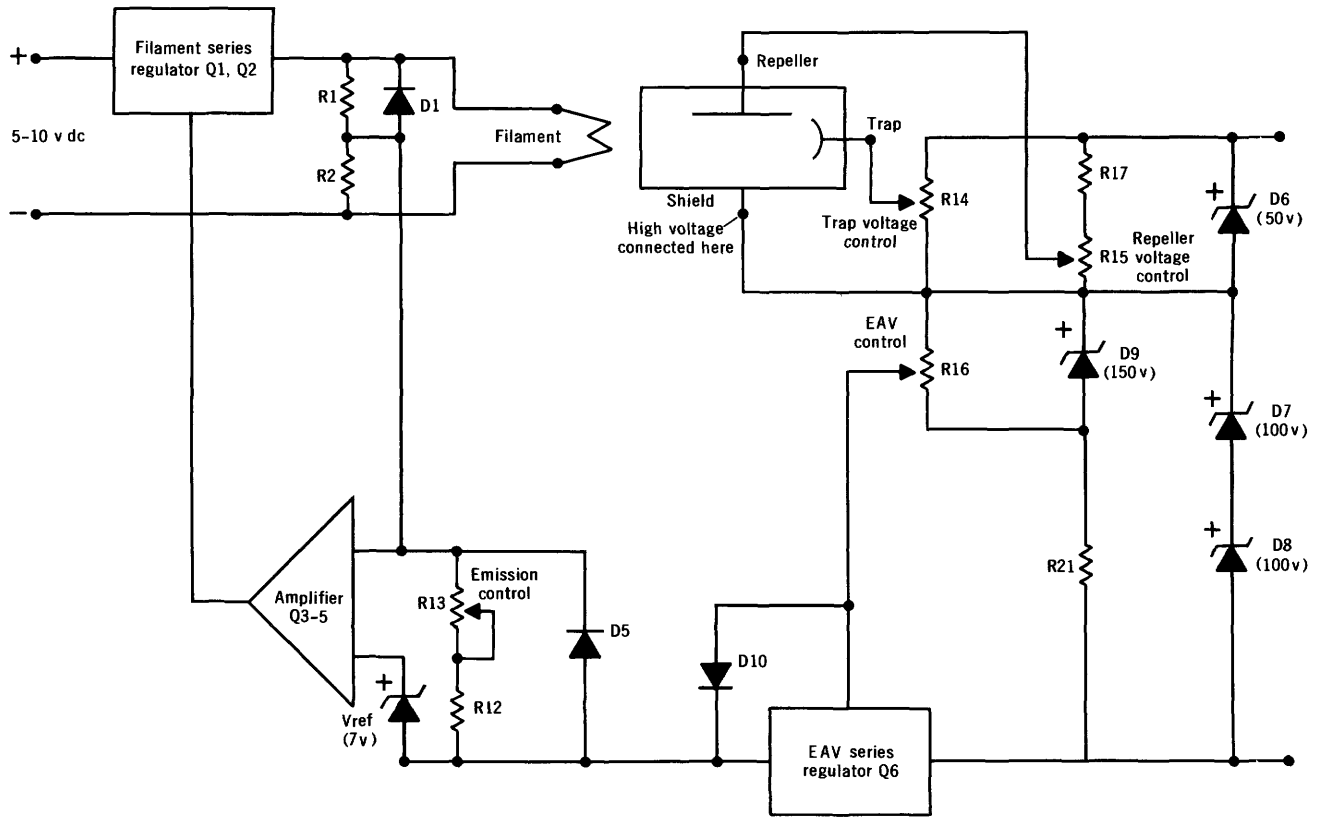

FIGURE 1.—Simplified diagram for filament emission regulator. EAV, electron accelerating voltage.

volts dc and should be connected to the secondary circuit "ground" as shown in figure 2.

At this point it must be noted that the incorporation of the screen in transformer T1 was intended to prevent a large 60 Hz ripple voltage from appearing in the control amplifier circuit. Should this trouble still occur, a 1:1 transformer must be connected into this secondary circuit of T1 in order to further isolate the filament from the line input. Such an arrangement was originally used in the circuit with an isolating transformer Triad type N51X.

When a new filament in the mass spectrometer is initially degassed, it is recommended that the emission regulator be connected to the main supply through a Variac transformer. The filament current can then be increased gradually. After the filament is conditioned, this procedure is useful to determine the correct tap for the secondary of the filament transformer. With the correct filament voltage, the circuit should start to regulate as the power input is increased to about 85–90 volts.

Summarized below are the main specifications and performance figures for this unit.

Specifications:

- Emission current ____ 1–5 ma.
- Filament current _____ 5 amps maximum (dc).
- Filament voltage _____ 6–10 v (given by 4 transformer taps).
- EAV _____ 0–150 v.
- Trap voltage _____ 0–50 v.
- Repeller voltage _____ 0–5 v.
- Transformer insulation, primary: secondary. 5,000 v (dc) working.

Performance:

Bench check:

- Total emission regulation _____ Better than 1 part in 20,000 for 10-percent line-voltage change.
- EAV regulation ____ Better than 1 part in 9,000 for 10-percent line-voltage change.
- Drift _____ Emission current drifted less than 1 part in 50,000 over a period of 2 hours at normal room temperature.

Operational check:

- Total ion beam regulation_____ Better than 1 part in 1,000 for 10-percent line-input change.
- Total ion beam fluctuations (that is, departures from a smooth decay curve) in our lead tetramethyl instrument are less than 1 part in 1,000 during the 30-minute period of an analysis.

Transformer specifications:

Transformers T1 and T2 are special transformers designed and manufactured for us by Transformer Electronics Co., Industrial Park, Boulder, Colo. Design details for T1 and T2 are listed on page B146 by permission of the manufacturers.

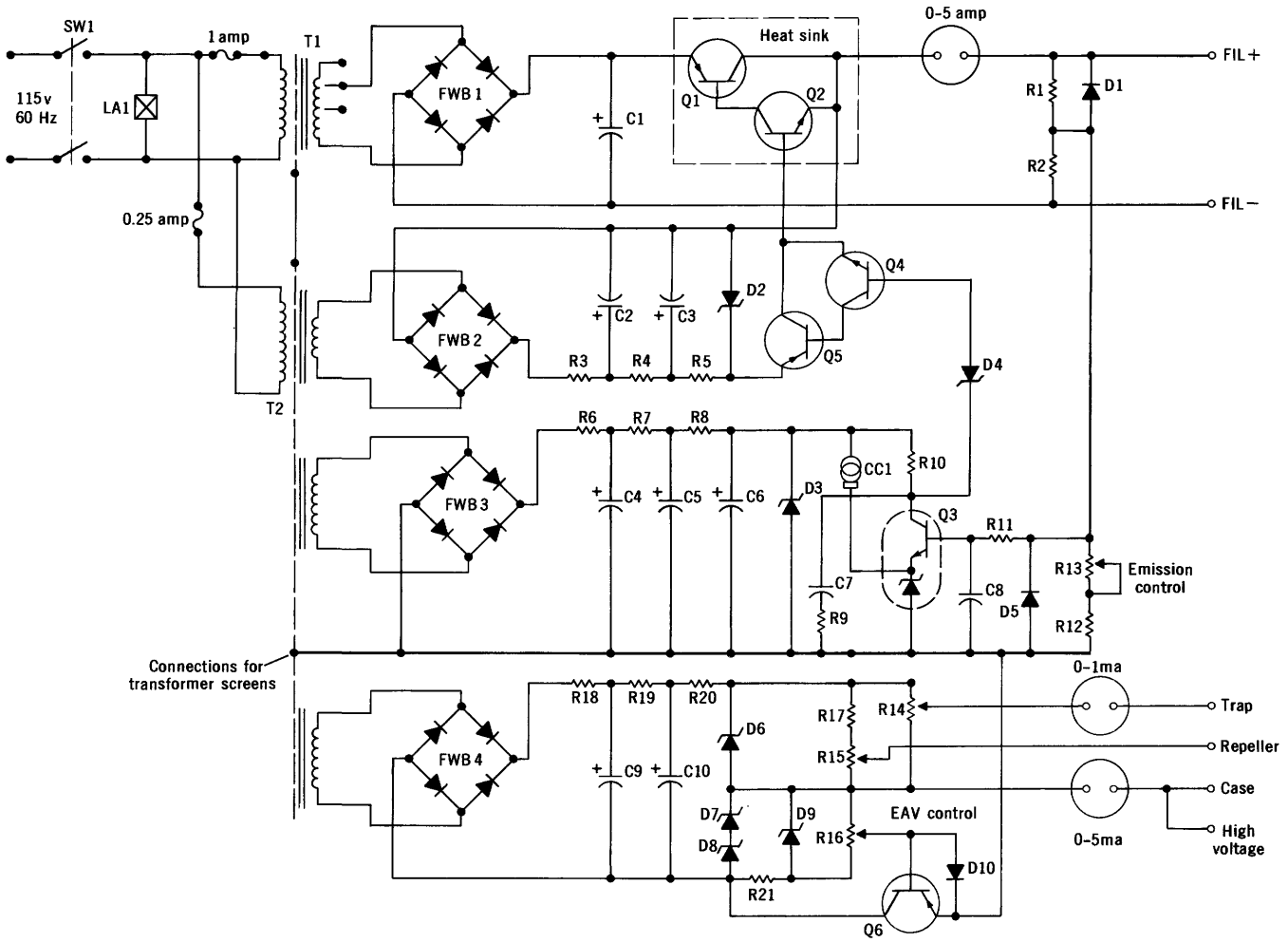

FIGURE 2.—Complete circuit diagram for filament emission regulator. EAV, electron accelerating voltage.

Transistors:

Q1 2N456A	Q3 RA–1 (G.E.)	Q5 2N525
Q2 2N656	Q4 2N336	Q6 2N3743

Constant current device: CCL C1–1300 (Motorola)

Resistors—all values in ohms ±5 percent, 0.25 watt (carbon film type) unless otherwise stated.

R1 100Ω	R8 5.1kΩ	R15 5kΩ, 10-turn
R2 100Ω	R9 510Ω	R16 30kΩ, 10-turn
R3 22Ω	R10 220kΩ	R17 47kΩ
R4 330Ω	R11 1kΩ	R18 22Ω
R5 3.3kΩ	R12 1.33kΩ	R19 330Ω
R6 22Ω	R13 5kΩ, 10-turn	R20 5kΩ (5 w)
R7 330Ω	R14 20kΩ, 10-turn	R21 4.7kΩ

Capacitors—all 50 v dc, unless otherwise stated.

C1 10,000 μf (10 v dc)	C5 30 μf	C8 0.05 μf, disk type
C2 30 μf	C6 8 μf	C9 10 μf (450 v)
C3 30 μf	C7 2 μf	C10 10 μf (450 v)
C4 30 μf		

Diodes:

D1 1N3010	D7 1N3005 (100-v, 10-w Zener)
D2 1N1512	D8 1N3005 (100-v, 10-w Zener)
D3 1N3031	D9 1N3011 (150-v, 10-w Zener)
D4 MPD400 (1.5 v, Zener)	D10 1N3010
D5 1N3010	FWB1 2AFB05AP (I.R.C.)
D6 1N2999 (50-v, 10-w Zener)	FWB2–4 3006A (Erie)

Transformer specifications (continued):

T1: Design No. 1408000, Transformer Electronics Co.
Primary: 806 turns 26 A.W.G. copper wire.
Secondary: 77 turns 16 A.W.G. copper wire, tapped at 46, 54, 61, 69 turns.
Core: Type AA9, Arnold Engineering Co.

T2: Design No. 1407000, Transformer Electronics Co.
Primary: 806 turns 26 A.W.G. copper wire.
Secondaries: a. 188 turns, 41 A.W.G. copper wire.
b. 326 turns, 23 A.W.G. copper wire.
c. 1,790 turns, 34 A.W.G. copper wire.
Core: Type A9, Westinghouse Co.

The primary windings of transformers T1 and T2 are insulated from both the secondary windings and the electrostatic screen for a working voltage of 5,000 v dc.

REFERENCE

Russell, R. D., and Kollar, Frank, 1960, Transistorized power supplies for a mass spectrometer: Canadian Jour. Physics, v. 38, p. 616–623.

CONTOUR FINDER—INEXPENSIVE DEVICE FOR RAPID, OBJECTIVE CONTOURING

By STANLEY P. SCHWEINFURTH, Washington, D.C.

Abstract.—The contour finder is a simple, graphical, inexpensive instrument designed to locate contours objectively and rapidly between any two adjacent map points. It is based on the principle of similar triangles, and it can be used with any map scale and any amount of dip.

The contour finder was designed by the author in 1962 to facilitate preparation of many structure contour maps based upon data from a relatively large number of core holes. The intention was to contour several datums as objectively as possible to determine whether or not structures in the area were formed during deposition of the sediments. The contour finder worked very well for this purpose. It will work equally well for objective contouring based on any kind of relatively closely spaced data, as for example, data from magnetic, gravity, and seismic surveys, and concentrations of elements found in geochemical surveys.

The design of the contour finder (fig. 1) is based on the geometry of similar triangles. Its advantage is that once it is set on two map points, all the contour values between the points can be read directly.

CONSTRUCTION

The author's model of the contour finder, consisting of a coordinate grid and arm (fig.1), was made out of readily available material for a nominal cost. (The device can be mass produced for less than $2.00 each.) Five inches square was determined to be a convenient size for the grid, and a pattern of 10 lines to the inch was found to provide adequate reference lines. The grid was inked on 0.007-inch-thick Cronaflex, and the horizontal lines were numbered from bottom to top for reference. The arm was cut out of 1/16-inch Plexiglas, and a thin reference line, darkened with India ink, was scratched into the bottom side. The top or receiving part of a small snap fastener was centered on the line and cemented to one end of the arm; bottom snaps were cemented onto corners of the grid at each of the two origin points "O". Finally, a narrow slot was cut into the Cronaflex along the bottom of the grid or base line. The grid can be reproduced photographically on Cronaflex or any similar material.

OPERATION

The instrument is operated as follows: Two control stations of unequal value are 2 to 4 inches apart on a map. The values differ at least 30 to 40 units (feet, gammas, percentage points, and so forth). A contour interval of 10 units is selected. To find the points through which selected contours must pass between these stations, place the right or left origin "O" of the contour finder over the point of lowest value and orient the device so that the base line passes through the higher point. Plot the difference between the values of the two stations on the ordinate of the grid above the higher valued station. Snap the arm over the origin used and swing it to intersect the point plotted. The ordinate or vertical scale of the grid is determined by the amount of difference between the stations. A vertical reference scale can be written on the grid and changed as necessary. The slope of the arm on the grid represents the gradient of the surface to be contoured.

To find the location of contours between these two points, enter the difference in value between the low point and the next regular contour line on the ordinate of the grid, using the same scale. Project that value parallel to the abscissa to intersection with the line on the arm, then down the ordinate to the slot at the base of the grid; plot a point on the map through the slot at that place. This point represents the location of the first contour between the control stations. Other contours are found in the same way by increasing successively the amounts entered along the side of the grid by the value of the contour interval.

U.S. GEOL. SURVEY PROF. PAPER 650-B, PAGES B147-B148

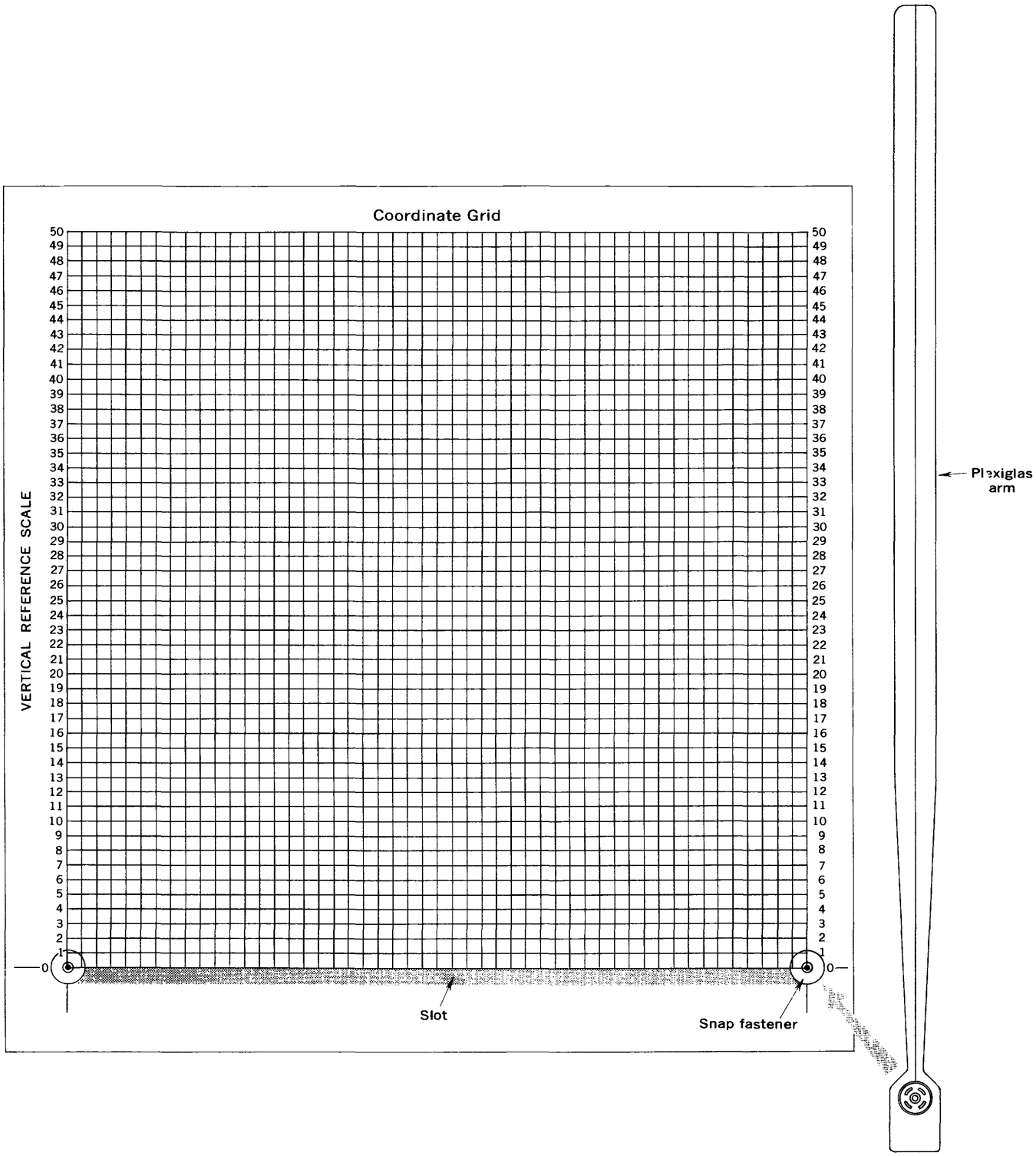

FIGURE 1.—Contour finder described in text.

DEVELOPMENT OF GROUND-WATER SUPPLIES ON THE PAJARITO PLATEAU, LOS ALAMOS COUNTY, NEW MEXICO

By WILLIAM D. PURTYMUN and JAMES B. COOPER,
Santa Fe, N. Mex., Albuquerque, N. Mex.

Work done in cooperation with the U.S. Atomic Energy Commission and the Los Alamos Scientific Laboratory

Abstract.—The Pajarito Mesa well field, completed in 1966 on the Pajarito Plateau, contributed 37 percent of the total water supply to Los Alamos in 1967. Two wells in the field are capable of yields of 1,400 gallons per minute each. This yield is about three times that of any of the other 13 supply wells in the water-supply system. The high yield of the two wells is attributed to the occurrence of coarse volcanic debris and arkosic sediment in the Puye and Tesuque Formations of the Santa Fe Group that make up the main aquifer beneath the Pajarito Plateau.

The town of Los Alamos and laboratories of the U.S. Atomic Energy Commission and the Los Alamos Scientific Laboratory are located on the Pajarito Plateau in north-central New Mexico (fig. 1). Since the community was established in 1943 the demand for water, created by population growth and the expansion of the laboratories, has equaled and at times exceeded the amount of water that had been developed.

The initial water supply was obtained from small streams and springs in the mountains west of the town. These sources soon became inadequate, and in 1949 a ground-water supply was established. Since conversion of the water-supply system to ground-water sources, the U.S. Geological Survey has assisted the U.S. Atomic Energy Commission in the development and management of the ground-water supply.

HYDROGEOLOGIC CONDITIONS OF THE PAJARITO PLATEAU

The Pajarito Plateau forms a topographically high area that slopes gently eastward from the flanks of the Sierra de los Valles toward the Rio Grande (Kelley, 1952, p. 93). The plateau is formed by rocks of the Santa Fe Group of middle (?) Miocene to Pleistocene(?) age, and volcanic rocks of Pliocene and Pleistocene age (Griggs, 1964, fig. 8). Figure 2 is a diagrammatic section showing the geologic units in the Los Alamos area.

The Santa Fe Group comprises the Tesuque and the Puye Formations, and the basaltic rocks of Chino Mesa. These formations crop out along the eastern margin of the Pajarito Plateau. The permeable sediments of the Tesuque Formation are the main aquifer penetrated by the wells in Los Alamos and Guaje Canyons.

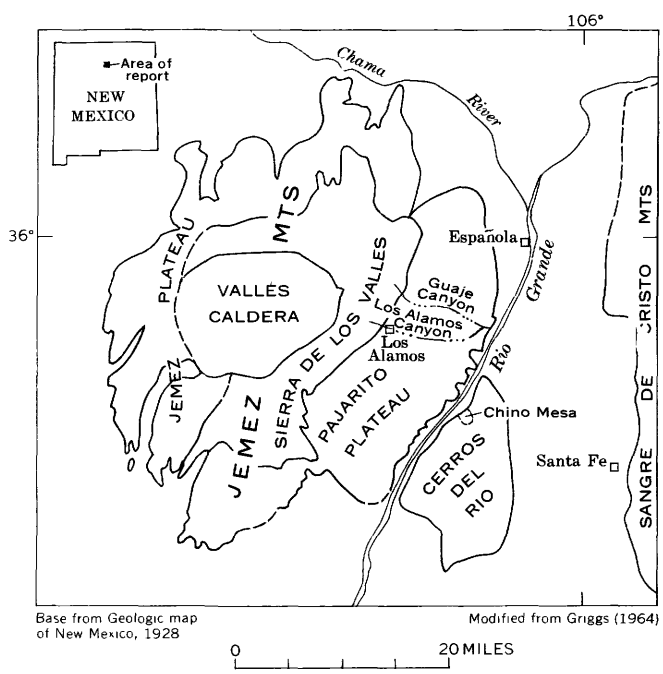

FIGURE 1.—Map of the Los Alamos area, showing topographic features mentioned in the text.

U.S. GEOL. SURVEY PROF. PAPER 650-B, PAGES B149-B153

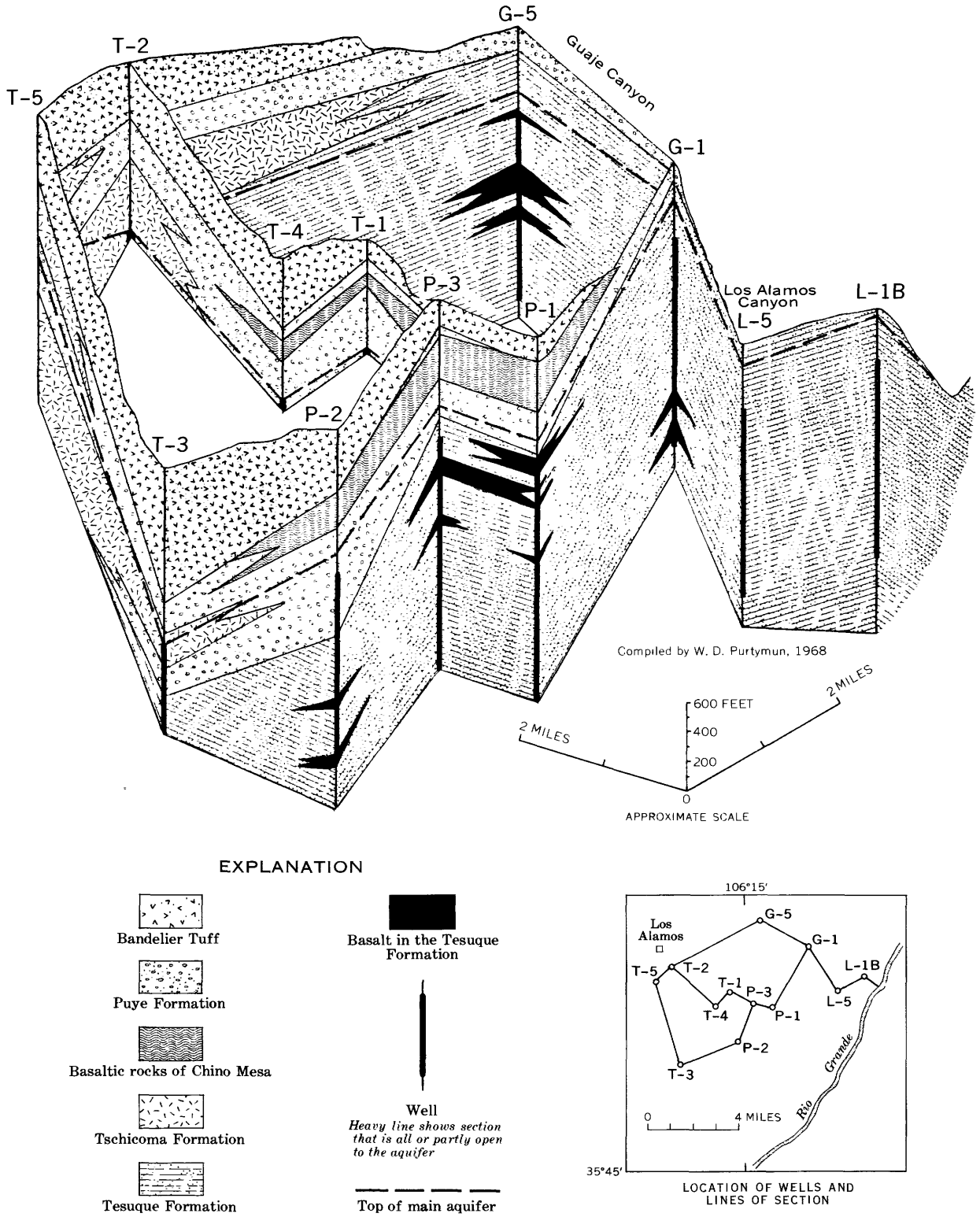

FIGURE 2.—Diagrammatic section of geologic units in the Los Alamos area.

The Tesuque Formation consists of friable to moderately well cemented light-pinkish-gray to light-brown siltstone and sandstone that contains lenses of conglomerate and clay and some interbedded basalt flows. The sedimentary rocks were derived from two sources. The lower part of the formation penetrated by wells in Los Alamos and Guaje Canyons consists principally of fine arkosic quartz sand derived from source areas to the east of the Rio Grande. The upper part consists of very coarse arkosic quartz sand, latitic gravels, and volcanic detritus, derived from sources both east and west of the Rio Grande (Griggs, 1964, p. 22).

The Puye Formation is a poorly consolidated conglomerate channel-fill deposit overlain by a fanglomerate composed of volcanic debris. The channel-fill deposits are gray and consist of fragments of quartzite, schist, gneiss, and granite, ranging in size from sand to boulders. The fanglomerate is generally gray and consists of pebbles and cobbles of rhyolite, latite, quartz-latite, and pumice, in a matrix of silt and sand. Sorting is poor, but tongues and lenses of fairly well sorted pumiceous siltstone and water-laid pumice are present within the fanglomerate. The rocks were derived from flows associated with the volcanic rocks of the Jemez Mountains.

The basaltic rocks of Chino Mesa consist of basalt and basalt breccia that overlie the Puye along the Rio Grande and interfinger with the conglomerate to the west beneath the Pajarito Plateau (fig. 2). The basalt, which thickens southward along the river and thins westward, originated from volcanic vents near Chino Mesa (fig. 1).

The volcanic rocks consist of the Tschicoma Formation of Pliocene age and the Bandelier Tuff of Pleistocene age. The Tschicoma Formation forms the mountains of the Sierra de los Valles, and is present in the subsurface beneath the western edge of the plateau (fig. 2). The deposits are composed of latite, quartz-latite flows, and pyroclastic rocks. The Tschicoma Formation is overlain by the Bandelier Tuff along the flanks of the mountains. The Bandelier Tuff, a series of ash flows and ash falls of rhyolitic tuff, caps the Pajarito Plateau and unconformably overlies the Puye Formation and basaltic rocks of Chino Mesa in the central and eastern parts of the plateau. The Tschicoma Formation, the Bandelier Tuff, and the basaltic rocks of Chino Mesa contain only small amounts of water, which usually is perched above a confining layer.

DEVELOPMENT OF GROUND-WATER SUPPLIES

The first water-supply wells drilled in the Las Alamos area were located along the eastern edge of the Pajarito Plateau in Los Alamos Canyon and Guaje Canyon, which are tributary to the Rio Grande (fig. 1). The wells were located in the canyons rather than in the higher elevations of the Pajarito Plateau in order to keep drilling depths to a minimum and to be as close as possible to the then-known aquifers in the Santa Fe Group. The wells yielded satisfactory quantities of water, 500 gallons per minute or more, and several of them have been in continuous service for 20 years or more. In 1967, six wells located in Los Alamos Canyon and seven wells located in Guaje Canyon supplied 63 percent of the total amount of water (1.3 billion gallons) used by Los Alamos (table 1).

In 1963, because of increasing water demands and lack of additional space for new wells in Los Alamos and Guaje Canyons, new locations were sought on the Pajarito Plateau. Test drilling on the plateau indicated that the main aquifer, entirely within the Tesuque Formation in the lower part of Los Alamos and Guaje Canyons, rises stratigraphically westward, and that beneath the central part of the plateau the lower part of the overlying Puye Formation is saturated and becomes a part of the aquifer.

These data, as well as extensive knowledge of the surface geology, suggested that the saturated portion of the Puye Formation and the sediments in the upper part of the Tesuque Formation would yield considerable quantities of water to a well that penetrated deeply into the zone of saturation. Even though wells on the plateau might need to be as much as a thousand

TABLE 1.—*Pumping rate, total pumpage, and specific capacities of wells in Los Alamos Canyon, Guaje Canyon, and Pajarito Mesa well fields, 1967*

Location	Number of wells	Pumping rate (gpm)			Total pumpage		Specific capacity (gpm per ft of drawdown)		
		Range		Average	Millions of gallons	Percent of total	Range		Average
		From	To				From	To	
Los Alamos Canyon	6	360	565	495	373	28	2	14	6
Guaje Canyon	7	395	560	425	465	35	2	13	6
Pajarito Mesa	[1] 2	635	1,425	1,030	481	37	15	26	20

[1] Does not include well P-3, which was added to the system in January 1968.

feet deeper than wells drilled at lower elevations in the canyons, the economic savings resulting from shorter pipelines and greater choice for well locations, made such drilling feasible.

The first deep well, P–1, of the Pajarito Mesa well field (well-field designation of the U.S. Atomic Energy Commission) was drilled in 1964 to a depth of 2,500 feet on the Pajarito Plateau. It penetrated about 1,800 feet of saturated sediments and volcanic rocks in the Puye and Tesuque Formations. The coefficient of transmissibility at the well and specific capacity of the well are greater than that of wells in the Los Alamos and Guaje Canyons (table 2).

Data from well P–1 enabled further interpretation of the geology and hydrology beneath the plateau, and sites for additional wells were established to the west, at even higher elevations on the plateau. In 1965 a second well (P–2) was completed at a depth of 2,300 feet, and in 1966 a third well (P–3) was completed at a depth of 2,550 feet. These wells were constructed to accommodate pumps capable of producing 1,400 gpm each. The specific capacity of these wells on the plateau is four to six times greater than that of the Los Alamos and Guaje Canyons wells (table 2).

QUALITY OF WATER

The chemical quality of water may vary within a well field owing to local conditions that exist in the aquifer in the vicinity of the well. In general the water from the supply wells is of good quality for domestic use (table 3), as it contains less than 500 parts per million of dissolved solids (U.S. Public Health Service, 1962, p. 33). In the Pajarito Mesa well field the quality and temperature of water from wells P–1 and P–3 are similar, but water from well P–2 is some what different. The major yield to wells P–1 and P–3 is from the coarse sediments of the Tesuque Formation, whereas a large part of the yield to P–2 is from a thick saturated section of Puye Formation. The section of each well that is open to the aquifer, either throughout the indicated section or at intervals within it, is shown on figure 2.

The silica concentration of water from the three wells ranges from 74 to 82 ppm. The silica and calcium-magnesium concentrations, particularly of P–1 and P–3, may require special treatment for some industrial uses inasmuch as these constituents will contribute scale to tubing and pipes when heated.

PRESENT YIELDS AND RECOMMENDATIONS FOR FUTURE SUPPLIES

Pumpage of ground water at Los Alamos in 1967 was 1.3 billion gallons. Two wells on the Pajarito Plateau produced 37 percent of this total (table 1); the heavy pumpage appeared to cause little or no change in water levels in the wells.

Information obtained from the drilling of the three deep wells on the Pajarito Plateau shows that the upper 1,000 feet of the Tesuque Formation is composed of coarse volcanic debris and arkosic sand. These coarse sediments yield larger amounts of water to wells than do the fine sediments that predominate in the formation farther to the east along the Rio Grande.

The Puye Formation attains greatest thickness in a north-trending depositional basin beneath the central part of the plateau (fig. 2). Partial saturation of the permeable conglomerate in the central part of the plateau contributes to the higher yields of the wells.

The main aquifer is at a depth of about 1,200 feet along the western edge of the plateau, and the depth

TABLE 2.—*Aquifer characteristics of selected wells in the Los Alamos area*

Supply well or test well [1]	Date drilled	Depth (feet) [2]	Depth to water (feet)	Pumping rate (gpm)	Specific capacity (gpm per ft of drawdown)	Aquifer [3]	Coefficient of transmissibility (gpd per sq ft)
L–1B	1960	1,750	40	560	5	QTst	17,000
L–5	1948	1,750	170	485	4	do	
G–1	1950	2,000	265	450	5	do	12,000
G–5	1951	1,840	445	555	7	do	12,000
P–1	1964	2,500	740	640	15	QTsp, QTst	55,000
P–2	1965	2,300	835	1,425	26	do	40,000
P–3	1966	2,550	740	1,400	38	do	343,000
T–1	1949	815	750	6	.5	QTsp	7,700
T–2	1950	1,205	1,166	2	.6	QTt	1,000
T–3	1960	1,821	1,173	88	6	QTsp, QTt, QTst	11,000
T–4	1960	1,065	968	16	2	QTsp	2,400
T–5	1949	2,000	970±5			QTsp, QTt	

[1] G, supply well in Guaje Canyon; L, supply well in Los Alamos Canyon; P, supply well on Pajarito Plateau; T, test well.
[2] Completed depth of well.
[3] QTsp, Puye Formation; QTst, Tesuque Formation; QTt, Tschicoma Formation.

TABLE 3.—*Chemical analyses of water from selected wells in Los Alamos Canyon, Guaje Canyon, and Pajarito Mesa well fields*

[Analyses by Group H-7 of the Los Alamos Scientific Laboratory]

Supply well [1]	Date Collected	Temperature (°F)	Chemical constituents (parts per million)												pH	Specific conductivity (micromhos at 25°C)
			Silica [2] (SiO_2)	Calcium (Ca)	Magnesium (Mg)	Sodium (Na)	Carbonate ($CaCO_3$)	Bicarbonate (HCO_3)	Chloride (Cl)	Fluoride (F)	Nitrate (NO_3)	Total dissolved solids	Total hardness (as $CaCO_3$)		
L-1B	5-28-68	87	37	8	1	195	0	262	17	2	0.2	409	24	8.1	600
L-5	6-18-68	78	36	10	0	105	0	134	0	.9	.2	191	26	8.3	232
G-1	5-28-68	80	84	12	.5	38	0	74	3	.4	.3	199	32	8.0	152
G-5	5-25-68	78	60	18	3	23	0	74	3	.4	.4	163	56	7.8	158
P-1	6-18-68	83	82	28	5	36	0	122	5	.3	.1	246	90	7.9	248
P-2	6-18-68	73	81	13	2	21	0	58	0	.3	.3	176	40	7.6	114
P-3	6-18-68	81	74	26	8	33	0	122	7	.3	.1	259	98	7.8	260

[1] G, supply well in Guaje Canyon; L, supply well in Los Alamos Canyon; P, supply well on Pajarito Plateau.
[2] Silica analyses are from samples collected in May 1967. Later samples have not been analyzed for silica.

decreases eastward with the gentle slope of the land surface to a depth of about 600 feet along the eastern edge (fig. 2). The water in the aquifer moves eastward toward the Rio Grande, which is the principal area for ground-water discharge (Cushman, 1965, p. D33).

Locations of future wells should be chosen carefully so as to avoid the relatively impermeable rocks of the Tschicoma Formation and the thick sections of basaltic rocks of Chino Mesa. These rocks are hard and are difficult to drill. Holes drilled in basalt are likely to be crooked because, in drilling, the bit may be deflected by joints or cavities. If rotary methods are used, it may be difficult to maintain fluid circulation in the hole at places where open joints occur. Additional wells capable of yielding from 1,000 to 1,500 gpm of water could be located at various sites near the center of the Pajarito Plateau.

REFERENCES

Cushman, R. L., 1965, An evaluation of aquifer and well characteristics of municipal well fields in Los Alamos and Guaje Canyons, near Los Alamos, New Mexico: U.S. Geol. Survey Water-Supply Paper 1809-D, 50 p.

Griggs, R. L., 1964, Geology and ground-water resources of the Los Alamos area, New Mexico: U.S. Geol. Survey Water-Supply Paper 1753, 107 p.

Kelley, V. C., 1952, Tectonics of the Rio Grande depression of central New Mexico, *in* New Mexico Geol. Soc. Guidebook, 3d Field Conf., The Rio Grande country: p. 93–105.

U.S. Public Health Service, 1962, Public Health Service drinking water standards, revised 1962: Public Health Service pub. 956, 61 p.

OCCURRENCE AND MOVEMENT OF GROUND WATER IN THE BRUNSWICK SHALE AT A SITE NEAR TRENTON, NEW JERSEY

By JOHN VECCHIOLI, LOUIS D. CARSWELL, and HAIG F. KASABACH [1], Trenton, N.J.

Work done in cooperation with the New Jersey Department of Conservation and Economic Development, Division of Water Policy and Supply and Bureau of Geology and Topography

Abstract.—Measurements of yield made during the drilling of 13 wells in the Brunswick Shale of Late Triassic age near Trenton, N.J., indicate that ground water occurs mainly in discrete zones controlled by bedding. Productivity of a well may be dependent on only one or on several zones; however, no relation was apparent between yield and the number of zones penetrated. Movement of water under pumping conditions, and presumably under natural conditions, is preferentially along strike, as indicated by drawdown observations made during several pumping tests. Wells situated along strike and thus tapping common producing zones had a greater drawdown than wells equidistant in transverse directions. Knowledge of a preferential direction of water movement in the Brunswick Shale is invaluable when locating a well with respect to a potential source of pollution or in attempting to minimize well interference.

The literature is replete with detailed accounts of the occurrence and movement of ground water in granular aquifers, but comparatively little has been presented regarding ground water in fractured-rock aquifers. Opportunity was afforded to conduct research into ground-water occurrence and movement in the Brunswick Shale—a principal aquifer throughout a large part of central and northeastern New Jersey—on a 20-acre site located 10 miles north of Trenton, N.J. (fig. 1). The site is on property dedicated for research by the Stony Brook–Millstone Watersheds Association and known as the New Land Research Reserve.

Acknowledgments.—Thanks are due the Stony Brook–Millstone Watersheds Association for allowing use of their land for this research, and in particular to Mr. Richard S. Thorsell, Resource Director of the Association, for coordinating the activities, and to Mr. L. H. Terpening, member of the Association, for personally bearing part of the test-drilling costs. Mr. Joseph W. Miller, Jr., Geologist, New Jersey Bureau of Geology and Topography assisted in interpreting

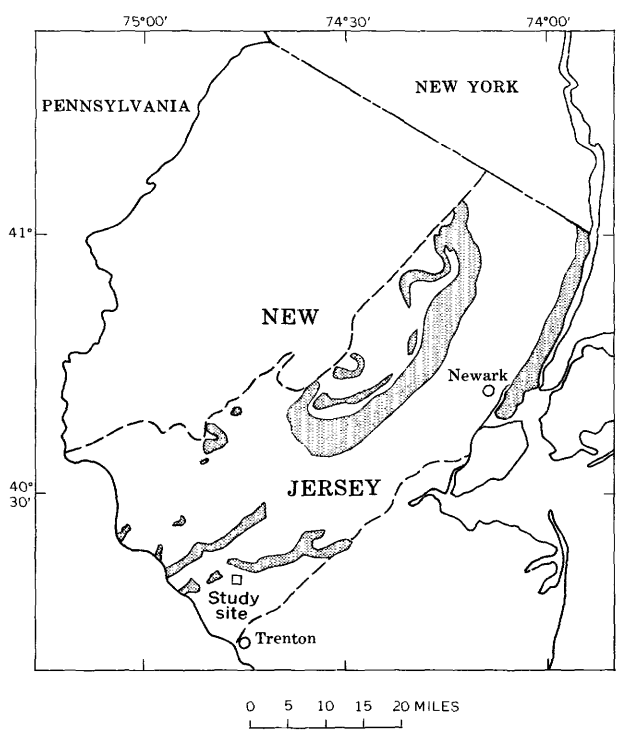

FIGURE 1.—Sketch map of northern New Jersey, showing location of study site and extent of outcrop area of Newark Group (dashed lines). Stippled areas are igneous rocks.

[1] Geologist, New Jersey Department of Conservation and Economic Development, Division of Water Policy and Supply.

U.S. GEOL. SURVEY PROF. PAPER 650-B, PAGES B154-B157

the geology of the site. The Dinunzi Well Drilling Co., Inc., cooperated fully in making special measurements while they were drilling the test wells.

GEOLOGY AND AQUIFER CHARACTERISTICS

The Brunswick Shale is the youngest, thickest, and most extensive unit of the Newark Group of Late Triassic age. The Newark Group crops out across northern New Jersey in a broad northeast-trending belt (fig. 1) that is part of the Triassic structural trough extending from southern New York through New Jersey, into Pennsylvania, and thence southward into Maryland and Virginia. At the site investigated the Brunswick Shale consists of alternating beds of red mudstone, shale, and siltstone. These beds are folded into a northwesterly plunging syncline. The site is characterized by gently rolling topography with more resistant beds forming minor ridges having a maximum relief of about 10 feet. The beds are broken by a dominant near-vertical joint set whose strike approximately parallels the strike of the beds. Secondary near-vertical joints are roughly perpendicular to the primary set, and random joints of minor importance are common. The intersecting fractures that have resulted from the jointing provide the principal means of storage and movement of ground water in the Brunswick.

Earlier work (Vecchioli, 1967) indicated in a general way that under pumping conditions the Brunswick Shale exhibits directional rather than isotropic hydraulic behavior, and that maximum and minimum directions of anisotropy are related to the structural orientation of the formation. For this study, test wells were located so as to provide more detailed information on the aquifer's anisotropy.

LOCATION OF TEST WELLS

The arrangement of the 13 wells in relation to geologic structure is shown in figure 2. Well 1, which was selected to be the pumping well, and 9 of the observation wells were drilled to a depth of about 150 feet on the west limb of the northwesterly plunging syncline where the beds strike east-west and dip an average of about 25° N. Eight of the observation wells were located radially from well 1 at a distance of 300 feet in directions parallel to the strike and dip of the beds and at an angle of 45° to the strike. Well 6 was drilled 100 feet downdip from well 1 and to a depth of 200 feet so as to fully penetrate all the beds present in well 1. Well 10 was drilled 600 feet west of and along strike from well 1 in an attempt to determine the shape of the drawdown cone in the strike direction.

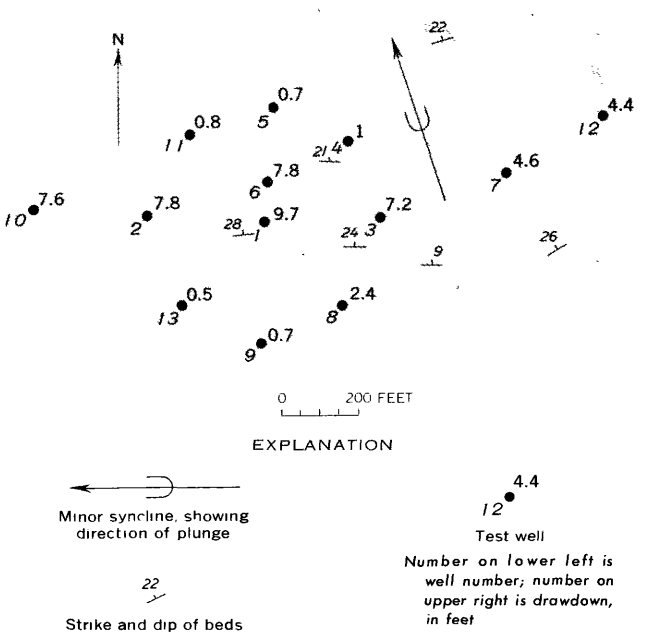

FIGURE 2.—Map showing geologic structure of the New Land Research Reserve site, location of test wells, and drawdown distribution at end of 8-hour pumping test of well 1 at 16 gpm.

Observation wells—7 and 12—were drilled to a depth of 150 feet on the east limb of the syncline where the beds strike east-northeast and dip about 25° N. These wells were drilled at a distance of 675 and 975 feet, respectively, from well 1 as measured along strike and were intended to fully penetrate the same sequence of beds as well 1 and the other wells alined along the strike with well 1. However, upon completion it was determined that these wells do not fully penetrate all the beds and producing zones present in well 1 as a result of a slight thickening of the sequence on the east limb of the syncline as well as the positioning of the wells slightly downdip from their designed locations because of terrain conditions.

DISTRIBUTION OF PRODUCING ZONES

All wells were drilled by the air-rotary method, a drilling method in which compressed air is forced out the end of a rotating bit and up the annular space between the drill column and the wall of the borehole. The "cuttings" and also the ground water entering the borehole are carried to the surface by the circulating air. This drilling method facilitates the identification of water-bearing zones as the well is deepened because the amount of water blown from the borehole can be measured and a log of discharge versus depth can thus be obtained. Discharge measurements were made at 10-foot intervals in all the wells during drilling, once the discharge of water started. In addition, the presence of wet chips or mud was

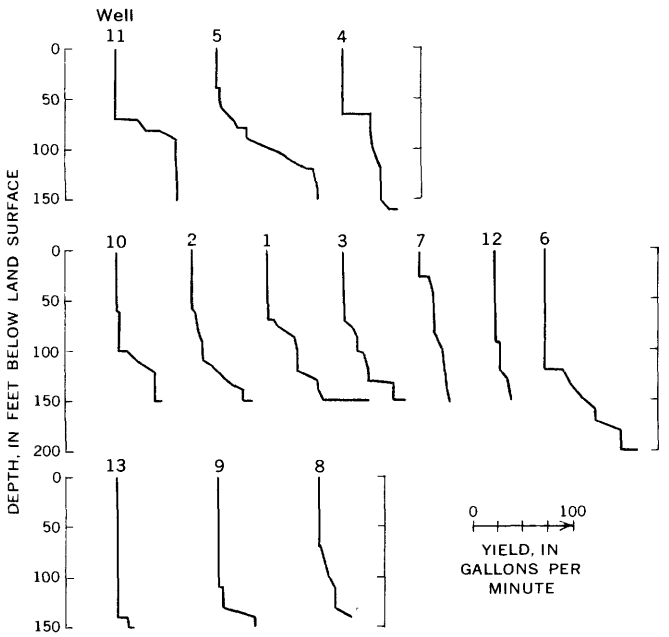

FIGURE 3.—Logs of well discharge at time of drilling.

recorded from zones above those zones that yield measurable quantities of water. Discharge logs are shown in figure 3.

The discharge logs of the wells are arranged in three "strike" groups from north to south across the site. Although the alinement of the wells with strike is not perfect, and minor adjustments for differences in land-surface elevation have not been made, the similarity of the logs within each group is readily apparent. The "stepped" character of the curves is also obvious, and indicates that the water is not evenly distributed throughout the formation, but that it occurs in discrete zones. Important producing zones are reflected on the logs by a sharp shift of the curve toward the right, which indicates that there was a marked increase in the water being discharged at this point in the drilling. The increase in yield of some of the wells at the finished depth reflects final development of the well and not necessarily a new producing horizon. It is not clear why the yield increases gradually with depth in parts of some wells (well 5, for example). It may be that the water-bearing zone in these places is thick and that the water is more evenly distributed throughout the interval, or that the gradually increasing yield may be a result of the more complete development of a discrete zone. The latter interpretation is favored here on the basis of supporting data obtained from borehole-velocity measurements in several wells, and on the fact that major caving started in well 5 just below a depth of 80 feet and that this zone continued to cave throughout the deepening of the hole.

Producing zones are restricted to favorable beds that are areally extensive along strike, as demonstrated by the similarity of the discharge logs and the pumping-test data discussed below. Along dip, however, the dip of the formation carries the water-producing zone to excessive depths within short distances. Figure 4 shows a section through the well field from south to north through wells 9, 1, 6, and 5, with wells 8 and 4 projected into the line of section. Some zones were present in only one borehole, whereas others were present in two or more boreholes alined in the dip direction.

Lithologically, the producing zones are similar to the nonproducing zones insofar as could be revealed by field examination of the drill cuttings. However, these zones appear to be distinctively fractured, as a greater percentage of the drill cuttings from the producing zones had chip faces that were smooth and planar, which suggests better defined jointing. In addition, many of the planar surfaces on these chips showed signs of having been altered by circulating ground water.

Although the productivity of a well may be from one zone or from several zones, no relation was apparent between the productivity of the wells and the number of zones penetrated by them.

PUMPING TESTS

An 8-hour pumping test at a constant rate of 16 gallons per minute was conducted on well 1, the centrally located well, and water-level declines were measured periodically in all the wells. The resulting time-drawdown curves fall into two general groups, with the exception of those from wells 7, 8, and 12. One group consists of curves from wells on the west limb of the syncline alined along strike with well 1. These

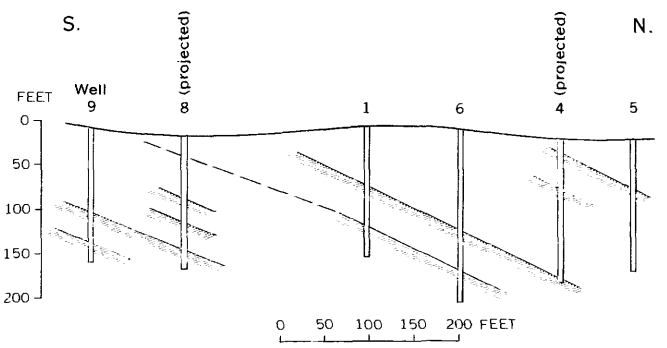

FIGURE 4.—Section showing extent of producing zones in the dip direction as determined from the wells. Producing zones shown by shading.

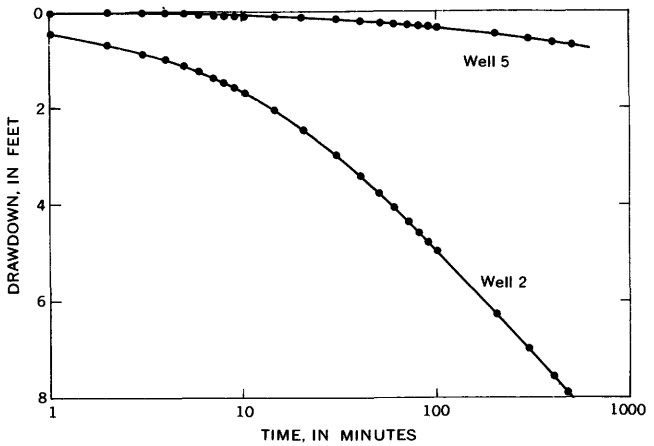

FIGURE 5.—Drawdown curves of wells 2 and 5 during pumping of well 1 at 16 gpm.

wells tap two common producing zones. Included in this group is the curve from well 6, which, although being downdip, was drilled deep enough to tap the same producing zones tapped by well 1. The other group includes the curves from wells alined in directions other than along strike. These wells do not tap the producing zones tapped in well 1. The drawdown trends of each group are shown in figure 5, where the curve for well 2 is typical of wells belonging to the first group, which tap the two major producing zones of well 1, whereas the curve for well 5 typifies those of the other group.

Figure 2 shows the drawdown distribution at the end of the 8-hour test. The drawdown in the wells alined parallel to strike is many times greater than in the wells alined in other directions—as much as 10 times more for those wells lying within 300 feet of well 1. The anomalous drawdown of 2.4 feet in well 8 probably results from its having penetrated the lower producing zone of well 1 (fig. 4). Although there was no measurable yield from this zone during the drilling of well 8, mud wadding on the bit when drilling through this interval suggests that the zone contains at least small amounts of water. The drawdown in wells 7 and 12 is somewhat less than that in the other wells of the strike group as a result of these wells having penetrated only the upper of the two major producing zones of well 1.

Shorter pumping tests of 2- to 3-hour duration have been run on most of the other wells. In these tests, the lowering of water levels in surrounding wells has been greatest in the direction of strike and much less in other directions, substantiating the hypothesis that the wells penetrate common producing zones that are laterally extensive along strike.

DISCUSSION

In general the literature contains a paucity of detailed pumping-test data for the Brunswick Shale. However, numerous pumping tests of wells throughout the outcrop area of the Brunswick Shale in New Jersey where drawdown observations have been made in more than one direction indicate that the aquifer has anisotropic hydraulic properties everywhere. The degree of anisotropy varies from place to place. In some areas it is considerably less than that shown here; in fact, it may even approach isotropy. Where mildly anisotropic conditions exist, one could conclude that discrete producing zones do not occur, but that the formation is thoroughly dissected by interconnecting fractures resulting in hydraulic continuity in all directions. Nonetheless, drawdown is always greatest along strike.

Practical implications of the hydraulic behavior of the Brunswick aquifer are as follows: If the water is able to move more freely in the direction of strike than in other directions, then the facility for the spread of a contaminant would be greatest along strike. Such a condition has been observed in Newark, N.J., where elongated tongues of salt water have encroached in directions parallel to strike (Herpers and Barksdale, 1951, p. 43). In addition, it is evident that well interference can be minimized by alining wells in directions other than parallel to strike. Moreover, knowledge of the anisotropic hydraulic behavior could also have application in planning housing developments that have private wells and waste disposal, so as to minimize the possibility of contaminating the ground-water supply to individual houses.

REFERENCES

Herpers, Henry, and Barksdale, H. C., 1951, Preliminary report on the geology and ground-water supply of the Newark, New Jersey, area: New Jersey Dept. Conserv. and Econ. Devel., Div. of Water Policy and Supply Spec. Rept. 10, 52 p.

Vecchioli, John, 1967, Directional hydraulic behavior of a fractured-shale aquifer in New Jersey, *in* International symposium on hydrology of fractured rocks, Yugoslavia 1965, Proc., v. 1: Internat. Assoc. Sci. Hydrology Pub. 73, p. 318–326.

CORRELATION OF CARBONATE ROCK UNITS IN NORTHWEST OHIO BY NATURAL GAMMA LOGGING

By STANLEY E. NORRIS and RICHARD E. FIDLER, Columbus, Ohio

Work done in cooperation with the Ohio Department of Natural Resources, Division of Water

Abstract.—Natural gamma logs are a basis for determining the contact between the principal carbonate rock units in northwest Ohio, those of the Niagara and Cayuga Groups. Logs of the upper part of the Niagara Group, a dolomite of high purity, show a relatively low intensity of radiation and are almost featureless, in marked contrast to logs of the slightly less pure dolomite of the overlying Cayuga rocks. A characteristic change in radioactivity at or near the contact is identifiable on most logs in the study area. Data from 26 wells, supplemented by that obtained from quarry exposures, have been used to construct a structure contour map which conforms closely to the known regional structure. This map will be a significant aid in the interpretation of the hydrogeologic system in northwest Ohio.

The Division of Water, Ohio Department of Natural Resources, has begun a program of ground-water exploration in northwest Ohio, in an area of approximately 9,000 square miles, which calls for drilling and testing about 90 wells in the carbonate rock aquifers. The U.S. Geological Survey is making geophysical logs of the test wells and of existing wells to establish criteria for stratigraphic correlation and identification of permeable zones. The logging is being done with portable, hand-operated equipment furnished by the Geological Survey Water Resources Division equipment unit at Denver. The equipment makes natural gamma, single-point resistance, self-potential, and temperature logs. So far in the study, with 6 test wells and about 20 existing wells having been logged, it is evident that natural gamma logs furnish a basis for determining the contact between the principal carbonate rock units in northwest Ohio, those of the Niagara and Cayuga Groups of Middle Silurian and Late Silurian age, respectively. Moreover, in areas of several tens of square miles, the natural gamma log furnishes for the entire carbonate rock section a characteristic "signature" which in many instances can be used with confidence to correlate the beds in relatively shallow wells and predict the depth of the contact.

PHYSICAL SETTING

The terrane in most of northwest Ohio is without appreciable relief, formed of lake sediments or glacial till overlying the limestone bedrock. In places, recessional moraines of the Wisconsin age glaciers occur as belts of slightly higher hummocky ground, typically 3 to 5 miles wide, extending in an east-west direction for many miles. These glacial moraines, composed chiefly of till, rise no more than 25 to 40 feet above the relatively flat terrane of the intermoraine areas. The till of the ground moraine in most places is no thicker than 30 to 40 feet. Bedrock of the Niagara and Cayuga Groups is exposed in quarries and the beds of shallow streams.

The Niagara Group in northwest Ohio is principally a dolomite of high purity. The rocks range in color from white, or very light gray, to dark bluish gray; generally they are thickly bedded to massive, and very porous, vuggy, and coarsely crystalline. Reefs are common in the upper part of the group. This upper unit, the Lockport Dolomite (Guelph Dolomite of local usage), is exposed at Carey in the quarry of the National Lime and Stone Co., where the reefs are revealed as massive structures 50 to 200 feet wide and at least 80 feet thick. The reefs have no discernible bedding; the beds on their flanks arch gently upward and grade imperceptibly into the reef masses. Rocks of the overlying Cayuga Group are more thinly and evenly bedded than those of the Niagara Group, and

U.S. GEOL. SURVEY PROF. PAPER 650-B, PAGES B158-B161

generally are darker than the latter, varying from brown to dark blue or almost black. Water occurs in joints, along bedding planes, and in other openings in these carbonate rock units which, together, constitute the principal aquifers in much of northwest Ohio.

In chemical composition, rocks of both groups are typical dolomites. Nine samples from the upper part of the Niagara Group, collected from quarries in four counties in northwest Ohio, ranged from 99.2 to 99.9 percent and averaged 99.5 percent dolomite. Nine samples from the lower part of the Cayuga Group, from the same quarries, ranged from 91.7 to 99.6 percent and averaged 97.1 percent dolomite (Stout, 1941, p. 271–390).

The Niagara rocks are exposed at the surface along the crest of the north-plunging Cincinnati arch, the main structural feature of northwest Ohio, and dip away from the crest at low angles to the east, north, and west beneath the Cayuga Group. Rocks of both groups thicken downdip; on the northeast side of the arch the Niagara rocks range in thickness from approximately 200 feet at Findlay, near the crest of the arch, to 350 feet at Fremont. They thicken similarly on the northwest side of the arch to approximately 350 feet at the Indiana line in Paulding County (Cohee, 1948, fig. 9). Rocks of the Cayuga Group pinch out at most points along the crest of the arch and thicken to about 600 feet near Fremont.

CHARACTERISTICS OF THE GAMMA LOGS

The most obvious characteristic of gamma logs of wells which penetrate both the Niagara and Cayuga sections is that the intensity of radiation decreases abruptly in the upper part of the Niagara rocks, and the logs become almost featureless, in marked contrast to logs of the overlying Cayuga rocks. The difference in log segments is illustrated in figure 1, which shows gamma logs made in wells at (*A*) Van Wert, (*B*) Delphos, (*C*) Vaughnsville, (*D*) Bluffton, and (*E*) Dunkirk.

The depths shown by arrows on these logs indicate the approximate contact between the Niagara and Cayuga Groups. This characteristic change in radioactivity is manifestly near the contact, but it probably does not indicate the exact position of the contact in all the logs. This is inferred from the character of the contact, which is not everywhere similar in northwest Ohio. In places the contact is disconformable, and the difference between the typically light gray, relatively thick beds of the Niagara Group and those of the overlying, thinner bedded and darker colored Cayuga Group is readily apparent on the outcrop. Locally,

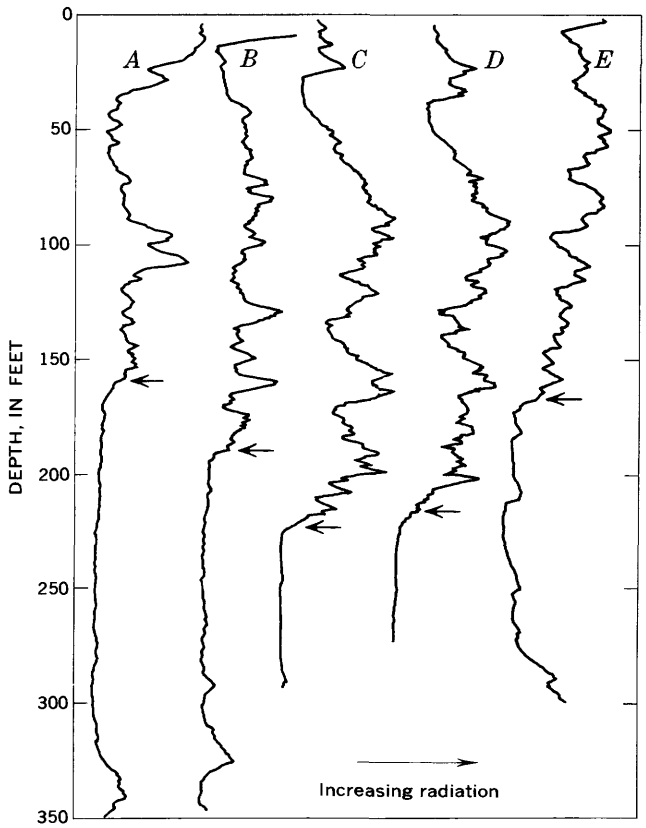

FIGURE 1.—Natural gamma logs of wells at five locations in northwest Ohio, showing contrast in radiation intensity between rocks of the Cayuga Group (top part) and those of the Niagara Group (bottom part). Arrows indicate the approximate depth of the contact. Location of wells: *A*, Van Wert; *B*, Delphos; *C*, Vaughnsville; *D*, Bluffton; and *E*, Dunkirk.

green shale and a thin layer of bituminous matter occur at the disconformity (Stout, 1941, p. 349–350). Commonly the green shale ranges in thickness from a fraction of an inch to about a foot; thicknesses of several feet have been reported as pockets filling erosional depressions. Elsewhere the contact is conformable and gradational, and typically is recognized on the outcrop by a change in color—usually taking place over several feet—from gray to light blue gray, which predominates in the Niagara Group, to brown or yellowish brown in the Cayuga Group.

In an effort to determine more precisely the position of the contact on the gamma logs, logs were made in shotholes at three quarries, where the holes were located close enough to the quarry walls so that the depth of the contact could be measured and accurately related to the logs. In two of these quarries the contact was disconformable; in the other it was conformable and gradational.

In one test the position of the contact as measured on the quarry wall coincided exactly with the characteristic change on the log identified as the contact in

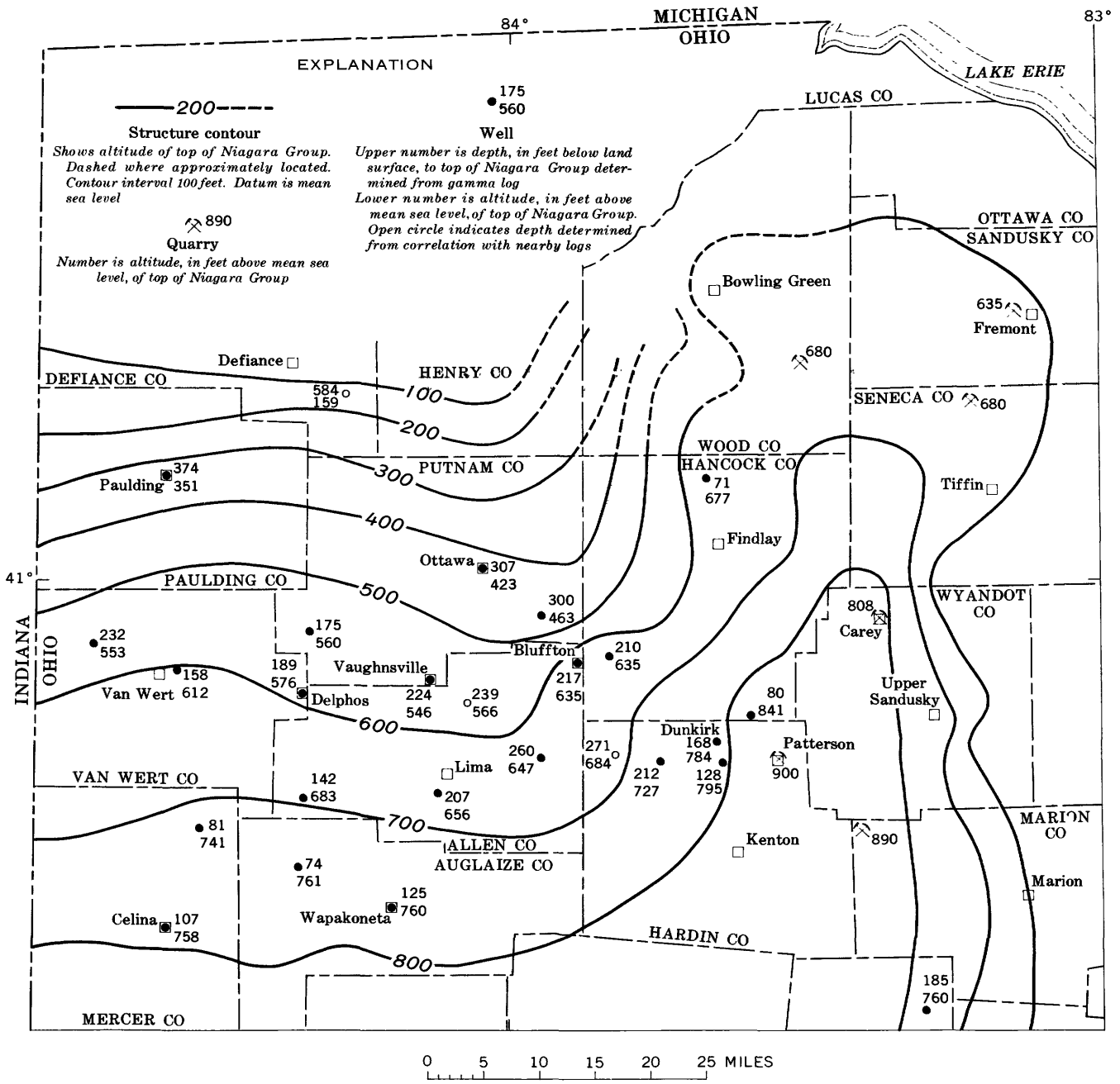

FIGURE 3.—Map of northwest Ohio, showing structure contours on top of Niagara Group. Based on data from gamma logs and quarries.

the examples shown here (fig. 1). This test was at Carey, in the quarry of the National Lime and Stone Co., where the contact is disconformable. The log was made in a 6-inch-diameter shothole that penetrated 13 feet each of the Cayuga and Niagara rocks (fig. 2).

Results of tests at the other two quarries indicate that locally the characteristic change in intensity on the log may occur a few feet above the actual contact. At the Herzog Lime and Stone Co. quarry near Patterson, where the contact is represented by a gradational zone 4 feet in thickness, the characteristic change on the log was 2 feet above the top of the gradational zone. At the Gottron Bros. quarry at Fremont, where the contact is disconformable, the change was 12 feet above the contact. The latter log did not appear typical, however, and the result is not considered conclusive. For practical purposes the change in radioactivity as here designated on the gamma logs can reasonably be taken to represent the contact between the Niagara and Cayuga Groups for correlation and regional studies.

APPLICATION OF RESULTS

The best evidence of the validity of the gamma-log interpretation is seen in the consistency of results when the data are used in mapping the regional structure. The map, figure 3, showing structure contours on the top of the Niagara Group in northwest Ohio, is based on data from the gamma logs and exposures of the contact between the Niagara and Cayuga Groups in quarries. Several of the control points used on the map were estimated from logs of wells too shallow to penetrate to the contact, by correlating those logs with the logs of nearby wells that did reach the contact. These estimated control points fit the regional structure pattern and contribute additional detail to the map. Because of the large number of shallow wells that can be logged in the study area, this correlation technique promises to add significantly to the data potentially available. Additional evidence that the contour map accurately depicts the regional structure in northwest Ohio lies in the fact that it conforms closely to a map prepared by Stout and others (1935, p. 899). Their map shows structure contours on the deep-seated rocks (Trenton Limestone), and was based on data from oil and gas wells.

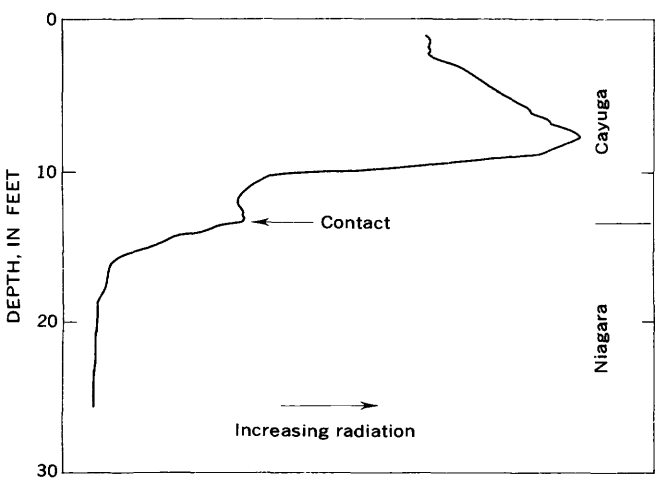

FIGURE 2.—Generalized trace of gamma log made in shothole in quarry at Carey, Ohio, showing contact between Niagara and Cayuga Groups.

CONCLUSIONS

A structure contour map of a key aquifer has been made for a large part of northwest Ohio by interpretation of the natural gamma logs. Because of the large number of wells that can be logged, the technique ultimately should provide a more detailed structure map of the carbonate rock aquifers than has heretofore been available. Such a map will be a valuable aid in the interpretation of the hydrogeologic system in northwest Ohio.

REFERENCES

Cohee, G. V., 1948, Thickness and lithology of Upper Ordovician and Lower and Middle Silurian rocks in the Michigan basic: U.S. Geol. Survey Oil and Gas Inv., prelim. chart 33, 2 sheets.

Stout, Wilber, 1941, Dolomites and limestones of western Ohio: Ohio Geol. Survey, 4th ser., Bull. 42, 468 p.

Stout, Wilber, Lamborn, R. E., Ring, D. T., Gillespie, J. S., and Lockett, J. R., 1935, Natural gas in central and eastern Ohio, *in* Geology of natural gas: Am. Assoc. Petroleum Geologists, p. 897–914, 3 figs. maps.

APPLICATION OF POISSON DISTRIBUTION TO FLOOD SERIES

By P. H. CARRIGAN, JR., Washington, D.C.

Work done in cooperation with the U.S. Atomic Energy Commission

Abstract.—The number of flood peaks per unit time (a year) above a selected base may be described by the Poisson distribution. The base magnitude must not be so low as to include carryover storage effects.

The Poisson distribution

$$p(x)=\frac{e^{-\lambda}\lambda^{x}}{x!} \quad x=0, 1, 2, \ldots \qquad (1)$$

in which $p(x)$=probability that x numbers of floods will occur in a unit time, and λ=the average number of floods in a unit time, may be applied to a partial-duration series of floods provided that:

(1) only one event occurs at a given instant and only a finite number of events occurs in any finite interval,
(2) the random variable x (number of floods per unit time) has independent increments, and
(3) the random variable x has stationary moments (Feller, 1957; Shane and Lynn, 1964).

By definition, the partial-duration series of floods satisfies the first condition (Langbein and Iseri, 1960). If the streamflow is free from secular trends, the third condition is satisfied; several investigators find streamflow free from secular trends (Carrigan and Huzzen, 1967; Hidore, 1966; and Yevdjevich, 1963). The second condition is reasonably satisfied if the number of floods per unit of time is not serially correlated.

We wish to show that the Poisson distribution is applicable to modern flood records meeting these conditions so that it can be applied in simulation of flood series and can be used to test randomness of series spanning much longer periods.

SCOPE AND METHODS

This study includes partial-duration series of floods at 22 streamflow stations in the United States (fig. 1). Insofar as practicable the flood records are from sites distributed throughout the country and represent runoff from a wide range of drainage areas (53—36,800 square miles). The floodflows are free of, or not overly affected by, regulation. The period of record ranges from 20 to 90 years.

A computer routine was developed (1) to count the number of floods per year exceeding a selected discharge (base), (2) to check the goodness-of-fit using the Kolmogorov-Smirnov test (Ostle, 1963, p. 471–472), (3) to compute λ in equation 1, and (4) to check the hypothesis that the number of floods per year was not serially correlated. If the goodness-of-fit test failed at the 5-percent level of significance or if serial correlation was found at the 5-percent level of significance, the base was increased and steps 1 to 4 were repeated until both criteria were satisfied. The base was increased in increments of one-tenth of the difference between the maximum flood for the period of record and the original base. The original base discharge was that published in reports of the U.S. Geological Survey (for example, see Green, 1964).

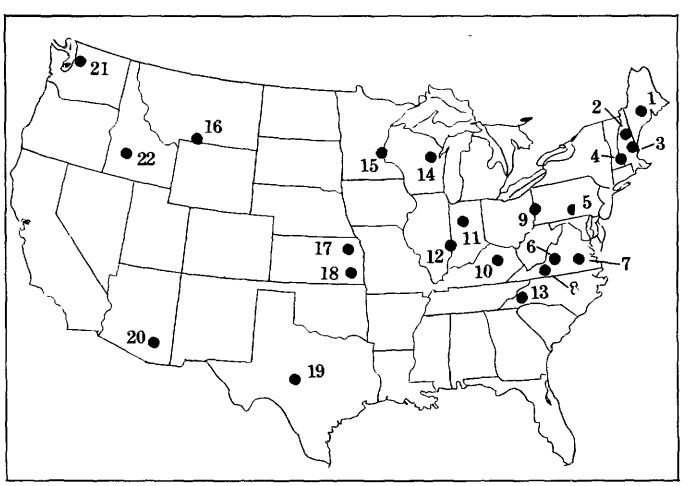

FIGURE 1.—Location of streamflow stations used in this study.

U.S. GEOL. SURVEY PROF. PAPER 650-B, PAGES B162-B163

RESULTS

In table 1 the Poisson parameter for peak discharges above a selected base—the base in cubic feet per second—and the serial-correlation coefficients for mean annual flows and for annual floods, are listed for the flood series included in this study.

TABLE 1.—*Poisson parameters, base discharges, and serial-correlation coefficients for selected flood series*

Station No. (fig. 1)	Station	Poisson parameter (peaks per year)	Base discharge (cfs)[1]	Serial-correlation coefficient	
				Mean annual flow	Annual flood
1	Piscataquis River near Dover-Foxcroft, Me.	2. 91	4, 000	0. 057	−0. 078
2	Pemigewasset River at Plymouth, N.H.	2. 18	12, 600	−. 047	−. 192
3	Souhegan River at Merrimack, N.H.	1. 91	2, 250	. 064	−. 171
4	Middle Branch Westfield River at Goss Heights, Mass.	2. 20	1, 650	−. 042	. 011
5	Susquehanna River at Harrisburg, Pa.	1. 85	290, 400	. 101	−. 111
6	James River at Buchanan, Va.	2. 76	21, 000	. 004	−. 024
7	James River at Cartersville, Va.	2. 68	40, 000	. 246	. 246
8	Roanoke River at Roanoke, Va.	2. 10	4, 000	. 108	−. 077
9	Little Beaver Creek near East Liverpool, Ohio	1. 00	9, 000 (5, 000)	. 344	. 088
10	Kentucky River at lock 10, near Winchester, Ky.	2. 18	40, 000	−. 011	−. 108
11	Wabash River at Lafayette, Ind.	3. 25	30, 000	. 288	. 170
12	Embarrass River at Ste. Marie, Ill.	2. 96	6, 500	. 179	. 196
13	French Broad River at Asheville, N.C.	1. 95	9, 000	. 216	−. 008
14	Oconto River near Gillett, Wis.	. 769	2, 790 (1, 500)	. 455	. 119
15	Mississippi River at St. Paul, Minn.	. 811	35, 400 (13, 000)	. 667	. 395
16	Clarks Fork Yellowstone River at Chance, Mont.	1. 80	5, 400	. 211	. 010
17	Marais des Cygnes River near Ottawa, Kans.	1. 26	7, 790 (3, 600)	. 287	. 053
18	Neosho River near Iola, Kans.	. 630	19, 500 (10, 000)	. 300	−. 020
19	Llano River near Junction, Tex.	2. 92	1, 500	. 207	. 235
20	Rillito Creek near Tucson, Ariz.	3. 44	1, 000	. 289	. 102
21	South Fork Skykomish River near Index, Wash.	3. 94	10, 000	. 261	. 149
22	Boise River near Twin Springs, Idaho	3. 11	3, 700	. 018	. 118

[1] Figures in parentheses are base discharges which were too low; goodness-of-fit test failed and (or) serial correlation was present in flood series for this base discharge.

Only five base discharges required upward adjustment so that the number of peaks per year would be free of serial correlation and would fit the Poisson distribution. The necessity of increasing the base may indicate that floods on some streams are enhanced by carryover storage, either as base flow or as a recession from previous high flows. Serial correlation of mean annual flows may be used as an indicator of the influence of carryover storage on the Poisson parameter. In a contingency test it was found that adjustments in base were significantly related to serial-correlation coefficients for annual flows greater than 0.28, at the 1-percent level of significance.

CONCLUSIONS

The Poisson distribution statistically describes the number of floods per unit time greater than a base, provided the base is of sufficient magnitude. Some rule of thumb for selection of the base, for example, an average of three peaks a year above base, may not ensure this sufficiency in base magnitude because the floods are affected by carryover storage.

If a partial-duration series of flood discharges or flood stages is adequately described by the Poisson distribution, then there is no reason to reject the hypothesis that the number of floods per unit of time occur randomly in time.

REFERENCES

Carrigan, P. H., Jr., and Huzzen, C. S., 1967, Serial correlation of annual floods: International Hydrology Symposium, Sept. 1967, Fort Collins, Colo.

Feller, William, 1957, An introduction to probability theory and its applications, v. 1: New York, John Wiley and Sons, 461 p.

Green, A. R., 1964, Magnitude and frequency of floods in the United States—Pt. 1–A. North Atlantic slope basins, Maine to Connecticut: U.S. Geol. Survey Water-Supply Paper 1671, 260 p.

Hidore, John, 1966, Fifty-year linear trends of runoff on selected watersheds in the United States: Jour. Hydrology, v. 4, p. 98–102.

Langbein, W. B., and Iseri, K. T., 1960, General introduction and hydrologic definitions: U.S. Geol. Survey Water-Supply Paper 1541A, 29 p.

Ostle, Bernard, 1963, Statistics in research: Ames, Iowa, Iowa State Univ. Press, 585 p.

Shane, R. M., and Lynn, W. R., 1964, Mathematical model for flood risk evaluation: Am. Soc. Civil Engineers Proc., v. 90, no. HY6, p. 1–20.

Yevdjevich, V. M., 1963, Climatic fluctuations studied by using annual flows and effective annual precipitations, *in* Climatic change: Arid Zone Research, v. 20, UNESCO, p. 183–199.

REDUCTION OF FLUORESCENCE OF TWO TRACER DYES BY CONTACT WITH A FINE SEDIMENT

By C. H. SCOTT, V. W. NORMAN, and F. K. FIELDS,
Albuquerque, N. Mex., Anchorage, Alaska, San Juan, Puerto Rico

Abstract.—Loss of dyes such as Rhodamine WT, Pontacyl Pink B, and Rhodamine B on clays and silts during discharge measurements in streams of the arid Southwest is a potential problem. A study of loss of fluorescence of Rhodamine WT and Pontacyl Pink B on fine sediment from the Rio Puerco near Bernardo, New Mexico showed that the loss was independent of the concentration of dye but was dependent on the concentration of sediment. Also, all the loss took place in less than 30 minutes. The loss of fluorescence may be related to characteristics of the sediment such as mineralogical composition, surface area per unit weight of material, and perhaps others.

The dilution method of measuring discharge has been known, but not widely used, for many years. With the development of relatively stable fluorescent dyes and instruments with which the dyes can be detected, the dilution method has become more practical to use. Dyes such as Rhodamine WT, Pontacyl Pink B, and Rhodamine B are relatively stable, and the first two are considered especially suitable for use in determining discharge by the dilution method. However, loss of these dyes on sediment and organic material in the bed and banks of the channel and in suspension in the flow may occur. Streams of the arid Southwest can have extremely high concentrations (in excess of 15 percent by weight) of sediment in the silt and clay size ranges (Beverage and Culbertson, 1964), and losses of dye on materials in these size ranges is a potential problem.

The purpose of this paper is to examine briefly the results of two experiments on losses of dye on sediments and to report the results of a study of losses of dye on a fine sediment. The study was made to determine the reduction of fluorescence of two kinds of dye by contact with fine sediment and to determine how the reduction was distributed in time.

OTHER INVESTIGATIONS

Feuerstein and Selleck (1963) used sediment from San Francisco Bay to determine the adsorption of Pontacyl Pink B, Rhodamine B, and fluorescein dyes. The sediment was 48 percent by weight in the clay size range and 42 percent by weight in the silt size range. Differential thermal and X-ray diffraction analyses on samples of similar material indicated abundances of illite, montmorillonite, kaolinite, and small amounts of quartz and chlorite. A constant concentration of 500 milligrams per liter of sediment and various concentrations of dye were used in the experiments.

Feuerstein and Selleck (1963) reported that Rhodamine B is adsorbed on the sediment, but that Pontacyl Pink B and fluorescein are not. They also reported that the amount of Rhodamine B the sediment adsorbed is a function of the concentration of sediment but is independent of the equilibrium concentration of the tracer. Also, the adsorption of the dye is a function of the concentration of salt in solution. The time required for adsorptive equilibrium to be obtained is not given, but it was stated that 1 hour is considered sufficient to obtain equilibrium.

James P. C. Watt (written commun., 1965) investigated loss of fluorescence caused by adsorption of Rhodamine B, Rhodamine WT, and Pontacyl Pink B dyes on a fine grade of filter sand, sand and silt from a mountain stream, and on rock fragments ⅛–½ inch in diameter. No size distribution or mineralogical analyses of the filter sand or sand and silt were given.

Ten grams of the filter sand or 20 grams of the sand and silt were introduced into 100-milliliter dye solutions, each containing 10, 100, and 1,000 parts per billion (J. P. C. Watt, written commun., 1965) of a single dye. The loss of fluorescence was expressed as

U.S. GEOL. SURVEY PROF. PAPER 650-B, PAGES B164-B168

a percentage of the initial fluorescence. The data indicated that the losses are time dependent; the loss of fluorescence after 116 hours is greater than the loss at 72 hours for all three dyes with the filter sand. Time dependency of loss was also shown for the sand and silt, but the experiment was ended after 18½ hours. In general, the loss of fluorescence is dependent on the concentration of the dye solution. The percentage loss of fluorescence after a given length of time decreased with increasing concentration. In general, the loss of fluorescence for a given initial concentration of tracer and after a given length of time is least for Pontacyl Pink B and greatest for Rhodamine B.

EXPERIMENTAL PROCEDURE

For this set of experiments Rhodamine WT and Pontacyl Pink B dyes were used. The Rhodamine WT dye, available in liquid form, has been used in discharge measurements but has not been previously used in experiments to determine the adsorption of the dye on fine sediments. The Pontacyl Pink B dye is available in powder form and is, in general, more difficult to handle than the dyes in liquid form. However, the Pontacyl Pink B dye was selected because the previous experiments had shown that the Pontacyl Pink B is, in general, less affected in the presence of sediments than are other dyes. The fine sediment used in these experiments is naturally occurring and was obtained from the Rio Puerco near Bernardo, N. Mex. The water-sediment mixture from the Rio Puerco contained a high concentration of sediment and was diluted with distilled water to a concentration of approximately 173,000 mg/l to facilitate treatment in the laboratory. The diluted mixture was allowed to settle for a few minutes to enable the removal of any sand by decanting. A sample of the decanted suspension was taken for a determination of concentration and for size analysis by the pipet method. The results of the size analysis are given in table 1.

TABLE 1.—*Size analysis, by pipet method, of fine material from the Rio Puerco, N. Mex.*

Sediment size (millimeters)	*Percent finer, by weight, than size indicated*
0.0625	99. 9
0.016	99. 5
0.004	85. 6
0.002	72. 5

No mineralogical analysis of the fine sediment was made, but Nordin (1963, table 7) reported that an analysis of material finer than 0.004 mm from the Rio Puerco showed a composition of 40–50 percent montmorillonite, 25–30 percent kaolinite, 10–15 percent illite, and the remainder made up of quartz, calcite, and amorphous material.

The initial water-sediment mixture, containing a concentration of 173,000 mg/l, was used to make 5 sets of stock mixtures having concentrations ranging from 650 mg/l to 23,000 mg/l. Dilutions of the initial mixture were made from Rio Grande water. Each of the 5 stock mixtures was then split into 6 parts, resulting in 5 sets of 6 bottles each. Two bottles of the initial mixture of 173,000 mg/l were used as a sixth set. Dye was added to 5 of the 6 bottles of each set of the stock mixtures in such quantities that the concentration of dye was increased incrementally in any single set containing the same sediment content. The sixth bottle in each set was retained as a control to determine apparent fluorescence caused solely by sediment in suspension. Controls containing dye but no sediment were made from Rio Grande water and from distilled water. The relationship of the different sets of stock mixtures and dye concentrations is shown schematically in figure 1 where "N" and "W" indicate Rio Grande and dis-

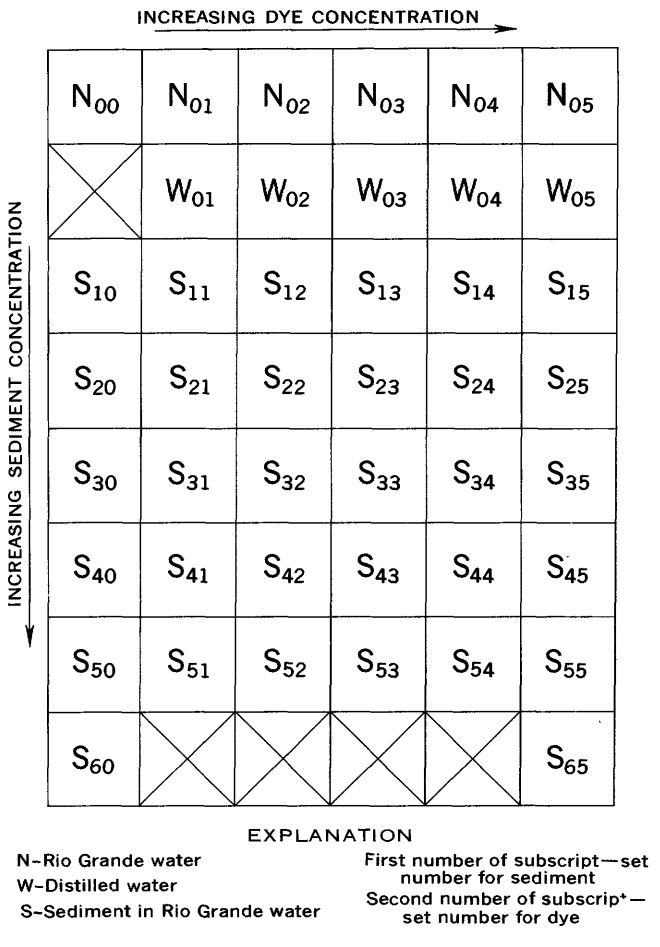

FIGURE 1.—Arrangement of sets of samples used in the fine-sediment–dye study.

tilled water, respectively, and "S" indicates sediment in Rio Grande water. The first digit of the subscript is the set number for the sediment—the larger this number, the higher the concentration of sediment. The second digit of the subscript indicates the same for the concentration of dye.

After the addition of the dye, the bottles were agitated for about 1 minute. Approximately 10 ml of the water-sediment-dye mixture was then withdrawn and centrifuged for 10 minutes to remove most of the sediment. Some sediment remained that could not be immediately removed by centrifuging. The samples of sediment with no dye were also centrifuged and were used to establish apparent background levels of fluorescence caused by fine sediment remaining in suspension. After temperature stabilization in a water bath at room temperature, the samples were analyzed by means of a Turner model 111 fluorometer. The fluorometer was calibrated with solutions of known concentration of dye prepared with distilled water.

The whole process, from introduction of dye to the first fluorometric analysis, required about 30 minutes. Centrifuging and fluorometric analyses were repeated after 4, 24, and 48 hours for the Rhodamine WT dye. The sediment apparently had flocculated, and centrifuging removed practically all the sediment from suspension for these analyses. At 72 hours after introduction of the Rhodamine WT, the bottles were again agitated and samples were centrifuged and analyzed on the fluorometer. Fluorometric analysis was repeated at 176 hours. For the Pontacyl Pink B, fluorometric analyses were made at 30 minutes and at 66 hours after introduction of the dye into the water-sediment mixture.

ANALYSIS OF DATA

The concentrations of dye determined by fluorometric analyses were plotted as a function of concentration of sediment as shown in figure 2. Time is shown as the third variable. Figure 2 shows that the concentrations of dye vary from about 10 to 12 percent with time, with the exception of the lowest concentration of approximately 1.5 μg/1 of dye. For this low concentration the scatter is somewhat greater. However, it should be noted that most of the scatter results

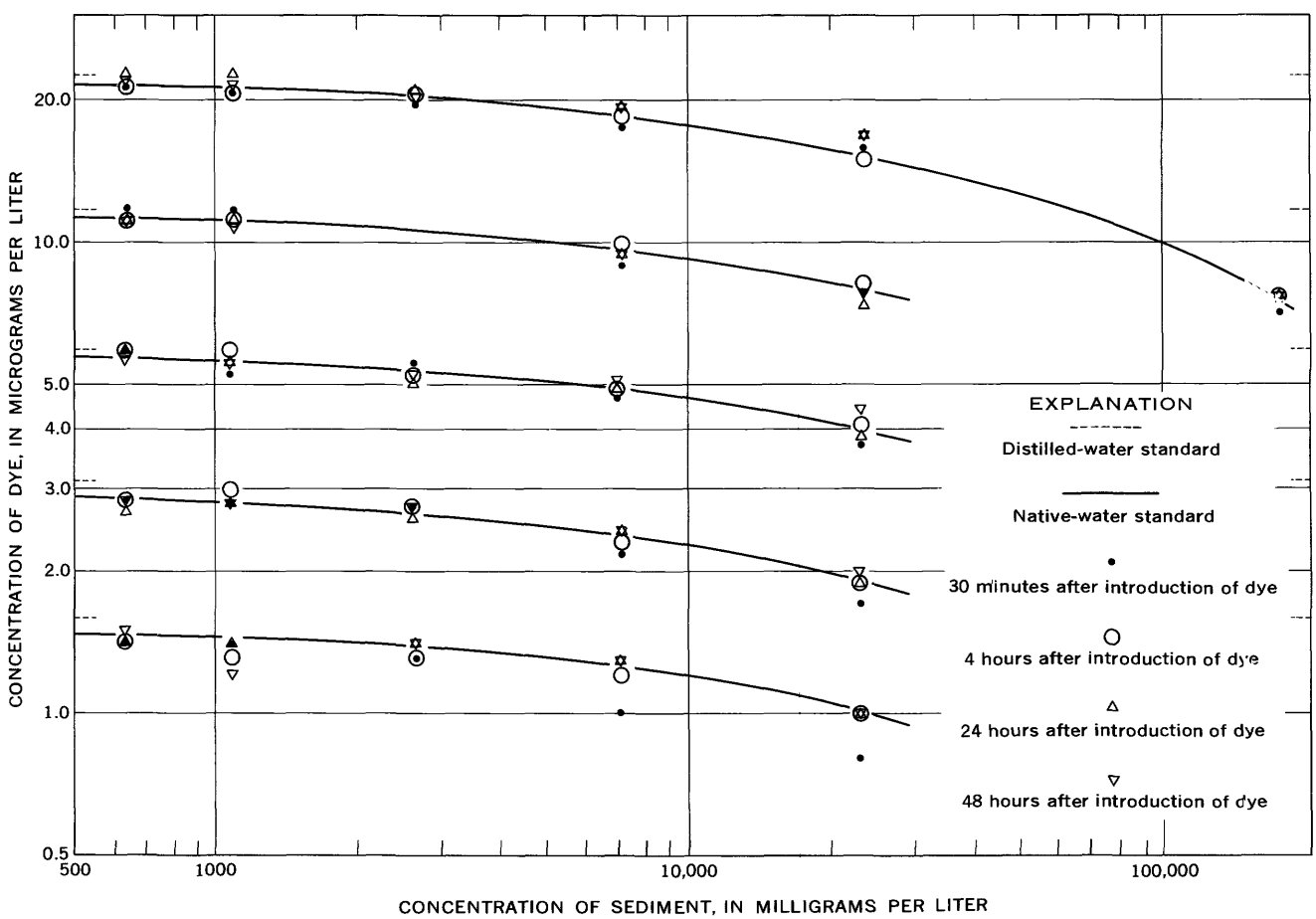

FIGURE 2.—Concentration of Rhodamine WT as a function of concentration of sediment.

from analyses of samples obtained approximately 30 minutes after the introduction of the dye. The concentrations of these samples generally are somewhat lower than the average as a result of quenching of the fluorescence in the presence of the fine sediment left in suspension after centrifuging. The quenching is caused by the scattering of light from the sediment particles, and evidently no way of correcting for this apparent loss exists. This effect is not noticeable for the higher concentrations, particularly concentrations higher than 5 μg/l of dye. It should also be noted that the concentrations of dye for the control standards of Rio Grande water are lower than the concentrations for control standards of distilled water, probably because of chemical quenching of the dye in the presence of the Rio Grande water. The concentration of dye from the control standard made up from Rio Grande water was used as the reference point from which the curves were drawn. For concentrations of sediment less than about 500 mg/l there appeared to be no noticeable reduction in fluorescence caused by losses on the fine sediment for either the Rhodamine WT or the Pontacyl Pink B dyes. No trend with time for the loss of fluorescence is apparent. All the loss of fluorescence occurred in less than 30 minutes, the shortest time after introduction of dye in which a measurement could be obtained. Even though apparent time dependence of loss of fluorescence is lacking in this experiment, the loss of fluorescence might show an apparent time dependence in a field stream because the dye could continuously contact uncontaminated sediment. This problem is, however, beyond the scope of this report. Figure 2 also shows that the percentage reduction in concentration of dye is a function of the concentration of sediment, but is not a function of the concentration of dye.

The curves of figure 2 were used to construct the curves shown in figure 3 in which the percentage reduction in fluorescence is shown as a function of the concentration of the fine sediment. Figure 3 shows that the Rhodamine WT is less subject to loss than the Pontacyl Pink B on the particular fine sediment used in this set of experiments. The loss of fluorescence of Pontacyl Pink B increases more rapidly with increase in concentration of fine sediment than the loss of fluorescence for the Rhodamine WT.

Rhodamine WT was not used by Feuerstein and Selleck (1963) in the study of the effects of fine sediment on dye, but the study by James P. C. Watt (written commun., 1965) with coarse material shows that the curves of figure 3 could not be used to determine loss of fluorescence in the presence of coarse sediment. The length of time in which the loss of fluorescence occurs and the dependence of the loss on the concentration of dye may be related to physical characteristics of the sediment such as mineralogical composition, surface area per unit weight of material, and perhaps others. All these factors may apply to fine as well as coarse sediment.

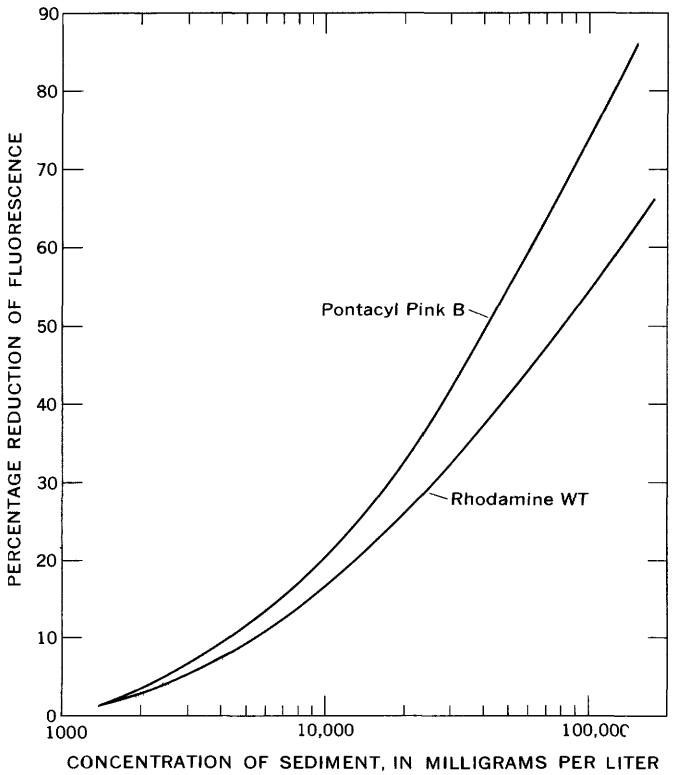

FIGURE 3.—Percentage reduction of fluorescence as a function of concentration of sediment.

CONCLUSIONS

The results of this and previous studies lead to the following conclusions:

1. In the presence of material finer than sands, the loss of fluorescence takes place in a short time and, practically speaking, time is not a factor. However, for material of sand size and coarser, the loss of fluorescence can take place over a relatively long period of time.

2. The loss of fluorescence in the presence of fine material is independent of the concentration of dye, but is dependent on the concentration of sediment. For coarse material, the loss of fluorescence is dependent on the concentration of dye.

3. The loss of fluorescence may be related to physical characteristics of the sediment such as mineralogical composition, surface area per unit weight of material,

and perhaps others. Therefore, it should not be assumed that the curves of figure 3 apply to losses of fluorescence in the presence of any sediment other than that used in this study.

4. This study indicates that the loss of fluorescence in the presence of fine sediment is appreciable for concentration of sediment greater than about 500 mg/l and that the losses for Rhodamine WT are less than for Pontacyl Pink B at a given concentration of sediment.

REFERENCES

Beverage, J. P., and Culbertson, J. K., 1964, Hyperconcentrations of suspended sediment: Am. Soc. Civil Engineers Proc., Jour. Hydraulics Div., v. 90, no. HY 6, p. 117–128.

Feuerstein, D. L., and Selleck, R. E., 1963, Fluorescent tracers for dispersion measurements: Am. Soc. Civil Engineers Proc., Jour. Sanitary Engineering Div., v. 89, no. SA 4, p. 1–21.

Nordin, C. F., Jr., 1963, A preliminary study of sediment transport parameters, Rio Puerco near Bernardo, N. Mex.: U.S. Geol. Survey Prof. Paper 462–C, p. C1–C21.

EFFECTS OF RESERVOIR FILLING ON A BURIED AQUIFER OF GLACIAL ORIGIN IN CAMPBELL COUNTY, SOUTH DAKOTA

By NEIL C. KOCH, Huron, S. Dak.

Work done in cooperation with the South Dakota Geological Survey

Abstract.—The filling of the Oahe Reservoir, which raised the reservoir surface west of Pollock, S. Dak., about 47 feet by December 1967, has produced a rise in the piezometric surface in a large buried artesian aquifer of glacial origin. The rise resulted in water-level rises of 34, 22, 20, and 17 feet in wells about 4, 11½, 16½, and 18 miles, respectively, from the reservoir. The piezometric surface 4 miles from the reservoir was about 13 feet above reservoir level as of December 1967. The aquifer is practically undeveloped. If development of the aquifer lowers the level of the piezometric surface below that of the reservoir surface, the hydraulic gradient would reverse and induce recharge from the Oahe Reservoir. This would provide a nearly unlimited water supply and would eventually improve the quality of water in the aquifer.

A major buried artesian aquifer of glacial origin underlies the Oahe Reservoir in the vicinity of Pollock, S. Dak. The aquifer is in a preglacial or glacial tributary of the ancient Grand River. Figure 1 shows the location of this tributary, which is referred to as the deep glacial aquifer. This article discusses the effects of changes in the stage of Oahe Reservoir on the hydrology of the aquifer.

ORIGIN OF THE DEEP GLACIAL AQUIFER

The origin of the deep glacial aquifer is associated with glacial events near the ice front in late Wisconsin time. During late Wisconsin glaciation, preglacial streams such as the Cannonball River in North Dakota were diverted to the southeast along the ice margin when the ice front, which had been advancing from the north and east, halted for some time. The ice margin crossed the present Missouri River at the mouth of Porcupine Creek in North Dakota and extended in a northwesterly direction through Timmer, N. Dak. (fig. 1). Blocked by the ice wall, Big Muddy Creek and the Cannonball River flowed into Porcupine Creek and cut a new channel along the present Missouri River to Spring Creek in South Dakota. At the mouth of Spring Creek, the diverted water followed the Spring Creek drainage but was stopped east of Herreid at the ice margin. The flow was then south along the ice front until it discharged into the ancient Grand River in southeast Campbell County, S. Dak. As the melt water flowed through this channel, it deposited considerable sand, gravel, and associated layers of reworked coal derived from Tertiary rocks. In Campbell County the ancient Grand River and its tributary were defined by L. S. Hedges and N. C. Koch (unpub. data).

The Missouri channel is older between Porcupine Creek and Spring Creek than it is to the north or south. This is shown by the fact that the Missouri channel is almost twice as wide between these two creeks as it is immediately to the north and south.

In late Wisconsin time the tributary to the ancient Grand River was filled with till, outwash, and lake deposits. Further local ice advances blocked the tributary and caused the present Missouri River channel to form between the mouths of Spring Creek and Grand River. Subsequent deposition of silt, sand, and gravel in the Missouri River channel has resulted in about 40 feet of sediment overlying the deep glacial aquifer.

HYDROLOGY OF THE DEEP GLACIAL AQUIFER

The deep glacial aquifer, composed mostly of outwash sand, gravel, silt, and coal, averages about 70 feet in thickness. The top of the aquifer ranges from 150 feet below land surface at Pollock to 225 feet below land surface east of Mound City. The aquifer slopes to the south and east, whereas the piezometric slope is to the west. This is apparent from the fact that

U.S. GEOL. SURVEY PROF. PAPER 650-B, PAGES B169-B173

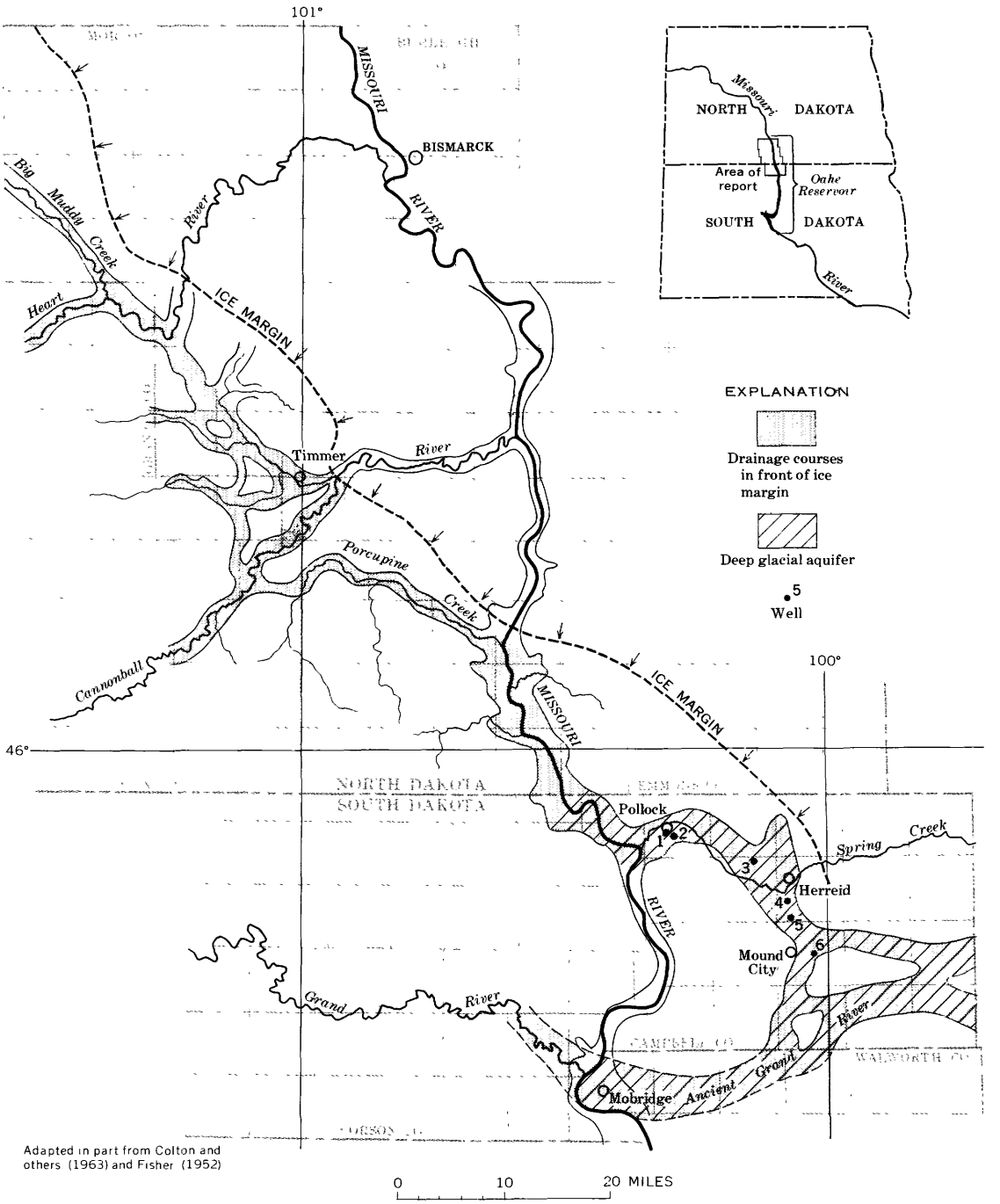

FIGURE 1.—Generalized map showing drainage courses in front of the ice margin. Well numbers are same as those on figures 3 and 4.

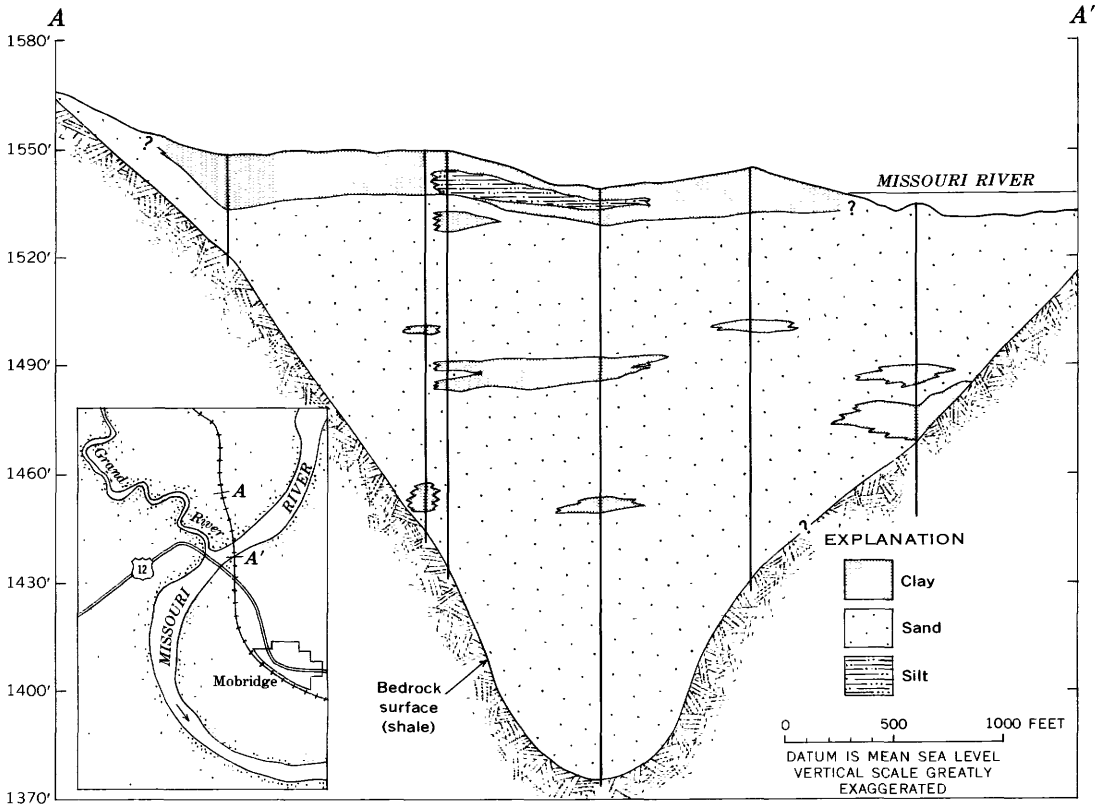

FIGURE 2.—Cross section showing the ancient Grand River sands connected to the Missouri River. Wells shown are U.S. Army Corps of Engineers test wells.

recharge occurs in and east of Campbell County, whereas discharge is to the Missouri River between Spring Creek and Porcupine Creek and in the area where the ancient Grand River channel underlies the Missouri River.

Test-well data (fig. 2) at Mobridge indicate that a permeable connection exists here between the Missouri River and the ancient Grand aquifer. Although no test-well data are available between Spring Creek and Porcupine Creek to show that a hydraulic connection exists there, other data indicate there is such a connection. Water levels show that the hydraulic gradient is toward the Missouri River both at Mobridge and in the area west of Pollock, suggesting that discharge is to the Missouri River in the area west of Pollock where the deep glacial aquifer underlies the river and also possibly to the Grand River west of Mobridge.

RELATION OF OAHE RESERVOIR TO THE AQUIFER

Storage of water in the Missouri River (Oahe Reservoir) was begun in August 1958. The river level, at an altitude of 1,560 feet, west of Pollock was unaffected until June 1962 at which time the reservoir level began a rise of 10 to 15 feet (see fig. 3). In September 1963 the water level dropped to the pre-reservoir altitude followed by an 8-foot rise in the spring of 1964. The main rise, which amounted to 38 feet, started in January 1965 and continued through April 1966.

The earliest available water-level records indicate that in 1955 the piezometric surface of the deep glacial aquifer was at an altitude of 1,585 feet at Pollock (about 4 miles from the river) at which time the altitude of the Missouri River was about 1,560 feet. As the piezometric surface of the discharging aquifer underlying the Missouri is about the same as the river's surface, the hydraulic gradient between Pollock and the river was 6 feet per mile in 1955. In April 1966, the water surface of the Oahe Reservoir was at an altitude of about 1,598 feet, a rise of 38 feet from the pre-reservoir level. During the same period the piezometric surface in the deep glacial aquifer at Pollock rose about 27 feet. About 11½ and 16½ miles from the reservoir, the piezometric surface rose 17 and 10 feet, respectively (see fig. 4). The hydraulic gradient in the aquifer at this time (1966) was 3½ to 4 feet per mile within 11 miles of the river. This lower

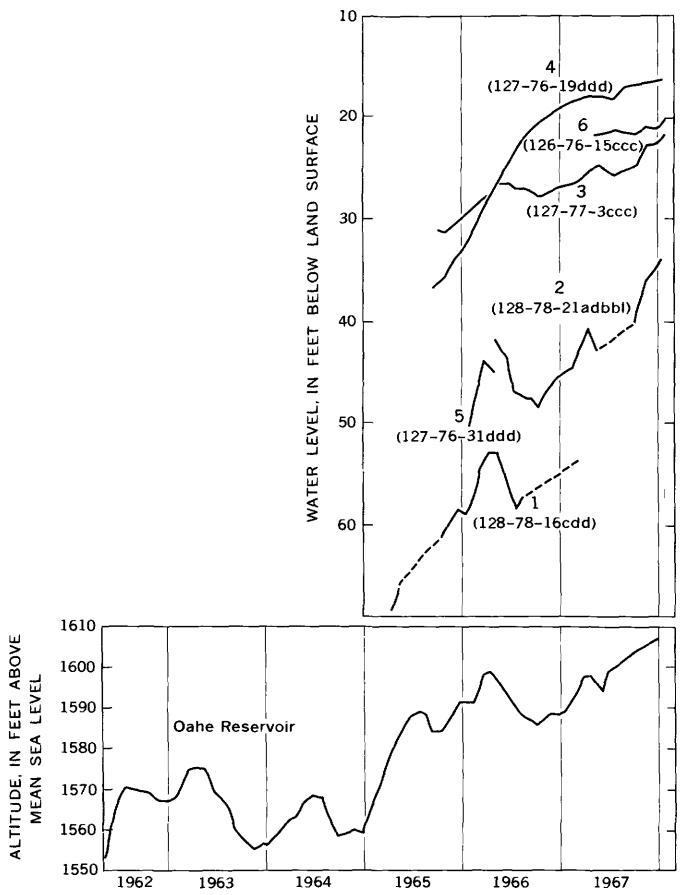

FIGURE 3.—Hydrograph of the water surface in wells in the deep glacial aquifier and of the Oahe Reservoir.

gradient indicates that the aquifer was discharging less water into the reservoir than it was before the reservoir began filling, and thus the availability of water from the aquifer has been increased by the presence of the reservoir.

The reservoir level dropped about 12 feet from April 1966 to October 1966. This resulted in a drop of the piezometric surface of 6 feet about 4 miles from the reservoir and a drop of about 1 foot 11½ miles from the reservoir. However, the piezometric surface continued to rise in a well 16½ miles from the reservoir, probably owing to a time-distance lag (fig. 4).

A 21-foot rise in the reservoir level took place from October 1966 to January 1968. This resulted in a 13-, 6-, and 4-foot rise in water levels in wells 4, 11½, and 16½ miles from the reservoir, respectively. A 6-foot drop in the reservoir level in May and June 1967 produced water-level drops in wells as far as 16½ miles from the reservoir. Water levels in wells 11½ miles or farther from the reservoir showed a 1-month lag in response to reservoir-level changes.

The maximum altitude of the Oahe Reservoir is to be 1,620 feet above mean sea level, an altitude which would raise the reservoir level 13 feet above the December 1967 level. On the basis of previous records, the piezometric surface should rise about 10 feet at Pollock and lesser amounts farther from the reservoir. As of December 1967, the reservoir surface had risen about 47 feet resulting in water-level rises of 34, 22, 20, and 17 feet in wells about 4, 11½, 16½, and 18 miles, respectively, from the reservoir.

When the transmissibility (T) of an aquifer is known, the quantity of water (Q) moving through an area can be computed by determining the hydraulic gradient (I) in feet per mile and the cross-sectional area (L) perpendicular to the direction of flow. By using the equation $Q=TIL$, where T=100,000 gallons per day per foot, I=6 feet per mile, and L=2½ miles, the quantity of water moving from the vicinity of Pollock toward the Missouri River prior to the filling of the Oahe Reservoir was calculated to be 1½ million gallons per day. As of December 1967 the quantity had dropped to half of the pre-reservoir discharge, or 750,000 gallons per day.

The piezometric surface at Pollock, 4 miles from the reservoir, was about 13 feet above reservoir level as of December 1967. The hydraulic gradient of the aquifer within 11 miles of the reservoir was 3–3½ feet per mile. The aquifer is now (1968) undeveloped, but if future development lowers the piezometric surface below the reservoir surface, the hydraulic gradient would reverse and induce recharge from the Oahe Reservoir. Thus, the aquifer would have available the water from the Oahe Reservoir.

The specific conductance of the water in the deep glacial aquifer averages about 1,831 micromhos per centimeter at 25°C, and the sodium-adsorption ratio is about 9.6. The reservoir water has a specific conductance of about 440 and a sodium-absorption ratio of 1. As the reservoir water moves into the aquifer, the quality of water in the aquifer would be greatly improved.

REFERENCES

Colton, R. B., Lemke, R. W., and Lindvall, R. M., 1963, Preliminary glacial map of North Dakota: U.S. Geol. Survey Misc. Geol. Inv. Map I-331.

Fisher, S. P., 1952, The geology of Emmons County, North Dakota: North Dakota Geol. Survey Bull. 26, 47 p.

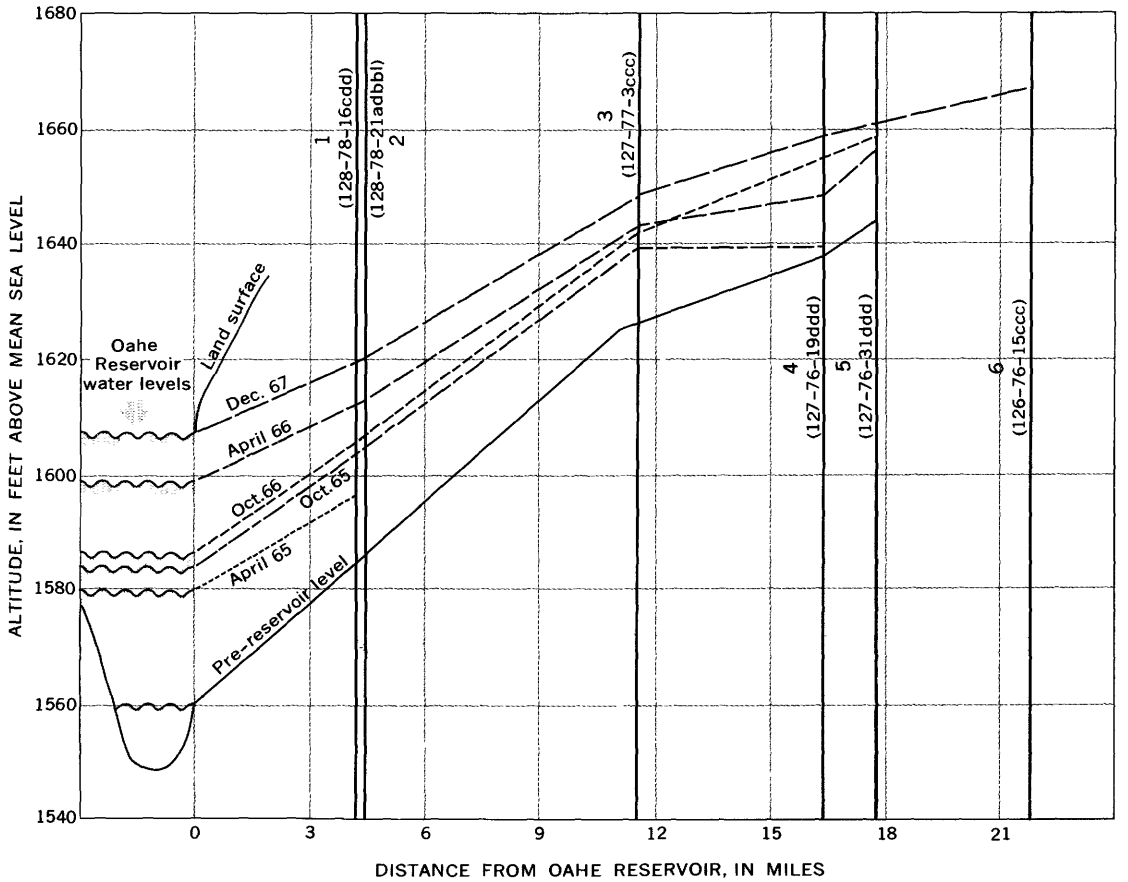

FIGURE 4.—Cross section showing relationship of water-surface changes in the aquifer (dashed and solid lines) to water-surface changes of the Oahe Reservoir (wavy lines).

TEMPERATURE ANALYSIS OF A STREAM

By M. R. COLLINGS, Tacoma, Wash.

Abstract.—Temperatures of a stream were fitted and defined by a harmonic analysis of the probable occurrence, at the 95-percent level, of maximum and minimum monthly temperatures and of median temperatures throughout the year. The 0.5-probability curve of maximum temperatures was found to have equivalent values of amplitude and phase angle to that of a curve fitting 9 years of monthly maximum temperatures. Investigations also were made to determine the acceptability of using spot-temperature observations, by harmonic analysis, to obtain mean monthly temperatures throughout the year. A comparison, by regression analysis, of the mean monthly temperatures, from the thermograph record, with the synthetically determined median monthly temperatures, from the spot measurements, showed a standard error of 1.6°C. Another comparison, between the average harmonic curve from 4 years of spot measurements and the median curve from the maximum and minimum monthly temperatures, showed a standard error of 0.9°C.

The temperature of a water body such as a stream is the result of both meteorological and physical effects. The governing factors of the meteorological effects are solar radiation, wind velocity, air temperature and vapor pressure. The governing physical phenomena are amount of surface area exposed, depth of the water, temperature of the source water, rate of water exchange (discharge), amount of mixing, shading from vegetation and land masses, impurities in the water, surface and subsurface inflows, temperature of surrounding land masses, and orientation of the stream.

The temperature of a stream is important to many water users, such as municipal, industrial, and fisheries agencies, and individual agriculture and domestic users. Temperature is a significant factor in the quality of the water. As the temperature of water bodies increases, the dissolved oxygen decreases, owing to (1) the decreasing saturation capacity of the water, and (2) the increased oxygen consumption of aquatic organisms. Also, increases in temperature raise the water's solution capability.

The desirable temperature for domestic drinking water is 10°C (50°F) and below. Water temperature in excess of 18°C (64.4°F) may have a noticeable taste and odor (Everts, 1963, p. 2).

Industries that use water for cooling usually return warmer water to the stream. This reduces the amount of dissolved oxygen and may have an effect on downstream aquatic life.

Fisheries and resource agencies are interested in the maximums, minimums and ranges of water temperature for selection of hatchery sites, development and preservation of spawning areas, and evaluation of the effects of regulation and water use on a stream. Fish affected by a rise of water temperature respond by increased metabolic rates, higher oxygen requirements, greater sensitivity to toxic materials, and reduced swimming speed. Lethal high and low temperatures vary as much as 18°C among different species. Also, some temperatures, not necessarily lethal, may favor competitors, predators, and diseases that can destroy a species of fish. After fish become acclimated to warm water they may be killed rapidly when they swim into appreciably colder water; the reverse also may be fatal.

The agriculturist prefers water at a temperature of about 15°C (59°F) for crop irrigation. Return-irrigation water usually increases temperatures in the receiving streams.

ANALYSIS OF A SITE WITH CONTINUOUS TEMPERATURE RECORDS

Monthly maximum temperatures

The periods of 1956–59 and 1962–66, covered by thermograph records of the Chehalis River near Grand Mound, Wash., were analyzed. (Years 1960–61 were not covered by complete records.) Using a harmonic analysis (Carson, 1963; Ward, 1963; Panofsky and Brier, 1965) of the first occurrence of the highest

[1] All temperatures given on the celsius scale unless indicated otherwise.

U.S. GEOL. SURVEY PROF. PAPER 650-B, PAGES B174-B179

temperature for the month for each of the 12 months, an evaluation of the constants of the equation

$$T=a[sin(bx+c)]+\bar{T}'$$

was made for each year of record (table 1). In the equation, T is the monthly maximum temperature of the stream; x is the calendar-year day on which the maximum temperature occurs, beginning with January 1 as $x=1$; b is a constant equal to $2\pi/365$, or 0.0172 radians per day; a is the amplitude, in degrees Celsius, of the curve above and below the mean annual maximum monthly temperature ($\bar{T}'$); and c is the phase angle in radians. The magnitude and day of occurrence of the highest and lowest maximum temperatures for the year are where T is equal to $(\bar{T}'+a)$ at x equal to $(3/\pi-c)$ $1/b$, and where T is equal to $(\bar{T}'-a)$ at x equal to $(\frac{1}{2}\pi-c)$ $1/b$, respectively.

As shown in table 1, the S.E. (standard error) of the monthly maximum temperatures around the fitted harmonic curve for each year averages 1.6°C for 9 years of data; about 68 percent of the data, for an average year, is within 1.6°C of the harmonic curve. Comparison of the amplitude, a, between the years shows a range of 2.4°C and an average of 8.2°C. The amplitude of a particular year is a characteristic of that year, thus differences between years are not entirely measurement error but rather, are indications of maximum monthly temperature variability from year to year. The highest maximum temperatures over the period ranged from 19.8° to 23.1°C between days 195 and 207. The lowest maximum temperatures ranged from 4.2° to 6.1°C between days 12 and 25.

Only the first harmonic was used to define the temperature variation within each year. The first harmonic, as indicated by "γ" in table 1, defines an average of 84 perecent of the variance, whereas the second harmonic defines only about 6 percent more of the variance. Thus, considering the error of the basic data, the amount of work involved, and the difficulties in physical interpretation of the constants, the first harmonic is considered adequate to define the temperature data.

From the basic data of monthly maximum temperatures, the frequency curve for each month over the period of record was determined (fig. 1). The data are assumed normally distributed, and a straight line was fitted to the points. The 0.5-probable temperature for each month (also the 0.95- and 0.05-probable temperatures) was determined from the monthly frequency curves in figure 1, and a harmonic curve (referred to as the 0.5-, 0.95-, or 0.05-probability curves, as the case may be) was fitted to each of these values. All data for 9 years were also fitted by the same method and the coefficients that were obtained are shown by the last two lines of table 1. There are no significant differences between the coefficients.

The slope of the probability frequencies in figure 1 may be obtained by using the standard deviation (in degrees Celsius) of the monthly maximum temperatures. The standard deviation of the maximum temperatures for a given month for all years is a measure

TABLE 1.—*Summary of analysis of annual highest and lowest monthly maximum water temperatures, in degrees Celsius*

[Based on first occurence of highest temperature during the particular month]

Calendar year	Number of pairs of data	[1] Harmonic coefficients			[2] S.E.	[3] γ (percent)	Annual maximum temperature		Annual minimum temperature	
		a	c	$\bar{T}'$			Degrees Celsius	Day from Jan. 1	Degrees Celsius	Day from Jan. 1
1956	12	8.5	4.33	13.0	1.8	81	21.6	204	4.5	22
1957	12	8.6	4.35	12.8	.8	92	21.4	203	4.2	21
1958	12	9.3	4.30	13.8	1.9	80	23.1	206	4.5	24
1959	12	8.4	4.30	13.5	2.3	80	21.9	206	5.1	24
1962	12	7.4	4.33	12.4	2.0	76	19.8	204	5.0	22
1963	12	7.5	4.50	13.5	1.6	85	21.0	195	6.0	12
1964	12	6.9	4.36	13.0	1.4	81	19.9	203	6.1	20
1965	12	9.0	4.39	13.4	1.8	88	22.4	201	4.4	19
1966	12	8.0	4.28	14.0	.6	91	22.0	207	6.0	25
Average of 9 years	12	8.2	4.35	13.3	1.6	84	21.5	203	5.1	21
Coefficients for all data for 9 years	108	8.2	4.36	13.3	----	88	21.5	203	5.1	21
Median year	12	8.2	4.36	13.3	----	85	21.5	203	5.1	21

[1] Type equation: $T=a[\sin(bx+c)]+T'$, where
T=temperature in degrees Celsius,
a=amplitude in degrees Celsius of the curve above and below the mean annual maximum monthly temperature ($\bar{T}'$),
b=0.0172 radians per day,
c=phase angle in radians,
x=day where x equals 1 on January 1, and
$\bar{T}'$=mean annual maximum monthly temperature.

[2] Standard error of data from harmonic within each year, in degrees Celsius.

[3] Variance of data defined by first harmonic.

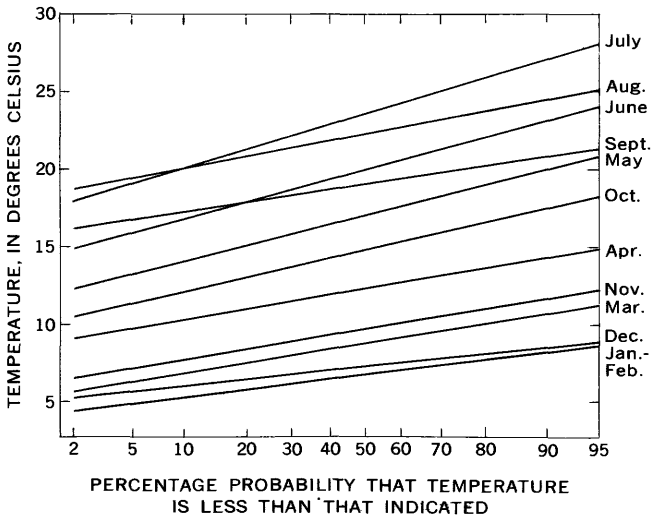

FIGURE 1.—Magnitude and probability of monthly maximum temperatures, by months, in degrees Celsius, for the periods 1956–59 and 1962–66, Chehalis River near Grand Mound, Wash.

of the variability in temperature of that month for that particular stream site.

A plot of the standard deviation of the monthly maximum and minimum temperatures is shown in figure 2. It may be noted that, from about the winter solstice in December, the standard deviation of maximum monthly temperatures gradually increases until the vernal equinox (late March), then a sharp increase occurs and continues through May. Thereafter, the magnitude of standard deviation nearly levels off through July, when a decline begins which lasts to about the autumnal equinox. The increase in October probably is caused by the changing climatic environment of the region (U.S. Weather Bureau, 1961). October is a transition month, being characterized by both summer and winter weather. This, in turn, results in a greater standard deviation of temperatures than in September or November. The plot of mean monthly sunlight duration (fig. 2) generally (except for October) follows the maximum-temperature standard-deviation trend. This suggests that solar radiation is related to temperature variability as well as to mean stream temperatures.

Because the harmonic fitting of the 0.5-probability curve of the monthly maximum temperatures is not different from the average of all the years or from the harmonic fitting of all the data for the 9 years (table 1), the probability analysis using the assumption of normality as an operational assumption may be justified. From the frequency curves of figure 1, the 90-percent confidence limits of the monthly maximum temperatures are defined by fitting a harmonic

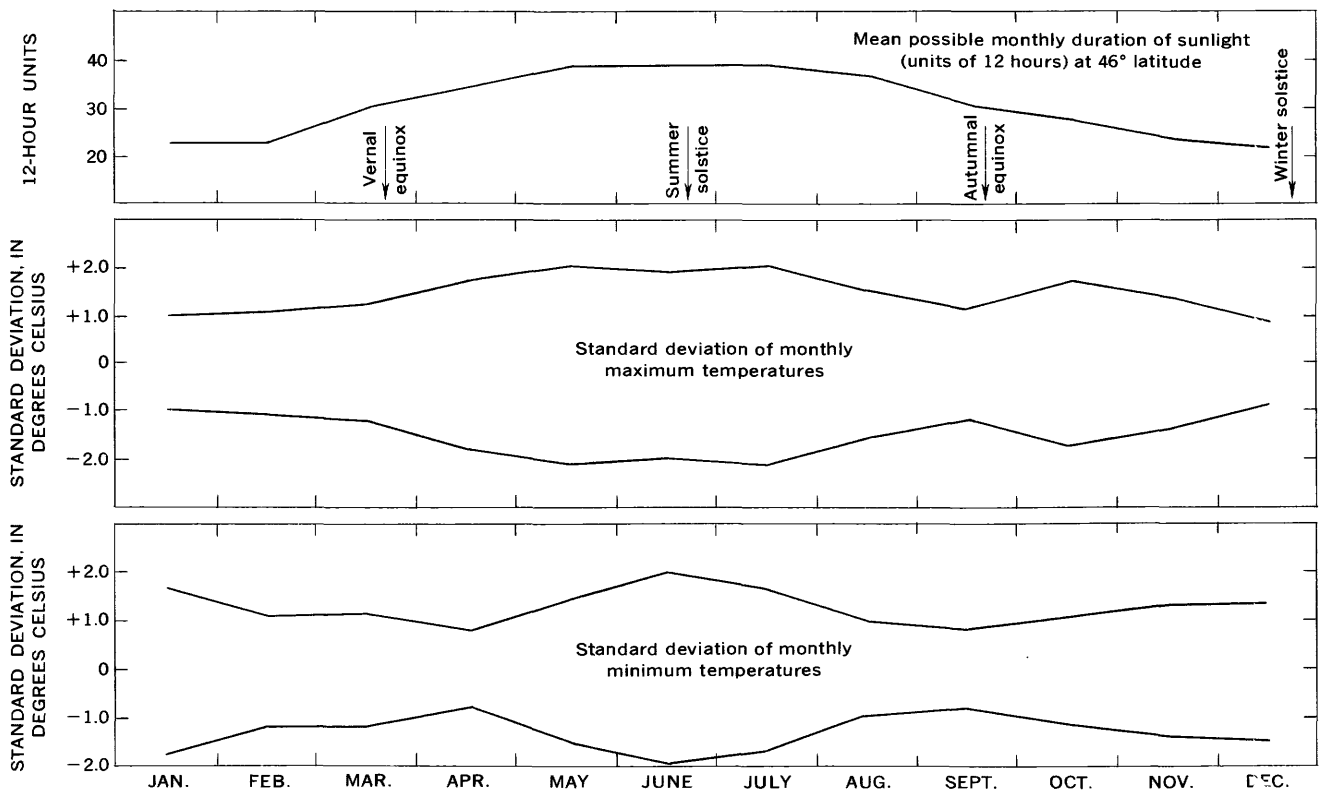

FIGURE 2.—Plot of magnitudes of standard deviations from the mean by month, for the monthly maximum and minimum temperatures.

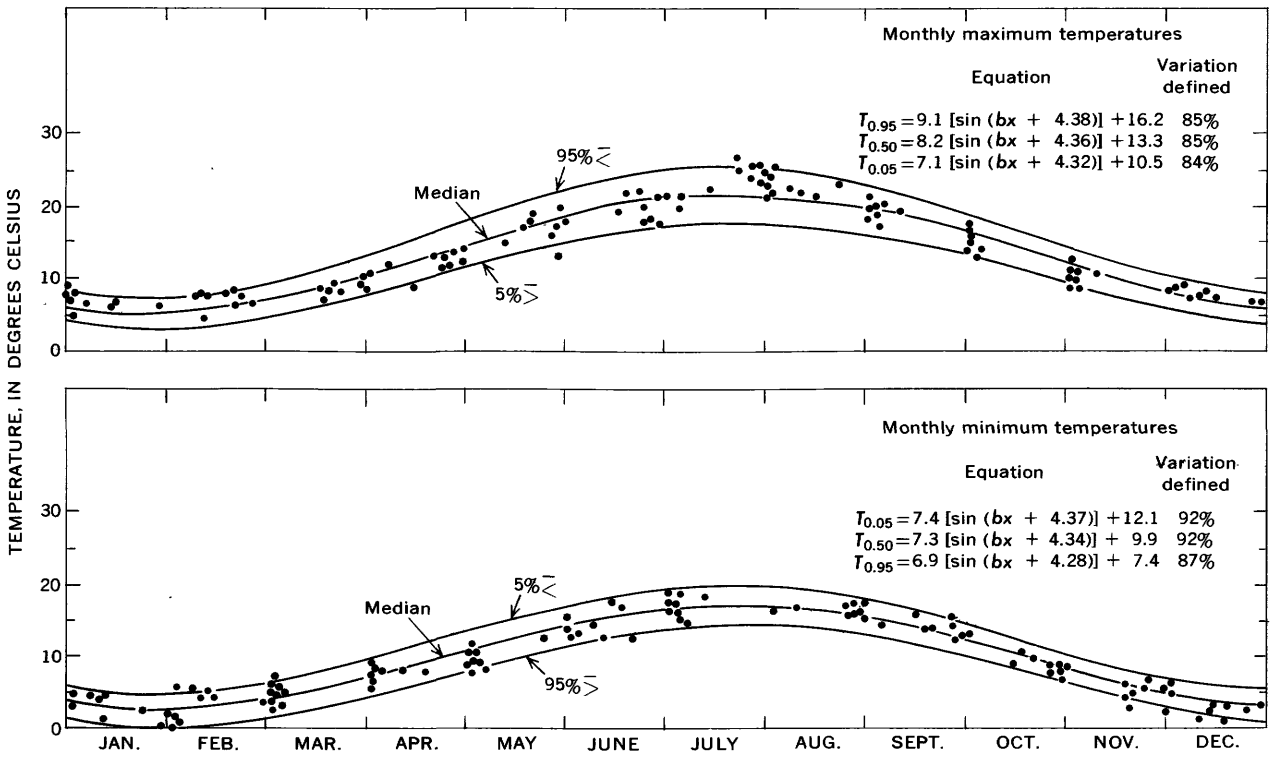

FIGURE 3.—Harmonic-curve fitting of the median, and of the 95- and 5-percent probability of occurrence for monthly maximum and monthly minimum temperatures.

curve to the 0.95- and to the 0.05-probability values (fig. 3).

Monthly minimum temperatures

The same method and time period used to analyze the monthly maximum temperatures were used to evaluate the monthly minimum temperatures. The magnitude and probability of the monthly minimum temperatures (fig. 4) show the same general pattern as that of the maximums—July temperatures are the highest and January and February temperatures are the lowest. April and September have the least standard deviation of monthly minimum temperatures (fig. 2), whereas June has the greatest standard deviation of minimums. Figure 2 shows a decrease in amplitude and confidence interval for the monthly minimum temperatures as compared to that of the monthly maximum temperatures (fig. 3).

Monthly maximum and minimum temperatures

The monthly maximum- and minimum-temperature data for the Chehalis River near Grand Mound are shown in figure 5 by the median and the 0.95-probability curve being equal to or less than that of the maximums, and the 0.95-probability curve being equal to or greater than that of the minimums. The curves show that (1) there is a 90-percent chance that the annual range in temperatures will not exceed 24.8°C (from 0.5°C to 25.3°C), (2) 50 percent of the time the annual water-temperature range will be 16°C, (3) the month with the greatest range in temperatures, from 14°C to 25.3°C, is also the warmest month (July), and (4) the coolest month (January) has the least variation (0.5°C to 7.8°C).

The Chehalis River is a major salmon-spawning stream, and the Chehalis River near Grand Mound would be adequate from the standpoint of water temperature, for most species of Pacific salmon (*Oncorhynchus*). For maximum productivity of *Oncorhynchus* the fresh-water temperature requirements range from 7.2° to 15.6°C (45° to 60°F) for upstream migration, from 5.8° to 12.8°C (42.5° to 55°F) for maximum survival at spawning, from 0° to 12.8°C (32° to 55°F) for egg incubation, and from 10° to 15.6°C (50° to 60°F) for the fingerling salmon (Burrows, 1963). Migration and spawning generally occur from July through December. Figure 5 shows that the 95-percent-maximum and the 95-percent-minimum curves of the river temperatures will encompass part of the maximum-productivity range (5.8°C to 15.6°C) for the July–December migration and spawning period. However, the July 0.95-probable- minimum temperature approaches the highest of the productivity range (15.6°C), and the December 0.95-probable-maximum temperature approaches the lowest value (5.8°C) of

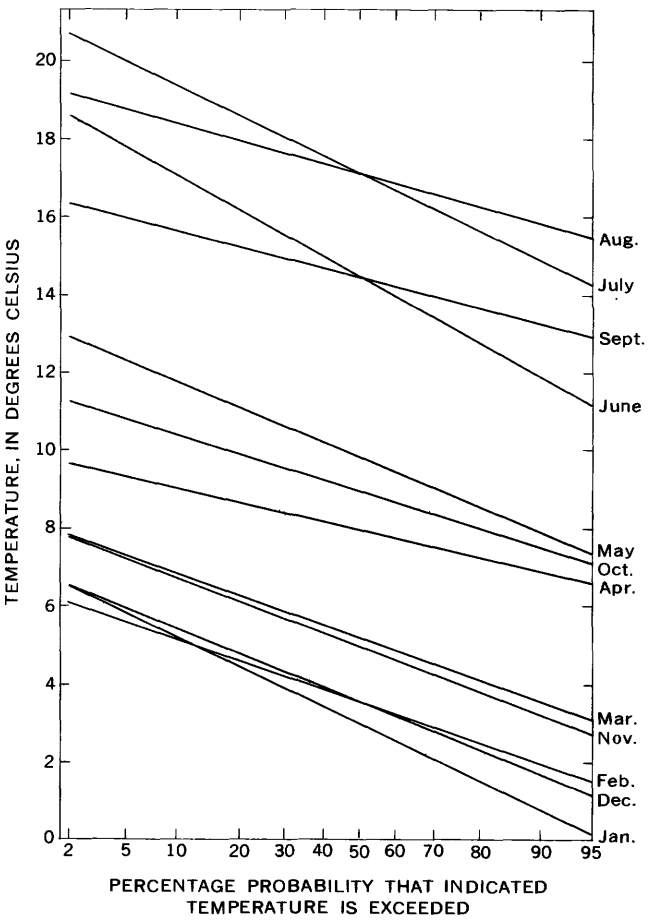

FIGURE 4.—Magnitude and probability of monthly minimum temperatures, by months, in degrees Celsius, for the periods 1956–59 and 1962–66, Chehalis River near Grand Mound, Wash.

the range. The maximum-productivity temperature range for egg incubation of Pacific salmon is between 0°C and 12.8°C, and the period of incubation is approximately from October through May. The 90-percent-temperature confidence limits over the October–May period are 0.5°C through 22°C, with every incubation month having part of the optimum range.

Median temperatures range from 16.5°C to 20.0°C during the growing season. This is somewhat higher than optimal irrigation-water temperatures.

ANALYSIS OF A SITE WITH SPOT OBSERVATIONS OF TEMPERATURES

Spot-temperature observations are made on many streams. To evaluate the acceptability of determining mean monthly temperatures from 10 to 12 spot-temperature measurements fairly well spaced throughout the year, harmonic curves calculated from 4 years of spot data were compared with the thermograph records for the Chehalis River near Grand Mound. The coefficients of the harmonic curves from the spot-temperature data of the 1960–63 water years are shown in table 2. Figure 6 shows the relation between thermograph records and temperatures as determined from a harmonic of spot-temperature data. The regression coefficients were tested by statistical methods and, at the 90-percent-confidence level, the line was found to pass through zero and the slope was not significantly different from 1.0. Thus, as should be expected, the final equation of the relation in figure 6 is, simply,

$$T_c = T_t,$$

with a standard error of estimate of 1.6°C (2.9°F). By averaging the mean monthly harmonic-curve tem-

Table 2.—*Summary of analysis of spot water-temperature data* [1]

Calendar year	Numbers of pairs of data	Harmonic coefficients			γ (percent)
		a	c	$\overline{T}'$	
1960	10	8.2	4.27	11.5	98
1961	10	7.5	4.28	12.1	92
1962	10	7.6	4.33	10.7	93
1963	11	9.8	4.56	11.6	87
Average		8.3	4.36	11.5	

[1] Coefficients are defined in table 1.

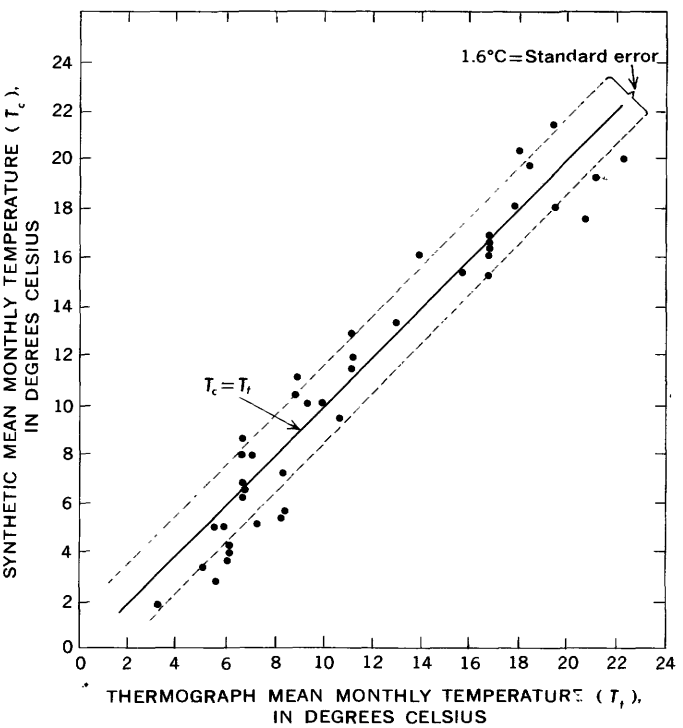

FIGURE 6.—Synthetic mean monthly temperatures (derived from spot-temperature harmonic curve) versus mean monthly temperatures (derived from continuous-recording thermograph) for a 4-year period, Chehalis River near Grand Mound, Wash.

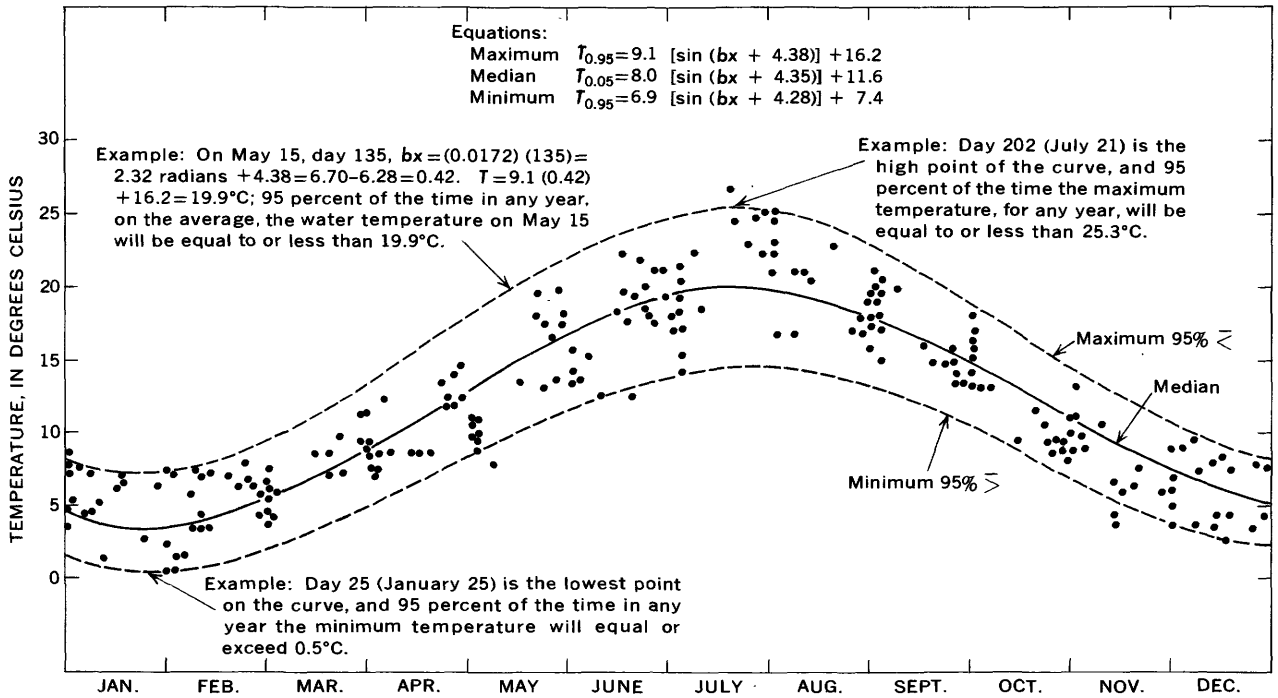

FIGURE 5.—95-percent-probability curves for maximum and minimum temperatures for the Chehalis River near Grand Mound, Wash.

peratures for each month over the 4 years of spot-temperature records (table 2) and comparing, by regression analysis, these values with mean monthly values from the median-probability harmonic curve of figure 5, a standard error of 0.9°C (1.6°F) was obtained. Only 41 (rather than 48) pairs of data for 4 years are represented in figure 6 because of incomplete thermograph records.

The determination of mean monthly water temperatures from routinely observed temperature data may be sufficiently accurate and acceptable for many situations. Such determinations may be useful in reconnaissance investigations that depict the broad spatial and seasonal variations of stream temperature, or in feasibility studies that determine whether additional temperature data are needed at a particular site. Also, the constants of the harmonic fitting (a and c) reflect characteristics of a stream and thus provide clues to differences between the temperature regimens of streams.

REFERENCES

Burrows, R. E., 1963, Water temperature requirements for maximum productivity of salmon, *in* Water temperature—influences, effects, and control: U.S. Pacific Northwest Water Laboratory, Pacific Northwest Symposium on Water Pollution Research, 12th, Corvallis [Oregon] 1963, Proc., p. 29–35.

Carson, J. E., 1963, Analysis of soil and air temperatures by Fourier techniques: Jour. Geophys. Research, v. 68, no. 8, April 15, p. 2217–2232.

Everts, C. M., 1963, Temperature as a water quality parameter, *in* Water temperature—influences, effects, and control: U.S. Pacific Northwest Water Laboratory, Pacific Northwest Symposium on Water Pollution Research, 12th, Corvallis [Oregon] Proc., p. 2–26.

Panofsky, H. A., and Brier, G. W., 1965, Some applications of statistics to meteorology: Pennsylvania State Univ., p. 128–134.

U.S. Weather Bureau, 1961, Climatic guide for Seattle, Washington and adjacent Puget Sound area: U.S. Weather Bur., Climatography of the United States, no. 40–45, p. 1–3.

Ward, J. C., 1963, Annual variation of stream water temperature: Jour. Sanitary Engineering Div., Am. Soc. Civil Engineers, v. 89, SA6, Proc., Dec. 1963, p. 3710 (1–16).

THE GIBBS FREE ENERGIES OF SUBSTANCES IN THE SYSTEM $Fe–O_2–H_2O–CO_2$ AT 25°C

By DONALD LANGMUIR, Trenton, N.J.[1]

Work done in cooperation with the New Jersey Department of Conservation and Economic Development

Abstract.—The Gibbs free energies of aqueous ionic and molecular species and solid phases in the system $Fe–O_2–H_2O–CO_2$ have been reevaluated, taking into account recently published thermochemical data and laboratory investigations conducted by previous workers and by the author. The study shows that a range of thermodynamic stabilities are possible for the ferric oxyhydroxides when they crystallize or are precipitated in water at temperatures near 25°C. Expressing these stabilities in terms of the activity products of the oxyhydroxides written as $K = (a\mathrm{Fe}^{+3})\ (a\mathrm{OH}^{-1})^3$, the following values are indicated: K (hematite) $\geqq 10^{-41.9\pm0.4}$*; K(maghemite) $\leqq 10^{-38.8\pm0.5}$; K(goethite) $\geqq 10^{-40.4\pm0.4}$ to $10^{-41.2\pm0.4}$*; K(lepidocrocite) $\leqq 10^{-38.7\pm0.5}$; and K(amorphous) $\leqq 10^{-37.1\pm0.6}$ to $\leqq 10^{-38.3\pm0.7}$. Also based on this study K(siderite) $= (a\mathrm{Fe}^{+2})\ (a\mathrm{CO_3}^{-2}) = 10^{-10.55\pm0.03}$*. Asterisks denote the activity products of thermodynamically most-stable forms.

In order to explain the occurrence of iron in ground waters of the Potomac-Raritan-Magothy aquifer system in New Jersey, it was necessary to reevaluate the available Gibbs free-energy data ($\Delta G_f°$) for a number of aqueous and solid iron species. The reevaluation is particularly appropriate in view of new thermochemical data for Fe^{+2}(aq), Fe^{+3}(aq), and goethite, which differ significantly from data previously published. The revised Gibbs free-energy values are listed in table 1. A brief explanation of each value is provided in footnotes accompanying the table. The text contains additional discussion of values in the table.

CARBONIC ACID (H_2CO_3), BICARBONATE ION (HCO_3^{-1}) AND CARBONATE ION (CO_3^{-2})

Wagman and others (1965) have published revised $\Delta G_f°$ data for H_2CO_3, HCO_3^{-1}, and CO_3^{-2}. In calculations of the activity product of calcite, Langmuir (1968) found that their data gave results which were not as internally consistent as results calculated using the corresponding $\Delta G_f°$ data in table 1. The data in the table, which are considered more accurate than the data of Wagman and others, are based on carbonic acid dissociation constants measured from 0° to 50°C by Harned and his coworkers (footnotes 2–4, table 1).

AQUEOUS IRON SPECIES

Latimer (1952) gives $\Delta G_f°$ (Fe^{+2}) = −20,300 calories per mole, and $\Delta G_f°(Fe^{+3}) = -2{,}530$ cal/mole. Larson and others (1968) have reevaluated the thermodynamic properties of Fe^{+2} on the basis of their own measurements and an appraisal of existing data, and find $\Delta G_f°(Fe^{+2}) = -21{,}800 \pm 500$ cal/mole. Their revised $\Delta G_f°(Fe^{+2})$ in table 1 introduces a corresponding change in $\Delta G_f°(Fe^{+3})$ and in the Gibbs free energies of all the other aqueous species of ferrous and ferric iron (footnotes 5–13, table 1). Similarly altered are $\Delta G_f°$ values for ferrous hydroxide, siderite, maghemite, lepidocrocite, and amorphous ferric oxyhydroxide, which are based on solubility measurements (footnotes 14–16, 18, table 1). However, in most instances, the differences in Gibbs free energy between these aqueous and solid species are changed little from similar differences published by Latimer (1952) or Hem and Cropper (1959). This reflects the fact that values in table 1 for the corresponding hydrolysis and equilibrium constants are similar or equal to the values for these constants adapted by previous workers.

The existence and stability of molecular $Fe(OH)_2°$ (aq) has not been adequately documented (Hem and Cropper, 1959), Thus, $\Delta G_f°$ [$Fe(OH)_2°$] in table 1 should be considered tentative. Gayer and Woontner (1956) proposed a solubility of $10^{-6.54}$ molar for molec-

[1] Present address: Department of Geochemistry and Mineralogy and Mineral Conservation Section, The Pennsylvania State University, University Park, Pa. 16802.

U.S. GEOL. SURVEY PROF. PAPER 650-B, PAGES B180–B184

TABLE 1.—*The Gibbs free energy ($\triangle G_f^\circ$) of certain substances at 25° C (298.15° K) and 1 atm total pressure*

[Nonitalicized values correspond to the hypothetical reference state of unit molality for the aqueous species, or in the case of solids to the most stable form. *Italicized* values are not strictly comparable (see footnotes 13, 16–18, and text)]

Substance	$\triangle G^\circ_f$ (cal/mole)	Sources (see footnotes)
$CO_2(g)$	$-94,257\pm40$	(1)
$H_2O(l)$	$-56,688\pm20$	(1)
$OH^{-1}(aq)$	$-37,594\pm10$	(1)
$H_2CO_3(aq)$	$-148,948\pm55$	(2)
$HCO_3^{-1}(aq)$	$-140,285\pm60$	(3)
$CO_3^{-2}(aq)$	$-126,196\pm70$	(4)
$Fe^{+2}(aq)$	$-21,800\pm500$	(5)
$FeOH^{+1}(aq)$	$-67,168\pm570$	(6)
$Fe(OH)_2^\circ(aq)$	$-111,173\pm600$	(7)
$Fe(OH)_3^{-1}(aq)$	$-148,249\pm600$	(8)
$Fe^{+3}(aq)$	$-4,020\pm500$	(9)
$FeOH^{+2}(aq)$	$-57,358\pm550$	(10)
$Fe(OH)_2^{+1}(aq)$	$-107,635\pm600$	(11)
$Fe(OH)_3^\circ(aq)$	$-155,595\pm600$	(12)
$Fe(OH)_4^{-1}(aq)$	*$-200,920\pm550$*	(13)
$Fe(OH)_2(s)$	$-117,584\pm570$	(14)
$FeCO_3$(siderite)	$-162,390\pm510$	(15)
Fe_3O_4(magnetite)	$-243,094\pm510$	(1)
α-Fe_2O_3(hematite)	$\geqq -177,728\pm310$	(1)
γ-Fe_2O_3(maghemite)	$\leqq$ *$-169,764\pm500$*	(16)
α-FeOOH(goethite)	$\geqq$ *$-115,280\pm160$* to $-116,375\pm160$	(17)
γ-FeOOH(lepidocrocite)	$\leqq$ *$-169,614\pm500$*	(16)
$Fe(OH)_3(s)$(amorphous)	$\leqq$ *$-167,460\pm600$* to $\leqq$ *$-169,040\pm1,100$*	(18)

[1] Robie and Waldbaum (1968) and for hematite also this article (see text).
[2] Based on $K=10^{-1.464}$ for $CO_2(g)+H_2O=H_2CO_3$ (Harned and Davis, 1943).
[3] Based on $K=10^{-6.331}$ for $H_2CO_3=H^{+1}+HCO_3^{-1}$ (Harned and Davis, 1943).
[4] Based on $K=10^{-10.329}$ for $HCO_3^{-1}=H^{+1}+CO_3^{-2}$ (Harned and Scholes, 1941).
[5] Larson and others (1968).
[6] Based on $K=10^{-9.40}$ for $Fe(OH)_2(s)=FeOH^{+1}+OH^{-1}$ (Leussing and Kolthoff, 1953).
[7] Based on $K=10^{-4.70}$ for $Fe(OH)_2^\circ(aq)=FeOH^{+1}+OH^{-1}$ (Hem and Cropper, 1959).
[8] Based on $K=10^{-5.08}$ for $Fe(OH)_2(s)+OH^{-1}=Fe(OH)_3^{-1}$ (Gayer and Woontner, 1956).
[9] Latimer (1952) gives $E^\circ=-0.771V$ for $Fe^{+2}=Fe^{+3}+e^{-1}$. Combined with ΔG_f° of $Fe^{+2}(aq)$ from table 1, this gives $\Delta G_f^\circ=-4,020\pm500$ cal/mole for $Fe^{+3}(aq)$.
[10] Based on $K=10^{-2.46}$ for $Fe^{+3}+H_2O=FeOH^{+2}+H^{+1}$ (Lamb and Jacques, 1938).
[11] Based on $K=10^{-4.70}$ for $FeOH^{+2}+H_2O=Fe(OH)_2^{+1}+H^{+1}$ (Lamb and Jacques, 1938).
[12] Based on $K=10^{-7.60}$ for $Fe(OH)_3^\circ(aq)=Fe(OH)_2^{+1}+OH^{-1}$ (Hem and Cropper, 1959).
[13] A rough estimate, based on $K=10^{34.11}$ for $Fe^{+3}+4OH^{-1}=Fe(OH)_4^{-1}$ in 3*M* $NaClO_4$ solution (Schindler, 1967).
[14] Based on $K=10^{-15.10}$ for $Fe(OH)_2(s)=Fe^{+2}+2OH^{-1}$ (Leussing and Kolthoff, 1953).
[15] ΔG_f° data given by Latimer (1952), and based chiefly on measurements by Smith (1918), corresponds to $K=10^{-10.68}$ at 25°C for $FeCO_3=Fe^{+2}+CO_3^{-2}$. Reevaluating the results of the 14 solubility runs from undersaturation by Smith, yields $K=10^{-10.55\pm0.03}$ at 30°C. ΔH_f° (siderite) $=-177,812\pm540$ cal/mole (Robie and Waldbaum, 1968), $\Delta H_f^\circ(Fe^{+2})=-22,100\pm500$ cal/mole (Larson and others, 1968), and $\Delta H_f^\circ(CO_3^{-2})=-161,736\pm120$ cal/mole (Langmuir, 1965), so that $\Delta H^\circ=-6,024\pm750$ cal for this reaction at 25°C. Assuming ΔH° constant, the integrated van't Hoff equation is: $\log K=-14.9'+1.316\times10^{+3}/T(°K)$, and $K=10^{-10.57\pm0.03}$ at 25°C. In good agreement, Langmuir (unpublished data) found $K=10^{-10.55\pm0.08}$ based on three solubility runs (one reversed) at 25°C. The latter K gives ΔG_f°(siderite) $=-162,390\pm510$ cal/mole.
[16] Eh-pH measurements by Doyle (1967) correspond to $K=10^{-38.7\pm0.5}$ for freshly precipitated lepidocrocite, and $10^{-36.8\pm0.5}$ for freshly precipitated maghemite. Doyle identified his crystalline phases by X-ray methods. Because more-soluble amorphous ferric oxyhydroxides could have also been present but not recognized (Feitknecht and Michaelis, 1962), these activity products may be too large. Welo and Baudisch (1934) and Feitknecht (1959) consider γ-FeOOH less soluble than γ-Fe_2O_3, and both phases less stable than their α polymorphs. Based on the evidence available, K values for the stable forms of these minerals are probably about 10^{-40}.
[17] Barany (1965) measured $\Delta H^\circ=-940\pm90$ cal for α-Fe_2O_3(stable)$+H_2O(l)=2(\alpha$-FeOOH)(stable). King and Barany (E. G. King, oral commun., 1968) measured $S^\circ_{298}=14.43$ gibbs/mole for stable goethite. Combined with enthropy and ΔG_f° data for stable hematite and water (Robie and Waldbaum, 1968) this yields $\Delta S^\circ=8.74\pm0.20$ gibbs/mole, $\Delta G^\circ=+1,666\pm60$ cal, and for stable goethite $\Delta G_f^\circ=-116,375\pm160$ cal/mole. The solution of goethite may be written α-FeOOH(stable)$+H_2O=Fe^{+3}+3OH^{-1}$. Based on ΔG_f° for stable goethite and other ΔG_f° data from table 1, the calculated equilibrium constant for this reaction is $K=(aFe^{+3})(aOH^{-1})^3=10^{-41.3\pm0.4}$. This may be compared with $K=10^{-41.3\pm0.8}$ for stable goethite measured in 3*M* $NaClO_4$ solutions by Schindler and others (1963). Solubility measurements described by Lengweiler and others (1961a, p. 801) showed that a fresh goethite precipitate which had been acid leached, had an activity product about 0.8 $\log_{10}$ units larger than K for most-stable goethite, or $K=10^{-40.4\pm0.4}$. This K is equivalent to $\Delta G_f^\circ=-115,280\pm160$ cal/mole. Presumably freshly precipitated goethite is somewhat less stable than this.
[18] Based on the reaction $Fe(OH)_3(s)$ (amorphous) $=Fe^{+3}+3OH^{-1}$, Elder (1930), Kriukov and Awsejewitsch (1933), and Evans and Pryor (1949) reported solubility products as large as $10^{-35.4}$ to $10^{-36.5}$ for the fresh precipitate. Reevaluating their solubility data considering Fe^{+3} complexes in table 1, and ion activities, gives activity products smaller than 10^{-37} (see Cooper, 1938). ΔG_f° data in Latimer (1952) correspond to $K=10^{-37.2}$ for what is described as $Fe(OH)_3(c)$. Lamb and Jacques (1938) measured a solubility of $10^{-8.70}$ molar $Fe(OH)_3^\circ(aq)$ in equilibrium with freshly precipitated amorphous ferric oxyhydroxide. Combined with ΔG_f° data from table 1, this gives $\Delta G_f^\circ=-167,460\pm600$ cal/mole and $K=10^{-37.1}$ for the fresh precipitate. Solubility measurements on an amorphous precipitate which had aged 4 days (Lengweiler and others, 1961a, p. 801), showed that the activity product of this material is 2.8 $\log_{10}$ units larger than it is for stable goethite, or $K=10^{-38.4}$. Feitknecht and Schindler (1963) assume that K for the same material is 1.1 $\log_{10}$ units smaller than it is for the fresh precipitate, or $K=10^{-38.2}$. The average of these values, $K=10^{-38.3}$, yields $\Delta G_f^\circ=-169,040\pm1,100$ cal/mole. The 4-day old precipitate contained particles smaller than 100 A in size, and so this K is presumably larger than it would be for longer-aged amorphous material.

ular $Fe(OH)_3^\circ(aq)$, however Lengweiler and others (1961 a, b) showed by ultracentrifugation and electron microsc py that the species presumed to be molecular $Fe(OH)_3^\circ$ in this case were chiefly colloidal-sized ferric oxyhydroxides.

The Gibbs free-energy data for the aqueous ferric species in table 1 indicate that the solubility of the ferric oxyhydroxides as ionic species and molecular $Fe(OH)_3^\circ(aq)$ is less than 2×10^{-7} molar (0.01 milligrams per liter as Fe) between pH 5 and 10. The large concentrations of ferric iron in many natural waters within this pH range (greater than 2×10^{-4} molar in some coastal plain ground waters; Langmuir, in press) are present as colloidal and suspended ferric oxyhydroxides.

THE FERRIC OXYHYDROXIDES

Experimental studies described by Welo and Baudisch (1934), Feitknecht (1959), and Feitknecht and Michaels (1962), show that the minerology of freshly precipitated ferric oxyhydroxides depends on the method or conditions of precipitation. For conditions of geologic interest, at ambient temperatures, the phases most often precipitated from solution are goethite and amorphous ferric oxyhydroxide. Goethite is precipitated by the slow oxidation of aqueous or solid ferrous iron species. The precipitation reaction is probably important only above pH 4 because Fe^{+2} oxidation rates are practically negligible at lower pH's. Amorphous ferric oxyhydroxide is precipitated by a rapid increase in pH and a concomitant rapid hydrolysis of dissolved ferric iron species. The hydrolysis is probably important below pH 4 or 5 where the total concentration of dissolved ferric species can exceed 0.01 mg/l.

Welo and Baudisch (1934) note that the amorphous precipitate tends to convert spontaneously into goethite, although in some instances conversion may be incomplete even after years of aging at ambient temperatures. If, however, the amorphous phase is precipitated in the presence of Fe^{+2}, it tends to completely recrystallize into goethite (Feitknecht and Michaelis 1962).

Lepidocrocite, maghemite, and hematite are uncommon as direct precipitates from aqueous solution at low temperatures. According to Welo and Baudisch

(1934) and Feitknecht (1959), lepidocrocite most often precipitates in the pH range of 2 to 6.5 by the oxidation of aqueous or solid ferrous iron species in the presence of Fe^{+2}-complexing anions. Maghemite is usually formed by the oxidation of magnetite, or by the dehydration of lepidocrocite. Hematite usually crystallizes from amorphous ferric oxyhydroxide by dehydration, or by long-term aging in solution.

Examination of ferric oxyhydroxide precipitates using X-rays, ultramicroscopy, electron microscopy, ultracentrifugation, changes in solubility with particle size, and thermal dehydration techniques show that when precipitation takes place in aqueous solutions at ambient temperatures, a wide range of particle sizes, degrees of crystallinity, and degrees of hydration are possible for amorphous ferric oxyhydroxide, goethite, lepidocrocite, hematite, and probably also maghemite (Welo and Baudisch, 1934; Lamb and Jacques, 1938; Suito and others, 1959; and Feitknecht and Michaelis, 1962). These same studies demonstrate that phases which are not thermodynamically stable relative to their better crystallized and larger particle-sized (stable) forms, sometimes remain virtually unchanged for long periods of time at ambient temperatures.

High-temperature measurements and calculations by Schmalz (1959), led to $\Delta G^\circ = -304$ cal at 25°C for the reaction

$$\alpha\text{-}Fe_2O_3 + H_2O(l) = 2[\alpha\text{-}FeOOH] \qquad (1)$$

between stable forms of hematite and goethite (see also Garrels and Christ, 1965). At the time of Schmalz's work no measured entropy or enthalpy data were available for goethite. Recent measurements described in table 1, permit a direct calculation of ΔG_f° for stable goethite, and give $\Delta G^\circ = 1{,}666 \pm 60$ cal for reaction 1 (see O'Connor, 1968). This value proves that goethite should dissociate spontaneously into hematite in water at 25°C. The fact that goethite is quite common in surface environments probably reflects its low nucleation energy in solution as compared to hematite, and the extremely slow kinetics of its dehydration and recrystallization to hematite at ambient temperatures.

The particle size of synthetic ferric oxyhydroxides has been studied in the laboratory by Lamb and Jacques (1938), Suito and others (1959), and Feitknecht and Michaelis (1962). The evidence proves that a continuum of sizes can exist from single $Fe(OH)_3^\circ$ molecules to macroscopic particles. The electron micrographs of Feitknecht (1959) and Feitknecht and Michaelis (1962) show that the particle size of the amorphous material is generally much smaller than that of coexisting goethite, and that precipitates of both forms may contain particles as small as 50–100 angstrom units in size which persist after years of aging. These same studies reveal that lepidocrocite and hematite crystals which are in some instances not much larger than 100 A in size can also persist as such for long periods of time.

It is instructive to estimate the effect of particle size on the Gibbs free energy of formation of such small crystals relative to ΔG_f° for macroscopic crystals of the stable phase. If we assume that the phase is fine-grained goethite, which has a formula weight of 88.86 grams, and a density of 4.28 grams per cubic centimeter, and that the individual particles are cubes with an edge length of x centimeters, then the molar volume is $V = 20.7$ cubic centimeters per mole. Each particle has a volume of x^3 cubic centimeters, and a surface area (s) of $6x^2$ square centimeters. There are thus $N = 20.7/x^3$ particles per mole with a total molar surface area of $S = (N)(s) = (124/x)$ square centimeters. From the foregoing, and the factor 4.184×10^7 ergs per calorie, the difference in Gibbs free energy between stable coarse-grained, and fine-grained material is

$$\delta G^\circ = \frac{Q}{x}(2.96 \times 10^{-6}) \text{ cal/mole} \qquad (2)$$

where Q is the surface energy of goethite in ergs per square centimeter. Schindler (1967) has discussed the surface energy of several metal oxides and hydroxides in aqueous solution (see also Dundon, 1928, and Hostetler, 1963). These findings show that the surface energy of goethite is probably between 200 and 800, and may be about 400 ergs per square centimeter. Equation 2 has been plotted in figure 1 for surface energies of 200, 400, and 800 ergs/cm^2.

Based on figure 1, the activity product of goethite particles smaller than 100 A should be at least 0.4–1.8 $\log_{10}$ units greater than that of stable material. The effect of particle size on the thermodynamic stability of the other ferric oxyhydroxides is probably similar to its estimated effort on the stability of goethite.

Experimental measurements which permit the calculation of actual differences in ΔG_f° between thermodynamically stable and unstable forms is largely lacking for the ferric oxyhydroxides. However, some such information is available for amorphous ferric oxyhydroxide and for goethite (table 1). A graphic summary of the stability data for the ferric oxyhydroxides is shown in figure 2. The activity products, $(a\mathrm{Fe}^{+3})(a\mathrm{OH}^{-1})^3$, for thermodynamically most stable hematite and goethite have been calculated from ΔG_f° data in table 1. The other activity-product information in the figure is based on solubility measurements described in the footnotes of table 1.

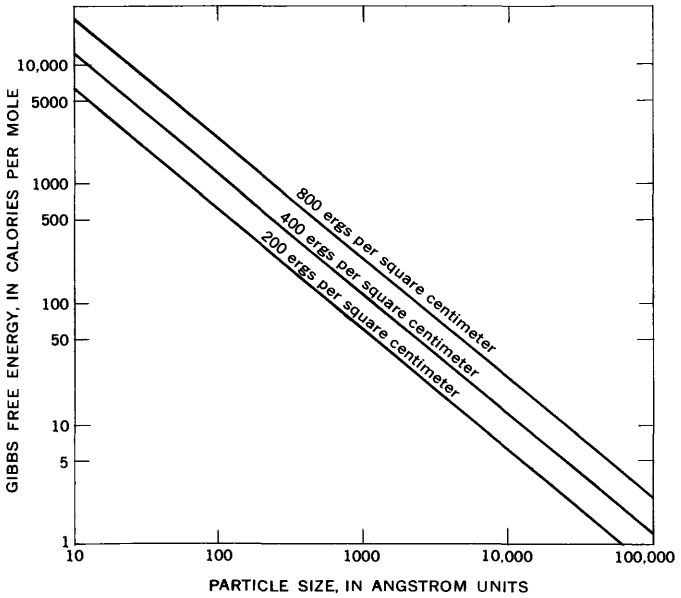

FIGURE 1.—The increase of Gibbs free energy ($\delta G°$), in calories per mole, resulting from decreasing particle size of goethite, assuming goethite surface energies of 200, 400, and 800 ergs/cm^2.

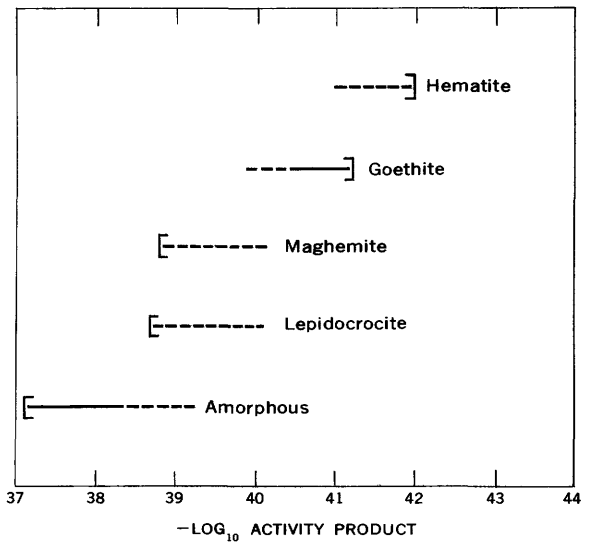

FIGURE 2.—Comparison of the possible ranges of stability of the ferric oxyhydroxides at 25°C and 1 atmosphere total pressure, expressed in terms of the activity product, $K=(aFe^{+3})\ (aOH^{-1})^3$. Brackets denote least-stable ([) or most-stable forms (]). Solid horizontal lines are known ranges of stability. Dashed horizontal lines are presumed ranges of stability, and as such their extent is conjectural.

REFERENCES

Barany, R., 1965, Heats of formation of geothite, ferrous vanadate, and manganese molybdate: U.S. Bur. Mines Rept. Inv. 6618, 10 p.

Cooper, L. H. N., 1938, Some conditions governing the solubility of iron: Proc. Royal Soc. London, ser. B, v. 124, p. 299–307.

Doyle, R. W., 1967, Eh and thermodynamic equilibrium in environments containing dissolved ferrous iron: Yale University, unpub. Ph. D. dissert., 100 p.

Dundon, M. L., 1923, Surface energy of several salts: Am. Chem. Soc. Jour., v. 45, p. 2658–2666.

Elder, L. W., 1930, A comparison of certain hydrogen ion electrodes in the presence of ferric iron: Electrochem. Soc. Trans., v. 57, p. 383–393.

Evans, U. R., and Pryor, M. J., 1949, The passivity of metals, Pt. IX. The solubility product of freshly precipitated ferric hydroxide: Chem. Soc. Jour. (London), pt. 5, p. 157–160.

Feitknecht, Walter, 1959, Über die Oxydation von festen Hydroxyverbindungen des Eisens in Wasserigen Lösungen: Zeitschr. Elektrochem., v. 63, p. 34–43.

Feitknecht, Walter, and Michaelis, Walter, 1962, Hydrolysis of iron(III) perchlorate solutions: Helvetica Chim. Acta, v. 45, p. 212–224.

Feitknecht, Walter, and Schindler, P. W., 1963, Solubility constants of metal oxides, metal hydroxides, and metal hydroxide salts in aqueous solution: Pure Appl. Chemistry, v. 6, no. 2, p. 130–159.

Garrels, R. M., and Christ, C. L., 1965, Solutions, minerals and equilibria: New York, Harper and Row, 450 p.

Gayer, K. H., and Woontner, Leo, 1956, The solubility of ferrous hydroxide and ferric hydroxide in acidic and basic media at 25°C: Phys. Chem. Jour., v. 60, p. 1569–1571.

Harned, H. S., and Davis, R., Jr., 1943, The ionization constant of carbonic acid in water and the solubility of carbon dioxide in water and aqueous salt solutions from 0° to 50°C: Am. Chem. Soc. Jour., v. 65, p. 2030–2037.

Harned, H. S., and Scholes, S. R., Jr., 1941, The ionization constant of HCO_3^{-1} from 0° to 50°C: Am. Chem. Soc. Jour., v. 63, p. 1706–1709.

Hem, J. D., and Cropper, W. H., 1959, Survey of ferrous-ferric chemical equilibria and redox potentials: U.S. Geol. Survey Water-Supply Paper 1459–A, 31 p.

Hostetler, P. B., 1963, The stability and surface energy of brucite in water at 25°C: Am. Jour. Sci., v. 261, p. 238–258.

Kriukov, P. A., and Awsejewitsch, G. P., 1933, Hydrolysis and oxidation-reduction potential in the ferrous-ferric system: Zeitschr. Elektrochem., v. 39, p. 884–891.

Lamb, A. B., and Jacques, A. G., 1938, The slow hydrolysis of ferric chloride in dilute solution. II. The change in hydrogen ion concentration: Am. Chem. Soc. Jour., v. 60, p. 1215–1225.

Langmuir, Donald, 1965, Stability of carbonates in the system $MgO–CO_2–H_2O$: Jour. Geology, v. 73, p. 730–754.

———1968, Stability of calcite based on aqueous solubility measurements: Geochim. et Cosmochim Acta, v. 32, no. 8, p. 835–852.

———1969, Iron in ground waters of the Magothy and Raritan Formations in Camden and Burlington Counties, New Jersey: New Jersey Dept. Conserv. and Econ. Devel., Water Resources Circ. [In press]

Larson, J. W., Cerutti, P., Garber, H. K., and Hepler, L. G., 1968, Electrode potentials and thermodynamic data for aqueous ions. Copper, zinc, cadmium, iron, cobalt, and nickel: Phys. Chem. Jour., v. 72, no. 8, p. 2902–2907.

Latimer, W. M., 1952, Oxidation potentials: New York, Prentice-Hall, 2d ed., 392 p.

Lengweiler, H., Buser, W., and Feitknecht, Walter, 1961a, Die Ermittlung der Löslichkeit von Eisen(III)-hydroxiden mit ^{59}Fe.I. Fällungsund Auflösungsversuche: Helvetica Chim. Acta, v. 44, no. 91, p. 796–805.

Lengweiler, H., Buser, W., and Feitknecht, Walter, 1961b, Die Ermittlung der Löslichkeit von Eisen(III)-hydroxiden mit ^{59}Fe.II Der Zustand kleinster Mengen Eisen(III)-hydroxid in Wässeriger Lösung: Helvetica Chim. Acta, v. 44, no. 92, p. 805–811.

Leussing, D. L., and Kolthoff, I. M., 1953, The solubility product of ferrous hydroxide and the ionization of the aquoferrous ion: Am. Chem. Soc. Jour., v. 75, p. 2476–2479.

O'Connor, J. T., 1968, Mineral stability at the Martian surface: Geophys. Research Jour., v. 73, no. 16, p. 5301–5311.

Robie, R. A., and Waldbaum, D. R., 1968, Thermodynamic properties of minerals and related substances at 298.15°K and one atmosphere pressure and at higher temperatures: U.S. Geol. Survey Bull. 1259, 256 p.

Schindler, P. W., 1967, Heterogeneous equilibria involving oxides, hydroxides, carbonates, and hydroxide carbonates, *in* Equilibrium concepts in natural water systems—a symposium: Am. Chem. Soc., Advances in Chem. Ser. 67, p. 196–221.

Schindler, P. W., Michaelis, W., and Feitknecht, Walter, 1963, Löslichkeits-produckte von Metalloxiden und-hydroxiden. VIII. Die Löslichkeit gealterter Eisen(III)-hydroxid-Fällungen: Helvetica Chim. Acta, v. 46, no. 46, p. 444–449.

Schmalz, R. F., 1959, A note on the system Fe_2O_3–H_2O: Geophys. Research Jour., v. 64, no. 5, p. 575–579.

Smith, H. J., 1918, On equilibrium in the system ferrous carbonate, carbon dioxide, and water: Am. Chem. Soc. Jour., v. 40, p. 879.

Suito, E., Ueda, Natsu, and Katsumi, M., 1959, Measurement of the size of colloidal particles by ultracentifugal methods and electron microscopy: Inst. Chem. Research Bull., Kyoto Univ., v. 36, no. 6, p. 197–205.

Wagman, D. D., Evans, W. H., Halow, I., Parker, V. B., Bailey, S. M., and Schumm, R. H., 1965, Selected values of chemical thermodynamic properties, Pt. I. Tables for the first 23 elements in the standard order of arrangement: Natl. Bur. Standards Tech. Note 270–1, U.S. Dept. Commerce, p. 124.

Welo, L. A., and Baudisch, Oskar, 1934, Active iron. II. Relationships among the oxide hydrates and oxides of iron and some of their properties: Chem. Rev., v. 15, p. 1–43.

THE SOURCES OF CARBON DIOXIDE IN THE ZONE OF AERATION OF THE BANDELIER TUFF, NEAR LOS ALAMOS, NEW MEXICO

By J. L. KUNKLER, Santa Fe, N. Mex.

Work done in cooperation with the U.S. Atomic Energy Commission and the Los Alamos Scientific Laboratory

Abstract.—Circulation of gas in the zone of aeration of the Bandelier Tuff in the vicinity of Los Alamos, N. Mex., has been under study for several years. Clues to the circulation pattern may be obtained from the carbon dioxide composition and concentration in the zone of aeration. Techniques for collection of samples of carbon dioxide for various analyses have been developed. Analyses of the data show that the carbon dioxide is of mixed origin, part is atmospheric and part is biogenic. Radiocarbon ages for the carbon dioxide could not be determined because of contamination in the zone of aeration by artificially produced radiocarbon.

Most reservoir rocks within the zone of aeration contain carbon dioxide (CO_2) derived from the decomposition of organic material, the solution of rock, the thermal decomposition of rock, the respiration of plant roots, and the atmosphere. The composition of reservoir CO_2 is related to the chemical composition of ground water through reactions that take place along the upper boundary of the zone of saturation; hence, studies of the composition of reservoir CO_2 probably have application to ground-water studies.

The purpose of this paper is to present a method for interpreting the source and movement of reservoir gas. The data presented were collected during a study of the dynamics of reservoir gas of the Bandelier Tuff, near Los Alamos, N. Mex.

Isotopes of light elements such as carbon may be separated by chemical processes. These processes, known as isotopic fractionation, are widespread in nature, and form the basis for interpretating many natural phenomena. A comprehensive dissertation on the mechanisms and geological significance of isotopic fractionation is beyond the scope of this paper, which summarizes only a few aspects of the subject. Interested readers will find a review of many studies summarized by Rankama (1963, p. 188–260).

Two of the three natural isotopes of carbon, carbon-12 (^{12}C) and carbon-13 (^{13}C), are stable. The third, carbon-14 or radiocarbon (^{14}C), is unstable, decaying with a beta emmission to form nitrogen-14 (^{14}N). The half life of this reaction is about 5,730 years. The stable isotope ratios are usually reported as $\delta^{13}C$, which is derived as follows:

$$\delta^{13}C=\left[\frac{^{13}C/^{12}C \text{ sample}}{^{13}C/^{12}C \text{ standard}}\right]-1\times 1{,}000$$

where the $^{13}C/^{12}C$ standard is the Peedee Belemnite (PDB) standard. The values of $\delta^{13}C$ are given in permil, and are preceded by a plus, or a minus, symbol which signify respectively that the ratio is enriched, or depleted, in ^{13}C compared to the PDB standard.

Radiocarbon is produced in the atmosphere by the bombardment of nitrogen atoms with cosmic rays. The zone of maximum production is probably about 12 kilometers above sea level. Some ^{14}C forms at lower altitudes, and an insignificant amount may form in the reservoir rock by this mechanism. During the last two decades, large amounts of ^{14}C have been added to the atmosphere as a byproduct of nuclear reactions. The amount of artificially produced ^{14}C in the atmosphere varies with time and place; it was estimated in 1959 to be 1¾ times natural amount (Hagemann and others, 1959, p. 550). Radiocarbon formed by these methods is readily oxidized to carbon dioxide; hence most atmospheric ^{14}C exists as $^{14}CO_2$.

Radiocarbon concentrations are reported in this paper as the percentage of a modern standard. The modern standard is defined as 0.95 of the ^{14}C activity

U.S. GEOL. SURVEY PROF. PAPER 650-B, PAGES B185-B188

in a standard oxalic acid prepared by the National Bureau of Standards. For practical purposes, any concentration of ^{14}C greater than 100 percent of the modern standard is contaminated with artificially produced ^{14}C.

The mean-residence age of reservoir-carbon dioxide can be computed for a given sample if the activity of that sample is compared with the activity of carbon dioxide of a known age. Mean-residence ages computed by this method are only apparent ages because they are a function of both the amount of radioactive decay that has taken place since the gas and its parent material were formed, and the amount of isotopic fractionation that has taken place during their subsurface history. The apparent ages are commonly corrected for the effect of isotopic fractionation by use of the stable isotopic ratios. These corrections are based on the assumption that the radiocarbon has been fractionated to an extent that is proportional to the fractionation of ^{13}C from ^{12}C.

A mean-residence age, corrected for isotopic fractionation, does not provide a mean age for the gas; it gives only the mean age of the carbon, which may be much older than the gas. For example, if the CO_2 has been recently evolved by the thermal decomposition of an ancient limestone, the mean-residence age of the gas may be a few months, but the mean-residence age of the carbon may be millions of years. It is apparent that the origin of the CO_2 must be inferred in order to interpret these data; this paper shows how the origin of CO_2 in the zone of aeration may be inferred.

DESCRIPTION OF TEST SITE

The data presented in this paper were collected from two test holes at a test site designated as TA–52, which is about 1½ miles south of Los Alamos, N. Mex. Two test holes were constructed, TA–52–22, 290 feet deep, and TA–52–23, 83 feet deep. The lower 19 feet of TA–52–22 and the lower 11 feet of TA–52–23 are gravel packed to form a test zone. Open pipes cemented in the holes lead from test zones to the land surface.

The test site is underlain by Bandelier Tuff which was described by Griggs (1964); surface altitude is about 7,200 feet. Canyons border the test site on the north and south, and within 100 yards horizontally from the site the bottoms of both canyons are lower than the bottom of test hole TA–52–23. The test site is covered with a thin layer of soil that is thick enough, in places, to support a few scrub oak, piñon pine, and juniper trees. Ponderosa pine grow on the floors and walls of the canyons where there is sufficient soil. Soil thickness probably does not exceed 2 feet anywhere except on the canyon floors. Rock is exposed at many places along the canyon walls.

The Bandelier Tuff is jointed to a depth of about 245 feet at the test site. It is likely that the Ponderosa pine extend their roots into these joints to depths of at least 50 feet. Tree roots have been observed at this depth in other test holes.

The Bandelier Tuff in the vicinity of the test site is generally unsaturated with water to a depth of about 1,000 feet; however, there may be perched water in alluvial material forming the canyon floors. The reservoir gas is saturated with water vapor at the reservoir temperature of about 25°C.

METHODS OF STUDY

Reservoir gas was pumped from the test zones through a scrubber that contained about 22 liters of 2.5*N* sodium hydroxide. The CO_2 was removed from the gas by reacting with the hydroxyl ion to form carbonate ion. The carbonate ion was precipitated as $BaCO_3$. The precipitates were washed, dried, and mailed to a commercial firm (Isotopes Inc.) for radiocarbon and stable-isotope determinations. Isotopic fractionation during sample collection was minimized by operating the scrubber at high efficiency. Carbon dioxide concentration determinations at the inlet and outlet of the scrubber indicate that about 97 percent of the CO_2 was removed from the reservoir gas.

The CO_2 concentrations were determined with a Kitagawa gas detector kit, a direct-reading colorimetric gas detector device. The analytical limitations of gas detector kits have been studied by many workers, and a typical conclusion is that they provide only semiquantitative data (Kusnetz and others, 1960, p. 373). In general, this conclusion may be warranted; however, the kit used in this study deserves a more commendable recommendation, perhaps because it is better than most.

The gas pump in the Kitagawa kit can be fitted with two types of CO_2 detector tubes, a low-range tube (0–7,000 parts per million by volume), or a high-range tube (0–26,000 ppm by volume). All field determinations were made in duplicate, most often with low-range detector tubes. These measurements were frequently checked with a determination from a high-range tube. Except for the determinations of very low concentrations the duplicate determinations usually checked within 5 percent; and determinations made with a high-range tube usually checked within 10 percent.

The concentration of atmospheric CO_2 was determined frequently as 300±50 ppm by volume, a value that agrees favorably with published determinations (Rankama and Sahama, 1949, p. 307). In addition, weighed masses of dry ice were sublimated in a gas chamber which contained air with an initial CO_2 concentration of 300–500 ppm by volume; the total CO_2 concentrations of the chamber were calculated and air from the chamber was sampled. The results of these tests are given in table 1.

TABLE 1.—*Calculated and determined CO_2 concentrations, in parts per million by volume, noted in laboratory testing of detector tubes*

[*A*, low-range tubes; *B*, high-range tubes]

Calculated	Determined	
	A	B
4,400±100	4, 300	
	4, 300	3, 900
8,150±100	8, 400	
	8, 600	8, 100

The reservoir gas pressures have been studied intermittently. These studies show that the reservoir pressures respond to changes in the atmospheric pressure. The response decreases with depth and is significant at depths of 100 feet, but is insignificant at the 290-foot depth.

INTERPRETATION OF DATA

Analysis of selected data given in table 2 provides some clues as to the origin of the reservoir CO_2.

TABLE 2.—*Selected data for CO_2 in samples of reservoir gas collected and discussed in this study*

Test hole	Depth of test zone (feet below land surface)	Date of collection	CO_2 (percent by volume)	^{14}C (percent of modern standard)	$\delta^{13}C$ (permil, relative to PDB standard)
TA–52–22	272–291	8–24–67	0.47	101	−18.5
		12– 4–67	.45		
TA–52–23	78–83	8– 5–67	.89	115	−17.9
		12– 5–67	.78		
		1– 8–68	.67		

1. The $\delta^{13}C$ from both test zones is nearly identical. It is surmised that the CO_2 at both depths is from the same source or sources (Craig, 1953, p. 53–92).

2. The high ^{14}C concentrations indicate a source that is atmospheric, biogenic, or some combination that includes one of these. The concentration of CO_2 in the atmosphere is about 0.03 percent by volume. The $\delta^{13}C$ of atmospheric CO_2 is about −7 permil (Craig, 1953, p. 60); hence, the source is not entirely atmospheric.

The value of $\delta^{13}C_B$ of the biogenic source can be calculated from the following relations:

$$\delta^{13}C_B = \frac{(V_R\delta^{13}C_R)-(V_A\delta^{13}C_A)}{(V_R-V_A)},$$

where V_A and V_R are respectively the percentage by volume of CO_2 of the atmosphere and of the reservoir gas, and $\delta^{13}C_A$ and $\delta^{13}C_R$ are the respective $\delta^{13}C$ values for atmospheric and reservoir CO_2. From this relation the $\delta^{13}C_B$ values of the shallow and deep test zones are −19.3 and −18.3 permil.

3. The variations of CO_2 concentrations of the reservoir gas from test hole TA–52–23 are much greater than those measured in the gas from test hole TA–52–22. This suggests a biogenic source that is nearer the 80-foot depth than the 290-foot depth.

Three specific biogenic sources are possible. The CO_2 may have been formed by the decomposition of deep tree roots or of soil humus, or it may have been respired by deep tree roots. The decomposition of deep tree roots probably is not a cyclic process, and the patterns of changes in reservoir gas pressures and the CO_2 concentrations do not support a shallow origin; hence, the most likely source is from respiring tree roots.

Respired CO_2 should be enriched with ^{13}C with respect to the wood by about 5 permil (Craig, 1954, p. 126). It may be significant that the $\delta^{13}C$ values of −19.3 and −18.3 determined for the biogenic CO_2 are enriched with ^{13}C with respect to wood by about this amount (Craig, 1953, p. 60).

4. Plant roots cannot survive in poorly aerated or unaerated soils because the CO_2 concentrations of the soil gas tends to be too high. It is commonly supposed that the CO_2 concentration of the soil gas in fertile soils is controlled by aeration, which is defined for this paper as any process that causes an exchange of reservoir gas with the atmosphere. The observed presence of deep tree roots and variations in CO_2 concentrations suggests that the reservoir is efficiently aerated to a depth of at least 80 feet. Aeration may be enhanced by the presence of nearby canyons which allow lateral movement of the reservoir gas. It is therefore assumed that the CO_2 in the reservoir gas has an origin that is in part biogenic and in part atmospheric and that some of the CO_2 is lost to the atmosphere through aeration.

Ground water may remove some CO_2 from the zone of aeration by solution and subsequent movement from the reservoir. Calculations made from analyses of ground water indicate a much lower concentration of CO_2 along the liquid-gas interface of the main aquifer than was measured at the 290-foot depth at the test site.

It is concluded, therefore, that the mechanisms of aeration and solution remove CO_2 from the reservoir, and as a consequence the CO_2 concentrations decrease with depth below the biogenic source. A further con-

sequence is that there must be a significant downward movement of CO_2 and that its mean age will increase with depth.

It has been shown that the data can be interpreted to give a tenuous origin for CO_2 in the reservoir air. The origin is a mixed one, part respiratory and part atmospheric. The significance of the interpretation is that the reservoir CO_2 has been a gas during its total residence and that any radiocarbon age will be a measure of the mean reservoir age of the CO_2.

Radiocarbon ages could not be calculated for either sample because of contamination in the zone of aeration with artificially produced ^{14}C; however, the very small amount of contamination in the sample collected from test hole TA–52–22 indicates that the reservoir gas at this depth has a minimum mean age of about two decades.

The data and interpretations given in this paper are understandably controversial. The presence of artificially produced ^{14}C in the reservoir gas at depths of nearly 300 feet is difficult to believe. The suggestion that aeration may be effective at depths of 80 feet or more may be viewed with skepticism, and the $\delta^{13}C_B$ values of −18.3 and −19.3 permil for the biogenic CO_2 are very different from the values estimated for biogenic CO_2 in ground water (Pearson and White, 1967, p. 253).

Because the data are difficult to believe, the methods and techniques of sample collection have been subjected to many searching reviews which have uncovered the following supporting evidence. Preliminary data from a related study by the author show that the $\delta^{13}C$ values of CO_2 dissolved in local ground water approach a value of −19 permil where the water has not been contaminated or has not dissolved a significant amount of lime. Three sampling systems, numbered 1, 2, and 3 in table 3, were built during this study. The data from these systems suggest that isotopic fractionation was restricted to negligible amounts in system 3, and it is these data that are given in table 2.

The values of $\delta^{13}C_B$ appear to confirm Craig's theory that respired CO_2 is fractionated with respect to wood; however, there are enough uncertainties about the geologic and biologic environments of the test site to make this confirmation tenuous. A better confirmation might be obtained from studies at a more appropriate test site.

TABLE 3.—*Data from three sampling systems designed during this study*

System	Depth of test zone (feet)	Efficiency of system (percent of CO_2 removed)	^{14}C (percent of modern standard)	$\delta^{13}C_B$ (permil)
1	70–100	[1] 30–60	[2] 106	[2] −29.0
2	78–83	[1] 70	112	−22.5
3	78–83	97	115	−17.9
2	272–291	[1] 70	98.8	−22.2
3	272–291	97	101	−18.5

[1] Estimated.
[2] Analyses by U.S. Geological Survey, Washington, D.C., and Denver, Colo.

Geochemical studies of ground water are usually predicated upon the assumption that there is chemical equilibrium between the ionic species in the water, the mineral species, and the gases in the reservoir rock. At many places there is reason to doubt the validity of this assumption. The methods described in this paper can be used for a variety of ground-water studies, however, their main utility lies in their capability of determining whether chemical equilibrium exists between water in the zone of saturation and CO_2 in the zone of aeration.

REFERENCES

Craig, Harmon, 1953, The geochemistry of the stable isotopes: Geochim. et Cosmochim. Acta, v. 3, p. 52–92.

———1954, Carbon 13 in plants and the relationship between carbon 13 and carbon 14 variations in nature: Jour. Geology, v. 62, p. 115–149.

Griggs, R. L., 1964, Geology and ground-water resources of the Los Alamos area, New Mexico: U.S. Geol. Survey Water-Supply Paper 1753, 104 p., 21 figs.

Hagemann, French; Gray, James, Jr.; Machta, Lester; Turkevich, Anthony; 1959, Stratopheric carbon 14, carbon dioxide, and tritium: Science, v. 130, no. 3375, p. 542–552.

Kusnetz, H. L., Saltzman, B. E., Lanier, M. E., 1960, Calibration and evaluation of gas detecting tubes: Indus. Hygiene Jour., Oct. 1960, p. 361–373.

Pearson, F. J., Jr., White, D. E., 1967, Carbon 14 ages and flow rates of water in Carrizo Sand, Atascosa County, Texas: Water Resources Research, v. 3, no. 1., p. 251–261.

Rankama, Kalervo, 1963, Progress in isotope geology: New York, Interscience Publishers, 705 p.

Rankama, Kalervo, Sahama, Th. G., 1949, Geochemistry: Chicago, Ill., Univ. of Chicago Press, 912 p.

MEASUREMENT OF WATER FLOW AND SUSPENDED-SEDIMENT LOAD, BOLINAS LAGOON, BOLINAS, CALIFORNIA

By JOHN R. RITTER, Menlo Park, Calif.

Prepared in cooperation with the Bolinas Harbor District, and Marin County, Calif.

Abstract.—Measurement of water flow and sediment load at the lagoon inlet for a 10-hour tidal period (floodtide and ebbtide) on June 22, 1967, revealed that in that specific period of time 152 tons of suspended sediment was carried into the lagoon by the floodtide, whereas only 36 tons was carried out of the lagoon by the ebbtide. However, the major ebbtide which was not measured probably carried the largest load of the day. Bedload made up as much as 18 percent of the total load during floodtide and 15 percent during ebbtide. Ten water measurements and seven sediment measurements were made during the floodtide (lower low water to lower high water). Six water measurements and five sediment measurements were made during the ebbtide (lower high water to higher low water). One measurement each of water and sediment was made during the second floodtide. The maximum measured water flow and maximum average velocity during floodtide were 5,810 cubic feet per second and 3.5 feet per second, respectively; during ebbtide the maximums were 3,720 cfs and 2.4 fps. The range of floodtide was about 4 feet, and ebbtide about 1.3 feet. Higher temperatures of water at the inlet possibly indicated lagoon water and ebbtide, and lower ones, ocean water and floodtide.

The U.S. Geological Survey's program to determine the rate of sediment deposition and erosion in Bolinas Lagoon includes estimating the quantity of sediment moving in and out of the inlet to the lagoon. On June 22, 1967, the first measurement of the sediment load for a tidal period was made at the inlet. The tide there is a mixed, predominantly semidiurnal type. Water flow was measured from 6:30 a.m. (lower low water) to 5:30 p.m. (one hour past higher low water) and suspended-sediment samples were collected from 6:30 a.m. (lower low water) to 10:00 p.m. (nearly higher high water). This paper presents the results of the measurements and relates them to the tidal stage.

Bolinas Lagoon, bordered by the towns of Bolinas and Stinson Beach (fig. 1), is about 15 miles north of San Francisco. The lagoon, about 3 miles long and about 1 mile wide at its maximum dimensions, has a triangular shape. At lower low water about 70 percent of the bottom of the lagoon is exposed, whereas at higher high water only two islands, one of which is insignificant in size, remain above water. Fresh-water inflow to the lagoon from the 16.7-square mile drainage area is negligible in the summer, when the measurements described here were made.

The inlet usually is bounded by sandy beaches on each shore; however, the western beach often is entirely eroded away during winter storms, leaving bedrock abutting a high cliff. During periods of calm,

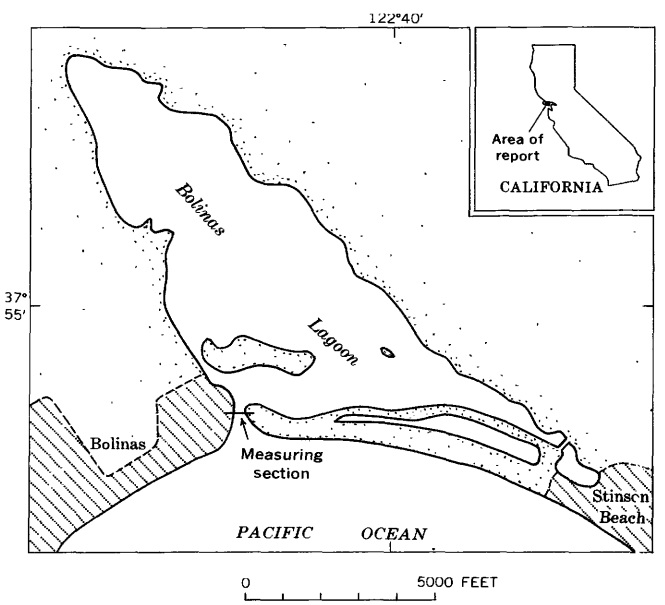

FIGURE 1.—Map of Bolinas Lagoon, Calif.

U.S. GEOL. SURVEY PROF. PAPER 650-B, PAGES B189-B193

the beach is reestablished. The middle of the inlet is lined with cobbles and bedrock.

Summer solstice occurred on June 22 and perigee was only 4 days earlier. This combination produced, on June 22, one of the highest tides of the year. The tide gage at Bolinas recorded a tidal range of from —1.97 to 4.10 feet (datum mean sea level) for the whole day, but the lower recording was erroneous because of ponding as explained later.

Waves during storms usually break in the inlet, but during the period of measurement storm waves were insignificant.

METHODS

A moving-boat technique, in which the boat moved at a rate of about 10 feet per minute along a cable stretched across the inlet, was used to measure water discharge. Two current meters, which were suspended from the boat and were adjusted for change in depth, measured the velocity of the current continuously at 0.2 and 0.8 of the depth. Direction of flow sensed by a current-orienting compass, depth of water, station, meter revolutions, and time were continuously registered on a panel of counters aboard the boat. The panel was photographed every 30 seconds by an automatically triggered 35-millimeter camera. The data on the film were tabulated, and water flow was then calculated by computer. The inlet was traversed 17 times, providing data for 17 flow measurements.

While flow was being measured, suspended-sediment samples were being collected on the same boat. Depth-integrated samples were collected at 5 to 7 stations during each measurement. On another boat, also in the inlet, point samples of sediment were collected from various depths, and samples of sediment moving along the bottom of the inlet were collected with an Arnhem sampler so that bedload could be calculated.

The temperature of the water, obtained with the samples of suspended sediment, was also measured.

RESULTS

Tidal stage, velocity, and flow

In figure 2 the results of the measurements at different tidal stages may be compared. The tide gage was about 900 feet north of the inlet in an area where ponding occurred during lower low water so that the water flowed out more slowly than it did in other parts of the lagoon. The tidal record was affected by the ponding until about 8:30 a.m. (fig. 2*A*). The tidal stage at the gage probably lagged behind that at the inlet by 15 to 30 minutes. Figure 2*A* shows the tidal stage for only the study period (6:30 a.m. to 5:30 p.m.); the maximum stage of 4.10 feet occurred at 11:30 p.m.

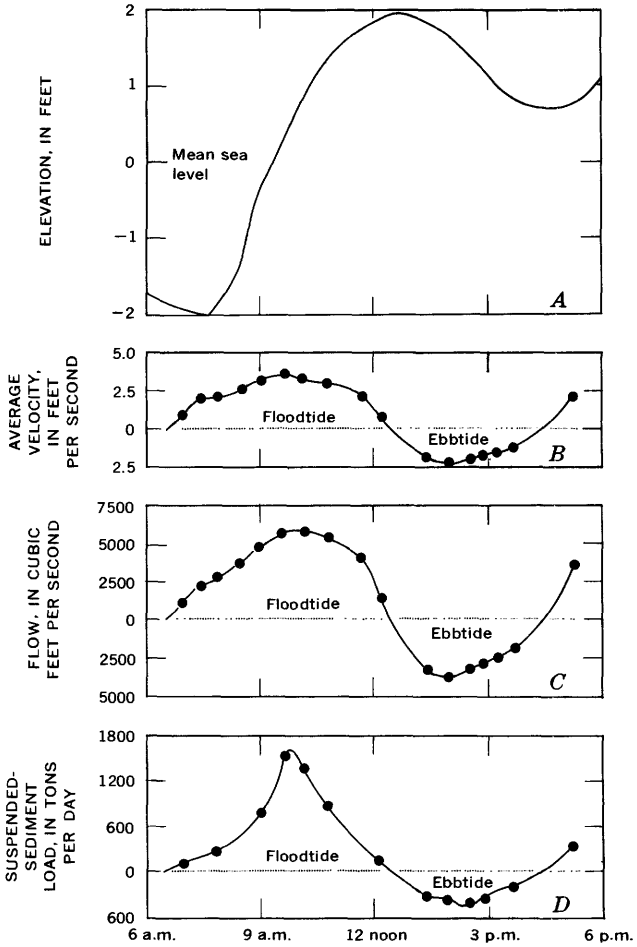

FIGURE 2.—Graphs of *A*, tidal stage; *B*, average velocity; *C*, water discharge; *D*, suspended-sediment load.

The average velocity in the inlet increased until about midtide and then decreased (fig. 2*B*). The maximum average velocity during floodtide was about 3.5 feet per second, and during ebbtide, about 2.4 fps.

The velocity in the cross section (fig. 3) was consistently higher in the middle of the channel than near the banks, except when the floodtide was about to change to ebbtide; then the higher velocity was near the west bank. During floodtide the position of maximum velocity ranged between stations 131 and 205. The two extremes occurred during the last two measurements of floodtide. The position of maximum velocity of ebbtide ranged between stations 135 and 192.

The maximum flow did not necessarily correspond to the maximum average velocity because during floodtide the area of the channel continued to increase after midtide while the velocity decreased. Conversely, during ebbtide the area decreased while the velocity increased until midtide. The maximum measured flow

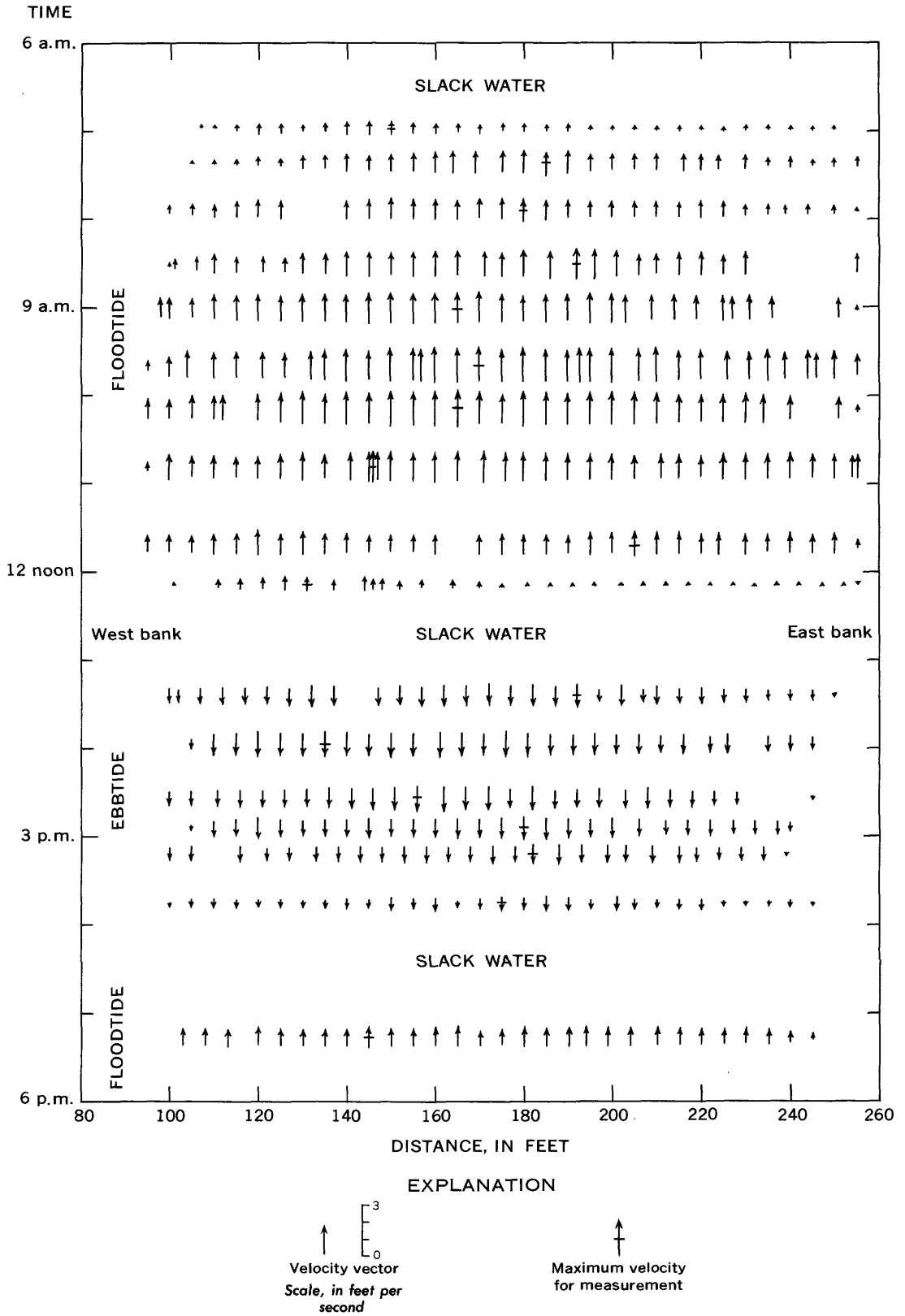

FIGURE 3.—Velocity variations in the inlet to Bolinas Lagoon, June 22, 1967. Each arrow represents a single velocity measurement, the amount of which is shown by the length of the arrow. Distances are from an arbitrary zero west of the channel.

328-687 O - 69 - 14

was 5,810 cfs during floodtide and 3,720 cfs during ebbtide (fig. 2*C*). During the 6-hour period of floodtide, 2,000 acre-feet of water flowed in through the inlet, and during the 4 hours of ebbtide 770 acre-feet flowed out.

Sediment transport

The quantity of suspended sediment, that sediment carried in suspension in water, transported into the lagoon was greater than the quantity that left the lagoon during the time of this study (fig. 2*D*) because (1) the duration of the floodtide was longer than that of the ebbtide, (2) the quantity of incoming water was much greater than the outgoing, and (3) the suspended-sediment concentration was higher during floodtide. About 152 tons of suspended sediment entered the lagoon and about 36 tons left; thus, 116 tons remained in the lagoon. Because the concentration of suspended sediment (fig. 4) was higher during the next floodtide (4:30 p.m. to 11:00 p.m.) probably much more sediment entered the lagoon during this later period. However, on the basis of the velocity of the following ebbtide (from higher high water to lower low water) which was observed to be much greater than that of the floodtides, all sediment carried into the lagoon during June 22 probably was carried out, and the net result probably was erosion in the lagoon. In more recent measurements throughout an entire tidal day, the major ebbtide transported more than three times the total suspended load of both floodtides.

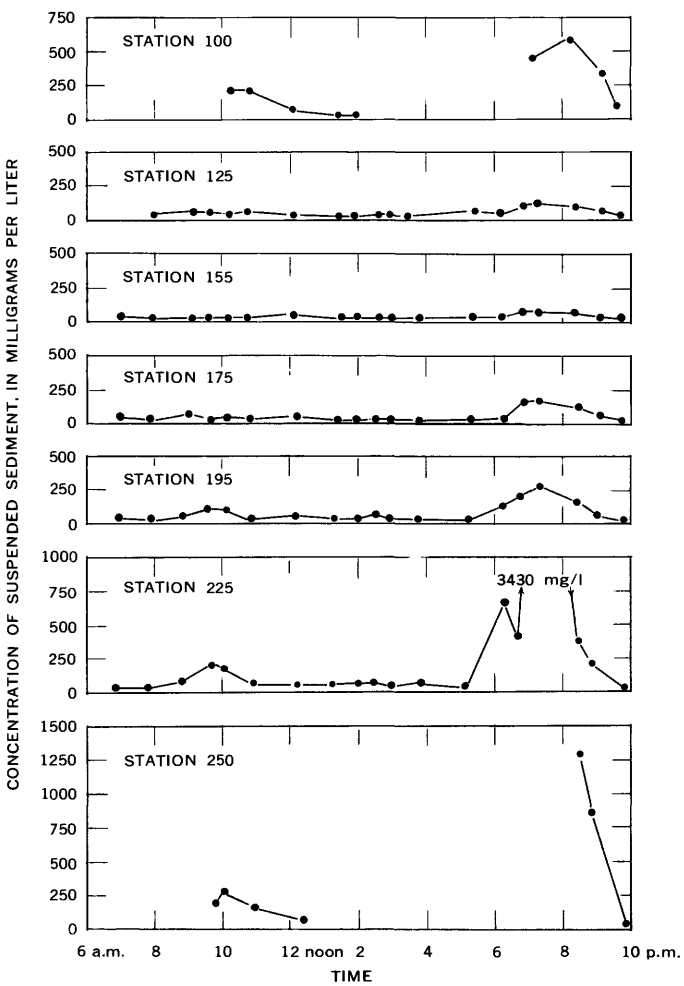

FIGURE 4.—Concentrations of suspended sediment at each sampling station on June 22, 1967. Stationing is according to the scale shown on the abcissa of figure 3.

Unfortunately, flow was not recorded during the higher floodtide because of a malfunction in the equipment. During the following ebbtide, conditions in the inlet became too hazardous to continue any measuring. Therefore, sediment loads from higher low water to lower low water are unknown.

The concentration of suspended sediment generally remained lower in the middle of the channel than near the banks (fig. 4). The banks, being composed of beach sand, contributed some sand to the channel when the velocity became high enough to erode the banks. Erosion of the banks was particularly noticeable during floodtide. The highest concentration of suspended sediment occurred during the period from higher low water to higher high water (4:30 p.m. to 11:00 p.m.), when the water reached its maximum extent over the banks. Even in the center of the channel (station 175), where the concentration had previously remained relatively constant, an increase in concentration was measured.

As shown in figure 5, the concentration of suspended sediment (silt and clay) finer than sand (<0.062 mm) remained almost constant throughout the cross section of the channel during each measurement. The increase in concentration, especially near the banks, was attributable to an increase in the quantity of sand carried in suspension. Thus, the major immediate sources of most of the transported sediment were the beaches adjacent to the channel.

Sampling indicated that the bedload, that part of the sediment load moving substantially in contact with the bed, made up as much as 18 percent of the total load, in effect bedload plus suspended load, during floodtide and 15 percent during ebbtide. The maximum bedload percentage was near the slack tide or at times when the suspended load was fairly low. At midtide, bedload was about 5 percent of the total load. The calculated maximum bedload rate was 950 tons per day at about the middle of floodtide.

Water temperature

The average temperature of the water along the measuring section ranged from 10.0°C to 16.7°C dur-

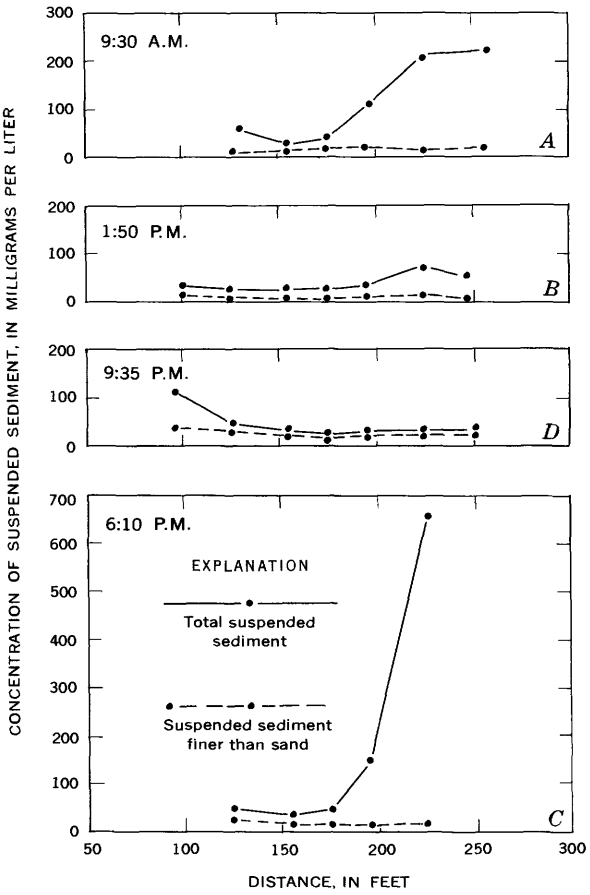

FIGURE 5.—Concentrations of total suspended sediment and that of suspended sediment finer than sand (<0.062 mm). Distances are from an arbitrary zero west of the channel.

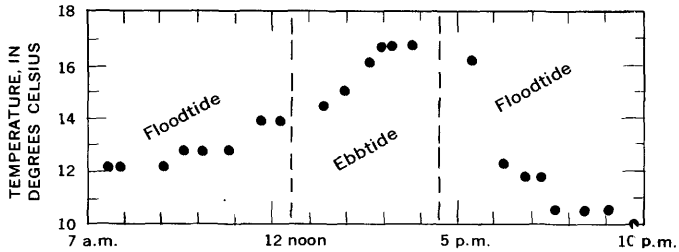

FIGURE 6.—Average water temperatures along measuring section (fig. 1) at inlet to Bolinas Lagoon, June 22, 1967.

ing the study period (fig. 6). The higher temperatures appeared to be associated with the lagoon water and ebbtide; the lower temperatures with ocean water and floodtide. The one high temperature noted during floodtide probably represents lagoon water that had not yet mixed with ocean water.

SUMMARY

Flow through the outlet during the 6-hour floodtide exceeded the flow during the 4-hour ebbtide by about 1,230 acre-feet. About 116 more tons of suspended sediment entered the lagoon than left during this period, which was only half a tidal day. The concentration of suspended silt and clay in the water passing through the outlet remained almost constant, while the concentration of sand increased and decreased with flow. Most of the suspended sediment was sand eroded from the beaches along the banks of the channel.

The calculated bedload was as much as 18 percent of the total load. The temperature of the water passing through the inlet is related to the residence time of the water in the lagoon.

SOIL-MOISTURE LOSSES IN THE UPPER THREE INCHES OF SOIL, CIBECUE RIDGE, ARIZONA

By M. R. COLLINGS, Tacoma, Wash.

Abstract.—Samples of the upper 3 inches of soil were collected on two small study areas in east-central Arizona. The samples have been collected intensively for 2 years during the period of summer rainfall to define a relation for predicting antecedent soil-moisture conditions. The data of available moisture (E) versus time (t) were found to fit an exponential regression of the type

$$E=b_0+be^{-ct},$$

where b_0, b, and c are constants, and e is the Napierian base. The regressions have 0.03-inch and 0.04-inch standard errors of estimate for areas 1 and 2, respectively. The findings indicate that antecedent soil moisture, in the upper 3 inches, may be predicted with 0.065-inch and 0.109-inch standard errors of estimate, respectively.

Cibecue Ridge is on the southwest edge of the Carrizo Creek drainage area, 2 miles southwest of the junction of Corduroy and Carrizo Creeks in east-central Arizona. The two small basins studied are situated in an area of coalescing alluvial fans on a relatively flat bench on the southeast side of Cibecue Ridge (fig. 1). Cibecue Ridge area 1 is 63 acres, and area 2 is 42 acres.

Basalt flows of Pleistocene age partly filled the Carrizo Creek valley and raised the base level of the tributary streams and the two basins, thereby causing deposition of the alluvial fan materials. Subsequent downcutting of the lava-filled main valley reentrenched the tributary streams to form the present drainage system.

The soils of the higher watershed, Cibecue Ridge area 1 (fig. 1), range in depth from 4 feet at the upper (west) end to 18 feet near the lower (east) end. The soils of the lower watershed, Cibecue Ridge area 2 (fig. 1), have a maximum depth of about 4 feet. Stones cover about 2 percent of the surface of area 1 as compared to more than 20 percent of area 2.

The vegetative cover is typical of the region and consists mainly of pinyon and juniper trees, chaparral, and, in open areas between trees, a partial ground cover of native grasses.

One of the areas ultimately will be cleared of the juniper and pinyon cover, and the other area will be used as a control to determine the effect of the clearing on water yield (Myrick and Collings, 1962; Collings and Myrick, 1966). Because loss by surface runoff at present accounts for only 5 percent of the water budget, a small change resulting from the clearing of vegetation may cause a large increase in the percentage of runoff.

A parameter to be considered in evaluating the amount of yield for a given storm is the antecedent soil moisture, or the moisture in the soil immediately preceding the storm. Therefore, to determine the regression equation and to predict the antecedent moisture conditions for precipitation-runoff relations, a study was made of the moisture losses in the upper 3 inches of soil in the 2 Cibecue Ridge areas.

DATA COLLECTION AND ANALYSIS

Near 5 sampling sites on Cibecue Ridge area 1 and near 6 sites on Cibecue Ridge area 2 (fig. 1), volumetric samples of the upper 3 inches of soil were collected in the 4 directions of the compass. From each of these samples, the soil density was determined. A statistical analysis indicated that the soil densities at the different sites were significantly different—the variance of the data being greater than could be defined by the error involved in sampling. However, a significant difference was not found within each sampling site. For subsequent calculation of percentage moisture by volume from samples taken for gravimetric determinations, the soil-density values established at each site were used. Periodic checks of these soil-density values demonstrated that they varied little with time and changes in moisture content.

Samples were collected intensively during two summer periods. Immediately after rainstorms, a sample was taken at each site and samples were collected two

U.S. GEOL. SURVEY PROF. PAPER 650-B, PAGES B194-B198

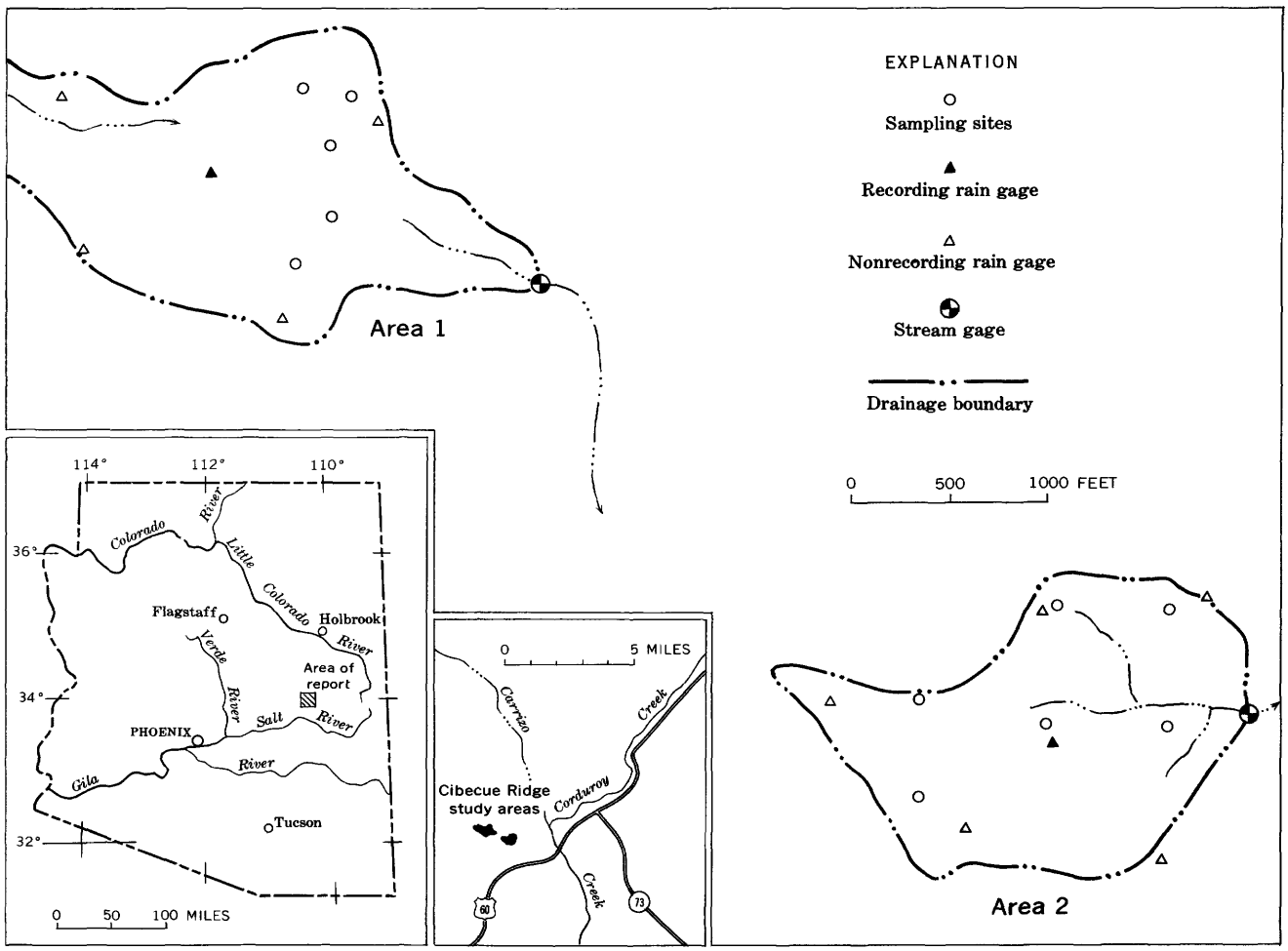

FIGURE 1.—Maps showing locations of the Cibecue Ridge study areas and soil-moisture sampling sites.

or more times a day. Between storms, during the soil-moisture depletion period, samples were collected twice daily whenever possible. The soil samples were weighed, dried and reweighed, and the volumetric moisture content was computed and converted to inches of moisture. Minimum values of moisture over the period of record were determined for each sampling site and substracted from the total number of inches of moisture. The average minimum values were 0.07 inch for area 1 and 0.10 inch for area 2. The values above the minimums were then referred to as available moisture.

The curve in figure 2 was fitted to the data by the least-squares method. The type relation was found to be an exponential regression of the type

$$E=be^{-ct}, \quad (1)$$

where E is available moisture, in inches; t is the time, in days; b and c are regression constants; and e is the Napierian base. Because the relation (fig. 2) is not linear in its parameters, a transformation and iterative methods of calculation are necessary (Williams, 1959).

The data plotted on figure 2 consist of mean available-moisture values from the 5 sampling sites in area 1 and from the 6 sites in area 2. These data were transformed by the e^{-ct} function; a least-squares fitting of the curve was then calculated. From an analysis of covariance of available moisture (E) versus e^{-ct} for area 1 and area 2, a significant difference in regressions was indicated at the 90-percent level, but not at the 95-percent level (table 1). By using the 90-percent confidence-level indication of different regressions, given by the statistics, it is possible to determine a least-squares curve of available moisture versus time for each area (fig. 3). The regression equation for area 1 was found to be

$$E=0.62e^{-0.32(t)} \quad (2)$$

with a standard error of estimate of 0.03 inch, and the equation for area 2 was found to be

$$E=0.52e^{-0.32(t)} \quad (3)$$

with a standard error of estimate of 0.4 inch.

As an experimental check of the fitted relations, the predicted available moisture was determined from

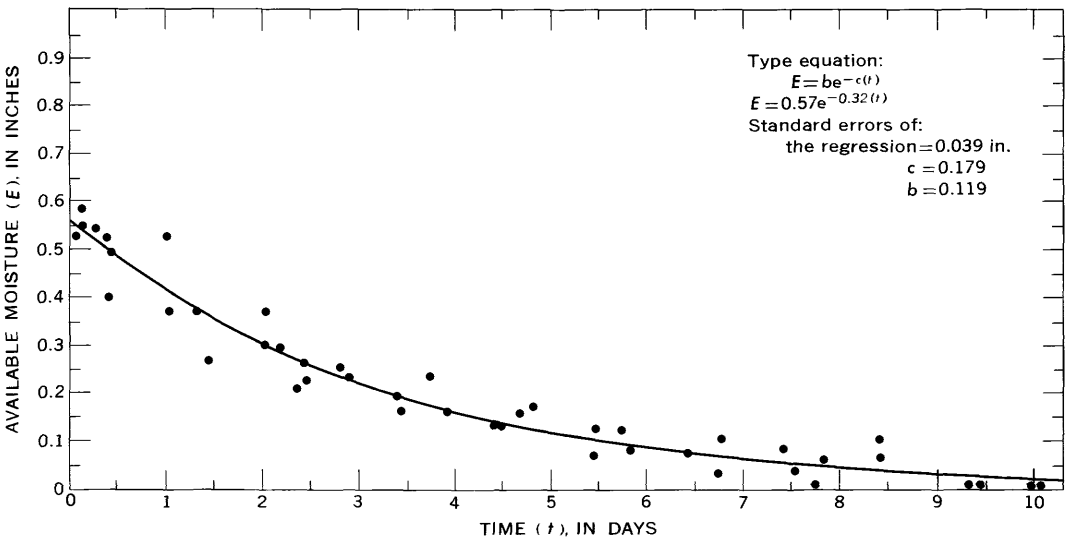

FIGURE 2.—Available moisture versus time for both Cibecue Ridge areas. Each point indicated on the graph is the mean value of either 5 samples from area 1 or 6 samples from area 2. The curve is representative of 110 samples from area 1 and 132 samples from area 2, a total of 242 samples.

TABLE 1.—*Analysis of covariance of available moisture* (E) *versus time* (t) *data transformed, for Cibecue Ridge areas 1 and 2*

Source of variance	Sum of squares			
	$(e^{-0.32t})$	$(e^{-0.32t})$ (E)	(E)	About the regression
Within each group:				
Area 1	1. 88905	1. 33193	0. 95753	0. 01841
Area 2	1. 83591	1. 15314	. 76173	. 03744
Among means	. 00001	. 00012	. 00218	. 00074
Within groups	3. 72496	2. 48507	1. 71926	. 06137
Total	3. 72497	2. 48519	1. 72144	. 06340

Tests:
1. For difference in mean values:
   $F=1.35$ $F_{0.90}$ (1, 41)=2.84, not significant.
2. To test if one regression line will fit all observations:
   $F=2.70$ $F_{0.90}$ (2, 40)=2.44, significant;
   $F_{0.95}$ (2, 40)=3.23, not significant.
3. To test if the slopes of the regression lines are the same:
   $F=3.95$ $F_{0.90}$ (1, 40)=2.84, significant;
   $F_{0.95}$ (1, 40)=4.08, not significant.

data that were not used to develop the curves by using the following method:

1. Starting with an available moisture (Ea) from an actual sample, the time (t_o) is obtained either from the curves (fig. 3) or by using equations 2 or 3. The time from sampling to the next rain (Δt_1) is added to t_o to obtain t_1.

2. From the value of t_1, the predicted antecedent moisture just before the rain (Ep_1) is calculated, using either equation 2 or 3.

3. The amount, in inches, of the next rain after t_1 (storms with no runoff were selected) is added to Ep_1 to obtain Ep_2, and then t_2 is calculated from the regression equation. Thus, t_2 is the starting point and Ep_2 is the available moisture immediately after the rain.

Knowing the difference in time (Δt_2) between the rain and the next sampling, t_3 is determined by adding $t_2+\Delta t_2$. Then Ep_3 is calculated from equation 2 or 3 and compared with the value of the actual sample.

In this way, 10 values of Ep_3 for each study area were compared with the actual data. The standard error of estimate of the predicted values versus the actual values is 0.06 inch for area 1 and 0.11 inch for area 2.

An example of computing predicted values of available moisture, to compare with actual values of available moisture, is given below:

The equation of the relation in figure 3, for area 1 is

$$E=0.62e^{-0.32(t)}.$$

The value of a soil sampling is $Ea=0.44$ inch, and

$$0.44=0.62e^{-0.32(t_0)}$$

$$t_0=1.04 \text{ days.}$$

After 0.4 day (Δt_1), 0.23 inch of rain fell (without runoff), and

$$t_1=t_o+\Delta t_1=1.04+0.4=1.44 \text{ days.}$$

The predicted available moisture at t_1 is

$$Ep_1=0.62e^{-0.32(1.44)}=0.39 \text{ inch.}$$

The predicted available moisture after 0.23 inch of rain is

$$Ep_2=Ep_1+\text{rain}=0.39+0.23=0.62 \text{ inch.}$$

After 1.0 days (Δt_2) another soil-moisture sample is taken, and the predicted value (Ep_3), starting at

$$0.62=0.62e^{-0.32(t_2)}, \text{ and}$$

$$t_2=0.0 \text{ day}$$

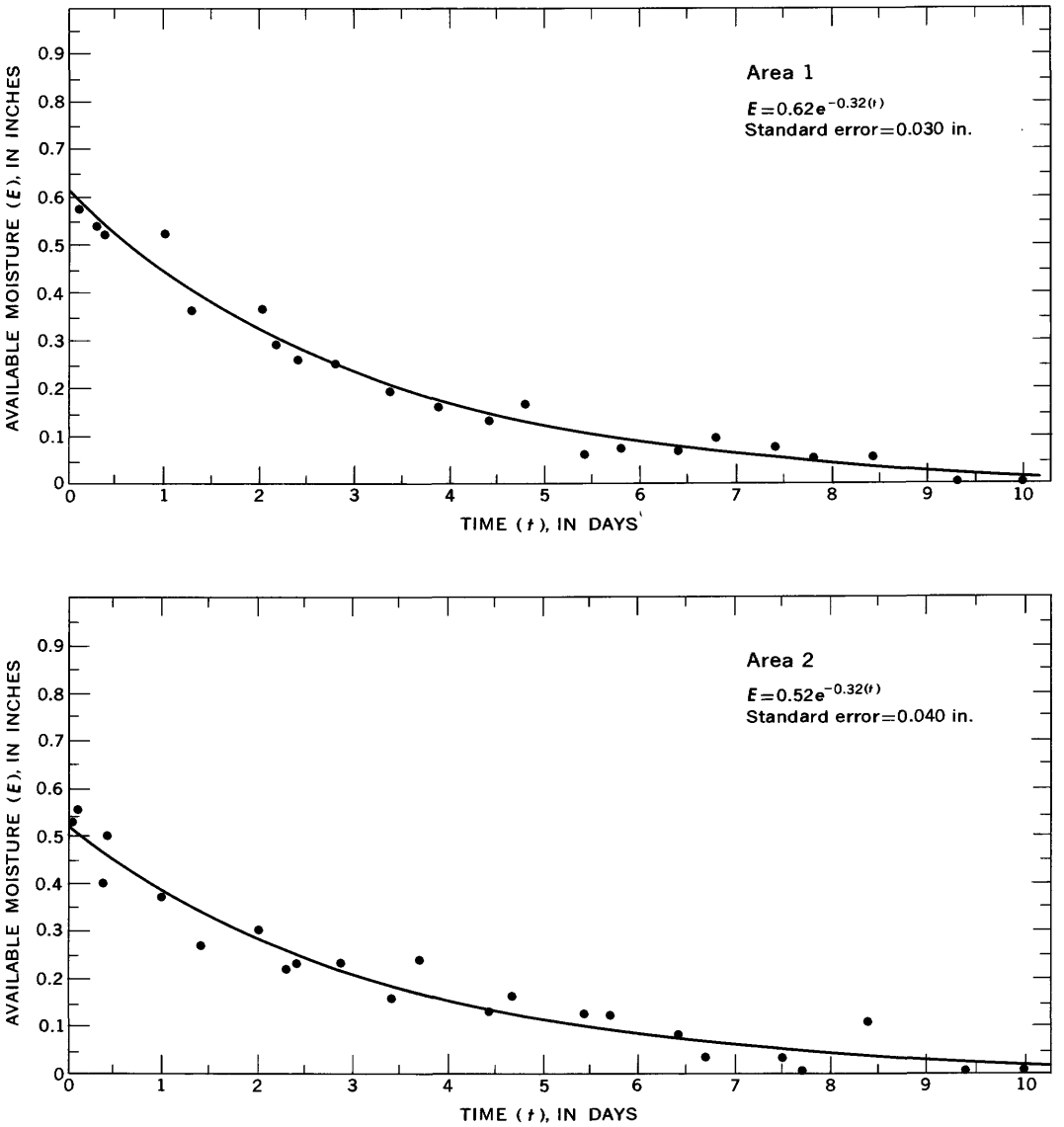

FIGURE 3.—Available moisture versus time for each Cibecue Ridge area. The relations show the decrease in available soil moisture with time for the mean of 5 sampling sites in area 1 and 6 sampling sites in area 2.

is

$$t_3=t_2+\Delta t_2=0.0+1.0=1.0 \text{ day, and}$$

$$Ep_3=0.62e^{-0.32(1.0)}=0.45 \text{ inch.}$$

The value of Ep_3 is then compared with the actual sampled value.

CONCLUSIONS

An analysis of the covariance of data from each area showed that the curves of figure 3 were different at the 90-percent significance level but not at the 95-percent level. Usually when there is no significant difference in mean values, one regression will fit all observations at the 95-percent level (table 1), and when the standard errors of estimate are acceptable, one relation would suffice (fig. 2). However, the standard error of estimate for area 1 is slightly lower in figure 3 than in the combined relation of figure 2, possibly because of the alinement and relative closeness of sampling sites in area 1 as compared to those in area 2 (fig. 1).

In addition to the improved curve fitting on area 1 it may also be desirable to define a relation for individual areas because area 2 is used as a control and area 1 will be cleared. If clearing causes a change in the available moisture relation this change would be more easily defined by evaluating pre- and post-clearing relations on both areas, rather than comparing the curve of the modified area 1 with a composite curve of areas 1 and 2.

REFERENCES

Collings, M. R., and Myrick, R. M., 1966, Effects of juniper and pinyon eradication on streamflow from Corduroy Creek basin, Arizona: U.S. Geol. Survey Prof. Paper 491–B, 12 p.

Myrick, R. M., and Collings, M. R., 1962, Hydrologic aspects of the pinyon and juniper eradication project on the Fort Apache Reservation, Arizona, *in* R. H. Weber and H. W. Peirce, eds., Guidebook of the Mogollon Rim region, east-central Arizona, Thirteenth Field Conference: New Mexico Geol. Soc., p. 140–142.

Williams, E. J., 1959, Regression analysis: New York, John Wiley and Sons, Inc., p. 62–64.

SUBJECT INDEX

[For major headings such as "Economic geology," "Geochemistry," "Ground water," see under State names or refer to table of contents]

AUTHOR INDEX

U.S. GOVERNMENT PRINTING OFFICE : 1969 O—328-687